

SUMMARY OF IHRA PEDESTRIAN SAFETY WG ACTIVITIES (2005) - PROPOSED TEST METHODS TO EVALUATE PEDESTRIAN PROTECTION AFFORDED BY PASSENGER CARS

Yoshiyuki Mizuno,

Chairman, on behalf of IHRA/ P.S. WG

Japan Automobile Standards Internationalization
Center (JASIC)

Japan

Paper Number 05-0138

ABSTRACT

This is the Summary Report of IHRA pedestrian safety working Group activities, which are completed in the past and will be completed in the near future.

INTRODUCTION

The primary tasks assigned to the IHRA/PS-WG were:

- a) investigating and analyzing the latest pedestrian accident data in the IHRA member countries, and
- b) establishing harmonized test procedures that would reflect such accident condition and would induce fatalities and alleviation of severe injuries in pedestrian vs. passenger car crashes.

These tasks would be carried out with the cooperation of all IHRA member countries.

The members of the IHRA Pedestrian safety Working Group (IHRA/PS-WG) is comprised of experts selected by the governments of Australia, Europe (EC/EEVC), Japan and U.S.A., and experts selected by the industrial organization of OICA and the chairperson selected by Japan.(see Table 11)

Approach of Application Systems

Biomechanics in the aspect of pedestrian accidents and the developments of test devices based on such bio-mechanics are still in the process of research.

A pedestrian dummy had not been developed at the beginning of this project. Also, pedestrian dummies have disadvantages when used as part of test methods to require protection for all statures of pedestrians. IHRA/PS-WG had to give up the idea of using a pedestrian dummy after consulting with the IHRA/Bio-WG. Beside this situation, the WG experts believe the subsystem test method has several merits such as repeatability, simplicity, impact locations of the vehicle can be freely chosen, and cost of the test.

One of the two primary tasks assigned to the IHRA/PS-WG was gathering the results of detailed research into the accidents Data to an agreed format has been collected from Australia, Europe, Japan and USA. The current dataset has been analyzed to determine the impact areas of vehicles, accidents frequency and injured regions of pedestrian vs. passenger car crashes and to decide research

priorities from these findings.

According to the priorities thus decided, the WG embarked on its research activities to develop adult and child head protection test methods, and adult lower leg/knee protection test method.

By the end of 2004, the WG has completed adult and child head test methods and adult lower leg/knee test method.

ACCIDENT DATA

The WG agreed that development of harmonized test procedures would be based upon real world crash data. Pertinent pedestrian and vehicle information contained in accident survey databases was accumulated. Pedestrian information included age, stature, gender, injured body region, and injury severity. Vehicle information included vehicle type, make, and year, mass, pedestrian contact location, damage pattern, and impact velocity. Other general accident information such as pedestrian crossing pattern, weather conditions, vehicle and pedestrian trajectories, alcohol use, etc. were also of interest if collected. Bicycle or motor-driven cyclists were not included in the study. Four injury databases from Australia, Germany, Japan, and United States were identified as containing much of this information. Multiple injuries per case were included in the dataset.

In Japan, pedestrian accident data collected by JARI between 1987 and 1988 and in-depth case study data of pedestrian accidents conducted by ITARDA between 1994 and 1998 were combined for inclusion into the IHRA accident dataset. A total of 240 cases were acquired in the cities surrounding the Japan Automobile Research Institute (JARI).

In Germany, investigation teams from both the Automotive Industry Research Association and Federal Road Research Institute collected accident information in a jointly conducted project called the German In-Depth Accident Study (GIDAS). A total of 783 cases collected between 1985 and 1998 were included from the cities of Dresden and Hanover and their surrounding rural areas. The teams selected accidents according to a strict selection process to avoid any bias in the database. Accidents where a passenger car collided with more than one pedestrian or one pedestrian collides with more than one passenger car were not considered. Furthermore, accidents in which the car ran over the pedestrian or the impact speed could not be established were not considered. The study included information such as environmental conditions, accident details, technical vehicle data, impact contact points, and information related to the people involved, such as weight, height, etc.

Detailed information from pedestrian crashes was collected in the United States through the Pedestrian Crash Data Study (PCDS). In this non-stratified study, a total of 521 cases were collected between 1994 and 1999. Cases were collected from six urban sites during weekdays. If, within 24 hours following the accident, the pedestrian could not be located and interviewed or the vehicle damage patterns documented, the case was eliminated from the study. In order for a case to qualify for the study, the vehicle had to be moving forward at the time of impact; the vehicle had to be a late model passenger car, light truck, or van; the pedestrian could not be sitting or lying down; the striking portion of the vehicle had to be equipped with original and previously undamaged equipment; pedestrian impacts had to be the vehicle's only impact; and the first point of contact between the vehicle and the pedestrian had to be forward of the top of the A-pillar.

The Australian data is from at-the-scene investigations in 1999 and 2000 of pedestrian collisions in the Adelaide metropolitan area, which has a general speed limit of 60 km/hr. The sample consists of 80 pedestrian/vehicle collisions, including 64 with passenger cars, SUV and 1-box type vehicles, where the pedestrian was standing, walking, or running, and where the main point of contact with the pedestrian on the vehicle was forward of the top of the A-pillar. Pedestrians and drivers were interviewed, wherever practicable, as part of the investigation process. The reconstruction of the impact speed of the vehicle was based on physical evidence collected at the scene. Injury information was obtained from hospital and coronial records, the South Australian Trauma Registry and, in minor injury cases, from an interview with the pedestrian.

Data from these four studies were combined into a single database for further analysis to develop a better basis for worldwide pedestrian impact conditions. From each of these studies, seven fields of information were identified which were common to all four studies and were crucial to providing guidance in test procedure development. For each injury, these seven fields of data were collected and input into the unified pedestrian accident database. The seven fields were country, case number, pedestrian age, impact speed, AIS injury level, body region injured, and vehicle source causing the injury. Injury body region and vehicle source were categorized as shown in Table 1.

The number of cases and total injuries represented in this combined database are shown in Table 2. Throughout the remainder of this report, this dataset is denoted as the IHRA Pedestrian Accident Dataset. It is recognized that pedestrian injuries in developing countries are not represented in this dataset; however, this data is the most comprehensive pedestrian accident database available to guide pedestrian

safety test procedure development. A total of 3,305 injuries of AIS 2-6 severity were observed, and there were 6,158 AIS=1 injuries observed (Table 2).

Table 1. Injury Body Regions and Sources

Injury Body Regions	Injury Sources
Head	Front Bumper
Face	Bonnet/Wing
Neck	Leading Edge
Chest	Windscreen Glass
Abdomen	Win. Frame/A-Pillars
Pelvis	Front Panel
Arms	Other Vehicle Source
Leg Overall	Indirect Contact Injury
Femur	Road Surface
Knee	Unknown Source
Lower Leg	
Foot	
Unknown Injury	

Table 2. IHRA Pedestrian Accident Dataset

Region	Cases	Injuries	AIS 1	AIS2-6
Australia	65	345	182	163
Germany	782	4056	2616	1440
Japan	240	883	523	360
U.S.A.	518	4179	2837	1342
Total	1605	9463	6158	3305

These minor (AIS=1) injuries were excluded in the following analysis because they were not believed to be crucial in test procedure development.

IHRA pedestrian injuries of AIS 2-6 severity are shown in Table 3 according to the part of the body that was injured.

As shown in Table 3, head (31.4%) and legs (32.6%) each accounted for about one-third of the AIS 2-6 pedestrian injuries. Of the 3,305 AIS 2-6 injuries, 2,790 (84%) were caused by contact with portions of the striking vehicle, with head and legs being the most frequently injured. Head injury accounted for 824 occurrences, and legs a total of 986 injuries when combining overall, femur, knee, lower leg, and foot body regions. Windscreen glass was the most frequent vehicle source of head injury, with the windscreen frame/A-pillars and top surface of bonnet/wing both being substantial additional sources of injury to the head. A further breakdown of the injuries and vehicle sources for children and adults is shown in Tables 5-7. For children, the top surface of the bonnet is the leading cause of head injury, while a substantial number of child head injuries also occur from windscreen glass contact. For adults, the windscreen glass is the leading source of head injury, followed by windscreen frame/A-pillars and top surface of the bonnet and

wing. Not surprisingly, the bumper was the leading source for both child and adult pedestrian leg injury. Distribution of pedestrian accident victims by age (all AIS levels) is shown in Table 4 and illustrated in Figure 1.

Table3.
Distributions of Pedestrian Injury (AIS 2-6)

Body Region	USA	Germany	Japan	Australia	TOTAL
Head	32.7%	29.9%	28.9%	39.3%	31.4%
Face	3.7%	5.2%	2.2%	3.7%	4.2%
Neck	0.0%	1.7%	4.7%	3.1%	1.4%
Chest	9.4%	11.7%	8.6%	10.4%	10.3%
Abdomen	7.7%	3.4%	4.7%	4.9%	5.4%
Pelvis	5.3%	7.9%	4.4%	4.9%	6.3%
Arms	7.9%	8.2%	9.2%	8.0%	8.2%
Legs	33.3%	31.6%	37.2%	25.8%	32.6%
Unknown	0.0%	0.4%	0.0%	0.0%	0.2%
TOTAL	100%	100%	100%	100%	100%

When broken into five-year age segments, Table 4 indicates that the 6–10 year old age group has the highest frequency of accident involvement at nearly 14% of all cases. In Japan, this age segment accounts for 20% of the cases, while the other three countries have lower involvements in this age group. The percentage involvement in the 11-15 year old group for Japan, however, drops considerably and is lower than for Germany, the U.S., or Australia. It is unclear why this sudden drop occurs in Japan and not in the other countries. In summary, over 31% of all cases involved pedestrians age 15 and younger. This percentage is 13% higher than the average overall population of individuals in this age group in the four countries (18%), which demonstrates the magnitude of the child pedestrian problem.

Table4. Distribution of Pedestrian Crashes by Age and Country

Age	US	Germany	Japan	Australia	IHRA
0-5	4.6%	9.0%	9.2%	4.3%	7.3%
6-10	13.8%	14.6%	20.0%	10.6%	14.1%
11-15	13.8%	9.8%	5.0%	11.0%	9.7%
16-20	6.2%	7.3%	3.3%	7.2%	6.6%
21-25	6.2%	4.5%	1.7%	8.7%	5.5%
26-30	4.6%	4.7%	1.7%	10.1%	6.0%
31-35	4.6%	4.2%	5.4%	5.8%	4.9%
36-40	3.1%	4.5%	5.0%	7.2%	5.4%
41-45	3.1%	3.6%	3.8%	6.2%	4.4%
46-50	3.1%	4.6%	5.4%	6.2%	5.2%
51-55	3.1%	5.4%	6.7%	3.3%	4.8%
56-60	1.5%	4.5%	10.0%	3.7%	4.9%
61-65	6.2%	5.8%	6.7%	3.9%	5.3%
66-70	7.7%	3.7%	3.8%	3.3%	3.7%
71-75	4.6%	3.8%	4.2%	3.7%	3.9%
76-80	3.1%	5.0%	2.5%	3.3%	4.0%
81-85	6.2%	3.8%	3.3%	0.8%	2.9%
86-90	4.6%	1.2%	2.1%	0.4%	1.2%
91-95	0.0%	0.1%	0.0%	0.6%	0.2%
96-100	0.0%	0.0%	0.4%	0.0%	0.1%

The age distribution data contained in Figure 1 also provides an opportunity to demonstrate that the IHRA Pedestrian Accident Dataset is representative of the pedestrian crash situation in the United States. In addition to the Germany, Japan, U.S., and Australian pedestrian datasets, data from the FARS and GES are also included. FARS is the Fatal Analysis Reporting System, which contains every fatal traffic accident in the U.S. The GES is the General Estimates System, and is obtained from a nationally representative sampling of police-reported crashes. In general, the age distribution of the GES data is similar to the others in Figure 1.

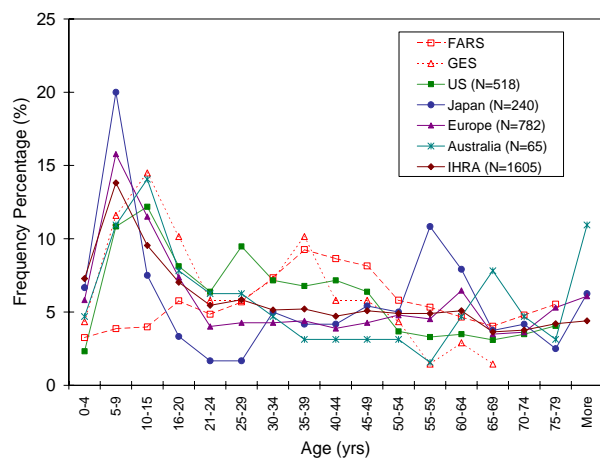


Figure1.
Frequency of Accidents by Age and Country

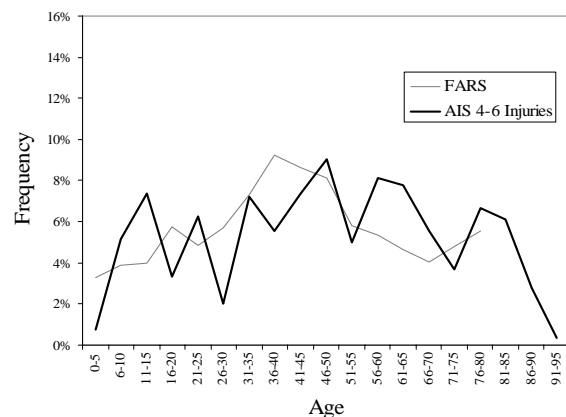


Figure 2.
IHRA AIS 4-6 Injuries vs. FARS Data by Age

Since the GES is designed to be a statistically representative sample, and since the U.S. PCDS and GES distributions are similar, this would imply that the PCDS is fairly statistically representative despite the non-stratified sampling scheme used to collect PCDS cases. However, the FARS distribution differs significantly from any of the others in Figure 1. Because FARS contains only fatal accidents, this may be an indication that the distribution of fatal and non-fatal injuries differs from each other. An ideal

comparison for the FARS data would have been with the IHRA pedestrian fatalities. But since the number of fatal cases is quite limited in the IHRA data, the FARS distribution was compared to the serious and fatal AIS \geq 4 injuries as shown in Figure 2. Although there is considerable variability remaining in this distribution due to small sample sizes, the FARS distribution has reasonable agreement with the IHRA data.

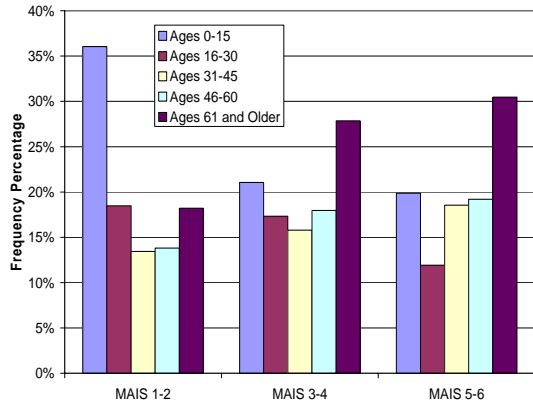


Figure 3. Distributions of MAIS Levels by Age

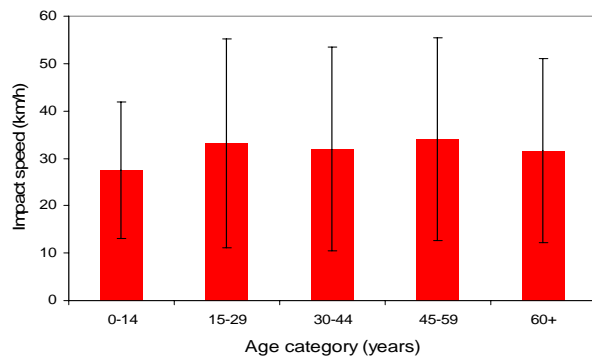


Figure 4. Average Impact Velocities by Age Group (MAIS 1-6)

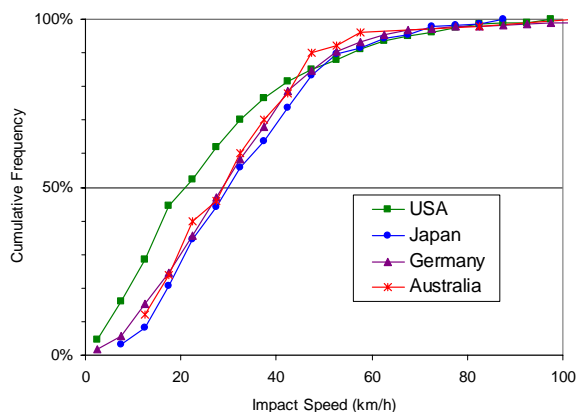


Figure 5. Impact Velocities by Country

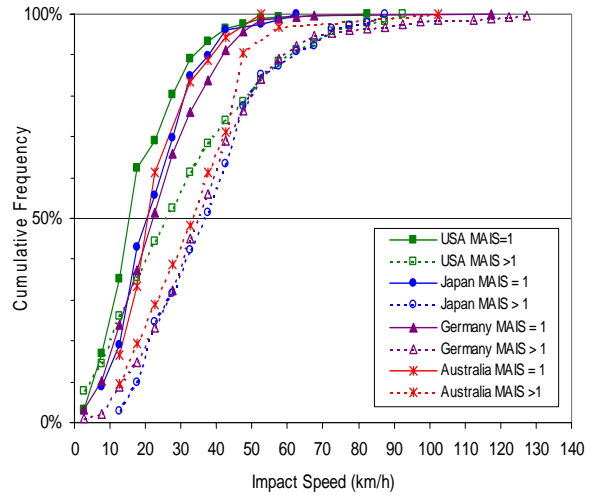


Figure 6. Impact Velocities by MAIS Level

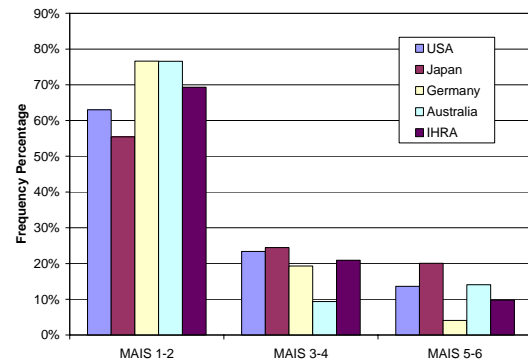


Figure 7. MAIS Injury by Country

Analysis of the injury level by age group is shown in Figure 3. This figure shows that children aged 15 and younger tend to have a higher proportion (25%) of AIS 1 and 2 injuries than adults, and persons aged 61 and older have the highest proportion (near 30%) of moderate and serious injuries. These observations are likely the result of two factors. First of all, exposure levels may differ for the various age groups. For example, younger children tend to be involved in pedestrian collisions with lower impact velocities. As shown in Figure 4, the average impact velocity for children aged 0-14 is about 28 km/h. This is approximately 5 km/h lower than for the other age groups. A second cause of the injury distribution observed in Figure 3 may be that those aged 60 years and older are generally more frail and less resilient, leading to higher severity injury for a given impact velocity. Figures 5 and 6 provide insight into the impact velocity distribution associated with pedestrian impacts. In Figure 5, the cumulative frequency of impact velocities on a per case basis for each country is similar although the U.S. has a larger percentage of injuries at lower velocities than the other three countries. This is broken down further in Figure 6, where lower MAIS injuries occur at lower velocities for all four countries. In Figure 7, the MAIS

injuries are broken into three categories for the four countries. For MAIS 1-2 injuries, Japan has the lowest frequency (55%) and Germany has the highest (77%). For MAIS 3-4 injuries, Australia has the lowest frequency percentage (9%) and Japan has the highest (24%). Finally, for the most severe injuries (MAIS 5-6), Germany has the lowest frequency (4%) and Japan has the highest likelihood of a life-threatening injury (20%).

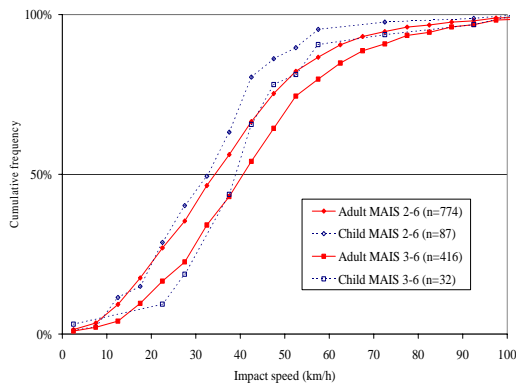


Figure 8. Impact Velocities by MAIS Level – All Body Regions

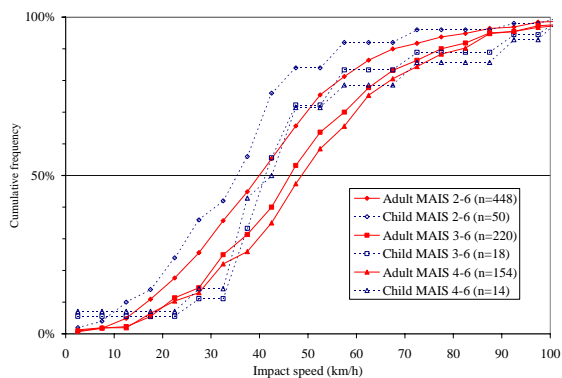


Figure 9. Impact Velocities by MAIS Level - Head Injuries

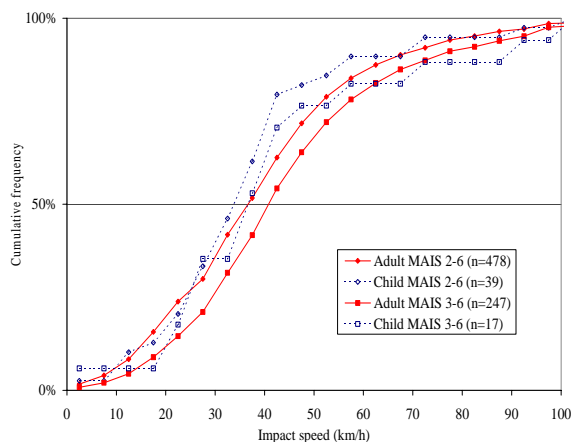


Figure 10. Impact Velocities by MAIS Level – Leg Injuries

The cumulative MAIS injury distributions are further broken down by age, body region, and injury severity in Figures 8 – 10. Age classifications are grouped as children (age 15 years and younger) and adults (age 16 years and older). All body regions are included for both children and adults in Figure 8, with distributions shown for MAIS 2-6 and MAIS 3-6 injuries. The injury distribution distinction between children and adults is evident in this figure. Children (ages 15 and under) are injured at slightly lower impact velocities than adults in most cases.

Head injury distributions are shown in Figure 9. For adults, the MAIS 3-6 and MAIS 4-6 injury distributions are almost identical, while the MAIS 2-6 distribution occurs at lower velocities. For children, there is similar separation between the MAIS 2-6, 3-6, and 4-6 injury curves, and the distributions are roughly the relationship between injury severity and impact velocity.

Injury distributions for children and adult leg injuries are shown in Figure 10. This figure shows that for leg injuries, injury severity is affected less by impact velocity than for head injuries. Once again, children suffer leg injuries at lower velocities than do adults.

The major conclusions from this analysis are:

1. The head and legs each account for almost one-third of the 9,463 injuries in the IHRA dataset.
2. For children, the top surface of the bonnet is the leading cause of head injury, while for adults the windscreen glass is the leading source of head injury.
3. Children (ages 15 and under) account for nearly one-third of all injuries in the dataset, even though they constitute only 18% of the population in the four countries.
4. Older individuals are more likely to suffer severe injuries in pedestrian crashes.
5. Children (ages 15 and under) are injured at lower impact velocities than are adults

This compilation of pedestrian accident data from Australia, Germany, Japan, and U.S.A. provides a unique and important dataset. In this section, MAIS for each case was used instead of all injuries in Figures 3 -10 to eliminate the possibility of cases with more injuries skewing the data. The cumulative injury distribution data will provide a basis for establishing component pedestrian protection test procedures, priorities, and potential benefits assessments.

Table 5.
IHRA Pedestrian Injuries by Body Region and Vehicle Contact Source – All Age Groups; AIS 2-6

Contact		Body Region							Legs					Unknown	Total
		Head	Face	Neck	Chest	Abdomen	Pelvis	Arms	Overall	Femur	Knee	Lower Leg	Foot		
Part of the Vehicle	Front Bumper	24	2		3	5	3	6	19	59	76	476	31	1	705
	Top surface of bonnet/wing	223	15	2	139	44	43	86	23	3	1	1	2	1	583
	Leading edge of bonnet/wing	15	2	4	43	78	85	35	50	40	6	30	1		389
	Windscreen glass	344	56	12	30	5	12	23	2			1	1	1	487
	Windscreen frame/A pillars	168	28	5	35	7	14	31	5	1				2	296
	Front Panel	5	1		9	13	7	6	9	14	11	35	3		113
	Others	45	7	1	38	12	13	15	15	9	5	39	18		217
	Sub-Total	824	111	24	297	164	177	202	123	126	99	582	56	5	2790
Indirect Contact Injury		13		17	1	1	7	1		3		1	2		46
Road Surface Contact		171	22	2	22	2	9	42	6	4	3	5	15	1	304
Unknown		27	6	3	19	10	16	25	1	7	9	32	3	7	165
Total		1035	139	46	339	177	209	270	130	140	111	620	76	13	3305

Table 6.
IHRA Pedestrian Injuries by Region and Vehicle Contact Source – Adult (Ages > 15); AIS 2-6

Contact Location		Body Region							Legs					Unknown	Total
		Head	Face	Neck	Chest	Abdomen	Pelvis	Arms	Overall	Femur	Knee	Lower Leg	Foot		
Part of the Vehicle	Front Bumper	20	2		2	3	3	3	16	29	69	429	29		605
	Top surface of bonnet/wing	140	9	1	122	39	35	73	21	3	1	1	2	1	448
	Leading edge of bonnet/wing	7	2	1	36	65	80	28	46	33	5	24	1		328
	Windscreen glass	303	52	11	28	3	10	22	1			1	1		432
	Windscreen frame/A pillars	159	28	5	34	7	14	29	5	1				2	284
	Front Panel		1		8	13	6	5	9	9	10	32	3		96
	Others	33	7		29	9	12	11	6	4	5	26	13		155
	Sub-Total	662	101	18	259	139	160	171	104	79	90	513	49	3	2348
Indirect Contact Injury		12		16	1		7			3		1	2		42
Road Surface Contact		125	18	2	21	2	8	32	6	4	3	5	14	1	241
Unknown		19	6	3	18	9	16	20	1	4	9	28	3	6	142
Total		818	125	39	299	150	191	223	111	90	102	547	68	10	2773

Table 7.
IHRA Pedestrian Injuries by Body Region and Vehicle Contact Source – Child (Ages < 16); AIS 2-6

Contact Location		Body Region							Legs					Unknown	Total
		Head	Face	Neck	Chest	Abdomen	Pelvis	Arms	Overall	Femur	Knee	Lower Leg	Foot		
Part of the Vehicle	Front Bumper	4			1	2		3	3	30	7	47	2	1	100
	Top surface of bonnet/wing	83	6	1	17	5	8	13	2						135
	Leading edge of bonnet/wing	8		3	7	13	5	7	4	7	1	6			61
	Windscreen glass	41	4	1	2	2	2	1	1					1	55
	Windscreen frame/A pillars	9			1			2							12
	Front Panel	5			1		1	1		5	1	3			17
	Others	12		1	9	3	1	4	9	5		13	5		62
	Sub-Total	162	10	6	38	25	17	31	19	47	9	69	7	2	442
Indirect Contact Injury		1		1		1		1							4
Road Surface Contact		46	4		1		1	10					1		63
Unknown		8			1	1		5		3		4		1	23
Total		217	14	7	40	27	18	47	19	50	9	73	8	3	532

VEHICLE SHAPES AND CATEGORIES

Front shape of passenger cars were investigated and categorized into three groups, Sedan, SUV (Sport Utility Vehicle) and 1-Box (One Box Vehicle), so that the effect of vehicle front shapes on the pedestrian impact were studied with computer simulations focusing on the head impact velocity, head impact angle, WAD (Wrap Around Distance) and head effective mass.

Figure 11 shows the car front shape corridors for the three groups obtained from current production cars in Europe, Japan and U.S.A. Each corridor consists of upper and lower boundaries of the bonnet and windscreen glass with the front skirt corridors.

Figure 12 shows the definitions of the measuring points for the bumper lead (BL), bumper center height (BCH), leading edge height (LEH), bonnet length, bonnet angle, windscreen angle and the bottom depth and height of the front skirt. These positions and angles for the lower, middle and upper boundaries of the corridors for each group were summarized in Table 8.

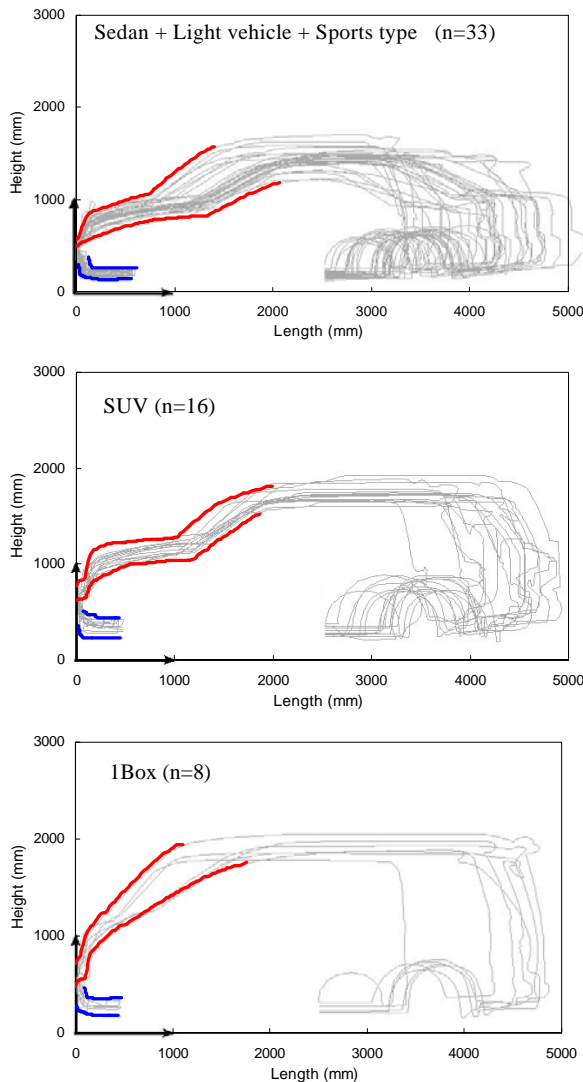


Figure 11. Car Front Shape Corridors

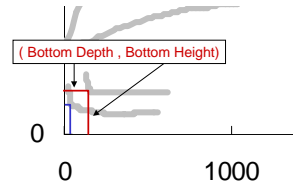
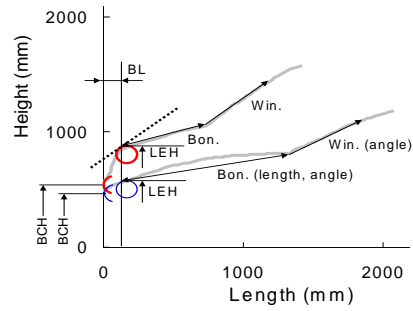


Figure 12. Definitions of Car Front Shape

Table 8. Car Fron Shape Corridors

Sedan + Light vehicle + Sports type				
		Lower	Middle	Upper
BL	(mm)	127	127	127
BCH	(mm)	435	475.5	516
LEH	(mm)	565	702	839
Bon. length	(mm)	1200	917.5	635
Bon. angle	(deg.)	11	14.5	18
Win. angle	(deg.)	29	34.5	40
Bottom depth	(mm)	42	98	154
Bottom height	(mm)	182	225.5	269
SUV				
		Lower	Middle	Upper
BL	(mm)	195	195	195
BCH	(mm)	544	640	736
LEH	(mm)	832	1000	1168
Bon. length	(mm)	1023	933.5	844
Bon. angle	(deg.)	11	9.75	8.5
Win. angle	(deg.)	36	39.5	43
Bottom depth	(mm)	48	123	198
Bottom height	(mm)	248	348	448
1Box				
		Lower	Middle	Upper
BL	(mm)	188	188	188
BCH	(mm)	448	576	704
LEH	(mm)	864	1004	1144
Bon. length	(mm)	361	259	157
Bon. angle	(deg.)	40	40	40
Win. angle	(deg.)	30	38	46
Bottom depth	(mm)	63	95	127
Bottom height	(mm)	214	292.5	371

BIOMECHANICS

Head Injury Biomechanics

The characteristics of the impact to the head of a pedestrian also differ, to a lesser degree, from those of the impact to the head of a vehicle occupant. The objects struck are, of course, different and the distribution of impact points on the head also differs, with the pedestrian's head being more likely to be

struck on the rear or the side compared with the predominantly frontal, with some lateral, impacts to the head of the vehicle occupant. (McLean et al, 1996A & B) However, for both pedestrians and car occupants, severe head injuries are most likely to be a consequence of a head impact with some part of the front of the vehicle, including the windscreen area and surrounds. A head impact with the road surface is less likely than a head impact with the car to be the cause of the most significant brain injury to a pedestrian. (Ashton et al, 1982)

The head is the most common site of fatal injuries to a pedestrian struck by a passenger car, either alone or in combination with one or more fatal injuries to other body regions.

The location of a pedestrian head impact on the striking car depends largely on the size and shape of the car and the height of the pedestrian. The speed of the car on impact also influences the head impact location on the vehicle. For an adult pedestrian the head impact location on the car is therefore usually towards the rear of the bonnet or on the windscreen or an A-pillar. It may extend back as far as the top of the windshield or, in exceptional cases, the roof of the car.

The head, and probably the upper torso, had been rotated through approximately 90 degrees about the longitudinal axis of the body in the 100 to 150 milliseconds between the bumper striking the legs and the head hitting the car. This whole body rotation is thought to be a consequence of the motion of the legs on impact by the front of the car.

Despite the rotation of the upper body and head of the pedestrian prior to the head striking the car, the high proportion of impacts on the back of the head indicates that the resulting acceleration of the head is likely to be predominantly linear rather than angular. This will be less so in those cases in which the impact is on the side of the head. (Ryan et al, 1989) However, even then, impacts which may result in a high level of angular acceleration of the head can also be expected to produce a high level of linear acceleration. The evidence for the roles of linear and angular acceleration in the production of brain injury is reviewed elsewhere. (McLean and Anderson, 1997)

For the purposes of this Working Group, emphasis has been placed on pedestrian head injuries resulting from head impact with the vehicle frontal structure, including the windscreen and A-pillars. The Head Injury Criterion (HIC) has been selected as the measure of the risk of brain injury resulting from these impacts. It is recognized that HIC evolved from the relationship between the duration of the impact applied to the frontal bone of the skull of a post mortem human subject, head acceleration, and the risk of the impact producing a skull fracture. It also does not allow for the influence of some factors, such as rotational acceleration of the head, or any effect of the location of the impact on the head, but it

has been selected here because, at present, it is used almost universally in crash injury research. The time window for the calculation of HIC has been set at a maximum of 15 milliseconds and the value of HIC shall not exceed 1000. That HIC level is thought to correspond to a 16 per cent risk of sustaining a head injury as severe as AIS 4 or greater. (Mertz et al, 1997)

Two head forms are proposed for use in subsystem testing, one representing the head of a 50th percentile adult and the other the head of a 6 year old child. The diameter of each head form is 165 mm and the mass is 4.5 kg for the adult head form and 3.5 kg for the child. The head forms are subject to performance, rather than design criteria. The head impact test areas on the vehicle for the child and adult head forms correspond to the areas commonly struck by the head of a child and an adult pedestrian, respectively.

Injuries to lower limbs

The pedestrian lower limb is typically loaded from the side (80-90%). Such loading conditions differ from those of lower limb of vehicle driver/occupant that are likely to be impacted in direction parallel to sagittal plane. These conditions result in injuries unique to the pedestrian-car collision. Such injuries are typically a consequence of contact between the lower limb and components of a car front, such as bumper, bonnet and bonnet leading edge. They are one of the most common types of injury in non-fatal pedestrian-car collisions. For instance, in the accident data investigated by Ashton and Mackay (1979) injuries to lower limbs were sustained by 67% of victims with minor injuries and 72% of victims with non-minor, non-life threatening injuries. Similarly, more recent Japanese data (ITARDA, 1996) have indicated that lower limbs are the most commonly injured body part (40%) with the most severe injury.

The pattern of lower limb injuries differs between children and adults, and it has been reported in the literature that the frequency of these injuries is higher for adults than for children (Ashton, 1986). Furthermore, children are less likely to sustain pelvic and leg fractures than adults. For instance, in the UK accident data analyzed by Ashton (1986), the leg fractures have not been observed in children aged below 5 years, and the children aged 0-4 years sustained mainly femur fractures. It is clear that this injury pattern is caused by the fact that the bumper directly impacts a young child thigh.

However, it seems that insufficient experimental data are available to quantify the responses of child lower limbs in pedestrian-car collision. Therefore, the present review is concentrated on injuries to the leg and knee joint of adult pedestrian.

Severity of Injuries to Lower Limbs

Injuries to the lower limbs are rarely fatal. They

involve fractures of fibula, tibia, and femur, as well as avulsion, rupture, and stretching of the knee joint ligaments. Such injuries are typically classified as AIS 1 to 3 (i.e., minor to serious injuries). However, they often require appreciably longer hospitalization and loss of working days than do injuries at the same AIS levels to other body regions. For instance, in the clinical study by Bunkentorp et al. (1982) healing time of tibia shaft fractures were 4-34 months, and only half of the fractures healed within 8 months. The healing time of knee and ankle injuries in their study was 2-7 months.

Injury Types and Injury Mechanisms to the Lower Limb of a Pedestrian

Injuries to the lower limb that have been observed in the PMHS experiments simulating pedestrian-car collisions and clinical studies are mainly fractures of tibia diaphysis (transverse and comminute fractures of the shaft), articular fractures of tibia, cartilage damages on femoral condyles, and avulsion/stretching of the knee joint ligaments (Bunkentorp, 1982; Kajzer et al., 1997 and 1999). The injury type depends on the following factors: 1) impact point, 2) car front part impacting the lower limb, and 3) the impact speed (e.g., fracture risk is likely to increase at high impact speed). According to Bunkentorp et al. (1982), a bumper impact at or just below the knee joint is correlated with high risk of serious knee injury. Such injury may be also caused by a prominent bonnet edge. However, the bumper seems to be the main cause of injury to leg and knee joint in adult pedestrians.

Injury Mechanisms

According to Kajzer et al. (1997, 1999) two fundamental mechanisms of injury to the knee joint can be distinguished: 1) shearing and 2) bending. The shearing mechanism is related to translational displacement in lateral direction between the proximal leg and distal thigh at the knee joint. On the other hand, the bending injury mechanism is related to angular displacement between the leg and thigh. Following these two injury mechanisms, two extreme loading conditions can be distinguished. The first of them corresponds to “the purest possible shearing deformation” of the knee joint (i.e., lateral impact to the leg slightly below the knee joint), whereas the second one — to “the purest possible bending deformation” of this joint (i.e., lateral impact to the distal leg end).

The typical initial injury (i.e., the injury that occurred first in a given test) associated with the shearing-type loading conditions observed by Kajzer et al. (1997, 1999) was articular fractures and anterior cruciate ligament avulsion in impacts using ram speeds of 40 km/h and 20 km/h, respectively. The articular fractures were caused by axial compressive force between femoral and tibial condyles (Fig. 13). On the other hand, typical initial

injury related to the bending-type loading at low impact speed (i.e., 20 km/h) reported by Kajzer et al. (1999) was avulsion/stretching of the collateral ligament on the leg side opposite to the struck area. Furthermore, based on analysis of both the experimental data obtained using PMHS and results of mathematical modeling, it has been suggested by Yang (1997) that the risk of tibia/fibula fracture and ligament avulsion/rupture may not be independent since such fracture may protect the knee joint ligaments from injury by absorbing the impact energy.

As for the long bone fracture, a bending moment and an accelerometer can be a candidate for the injury criterion.

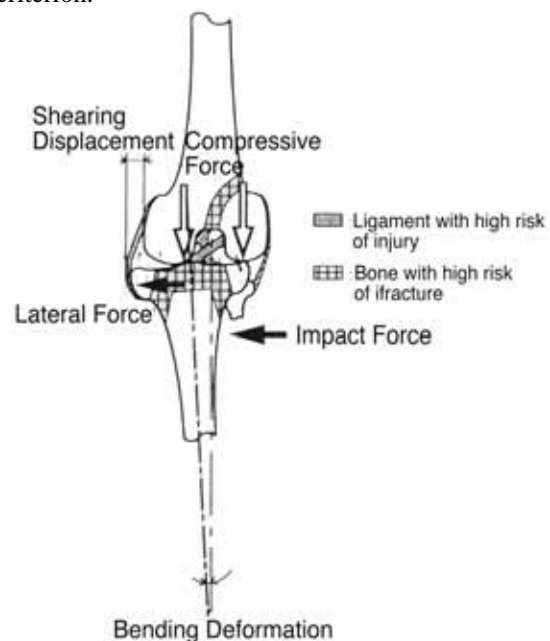


Figure 13. Injuries resulting from shearing-type loading conditions at ram speed of 40 km/h. Based on Kajzer et al. (1997).

Indicators of Injury Risk to Leg and Knee Joint Suggestions for Biofidelity Requirements for Leg-form

Summary of shearing and bending injury mechanisms presented in the previous section suggests that the injury risk to the leg and knee joint can be described by means of the following four variables: 1) shearing displacement (i.e., lateral displacement between proximal leg and distal thigh at the knee joint), 2) knee joint angle (i.e., relative angular displacement between the leg and thigh), 3) impact force (i.e., force between the leg and object striking it), and 4) knee ligaments (MCL, ACL, PCL, LCL) elongations. It seems reasonable to use these variables in evaluation of the biofidelity of legform impactors.

Corridors (average +/- standard deviation) of impact force, shearing displacement and knee angle-time histories for such evaluation have been determined by Matsui et al. (1999) and Wittek et. al. (2000)

using the PMHS experimental data of Kajzer et al. (1997, 1999). Cesari D. et. al. (2004) also developed pedestrian lower extremity corridors using the PMHS experimental data of Kajzer et. al. (1991, 1994). Besides these works, Ivarsson et. al. (2004) developed thigh, leg, and knee joint response corridor, and these corridors are can be utilized to evaluate a legform impactor biofidelity.

COMPUTER SIMULATION OF PEDESTRIAN HEAD IMPACTS

Computer simulation has been used by the Pedestrian Safety Working Group to study the influence of vehicle shape and pedestrian anthropometry and posture on the impact conditions required of sub-system testing. These impact conditions are the mass, speed and angle of the subsystem impactors, with reference at this stage to the reconstruction of head impacts involving a 50th percentile male. Computer simulation also shows promise for use in the study of possible interactions between the results of subsystem tests. For example, is it possible that a particular measure that reduces the risk of a severe injury to the knee joint may increase the risk of a severe head injury?

The pedestrian-vehicle simulations that have been performed have made use of multi body dynamic codes such as MADYMO (TNO, Delft, the Netherlands) in which the pedestrian is represented by a tree structure of rigid links, connected with kinematics joints. Properties of the model that are specified include the mass and moments of inertia of each link, the properties of the kinematics joints, the geometry of the contact surfaces of each link and their contact properties. The front of the vehicle,

back to the upper frame of the windscreen, is similarly described.

The properties of such models are based on studies of the joints and body segments of post-mortem human subjects and/or human volunteers. The behavior of the model can be validated by confirming that its response is similar to the response of human joints and body segments when subjected to dynamic loads in experiments. Pedestrian models can also be compared to the kinematics of post mortem human subjects subjected to experimental impacts by a vehicle and also to the results of detailed investigations of actual pedestrian-vehicle collisions in those cases in which a reasonable estimate of the impact speed of the striking vehicle is available.

Three computer models have been used by the Japan Automobile Research Institute, the United States National Highway Traffic Safety Administration (using a TNO computer model), and the Centre for Automotive Safety Research (previously the Road Accident Research Unit) of Adelaide University, Australia, for the purposes of this Working Group. Each of the models was used to simulate experiments with cadavers, as an initial assessment of the biofidelity of the kinematics of the model. The results for three output parameters relating to head impacts with the bonnet, where relevant, and the windscreen are summarized in Tables 9-10 for three categories of vehicle frontal shape. These parameters are:

- (1) Head impact speed divided by the vehicle impact speed (values shown are average +/- 1 SD)
- (2) Head impact angle (values shown are average +/- 1 SD)

Table 9. Summary of Parameter Study for Adult (Car Impact Speed: 30, 40 and 50 Km/h)

For Adult							
Shape Corridor	Car impact speed 30km/h						
	Impact Velocity (km/h)			Impact Angle (deg.)			
	Bonnet	Windsheld	BLE/Grille	Bonnet	Windsheld	BLE/Grille	
Sedan + SUV	23.7 +/- 6.0	27.3 +/- 5.4	nc	78.3 +/- 5.6	48.8 +/- 9.9	nc	
One box	26.4 +/- 3.6	nc	nc	73.8 +/- 21.5	nc	nc	
	nc	20.4 +/- 3.6	nc	nc	55.1 +/- 10.4	nc	

Car impact speed 40km/h							
Shaep Corridor	Impact Velocity (km/h)			Impact Angle (deg.)			
	Bonnet	Windsheld	BLE/Grille	Bonnet	Windsheld	BLE/Grille	
	Sedan + SUV	30.4 +/- 7.2	35.2 +/- 6.8	nc	66.0 +/- 14.0	38.4 +/- 10.9	nc
One box	30.8 +/- 8.8	nc	nc	76.7 +/- 22.2	nc	nc	
	nc	29.6 +/- 3.2	nc	nc	47.3 +/- 9.6	nc	

Car impact speed 50km/h							
Shaep Corridor	Impact Velocity (km/h)			Impact Angle (deg.)			
	Bonnet	Windsheld	BLE/Grille	Bonnet	Windsheld	BLE/Grille	
	Sedan + SUV	37.5 +/- 9.5	46.5 +/- 11.0	nc	56.8 +/- 11.5	33.5 +/- 11.3	nc
One box	39.5 +/- 11.0	nc	nc	73.5 +/- 25.2	nc	nc	
	nc	43.0 +/- 6.0	nc	nc	38.4 +/- 12.3	nc	

*nc: No Contact

** Linear interpretation to be used to determine impact conditions for in-between speeds if required.

**Table 10. Summary of Parameter Study for Child
(Car Impact Speed: 30, 40, and 50 Km/h)**

For Child		Car impact speed					
Shaep Corridor	30km/h						
	Impact Velocity (km/h)			Impact Angle (deg.)			
	Bonnet	Windsheld	BLE/Grille	Bonnet	Windsheld	BLE/Grille	
Sedan +	21.6 +/- 3.0	nc	nc	65.1 +/- 0.8	nc	nc	
SUV	21.3 +/- 1.2	nc	21.3 +/- 6.0	55.6 +/- 5.5	nc	26.0 +/- 7.5	
One box	20.1 +/- 0.6	nc	21.9 +/- 5.1	47.5 +/- 2.8	nc	20.3 +/- 8.0	

Shaep Corridor		Car impact speed					
Shaep Corridor	40km/h						
	Impact Velocity (km/h)			Impact Angle (deg.)			
	Bonnet	Windsheld	BLE/Grille	Bonnet	Windsheld	BLE/Grille	
Sedan +	30.0 +/- 4.0	nc	nc	66.0 +/- 6.3	nc	nc	
SUV	27.2 +/- 1.6	nc	32.0 +/- 3.6	59.2 +/- 2.6	nc	22.5 +/- 4.2	
One box	27.6 +/- 0.8	nc	33.2 +/- 3.2	49.8 +/- 1.8	nc	17.4 +/- 6.1	

Shaep Corridor		Car impact speed					
Shaep Corridor	50km/h						
	Impact Velocity (km/h)			Impact Angle (deg.)			
	Bonnet	Windsheld	BLE/Grille	Bonnet	Windsheld	BLE/Grille	
Sedan +	38.5 +/- 5.0	nc	nc	65.2 +/- 6.5	nc	nc	
SUV	34.0 +/- 1.5	nc	44.5 +/- 1.0	61.9 +/- 3.8	nc	18.1 +/- 3.8	
One box	36 +/- 0.5	nc	46.5 +/- 2.0	47.4 +/- 2.1	nc	14.8 +/- 3.6	

*nc: No Contact

** Linear interpretation to be used to determine impact conditions for in-between speeds if required.

TEST METHODS

IHRA/PS decided to adopt head and leg sub-system test methods and to establish specifications. That means that test procedures were drafted for each of the sub-systems. Two head-forms are proposed for use in head sub-system testing, one to represent an adult pedestrian head and one to represent a child pedestrian head. They are defined as falling in the height range of typical adults or children respectively, provided that short adults are included in the height range of children. The group also set forth a leg test procedure, for which the specifications of a leg-form are defined. The test procedures are such that these head-forms and leg-forms are subject to performance rather than selection of particular design.

HEAD

Mathematical simulations of head impact against different categories of shapes of cars, defined previously, were performed. They focused on head effective mass, head impact speed and angle at impact, and also wrap around distance at the head contact point, as described in the former section.

Head-form Specifications

Mass and dimensions

The results of these simulations indicated that the effective head mass of the head varied throughout the contact period and so some averaging of the effective mass function over the relevant impact period was required to determine a single value for the effective mass. The simulation results also

showed a large variation in head effective mass depending on vehicle shape. Within the test method, it was also clearly undesirable to require head-forms of different masses for vehicles of different front shapes, as IHRA/PS wanted to produce simple and repetitive test procedures.

It was noted that for the average effective mass for all vehicle shapes simulated was almost comparable to the head mass itself for cases of bonnet contacts, whereas the average effective mass is about 80 % of the head mass for cases of windscreen contacts. Therefore, based on this and engineer judgment, IHRA/PS decided to take the average effective mass for all vehicle shapes and to specify only one value of mass for an adult headform and one value for a child headform.

The mass for the adult headform was chosen to be 4.5 kg, which is the mass of the head of the 50th percentile male human being. This is the total impactor mass including instrumentation. Based on studies of human head dimension, a diameter was chosen which the same is as both EEVC and ISO test procedures of 165 mm. This value was reportedly based on existing documents including SAE J921 and was considered to represent the diameter mainly of the forehead portion.

The distribution of pedestrian victims by group of age indicates that the age group around 6 years old has the highest frequency of pedestrian accidents involvement at nearly 14% of all the cases. For this reason, it was decided to consider a head-form representing the head of a six years old child.

According to the recommendations of ISO working group of Biomechanics (ISO/TC22/SC12/WG5), the average mass of the six year old child head is 3.48

kg, which has been rounded to 3.5 kg. IHRA decided to also select 3.5kg for the mass of the child headform.

The only data available for the dimensions of a 6-years old child head are the circumference of the head which is 523 mm, the width which is 141 mm and the A-P length which is 180 mm. From these values one can determine the diameter, either by taking the average of the two dimensions, A-P and width, $(141 + 180)/2 = 161$ mm or from the circumference, which leads to a value of 166 mm. So it is decided, for the child head-form, to use the same value as for the adult head-form of 165mm.

Moment of inertia

With regard to the moments of inertia, a comprehensive study on the influence of moment of inertia of a head-form impactor on HIC was conducted, and it was concluded that the influence is not significant. Consequently, IHRA/PS WG decided the moment of inertia specification for the adult and child head-form impactor should be $0.0075 - 0.02 \text{ kgm}^2$.

Test procedures

The test procedures are based on the accident statistics, the results of the computer simulations, cadaver tests, and engineering judgment. The latter is applied to create sufficiently simple and repeatable tests suitable for use in regulations.

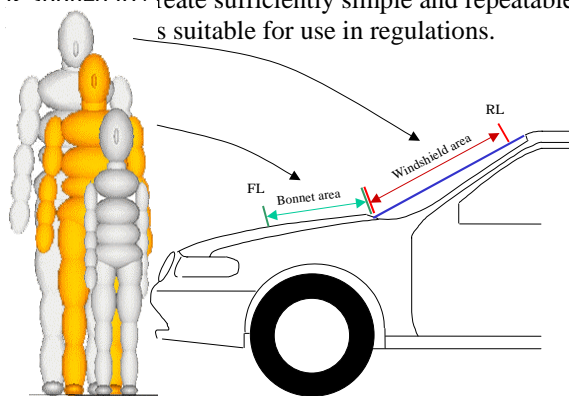


Figure 14. Principles of headform impactor test

According to the accident data of Australia, Europe, Japan, and United States, the 50th percentile impact speed between a pedestrian and a car was 25-30 km/h. For the injury level of AIS 3 or over, the corresponding speed was 50-55 km/h. According to the accident data of Australia, the 50th percentile impact speed was 50-60 km/h. The computer simulations for a child indicated that the head impact speed equals to 80% of the car impact speed. On the other hand, a PMHS test for adult indicated that such ratio for the head impact speed against car impact speed varies widely between 80% and 150%. The values for the head impact speed related to the vehicle impact speed in simulations of a head

collision with the bonnet or the windshield show significantly different results according to the simulation model and vehicle shape used; the average ratio varies significantly from 0.7 to 1.1 according to vehicle shape. Also, there are differences between contacts on the bonnet and contacts on the windscreen, due to the big differences in terms of impact conditions. Based on the PMHS test and simulation result data variations as well as concerns about the biofidelity of the human models used in the computer simulation, the IHRA PS WG could not come to a solid conclusion to use average ratio of head-to-vehicle ratio for all vehicle shapes. However, the IHRA/PS group believed the information is best available information at the present time. Finally, a lookup table is provided by average +/- 1 SD, that give the user the option to test anywhere within the tolerance window depending upon the desired level of stringency.

For future work, the JARI pedestrian model was selected as a base model, and now IHRA/PS members are developing an IHRA pedestrian model (IHRA-PED). Therefore, in the future, the IHRA-PED will be developed and will be used to update the current IHRA/PS lookup table. However, before the table is finalized, IHRA/PS WG group believes the current lookup table represents the best available information for the head-form impactor test conditions.

The head impact test areas on the vehicle, defined on the basis of wrap around distances for the child and adult head-forms correspond to the areas that accident data shows are commonly struck by the head of a child and an adult pedestrian respectively. The final WAD value derived from the accident data of Australia, Europe, Japan and the US was 1000-1700 mm for child head-form and 1400-2400 mm for adult head-form. Consequently a WAD 1400-1700 mm was shared by both adult and child head-forms and was named “transition zone”. Ishikawa showed that there is no added benefit from having a transition zone instead of a boundary line. So, there was a proposal to leave the use of the transition zone to the discretion of each national government.

The values for head impact velocity, head impact angle and wrap around distances are given in the detail test procedure, which describes the test conditions for the different categories of vehicle shapes and according to the fact that the impacts are on the bonnet or in the windshield.

Injury criteria

For the purpose of this working group, emphasis has been placed on pedestrian head injuries resulting from head impact with the vehicle frontal structure, including the windscreen and the A-pillars. The HIC has been selected as the measure of the risk of brain injuries resulting from such an impact.

HIC has been selected, despite the fact that it doesn't take into account the influence of some factors such as the rotational acceleration of the head, because it is used universally in crash injury research and prevention and the threshold was set at a current 1000 after consideration of existing pass/fail threshold values and the new values being studied by NHTSA.

Taking into account the short duration of this type of head impact, the time window for the HIC calculation has been set at 15 ms. Due to the short duration of the impact, a HIC window of 15ms will normally give the same result as a window of 36 ms, but the 15 ms window will help to reduce the risk of signals from spurious secondary impacts being accidentally included in the calculation

LEG

The IHRA proposal specifies a test method to simulate the impact of the leg of an adult pedestrian against the front face of a passenger car for impact speeds up to 40km/h.

The basic concept is to develop a mechanical impactor, with a controlled motion at knee joint level, to simulate a human knee impact in lateral direction. The characteristics of the leg-form impactor are that it must be a device representing an adult human leg sensitive to the front face characteristics of a vehicle. According to the agreement of the IHRA Pedestrian Safety Working group, the physical properties of the impactor are listed below.

Leg-form Specifications

Mass and Dimensions

The IHRA/PS decided that a leg-form used to test vehicle structures should be consistent with the anthropometry of a 50th percentile human leg. The size and mass of a 50th percentile human leg are documented in a report by the University of Michigan Transportation Research Institute (UMTRI), which was used by the IHRA Biomechanics WG. There was considerable discussion about whether the dimensions should reflect a 50th percentile male, 50th percentile female, or an average of the two. It was concluded that since the 50th percentile male is reflective of the most common knee height in pedestrian collisions according to accident data, it would be used in the initially proposed test procedure. The lower leg should be 493 ± 5 mm from bottom of foot to knee joint center, with a center of gravity 233 ± 10 mm from the knee joint center. The thigh should be 428 ± 5 mm long, with a center of gravity 210 ± 10 mm from the knee joint center. The leg-form mass should be 13.4 ± 0.1 kg, divided into 8.6 kg for the thigh (including skin and foam) and 4.8 kg for the lower leg.

Moments of Inertia

Like the mass and dimensions, the moments of inertia are also consistent with the UMTRI anthropometry data. For the tibia, the MOI specification about the y-axis is 0.120 ± 0.001 kg-m². For the femur, the specification is 0.127 ± 0.002 kg-m². These values are taken with respect to the origin located at the end of each bone. With respect to each individual segment's CG location, the MOI values for the tibia and femur are 0.054 kg-m² and 0.132 kg-m², respectively

An adapter can be fitted to the top of the thigh to permit the attachment of the leg-form impactor to the propulsion system. If an adapter is used, the thigh with adapter must still comply with the thigh requirements of mass, centre of gravity, and moment of inertia.

There shall be a flesh and/or a skin on the outer surface of the leg-form impactor. This material shall be human-like.

The shape of the leg-form impactor shall be cylindrical. The outer diameter of the thigh and leg shall be the same. Outer diameter is 120 ± 10 mm including flesh thickness of 30 ± 5 mm.

Test Procedures

The test will consist of a projectile legform being launched into a stationary vehicle front at a speed consistent with the mean vehicle speed in the pedestrian accident data.

The direction of the impact velocity vector shall be in the horizontal plane and parallel to the longitudinal vertical plane of the vehicle. The axis of the leg-form shall be perpendicular to the horizontal plane with a tolerance of $\pm 2^\circ$ in the lateral and longitudinal plane (see Figure 15). The horizontal, longitudinal and lateral planes are orthogonal to each other.

The bottom of the leg-form impactor shall be at 25mm above the Ground Reference Level at the time of first contact with the bumper (see Figure 16), with a ± 10 mm tolerance.

When setting the height of the propulsion system, an allowance must be made for the influence of gravity during the period of free flight of the leg-form impactor.

At the time of first contact the impactor shall have the intended orientation about its vertical axis, for the correct operation of its knee joint with a tolerance of $\pm 5^\circ$ (see Figure 15)

Tests shall be made to the front face of the vehicle, between the bumper corners. The center of each impact shall be a minimum of half leg-form diameter inside defined bumper corners. Sufficient test points shall be selected to evaluate the vehicle structure.

This test method is intended to cover impact velocity up to 40 km/h. The velocity of the impactor shall be measured at some point during the free flight before impact.

The IHRA PS WG discussed application of an upper

body mass to the legform to simulate the upper body of the pedestrian.

While the group maintained that upper body mass should not be included when looking at lower leg and knee impacts, it was agreed that this issue would be re-opened at a time when it is necessary to look at upper leg/thigh injury.

Figure 15.

During contact between the leg-form impactor and the vehicle, the leg-form impactor shall not contact the ground or any object not part of the vehicle.

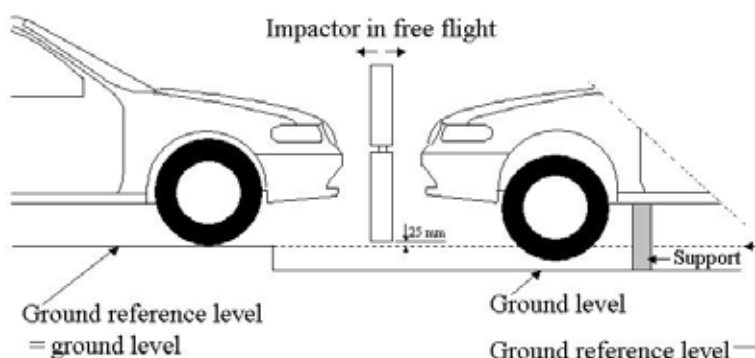
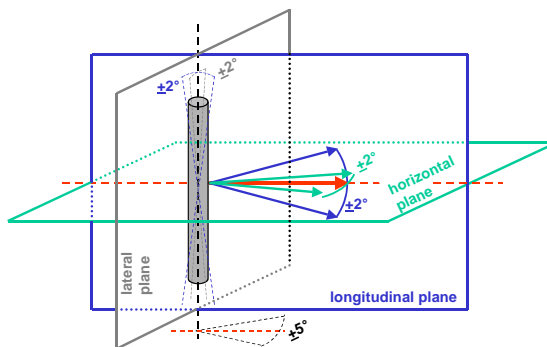


Figure 16.

Legform to bumper tests for complete vehicle in normal ride attitude (left) and for complete vehicle or sub-system mounted on supports (right)

Dynamic Response Corridors

The University of Virginia conducted a number of tests assessing the response of the human leg in a bending mode. Historical PMHS data was also used to generate adapted time history corridors in both bending and shearing modes. Dynamic response corridors were created and normalized for;

- Force vs. Deflection (Lower Leg and Thigh)
- Moment vs. Deflection (Lower Leg and Thigh)
- Knee Moment vs. Angle
- Impact Force vs. Time (Bending & Shearing Mode, 20 and 40 km/hr)
- Bending Angle vs. Time (Bending Mode, 20 and 40 km/hr)
- Shear Displacement vs. Time (Shearing Mode, 20 and 40 km/hr)

Bio-ranking method

A Bio-ranking method was developed by NHTSA to quantitatively and objectively evaluate leg-form impactor biofidelity using dynamic response corridors and impactor response data. The leg-form impactor should have a sufficiently high biofidelic score to conduct to properly assess leg injury

potential due to vehicle impact.

Injury Risk Curves

Injury risk curves were developed by the University of Virginia for the thigh and lower leg using logistic regression. They developed two sets of risk curves for the knee and lower leg, one using maximum moment and the other using an acoustic sensor to detect the time of injury.

CONTINUATION OF IHRA/PS ACTIVITIES

The aim of the IHRA/PS WG is to propose test procedures for the child and adult head, and the adult leg as the high priority body regions, for presentation at the ESV Conference in 2003 and 2005, together with recommendations for research activities that will be needed to develop other test procedures for the further improvement of pedestrian protection.

In the field of pedestrian crash injury biomechanics there are still areas which must be investigated and their practical applications explored. We plan to first clarify the issues, necessities and research responsibilities through detailed investigations. The following issues will be studied.

- (1) Methods employing a computer simulation program based on the best such programs currently available.
- (2) Clarification of the importance of injury mechanisms to areas other than the head or legs; also, R&D on impactors to confirm such injury mechanisms
- (3) The Research for Adult Leg vs. High Bumper vehicles Test method and its tool
 1st step: Analyze the current IHRA Adult Leg test method limitation using computer simulation model. Comparative evaluation of the results of, and interactions between, subsystem test methods and test
 2nd step: If the current Adult Leg test method can not apply for the high bumper vehicles, an Adult Leg test method for the high bumper vehicles and tools will be developed.
- (4) Development of the Adult Upper Leg vs. BLE test method
 1st step, focusing on in-depth study for pedestrian accidents for these area, and if we find out the necessity of the development of the test method and tool, we will conduct such research to develop the test method and its tool.

This work will be greatly facilitated if member countries are prepared to cooperate and share the cost, conduct further studies, and assist in the development of essential test procedures.

Table 11.
Members of IHRA Pedestrian Safety WG

Name	Organization
Chair person, Yoshiyuki Mizuno	JASIC Japan
Jack McLean	University of Adelaide Australia
Dominique Cesari	INRETS EEVC/EC
Graham Lawrence	TRL EEVC/EC
Bruce Donnelly	NHTSA USA
Hirotoishi Ishikawa	JARI Japan
Atsuhiro Konosu	JARI Japan
Oskar Ries	VW ACEA
Françoise Brun-Cassan	LAB,PSA/RENAULT ACEA
Masaaki Tanahashi	Honda R&D JAMA/Japan
Sukhbir Bilkhu	Daimler Chrysler AAM
Yoshihiro Yazawa	Nissan/JASIC Japan

Predecessor, contributed to the IHRA/PS-WG

Akira Sasaki (1996-2000)	Honda R&D JAMA/Japan
Roger Saul (1996-2000)	NHTSA USA
Hirotoishi Ishimaru (1996-2000)	JSAE Japan
Norbert Jaehn (1996-2000)	ACEA
Manuel Bartolo (1996-2000)	Ford AAM
Jacques Provensal (1999-2001)	ACEA
Edgar Janssen (1996-2002)	TNO EEVC/EC

Reference:

International Harmonized research Activities,
 Pedestrian safety Working group 2005 Report

ASSESSING FEMUR AND PELVIS INJURY RISK IN CAR-PEDESTRIAN COLLISIONS: COMPARISON OF FULL BODY PMTO IMPACTS, AND A HUMAN BODY FINITE ELEMENT MODEL

Jess G. Snedeker

Felix H. Walz

Markus H. Muser

Christian Lanz

Working Group on Accident Mechanics, Institute of Biomedical Engineering, University and Swiss Federal Institute of Technology, Zurich
Switzerland

Günter Schroeder

Institute of Legal Medicine, Hanover Medical School
Germany

Paper number 05-103

ABSTRACT

A considerable potential for reducing fatalities of pedestrians and other vulnerable road users lies in the design of car front shapes. Vehicle safety tests have been proposed by the EEVC WG17, and are currently in discussion by legal entities, as well as car makers.

In this study, we first present numerical simulations of various pedestrian impacts against several different simplified hood shapes. Impacts were simulated using a detailed finite element model of a mid-size pedestrian that has been extensively validated in previous studies. As expected, the model revealed that biomechanical loading patterns are heavily influenced by hood leading edge shape.

In a second step, femoral and pelvic bone surface strains were measured in five full body PMTO impacts at 40 kph using physical representations of the simulated car shapes. Each PMTO was instrumented with strain gauges on the impact side: four on the femoral shaft, three on the femoral neck, and three on the superior ramus of the pelvis. Accelerometers were placed on the dorsal aspect of vertebra T6 and L5. High speed digital video was recorded at 1,000 frames per second from the side. Fracture risk was examined with respect to car geometry, pedestrian stature, and bone quality as indicated by peripheral quantitative computed tomography (pQCT) of the femoral neck.

Experimental results indicated a remarkable predictive ability of the finite element model in

assessing femur and pelvic injury risk. Strain data yielded valuable insight into the failure threshold of the pelvic rami, which was observed to fracture in three of the tests. The largest factor in pelvic fracture was low bone quality, rather than car geometry. Based upon results of the model and PMTO experiments, recommendations are offered for a more appropriate characterization of the hood shape with regard to pelvis and femur injury risk.

INTRODUCTION

Pedestrians and bicyclists represent an extremely vulnerable population of road users, and thousands are severely injured or killed every year. It has been reported that upper leg and pelvis injury occur in just over 10% of pedestrian-vehicle impacts (Matsui et al., 1998). Vehicle-pedestrian crashes are responsible for 10% to 20% of all adult pelvic fractures and 60% to 80% of pediatric pelvic fractures (Sheppard, 2001).

The intelligent design of automotive front-end geometry holds a large potential for reducing injuries in unprotected road users. In order to assess the risk posed to a pedestrian by an automobile, the European Experimental Vehicles Committee (EEVC) has proposed three subsystem pedestrian dummy tests (EEVC Working Group 17, 1998). These tests represent a significant investment of the limited resources available for pedestrian protection. For such tests to be useful, it is essential to concentrate on the most relevant aspects of automotive design, and

employ testing protocols that are capable of successfully identifying high-risk vehicles. This study focuses on the upper leg (UL) impact portion of the EEVC protocol, which is intended to assess the risk of femur and pelvis injury in a struck pedestrian.

Vehicle front end geometry plays a critical part in the resulting kinematics of pelvic/upper leg impact. The EEVC prescribes a systematic method for characterizing the front end geometry of an automobile. With regard to the UL subsystem test protocol, three geometric parameters are considered:

- 1) Upper Bumper Edge Height (BH) – The upper limit to significant points of pedestrian contact with the bumper. It is defined as the vertical distance between the ground, and the uppermost point of contact between a 700 mm long reference line and the bumper when the line is inclined rearwards by 20 degrees, and traversed across the car front at ground level.
- 2) Hood Leading Edge Height (LEH) – Defined as the point of contact between a reference line 1000 mm long and the front surface of the hood when the line is inclined rearwards by 50°, with the lower end 600 mm above ground.
- 3) Bumper Lead (BL) – is the horizontal distance between the upper bumper reference line and the hood leading edge reference line.

The EEVC WG17 test protocol employs these characteristics within a system of look-up tables based on kinematic analysis of cadaver and dummy impact experiments. The look-up tables are intended to incorporate pedestrian impact kinematics into the UL testing protocol. Previous studies have identified an apparent discrepancy between injury risk as assessed by the EEVC UL test protocol, and real-world accident experience (Matsui et al. 1998, Konosu et al. 1998, EEVC WG17 1998, Konosu et al., 2001, Okamoto et al. 2001, Snedeker et al., 2003). This discrepancy has been primarily attributed to the simplification of the complicated three dimensional kinematics of vehicle-pedestrian impact, to a one dimensional impact test.

The current study examines the possibility that this discrepancy also arises from an inadequate characterization of vehicular front end geometry. The geometric characteristics that play a critical role in pedestrian impact are examined with the goal of identifying potentially important considerations that are neglected or improperly accounted by the current version of the EEVC protocol.

METHODS

In this study, we first performed numerical simulations of various pedestrian impacts against different simplified hood shapes. Impacts were simulated using a detailed finite element (FE) model of a mid-size pedestrian (THUMS) that has been extensively validated against PMTO experiments in previous studies (Iwamoto et al., 2002) and specifically validated for use in the study of pedestrian impact (Snedeker et al. 2003).

In a second step, measurements of femoral and pelvic cortical bone surface strains were recorded in five full body PMTO impacts at 40 kph against physical representations of the simplified car shapes used in the FE simulations. Each PMTO was instrumented with strain gauges on the impact side femur and pelvis, as well as with accelerometers on the dorsal aspect of the spine. The results from the impact tests were then compared with the corresponding simulations.

Finally, insights obtained from the first two steps were used to critically reexamine the EEVC UL test protocol. Specifically, an attempt was made to redefine the important aspects of car geometry, and implement them into a revised protocol.

Creation of the simplified automotive geometries

Fifteen simplified automotive car shapes were created for FE simulation of pedestrian impact. The car geometries were equally divided among three classes: Sedans, SUVs, and Vans/One-Box. Five to six actual production vehicles from each class were individually measured to produce a geometric template for the class. The geometric parameters used to create each template are illustrated in Figure 1. Class average and standard deviations for each class are listed in Table 1.

Within each class, five geometries were created by varying the radius of the hood leading edge, while keeping all other parameters constant. Radii of 0, 50, 100, 250 and 500 mm were created. Thus within a given class, all geometries had identical bumper height, bumper width, bumper lead, leading edge height, hood pitch, and windscreen position, but differing hood leading edge roundedness.

In the FE simulations, each automotive geometry was modeled using a total of 1,000 quadratic shell elements. The front end was represented by a 0.8 mm thick sheet metal (ASTM-A36) hood supported with a stiff steel frame. The bumper was modeled as 2 mm thick ASTM-A36 steel plate covered by a 50 mm thick hard PVC shell. A plastic hardening function

was employed to represent the yield behavior of steel. Thicknesses of the hood sheet metal and bumper materials were set to accord with realistic deformations as reported in the literature (Matsui et al., 1998, Ishikawa et al., 1993, Bunketorp et al. 1983).

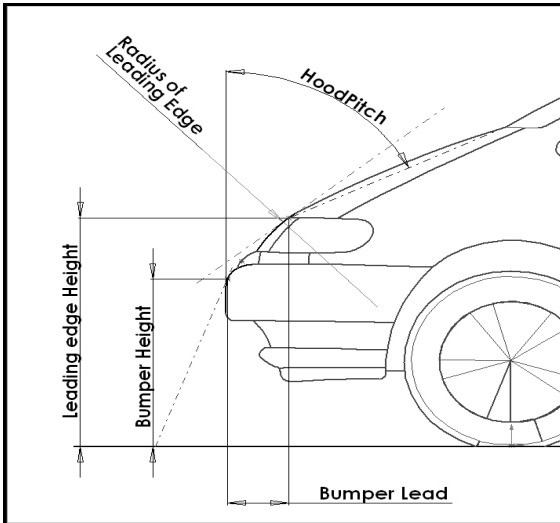


Figure 1. The geometric characteristics used to create each automotive class temp

Table 1. Average measurements (lengths in mm; angles in degrees) and standard deviations for the geometric parameters used to create an automotive class template.

	Sedan		SUV		Van / A-Box	
	Class Avg.	STD	Class Avg.	STD	Class Avg.	STD
Model Year	1996	2.9	1998	1.4	1997	1.7
BH	500	20	640	30	580	60
BL	140	20	140	50	160	60
LEH	740	50	1020	90	860	130
Rad. LE	230	130	410	370	730	530
Hood Pitch	79	1.5	80	2.9	65	4.5

Pedestrian impact finite element simulation

The FE model used to simulate pedestrian impact was the Total Human Model for Safety (THUMS), provided by Toyota Central R&D Lab., Inc., and implemented within the PAM-Crash® v2001 FE software. The THUMS model consisted of nearly 85,000 elements, and over 1,000 separate material models. In addition to bone structures and soft tissues, the model included relevant muscles, ligaments, and tendons. For specific information on

the construction of the human FE model, the car geometry FE models, and the validation of the THUMS femur and pelvis for use in simulating femur and pelvic injury, the reader is referred to Snedeker et al., 2003.

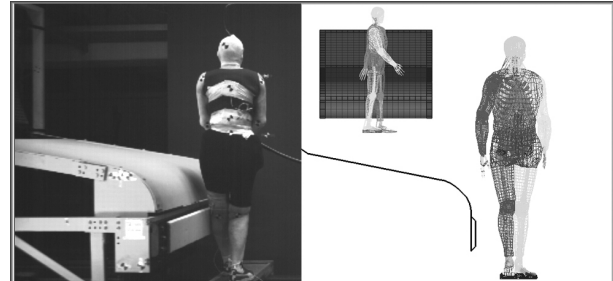


Figure 2. Simplified vehicle geometries were constructed for actual PMTO impacts (left). The vehicles were constructed according to the specifications used in FE simulations (right).

In each simulation, the THUMS model was permitted to settle under the load of gravity such that each leg supported 50% body weight at the time of impact. The foot/ground coefficient of friction was set at 0.65. The coefficient of friction between the car surfaces and impacted body parts was set at 0.25. The initial velocity of the car was 40 kph (11.1 m/s) at time of impact, and the car was decelerated at 6.9 m/s², to replicate braking by the driver.

Construction of the PMTO impact vehicle geometries

In the PMTO impacts, four vehicle fronts were constructed according to the same physical specification as used in the FE simulations. The sheet metal thickness was adjusted until force deflection characteristics matched those of the FE model. The geometries constructed for the PMTO tests consisted of: a sedan with a 50 mm radius hood leading edge (Sed050), a sedan with a 250 mm radius hood leading edge (Sed250), a van with a 50 mm radius hood leading edge (Van050), and a van with a 250 mm radius hood leading edge (Van250).

PMTO impact experiments

All PMTO tests were performed in accordance with German federal and local laws regarding the use of human test subjects. Cadavers were obtained from the Medical University of Hanover anatomy department.

As indicated in Table 2, the PMTOs varied in age, sex and stature. Test subjects were excluded from the study for pre-existing bone fractures of the legs and pelvis, as indicated by diagnostic radiograph

images. Each PMTO was instrumented with ten strain gauges (*Vishay Micro-Measurements, Inc., Raleigh, NC, USA*) to measure cortical bone surface strains. Strain gauges were applied using well established techniques (Cordey, 1998). Briefly, the periosteum was scraped away using a scalpel blade and surgeon's rasp, the gauging area was cleaned with a chemical solvent to remove lipid contaminants, and a combination activator-cyanoacrylate bonding agent was applied to the back of the gauge before mounting.

Table 2. PMTO specifications

ID	Sex	Age	Height (cm)	Mass (kg)
T1	F	52	160	50
T2	F	76	166	74
T3	M	32	177	75
T4	M	78	180	64
T5	M	76	172	60

An anterior, inverted - "L" shaped incision was made from the left knee to the hip, and then from the hip to the pubic symphysis. Care was taken to minimize disruption of ligaments and tendons; however, access to the femoral neck required partial dissection of the hip joint. It should be noted here that no hip dislocations were observed in post-impact autopsy. A single axis strain gauge was centered on the midpoint of the lateral aspect of the femoral shaft, with the principal axis of the gauge aligned with the long axis of the bone. A strain gauge rosette was placed on the medial aspect of the femur, with the axis of the center gauge aligned with the long axis of the bone. A second strain gauge rosette was placed on the inferior/anterior aspect of the femoral neck, and another on the superior/anterior aspect of the superior ramus of the pelvis. All gauges were placed on the left (impact) side of the PMTO according to Figure 3. Location of the strain gauges necessarily varied between subjects due to anatomical differences in bone geometry and obstruction of the gauge installation site by tendon and ligament insertions.

Strain gauges were excited in a quarter-bridge configuration using a DC-amplifier and signal conditioner (*Vishay model 2100, Vishay Micro-Measurements, Inc., Raleigh, NC, USA*). Output signals were digitized and recorded using a 16 bit

analog/digital data acquisition system (*Labview v7.0 and NI DAQCard-6036E, National Instruments Corporation, Austin TX, USA*). Triaxial accelerometers (*Endevco Corporation, San Juan Capistrano, CA, USA*) were screwed into the dorsal aspect of vertebrae T6, and vertebrae L5.

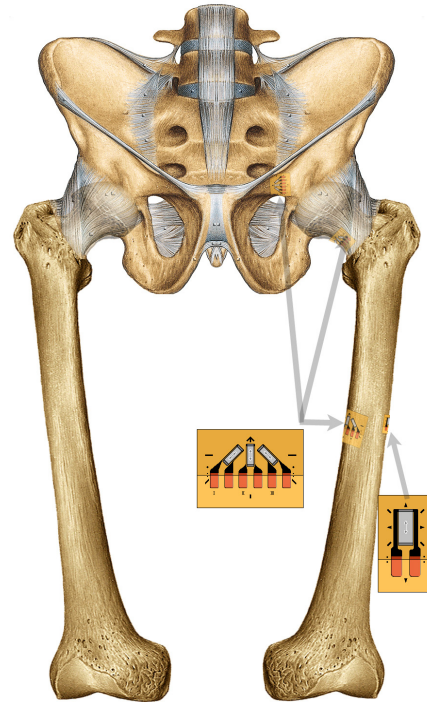


Figure 3. Strain gauge placement (Anatomy adapted from Sabotta, 1993)

Prior to impact, the PMTO was positioned in the stance phase of gait, with the left foot forward. To prevent the arms from obstructing contact with the car front, the hands were bound at the wrist in front of the subject. At 65 ms prior to impact, the subject was released from an overhead support using an electro-mechanical switch. The PMTO was thus permitted to settle under the load of gravity for 65 ms before being impacted from the left side.

For each PMTO, one of the four automotive geometries described above was bolted to the test sled. The initial velocity of the sled was 40.0 ± 0.3 kph at time of impact, and the sled was decelerated at 13 m/s^2 after contact. Details about the impact conditions of each test are listed in Table 3. Impact and post-impact kinematics were recorded at 1,000 frames per second from two high speed digital video cameras mounted perpendicularly to the sled track. A lateral view of the car geometries and relative statures of the PMTOs is shown in Figure 4.

Table 3. The LEH/Hip ratio gives an indication of the hood edge contact point on the leg. For example, in the case of 100%, the hood edge strikes the greater trochanter. A ratio of 75% would correspond roughly to contact with the midshaft of the femur.

PMTO	Geometry	Impact Speed	Ratio LEH to Hip height
T1	Sedan 250	40.1	97%
T2	Sedan 250	40.0	91%
T3	Sedan 050	40.0	83%
T4	Van 050	39.8	96%
T5	Van 250	39.7	100%



Figure 4. While geometries for a given vehicle class have identical hood edge height as defined by the current EEVC protocol, the effective hood leading edge height is higher with respect to smaller stature pedestrians.

After impact, diagnostic radiographs were made of the struck-side femur, tibia/fibula, knee joint, hip joint, and pelvis. The body was then autopsied by a qualified forensic medical doctor, and impact-related injuries were catalogued. Sections of bone specimens were removed at the strain gauge location, and were assessed for bone quality using a peripheral quantitative computer tomography (pQCT, *Scanco Medical, Bassersdorf, Switzerland*). The pQCT scans

with a spatial resolution 90 μm were analyzed for cortical and trabecular bone architecture, and were assessed with regard to osteoporosis. According to World Health Organization standards, subjects with bone quality more than 1 standard deviation below average of a healthy population are considered “low-bone” and subjects more than 2.5 standard deviations below are clinically diagnosed as having osteoporosis. It should be noted that pQCT provides vastly superior spatial resolution over two-dimensional diagnostic techniques, and provides the capability to analyze bone structure geometrically. However, baseline data-sets published in the literature are limited. The baseline dataset (n=60) used in this study comes from Hirokoshi et al., 1999.

Data analysis

Raw strain gauge data were filtered using a low-pass CFC-600 filter, and converted to strain data using the calibration gauge factors provided by the manufacturer. Bone stresses and bending moments were calculated by multiplying strain by an assumed elastic modulus of 17 GPa (McElhane, 1966). Bending moments at the femur were calculated using classical beam theory:

$$M = \frac{\varepsilon * E * I}{r_o} \quad \text{where,} \quad I = \frac{\pi}{4} [r_o^4 - r_i^4],$$

ε is measured strain, E is the elastic modulus, I is the moment of inertia for a hollow cylinder, and r_i and r_o are mean femoral midshaft internal and external radii, respectively. The midshaft radii were obtained during autopsy by averaging five measurements of periosteal shaft diameter and cortical wall thickness.

Kinematic analysis of the high-speed video was performed to assess the danger presented to the pedestrian for a head first secondary impact with the road. A qualitative comparison between the kinematics of the FE model and those of the PMTOs was also performed. Video was further analyzed to estimate the closing speed of contact between the car hood leading edge and the leg or pelvis of the PMTO. Finally, the measured bone strains, bone stresses, and observed injuries were analyzed with respect to car geometry and bone quality as assessed by pQCT.

Proposed Modifications to the EEVC Upper-leg Testing Protocol

An attempt to improve the current EEVC UL impact protocol was made via a modification of the test conditions. It was hoped to increase bio-fidelity of the test protocol with minimal changes to the

impactor itself. Modifications of impact velocity, impactor mass, impact angle, and impact height (leading edge height) were based on simplified geometric/anatomical principles and observations from both the FE simulations and PMTO experiments. Madymo® simulations employing the proposed protocol changes were then compared against the default EEVC conditions, the results of the FE model, and the PMTO impact results.

RESULTS

Bone fracture, and other injuries: Simulation vs. PMTO experiments

Three PMTO fractures of the struck-side superior ramus were observed, including the sedan 250 (T2) and both van geometries (T4 and T5). Fractures of the acetabulum were also observed in both van impacts (T4 and T5). FE simulation predicted pelvic fractures for only the small radius van geometry (Van050). Acetabular fractures were not predicted by the THUMS for any car/van geometry. No PMTO femoral fractures were observed, nor were they predicted by the FE simulations for any of the test geometries. Fractures of the lower legs were not analyzed using the model.

Kinematic analysis revealed a straightforward mechanism of pelvic loading when impacted by high leading edge geometry (LEH \geq hip height); the hood leading edge contacted the femur at or above the greater trochanter, loading the pelvis obliquely through the axis of the femoral neck (the PMTO pelvis was rotated 20 degrees (cw) in the coronal plane with respect to the impact direction). However, for automotive geometries with hood leading edges lower than the hip, the soft tissues of the thigh make first contact, and the loading path to pelvic structures is considerably more complicated.

Only PMTO T3 (a 50th% man impacted by Sed050) was clearly a case of leading edge contact with the midshaft of the femur. This can be seen qualitatively in Figure 4 above, and quantitatively in Table 3 as the ratio of LEH/hip-height. The other PMTO trials, including PMTO T2 (impacted by Sed250), were to a much greater extent impacted at the proximal femur and pelvis.

Bone quality measured by pQCT

To investigate the possible influence of bone quality on the observed fracture patterns, the femoral necks of all five PMTOs were scanned using pQCT (Table 4, Figure 5) and analyzed for bone quality.

Consistent with their age group, subjects T1 and T3 had healthy trabecular bone, cortical bone, and overall total bone quality, while subjects T2, T4 and T5, had poorer trabecular density, trabecular connectivity, cortical bone density, and lower overall bone density.

Table 4. PMTO bone quality and geometry (* = low bone, ** = Osteoporosis). The bone mineral density of the PMTOs in terms of trabecular, cortical, and overall bone mineral density are normalized to values from Horikoshi et al, 1999.

PMTO ID	Trabecular Bone (Z-Score)	Cortical Bone (Z-Score)	Total Bone (Z-Score)	Fem Shaft OD mm	Fem Shaft thick mm	Fem Neck OD mm	S. Ramus OD mm
T1	0.3	1.5	0.9	24	6	22	12
T2	-2.8**	4.2	0.1	29	7.5	28.5	13.5
T3	6.0	2.7	2.8	31	7	31.5	14.5
T4	-1.2	-5.5**	-1.9*	30	7	39	21
T5	-3.9**	2.2	-1.7*	32	7	36	N/A

The observed fractures corresponded heavily to relative bone quality of the PMTO, with all pelvic and acetabular fractures occurring in the lowest bone quality subjects. Thus analysis of the resulting injuries with respect to car geometry, age, and bone quality shows that bone quality seems to be a major factor for a pelvic/acetabulum fracture (Table 5). It also appears that acetabulum fracture is more likely with a high leading edge, such as present on the van geometries. Finally, femur fracture did not occur for any hood leading edge shape, regardless of bone quality. It should be noted, that the large bumper lead of the tested geometries may have helped prevent femur fracture for even sharp hood edges.

Loading mechanism of the femur in lateral pedestrian impact: Finite element results

In the simulations, the automotive front-end geometry had a large effect on the nature of the bending stresses in the femur. In the case of the sedan, the relatively low hood leading edge (745 mm) and moderate bumper lead (150 mm) delays the first contact of the thigh with the hood. This permits the pelvis and proximal femur to accelerate before first contact, thus reducing the closing speed between the thigh and the hood leading edge to between 1 and 6 m/s, depending on the hood leading edge radius. In

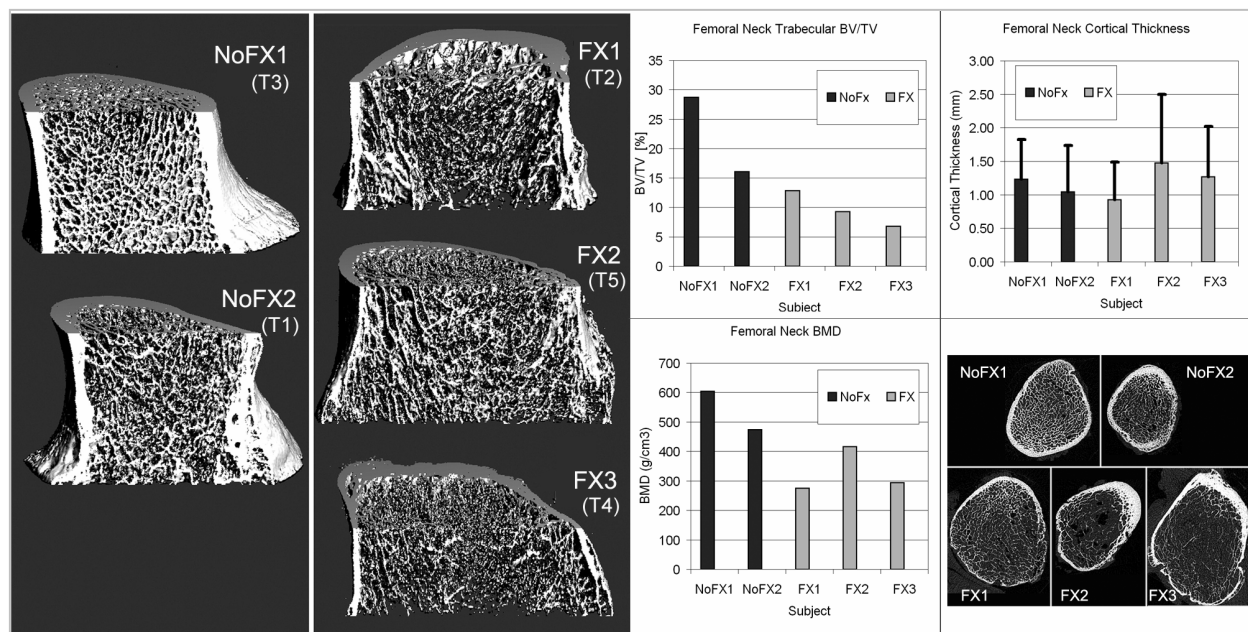


Figure 5. Bone quality was assessed using pQCT scans of the femoral neck.

Table 5. Lower extremity injury related to car geometry, age, pedestrian stature, bone quality.

Trial	Sedan	Sedan	Sedan	Van	Van
	T3	T1	T2	T5	T4
Hood Radius	50 mm	250 mm	250mm	250 mm	50 mm
Age	35	52	76	76	78
Hood Height (% of Hip Height)	83%	97%	91%	100%	96%
Bone Quality	Good	Good	Poor	Poor	Poor
Lower Leg Fracture	No	Yes	Yes	Yes	Yes
Pelvic Ramus Fracture	No	No	Yes	Yes	Yes
Pelvic Acetabulum Fracture	No	No	No	Yes	Yes
Femur Shaft Fracture	No	No	No	No	No

the case of the van/one-box construction (or a sedan with high LEH and/or short BL), the pelvis and proximal thigh do not considerably accelerate before contact with the hood leading edge. Hence, the contact closing velocity is much higher than that of the sedan, and the bending induced by this contact is more severe. In car geometries that involve a hood leading edge lower than the height of the hip, it appears that the bending of the femur, and consequently the associated risk of fracture, are directly related to the closing speed of contact between the thigh and the hood leading edge (Figure 6). According to the model (and verified by the PMTO tests), the roundness of the hood leading edge

imparts a rolling motion to the thigh, which reduces the closing speed of contact.

Loading of the femur in lateral pedestrian impact: PMTO results

In general, the mechanism of femoral loading and the corresponding femur shaft cortical strains and bending moments (both magnitude and time history) in the PMTO femur corresponded very well to those predicted by the THUMS model (Figures 7 and 8). However discrepancies arose due to differences in stature between the THUMS and the PMTOs. In tests T1 and T5, the small stature of the subject with respect to the hood edge causes the hip to be

contacted by the hood before the femoral bending moment (and stresses) can fully develop. With respect to hip height, Trials T1 and T5 are more similar to an SUV type impact on a 50th% man, for which the hood edge engages the hip/pelvis at or above the greater trochanter.

In no case was femoral fracture observed. Consistent with this observation, peak recorded femoral shaft cortical bone strain never approached the 2500 $\mu\epsilon$ threshold associated with fracture (McElhaney, 1966). The measured bone strains and corresponding bending moments of the first peak tend to be less than those predicted by the THUMS model. This may indicate that the THUMS knee is more rigid than that of the PMTO, where skeletal tissues tend to dissipate or absorb impact energy

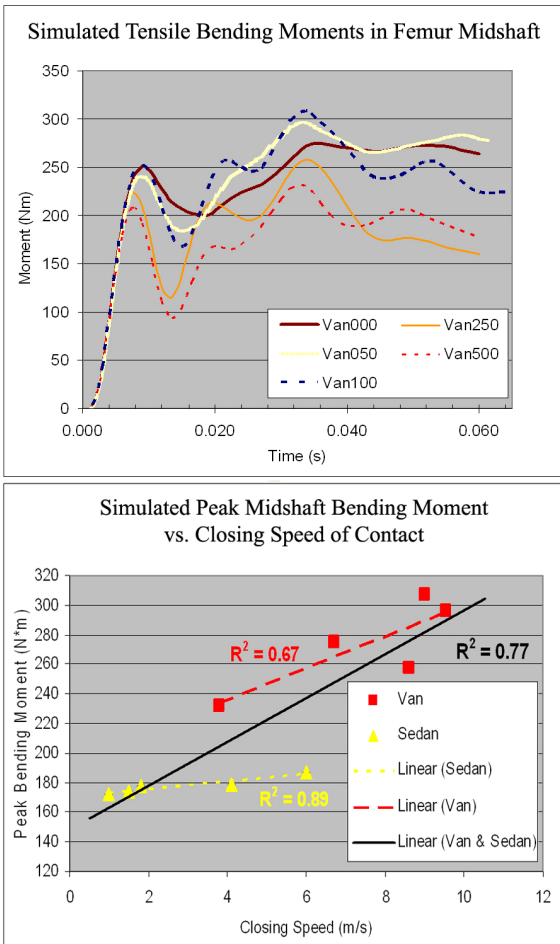


Figure 6. (Top) The larger leading edge radii impart a rolling motion to the thigh. This effectively reduces the closing velocity, and consequently, the peak bending moment in the femur. (Bottom) As closing speed increases, so does the bending load applied to the femoral shaft due to hood contact. These trends were also observed in the PMTO experiments.

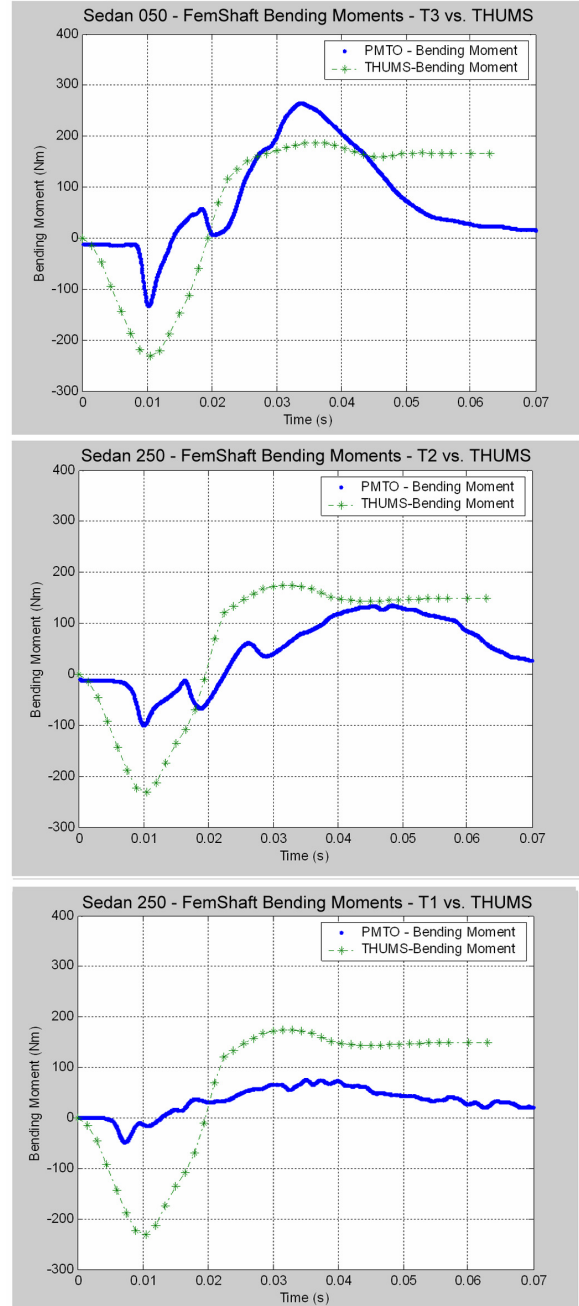


Figure 7. The bending moment in the medial femoral shaft impacted against the sedan. (Top) In PMTO T3, the stature of the subject is very similar to the THUMS. Accordingly, there is particularly good agreement between the experimentally measured bending moments and those predicted by the THUMS model. In PMTO T2 (Middle) and T1(Bottom), the smaller stature of the subject causes hip contact with the hood before the bending moment can fully develop. With respect to hip height, trial T1 is more similar to a van/SUV type impact on a 50th% man. A resulting fracture of the superior pubic ramus in T2 may have also influenced the resulting loads.

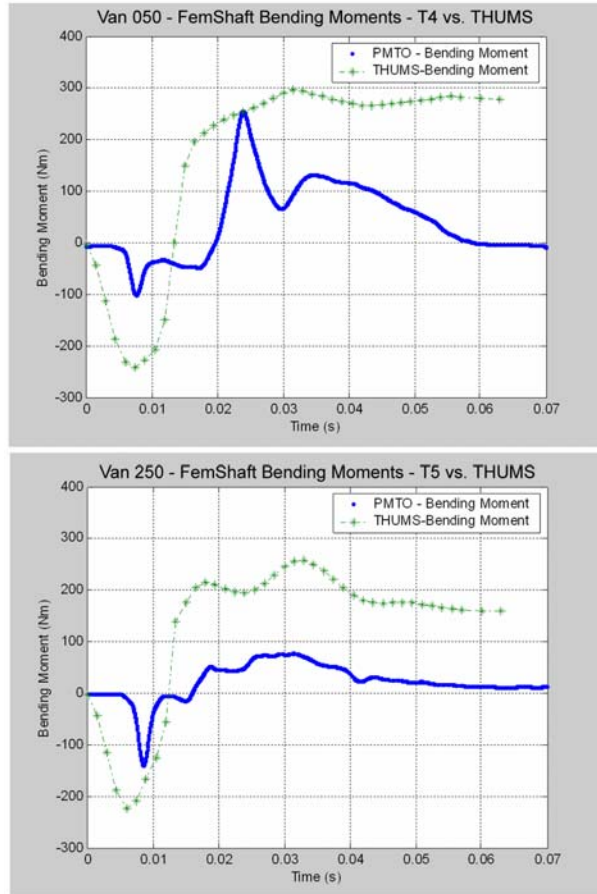


Figure 8. In both van impacts, a catastrophic failure of the acetabulum and superior pubic ramus on the struck side of the PMTO may have contributed to decreased loading of the femur.

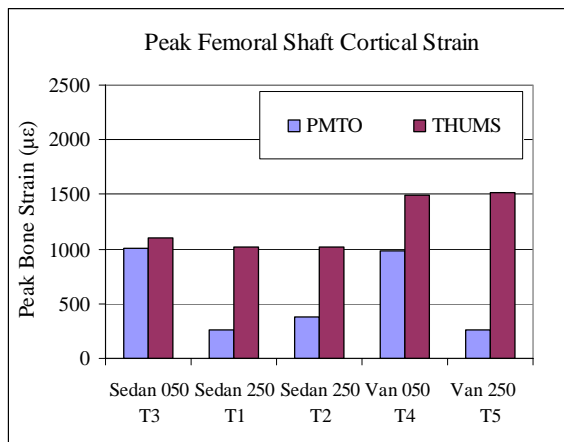


Figure 9. Summary of peak femoral shaft cortical bone strain for the PMTO test series and the corresponding THUMS simulations. Peak tensile strains are less than thresholds associated with tensile fracture (2500 µε), consistent with no observed femoral fractures.

Loading of the pubic ramus in lateral pedestrian impact

The recorded pubic rami strains were similar for all PMTO's (Figure 10). Bone strain increased rapidly after contact between the thigh/buttocks and the hood, then either dropped immediately in the case of pelvic fracture, or continued to rise and then gradually decrease in cases of non-fracture.

The measured peak stress magnitudes in the PMTO pubic rami are consistent with those predicted by the THUMS model (Figure 11). The fracture of the strain-gauged pubic rami observed in PMTO T2, T4, and T5 provide insight into the failure behavior of this structure. Analysis of bone quality by pQCT shows that the discrepancy between the ultimate strains of the fracture cases and the non-fracture cases is most likely due to differences in bone quality (age-related osteoporosis).

Loading of the femoral neck in lateral pedestrian impact

Surgical access to the femoral neck was hindered by the ligaments at the hip. Generally the strain gauges were placed on the inferior/anterior aspect of the femoral neck. Since the gauge placement was variable between trials, the direct comparison of PMTO and FE model femoral neck stresses is complicated.

As can be seen in Figure 12, a prominent peak in the stress vs. time curves can be seen in T2, T4, and T5 at approximately 20 ms after impact. Video analysis indicated that this peak coincided with contact between the hip and hood leading edge.

Analysis of high-speed video: secondary road impact

Video analysis revealed that all PMTOs were rotated between 190 and 270 degrees in the sagittal plane depending upon the shape of the vehicular hood. The pedestrians struck by the sedan geometries often made a secondary impact with the hood before landing on the ground. This secondary impact provided additional rotation of the body, and prevented the PMTO from landing head-first on the test track. The shorter, angled hoods of the van geometries, and head contact with the van windscreen caused PMTOs T4 and T5 to rotate approximately 190 degrees, thus resulting in a head-first contact with the ground (Figure 13). It should be noted that PMTO T4 had a cranial fracture, and PMTO T4 and T5 both experienced cervical spine fractures at C7. However, it is not clear whether these injuries occurred as a result of primary, or secondary impact.

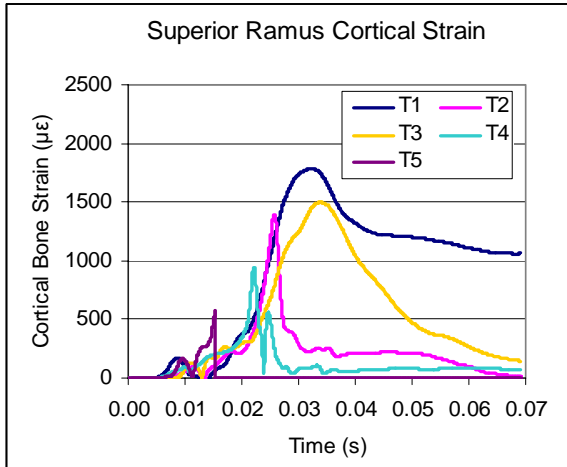


Figure 10. Cortical bone stresses in the superior pubic ramus. Pelvises of T2, T4, and T5 were fractured during impact, as indicated by the sharp drop in strain.

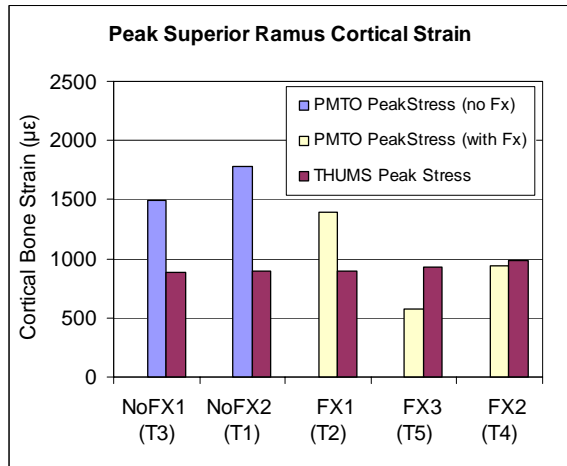


Figure 11. Peak superior pubic ramus tensile cortical strain for the PMTO and THUMS simulations.

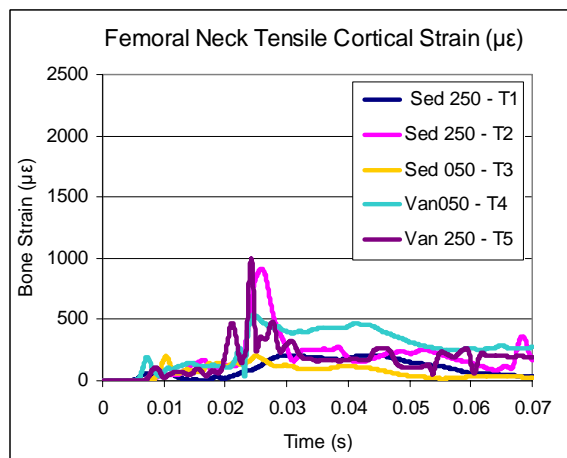


Figure 12. Cortical bone strains in the femoral neck.



Figure 13. Secondary road impact is a very important design consideration that is often neglected. PMTOs struck by the sedan landed on their sides. PMTOs struck by the vans were thrown onto their heads. Notice the use of ground padding cushioned secondary impact, possibly resulting in fewer injuries than would be observed against a rigid road surface.

Proposed Modifications to the EEVC Upper-leg Testing Protocol

Observations from the THUMS simulations and PMTO experiments indicate that EEVC designated hood leading edge is often not the first point of contact with the pedestrian P/UL. The proposed changes to the method of geometric characterization define the hood leading edge height using a “wrap around” contact definition method similar to that already employed for the EEVC headform test protocol. In the proposed modification, hood leading edge height is defined as the first point of contact between the hood and a 1,000 mm long string rotated from the EEVC upper bumper reference line. The impact angle is defined as the angle between the string and the vertical plane (Figure 14).

Results from the present study show that for hood leading edge heights exceeding approximately **90 cm** (defined as per the modified method), the threat of fracture posed to the femur is reduced, and the likelihood that a pelvic fracture will occur is raised. Thus, this LEH threshold is proposed as a transition from test conditions and failure criteria suited to the femur to conditions appropriate for assessing pelvic fracture risk. The test conditions for each of these cases are outlined below in Table 7. The impact tests are executed in exactly the same manner, regardless of whether the pelvis is being tested, or the femur. The difference lies in the selection of the impactor mass, and the pass/failure criteria applied when analyzing the test results.

In particular, the current EEVC UL test protocol fails to reflect the true closing speed of contact between the pedestrian UL and the hood leading edge. This inaccuracy is especially important since impact energy (a critical value with regard to injury likelihood) varies quadratically with impact velocity. With certain velocity assumptions (Figure 14), the closing contact velocity (normal to the long axis of the femur) is a simple geometric relationship. The proposed method uses this geometrical relationship for determining a more appropriate impactor velocity. The selection of the impactor mass is based upon the mass of the involved body segments. For a 50% male pedestrian, the mass of the upper leg (thigh) is approximately 7.5 kg. This is the mass then designated for impact tests of vehicles with a LEH \leq 90 cm. The 11.1 kg mass for LEH > 90 cm, corresponds to the mass of the 50% male pelvis plus 10% of the upper leg mass. It should be noted that an impact mass of 7.5kg is 2kg less than the default weight of the current EEVC UL impactor. Thus for testing geometries with LEH \leq 90 cm, modification to the default impactor will be necessary.

The impactor trajectory should follow the measured impact angle along a path such that the impactor shaft centerline coincides with the newly defined leading edge height (Figure 15). Unlike the current version of the EEVC UL protocol, the impact angle and the point of first contact between the impactor and the car front is roughly the same as the actual pedestrian impact.

The proposed test pass/failure criteria (Table 7) are based upon the following observations:

- 1) The femoral shaft is likely to fail in lateral impact due to stress induced by bending moments. A nominal threshold of 320Nm is suggested based upon quasi static tests of Yamada (1971), and dynamic tests of Powell et

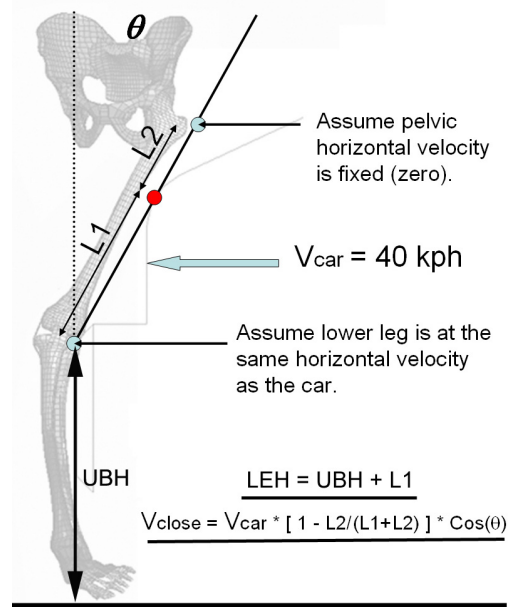


Figure 14. The proposed method for determining the EEVC leading edge height.

Table 7. Description of differences in pelvic vs. femur UL test

Region	LEH (cm)	Impact Mass	Failure Criteria
Femur	≤ 90	7.5 kg	Average Bending Moment > 320 Nm (Yamada 1971, Powell et al. 1975, Kress et al. 2001,)
Pelvis	> 90	11.1 kg	Peak Average Force > 10 kN (Cesari 1982)

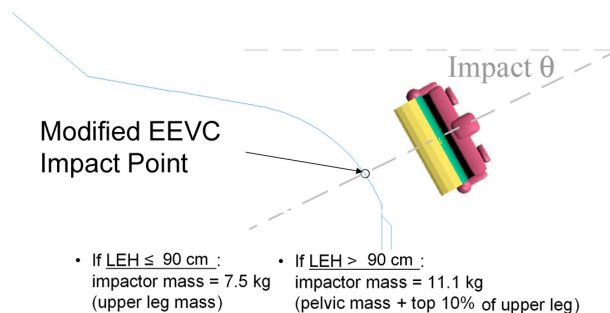


Figure 15. The impactor is directed along a trajectory such that the impactor centerline is aligned with the Mod-EEVC LEH reference point. Impact masses are determined by the mass of the involved body segments. The test impact mass values are derived from the anthropometric study of Roebuck et al. 1975.

al. (1975) and Kress et al. (2001). Peak bending moments observed in the present PMTO study also suggest that this threshold is reasonable.

- 2) To our knowledge, no comprehensive data set exists for injury tolerance of the femoral neck and greater trochanter under lateral impact loading.
- 3) The PMHS studies of Cesari et al. (1982) establish a peak force limit of 10 kN for lateral impacts directed at the greater trochanter, and along the axis of the femoral neck. This is the best suited criteria given the information available from the EEVC UL impactor sensors.

Assessment of the proposed modifications to the EEVC UL Protocol

The proposed modifications to the EEVC UL test protocol were employed in simulated EEVC testing of several automotive geometries. The fifteen simplified car geometries used in this study were tested using the Madymo® FE model of the EEVC UL impactor. The simulation results from the modified protocol were then compared to those of the original protocol, as well as against the results from the THUMS FE model and PMTO results.

Generally, the modified EEVC protocol methods employed substantially lower impact velocities than those prescribed by the original version of the EEVC UL testing protocol. This is due a more appropriate characterization of the leading edge and contact velocity between the thigh and the hood.

The proposed modifications to the EEVC test conditions greatly improved correlation to both the THUMS pedestrian model and PMTO impact results for bending moments (Figure 16). However, the modified EEVC simulations still predict higher bending moments than the THUMS simulations or PMTO tests.

A separate test condition (11.1 kg impact mass instead of 7.5 kg) and failure criterion (10kN peak impact force) were applied to those vehicles with an Mod-EEVC LEH greater than 90 cm. Thus, the Van000 geometry and all SUV geometries except SUV500, were tested for pelvic impact. As can be seen in Figure 17, the 10 kN peak impactor force threshold yielded a good correlation with THUMS injury prediction. However, the modified EEVC protocol simulation predicts that a van geometry with no leading edge radius (Van000) will cause no pelvic fracture, while the THUMS model and PMTO experiments predict that this geometry will cause a pelvic fracture to occur. The modified EEVC test

protocol also inherently assumes that no pelvic fracture will occur in vehicles with Mod-EEVC LEH < 90 cm.

Thus the SUV000 and Van050 geometries, for which THUMS simulations predicted pelvic fracture and for the latter of which PMTO tests showed pelvic fracture, were not tested for pelvic injury risk according to the modified EEVC proposal. As indicated by the PMTO test results, it may therefore be necessary to apply both force and bending moment injury criteria to vehicles with LEH near the pelvis/femur decision threshold.

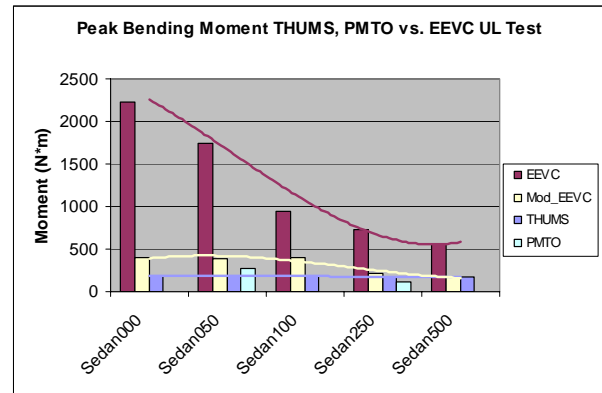


Figure 16. Comparison of the peak bending moments for impact against sedan geometries.

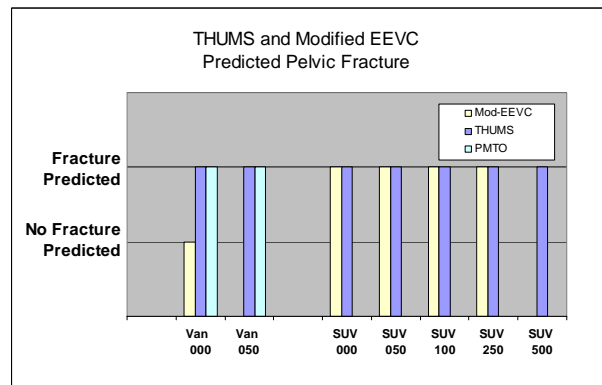


Figure 17. Comparison of pelvic fracture predictions between the modified EEVC protocol, PMTO test results, and the THUMS model.

DISCUSSION

The intelligent design of automotive front-end geometry holds a large potential for reducing injuries to vulnerable road users. In order to assess the risk posed to a pedestrian by an automobile, the European Enhanced Vehicle-Safety Committee has proposed three subsystem pedestrian dummy tests. These tests

are currently in use on production vehicles, and are published regularly by EuroNCAP. For such tests to be useful, it is necessary to concentrate on the most important aspects of automotive design, and employ testing protocols that are capable of successfully identifying high-risk vehicles. The current study focuses on the upper leg impact portion of the EEVC protocol, which is intended to assess the risk presented to the thigh and pelvis of a struck pedestrian.

Vehicle front end design, including hood leading edge height, bumper height, and bumper lead play a critical part in determining the complicated kinematics of pelvic/upper leg contact with the hood leading edge. The EEVC test conditions, which have been based on kinematic analysis of PMTO and dummy impact experiments, intend to incorporate these kinematics into the UL testing protocol. However, the reduction of a complicated three dimensional impact into a simplified, one dimensional impact test appears to fall short in replicating the complex nature of actual upper leg/pelvic impacts (Konosu et al., 2001, Okamoto et al. 2001, Snedeker et al. 2003).

In the current study, a full body FE model, THUMS, was used to simulate pedestrian impact against several simplified automotive geometries. The results from these simulations indicate that hood leading edge radius is an important factor in determining the injury risk posed to a pedestrian by a given automotive form. The model also indicates that acceleration of the distal femur by the bumper and rolling motion imparted to the thigh by the hood radius drastically reduce the closing speed of contact in appropriately designed vehicles. In a previous study we have shown that the current EEVC WG17 upper-leg testing protocol does not reflect these critical factors (Snedeker et al., 2003). The purpose of the present study was to validate the THUMS model predictions against actual PMTO experiments, use the PMTO experiments to deepen our understanding of femur and pelvic injury mechanisms, and use this insight to make recommendations for an improved characterization of vehicle geometry.

In general, the predictive capacity of the THUMS pedestrian model was excellent. The predicted femoral bone strains and bending moments corresponded very well to the experimental PMTO measurements. The model tends to over-estimate the “first-peak” bending moment imparted to the thigh by contact with the bumper. This may imply that the model knee is more rigid than that of the PMTO, in

which the soft tissues of the knee dissipate impact energy, and force transmission from the lower leg to the femur is dampened. It may also be due, in part, to the fact that the THUMS model does not account for soft tissue injuries or fracture of the tibia or fibula. Such injuries were observed in three of the five trials, and would serve to inhibit force transmission to the femur.

Interpretation of the strain gauge data from the pubic ramus and femoral neck is more difficult, since the precise loading mechanism of these structures is relatively unknown. These measurements were also complicated by variability in the anatomical placement of the gauges due to individual differences in bone geometry, and difficulty in accessing bone surfaces heavily invested by connective tissue. In an effort to compare the measured bone strain data with the THUMS model, the time history of cortical bone strain was compared against individual finite elements located in corresponding anatomical positions. The element strains in the THUMS pubic rami vary widely between even neighboring elements, suggesting both that the strain distribution in these bone structures is complex and that the mesh discretization was perhaps too coarse. However, the strain time history of certain THUMS elements in each case was similar to that measured with the PMTO strain gauges, and the predicted THUMS stress magnitudes are appropriately matched to the corresponding measurements of PMTO stress magnitude (Figure 11 above).

When considering automotive front end geometry, the observed PMTO injury patterns were surprising. The THUMS model predicted no injuries for any geometry except the van with a sharper hood edge (Van050). It was anticipated that the large bumper lead and hood radius of the sedans, and the van with the rounded hood edge (Van250) would permit sufficient acceleration of the distal femur prior to contact with the hood, such that the closing speed would be reduced and no injury would result. In fact, no injuries to the femur were observed. However, two factors are likely causes to why this hypothesis failed with regard to the pelvis: bone quality and victim stature.

In an attempt to explain the prevalence of pubic rami fracture in PMTOs T2, T4, and T5, test subject bone quality was assessed using pQCT. As can be readily seen in Figure 5, marked differences in bone quality existed between subjects. Further, the three impacts that resulted in pelvic fracture all involved subjects with compromised bone integrity. While these subjects had diminished bone quality with

respect to young healthy adults, their bone quality was typical of the older pedestrians that represent a significant proportion of pedestrian victims. Thus, it appears that age and age-related bone loss may be at least as important as car geometric design when it comes to the injury outcome of a car-pedestrian collision.

Victim stature with respect to leading edge height is the second factor that explains the prevalence of hip and pelvis injuries in these experiments. All THUMS simulations, and indeed most reported biomechanical studies, involve the anatomy of a 50th% man or have data normalized to this standard. Only two of the subjects tested in the present study are representative of such a subject, and the other three subjects were considerably smaller in stature. Thus the hood of a sedan with a leading edge height of 765 mm will most certainly contact a standing 50th% man on the femoral midshaft, but shorter pedestrians are likely to be struck at the hip or pelvis. With regard to PMTOs T1, T2, and T5, the hood front contacted the pedestrian at the hip, and thus these impacts are perhaps better compared to the THUMS being struck by an SUV or van with a high leading edge height. With regard to the hip and pelvic fracture of subject T4, it is possible that the violent loading of the femur due to the sharp hood edge, may have caused a “push-through” fracture of the acetabulum, and a subsequent fracture of the superior ramus.

CONCLUSIONS:

- A method for dynamic measurement of femoral and pelvic bone strains in a laterally struck pedestrian has been successfully established
- The THUMS pedestrian model is capable of accurately assessing pelvic and femoral injury risk in laterally struck pedestrians.
- It may be possible that “safe” cars can be identified using only geometric measurement, and that an UL impactor is unnecessary.
- A car sufficiently exhibiting: low hood leading edge height, large hood edge radius, moderate bumper lead, and high bumper edge height would practically exclude the possibility of a femoral fracture in primary lateral impact of a 50th percentile male pedestrian at impact velocities less than 40 kph.
- Bone quality and pedestrian stature are critical considerations with regard to injury outcome that are not considered by the current EEVC UL test protocol.

- The hood leading edge roundness has an important effect on the upper leg kinematics of pedestrian impact. This effect is not sufficiently encompassed by the one dimensional impactor or the test condition look-up graphs employed in the current version of the EEVC test protocol.
- The closing speed of contact between the thigh and car hood is a critical factor in injury likelihood that does not appear to be sufficiently accounted for in the current EEVC test protocol. The closing speed is often not equivalent to vehicular speed, and can largely depend on the roundedness of the hood leading edge.
- Separate test conditions and test pass/fail criteria should be implemented for low leading edge height (LEH < hip height) and high leading edge height vehicles (LEH > hip height). Specifically, low LEH vehicles should be tested with regard to the femur, and high LEH vehicles should be tested with respect to the pelvis.
- A modified EEVC UL test protocol has been offered. The modified EEVC protocol is based on a logical geometric determination of impact conditions derived from pedestrian anthropometry and vehicle front end shape.
- The modified proposal accounts for reduced impact velocity in cases where the impacted femur has been accelerated by the bumper prior to impact with the hood leading edge thus reducing impact energy.
- The modifications to the EEVC protocol yield impactor bending moments that correspond much better with those predicted by the THUMS pedestrian model and PMTO experiments. It is therefore deemed to be a significant improvement on the current EEVC protocol.
- Validated numerical models provide a powerful low-cost alternative to the use of impactors in assessing pedestrian injury risk.

OUTLOOK

The present study represents a significant leap forward in the assessment of pedestrian injury risk through the use of numerical models. The THUMS pedestrian model has been shown to predict with a high degree of accuracy the resulting pelvic and femoral loading patterns in laterally struck pedestrians. However, there is still work to be done.

The proposed modifications to the EEVC UL test protocol are based upon numerical simulations that require experimental validation. Additionally, the effects of pedestrian stature should be investigated

using numerical models of varying dimensional scale. Finally, the effect of hood stiffness was not addressed in the current work, and a parametric study of hood force-deformation characteristics could provide valuable insight automotive design insight.

ACKNOWLEDGMENTS

The authors gratefully acknowledge Toyota Motor Corporation and Toyota Central R&D Labs., Inc. for support of this study.

REFERENCES

- Bunketorp, O., Romanus, B., Hansson, T., Aldman, B., Thorngren, L., Eppinger, R.H. (1983) Experimental study of a compliant bumper system. Proc. 27th Stapp Car Crash Conference, pp. 287-297.
- Cesari, D., Ramet, M. (1982) Pelvic tolerance and protection criteria in side impact. Proc. 26th Stapp Car Crash Conference, pp. 145-154.
- Cordey J, Gautier E. Strain gauges used in the mechanical testing of bones. Part II: "In vitro" and "in vivo" technique. *Injury*. 1999;30:A14-20.
- EEVC (1998) EEVC-proposal of the EEVC Working Group 17 Report: Improved test methods to evaluate pedestrian protection afforded by passenger cars. Brussels.
- Horikoshi T, Endo N, Uchiyama T, Tanizawa T, Takahashi HE. Peripheral quantitative computed tomography of the femoral neck in 60 Japanese women. (1999) *Calcif Tissue Int*.
- Ishikawa, H., Kajzer, J., Schroeder, G. (1993) Computer simulation of impact response of the human body in car-pedestrian accidents. 37th Stapp Car Crash Conference, pp. 235-248.
- Iwamoto, M. Kisanuki, Y., Watanabe, I., Furusu, K., Miki, K., Hasegawa, J. (2002) Development of a Finite Element Model of the Total Human Model for Safety (THUMS) and Application to Injury Reconstruction, Proc. 2002 International Research Council on the Biomechanics of Impact (IRCOBI).
- Konosu, A., Ishikawa H., Sasaki, A. (1998) A study on pedestrian impact test procedure by computer simulation. In: Proc. 16th International Conference on the Enhanced Safety of Vehicles (ESV).
- Konosu A., Ishikawa H., Tanahashi M. (2001) Reconsideration of injury criteria for pedestrian subsystem legform testproblems of rigid legform impactor. In: Proc. of the 17th International Conference on the Enhanced Safety of Vehicles (ESV).
- Kress, T A and Porta, D J. (2001) Characterization of Leg Injuries from Motor Vehicle Impacts. In: Proc. of the 17th International Technical Conference on the Enhanced Safety of Vehicles (ESV).
- Matsui Y, Ishikawa H, Sasaki A (1998). Validation of Pedestrian Upper Legform Impact Test – Reconstruction of Pedestrian Accidents, Proc. of the 16th International Technical Conference on the Enhanced Safety of Vehicles (ESV).
- Matsui Y, Ishikawa H, Sasaki A. (1999) Pedestrian injuries induced by the bonnet leading edge in current car-pedestrian accidents. SAE International Congress and Exposition, Society of Automotive Engineers, Warrendale, Pennsylvania, USA.
- McElhaney J.H. (1966), Dynamic Response of Bone and Muscle Tissue. *Journal of Applied Physiology*, 21, pp. 1231-1236.
- Okamoto, Y., Akiyama, A., Okamoto, M., Kikuchi, Y. (2001) A study of the upper leg component tests compared with pedestrian dummy tests. In: Proc. of the 17th International Technical Conference on the Enhanced Safety of Vehicles (ESV).
- Powell, W. R., Odala, S. J., Advani, S. H., and Martin, R. B. (1975) Cadaver Femur Responses to Longitudinal Impacts. SAE 751160, Proceedings of the Nineteenth Stapp Car Crash Conference.
- Roebuck, J.A., Kroemer, K.H.E., Thomson, W.G. (1975) *Engineering Anthropometry Methods*. Wiley, New York
- Sheppard, C.(2001) "Pelvic Fractures", *eMedicine Journal* , (www.emedicine.com) 2:6.
- Sabotta J., (1993) Sobotta, *Atlas der Anatomie des Menschen Band 2*. Urban & Fischer.
- Snedeker J.G., Muser M.H., Walz F.: Assessment of pelvis and upper leg injury risk in car-pedestrian collisions: Comparison of accident statistics, impactor tests and a human body finite element model. *STAPP Car Crash Journal* 2003; 47:437-457.
- TNO Corporation (2001) *Madymo V6.0 Database Manual*, Delft, Netherlands
- Yamada H. (1971) *Strength of Biologic Materials*. Krieger, Huntingdon.

TORSO INJURY TRENDS FOR PEDESTRIANS STRUCK BY CARS AND LTVs

Douglas Longhitano

Honda R&D Americas Inc.

Johan Ivarsson

Basem Henary

Jeff Crandall

University of Virginia

USA

Paper Number 05-0411

ABSTRACT

As light trucks become more prevalent in the vehicle fleet, it becomes important to consider the implication of vehicle geometry variations on pedestrian injury patterns. Historically, studies have shown that the body region priorities should be the head and lower extremity for pedestrians struck by motor vehicles. More recent studies have found that the injury pattern for pedestrians struck by Light Trucks, Vans, and Sport Utility Vehicles (LTVs) is different from that of those struck by passenger cars. Data from the Pedestrian Crash Data Study (PCDS) during the period 1994 to 1998 has shown that the torso should be a significant focus area, preceded only by the head, for pedestrian struck by LTVs. In this study we analyzed the type and severity of AIS 2+ torso injuries recorded in PCDS for adults age 18 to 50. Regardless of impacting vehicle type, the most frequently injured torso structures at the AIS 2+ level are the ribcage, liver, and lung. Considering instead the AIS 4+ level, the most commonly injured torso structures are the aorta, ribcage, and spleen in pedestrians struck by LTVs and the lung, ribcage, and liver in those struck by passenger cars. The results of this study suggest that while the overall torso injury trends may be similar for passenger cars and LTVs, somewhat different injury patterns are occurring at higher severity and may be a result of differences in vehicle geometry and injury mechanisms.

INTRODUCTION

Since the 1970's, pedestrian impact protection has been a significant focus area for automotive safety researchers. Accident data shows that pedestrian impact consistently accounts for more than 10% of the annual fatalities on roadways in the United States (NHTSA, 2004a). In 2003, there were 4,749 pedestrian fatalities and 70,000 injuries in the

US (NHTSA, 2004b). 45% of the fatalities and 62% of the injuries are associated with passenger cars, while 39% of the fatalities and 31% of the injuries are associated with LTVs (NHTSA, 2004a).

LTVs have been increasing in popularity in the US since the early 1990's. By 1999, they accounted for nearly 50% of new vehicle sales. This trend has been accompanied by an increasing trend in pedestrian fatalities associated with LTVs (Lefler and Gabler, 2004). Numerous studies have been conducted to understand the pedestrian injury and fatality risk from cars, however only a few investigations have focused on pedestrian interaction with specific vehicle types such as LTVs.

In a 1998 study using the Pedestrian Crash Data Study (PCDS) database, Jarrett and Saul noted that LTVs might pose a more serious threat to pedestrians than cars since LTV impacts dominate the highest levels of injury severity.

A 1999 study by Mizuno and Kajzer looked into the influence of vehicle geometry on pedestrian injury risk using Japanese data (Mizuno and Kajzer, 1999). They found that the risk of fatality for pedestrians is independent of vehicle type for vehicles weighing less than 1400 kg. However, they found that fatality risk is dependent upon the vehicle type for vehicles over 1400 kg,

Lefler and Gabler published a 1998 study looking at pedestrian injury risk from LTVs. This study, revised and updated in 2004 (Lefler and Gabler, 2004), indicates that a pedestrian struck by an LTV has a 2 to 3 times greater likelihood of dying than if struck by a car. The study is based on 543 cases in the PCDS database and includes pedestrians of all ages. The results indicate that the probability of AIS 4 to AIS 6 injury is greater for LTVs and that LTV impacts result in a greater probability of serious head and thorax injury.

Using the PCDS database, Henary et al. (2003) found that LTVs present a significantly greater risk of serious injury and fatality than passenger cars in lower speed impacts. The statistically adjusted odds

ratios for serious injury and fatality were 3.34 and 1.87 respectively when comparing LTVs to cars.

Ballesteros et al. (2004) used 1995-1999 data from the Maryland Trauma Registry and found the risk of fatality and high injury severity to be greater for LTVs. He concluded that, compared to cars, SUVs and pickups present a greater risk of serious injury to the brain, thorax, and abdomen, but a lower risk of injury to the region below the knee.

Based on the most frequent pedestrian injuries and consequent HARM, Fildes et al. (2004) set out to determine priorities for vehicle design. The study based on Australian and German data reported that 96% of all fatal pedestrian cases have injuries equivalent to AIS 4 or greater and 59% of the fatalities have some AIS 4+ torso injury.

Using the PCDS database Longhitano et al. (2005) studied differences in adult pedestrian injury patterns and injury sources based on vehicle type. The study looked at the number of injuries per body region sustained by pedestrians struck by passenger cars compared to those struck by light truck vehicles such as SUVs, vans, and pickup trucks (Figure 1). One significant finding was that serious injuries to the torso are much more frequent for pedestrians struck by LTVs than for those struck by cars. For LTVs, torso injuries are preceded by head injuries, but occur in greater numbers than lower extremity injuries.

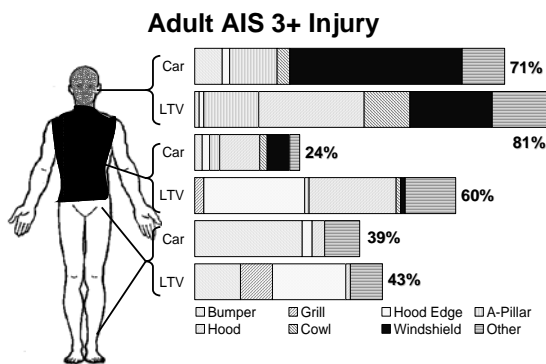


Figure 1 – Distribution of AIS 3+ Injuries by Body Region, Vehicle Type, and Injury Source.

Based on these previous studies it is evident that torso injury is an important area of consideration for mitigating pedestrian injuries and fatalities. This study was designed to focus on the specific type and severity of torso injuries recorded for adult pedestrians in the PCDS database. The purpose is to identify the organs and structures which sustain injury so that future countermeasures can be developed to mitigate their frequency.

METHODOLOGY

Data Source

The PCDS database was used as the primary source of data for this study. PCDS contains data for 552 pedestrian impacts and includes approximately 4,500 pedestrian injuries. The data was collected for late model vehicles from 6 US cities in the years 1994 to 1998 (Chidester and Isenberg, 2001). The database contains information on crashes of all severities for pedestrians struck by passenger vehicles including passenger cars, SUVs, vans, and light trucks.

Inclusion and Exclusion

For the purpose of this study, we limited the data to adult pedestrians aged 19 to 50 years. Children of age 18 and under were excluded due to numerous confounding factors such as size and biomechanical characteristics associated with growth and development. Adults over 50 were also excluded to avoid age related issues such as degradation in bone mineral density. In addition, cases which included multiple vehicles and/or multiple pedestrians were excluded.

The remaining data was divided into two categories: Car cases, which contains cases in which the impacting vehicle was a passenger car; and LTV cases, which includes cases in which the impacting vehicle was an SUV, van, or light truck. Within each of these subsets, the torso injury data was then filtered at the AIS 2+, AIS 3+, and AIS4+ levels. Torso injuries were defined as those injuries with an AIS code associated with the thorax, thoracic spine, abdomen, or lumbar spine.

The AIS 1 level injury has been excluded from this study as they are largely skin or other non-specific injuries that would not improve the analysis and may even mask other existing relations.

To focus on vehicle related factors, ground contact injuries were also excluded. This was accomplished by filtering all injuries that the PCDS crash investigators attributed to ground or other non-vehicle contact.

Torso Injury Type & Severity

For each division of AIS injury level the recorded torso injuries were divided into groups by the organ or structure injured. These groups were determined by the organ classification of the AIS code for each recorded injury. These classifications included aorta, lung, thoracic cavity, ribcage, liver, spleen, kidney, and other. Items were classified as

other because either the specific portion of the torso was unclear or because the total number of injuries was relatively low. This data was then taken and each injury classification was shown as a fraction of the cumulative injury at that level for each vehicle type.

Relative HARM Assessment

A HARM approximation was used in order to differentiate the relative importance of torso injuries as a function of frequency and severity. This is accomplished by assigning a societal cost factor to each AIS injury level (Malliaris, 1982).

The PCDS data was divided by injury severity level at AIS 2, 3, 4, and 5+ for each injury classification and vehicle type. AIS 5 and 6 injuries were combined because AIS 5 would normally be weighted higher than AIS 6 due to the cost of medical treatment associated with the AIS 5 injuries. (AIS 6 injuries are by definition not treatable, therefore associated medical costs are greatly reduced when compared to AIS 5 injuries.)

Each injury was assigned a HARM weighting factor based solely on the AIS level. These factors are 2.7, 7.1, 38.8, and 186.6 for AIS 2, 3, 4, and 5+ injuries respectively. For each injury classification region, the cumulative cost factor was calculated and normalized by dividing by the cumulative cost for the vehicle type classification. These calculations were performed for the cars, LTVs, and the overall vehicle sample.

RESULTS

After filtering the data by age and vehicle type there were 169 car cases and 85 LTV cases remaining for further analysis. In the passenger car cases there were 67 AIS 2 or greater (AIS 2+) torso injuries recorded and there were 77 AIS 2+ torso injuries in the LTV cases. The number of torso injuries at AIS 3+ is reduced to 40 and 46 for cars and LTVs respectively. At AIS 4+ there are 18 and 21 torso injuries recorded for car and LTVs respectively.

Table 1. Adult Torso Injuries in PCDS.

	Cars	LTVs	Total
AIS 2+	67	77	144
AIS 3+	40	46	86
AIS 4+	18	21	39

AIS 2+ Torso Injuries

There were 144 torso injuries of moderate or greater severity (AIS 2+) included in the sample of the PCDS database studied. Figure 2 shows the breakdown of these injuries by organ or structure as indicated by the AIS injury coding. This data indicates that of the major organs and structures the ribcage sustains injury at the greatest frequency, followed by the liver and lung.

The breakdown for passenger cars (figure 3) shows a similar trend to the overall breakdown, with the ribcage being the most frequently injured followed by the lung and liver. For LTVs, the breakdown (figure 4) is also similar though the frequency of spleen injury is greater than observed for passenger cars.

AIS 3+ Torso Injuries

When the PCDS sample was filtered for torso injuries of AIS 3 severity or greater, 86 injuries remained. Figure 5 indicates that in terms of serious injury the ribcage and lung are injured with the greatest frequency.

In the case of passenger cars, the distribution of AIS 3+ injuries again follows a similar trend to the data for all vehicles (figure 6). One notable difference is that there is an increased fraction of representing injury to the thoracic cavity.

Ribcage and lung continue to be of greatest importance at the AIS 3+ level for LTVs. (figure 7). The spleen also continues to be an appreciable fraction for LTVs, and the fraction associated with the aorta is of increasing importance.

AIS 4+ Torso Injuries

At AIS 4+, all but the most severe injuries are filtered out. In figure 8, we can see that the aorta encompasses a much greater fraction than at the AIS 3+ or AIS 2+ levels. The lung and ribcage, however, retain the greatest number of injuries.

The injury breakdown for passenger cars shown in figure 9 indicates that the lung and ribcage continue to be the predominant torso injuries even at the greatest severity levels for this classification.

For light trucks, the aorta and spleen occur at a frequency level in excess of the lung for severe torso injuries (figure 10). The spleen accounts for approximately 14 percent of the AIS 4+ injuries and the ribcage and aorta each account for approximately 23%.

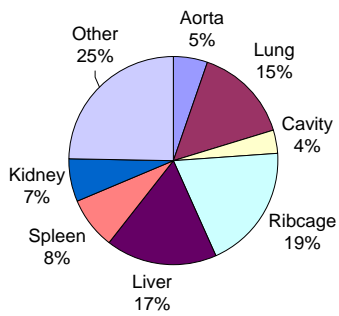


Figure 2. AIS 2+ Torso Injury Distribution For All Vehicles.

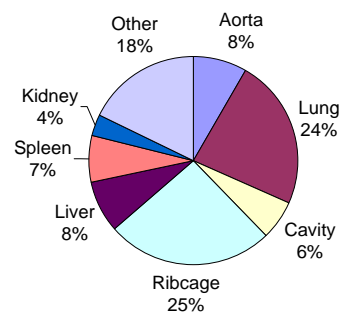


Figure 5. AIS 3+ Torso Injury Distribution For All Vehicles.

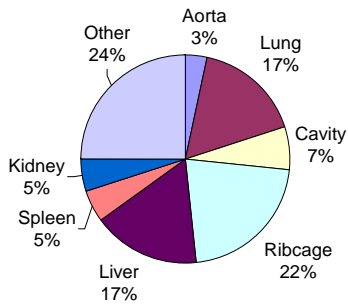


Figure 3. AIS 2+ Torso Injury Distribution For Passenger Cars.

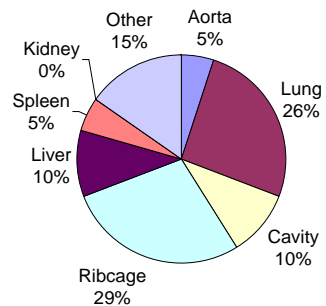


Figure 6. AIS 3+ Torso Injury Distribution For Passenger Cars.

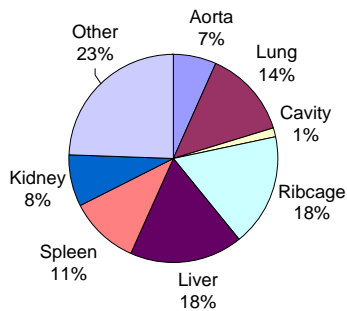


Figure 4. AIS 2+ Torso Injury Distribution For LTVs.

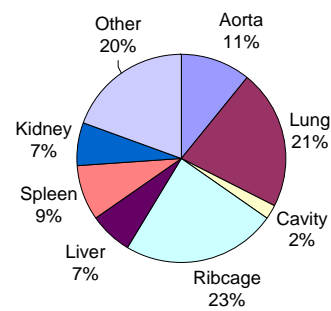


Figure 7. AIS 3+ Torso Injury Distribution For LTVs.

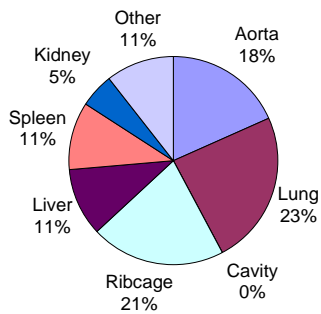


Figure 8. AIS 4+ Torso Injury Distribution For All Vehicles.

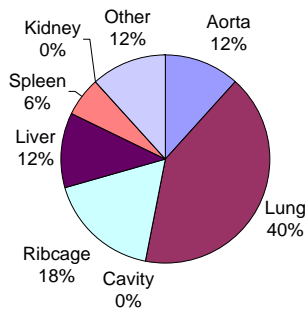


Figure 9. AIS 4+ Torso Injury Distribution For Passenger Cars.

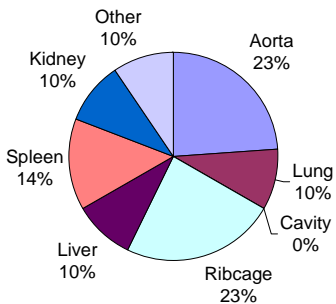


Figure 10. AIS 4+ Torso Injury Distribution For LTVs.

Cumulative HARM

Since it can be difficult to ascertain the relative importance of each injured organ or structure across a range of injury severities, a simplified relative HARM analysis was performed. For the cases studies, the percentage of total HARM within the torso was calculated for each major organ and structure for LTVs, cars, and the overall sample (Figure 11).

The data in Figure 11 indicates that the lung and aorta are the torso components at the greatest risk for HARM in pedestrian impacts. The lung predominates in cases with passenger cars due to a number of incidences where AIS 5+ lung injury is reported. For LTVs, the aorta is the most significant component, which is again due largely to the severity being recorded as AIS 5+.

A breakdown of injured torso region by injury severity and vehicle classification can be found in Appendix A.

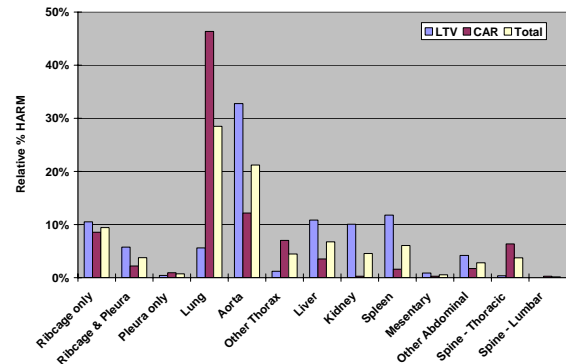


Figure 11. Relative Percentage of Torso HARM.

DISCUSSION

When looking at the distribution of AIS2+ torso injuries, it at first appears that the types of injuries sustained when struck by an LTV are similar to those for a passenger car. The ribcage is the dominant area of injury, followed by injuries to the lung, liver, spleen, and thoracic cavity.

This distribution changes noticeably when looking at higher severity injuries, AIS 4+. At the severe injury level, lung and ribcage injury dominate the passenger car dataset; while lung, ribcage, aorta, and spleen are all important for LTVs.

HARM analysis shows a further divergence between cars and LTVs. For cars, 45 percent of the cumulative HARM is associated with lung injury.

This is due to a number of instances of AIS 5 lung injury in the passenger car dataset. In the LTV dataset, the lung is not as significant. For LTVs, it is the aorta which indicates the greatest cumulative HARM accounting for over 30 percent. This is due to a large number of AIS 5 and 6 aorta injuries in the LTV sample. Liver, kidney, and spleen injuries are also evident in the LTV HARM analysis, but not for the passenger cars. The ribcage is also of importance in both datasets, where it sustains approximately 10 percent of the cumulative HARM.

This shift of injury distribution is indicative of the change in loading characteristics between passenger cars and LTVs. High leading edge profiles of LTVs produce an inherently different interaction with the pedestrian. When struck by a car, a pedestrian will normally wrap the front of the vehicle with the thigh interacting at the hood edge before being thrown forward. For LTVs, the hood edge strikes between the pelvis and thorax of the pedestrian. This results in a more direct penetrating loading for the torso.

CONCLUSIONS

Torso injury is an important area of consideration for the mitigation of pedestrian injuries and fatalities. At lower AIS levels, the distribution of torso injuries is substantially similar between vehicle types with the ribcage being the dominant area of injury followed by the lung and liver. At higher AIS levels, the injury pattern shifts. For cars at the AIS 4+ level, injury to the lung and ribcage is still dominant. For LTVs at this higher level the aorta and spleen also account for large percentages of the injuries.

When these injury distributions are looked at in terms of HARM, the focus shifts. For cars, the lung is the dominant area accounting for 45% of the HARM. For LTVs it is the aorta that dominates with over 30% of the HARM. The ribcage, liver, kidney, and spleen are also significant components of HARM in the case of LTVs.

Based on these findings, further work is necessary to better understand mechanisms for the injuries occurring so that tools can be developed to evaluate the risk of these injuries during vehicle development.

REFERENCES

- Ballesteros M, Dischinger P, and Langenberg P (2004). Pedestrian injuries and vehicle type in Maryland, 1995-1999, *Accid. Anal. Prev.* 36, pp. 73-81.
- Chidester A & Isenberg R (2001). Final report – the pedestrian crash data study, Proc. 17th International Conference for the Enhanced Safety of Vehicles, Paper 248, Amsterdam, Netherlands.
- Fildes B, Gabler HC, Otte D, Linder A, & Sparke L (2004). Pedestrian impact priorities using real-world crash data and harm, Proc. IRCOBI conference, Graz, Austria
- Henry B, Crandall J, Bhalla K, Mock, N & Roudsari B. (2003). Child and adult pedestrian impact: the influence of vehicle type on injury severity, Proc. AAAM conference, Lisbon, Portugal.
- Jarret K & Saul R (1998). Pedestrian injury analysis of the PCDS field collision data, Proc. 16th International Conference for the Enhanced Safety of Vehicles, Paper 98-S6-O-04, pp. 1204-1211.
- Lefler D & Gabler HC (2004). The fatality and injury risk of light truck impacts with pedestrians in the United States, *Accid. Anal. Prev.* 36, pp. 295-304.
- Longhitano D, Henry B, Bhalla K, Ivarsson J, & Crandall J (2005). Influence of Vehicle Body Type on Pedestrian Injury Distribution, SAE Paper #2005-01-1876, Society of Automotive Engineers, Warrendale, PA.
- Malliaris A, Hitchcock R, & Hedlund J (1982). A Search for Priorities in Crash Protection, SAE Paper #820242, Society of Automotive Engineers, Warrendale, PA.
- Mizuno K & Kajzer J (1999) Compatibility problems in frontal, side, single car collisions and car-to-car-pedestrian accidents in Japan, *Accid. Anal. Prev.* 31, pp. 381-391.
- National Highway Traffic Safety Administration (2004a). Traffic Safety Facts 2002. US Department of Transportation, Washington, DC.
- National Highway Traffic Safety Administration (2004b). Traffic Safety Facts 2003 – Pedestrians, US Department of Transportation, Washington, DC.

APPENDIX A

**Table A1.
Passenger Car Injury by Organ and Severity.**

<u>Car</u>	AIS 2	AIS 3	AIS 4	AIS 5	AIS 6
Ribcage only	3	4	1	1	
Ribcage & Pleura		4	1		
Pleura only		4			
Lung			3	7	
Aorta				1	1
Other Thorax		4			1
Liver	6	2	2		
Kidney	3				
Spleen	1	1	1		
Mesentary	3				
Other Abdominal	5		1		
Spine - Thoracic	3			1	
Spine - Lumbar	3				

**Table A2.
LTV Car Injury by Organ and Severity.**

<u>LTV</u>	AIS 2	AIS 3	AIS 4	AIS 5	AIS 6
Ribcage only	2	3	1	1	
Ribcage & Pleura		3	3		
Pleura only	1	1			
Lung		8	2		
Aorta			1	3	1
Other Thorax		4			
Liver	10	1	1	1	
Kidney	3	1	1	1	
Spleen	4	1	2	1	
Mesentary	5	1			
Other Abdominal	3	2	2		
Spine - Thoracic	3				
Spine - Lumbar					

PEDESTRIAN INJURY MECHANISMS & CRITERIA A COUPLED EXPERIMENTAL AND FINITE ELEMENT APPROACH

Catherine Masson
Pierre-Jean Arnoux
Christian Brunet

Laboratory of Applied Biomechanics. French National Institute for Transport and Safety Research-Faculty of Medicine of Marseille, Marseille, France

Dominique Cesari

Scientific Direction. French National Institute for Transport and Safety Research. Bron, France
Paper number 05-0335

ABSTRACT

In pedestrian injury biomechanics, knees and lower legs are highly recruited, leading to joint damage and bones failures. Safety improvements should mainly focus on knee ligaments injury minimization. To investigate the corresponding injury mechanisms and postulate on injury criteria risk, both experimental and finite element simulation approaches were performed. The lower limb behavior was first studied in lateral bending and then in lateral shearing impact tests in order to isolate injury mechanisms effects. The tests consisted in evaluating lower limb forces and kinematic through a 37kg guided impact with velocities ranged between 15 & 20kph. 35 tests were performed on isolated PMHS lower limbs. Response corridors for the time history about the mean response curve \pm one standard deviation with the Maltese procedure were established. The observed damages were contact injuries (head of fibula and lateral tibial condyle fractures), ligament injuries (cruciates and collaterals ligaments according to the tests) and bone fractures (extra and diaphysis). These experimental tests were simulated using a finite element model of the lower limb (with extended impact velocities). The model response analysis (bone Von Mises stress levels, Ligaments global and local strain levels, knee rotation and shearing measurements) was performed during each step of the impact chronology. It leads to postulate on injury criteria for knee soft tissues based on the knee ultimate lateral bending ($\sim 16^\circ$) and shearing levels ($\sim 15\text{mm}$). These approaches by coupling PMHS experimentation and numerical simulation ensure an accurate description of pedestrian lower limb trauma in terms of injury chronology and threshold. These results were also relevant with accidentology and clinical knowledge, especially with the evaluated potential injuries.

INTRODUCTION

Although the number of pedestrian suffering severe or fatal injuries has decreased since 1991 in EU (Kallina, 2002), pedestrian safety has become a major issue of society and is one of the most discussed topics in vehicle safety. If pedestrian sustain multisystem injuries, head and lower extremities injuries are the most frequently injured body regions. Particularly, lower limbs are highly loaded during crash situations (AIS from 2 to 6) with joints damages and bones failures (IHRA 2001, Stutts 1999). To improve understanding of the mechanisms and establishing tolerance criteria for this specific body part, coupled experimental and numerical studies were conducted.

Experimental studies were performed to represent condition of pedestrian accident focusing on the lower limb. The tests should have reflected the nature and the severity of the injuries sustained from this kind of impact. There is little data available from experimental studies measuring the response of the human knee joint in the pedestrian environment. Aekbote et al (Aekbote, 2003) reviewed the biomechanical studies conducted over the last three decades. He noted that mainly the injury mechanisms of the lower extremity were investigated. Tests were conducted in pure lateral shear loads, in pure bending moments or a combination of lateral shearing and bending of the knee (Kajzer 1990, Kajzer 1993, Grzegorz 2001). On cadavers full leg experiments, Kajzer (1990, 1993) focused on lower limb response under shearing and bending solicitation. He showed that pure shearing induces collateral tibial and anterior cruciate ligaments failure while a primarily bending mainly induces medial collateral ligament failure. More generally, three primary injury mechanisms were underlined: acceleration of the leg induced contact injuries as fracture of the femur and/or tibial shaft, shear force through the knee joint led to ACL rupture/avulsion, tibial intercondylar eminence fracture and femoral cartilage injury, and injuries due to bending moment at the knee joint are compression fracture of lateral femur condyle, tibial plateau fracture and MCL rupture.

These last years, recent studies have reported the response of the isolated knee joint to bending and shearing forces (Kerrigan, 2003). These tests aimed to investigate into the failure thresholds of the lower extremity. In bending tests, femoral and tibia ends were held. In this experimental configuration, MCL injuries were the most common. In shearing tests, damage to the ACL was the only relevant ligamentous injury. More recently, Bose (2004) performed 3-point bending tests on isolated knee joints in order to obtain a combination of shearing and bending effects, and confirmed injuries to medial collateral and anterior cruciate ligaments. It can be noted that knee injuries are not restricted to the injuries described above. Tibia fractures (especially with at the tibial eminence in contact with the intercondylar notch at impact), PCL injuries, fibula and femur fractures can also be observed. From all these studies, it appears that the main challenge for improving leg protection should focus on knee ligament damage and failure minimization.

Much of the most recent researches on pedestrian injury using PMHS has solely focused on sustained injuries. They reported in details bone and ligament injuries, proposed injury criteria and gave only typical load or accelerometric responses of the lower limb. These data are not always sufficient to assure a satisfactory validation of the model (Bhalla, 2003; Kerrigan, 2003; Bose, 2004; Ivarsson, 2004; Ivarsson, 2005). Very few presented response corridors to impact though they are useful to validate pedestrian surrogate models for biofidelity against PMHS test data. That why we decided to re-analyse the results of previous studies performed in Inrets-LBA (Kajzer, 1990, 1993) and to establish force-versus time corridors for bending and shearing tests.

In order to more accurately describe the injury mechanisms involved in such trauma situations, finite element simulations are more and more useful as they can provide data unavailable experimentally. In the literature, many finite element models have been designed to study very specific points of the leg behaviour under crash situations. Some ankle-foot models focused on the kinematics (Beaugonin, 1996; Beillas, 1999), others on material properties (Beaugonin, 1997; Tannous, 1996) and others else on an accurate description of geometry (Beillas, 1999). Knee models were also developed both for frontal impacts (Hayashi, 1996; Atkinson, 1998) and pedestrians (Yang, 1997; Schuster, 2000; Takahashi, 2003). Lastly, Bedewi (1996) included mathematical joints in order to control the kinematics of a full lower limb model. The THUMS model (Chawla, 2004) or the LLMS model (Arnoux, 2001-2004; Beillas, 2001) are advanced finite element models of the whole lower

limb. This last model was based on an accurate description of all anatomical parts of the lower limb, and its validation was performed in various impact situations (isolated materials, sub-segments up to the whole model). It has been used to complete experimental results analysis by focussing on ligaments strain levels as a function of lateral shearing or flexion according to the load cases with an extended range of velocity.

EXPERIMENTAL STUDY

Material and methods

A linear impactor rig was used to perform dynamic PMHS tests, Figure 1. The cylinder had a mass of 37kg including instrumentation. The contact area was a flat piece with 50 mm Styrodur padding surface.

Impact experiments were conducted on 34 pairs of human lower limbs. The subjects are Post Mortem Human Subjects (PMHS) who have given voluntary before dying their body to the science. The cadaver specimens are from a population with considerably advanced age. Haut (Haut, 1995) reported that cadaver age is not significant predictor of impact biomechanics or injury to the human knee. All subjects were preserved at 3°C in Winkler's preparation (Winkler, 1974). These injection methods allow to keep supple the sampling and to preserve for several months the soft tissues elasticity. The joint range of physiological mobility was checked by medical team. Measurements of valgus-varus and knee laxity were performed. X-Rays radiographs of the body were taken and the osseous integrity in 2 planes (sagittal plane and frontal plane) was checked by an anatomist surgeon. The subjects chosen were with an average age of 78±8 years, average weight of 66±11kg, and average height of 161±21cm. Anthropometric details of the subjects are reported in Table 1. These values are both large as compared to the 50th percentile male dummy specifications of 1.73m in height and 74.5 kg in weight.

Table 1.
Cadaver Physical data.

	Age	Weight (kg)	Height (cm)	Limb Weight (kg)
Bending tests at 4.4m/s	76±6	70±8	166±4	14.4±1.9
Bending tests at 5.5m/s	75±11	60±5	168±7	13.2±1.4
Shearing tests at 4.2m/s	79±6	62±9	167±10	12.1±1.9
Shearing tests at 5.5m/s	79±8	71±16	162±6	12.8±2.2

The experiment consisted in lateral impacting an isolated lower limb (leg-thigh-half pelvis) stood up straight. The thigh was blocked with 2 foam-padded plates, called the “upper plate” and the “lower plate”. One was placed on the external face at femoral condyle level, about 2 cm below the knee joint line. The second was placed on the internal face at pubic bone level. The foot was on a mobile plate to minimize ground friction and a mass of 40kg allowed preloading the lower limb (Figure 1).

Bending impacts were performed by loading the leg just above the ankle joint. The impactor was equipped with a foam-padded face of 50mm of Styrodur and 150mm×50mm of size. Distance between the knee joint line and impactor axis on the one hand and between the knee joint line and the lower plate on the other hand were recorded before test. The impact tests were performed at two impact velocities: 4.4m/s (MFG01-MFG06) and 5.5m/s (MFG07-MFG15).

Shearing tests were performed by loading the leg with 2 impact plates fixed on the impactor, one loading the leg at the proximal end of tibia and head of fibula named the “upper impact face”, and one loading the leg just above the ankle joint and named the “lower impact face”. Distance between the lower plate and the upper impact interface was chosen to be 40mm. A minimize contact injuries, two foam-padded interfaces were fixed on the plates (50mm of Styrodur). These impact tests were performed at two impact velocities: 4.2m/s (FCG06-FCG15) and 5.5m/s (FCG17-FCG26).

Instrumentation and measurement

An accelerometer (Entran EGA, 250g) and a force transducer (SEDEME 20kN) equipped the face of the impactor in bending tests. They measured the impactor acceleration and the impactor force presented Figures 2-3. The lower reaction force was given by a force transducer fixed on the lower plate (SEDEME, 20kN).

In shearing tests lower impact forces were measured with a force transducer fixed to the lower impact face and presented Figures 7-8. The upper impact face was equipped with an accelerometer (Entran EGA, 250g) and a force transducer (SEDEME 20kN). The measurements of the upper impact force were given in Figures 9-10. A force transducer equipped the lower plate and recorded the femur reaction force presented Figure 11-12.

A unit, comprising 32 measurement channels ensured the conditioning, analog-digital conversion and memorisation of signal. All the channels were sampled at 10kHz for a duration of 5 sec. The data

acquisition system was triggered by a contact plate on the impactor connecting with two contacts on the knee. Data was transferred to a computer for processing. Loads were collected and filtered at 180Hz. Two high-speed cameras operating at 1000 frames per second were used to provide a visual record of the tests and to allow a cinematic analysis. The locations of all high-speed cameras were measured with respect to the impact location.

Test Matrix

A total of 35 tests were performed on knee joints from PMHS. In pure bending, all tests were performed from male subjects, six tests at 4.4m/s and nine tests at 5.5m/s. In shear loading, ten tests were carried out at 4.2m/s and ten tests at 5.5 m/s. In order to study repeatability of the test procedure, tests were performed on matched pairs of knees from the same subject.

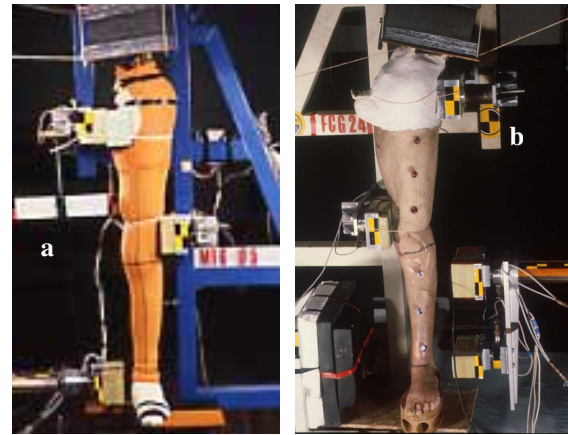


Figure 1. Setup for the bending tests (a) and for the shearing tests (b)

Corridor construction

There is not a standard methodology to construct biofidelity corridors around the cadaveric data despite the fact that the way corridors are derived is an important issue on which the biofidelity rating depends. Maltese et al (Maltese, 2002) have proposed a process for calculating corridors from test data. The first step was to scale data employing mass scaling developed by Eppinger (Eppinger, 1984) to normalize the data to a 50th percentile male subject. The scaling variable λ and the scaled test parameters with subscript s are expressed in terms of the initial parameters with subscript i in following equations.

$$\text{Scaling variable} \quad \lambda = (75/M_i)^{1/3} \quad (1)$$

$$\text{Velocity} \quad V_s = V_i \quad (2)$$

Acceleration $A_s = A_i / \lambda$ (3)

Time $T_s = \lambda \times T_i$ (4)

Force $F_s = \lambda^2 F_i$ (5)

Then signals were aligned by time shifting. For each sensor, one signal was chosen as characteristic response. The cumulative variance between this typical signal and each signal was calculated shifting forward then backward in time by one time step until a minimum variance (Equation 6). The calculation of cumulative variance continued until the signal was shifted in time by an amount equal to one-third of this duration in both directions

$$V_{s,k} = \sum_{i=1}^{i^2} (s_i - k_i)^2 \quad (6)$$

where

s_i is the magnitude of the typical signal s at $t=i$

k_i is the magnitude of the signal k at $t=i$

After time alignment, the mean response and the standard deviation was calculated at each time. To finish, mean \pm one standard deviation corridors were developed. Straight lines were constructed around the mean from the defined requirements.

Experimental results

Results from bending tests

The impact force versus time corridors for the two impact velocities are presented Figures 2-3. The corridors mean shape is similar in both cases, with a linear increasing phase slightly greater at 5.5m/s. The mean peak force is 1860N at 4.4m/s and 2850N at 5.5m/s with a greater standard deviation. The duration of solicitation is comparable for both impact velocities, with a same increasing slope.

The lower reaction force corridors is plotted as a function of time for both impact velocities in Figures 4-5. The corridors show similar trends in both cases, with a first linear phase during 20ms following by a local peak. This first mean local peak is 615N at 4.4m/s and 1628N at 5.5m/s. A second peak is noticed around 50ms, slightly greater: 693 N at 4.4m/s and 1728 N at 5.5m/s.

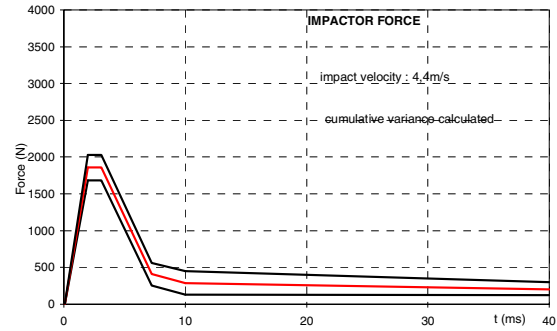


Figure 2. Impactor force corridors in bending tests at 4.4m/s.

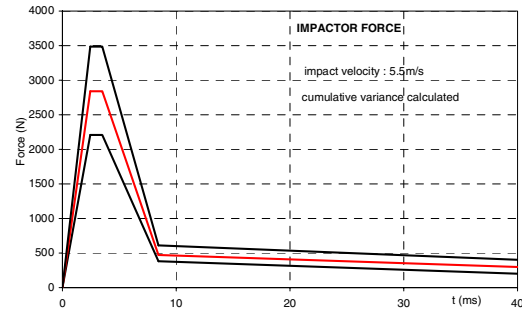


Figure 3. Impactor force corridors in bending tests at 5.5m/s.

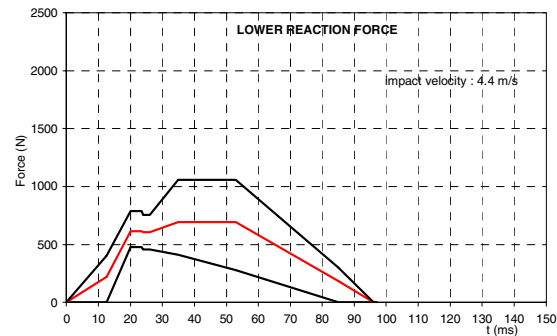


Figure 4. Lower reaction force corridors in bending tests at 4.4m/s

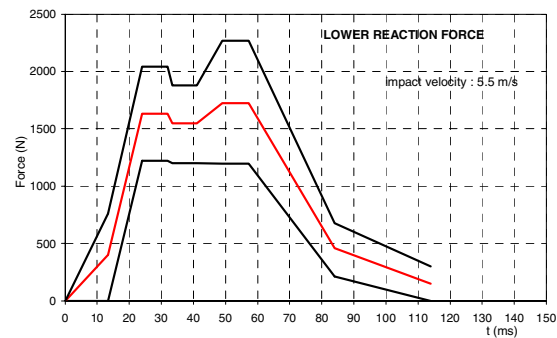


Figure 5. Lower reaction force corridors in bending tests at 5.5m/s.

A cinematic analysis was performed. The high speed images analysis provided the position at each ms. From the relative displacement of the leg against the thigh in frontal view, the lateral flexion angle of the knee was calculated (Figure 6). No significant difference appeared between 4.4m/s and 5.5m/s. It is estimated that the knee bending rate in the bending tests is approximately 1°/ms up to 13ms then is 0.5°/ms.

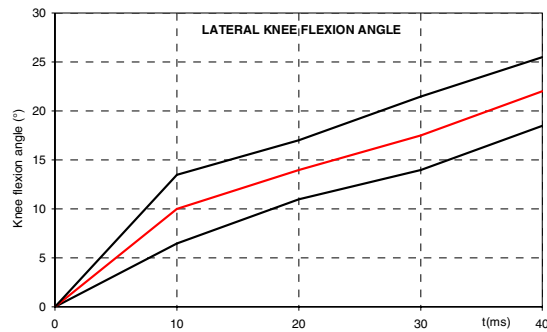


Figure 6. Knee flexion angle versus time

After testing, radiographs were taken and pre- and post-radiographs were analysed and compared. Each lower limb was then autopsied. Tables 2 and 3 list the injuries for both series of test. Bone damage was seldom observed, only in two tests at 5.5m/s. In contrary ligament damage was observed in 70% of tests and the medial collateral ligament was always injured. The posterior cruciate ligament was never injured and damage were observed on the anterior cruciate ligament in 3 tests at 5.5m/s

Table 2.
Injuries caused in bending tests at 4.4m/s.

MFG01	MCL: avulsion at the femoral insertion
MFG02	MCL: avulsion at the femoral insertion (80%)
MFG03	MCL avulsion at the femoral insertion
MFG04	LCL : rupture (80%) in the ligament MCL : avulsion (30%) at the femoral insertion
MFG05	None
MFG06	None

Table 3.
Injuries caused in bending tests at 5.5m/s.

MFG07	LCL : partial avulsion at the femoral insertion ACL : partial avulsion at the tibial insertion
MFG08	None
MFG09	MCL: avulsion at the tibial insertion
MFG10	Tibial plate fracture
MFG11	None
MFG12	MCL: total avulsion at the femoral insertion
MFG13	MCL : avulsion at the femoral insertion Tibial plate fracture
MFG14	MCL: avulsion at the femoral insertion ACL: avulsion at the femoral insertion
MFG15	MCL: total avulsion at the femoral insertion ACL: avulsion at the femoral insertion

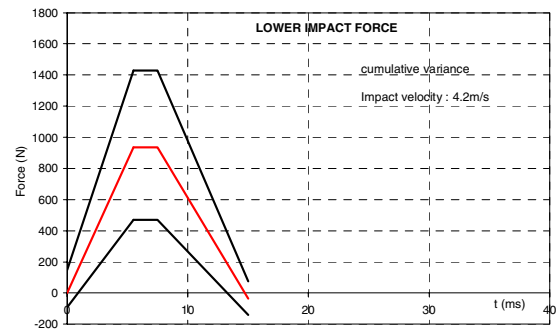


Figure 7. Lower impact force corridors in shearing tests at 4.2m/s.

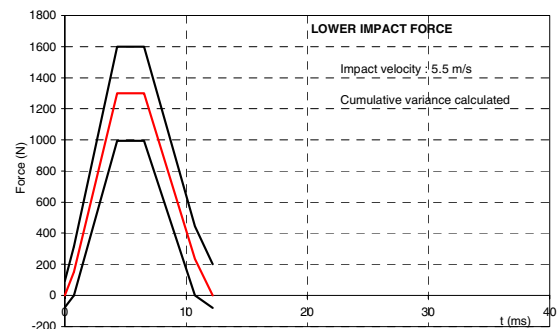


Figure 8. Lower impact force corridors in shearing tests at 5.5m/s.

Results from shearing tests

Lower impact force versus time corridors for the two impact velocities are presented Figures 7-8. The mean peak force is 935N at 4.2m/s and 1300N at 5.5m/s. The increasing phase is stiffer at 5.5m/s with a slope of 300N/ms against 170N/ms at 4.2m/s. The impact forces peak at 5.5 ms for the lower impact velocity, at 4.3ms for the second velocity and then drop to 0 by 14.8ms and 16.2ms respectively.

Figures 9-10 show upper impact force versus time corridors for both impact velocities. Three peaks are noted at 4.2m/s against only two peaks at 5.5m/s with a decreasing of the force occurring much later (60ms) than for the lowest impact velocity. If the values of the first peak differ according impact velocity (1708N and respectively 2421N), peak values on all duration are approximately the same (3000N) but appear at different times (20ms and 60ms).

Femur reaction force versus time corridors for both impact velocities are presented Figure 11-12. The corridor at 4.2m/s is very larger in time. The peak values are similar in both cases with nevertheless a slope in the increasing phase greater at 5.5m/s than at 4.2m/s (143N/ms and 306N/ms).

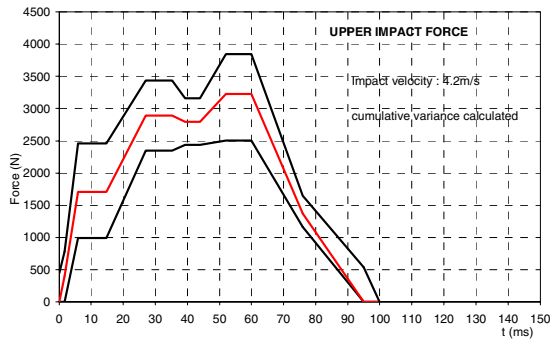


Figure 9. Upper impact force corridors in shearing tests at 4.2m/s.

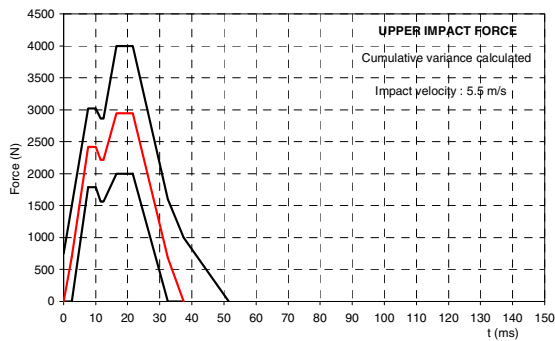


Figure 10. Upper impact force corridors in shearing tests at 5.5m/s.

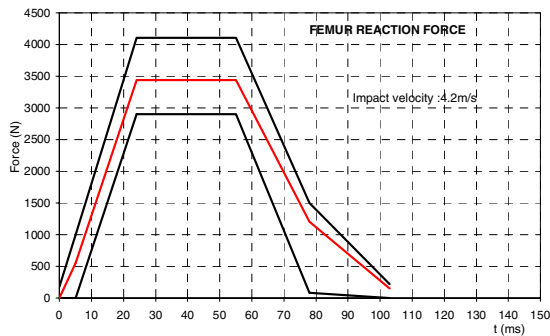


Figure 11. Femur reaction force corridors in shearing tests at 4.2m/s.

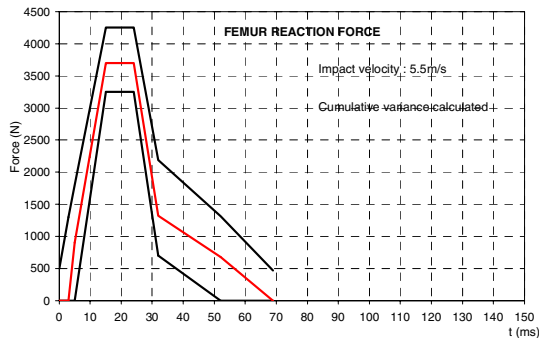


Figure 12. Femur reaction force corridors in shearing tests at 5.5m/s.

After testing, radiographs were taken and pre- and post-radiographs were analysed and compared. Each lower limb was then autopsied. Injuries are listed in Tables 4-5 and concern as well knee ligaments as lower limb bones. At 4.2m/s, concerning ligament, there were no injuries to any of the posterior cruciate ligament and only one injury to medial collateral ligament. The anterior cruciate ligament was the most often injured (in seven tests) with in six tests injury of lateral collateral ligament. Bone injuries were mainly fracture of fibula (75% of tests) and fracture of the tibial intercondylar eminence associated with femoral cartilage injury. There were no fractures to femoral diaphysis and one to tibial diaphysis. Only one knee showed no signs of fracture or any ligamentous injury. At 5.5m/s, ligament injuries were mainly anterior cruciate ligament injuries (seven tests). There were no injuries to any of the posterior cruciate ligament and few lateral ligament injuries (in 2 tests for the medial collateral and in 2 cases for the lateral collateral). Concerning bone injuries, in all cases, a fracture of the fibula was noted. We noted proportionally less tibial intercondylar eminence fracture but more tibia condyle fracture.

Table 4. Injuries caused in shearing tests at 4.2m/s.

FCG06	None
FCG07	MCL: avulsion at the tibia insertion
FCG08	ACL avulsion at the tibia insertion, tibial intercondylar eminence crushing, femoral cartilage
FCG09	LCL : avulsion at the fibula insertion, ACL: avulsion at the tibial insertion Fracture of the lateral tibia plate Avulsion of tibial intercondylar eminence
FCG10	LCL : avulsion at the fibula insertion ACL: avulsion at the tibial insertion Avulsion of tibial intercondylar eminence
FCG11	LCL : avulsion at the fibula insertion ACL: peeling Crushing of the tibial intercondylar eminence
FCG12	LCL : avulsion at the fibula insertion ACL: peeling and partial avulsion at the tibial insertion Fracture of the fibula Crushing of the tibial intercondylar eminence
FCG13	LCL: rupture ACL: rupture at the tibial insertion Fracture of the tibia Fracture of femoral condyles
FCG14	LCL :damage ACL : avulsion (70%) at the tibial insertion Fracture of the fibula neck

Table 5.
Injuries caused in shearing tests at 5.5m/s.

FCG17	Fracture of the femoral diaphysis Fracture of the medial malleolus Fracture of the fibula (proximal end) ACL: Partial rupture (80%)
FCG18	ACL : Avulsion at the tibial insertion Fracture of the fibula diaphysis Fracture of the fibula (proximal end) Fracture of the tibia (proximal end)
FCG19	ACL : Avulsion at the tibial insertion Fracture of the fibula (proximal end) Fracture of tibial intercondylar eminence Fracture of tibial spinal tuberosity
FCG20	Crushing fracture of the medial femoral condyle Fracture of tibial intercondylar eminence Fracture of tibial spinal tuberosity Tibial cartilage injury Fracture of the fibula neck ACL: partial (80%) avulsion at the tibial insertion MCL: partial rupture
FCG21	Fracture of the femoral diaphysis Fracture of tibial intercondylar eminence Fracture of the fibula neck ACL: partial (80%) avulsion at the femoral insertion
FCG22	Fracture of the fibula (proximal end) MCL: partial rupture ACL: partial (80%) avulsion at the femoral insertion
FCG23	Fracture of the tibial diaphysis Fracture of the fibula neck
FCG24	Fracture of the fibula (proximal end) LCL: avulsion at the fibula insertion
FCG25	Fracture of tibial intercondylar eminence Fracture of the fibula diaphysis Fracture of the fibula (proximal end) ACL: avulsion at the tibial insertion
FCG26	Fracture of the fibula (proximal end) LCL : avulsion at the fibula insertion

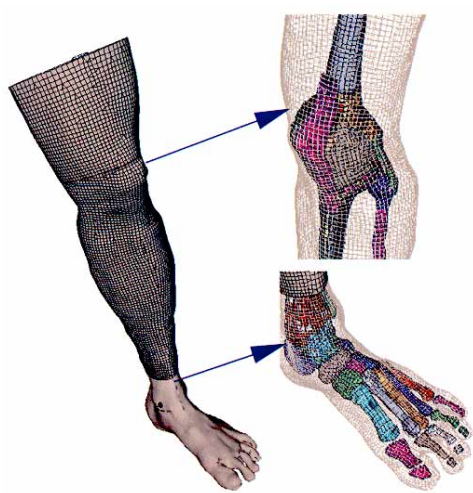


Figure 13. General overview of the Lower Limb Model for Safety (LLMS).

NUMERICAL STUDY

To complete the analysis of experimental results, a finite elements model of the lower limb (the Lower Limb Model for Safety) was used (Figure 13). As this model (validation, applications, model features) has already been presented in previously published papers (Arnoux 2001- 2004, Behr 2003- 2005, Beillas 2001), we only focus here on the use of this model to determine injury criteria assumption on the base of pedestrian related impact situations performed during experiments. In a first step model response was evaluated by comparison between simulation and reanalysis of experimental results performed in this work. Then, an analysis of model kinematics, bones Von Mises and lastly soft tissues strain levels was performed (Arnoux 2004) in order to postulate on injury assumptions

Model comparison with experiments

In Kajzer (1990) bending tests (Figure14) the upper leg was allowed to freely translate in the vertical direction, while a 22 kg dead weight was attached to the proximal femur to simulate the weight of the body. The foot was placed on a plate which allowed free translation along the direction of impact. A 40 kg impactor was used to load the distal tibia with impact velocities of 16 and 20 Kph. The model validation was achieved by comparing forces versus time recorded on the impactor face and lateral flexion by analysis of high speed video data regarding model response through new experimental corridors defined above. Results reported were relevant with experiments. Note that time amplitude was higher than experiment especially concerning unloading phase. This could be linked to soft tissue behaviour laws where physical failure was not implemented in the model.

In Kajzer (1993) shearing tests (Figure15), the leg was put in same conditions as the previous test. The impactor consists in two impacting surfaces applied simultaneously on both proximal and distal extremities of fibula and tibia. Model response was relevant with experimental corridors but do not describe complete time duration of the test. The two-stage injury mechanism experimentally identified, with the two peaks in the force time curve, was not reproduced with the LLMS model. The first injury mechanism, which occurred in 10th ms after impact, is directly related to the knee impact force. It can be described as a contact injury and can induce bone fractures (head of fibula, tibia or femur). This phenomenon was relevant with Von Mises stress level recorded between tibia and fibula (Figure 16).

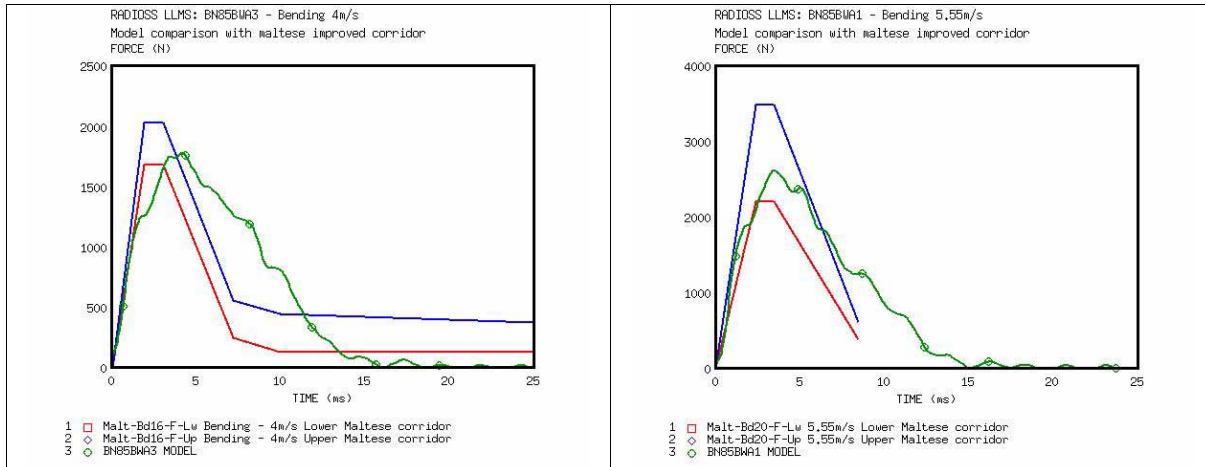


Figure 14. Comparison between simulated model and experiments of impact forces in bending tests for 16 and 20 kph impact velocities.

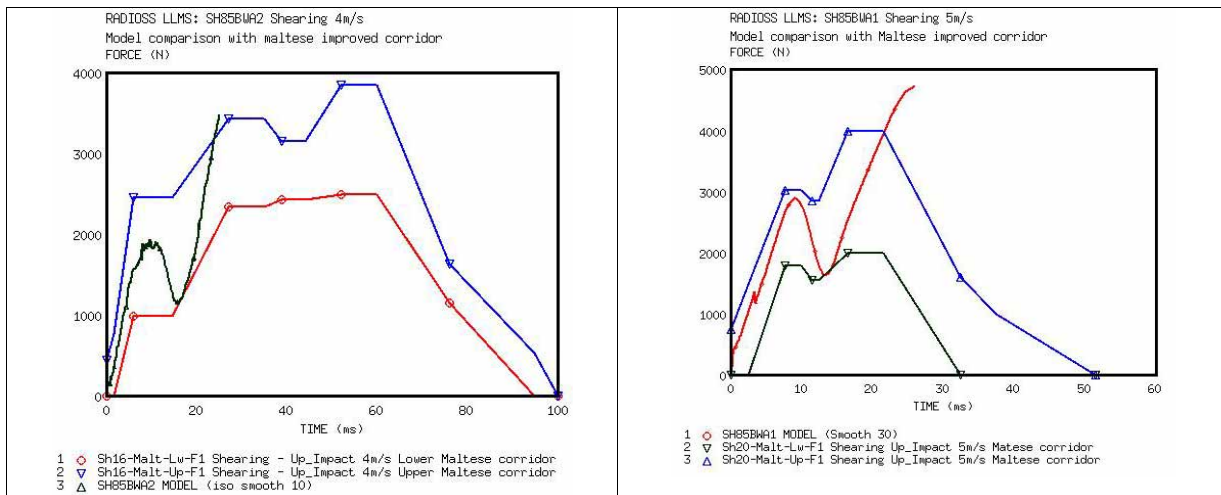


Figure 15. Comparison between simulated model and experiments of impact forces in shearing tests for 16 and 20 kph impacts velocities.

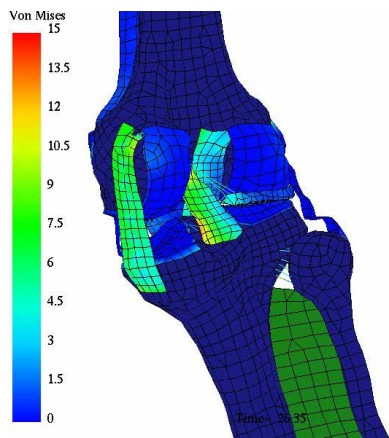


Figure 16. Illustration of Von Mises stress level in joints and recruitment level of knee ligaments. Injury criteria evaluation

The second injury mechanism is correlated to forces transferred through the knee during acceleration of the thigh (relative shearing of tibia versus femur) which lead to soft tissues injuries. This could be linked to soft tissue behaviour laws where physical failure was not implemented in the model. Consequently, the model analysis was bounded to first part of the tests until the strain failure level on ligaments were reach. Additionally, the locations of stress concentrations predicted by the model, including the cruciate ligament insertions, the tibia eminence and the tibia fibular joint, were in agreement with the injury locations found during the autopsies (Figure 17).

Injury criteria evaluation

Taking care to the validity domain, loading cases can be extended and, from model analysis, it remains possible to compute data that is not usually recordable experimentally:

- The stress level and distribution in bones provide an estimation of damage on bone structures when stress reaches the Yield stress values.
- The kinematics was recorded to check the correct relative movements between the corresponding bones or soft tissues through knee torsion, lateral bending and frontal bending in the different planes and for each test. Therefore, the lateral relative displacement between the tibial eminence and the intercondylar notch was calculated to accurately identify knee lateral shearing at the joint level.
- Damage properties of soft tissues can be described in terms of ultimate strain levels in soft tissue structures (Arnoux 2000, Subit 2004). The results led to consider ligament failure with a strain criterion. Ultimate strain levels were calculated for the four knee ligaments and used in this study to identify potential failure. Note that literature gives various values for ultimate strain (Table 6) obtained in different experimental conditions (loading, preconditioning, conservation method...). In the present study, the ultimate values used to postulate on damage were assumed to be 28% for lateral ligaments, and 22% for cruciate ligaments. For each of the four knee ligaments, strain sensors were inserted in the model. These sensors consist in a series of springs along the main fiber axis. For the cruciate and lateral ligaments, it was also possible to compute the global strain level, the average strain level as well as the curve of maximum strain recorded at various levels in the ligament. A first step in the investigation knee joint injury criteria was to focus on previous experiments with extended impact velocities which are 2 m/s, 4 m/s, 5.55 m/s, 7 m/s and 10 m/s.

Table 6.
Overview of ultimate strain levels recorded for knee ligaments.

Author	Collateral tibial	Collateral medial	Posterior cruciate	Anterior cruciate
Viidick (1973)	30%	40%	60%	60%
Kennedy (1976)			24 (±6) %	
Marinozzi (1982)			20 (±5) %	
Prietto (1992)			28 (±9) %	
Race (1994)			18 (±5)	
Arnoux (2000)	24-38%	22-38%	15-23%	18-24%
Kerrigan (2003)	7-10%	11-20%		

For both impact situations, the Von Mises stress levels on bones were located on the proximal tibial metaphysis and distal femoral metaphysis (Figure 17). With impact velocity upper than 7m/s Von Mises stress reach 120-130MPa which is closed to failure. Bone failure on shell element was obtained by deleting elements once ultimate strain is reach. Note that model stress distribution and failure location were relevant with experiments (with lower impact velocities).

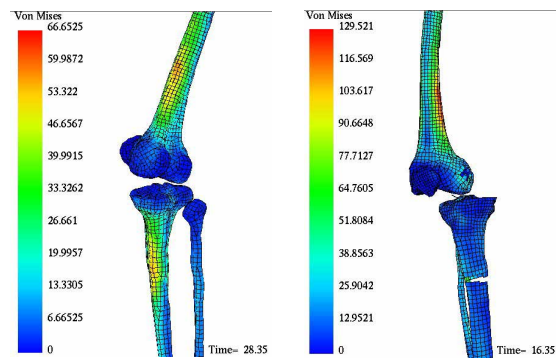


Figure 17. Typical Von Mises stress on bones for bending and shearing impact.

Model kinematics in bending tests exhibit typical lateral rotation between the tibia and the femur which seems to be correlated with velocity. The frontal rotation is stable whereas torsion effect seems to be important and correlated to the impact velocity (Figures 18 and 19). Variations of angles reach values ranging from 2° to 8°, depending on the impact velocity.

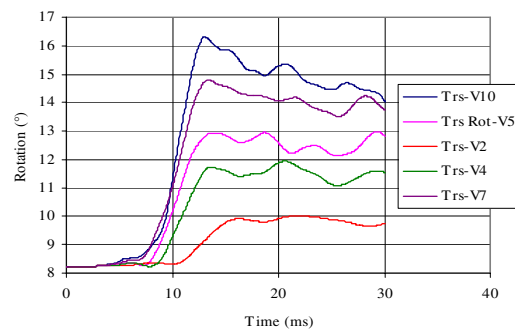


Figure 18. Knee torsion in the bending test.

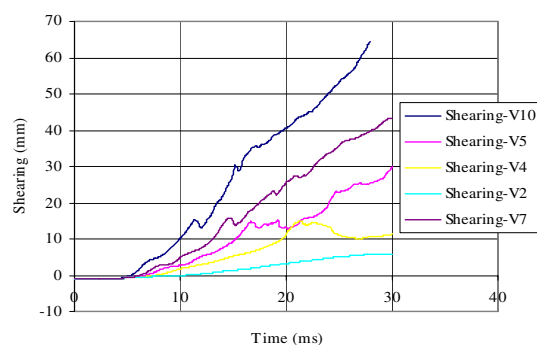


Figure 19. Knee lateral shearing in the shearing test.

In shearing tests, the two main kinematics aspects are the lateral shearing and the knee torsion (Figure 19). The lateral shearing seems to be correlated with velocity and rapidly reaches high values which are not relevant with geometrical characteristics of the proximal tibia and distal femur. At 15mm of shearing the curves reach a steady state which could result from the contact between intercondylar notch and tibia eminence. In the first 15 ms, the knee torsion reaches amplitudes ranging from 2° to 10° depending on the impact velocity (Figure 20).

For both impact situation rotation effects have to be linked to the asymmetrical geometry of the femoral condyle and the tibial glena. From a medical point of view, this torsion effect is described as a natural safety countermeasure of the human body during trauma situations in order to avoid (or limit) damage to ligaments.

The strain level recorded on each ligament (cruciate and lateral) and correlated to rotation or shearing effects were computed in total strain curve on the whole ligament and the maximum strain curve of local maximum strain level (Arnoux 2004). In this model analysis, the maximum strain can be considered as a first sensor to locate damage in the structure whereas the total strain gives a global overview of the whole structure. If the maximum strain reaches the ultimate strain level, we assume that damage can occur in the ligament. Moreover, if the ultimate strain level is reached on the total strain curve, the ligament complete failure can be postulated with a high probability.

For lateral bending tests, the lateral medial and the posterior cruciate ligaments were highly loaded and strain versus lateral bending seems to be independent of impact velocity (Figure 20). A small difference between maximum strain level and total strain level seems to show that the medial collateral ligament in the model has homogeneous strain distribution. Its maximum strain or total strain level used to postulate on damage in the ligaments is obtained with a lateral rotation ranging from 20° to 24°. For the posterior cruciate ligament, the difference between global strain (maximum strain) and local strain (maximum strain) seems to be confirmed local high strain levels. They were obtained on ligaments insertion and illustrated with Von Mises curve processing. Local damage could occur for knee rotation between 12° and 15°, whereas global damage for knee lateral rotations was close to 26° (which seems to be very high).

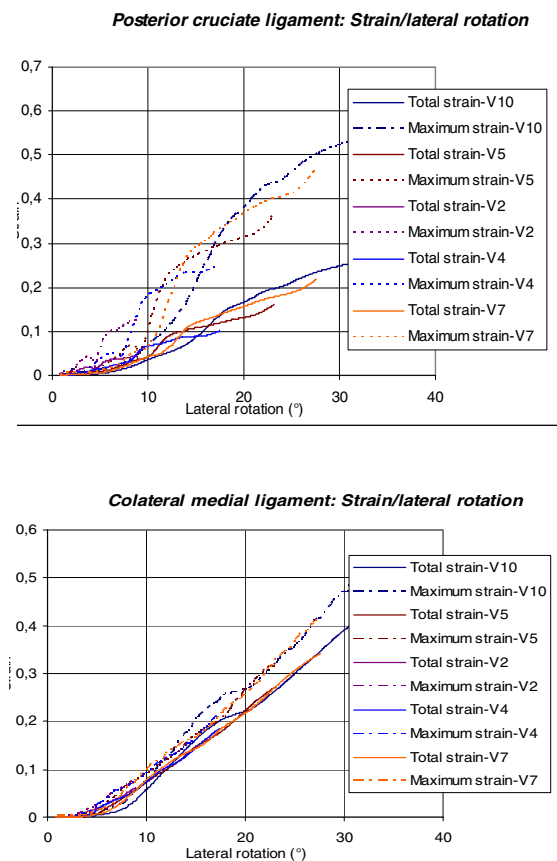


Figure 20. Posterior cruciate ligament total and maximum strain curves versus lateral rotation. Collateral medial ligament total and maximum strain curves versus lateral rotation.

For the shearing tests, the two cruciate and the tibial collateral ligaments were highly loaded (Figure 21). In that situation, impact velocity had no effects on strain versus knee shearing curves. The failure or damage could start at a 13 to 15 mm knee shearing. For the posterior cruciate ligament, the strain being not homogeneous on the structure, only maximum strain levels were computed, and they show that damage could occur for shear values ranging from 12 to 14 mm. Finally, for the collateral tibial ligament, the maximum strain reaches up to 14-17mm according to the impact velocity.

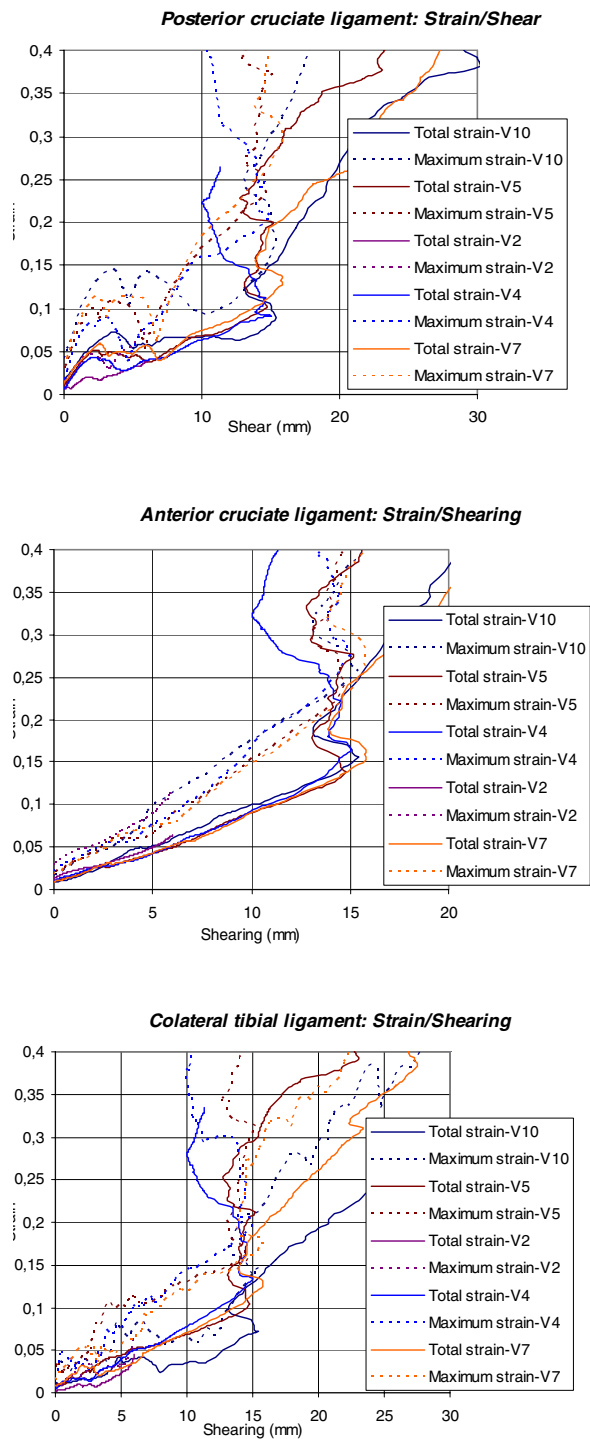


Figure 21. Total and maximum strain curves versus lateral shearing for the posterior cruciate ligament, the anterior cruciate ligament and the collateral tibial ligament.

DISCUSSION -CONCLUSION

Four test series were presented with the objective to evaluate the response of the lower limb to bending or shearing force. Impact tests were performed on isolated lower extremities of Post Mortem Human

Subjects and biomechanical corridors have been proposed.

In bending tests, the differences between lower reaction force corridors for both impact velocities were only in magnitude, the rise time and the duration were equivalent. The first lower reaction force peak appears between 20 and 23 ms corresponding to a knee lateral flexion angle of 15-16°. Damage to the MCL was the most common joint damage induced in this test configuration; this is agreement with real word pedestrian accident injuries (Bhalla, 2003). Two fractures of the tibial plateau were noted for a 5.5m/s impact velocity (MFG10-MFG13). These damages could be induced by a greater valgus rotation of the knee at this speed causing a compression force on the tibial plateau. A vertical rotation of the lower limb was noted in all tests and is due to the no symmetric of the knee joint. The influence of this movement on the global response of the knee joint and the type/time of injury is unknown but may induce tensional forces in the knee joint ligaments.

In shearing experimental test, the upper impact load induced firstly bone injuries located near impact point as fracture of fibula head, lateral tibial condyles fractures or diaphysis fracture. These injuries could be tied to the first peak force, corresponding to a mean level of 1700N for an impact velocity of 4.2m/s and 2400N for an impact velocity of 5.5m/s. The following peaks are related to intra articular injuries as avulsion or rupture of the anterior cruciate ligament, and femoral cartilage injury. Note that tibial intercondylar eminence fractures were typical due to the shear force through the knee joint. In our tests, they were always associated with ACL damage.

Coupling such results with model analysis which allowed to record data unavailable experimentally and then to follow their evolution during the test, it was possible to complete injury mechanisms description and make correlation between peak in force and failure level reach on ligaments.

For the bending tests, the knee injury mechanism consisted in a lateral rotation around the contact area between the lateral femoral condyle the and tibial glena. This rotation simultaneously induces a high deflection of both anterior cruciate and medial collateral ligaments, assumed to be injured for rotations over 15 and 20 °respectively. These results were not sensitive to impact velocities, and seem to be relevant with those identified experimentally. Consequently, a conservative value of 15° for lateral rotation can be considered as ligaments injury criteria. For pure shearing impacts, the anterior, posterior cruciate

and tibial collateral ligaments were concerned. The ultimate shearing level was computed by recording the distance between the tibial eminence and the condylar notch that reached up to 13 to 15 mm whatever the impact velocity. Consequently, a conservative value of 13mm for shearing rotation can be considered as ligaments injury criteria.

The criteria postulated above were strongly dependant on the material properties. Model improvement with tissues a damage model as well as a parametric study around the failure criteria should be performed in order not to summarize the injury criteria to a single couple of value (lateral rotation and shearing) but also to define injury risk curves.

The strain versus time curves show the influence of impact velocity and the time dependent answer of the whole structure which could be mainly attributed to structure effects and also soft tissue viscoelastic properties. It also underlines the differences in strain distribution between cruciate and collateral ligaments. For the cruciate ligaments, high strain levels were recorded on ligaments insertions (in agreement with experimental results), that underlines failure properties of cruciate ligaments at their insertions.

Von Mises distribution was systematically located on the same metaphysis areas of the lower femur and upper tibia but also in the knee joint with contact area during shocks. This distribution could indicate a bending effect on the two bones. It was also observed that for impact velocities overs 10m/s, and according to the damping properties of the impacting surface, the failure risk for bones seems to be very high. Therefore, with numerical simulations, it was observed that even in pure loading, pure shearing or pure bending can not be obtained alone. The two mechanisms seem to be coupled with a majority of shearing or bending according to the loading conditions.

In perspective, new tests will be performed on suitably instrumented PMHS with objective to compare the effects of varying proportions of moment and shear applied at the knee joint. Further numerical simulations will be done in order to widen model capabilities by focussing on material properties and to improve injury criteria accuracy. The new experimental tests will be included in model validation process.

ACKNOWLEDGEMENT

We would like to thank MECALOG for their partnership in LLMS model designing.

REFERENCES

- Aekbote K., Schuster P., Kankanala S., Sundararajan S., Rouhana W. 2003. "The biomechanical aspects of pedestrian protection". *Int. J. Vehicle Design*, Vol. 32. 28-52
- Arnoux P.J. 2000. « Modélisation des ligaments des membres porteurs », Ph D. Thesis.
- Arnoux P.J., Kang H.S., Kayvantash K., Brunet C., Cavallero C., Beillas P., Yang H. 2001. "The Radioss Lower Limb Model for safety: application to lateral impacts", *International Radioss user Conference*. Sophia
- Arnoux P.J., Kang H. S., Kayvantash K. 2001. "The Radioss Human model for Safety", *Archives of Physiology and Biochemistry*, vol. 109, 109.
- Arnoux P.J., Cavallero C., Chabrand P., Brunet C. 2002. "Knee ligaments failure under dynamic loadings". *International Journal of Crashworthiness*, Vol 7 (3), 255 – 268.
- Arnoux P. J., Thollon L., Kayvantash K., Behr M., Cavallero C., Brunet C. 2002. "Advanced lower limb model with Radioss, application to frontal and lateral impact Radioss lower limb model for safety". *Proceedings of the IRCOBI Conference*.
- Arnoux P. J., Cesari D., Behr M., Thollon L., Brunet C. 2004. "Pedestrian lower limb injury criteria evaluation a finite element approach", under submission to *Traffic Injury Prevention Journal*.
- Atkinson P., A stress based damage criterion to predict articular joint injury from subfracture insult, Ph.D. thesis, 1998.
- Atkinson P.J., Haut R., Eusebi C., Maripudi V., Hill T., Sambatur K. 1998. "Development of injury criteria for human surrogates to address current trends in knee-to-instrument panel injury", *Stapp Car Crash Conference Proceedings*. 13-28.
- Beaugonin M., Haug E., Cesari D. 1996. "A numerical model of the human ankle/foot under impact loading in inversion and eversion", *40th Stapp Car Crash Conference Proceedings*.
- Beaugonin M., Haug E., Cesari D. 1997. "Improvement of numerical ankle/foot model: modeling of deformable bone", *41th Stapp Car Crash Conference Proc.*
- Bedewi P.G., Bedewi N.E. 1996. "Modelling of occupant biomechanics with emphasis on the analysis of lower extremities injuries". *International Journal of Crash*, Vol. (1). 50-72.

- Behr M., Arnoux P. J., Serre T., Bidal S., Kang H.S., Thollon L., Cavallero C., Kayvantash K., Brunet C. 2003. "A Human model for Road Safety : From geometrical acquisition to Model Validation with Radioss", *International Journal on Computer Methods in Biomechanics and Biomedical Engineering*, vol 6 issue 4.
- Behr M., Arnoux P.J., Thollon L., Serre T., Cavallero C., Brunet C. 2003. "Towards integration of muscle tone in lower limbs subjectes to impacts", *IX International Symposium on Computer Simulation in Biomechanics*, Sydney, Australia.
- Behr, M., Arnoux, P.J., Serre, T., Kayvantash, K., Brunet, C. 2005. "Modeling active muscle behavior for emergency braking simulations". *Computational Fluid and Solid Mechanics*, Ed. Bathe. 60-64.
- Beillas P., Modélisation des membres inférieurs en situation de choc automobile, Ph.D. thesis, École Nationale Supérieure d'Arts et Métiers, Paris, France, 1999
- Beillas P., Lavaste F., Nicoloupoulos D., Kayventash K., Yang K. H., Robin S. 1999. "Foot and ankle finite element modeling using CT-scan data", *Stapp Car Crash Conference Proc.*
- Beillas P., Arnoux P. J., Brunet C., Begeman P., Cavallero C., Yang K., King A., Kang H. S., Kayvantash K., Prasad P. 2001. "Lower Limb: Advanced FE Model and New Experimental Data", *International Journal of STAPP - ASME*, vol. 45, 469-493.
- Bhalla K., Bose D., Madeley N.J., Kerrigan J., Crandall J., Longhitano D., Takahashi Y. 2003. "Evaluation of the Response of Mechanical Pedestrian Knee Joint Impactors in Bending and Shear Loading". *18th International Conference on the Enhanced Safety of Vehicles*.
- Bose D., Bhalla K., Rooij L., Millington S., Studley A., Crandall J. 2004. "Response of the Knee joint to the pedestrian impact loading environment", *SAE World Congress*, paper 2004-01-1608.
- Chawla A., Mukherjee S., Mohan D., Parihar A.. 2004. "Validation of Lower Extremity Model in THUMS". *IRCOBI Conf.* 155-166
- Eppinger R, Marcus J., Morgan R. 1984. 'Development of Dummy and injury index for NHTSA's Thoracic side impact protection research program', *SAE 840885*, 28th Stapp Car Crash Conference, Warrendale, PA.
- Grzegorz Teresinski, Roman Madro. 2001. "Pelvis and hip injuries as a reconstructive factors in car-to-pedestrian accidents", *Forensic Science International* 124. 68-73.
- Haut R. C., Atkinson P. J. 1995. "Insult to the human cadaver patellofemoral joint : effect of age on fracture tolerance and occult injury", *39th Stapp Car Crash Conference Proc.*, SAE. 952729.
- Hayashi S., Choi H.Y., Levine R.S., Yang K.H., King A.I. 1996. "Experimental and analytical study of knee fracture mechanisms in a frontal knee impact", *40th Stapp Car Crash Conf. Proc.* 161.
- IHRA/PS/200. 2001. *International Harmonized Research Activities, Pedestrian Safety Working Group Report.*
- Ivarsson J, Lessley D, Kerrigan J, Bhalla K, Bose D., Crandall J, Kent R. 2004. "Dynamic Response Corridors and Injury Thresholds of the Pedestrian Lower Extremities. *IRCOBI Conference on the Biomechanics of Impacts.*
- Ivarsson J, Kerrigan J, Lessley D, Drinkwater C, Kam C, Murphy D, Crandall J, Kent R. 2005. "Dynamic "Response Corridors of the Human Thigh and Leg in Non-Midpoint Three-Point Bending." *Society of Automotive Engineers World Congress. Paper Number 05B-218.*
- Kajzer J., Cavallero C., Bonnoit J., Morjane A., Ghanouchi S. 1990. "Response of the knee joint in lateral impact: Effect of shearing loads". *Proc. IRCOBI.* 293-304.
- Kajzer J., Cavallero C., Bonnoit J., Morjane A., Ghanouchi S. 1993. "Response of the knee joint in lateral impact: Effect of bending moment." *Proc. IRCOBI.* 105-116.
- Kallina I, 2002. "Pedestrian Protection. Looking for Potentials". *Proc. IRCOBI.* 1-15.
- Kerrigan J.R., Ivarsson B.J., Bose D., Madeley N.J., Millington S.A., Bhalla K. S., Crandall J.R. 2003. "Rate sensitive constitutive and failure properties of human collateral knee ligaments", *IRCOBI conference.* 193
- Maltese M.R., Eppinger R. H., Rhule H., Donnelly B., Pintar F. A., Yoganandan N. 2002. "Response Corridors of Human Surrogates in lateral impacts". *Stapp Car Crash Journal*, vol. 46.
- Schuster P.J., Chou C.C., Prasad P., Jayaraman G. 2000. "Development and Validation of a Pedestrian Lower Limb Non-Linear 3-D Finite Element

Model". 44th Stapp Car Crash Conference Proceedings. Atlanta, 2000-01-SC21.

application of Human-Body mathematical models". Ph.D. thesis.

Stutts J.C., Hunter, W.W. 1999. "Motor vehicle and roadway factors in pedestrian and bicyclists injuries: an examination based on emergency department data", *Accident analysis and prevention*. Volume 31, Issue 5, Pages 505-514.

Subit D. 2004. "Modélisation de la liaison os ligament dans l'articulation du genou", PhD. Thesis, Université de la Méditerranée.

Subit D., Chabrand P., Masson C., Brunet C. 2004. "Modelling of the mechanical behaviour of the insertion of the ligament to bone in knee joint." Congress of European Society of Biomechanics, s'-Hertogenbosch.

Subit D., Chabrand P., Masson C., Brunet C. 2004 "Behaviour of human knee ligaments : tensile tests in flexion and extension." 12th International Conference On Experimental Mechanics. Bari.

Takahashi Y., Kikuchi, Y., Mori, F., and Konosu, A., 2003 "Advanced FE Lower Limb Model for Pedestrians". 18th International Conference on the Enhanced Safety of Vehicles.

Tannous R.E., Bandak F.A., Toridis T.G., Eppinger R.H. 1996. "A three-dimensional finite element model of the human ankle: development and preliminary application to axial impulsive loading", 40th Stapp Car Crash Conference Proc., SAE. 219-238.

Winkler G. 1974. *Manuel d'Anatomie Topographique et Fonctionnelle*, 2nd ed. Masson, Paris.

Yang J. 1997. "Injury Biomechanics in car pedestrian collisions: development, validation and

CHARACTERIZATION OF THE LOWER LIMB SOFT TISSUES IN PEDESTRIAN FINITE ELEMENT MODELS

Costin Untaroiu

Kurosh Darvish

Jeff Crandall

Center of Applied Biomechanics, University of Virginia

Bing Deng

Jenne-Tai Wang

General Motors Research & Development, Warren, MI
United States

Paper Number 05-0250

ABSTRACT

Current finite element (FE) models of the human lower extremity lack accurate material properties of the soft tissues (flesh, fat, and knee ligaments), which are needed for computational evaluation of pedestrian injuries. Medial collateral ligament (MCL) is the most frequently injured ligament in lateral impacts. Therefore, the accuracy of the viscoelastic mechanical properties of the MCL FE model is of crucial importance in modeling pedestrian impacts. During automotive impacts, the flesh and fat get compressed, absorb part of the impact energy, and transfer and distribute the rest of energy to the skeleton. Therefore, the compressive response of these soft tissues can affect the accuracy of bone fracture predictions and as a result the overall kinematics of the FE pedestrian model. Quasi-Linear Viscoelastic (QLV) constitutive material models were assumed for MCL, flesh, and fat. Their global properties in terms of material parameters were derived using uni-axial step and hold tests on cadaveric specimens. The material models coefficients were derived by optimization. The flesh/fat models were validated in lateral leg impact tests at 2.5 m/s. The force-deflection results of the impactor, compared to other models, showed more biofidelity with respect to the cadaveric and volunteer data.

INTRODUCTION

In the past decade, several finite element (FE) lower limb models have been developed in order to reproduce lower limb injuries in the car-to-pedestrian collisions (CPC). Initially (e.g. Bermond et al. [1]) the surrounding muscles and the skin were neglected, and the knee ligaments were modeled usually by spring elements. Recently, due to rapid and continuously increasing of the speed of

computers, more sophisticated FE lower limb models have been developed. These models have accurate geometry obtained from CT and MRI scans from human volunteers (Beillas et al. [2], Takahashi et al [3]) or from Visible Human Database (Untaroiu et al. [4]), and the flesh and knee ligaments were meshed with shell and solid elements. However, the accuracy of FE models depends not only on the quality of the model geometry (e.g. anatomical surfaces, the number of components modeled, or mesh quality), but also on the biofidelity of the material properties assigned to the FE components.

Flesh and skin (fat) cover long bones of the lower limb. During automotive impacts, these soft tissues get compressed, absorb part of the impact energy, and transfer and distribute the rest of energy to the skeleton. Therefore, the compressive response of these soft tissues affect the severity of bone injuries and as a result the overall kinematics of the FE pedestrian/occupant model. McElhaney [5] conducted in-vitro compression tests of bovine muscle along the direction of the fibers. He published the loading stress-strain curves at various strain rates, but the strain data was limited to strains above 35%. The loading in a pedestrian impact is typically transverse to the muscle fiber direction. Therefore, the material properties derived in [5] may not be applicable. However, due to the lack of additional test data, in human FE models reported in the literature (e.g. [2]), it was assumed that the muscle and fat were linear elastic with Young's modulus about 1 MPa based McElhaney's stress-strain curves. In lower extremities of the H-Model [6] the flesh properties were estimated using impact tests on anterior and posterior thigh and the greater trochanter of human volunteers. The flesh material properties were expressed in the form of a nonlinear viscoelastic model that consisted of a nonlinear elastic stiffness in parallel with a viscous damper.

The nonlinearity of spring and damper depended on the ratio of the current to the initial volume. Considering the fact that soft tissues are almost incompressible (volume ratio is almost one) and highly viscoelastic, this material model could simplify their behavior. Snedeker et al. [7] and Ruan et al. [8] used the linear viscoelastic materials for flesh FE models and elastic material for skin models, but significant differences (more ten times) appear between their parameters. All these facts suggest the need for further investigation of the material properties of lower limb flesh and skin.

Medial collateral ligament (MCL) is the most frequently injured ligament in lateral impacts. Therefore, the accuracy of the viscoelastic mechanical properties of the MCL FE model is of crucial importance in modeling pedestrian impacts. MCL, as all knee ligaments, is highly anisotropic material consisting of a ground substance material reinforced by collagen and elastin (Weiss and Gardiner [9]). Collagen provides the major resistance in tension and negligible resistance in compression. In the literature, the mechanical properties of ligaments are provided as structural properties (derived from tensile test of the bone-ligament-bone structures), or material properties (derived from tests on isolated ligaments tissues). Structural properties depend on the global material properties, the direction in which the ligament is pulled, and the rate of loading. In FE models, the structural properties can be used only if the ligaments are modeled with one-dimensional elements (linear or non-linear springs). However, this approach is incapable of simulating the bone-ligament and ligament-ligament contacts, cross-sectional variation of ligament, and the stress distribution around the insertion sites. For two-dimensional (shell) or three-dimensional (solid) representations of ligaments, the material constitutive properties are needed. However, in the literature only one study reported material property data of MCL. Quapp and Weiss [10] conducted tensile tests at a strain rate of 1% sec⁻¹ on dog-bone shaped samples taken from the anterior-central two-third regions of ten human MCLs along the collagen fiber direction (longitudinal). The material properties obtained along the collagen axis were close to the average data reported by Butler et al. [11] (average of LCL, PCL, and ACL), and it was twenty times stiffer than the properties found in the transverse direction. Anisotropic hyper-elastic constitutive models were used to describe the tensile properties in both directions. The material coefficients were obtained by optimization. MCL is also a viscoelastic material, but its viscoelasticity in the domain of milliseconds, characteristic to the car crashes, is poorly understood. Woo et al [12] determined the material properties of

rabbit MCLs at five strain rates, from 0.008 mm/sec to 113 mm/sec. Tensile strength and ultimate strain increased slightly with increasing strain rate, whereas tangent modulus remained essentially unchanged. Based on this Weiss and Gardiner [9] concluded that the strain rate dependency had relatively small effects on ligament material properties. Yamamoto et al. [13] conducted dynamic tensile tests with femur-MCL-tibia complex obtained from female Japanese white rabbits. The strain rate was changed from 0.01 mm/sec to 300 mm/sec and a significant strain rate dependency was observed for the entire region of the stress-strain curve. The brief review of the reported material properties for MCL shows that its material properties, especially the viscoelastic ones, are poorly understood and need for further investigation.

The objectives of this work were to determine the material properties of lower limb soft tissues (flesh, fat, and MCL) and to evaluate their ability to describe the global response of the corresponding human tissues. To achieve these objectives, step and hold uniaxial tests on cadaveric specimens were performed. According to the main loadings which appear in the soft tissues during the pedestrian accidents, the flesh and fat samples were loaded in compression, while bone-MCL-bone complex was loaded in tension. The quasi-linear viscoelastic theory (QLV) [14] was selected to characterize the properties of the soft tissues under study. The material model coefficients were derived by optimization.

MATERIAL IDENTIFICATION

Quasi-Linear Viscoelastic (QLV) Theory

Soft tissues have a time-dependent behavior which can arise from fluid flow in and out of the tissue, or from inherent viscoelasticity of the solid phase (Weiss and Gardiner [9]). Fung [14] has proposed the QLV theory which had been widely used in mechanics in order to describe the soft tissue behavior. The main assumption of this theory is that the elastic response and the relaxation function are separated in the convolution integral representation of the stress, as shown in the following expression for a uniaxial loading condition:

$$\sigma(t) = \int_0^t G(t-\tau) \frac{\partial \sigma^e[\lambda(\tau)]}{\partial \tau} d\tau \quad (1).$$

where σ^e is the elastic response, $G(t)$ the relaxation function, and $\lambda(t)$ is the stretch ratio time history. A material model with this formulation implemented in Ls-Dyna was used in the material identification processes. A brief description of this material model is provided in this section.

The soft tissue is considered as a composite material which consists of collagen fibers embedded in a softer isotropic (ground) material. The strain energy function of the soft tissue material, as was formulated by Weiss [15], has three terms:

$$W = W_1 + W_2 + W_3 \quad (2).$$

The first term models the ground substance matrix as a Mooney-Rivlin material:

$$W_1 = C_1(I_1 - 3) + C_2(I_2 - 3) \quad (3).$$

where I_1 and I_2 are the invariants of the right Cauchy deformation tensor. The second term $W_2 = F(\lambda)$ is defined to capture the behavior of crimped collagen in tension and it works only in the fiber direction defined in the model. Its derivative (i.e., stress) has an exponential function which describes the straightening of the fibers and a linear function once they are straightened past a critical stretch level λ^* :

$$\frac{\partial F(\lambda)}{\partial \lambda} = \begin{cases} 0 & \lambda < 1 \\ \frac{C_3}{\lambda} [\exp(C_4(\lambda - 1)) - 1] & \lambda < \lambda^* \\ \frac{1}{\lambda} (C_5\lambda + C_6) & \lambda \geq \lambda^* \end{cases} \quad (4).$$

The role of the last term in the strain energy function is to ensure nearly-incompressible material behavior:

$$W_3 = \frac{1}{2} K [\ln(J)]^2 \quad (5).$$

where $J = \det \mathbf{F}$ is the third invariant of the deformation tensor (change in volume) and K is the bulk modulus. It is recommended that the bulk modulus should be two-three orders of magnitude larger than C_1 . The reduced relaxation function $G(t)$ was represented by a Prony series:

$$G(t) = \sum_{i=1}^3 S_i \exp\left(\frac{-t}{T_i}\right) \quad (6).$$

where S_i and T_i terms are the spectral strengths and characteristics times. Three terms were used for MCL and two terms for flesh and skin,

MCL Material Identification

A representative bone-MCL-bone specimen was extracted while its ends were potted in the fully extended position. The proximal potting cup was rigidly fixed and the distal cup was pulled along the longitudinal axis of tibia. First, the specimen was subjected to a ramp-and-hold test with constant tensile ramp of 3 mm in 30 ms and approximately

600 seconds hold time. The second test was a quasi-static test to failure on the same specimen. In both tests the time histories of force and displacement were recorded. For MCL material identification, the components of the UVA-GM FE model [4] were used (Figure 1).

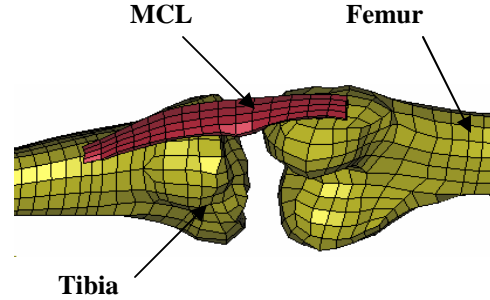


Figure 1. FE Simulation of the MCL Tensile Tests.

The MCL specimen had geometrical characteristics (length and medial cross-section) close to the MCL FE model. The insertion sites in the model were created using tied contact between bones and ligament. The direction of anisotropy (of collagen fibers) was defined in the material definition as the element normal in the longitudinal direction as illustrated in Figure 2.

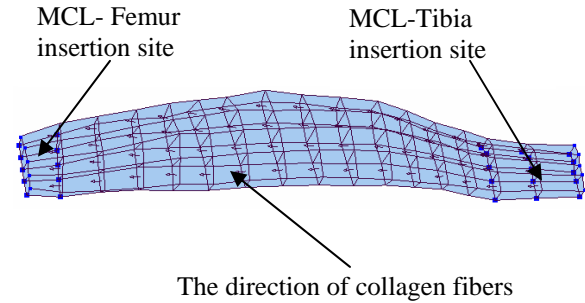


Figure 2. The insertion sites of MCL FE model and the direction of collagen fibers.

First, the quasi-static test was simulated. The material coefficients were optimized, assuming the quasi-static test data as the target values and defining minimization of the root-mean-square (RMS) error as the objective function. The optimization process was performed using the response surface methodology (RSM), a statistical method implemented in LS-Opt [16], used usually in design optimization. The hyperelastic coefficients (C_1 - C_5) were considered as design variables (independent parameters). The design space (a multi-dimensional space) was defined

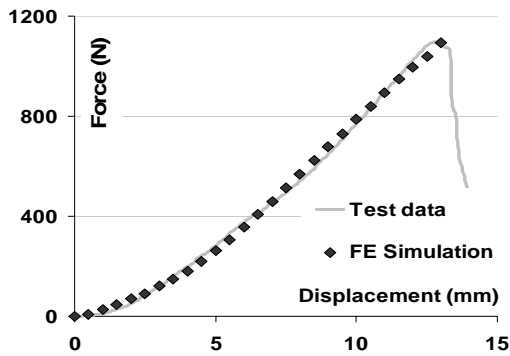


Figure 3. Quasistatic tensile test of MCL; Comparison between the test data and FE simulation results.

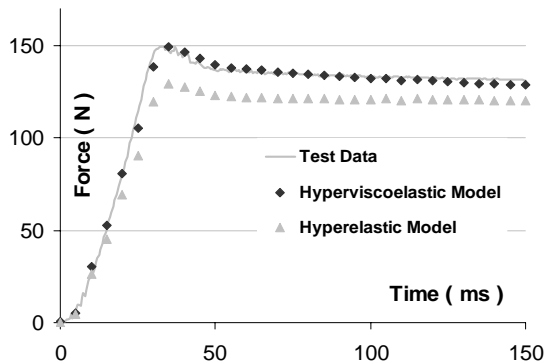


Figure 4. Dynamic tensile test of MCL; Comparison between test data and FE simulation results.

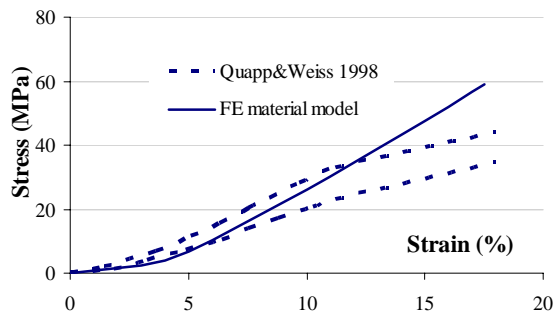


Figure 5. MCL stress-strain relationship; comparison between the material model determined from FE optimization and data reported by Quapp and Weiss [10].

as the ranges of hyperelastic coefficients, which were based on the data reported in [10]. The “best” design point (the set of hyperelastic coefficients provided in Table 1) were determined iteratively based on the

Table 1. Optimized MCL material properties.

K (GPa)	C ₁ (MPa)	C ₃ (MPa)	C ₄ -	C ₅ (MPa)	S ₁ -
3.75	7.85	0.25	60.4	307.5	0.15
S ₂ -	S ₃ -	T ₁ (ms)	T ₂ (ms)	T ₃ (ms)	λ
0.026	0.348	100	11,710	162,633	1.05

responses (RMS errors) at the design points, which were optimally distributed throughout the design space.

The viscoelastic properties of the ligament were then determined from the dynamic ramp and hold test. A three-term Prony series was considered to characterize the MCL relaxation behavior. The long-term Prony coefficients (S₃ and T₃) were estimated directly from the relaxation data. The two additional Prony coefficients (S₁, T₁, S₂, and T₂) were determined by considering both the ramp and hold periods and the same FE optimization procedure described above was conducted. All MCL material coefficients obtained by FE optimization are provided in Table 1.

The results of the simulations of quasi-static failure tests and dynamic ramp-and-hold tensile tests of MCL in comparison with experimental data are shown in Figures 3, and 4 respectively. The elastic stress-strain relationship in a cubic sample of MCL in tension along the collagen fibers with optimized parameters was compared with the corridor provided in Quapp and Weiss [10].

Flesh and Fat Material Identification

The dynamic passive properties of flesh and fat were determined from step and hold unconfined compression tests on cadaveric samples, as shown in Figure 6. Rectangular samples (20mm length and width, and 7 mm thickness) were excised perpendicular to the longitudinal axis of the leg from anterior thigh muscles and fat. Four flesh sample and one fat sample were tested. Approximately 20% compression was applied in 60 ms.

Structurally, fat tissue has no preferred direction and therefore can be considered to be isotropic. Muscle tissue however can be assumed to be transversely isotropic with the axis of anisotropy being along the longitudinal axis of the muscle. Since compression tests were performed perpendicular to this axis, the muscle samples were assumed also to be isotropic. As most of the other soft tissues, both muscle and fat were assumed to be nearly incompressible. The material properties were

assumed to be visco-hyperelastic with a Mooney-Rivlin strain energy function (Equation 3).

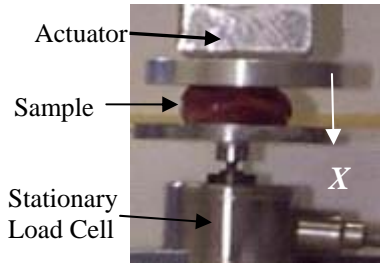


Figure 6. The apparatus for unconfined compression tests with a muscle sample.

Based on the boundary conditions on the unloaded faces (X_2 and X_3) of the sample and the incompressibility condition, the elastic stress in the compression direction (X_1) can be derived as:

$$\sigma_{1m}^e = \frac{2(\lambda_1^3 - 1)}{\lambda_1^2} (C_1 \lambda_1 + C_2) \quad (7).$$

Where $\lambda_1(t)$ is the stretch ratio history that was derived from the actuator displacement. The experimental Cauchy stress history was calculated based on the compression force history $F(t)$ measured by the load cell and the initial cross-sectional area A_0 with the following formula:

$$\sigma_{1\text{exp}}^e(t) = \frac{F(t)}{A_0 \lambda_1^2(t)} \quad (8).$$

Assuming a relaxation function of exponential form as shown in (6), the model and experimental Cauchy time histories were derived recursively from the convolution integral (Equation 1). The actual ramp and hold inputs were used as arbitrary inputs and the convolution integral of Equation (1) was carried out numerically as in Puso and Weiss [17]. The material coefficients C_i and the coefficients of Prony series S_i and T_i were optimized, assuming the experimental Cauchy stresses (Equation 8) as the target values and defining minimization of the root-mean-square (RMS) error as the objective function. Minimization was carried out using the Solver package of Microsoft Excel, which uses a quasi-Newton search algorithm. A comparison between the Cauchy stress obtained from experimental data and the stress calculated from the model using the optimized parameters is shown in Figure 7. The average reduced relaxation function of flesh (muscle) and the reduced relaxation function of fat are shown in

Figure 8. The average material properties obtained from flesh tests and fat data are provided in Table 2.

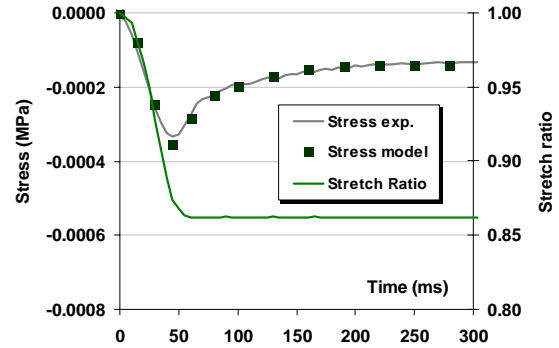


Figure 7. Comparison between the experimental and model results for flesh.

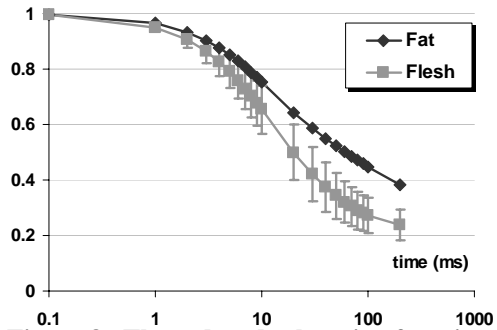


Figure 8. The reduced relaxation functions of flesh and fat.

Table 2. Material Properties of Flesh and Fat.

Tissue	C_1 (kPa)	C_2 (kPa)	S_1	S_2	T_1 ms	T_2 ms	K MPa
Muscle	0.12	0.25	1.2	0.8	23	63	20
Fat	0.19	0.18	1.0	0.9	10	84	20

FLESH VALIDATION AT LATERAL IMPACT

In order to verify the global response of the QLV material models of flesh and skin developed in this study, the lateral impact tests to the leg performed by Dhaliwal et al. [18] were simulated. The optimized material properties were assigned to the flesh and skin in the lower limb finite element (FE) model of the 50th percent male developed by Untaroiu et al [4].

The femoral head, distal fibula/tibia, and the skin nodes in contact with rigid foam blocks (on the opposite side of the impact) were rigidly constrained.

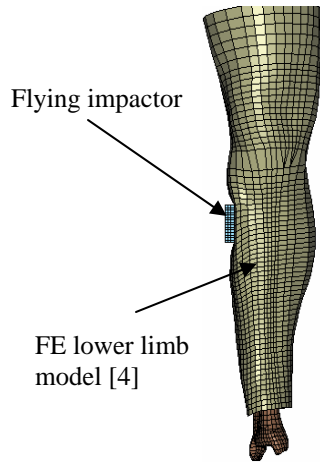


Figure 9. The impactor hitting the FE model.

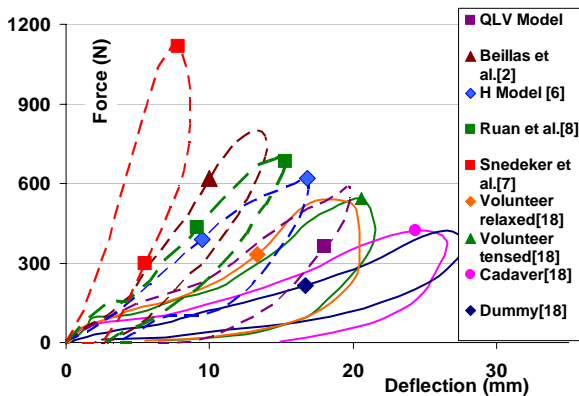


Figure 10. Force-deflection response; Comparison between FE simulation with QLV skin/flesh material models, other published models, and typical test data [18].

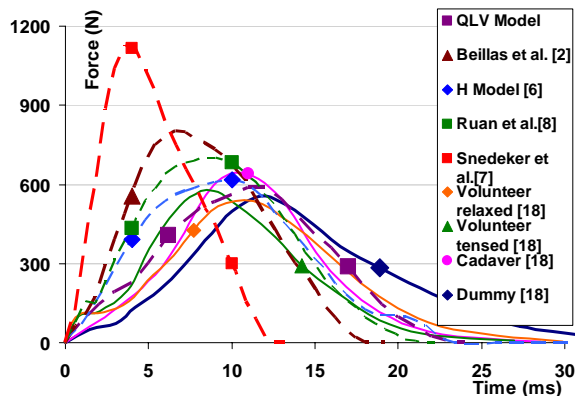


Figure 11. Impact Force time histories; Comparison between FE simulation with QLV skin/flesh material models, other published models, and typical test data [18].

The free flying impactor was a plate (45 mm by 142 mm – impact area) with 1.84 kg mass and 2.5 m/s initial velocity, as illustrated in Figure 9. The impact direction was inclined 30 degrees from the lateral direction as in [18] to protect the fibula. The densities of muscle and fat were assigned as 1000, and 800 kg/m³ respectively. In simulations, the impactor force and displacement of one point of the impactor were calculated. The ratio of the energy lost by the impactor was obtained based on the initial velocity $V_{initial}$ and the rebounded velocity $V_{rebound}$, as in [18]:

$$E = \left[1 - \left(\frac{V_{rebound}}{V_{initial}} \right)^2 \right] \cdot 100 \quad (9).$$

Several simulations of the lateral impact test were run with other published flesh/skin material models mentioned before. Their simulation results, the results of the FE model with QLV skin/flesh models, typical test data of cadavers, Hybrid III dummy, and volunteers with relaxed and tensed muscles [18] were compared in terms of force-deflection response and the impact force histories in Figures 10, and 11 respectively. Some characteristic parameters reported in [18] and their range from test data were compared to FE simulation results in the Table 3.

Table 3. Comparison between test data [18] and FE simulation results for different flesh/skin material models used in the FE lower limb model. (Numbers in paranthesis indicate S.D.)

Specimen/ FEM - skin/flesh material models	Max. Force (N)	Max. defl. (mm)	Impact Time (ms)	Energy Lost Ratio (%)
Relaxed Volunteer	498 (52)	21 (3)	24 (2)	82 (4)
Tensed Volunteer	521 (62)	20 (4)	24 (1.8)	74 (4)
Cadaver	596 (168)	22 (3)	24.2 (5.6)	82 (2)
Dummy	535 (8)	24 (0.1)	34.2 (0.5)	60 (1)
FEM – [2]	802	14	18	45
FEM – [6]	617	17	24	56
FEM – [7]	1114	8.7	12.2	64
FEM – [8]	702	15.3	21.5	41
QLV material	592	20	24	64

DISCUSSION

The QLV material model developed in this study for MCL showed good agreement with experimental data in tensile tests. In the dynamic test with 0.1 mm/ms displacement rate, approximately 15% increase in the peak dynamic force was observed, which suggests that tissue viscoelasticity plays an important role in the response during impact scenarios. The elastic stress-strain relationship of the model in tension along the collagen fibers was compared with the corridor provided in Quapp and Weiss [10]. The current material model was slightly stiffer at strains above 13% (Figure 5). This material model was determined by assuming a homogeneous anisotropic material for the whole MCL and optimizing its global tensile properties. However, MCL is inhomogeneous, particularly at the insertion sites, which could explain the difference observed in its local and global properties.

The global responses of the QLV skin/flesh material models developed in this study and other material models from the literature were compared with the published experimental data [18] for cadavers, Hybrid III dummy, and volunteers with relaxed and tensed muscles. The model results using the identified material properties showed good agreement with the cadaver data in terms of the maximum force and displacement. The ratio of energy loss (calculated based on the initial and rebound velocities) was 64%, which was smaller than the volunteer data (70-86%), but larger than the dummy data (60%), or other published material models (41-64%). Such difference could appear due to inaccuracies in the determination of the Pony series coefficients as a result of the optimization procedure, the number of relaxation terms (three), the hold time (500 ms), and the limited number of cadaveric specimens tested. Also friction at the impactor/skin interface contributes to the energy loss whereas in the FE simulation no friction was applied at the contact interface. Overall, the model with QLV material property showed significantly better biofidelity than the model with linear elastic property in low speed impact tests.

The main limitation of the QLV soft tissues material models developed in this study is determined by the small number of samples used in the material identification processes. Since the MCL geometry is not identical in all subjects, it is advisable that an FE model should be developed for each specimen based on its surface digitization. In case of compressive material properties of flesh/skin, more validations are needed especially at high speed impacts.

CONCLUSIONS

The global viscoelastic material properties of a representative MCL specimen were derived by FE optimization. Results showed a higher stiffness at high strain values than the local properties derived in a previous study. The viscoelastic properties obtained from the stress relaxation tests showed that tissue viscoelasticity increases the peak dynamic force by 15% at 0.1 mm/ms displacement rate. Studies of more specimens are underway and will be reported in the future.

The passive material properties of muscle and fat were identified from unconfined compression tests on cadaveric samples using a QLV constitutive material model. The global validation performed against published lateral impact test data using actual flesh/skin models showed more biofidelity than other material models used in the literature. The high stiffness of several published muscle/skin models poses a question over the accuracy of the global validation results in which the skin was impacted. More validation tests are needed for the wide range of impact speeds observed in car-to-pedestrian collisions.

REFERENCES

- [1] Bermond, F.; M. Ramet; R. Bouquet and D. Cesari (1994). "A finite element model of the pedestrian leg in lateral impact." 14th ESV.
- [2] Beillas, P.; P.C. Bageman; K.H. Yang; A.I. King; P.J. Arnoux; H.S. Kang; K. Kayvantash; C. Brunet C.; C. Cavallero and P. Prasad P., 2001, "Lower Limb: Advanced FE Model and New Experimental Data." *Stapp Car Crash Journal* 45: 469-494.
- [3] Takahashi, Y.; Y. Kikuki; F. Mori, and A. Konosu (2003). "Advanced FE Lower Limb for Pedestrians.", 18th ESV Conference
- [4] Untaroiu, C., Darvish, K., Crandall, J., Deng, B., and Wang J.T., 2004, "Development and Validation of a Finite Element Model of the Lower Limb", IMECE 2004-61583, 2004 ASME Congress.
- [5] McElhaney, J., 1966, "Dynamic response of bone and muscle tissue," *Journal of Applied Physiology*, 21(4): 1231-1236.
- [6] "H-Dummy™ Version 2.1 User's Manual", (1999). Hankook ESI, Engineering Systems International

[7] Snedeker, J.G., M.H. Muser, and F.H. Walz (2003). "Assessment of Pelvis and Upper Leg Injury Risk in Car-Pedestrian Collisions: Comparison of Accident Statistics, Impactor Tests and a Human Body Finite Element Model", *Stapp Car Crash Journal*, 47:437-457

[8] Ruan, J., R. El-Jawahri, L. Chai, S. Barbat, and P. Prasad (2003). "Prediction and Analysis of Human Thoracic Impact Responses and Injuries in Cadaver Impacts Using a Full Human Body Finite Element Model" *Stapp Car Crash Journal*, 47:299-321

[9] Weiss, J.A. and J.C. Gardiner (2001). "Computational Modeling of Ligament Mechanics." *Critical Reviews in Biomedical Engineering* 29(4): 1-70

[10] Quapp, K.M. and J.A. Weiss (1998). "Material Characterization of Human Medial Collateral Ligament." *Journal of Biomechanical Engineering* 120: 757-763.

[11] Butler, D.L.; M.D. Kay, and D.C. Stouffer (1986). "Comparison of Material Properties in Fascicle-Bone Units from Human Patellar Tendon and Knee Ligaments." *Journal of Biomechanics* 19(6): 425-432.

[12] Woo, S.L.; M.A. Gomez, and W.H. Akeson, (1981). "The time and history-dependent viscoelasticity properties of the canine medial collateral ligament." *Journal of Biomechanical Engineering* 103: 293-298.

[13] Yamamoto S., Kajzer, J., and E. Tanaka, (2000). "Development of high-speed tensile test system for ligaments and skeletal muscles", In *Human Biomechanics and Injury Prevention*, Ed. Kajzer J., Tanaka E., Yamada H., Springer: 167 – 172.

[14] Fung YC. (1967). "Elasticity of soft tissues in simple elongation." *Am J Physiol*; 213: 1532–1544.

[15] Weiss, J.A. (1994). "A constitutive model and finite element representation for transversely isotropic soft tissues." Ph.D. Dissertation, Department of Bioengineering, University of Utah; 1994.

[16] Stander, N., Eggleston T., Craig K., and W. Roux (2003), "LS-OPT User's Manual", Livermore Software Technology Corporation.

[17] Puso, M.A.. and Weiss J.A., 1998, "Finite Element Implementation of Anisotropic Quasi-Linear

Viscoelasticity Using a Discrete Spectrum Approximation," *J. Biomech. Eng.* 120: 62-70.

[18] Dhaliwal, T.S.; Beillas, P.; Chou, C.C.; Prasad, P.; Yang, K.H., and King, A.I., 2002, "Structural Response of Lower Leg Muscles in Compression: A Low Impact Energy Study Employing Volunteers, Cadavers and the Hybrid III" *Stapp Car Crash Journal* 46: 229-243.

DEVELOPMENT OF A PEDESTRIAN LOWER EXTREMITY PROTECTION CAR USING A BIOFIDELIC FLEXIBLE PEDESTRIAN LEGFORM IMPACTOR

Atsuhiko Konosu, Takahiro Issiki

Japan Automobile Research Institute (JARI)

Masaaki Tanahashi

Japan Automobile Manufacturers Association, Inc. (JAMA)

Paper Number 05-0106

ABSTRACT

The Japan Automobile Manufacturers Association, Inc. and the Japan Automobile Research Institute are jointly engaged in the development of a flexible pedestrian legform impactor (hereafter referred to as "Flex-PLI"). However, a study for the development of a pedestrian lower extremity protection car using the Flex-PLI has not been reported.

In this study, development of sedan, minivan and SUV type cars for pedestrian lower extremity protection was conducted using a Flex-PLI. This study results indicated a good possibility of lower-extremity protection in collisions by pushing the pedestrian's legs forward within the extent of not causing bone fractures. However, such protection methodology is difficult for SUVs because they need high ground clearance and large approach angle as for rough road condition running purpose.

This study is the first trial study for the development of pedestrian lower extremity protection car using a Flex-PLI, therefore, additional similar studies are necessary.

INTRODUCTION

The Japan Automobile Manufacturers Association, Inc. and the Japan Automobile Research Institute are jointly engaged in the development of a flexible pedestrian legform impactor (hereafter referred to as "Flex-PLI") [1][2][3]. The bone and knee of the Flex-PLI have a bending deformation characteristic equivalent to those of the human lower-extremity. The Flex-PLI is equipped with more built-in measuring instruments than are conventional pedestrian legform impactors.

It is reasonable to consider that the Flex-PLI is more suited for the development of proper pedestrian lower-extremity protection car; however, there has been no report of such vehicle development using a Flex-PLI before. In the present study, therefore, pedestrian lower-extremity protection methods for

various types of cars were examined using a Flex-PLI.

METHODOLOGY

Pedestrian Legform Impactor

The pedestrian legform impactor employed in the present study is shown in Figure 1. It is the latest-version model developed in 2004 and is called Flex-PLI 2004 [3] (hereafter simply "Flex-PLI"). As listed in Figure 2, the Flex-PLI has a total of 10 measurement items including bone core strain and knee ligament elongation. Based on the relationship between the strain and bending moment of the bone core derived from bone core calibration tests (see Appendix B), it is possible to calculate from the measured value of strain the value of bending moment applied to the bone core.

In the present study, measurement of the elongation of the lateral collateral ligament ("LCL") was omitted since the LCL could not be elongated by the types of vehicles used in the present study.

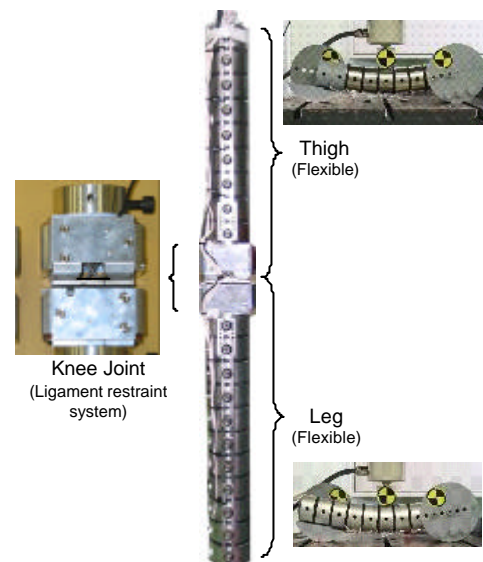


Figure 1. Overall design of Flex-PLI.

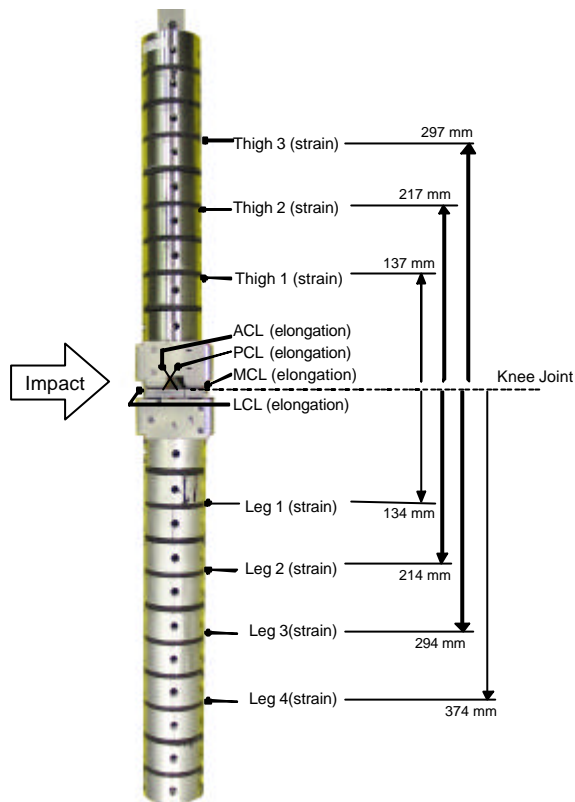


Figure 2. Measurement items of Flex-PLI (2004).

Test Vehicles

The four types of cars used in the present study are shown in Figure 3 and Table 1. They were two sedans, a minivan and an SUV (Sedan 1, Sedan 2, Minivan, SUV).

For each car type, the test was conducted with the car in its original parts. Then, based on the test results, the car was modified and tested to determine suitable methods to protect the pedestrian lower- extremity.

Test Conditions

The test conditions are introduced in Figure 4. The initial impact speed of Flex-PLI was 11.1 m/s, and the impact position was at the center of the vehicle's front face. In accordance with a conclusion drawn by the International Harmonized Research Activity Pedestrian Safety Working Group [4], the lowest point of Flex-PLI was set 25 mm above the ground to allow for the shoe sole height.

Injury Risk Levels (tentative)

The tentative 50% injury risk levels assumed for the present study are listed in Table 2. These tentative 50% injury risk levels for the American 50 percentile male were derived from available literatures for the present study [5][6][7][8][9].

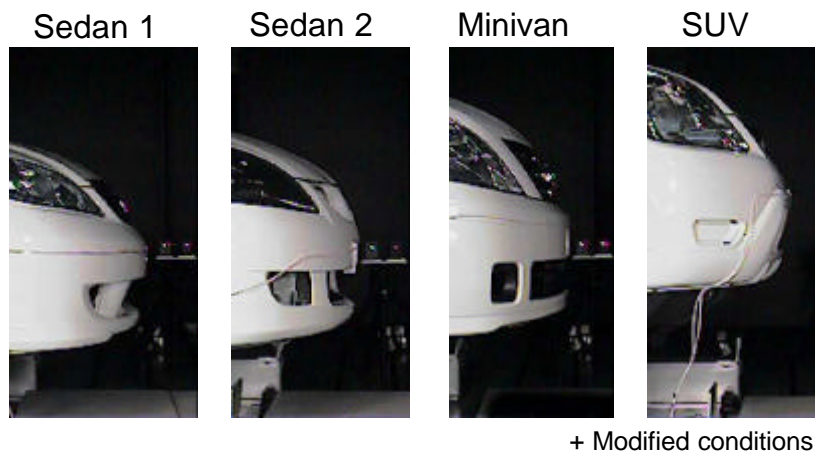


Figure 3. Test cars.

Table 1. Dimensions of test cars.

Car Type	LEH* (mm)	BL** (mm)
Sedan 1	703	157
Sedan 2	765	185
Minivan	829	164
SUV	925	211

* LEH: bonnet leading edge height.

** BL: bumper lead.

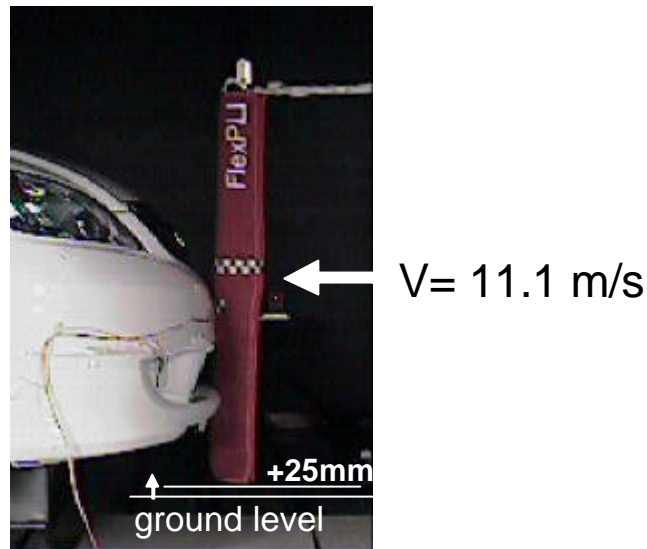


Figure 4. Test conditions.

Table 2. Injury risk levels (tentative).

Body regions	50% injury risk level for 50 percentile American male (tentative)	References
Leg	BM (312 - 350 Nm)	BM (312 Nm): Kerrigan et al., 2004 BM (350 Nm): INF GR/PS/82
Knee	MCL	EL (18 - 20 mm)**
	ACL	EL (10 mm)***
	PCL	EL (10 mm)***
Thigh	BM (372-447 Nm)	BM (372 - 447 Nm): Kerrigan et al., 2004 BM (390 - 395 Nm): Kennedy et al., 2004

* BM: Bending moment, EL: Elongation, BA: Bending angle, SD: Shearing displacement.

** Estimated from BA (18-20 deg.), *** Estimated from SD (10 mm)

RESULTS

Sedan 1

Test results with the original Sedan 1 are given in Figure 5. In a collision with Sedan 1 the risk of causing a thigh or leg fracture to the pedestrian proved to be low, but the risk of an injury to the medial collateral ligament (MCL) of the knee might be high (located in the tentative injury risk level). The reason: although the bumper rigidity was insufficient to cause a fracture, the bumper also lacked sufficient force to push the pedestrian's legs forward, thus generating a large bending of the knee.

In view of the above results, Sedan 1 was modified as shown in Figure 6. A second bumper face and a pad were added to the bumper's lower section in order to increase the bumper rigidity.

As shown in Figure 7, the modified Sedan 1 yielded test results that were clearly below the injury risk level for the thigh, leg and knee alike, thus indicating a high pedestrian lower-extremity protection capability of the modified Sedan 1.

The test results with the original Sedan 1 and the modified Sedan 1 were compared in Figure 8. The modified sedan recorded lower bending moment and elongation values at the various positions on the Flex-PLI except the Leg 4 position, as compared to the original sedan. This was attributed to the 'leg sweeping structure' of the modified bumper, whereby the overall load on the lower-extremity was lightened by pushing the leg region forward.

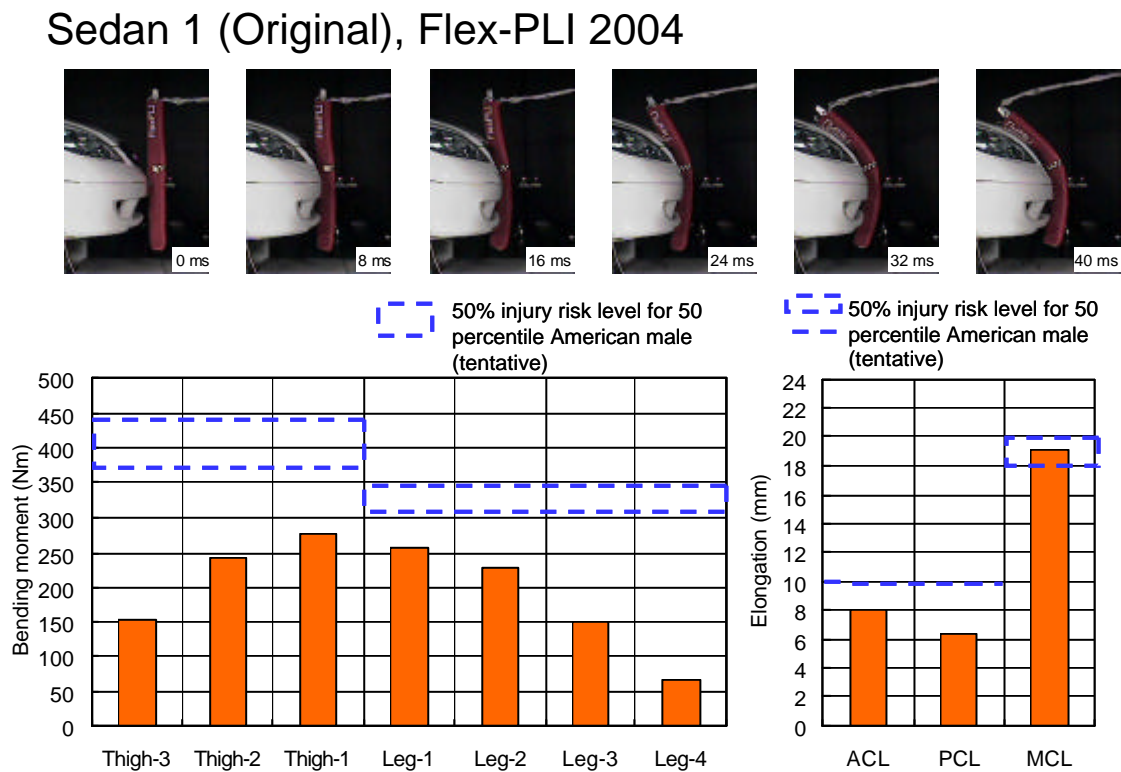


Figure 5. Test results of Sedan 1 (Original).

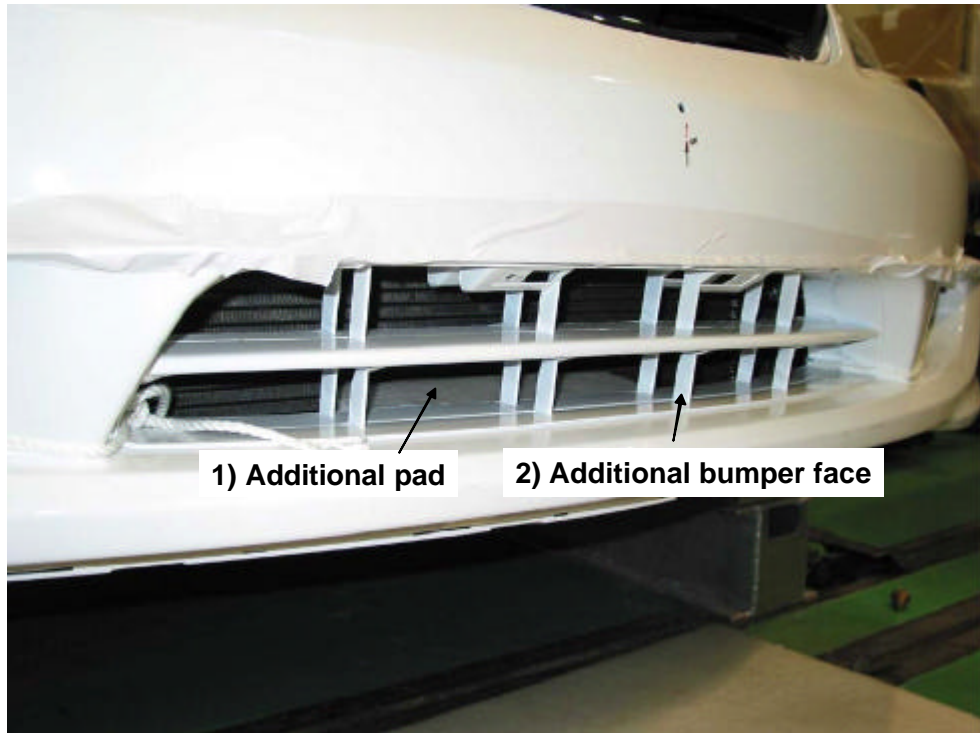


Figure 6. Modifications to Sedan 1.

Sedan 1 (Modified), Flex-PLI 2004

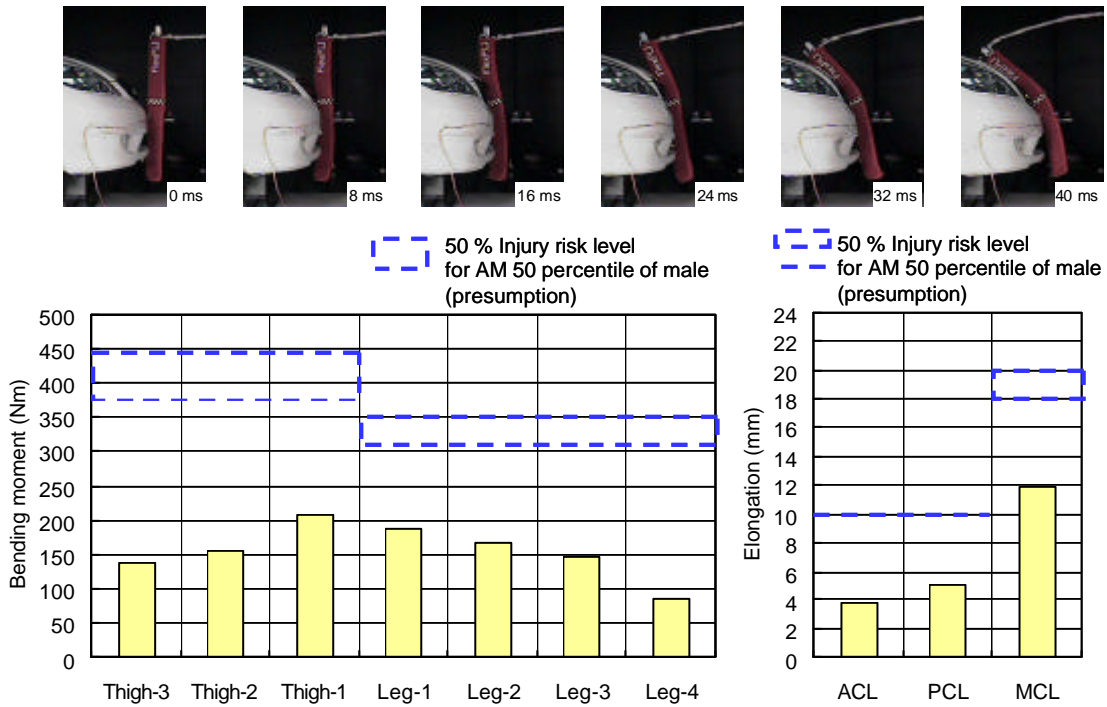


Figure 7. Test results of Sedan 1 (Modified).

Sedan 1 (Original), Flex-PLI 2004



Sedan 1 (Modified), Flex-PLI 2004

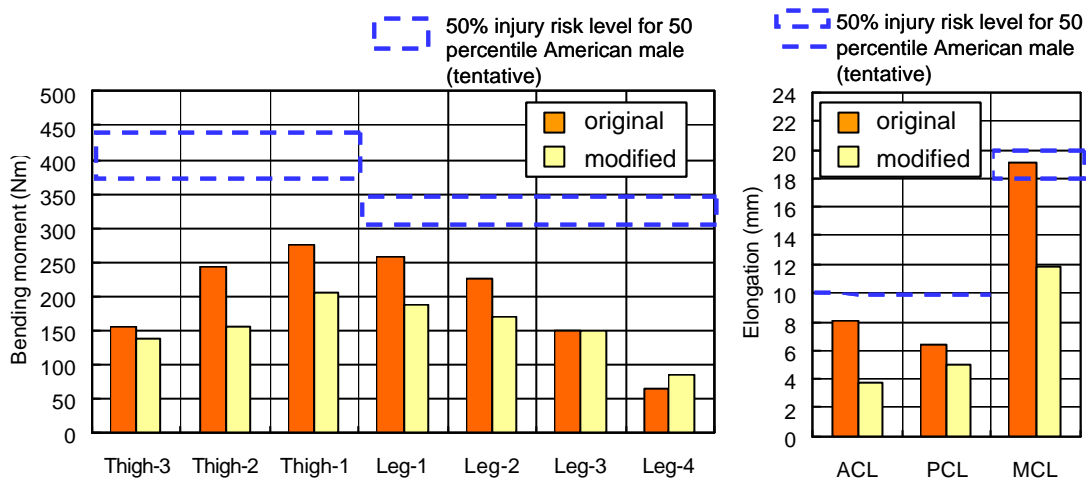


Figure 8. Comparison of the test results between the Original and Modified Sedan 1.

Sedan 2

Test results with Sedan 2 are shown in Figure 9. Sedan 2 was found to be similar to Sedan 1 in that, although the risk of thigh or leg fracture proved to be low, the risk of knee injury might to be high. The reason: similar to Sedan 1, Sedan 2 lacked a sufficient bumper force to push the pedestrian's leg forward, although the bumper rigidity was low enough to prevent thigh or leg fractures. Thus, a large bending of the knee was observed.

The pedestrian lower-extremity protection methods adopted to Sedan 2 are shown in Figure 10. A pad was added so as to increase the rigidity of the bumper's lower portion.

The test results with this modified sedan are given in Figure 11. The measured bending moment and elongation values at all the positions on the thigh, knee and leg of the Flex-PLI were measured to be below the injury risk level, thus affirming a capability of the modified Sedan 2 to protect the pedestrian lower-extremity in a collision.

The test results with the original Sedan 2 and the modified Sedan 2 were compared in Figure 12. The modified sedan recorded lower bending moment and elongation values at the various positions on the Flex-PLI except the Leg 3 and Leg 4 positions, when compared to the original sedan.

Sedan 2 (Original) – Flex-PLI 2004

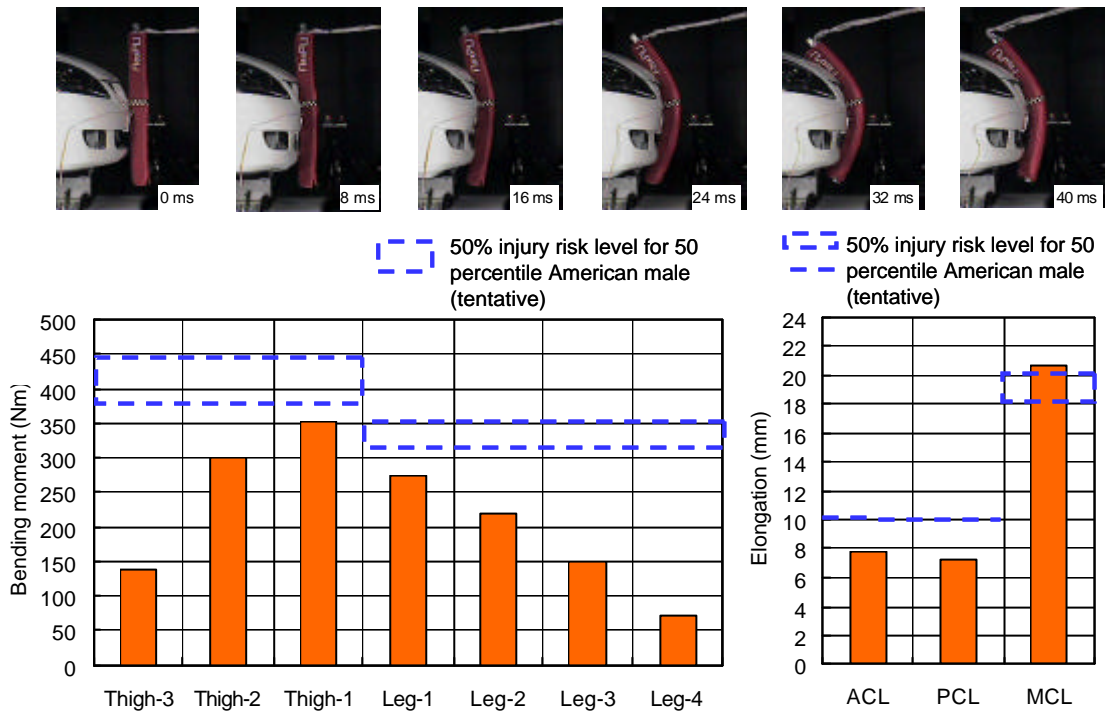


Figure 9. Test results of Sedan 2 (Original).



Figure 10. Modifications to Sedan 2.

Sedan 2 (Modified), Flex-PLI 2004

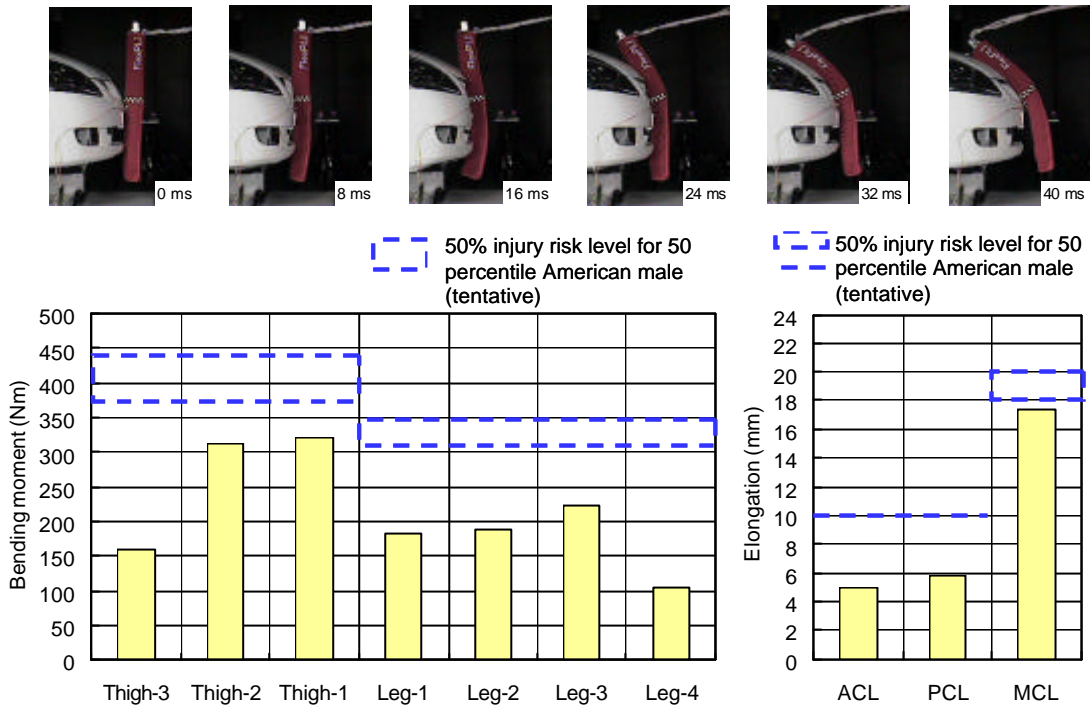
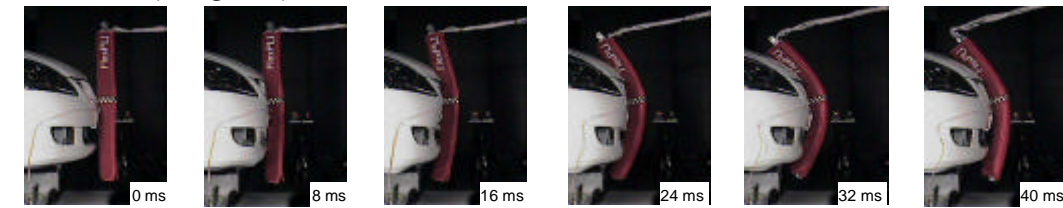


Figure 11. Test results of Sedan 2 (Modified).

Sedan 2 (Original), Flex-PLI 2004



Sedan 2 (Modified), Flex-PLI 2004

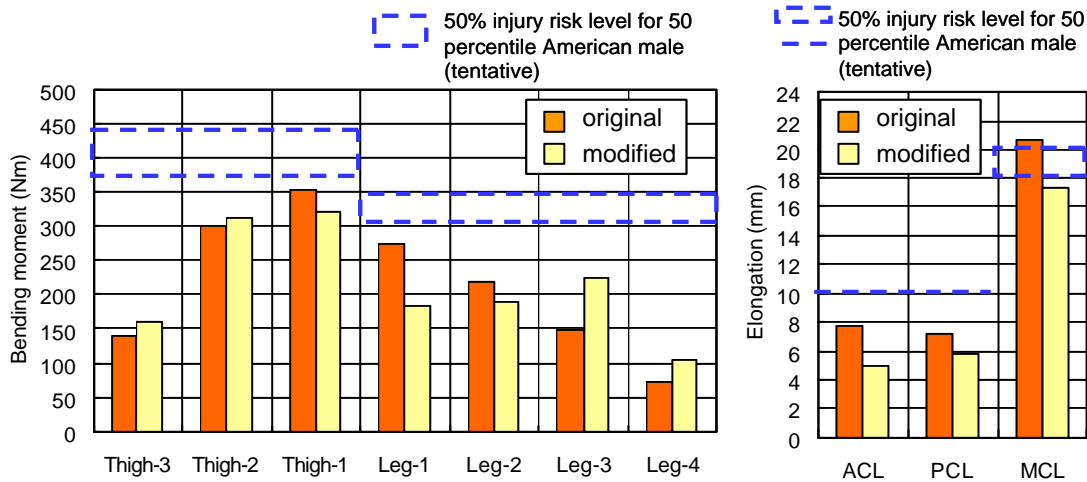
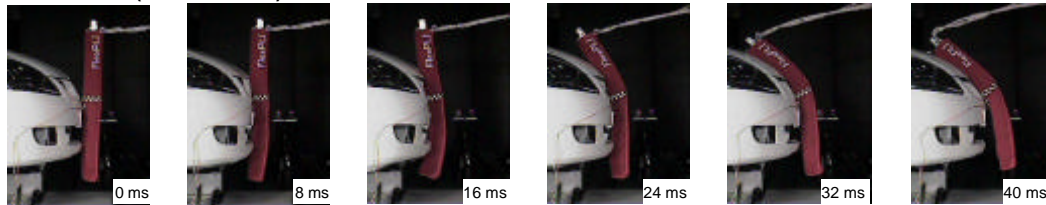


Figure 12. Comparison of the test results between the Original and Modified Sedan 2.

Minivan

Test results with the original Minivan are given in Figure 13. Similar to Sedans 1 and 2, although its bone fracture risk was low, the risk of knee injury might be high. The reason: similar to Sedans 1 and 2, the Minivan lacked a sufficient bumper force to push the pedestrian's leg forward, although the bumper rigidity was low enough to prevent thigh or leg fractures. Thus, a large bending of the knee was manifested.

The pedestrian lower-extremity protection introduced into the Minivan is shown in Figure 14. A pad was added so as to increase the rigidity of the bumper's lower portion. The test results with this modified Minivan are given in Figure 15. The measured MCL elongation remained at the tentative injury risk level, and it was evident that the addition of the pad was ineffective.

The test results with the original and modified Minivans were compared in Figure 16. The protection employed in the modified Minivan proved to be ineffective, except that elongation values for the knee slightly improved. This was attributed to the fact that because several pads already existed in the bumper area of the original Minivan (see Figure 14), the additional pad had to be placed on top of them in a higher position comparing to the Sedan 1 and Sedan 2 (see Figure 17).

The lower the impact point on the leg, the more the rotating motion of the entire lower-extremity. To reduce the load on the knee, therefore, the position of the added pad needs to be lowered and/or the rigidity of the pads used in the original Minivan must be increased within the extent of not causing bone fractures.

Minivan (Original), Flex-PLI 2004

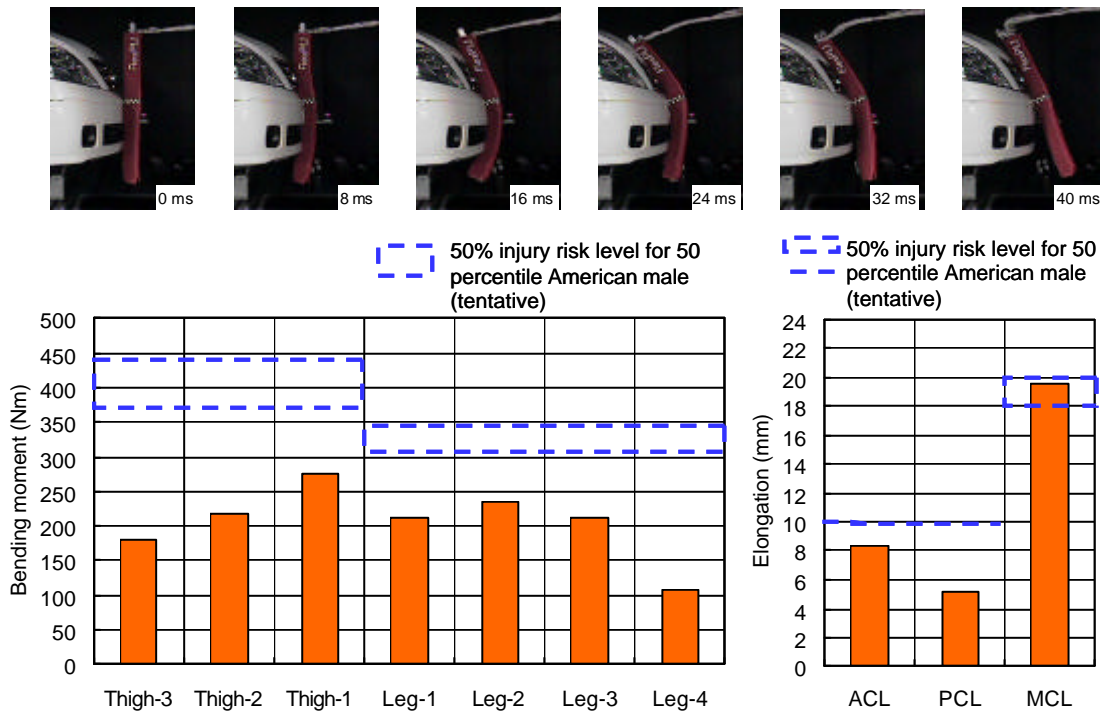


Figure 13. Test results of Minivan (Original).

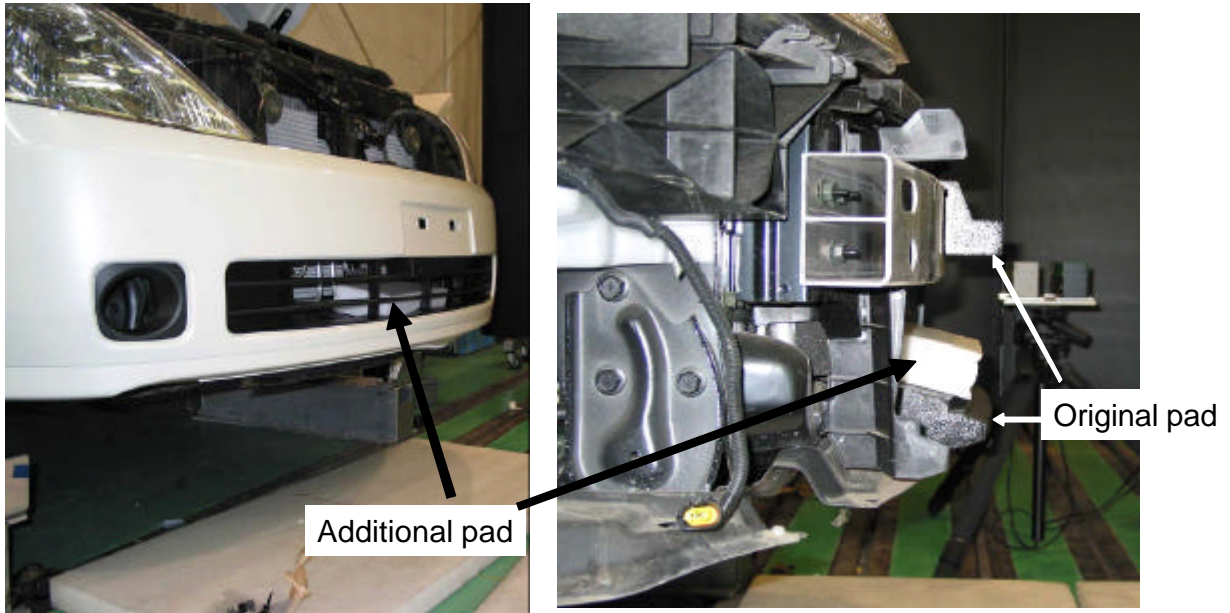


Figure 14. Modifications to Minivan.

Minivan (Modified), Flex-PLI 2004

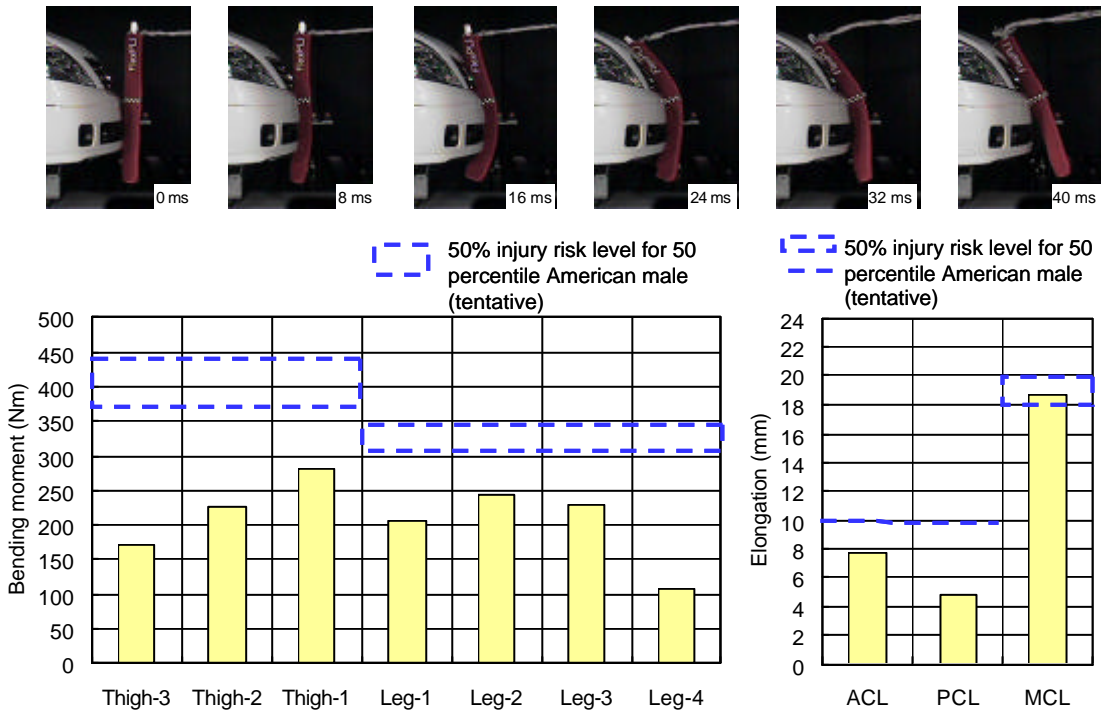
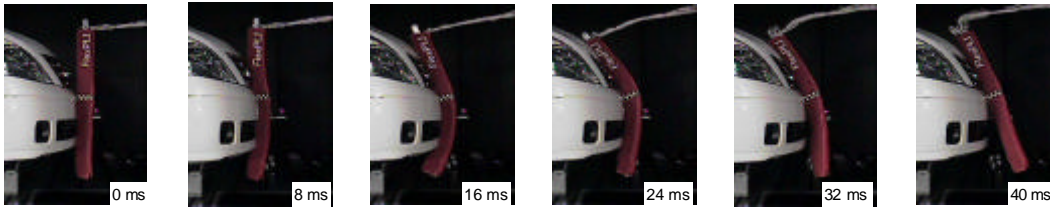


Figure 15. Test results of Minivan (Modified).

Minivan (Original), Flex-PLI 2004



Minivan (Modified), Flex-PLI 2004

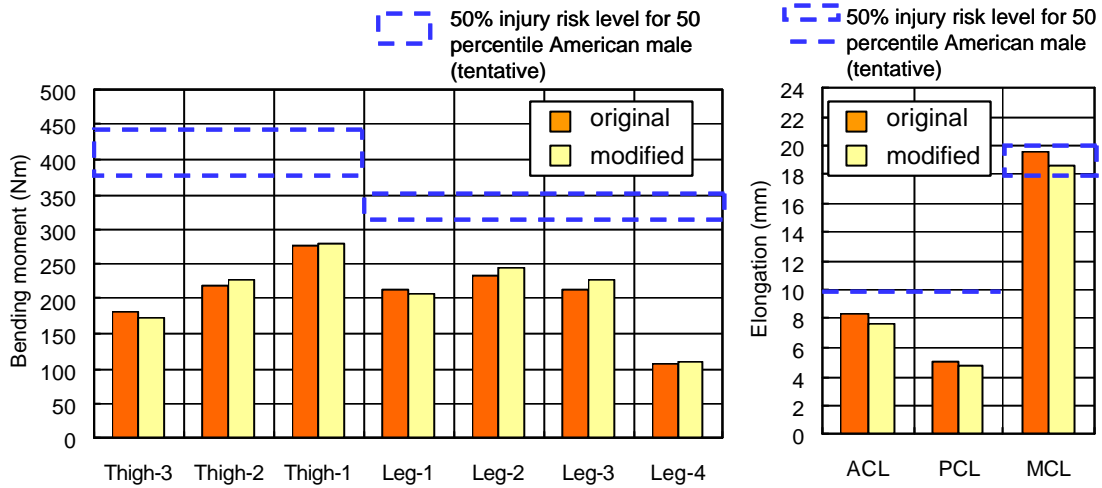
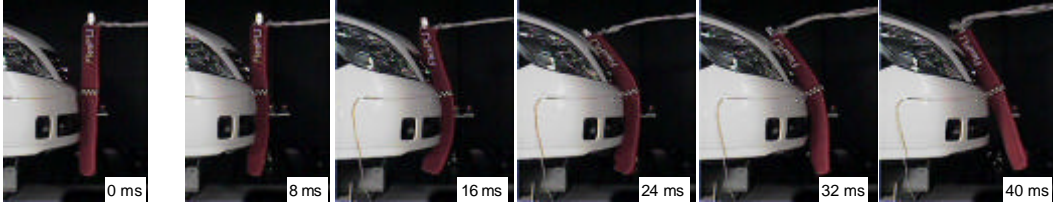


Figure 16. Comparison of the test results between the Original and Modified Minivan.

----- Additional pad position



Sedan 1 (Modified)

Sedan 2 (Modified)

Minivan (Modified)

Figure 17. Comparison of the additional pad position.

SUV

Test results with the original SUV are given in Figure 18. In a collision with the SUV the risk of causing a thigh or knee injury proved to be low, but the risk of leg fracture was high. The reason: while the bumper rigidity was insufficient to cause a thigh fracture or a knee ligament injury, the original SUV lacked a structural member to support the lower part of the leg because SUVs are required to have a high ground clearance and a large approach angle. As a result, a large bending load was applied to the leg.

Accordingly, the Minivan was modified as shown in Figure 19. An additional bumper face was installed underneath the standard bumper to support the pedestrian's leg. Although the introduction of this

additional bumper face may make the vehicle deviate from the definition of an SUV, this step was taken because no other effective protections could be found at this stage. As shown in Figure 20, the modified SUV clearly reduced the leg fracture risk.

The test results with the original and modified SUV were compared in Figure 21. The modified SUV was able to reduce the general lower-extremity injury risk thanks to the addition of a bumper face that supported the lower leg part. To further reduce the injury risk to a satisfactory level, however, additional steps will be necessary, for example the padding of the back of the added bumper face.

SUV (Original), Flex-PLI 2004

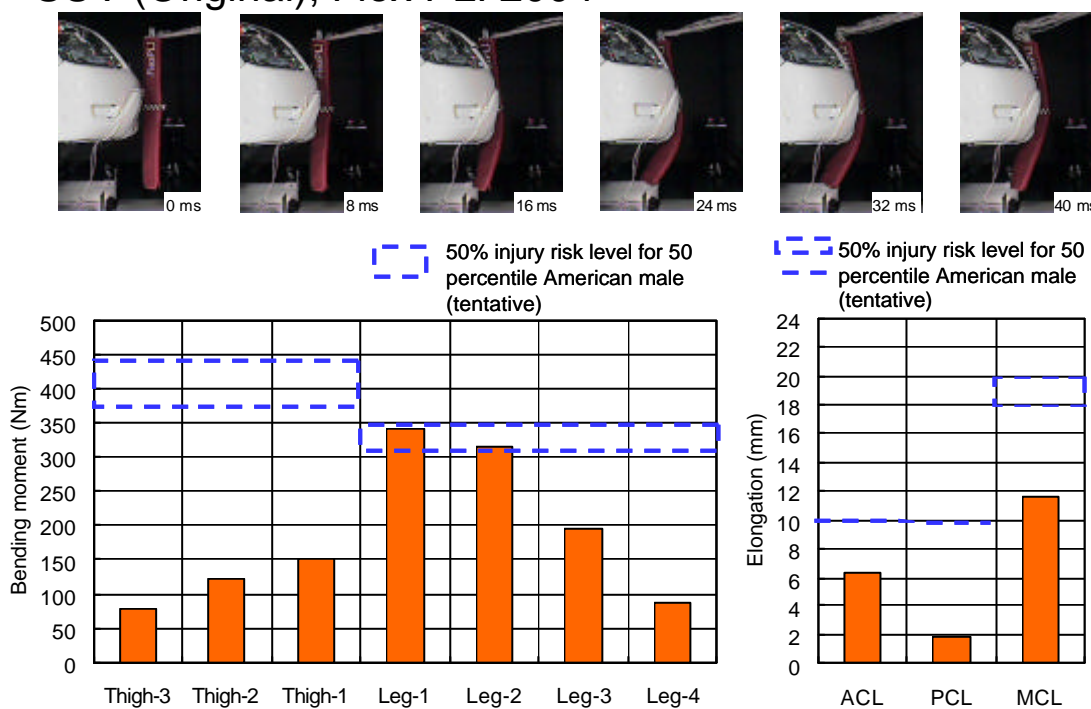


Figure 18. Test results of SUV (Original).



Additional bumper face
(No pad inside and no bumper support)

Figure 19. Modifications to SUV.

SUV (Modified), Flex-PLI 2004

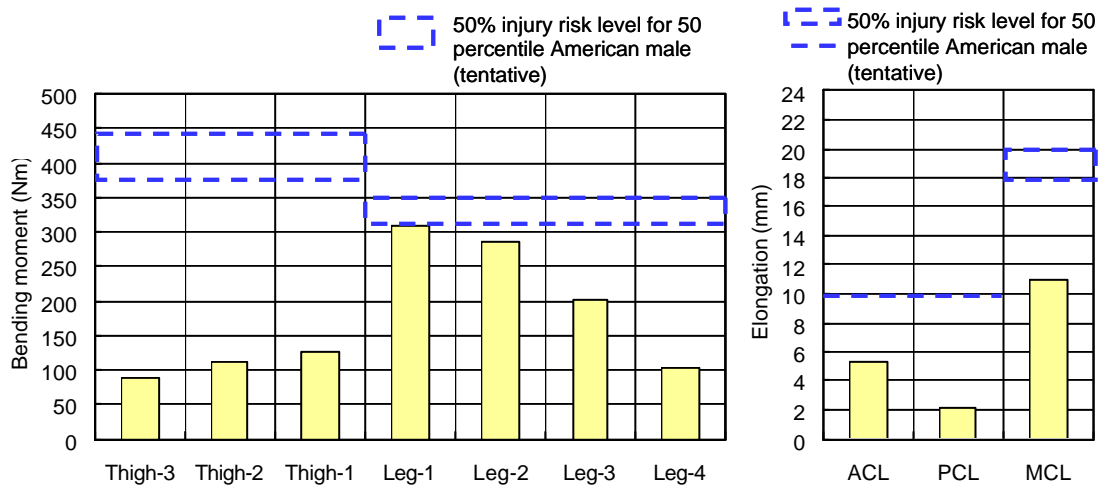
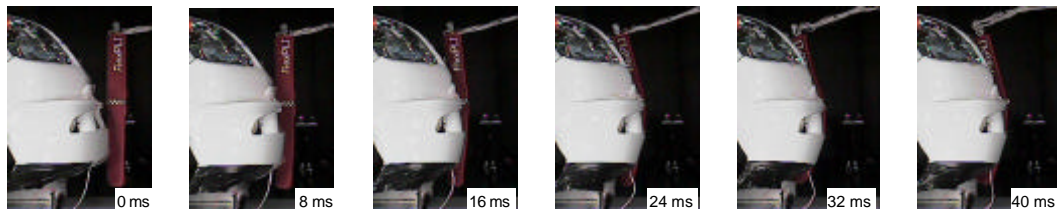
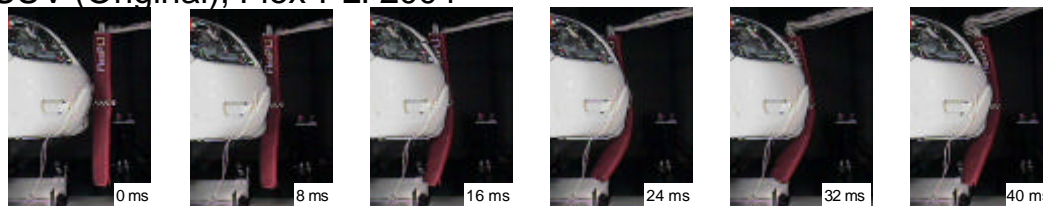


Figure 20. Test results of SUV (Modified).

SUV (Original), Flex-PLI 2004



SUV (Modified), Flex-PLI 2004

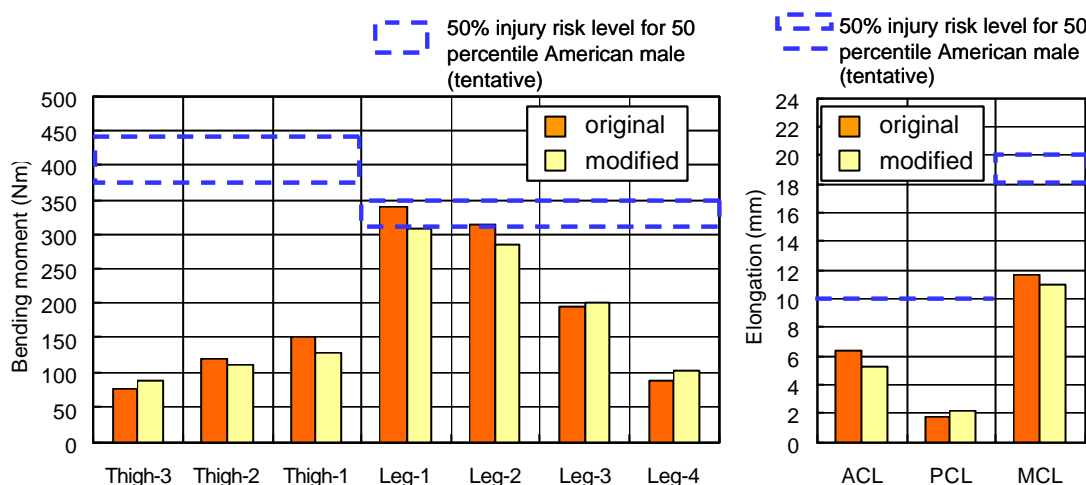
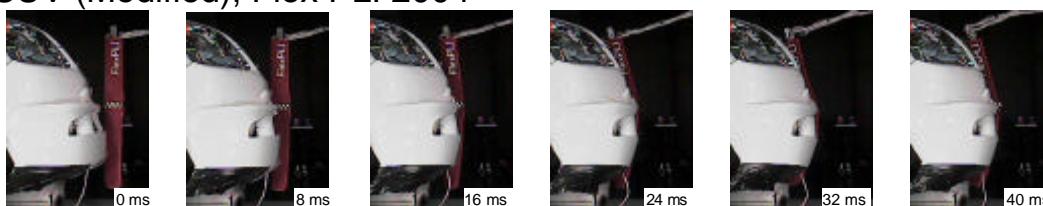


Figure 21. Comparison of the test results between the Original and Modified SUV.

DISCUSSION

In the present study, lower-extremity protection possibilities were examined for sedan, minivan and SUV types of vehicles. The results indicated a good possibility of protecting the pedestrian lower-extremities for all the vehicle types by pushing the legs forward within the extent of not causing leg fractures. This possibility was most saliently observed in Sedan 1 and Sedan 2.

In the case of the Minivan, the present study failed to obtain satisfactory injury risk values. However, to lower the position of the additional pad position and/or by increasing the rigidity of the standard pads within the extent of not causing bone fractures, the Minivan output also has a high possibility to be lower the injury risk level.

As for the SUV, it was considered difficult for this type of vehicle to provide sufficient lower-extremity protection because the requirement of a high ground clearance and large approach angle makes it difficult to introduce methods of pushing the pedestrian's legs forward.

However, this study is the first trial study for the development of pedestrian lower extremity protection car using a Flex-PLI, therefore, additional similar studies are necessary.

CONCLUSIONS

- In the present study the pedestrian lower-extremity protection performances of sedan, minivan and SUV types of cars were tested using a Flex-PLI.
- The test results indicated a good possibility of lower-extremity protection in collisions by pushing the pedestrian's legs forward within the extent of not causing bone fractures.
- In the case of SUVs, however, it was found difficult to provide such protection because of their high ground clearance and large approach angle which make difficult the introduction of methods to push the pedestrian's legs forward.
- This study is the first trial study for the development of pedestrian lower extremity protection car using a Flex-PLI, therefore, additional similar studies are necessary.

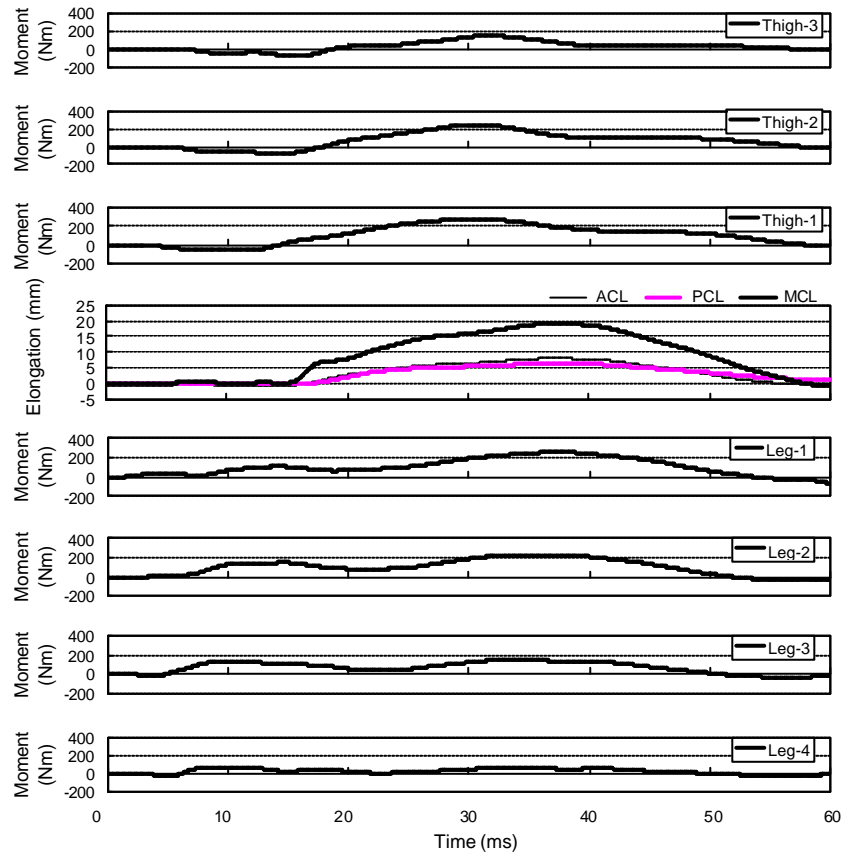
REFERNECES

- [1] Konosu, A., Tanahashi, M. (2003) Development of a biofidelic pedestrian legform impactor: Introduction of JAMA-JARI legform impactor ver. 2002, Proc. 18th International Technical Conference on the Enhanced Safety of Vehicle, Paper No. 378.
- [2] Konosu, A., Tanahashi, M. (2003) Development of a biofidelic flexible pedestrian legform impactor, Stapp Car Crash Journal, Vol. 47, pp. 459-472.
- [3] Konosu, A., Issiki, T., Tanahashi, M. (2005) Development of a Biofidelic Flexible Pedestrian Leg-form Impactor (Flex-PLI 2004) and Evaluation of its Biofidelity at the Component Level and at the Assembly Level, SAE technical paper series, 2005-01-1879.
- [4] International Harmonized Research Activity, Pedestrian Safety Working Group, IHRA/PS/295.
- [5] Kerrigan, J.R., Drinkwater, D.C., Kam, C.Y., Murphy, D.B., Ivarsson, B.J., Crandall, J.R., Patrie, J. (2004) Tolerance of the Human Leg and Thigh in Dynamic Latero-Medial Bending, ICRAASH 2004.
- [6] United Nations, ECE/WP29/GRSP/Informal Working Group on Pedestrian Safety, INF/GR/PS/82.
- [7] Ivarsson, B.J., Lessley, D., Kerrigan, J.R., Bhalla, K.S., Bose, D., Crandall, J.R., Kent, R. (2004) Dynamic Response Corridors and Injury Thresholds of the Pedestrian Lower Extremities, Proc. International IRCOBI Conference on the Biomechanics of Impacts, pp. 179-191.
- [8] International Harmonized Research Activity, Pedestrian Safety Working Group, IHRA/PS/309.

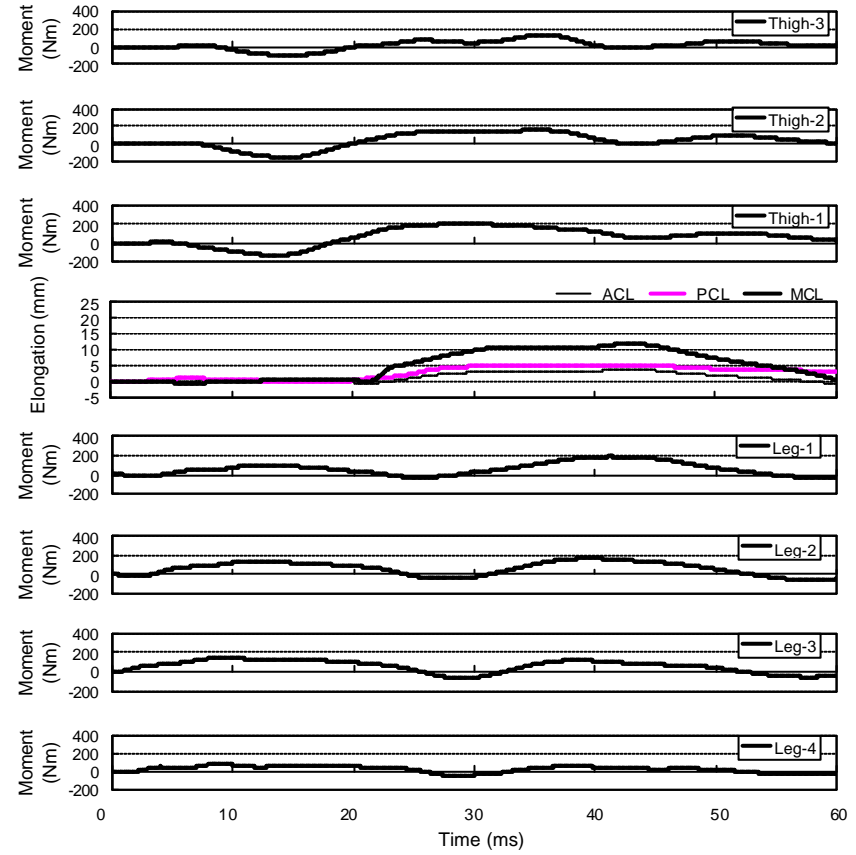
- [9] Kennedy, E.A., Hurst, W.J., Stitzel, J.D., Cormier, J.M., Hansen, GA., Smith, E.P., Duma, S.M. (2004) Lateral and Posterior Dynamic Bending of the Mid-Shaft Femur: Fracture Risk Curves for the Adult Population, Stapp Car Crash Journal, Vol. 48, pp. 22-51.

Appendix A: Measured Waveforms

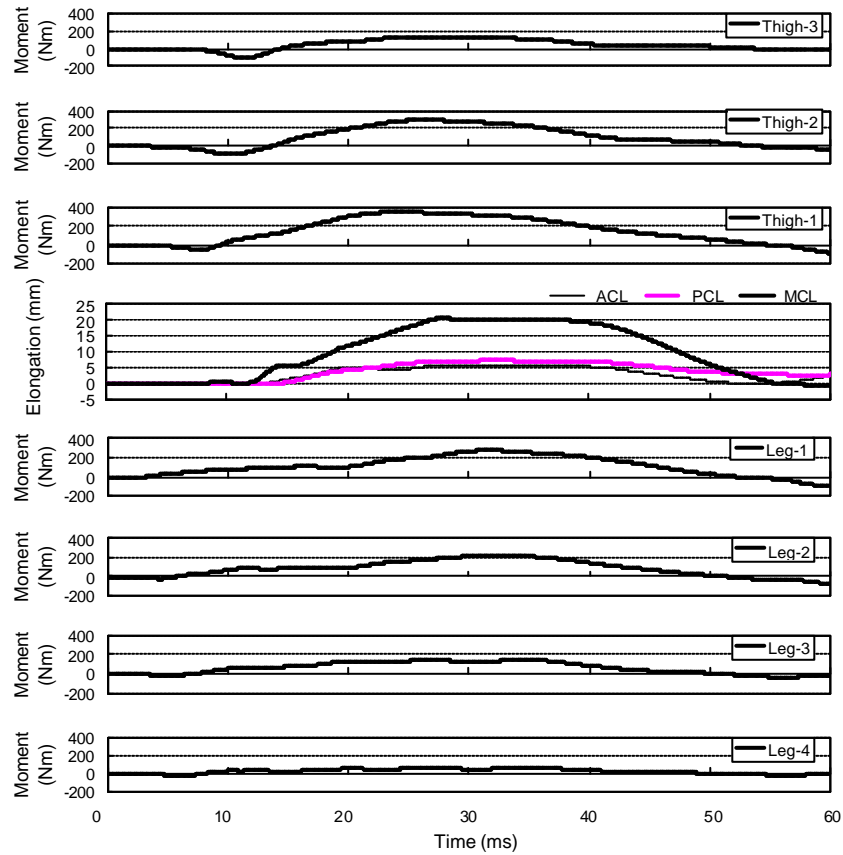
Sedan 1 (Original), Flex-PLI 2004



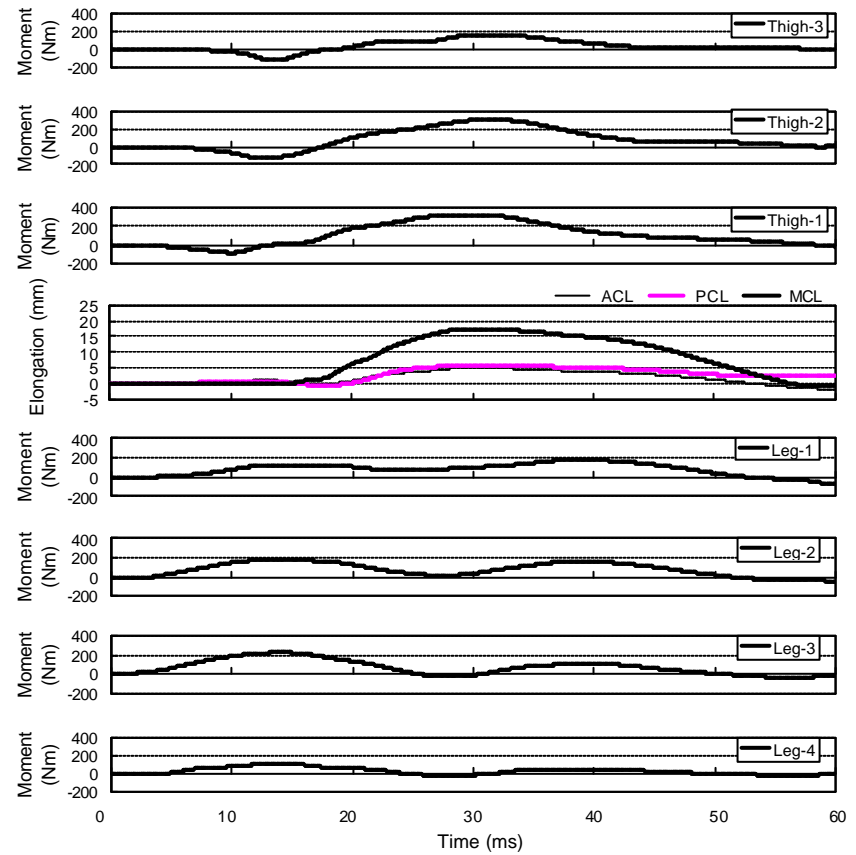
Sedan 1 (Modified), Flex-PLI 2004



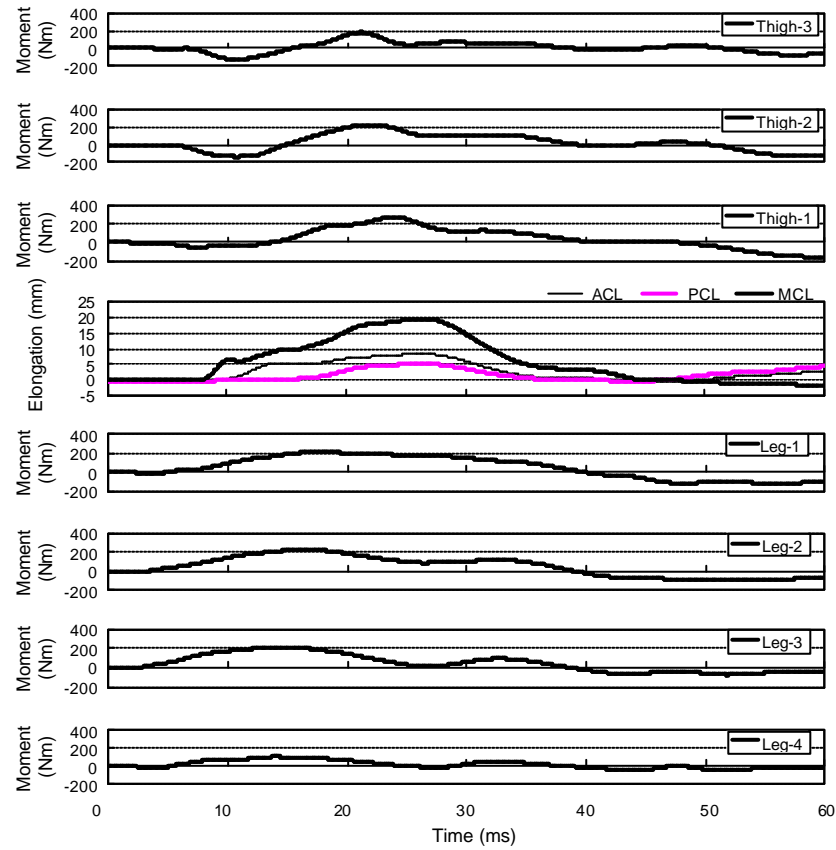
Sedan 2 (Original), Flex-PLI 2004



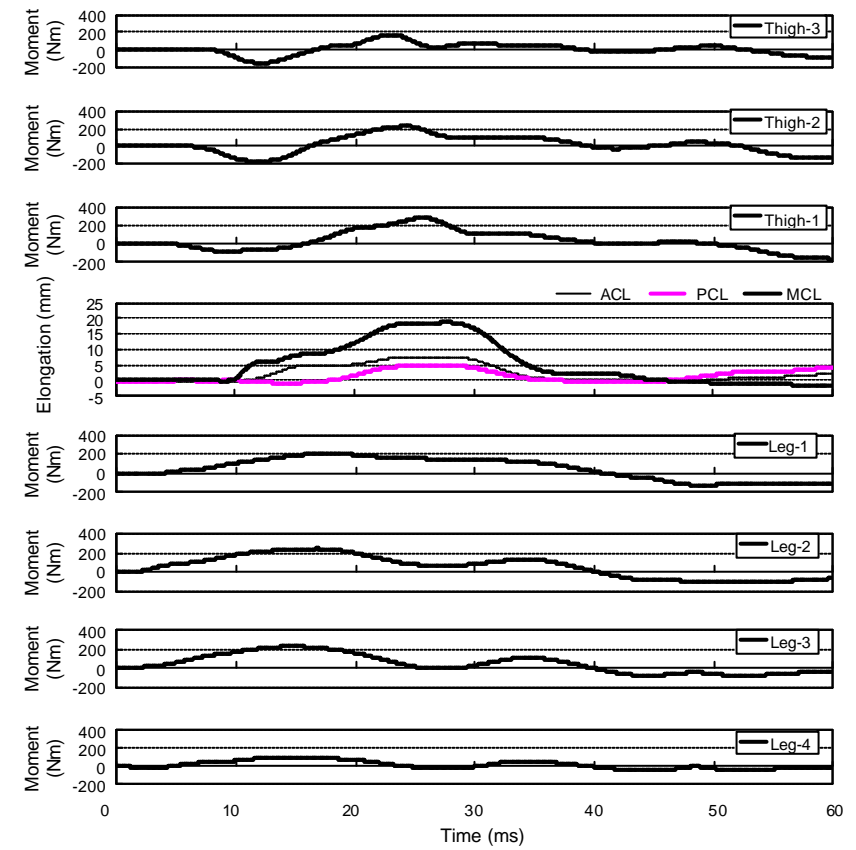
Sedan 2 (Modified), Flex-PLI 2004



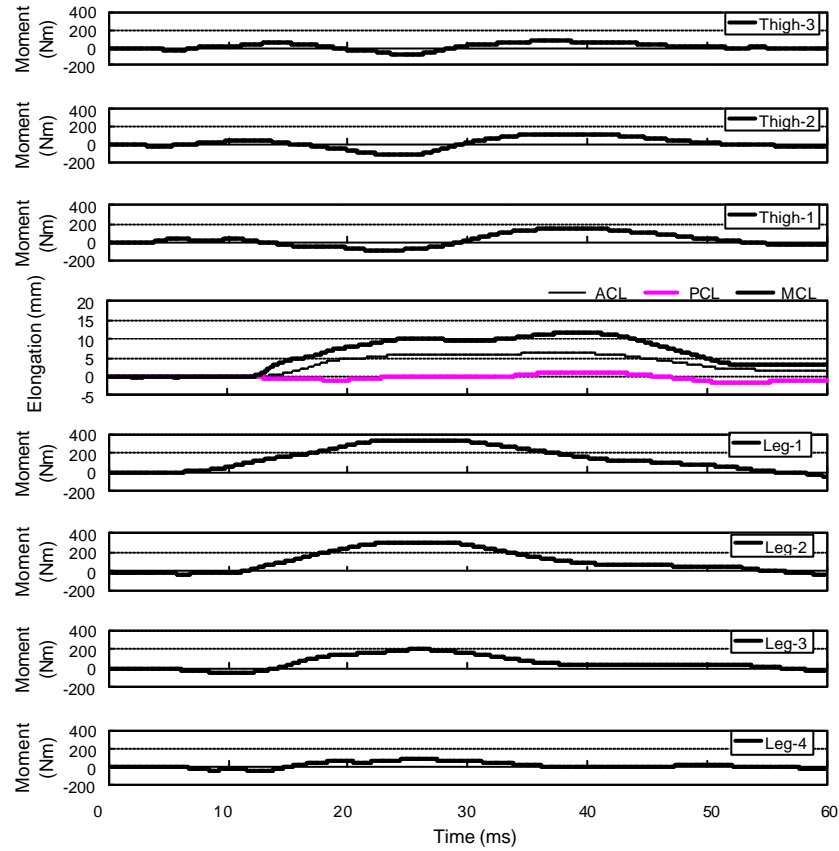
Minivan (Original), Flex-PLI 2004



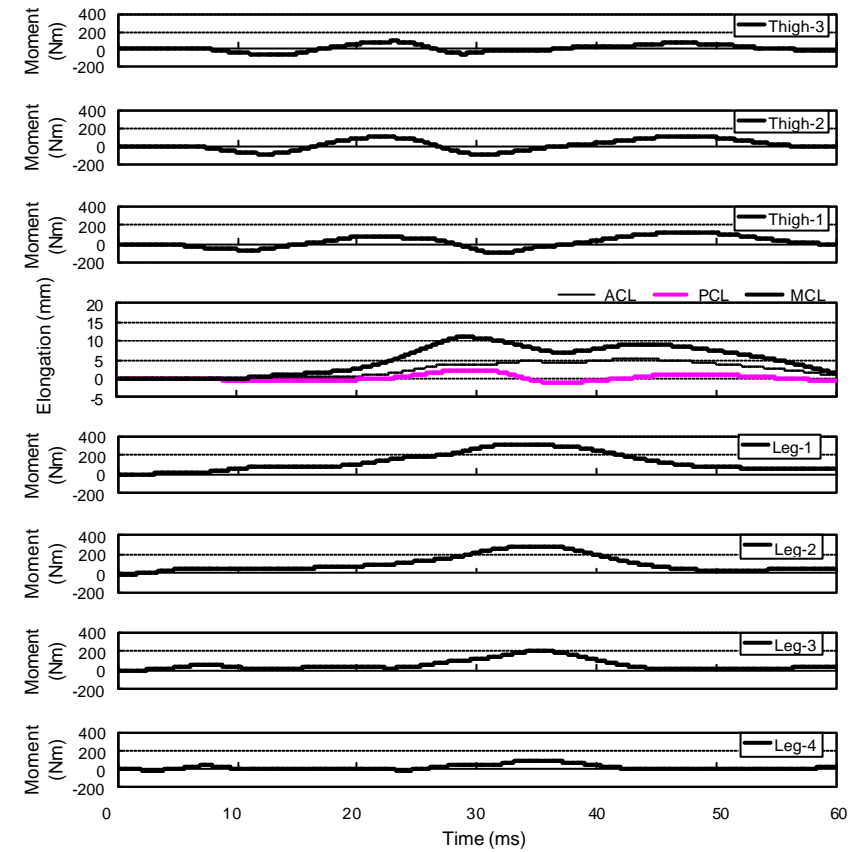
Minivan (Modified), Flex-PLI 2004



SUV (Original), Flex-PLI 2004

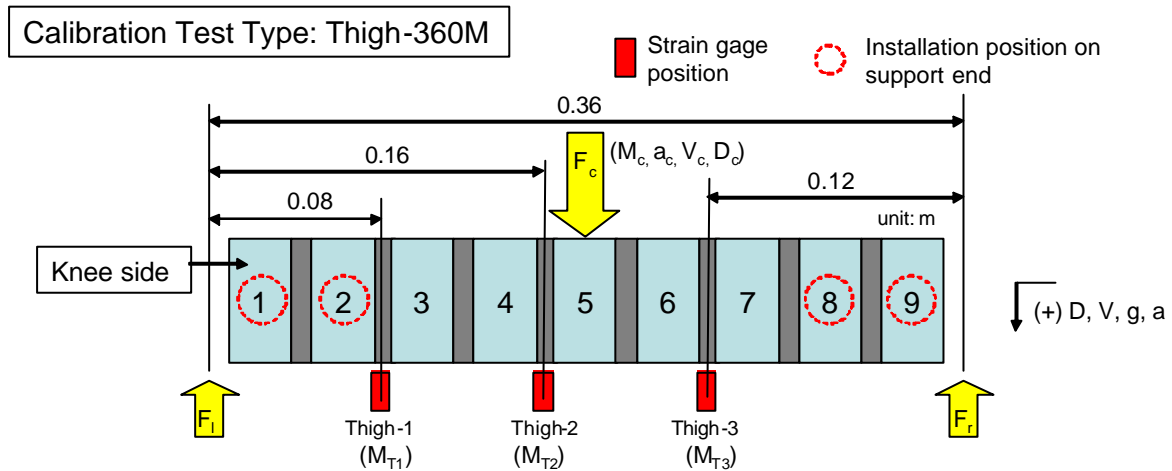
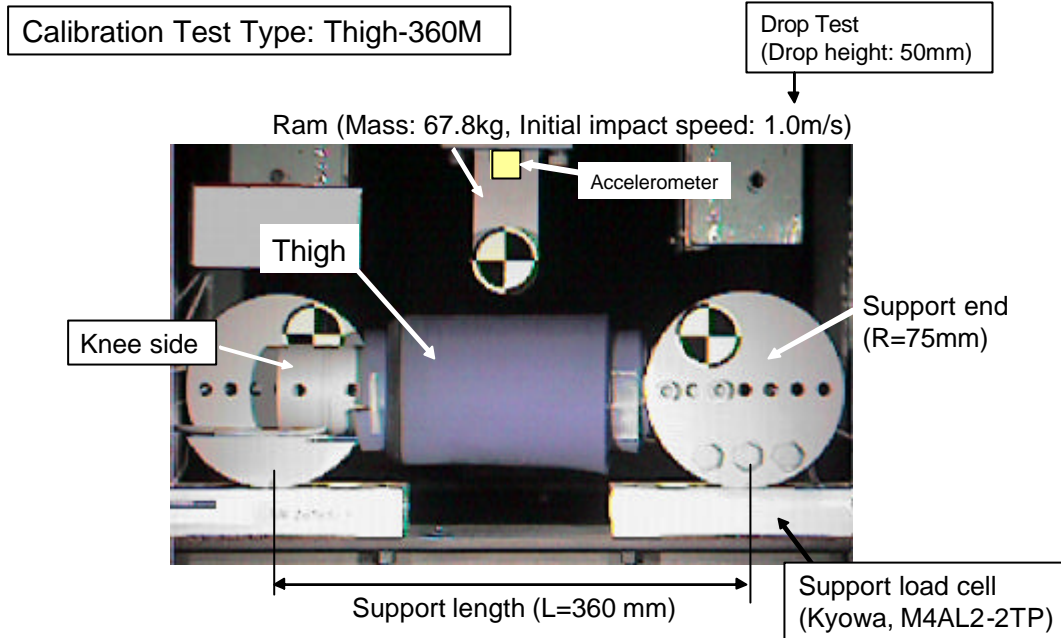


SUV (Modified), Flex-PLI 2004



Appendix B:
Dynamic Component Calibration Test Procedure
for Thigh and Leg of Flex-PLI 2004

B1: Dynamic Component Calibration Test Procedure for Thigh of Flex-PLI 2004



Bending moment estimation equation at loading center

$$M_c(t) \cong \left| \frac{F_l(t) \times F_r(t)}{F_l(t) + F_r(t)} \times 0.36 \right|$$

Deflection estimation equation at loading center

$$D_c(t) \cong V_{c_init} t + \frac{1}{2} g t^2 + \iint a(t) dt$$

Bending moment estimation equations at strain gage positions

$$M_{T1}(t) \cong |F_l(t) \times 0.08|$$

$$M_{T2}(t) \cong |F_l(t) \times 0.16|$$

$$M_{T3}(t) \cong |F_r(t) \times 0.12|$$

M : Bending Moment (Nm)

F : Force (N)

D : Deflection (m)

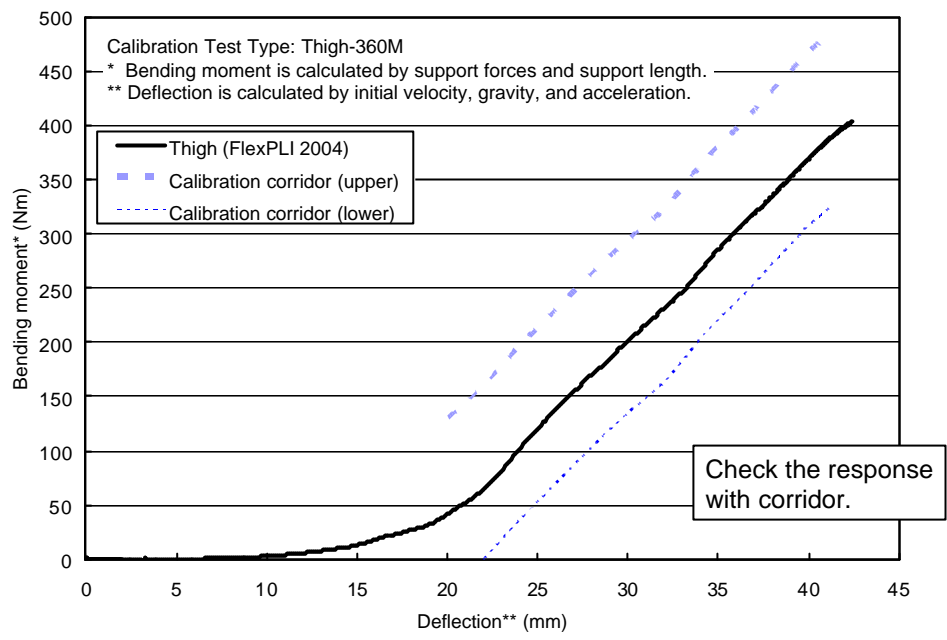
V : Velocity (m/s)

g : Gravity (m/s²)

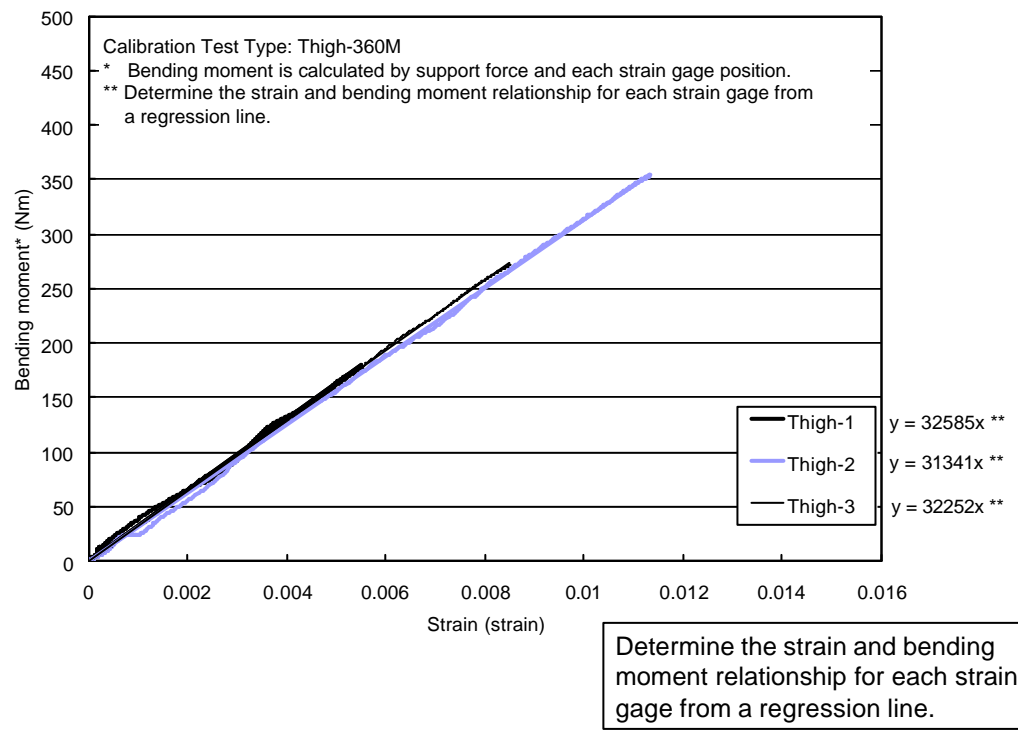
a : Acceleration (m/s²)

t : time (s)

Step 1: Check the Bending moment and Deflection characteristics of thigh - Comparison with a calibration corridor -



Step 2: Obtain calibration values derived from Strain and Bending moment relations

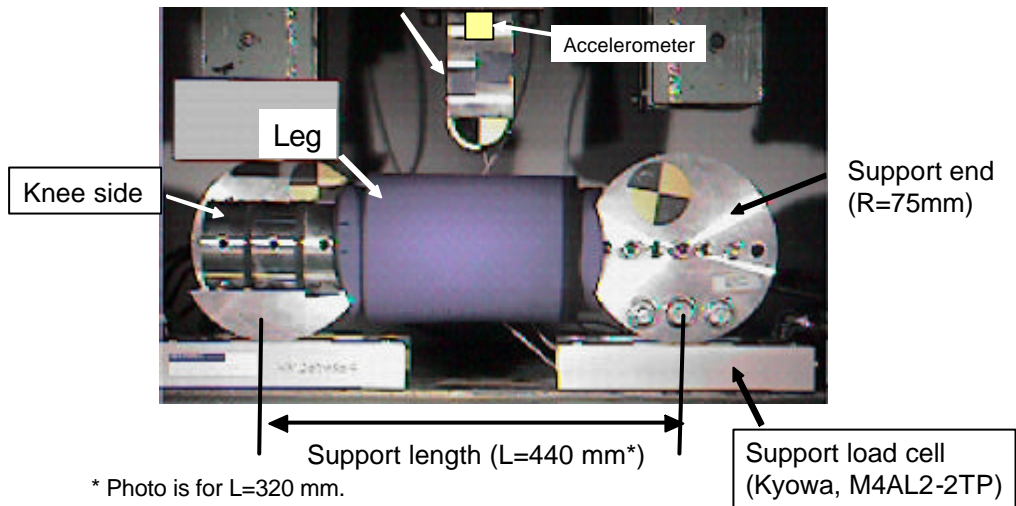


B2: Dynamic Component Calibration Test Procedure for Leg of Flex-PLI 2004

Calibration Test Type: Leg-440M

Drop Test
(Drop height: 50mm)

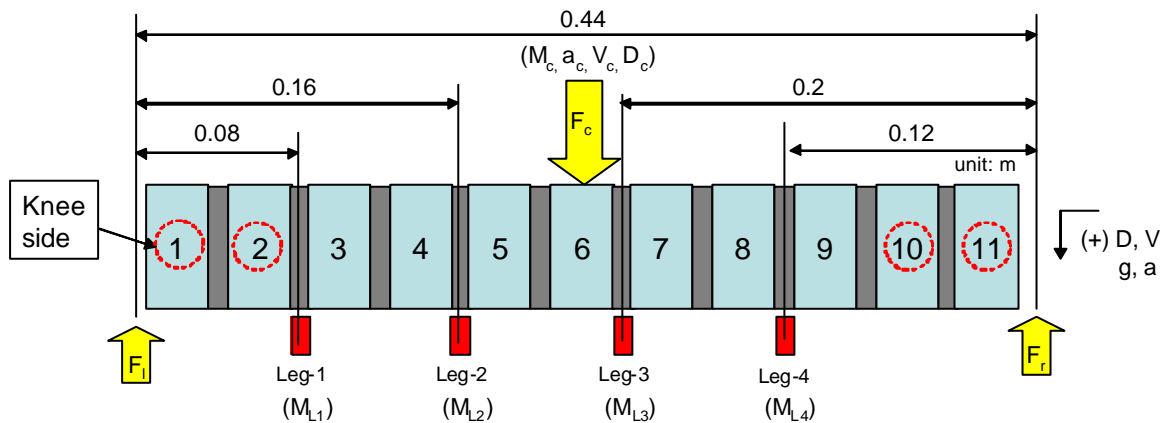
Ram (Mass: 67.8kg, Initial impact speed: 1.0m/s)



Calibration Test Type: Leg-440M

Strain gage position

Installation position on support end



Bending moment estimation equation
at center of loading

$$M_c(t) \cong \left| \frac{F_l(t) \times F_r(t)}{F_l(t) + F_r(t)} \times 0.44 \right|$$

Deflection estimation equation
at center of loading

$$D_c(t) \cong V_{c_init} t + \frac{1}{2} g t^2 + \iint a(t) dt$$

Bending moment estimation equations
at strain gage positions

$$M_{L1}(t) \cong |F_l(t) \times 0.08|$$

$$M_{L2}(t) \cong |F_l(t) \times 0.16|$$

$$M_{L3}(t) \cong |F_r(t) \times 0.20|$$

$$M_{L4}(t) \cong |F_r(t) \times 0.12|$$

M : Bending Moment (Nm)

F : Force (N)

D : Deflection (m)

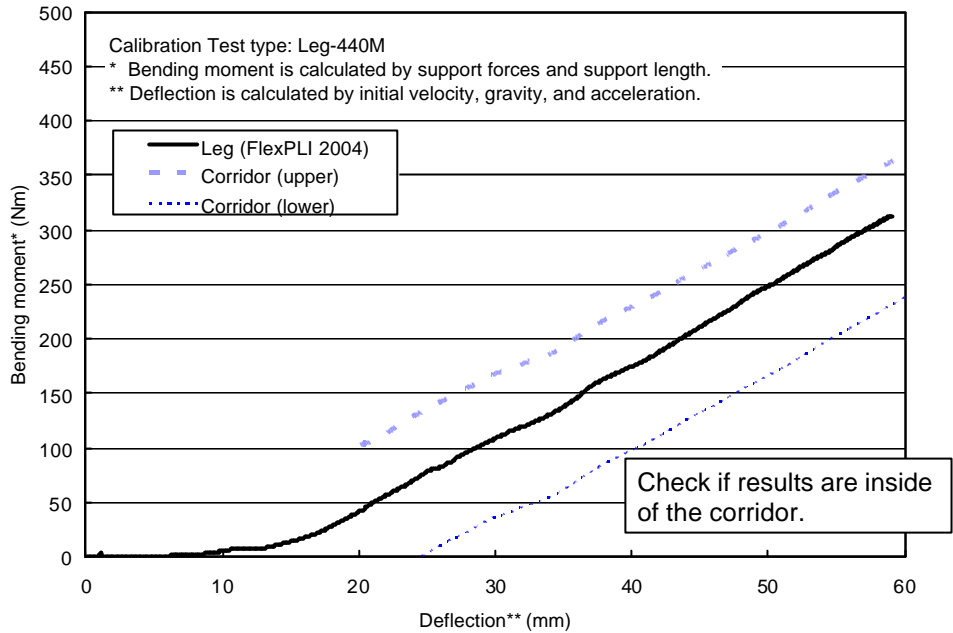
V : Velocity (m/s)

g : Gravity (m/s²)

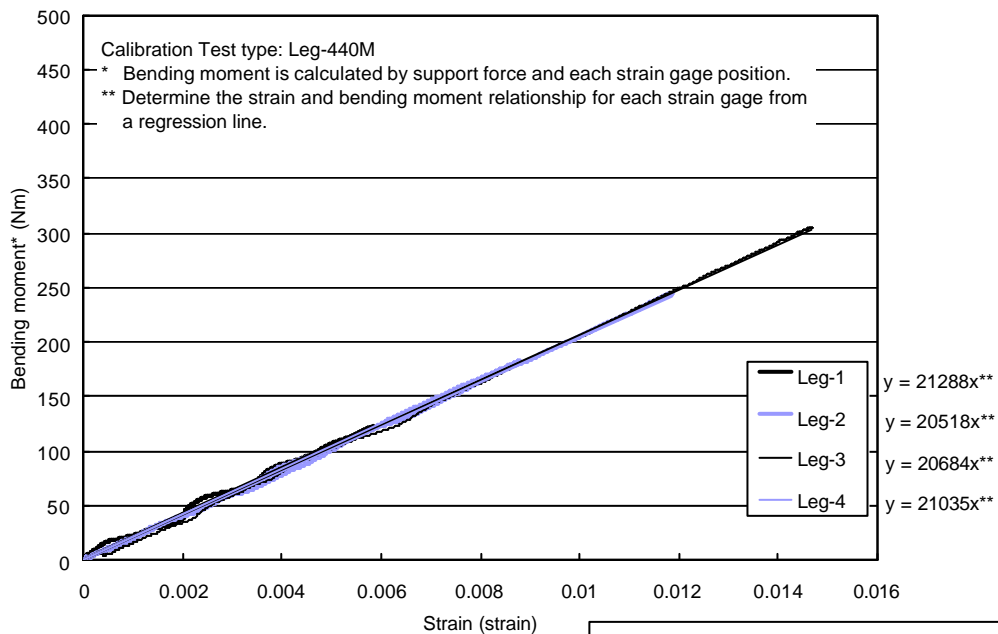
a : Acceleration (m/s²)

t : time (s)

**Step 1: Check the Bending moment and Deflection characteristics of leg
- Comparison with a calibration corridor -**



Step 2: Obtain calibration values derived from Strain and Bending moment relations



Determine the strain and bending moment relationship for each strain gage from a regression line.

KINEMATIC CORRIDORS FOR PMHS TESTED IN FULL-SCALE PEDESTRIAN IMPACT TESTS

Jason R. Kerrigan
Drew B. Murphy
D. Chris Drinkwater
Check Y. Kam
Dipan Bose
Jeff R. Crandall

University of Virginia Center for Applied Biomechanics
United States
Paper Number 05-0394

ABSTRACT

A primary function of pedestrian dummies is biofidelic representation of whole body kinematics. To assess the biofidelity of a pedestrian dummy, corridors for the kinematic response of post-mortem human surrogates (PMHS) tested in full-scale pedestrian impact tests were developed. Three PMHS were tested in full-scale pedestrian impact tests using a late-model small sedan with an impact velocity of 40 km/h. Three additional tests using the Polar-II dummy were conducted in identical conditions to those used in the PMHS tests.

All impacts were conducted with the PMHS or dummy positioned laterally at the center line of the vehicle, in a mid-stance gait position, with the struck-side limb positioned posteriorly and the upper limbs placed anterior to the torso. Initially supported by a harness, each surrogate was released prior to impact and was unconstrained through a 250 ms interaction with the vehicle.

Using photo targets mounted at the equivalent locations of the head center of gravity (CG), top of the thorax, thorax CG, and pelvis CG, the kinematic response of the pedestrian surrogates was evaluated using parametric trajectory data. To account for simultaneous variability in multiple kinematic parameters, boxed-corridors based on a percentage of trajectory path length were developed from the trajectory data. Given the significance of head impact for pedestrian injury outcome, head velocity-time corridors were also developed.

Comparing dummy response and PMHS corridors, the Polar-II generally replicated the complex kinematics of the PMHS and demonstrated good overall biofidelity. Greater sliding up the hood by the PMHS, and lack of neck muscle tension in the PMHS have been identified as potential causes for differences in the length and shape of body segment trajectories. More testing is necessary to assess the effects differences in pre-test orientation, surrogate stature, and clothing will have on surrogate response.

INTRODUCTION

Pedestrians killed in pedestrian-vehicle collisions represent 65% of all road traffic fatalities worldwide (World Bank 2001). While the percentage of pedestrian fatalities is much higher in developing nations than in industrialized nations, pedestrians still make up 11%-30% of road traffic fatalities in the US, the European Union, and Japan (NHTSA, 2003, NPA, 2003, CARE, 2002).

To combat this serious public health problem, researchers have been developing pedestrian surrogates like pedestrian dummies and pedestrian computational models to further understand pedestrian injury mechanisms and to evaluate the level of safety afforded to pedestrians by all motor vehicles. Numerous studies presenting data from pedestrian impact tests with different pedestrian dummies were published in the late 1970's and early 1980's. More recently, most of the public research regarding the development and validation of pedestrian dummies has been with regard to one particular dummy, the Polar dummy. Development of the Polar dummies began in the late 1990's by Honda R&D Co., Ltd. in collaboration with GESAC Inc. and the Japan Automobile Research Institute.

The first version of the Polar dummy, the Polar-I, was developed by combining and modifying components from the Hybrid III and THOR dummies (Akiyama *et al.* 1999a and 1999b, Huang *et al.* 1999). Modifications made to the Hybrid III and THOR parts included additional foam in the knee joint flesh, a compliant element in the tibia, and two additional joints to the thoracic/lumbar spine to permit more lateral bending compliance spine. Full-scale tests and component-level tests were performed to assess the biofidelity of the dummy (Akiyama *et al.* 1999a and 1999b, Huang *et al.* 1999).

Based on the results of computer simulations and experiments, modifications to the femur, knee joint and lower extremity flesh were made (Huang *et al.* 1999). An additional series of full-scale pedestrian tests was performed. This new version of the dummy, Polar-I.2,

provided a more biofidelic response than the Polar-I version, but additional improvements were required for biofidelity at vehicle speeds of 32 km/h.

A new version of the dummy, called Polar-II (Figure 1), was developed to improve the kinematic response of the dummy (Akiyama *et al.* 2001). A new knee joint (Figure 1) with human-like geometry and a new flexible tibia were added to improve lower extremity biofidelity. The shoulder joint was also modified to decrease the stiffness for motions within the normal human range. Additionally more instrumentation was added to obtain kinetic data in the lower extremity and deflection data in the thorax and abdomen (Akiyama *et al.* 2001). Full-scale pedestrian impact tests were performed on the Polar-II with six different sized vehicles to further understand how differing vehicle shapes affect pedestrian kinematics (Akiyama *et al.* 2001 and Okamoto *et al.* 2001).



Figure 1. Polar-II dummy with human-like knee joint inset. (Akiyama, 2001)

The biofidelity of the Polar dummy has been evaluated by comparing its response in full-scale impact tests to the response of PMHS in similar experiments (Akiyama *et al.* 1999a and 1999b, Huang *et al.* 1999, Akiyama *et al.* 2001). The experiments on the PMHS, discussed in Ishikawa *et al.* (1993), were performed using a similar, not identical, vehicle as the full-scale tests performed using the Polar-II dummy (Akiyama 2001).

Numerous other studies have documented the results of full-scale pedestrian impact testing on hundreds of PMHS. While the previous studies provide valuable information regarding full-scale test methodology, many of the tests were performed on vehicles not representative of the current vehicle fleet (Kam *et al.* 2005). Additionally, many of the previous full-scale impact test studies do not provide kinematics

data in enough detail to permit use of the data in validation studies (Kam *et al.* 2005).

Thus, there is a need for additional study of full-scale pedestrian impact tests on PMHS with late-model vehicles to develop detailed kinematics data. For further assessment of the biofidelity of the Polar-II, full-scale pedestrian impact tests should ideally be performed using identical test conditions so that the Polar-II response can be directly compared to the PMHS response. The goals of this study are threefold:

- to perform full-scale pedestrian impact tests on PMHS with late-model small sedan,
- to develop kinematic response corridors for upper-body trajectories, and
- to evaluate the response of the Polar-II dummy, tested using identical conditions as in the PMHS tests.

FULL-SCALE TEST METHODOLOGY

Six full-scale pedestrian impact experiments were performed with a small sedan. Three tests were performed using PMHS and three tests were performed using the Polar-II dummy. The test conditions remained identical in all six tests to minimize variability in the results and facilitate a biofidelity evaluation of the Polar-II dummy.

Sled System

The vehicle used in all six tests was a recent model small sedan. A scaled dimensioned drawing of the center line contour for the front of the vehicle is given in Figure 2. The vehicle was cut in half at the B-pillar and mounted on a sled fit to the deceleration sled system at the UVA Center for Applied Biomechanics. A hydraulic decelerator was positioned at the impact end of the sled tracks to stop the vehicle at the end of the surrogate (dummy or PMHS) interaction.

Since the sled tracks at UVA are above ground, an additional sled was necessary to serve as the ground level surface on which the pedestrian surrogate (PMHS or dummy) would be positioned. Thus a small, light sled was constructed to hold two pieces of plywood used to simulate the ground surface. Plywood has been shown to possess frictional characteristics similar to road surfaces (Kam *et al.* 2005). This “pedestrian sled” was positioned before each test in a location that permitted the vehicle to interact with the pedestrian surrogate for approximately 250 ms between initial bumper contact and vehicle deceleration (Figure 3). For more discussion on why a 250 ms interaction time was chosen, see Kam *et al.*(2005).

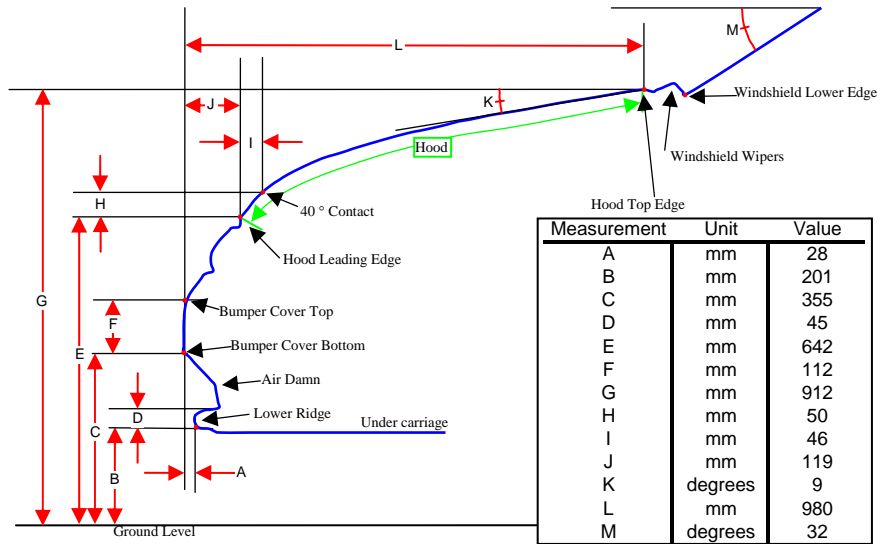


Figure 2. Scaled, dimensioned drawing of the front of the small sedan used in all tests in the current study.

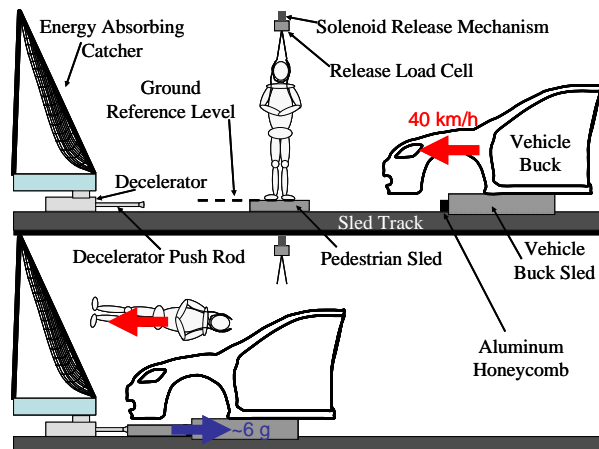


Figure 3. Schematic of full-scale pedestrian impact test system. Not to scale.

The primary objective of the current study was to examine only the interaction of the pedestrian and the vehicle. Secondary contact with the ground, road structures or other vehicles was not studied. Therefore an energy-absorbing catching structure was constructed at the impact end of the sled to catch the pedestrian surrogate, and lay it softly on an energy absorbing bed. The purpose of the catching structure was to reduce the potential to cause additional injuries to the PMHS during vehicle deceleration.

During the impact event, the vehicle sled was accelerated to 40 km/h, and it subsequently struck the pedestrian surrogate. Approximately 50 ms later, the vehicle impacted and accelerated the pedestrian sled (Figure 3). By this time, the pedestrian surrogate had long since relinquished contact with the ground level surface of the pedestrian sled. About 250 ms after the

vehicle initially contacted the pedestrian surrogate, the pedestrian sled, now coupled to the vehicle sled, contacted the decelerator, slowing them to a stop at a rate of approximately 6 g. At this time the pedestrian surrogate was lofted forward into the energy absorbing catching structure (Figure 3). For more information regarding the UVA sled system, and how it is configured for full-scale pedestrian collisions, see Kam *et al.* (2005).

PMHS Preparation

The criteria used to select the three PMHS (Table 1) used in this study include stature, weight, and cause of death. Specimens were chosen that had a stature between 170 and 175 cm, a weight between 50 and 85 kg and a cause of death that didn't involve traumatic injury. Pre-test CT scans were used to confirm the absence of pre-existing fractures, lesions and other bone pathology in all skeletal structures. All PMHS were preserved by a combination of refrigeration and freezing (Crandall, 1994). All PMHS were obtained and treated in accordance with the ethical guidelines approved by the Human Usage Review Panel, National Highway Traffic Safety Administration, and all PMHS testing and handling procedures were approved by the University of Virginia (UVA) institutional review board.

Approximately four days prior to testing, each PMHS was removed from the freezer and allowed to thaw at room temperature over a three day period. Approximately one day before each test, the specimen preparation began. During preparation, a series of hardware mounts, used to fix sensor cubes to PMHS osseous structures, were fix on each specimen.

Table 1. Description of the 3 PMHS used in this study.

Test #/PMHS ID	C-1/196	C-2/191	C-3/220	Average	Range
Age at Death/Gender	61/F	70/M	62/M	64	9
Weight (kg)	80.7	54.4	81.6	72.3	27.2
Post-Mortem Stature ¹ (mm)	1727	1701	1752	1727	51
Stretched Stature ² (mm)	1870	1785	1859	1838	85
Height Change ³ (%)	8.3%	4.9%	6.1%	6.4%	3.3%
Cause of Death	Ovarian Cancer/ Pulmonary Edema	Cardiac Arrest	Liver Cancer		

1- Height measured post-mortem with each PMHS lying supine.

2- Height measured by scaling a video image of PMHS in pre-test position.

3. Height change is a measure of how much the stature of each PMHS increased by vertically supporting the PMHS by the upper body.

Most notably mounts were installed at the head near the posterior projection of the head center of gravity (CG), on the first thoracic vertebra (T1) where the neck meets the thorax, on the eighth thoracic vertebra (T8) near the thorax CG, and on the sacrum near the pelvis CG. Mounts on the head, T1 and sacrum were used to hold one type sensor cube (44 mm x 44 mm x 31 mm, 180g), and the one at T8 was used to hold a smaller sensor cube (21 mm x 21 mm x 15 mm, 13 g).

On the head, the mount was a 52 x 52 mm piece of 3.2 mm thick aluminum plate attached with bone screws directly to the posterior skull. On T1, the mount was a “U”-shaped aluminum structure that straddled the spinous processes of the vertebral column and bolted directly to the vertebral body of the T1 vertebra. The mount at T8 was simply a deep threaded bone screw with a 20 x 20 mm 3.2 mm thick aluminum plate brazed to its head. The mount was screwed directly into the vertebral body just to the right of the spinous process. The mount on the sacrum was a 35 mm x 90 mm x 3.2 mm thick piece of aluminum screwed directly to the sacrum between the second and third sacral foramen with two bone screws.

The location of the head CG was found by first marking the Frankfurt planes on each PMHS’ head. The lateral projections of the head CG were marked at a location 8.5 mm anterior to the trignon and 25% of the vertical distance from the Frankfurt plane to the top of the head above the Frankfurt plane (Robbins, 1983). The posterior projection of the head CG was marked at a location determined by bisecting a head exterior contour that connected the two lateral projections of the head CG. If the head instrumentation mount could not be mounted at this location due to skull curvature, the head instrumentation mount was attached superior to this point. In these cases, a screw was used to mark the posterior projection of the head CG.

After preparation each specimen was returned to the refrigerator until the day of the test. On the day of the test, the specimen was removed from the

refrigerator to allow the core body temperature to equilibrate with the room temperature (22 °C ± 3 °C) prior to the test. At this time the sensor cubes were mounted to the specified locations using screws. The specimens were clothed in a semi-permeable TYVEK[®] shirt and pants interiorly, a cotton/elastic blend shirt and pants exteriorly, and a new pair of athletic shoes (Corey, Athletic Works, from Wal-Mart Stores Inc., Little Rock, AK).

A wireless data acquisition system (TDAS G5, DTS, Seal Beach, CA), used to sample the data from the instrumentation, was padded and inserted into a cylindrical dry-bag with radius 9 cm and length 32 cm (3.4 kg with the data acquisition system). The bag was attached to the PMHS posteriorly over the lumbar spine using plastic tie-wraps (see Figure 5).

Dummy Preparation

The dummy was prepared as specified by its developers. The dummy was clothed in the standard shoes, standard shorts, and all of the flesh and jacket was positioned appropriately.

The dummy was equipped with similar external sensor cubes as used on the top of the thorax and pelvis of the PMHS. On the head however, no external instrumentation was used. Finally the instrumentation bag used in the PMHS was mounted to the dummy’s lumbar area via plastic tie-wraps.

Support

After the dummy and PMHS were prepared, they were outfitted with harness straps to facilitate positioning for the test. In the dummy, the harness consisted of a rope that was tied through the eye bolts of the shoulders on the dummy (Figure 4). The harness for the PMHS consisted of two sections of seatbelt webbing. One longer piece (the shoulder strap) was directed under the arms of the PMHS anteriorly and across the posterior thorax. The second seatbelt strap

was split longitudinally in the middle so that half of the strap could be positioned under the PMHS chin and the other half could slip under the occiput (Figure 4).

At this time, the surrogate was hoisted into position over the pedestrian sled. The harness was then transferred to the release hardware. It should be noted that the lengths of the two harness straps used in the PMHS tests were such that the majority of the weight of the PMHS was being supported by the shoulder strap. The head strap is only used to orient the head in a neutral position prior to the test.

The release hardware consisted of a plate rigidly mounted to the laboratory roof, with a threaded rod going through the plate. At the end of the threaded rod, a tension load cell was attached to determine the timing of surrogate release (Figure 4). A solenoid release mechanism, mounted below the load cell, was used to release the support harness just prior to vehicle impact.

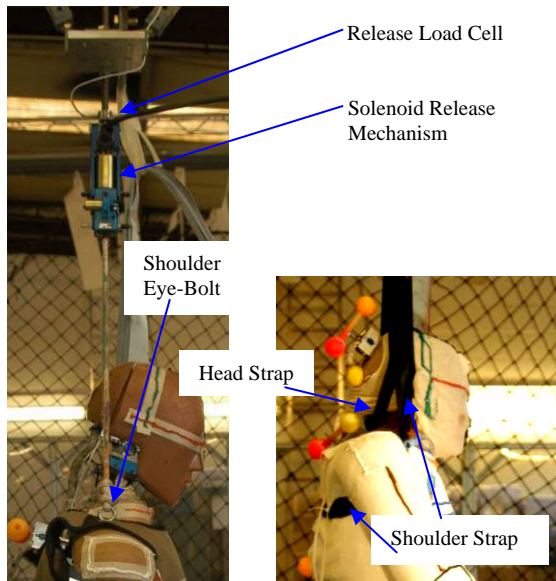


Figure 4. Support methods for both the dummy (left) and PMHS(right). Note that the shoulder strap used with the PMHS (right) mostly obscures the head strap. Only half of the split strap can be seen as it passes under occiput of the PMHS.

Positioning

Data from the pedestrian crash data study (PCDS) suggest that the majority of pedestrians are struck laterally with their lower extremities positioned in a gait-like position (Kam *et al.* 2005). Thus, all surrogates in this study were positioned laterally at the vehicle center line in a mid-stance gait position (Figure 5). Since arm position can potentially affect upper body kinematics to a level that would reduce the severity of thoracic and head loading (Kam *et al.* 2005), the arms were bound at the wrists anterior to the

surrogate. The right wrist was placed farthest from the body and the left wrist was placed closest to the body when the wrists were bound. This positions the struck-side elbow slightly anterior to the thorax and thus reduces the potential for the arm to affect the upper body kinematics (Kam *et al.* 2005).

The height of the dummy, as measured after positioning in each test, varied between 173 cm and 174 cm. The standing height of each PMHS after positioning is given in Table 1 as the “stretched stature”.

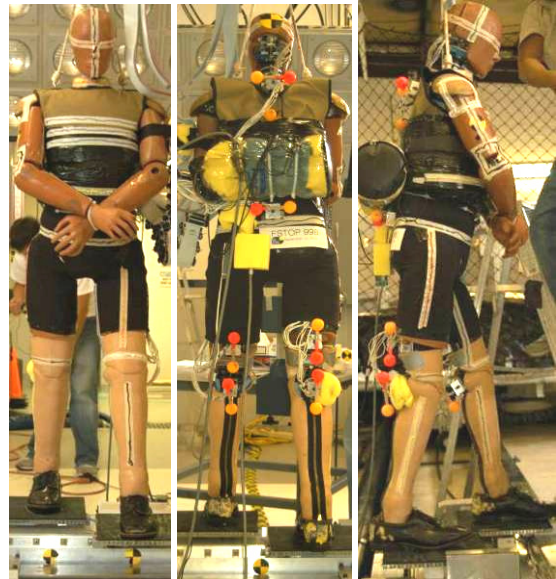


Figure 5a. Typical position of the dummy prior to each test.



Figure 5b. Typical position of the PMHS immediately prior to each test.

Test Event

After positioning of the surrogate was complete, the vehicle sled was propelled down the tracks toward the pedestrian. The vehicle sled passed an inductive sensor on the track that triggered the release of the surrogate between 19 and 26 ms before initial bumper contact (Table 2). The vehicle speed was recorded using a similar sensor, and was approximately 40 km/h in each test (Table 2).

After the vehicle struck the pedestrian surrogate, then impacted and accelerated the pedestrian sled, and approximately 200 ms later, both sleds contacted the decelerator. This caused the vehicle to decelerate, and pedestrian surrogate to be lofted forward into the catching mechanism. After the test the wrap around distance (WAD) to head strike was measured (Table 2).

KINEMATICS MEASUREMENT

Analysis of pedestrian surrogate kinematics during the impact event were performed using high speed video images taken from an off-board camera on the driver's side of the vehicle during all of the tests. The camera used to capture the high speed video (Phantom V5.0, Vision Research, Wayne, NJ) sampled 1024 pixel by 1024 pixel (1.0 mega pixel) images at 1000 Hz during all of the tests.

The camera's field of view stretched 3.78 m horizontally from approximately 30 cm up the tracks from the positioned surrogate to about 60 cm down past the tip of the decelerator push rod. The field of view of the imager was sufficient to permit motion tracking of all points on each surrogate and the vehicle from 40 ms prior to initial contact, to the time that the vehicle began to decelerate. High speed video images (at 20 ms intervals) from a representative dummy and PMHS test are given in Figure 6.

Table 2. Vehicle velocity, surrogate release time and wrap around distance (WAD) to head strike for all six tests.

	Test #	Vehicle Velocity km/h	Release Time ¹ ms	Head Strike (WAD) mm
Dummy	D-1	39.69	-19.6	1930
	D-2	40.02	-26.3	1940
	D-3	39.88	-21.6	1970
PMHS	C-1	39.75	-20.2	2410
	C-2	39.56	-25.6	2200
	C-3	39.88	-24.7	2320

1-Time zero is defined as the initial contact between the vehicle's bumper and the surrogate's lower extremity

Photo Targets

Since no external instrumentation mount was used on the dummy's head, a quadrant type photo target was mounted on the dummy's head at the posterior projection of the CG for all tests (as determined by the drawing of the head).

Most of the other photo targets used were dumbbell-type targets consisting of two 38 mm diameter table tennis balls, painted in contrasting colors, mounted at both ends of a wooden rod (63.5 mm in length). Each photo target was fixed to the outer surface of each sensor cube with a piece of threaded rod. The dumbbell photo targets were positioned so that the center of the wooden rod was directly over the center of the sensor cube (and thus directly over the center of the mount location) and approximately 38 mm from the sensor cube's outer face (Figure 7).

Dumbbell-type photo targets were mounted to the sensor cubes on the dummy near the pelvis CG, and at the top of the thorax (T1). On the PMHS, dumbbell-type photo targets were mounted to sensor cubes at the head, T1, and pelvis.

A single 38 mm table tennis ball was used as a photo target at the thorax CG for both the Polar-II and PMHS. In the Polar-II, a specially designed mount was installed near the CG of the thorax that permitted the ball (attached to a plastic tube) to be positioned directly over the posterior projection of the thorax CG point (Figure 7). For the PMHS, duct tape was added over the sensor cube and the ball was attached to the duct tape with foam tape.

Whenever possible the sensor cube mounted on the PMHS head was mounted at the posterior projection of the head CG (permitting the dumbbell type photo target mounted to the cube to be used to track head motion). However, when the instrumentation mount had to be mounted superior to this point, table tennis ball was screwed directly to the PMHS skull at the posterior projection of the CG point. In all cases, all of the targets were rigidly secured to either the steel structure of the dummy or osseous structures in the PMHS.

Phototarget Tracking

The motion of all of the photo targets (head CG projection, T1 or top of thorax, T8 or thorax CG projection and pelvis CG projection for both the dummy and the PMHS) were tracked throughout the impact event (Figure 8). In all cases that the motion of a dumbbell type photo target was measured, the motions of both target balls were measured.

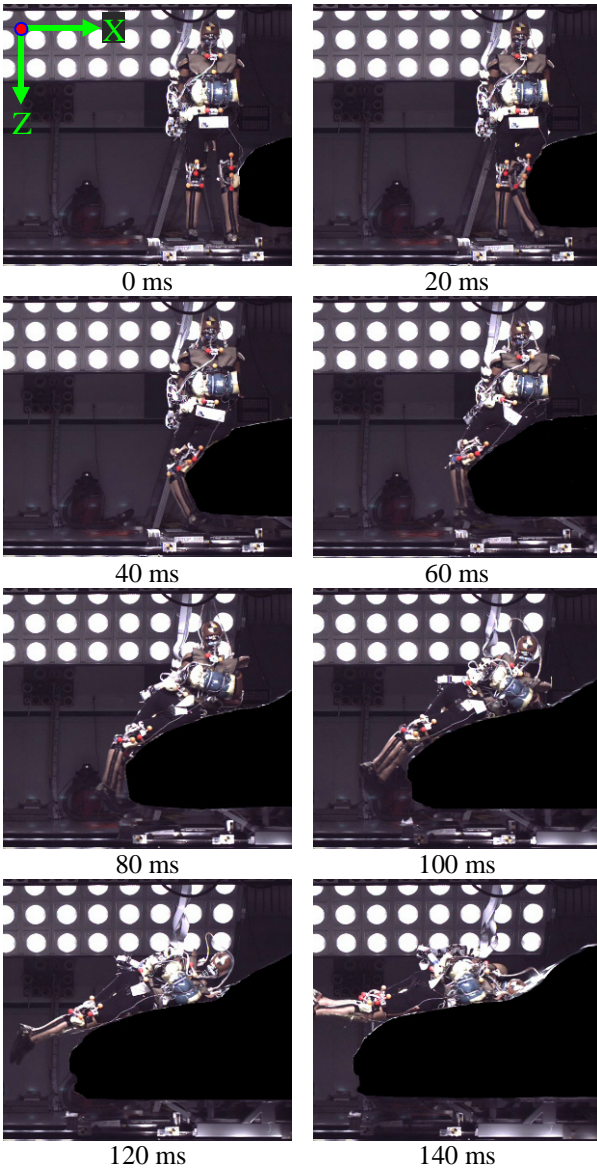


Figure 6a. High speed video images of a typical dummy test.

The motion of each photo target was measured by recording the location, in pixels, of each photo target from high speed video images that were re-sampled at 250 Hz. The time of initial contact between the vehicle bumper and the surrogate's lower extremity was defined to be $t=0$. The first video analysis frame was 40 ms prior to $t=0$, at $t=-40$ ms.

The time of head strike was determined to mark the end of the time interval of interest for computing kinematic trajectory data. In each test the time of head strike was determined by visual examination of the video data. Since the trajectory data are only sampled at 250 Hz, the time of head strike was then rounded to the nearest 4 ms so that it corresponded with an analysis frame (Table 3). To facilitate accurate head

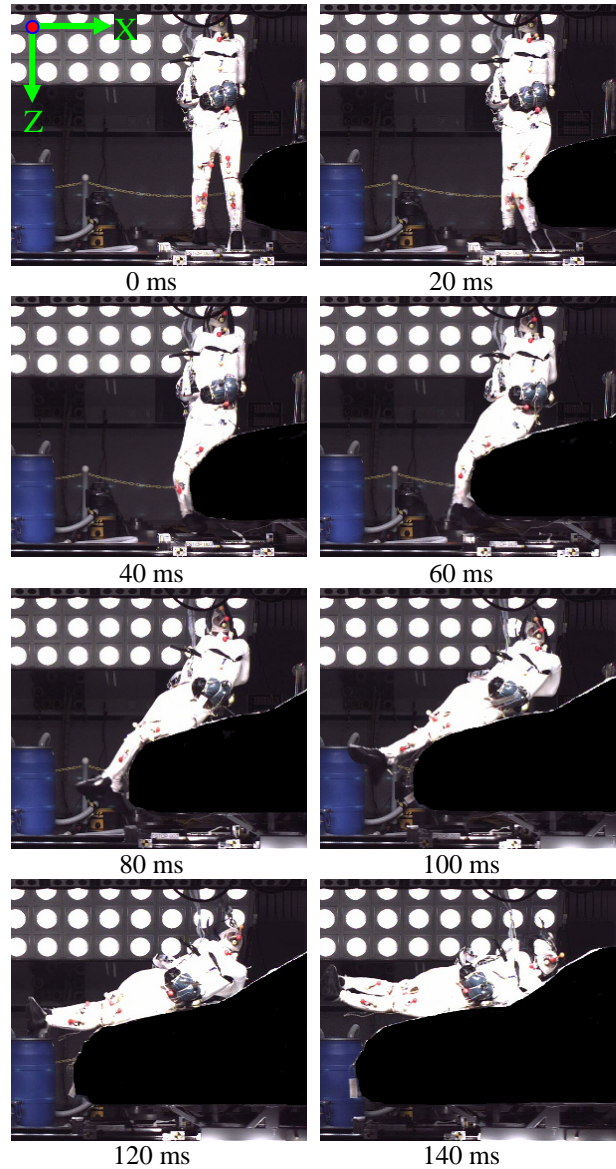


Figure 6b. High speed video images of a typical PMHS test

velocity measurement during head strike, the last video frame that was digitized was the frame 20 ms after the head-strike frame (Table 3).

Data Analysis

For the discussion of the methodology used to analyze the trajectory data, two coordinate systems must be defined. The frame coordinate system, defined by the view of the high speed imager, is fixed with respect to the laboratory. The x and z directions are defined as the horizontal and vertical axes of the imager frame, respectively. Positive x is to the right (the vehicle travels in the negative x direction) and positive z points down. The motions of all of the photo

targets were tracked in the frame coordinate system. The second coordinate system, the vehicle coordinate system, will be defined later.

To obtain the motion of the center of the dumbbell-type targets, the x and z coordinates (in the frame coordinate system) of each ball on the target were averaged at each sampled frame. Then all of the parametric trajectory signals (each target had $x(t)$ and $z(t)$ signals) were de-biased so that each signal's value was 0 pixels at the first time step (-40 ms).

Then each of the trajectory signals was converted to a measurement in mm by multiplying each signal by 3.695 mm/pixel and each vehicle signal by 3.243 mm/pixel. These values for the spatial resolution of the imager at the surrogate plane and at the driver's-side vehicle exterior plane (where the motion of the vehicle was tracked) were determined prior to the test. The absence of significant edge effects was determined because a maximum difference in spatial resolution of only 0.2 mm/pixel was measured at the edges of the camera's field of view.

The filtering convention specified in ISO/DIS 13432-4 (ISO, 2004) was adopted to smooth the position data. All signals were filtered with four passes of the moving average filter given in Equation 1.

$$x_{i,f} = \frac{x_{i-1,fc} + 2x_{i,fc} + x_{i+1,fc}}{4} \quad (1)$$

$$z_{i,f} = \frac{z_{i-1,fc} + 2z_{i,fc} + z_{i+1,fc}}{4}$$

In Equation 1,

- $x_{i,f}$ and $z_{i,f}$ are the filtered x and z positions, in the frame coordinate system, at frame i , in mm, and
- $x_{i,fc}$ and $z_{i,fc}$ are the unfiltered (or filtered on the previous pass) x and z positions, in the frame coordinate system at frame i , in mm.

The second coordinate system important to this analysis is the vehicle coordinate system. The vehicle coordinate system is defined to be fixed with respect to the vehicle's motion. The origin is defined by the x coordinate of the head CG photo target at the analysis frame taken at time $t=0$ ms, and by the z coordinate of the simulated ground level (the level of the platforms on the pedestrian sled) (Figure 9). In the vehicle coordinate system the positive z direction points down and the frame coordinate system (fixed with respect to the lab) moves in the positive x direction. It is important to note that the location of the origin in the x direction is defined separately in each individual test,

while the location of the origin in the z direction remains constant from test to test.

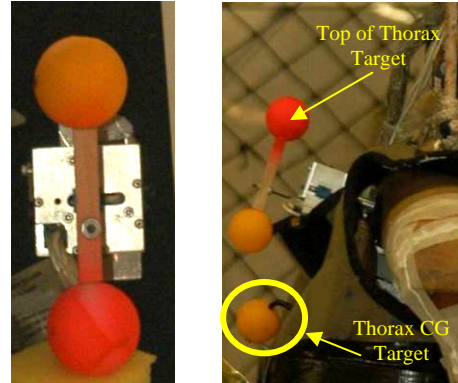


Figure 7. Dumbbell-type photo targets. At left, a dumbbell-type photo target is shown. The image on the right shows how a dumbbell-type photo target was mounted to the sensor cube at the T1 location in the dummy. The single-ball photo target used to track the thorax CG of the dummy is also shown.

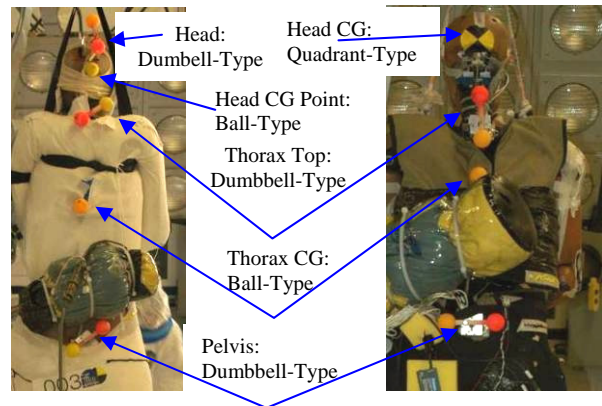


Figure 8. Photo targets used in the dummy (top) and PMHS (bottom) tests. Note these images are not at the same scale.

Table 3. Test type, time of head strike, digitized frame closest to the time of head strike and last frame digitized for each test in the study.

	Test	Time of Head Strike (ms)	Head Strike Imager Frame	Last Frame Analyzed
Dummy	D-1	126	128	148
	D-2	126	128	148
	D-3	131	132	152
PMHS	C-1	152	152	172
	C-2	138	136	156
	C-3	144	144	164

To compute the trajectory signals in the vehicle coordinate system, the motion of each target had to be subtracted from the vehicle motion and the origin of each signal had to be shifted in space to its origin as defined by the vehicle coordinate system.

The distances between each body segment's photo target (and the origin of its trajectory) and the origin of the vehicle coordinate system in the x and z directions, s_x and s_z , were measured in pixels and converted to mm using the frame taken at $t=0$.

Equation 2 explains how frame coordinate system parametric trajectory signals were transferred to the vehicle coordinate system by subtracting the vehicle's motion and shifting the trajectory origin.

$$\begin{aligned} x_i &= s_x + (x_{i,f} - v_{x,i,f}) - (x_{0,f} - v_{x,0,f}) \\ z_i &= s_z - (z_{i,f} - v_{z,i,f}) + (z_{0,f} - v_{z,0,f}) \end{aligned} \quad (2).$$

In Equation 2,

- x_i, z_i are the x and z coordinates, of each body segment's trajectory, in the vehicle coordinate system, at frame i , in mm,
- $v_{x,i,f}, v_{z,i,f}$ are the filtered x and z positions of the vehicle photo target at frame i , in mm,
- $x_{0,f}, z_{0,f}$ are the filtered x and z positions of each of the surrogate photo targets at frame zero (corresponding to time $t=0$), in mm, and
- $v_{x,0,f}, v_{z,0,f}$ are the filtered x and z positions of the vehicle photo target at frame zero (corresponding to time $t=0$), in mm.

The velocity of the head was calculated by adopting the methodology used in ISO/DIS 13232-5 (ISO, 2004) and given in Equation 3.

$$\begin{aligned} V_{x,i} &= \frac{x_{i+1} - x_{i-1}}{t_{i+1} - t_{i-1}} \\ V_{z,i} &= \frac{z_{i+1} - z_{i-1}}{t_{i+1} - t_{i-1}} \end{aligned} \quad (3).$$

In Equation 3,

- $V_{x,i}, V_{z,i}$ are the head photo target's velocity, in m/s, in the x and z directions at frame i , and
- t_i is the time, in ms, at frame i .

The resultant of the velocity signal is then computed by calculating the magnitude of the velocity vector defined by the parametric components in Equation 3 at each time step.



Figure 9. Vehicle coordinate system. The green cross represents the vehicle coordinate system origin.

PMHS KINEMATICS

Trajectory data for the head CG, T1, T8 and the pelvis are given in the vehicle coordinate system (Equation 2) for the PMHS tests in Figure 10. In each of the three plots given in Figure 10, the vehicle center line contour is added for reference. To provide an indication of the time scale, lines connecting each segment's trajectory at 12 ms intervals are also included. In each test, the trajectory signal is plotted from time $t=0$ to the time of head strike (also given in Table 3). Time histories of head resultant velocity from each of the PMHS tests are given in Figure 11.

KINEMATIC TRAJECTORY CORRIDORS

Scaling Kinematics Data

To provide a basis for comparing surrogate kinematics, it is common to scale PMHS response using a length scale factor. A scale factor is used to scale the geometry of the PMHS to a reference geometry. Since one goal of this study is to compare the kinematic response of the PMHS and the dummy, the dummy geometry was chosen as the standard, or reference geometry, to use in scaling the PMHS kinematics data.

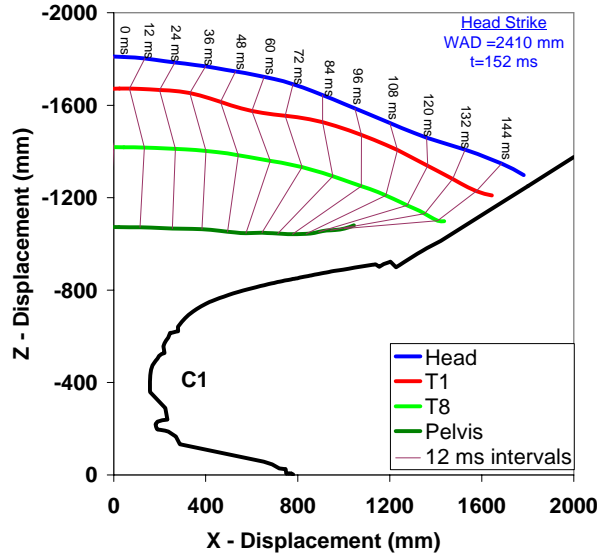


Figure 10a. Vehicle coordinate system trajectories for test C-1. The vehicle center line contour is in black. Purple lines, labeled “12 ms intervals”, connect body segments at each specified time.

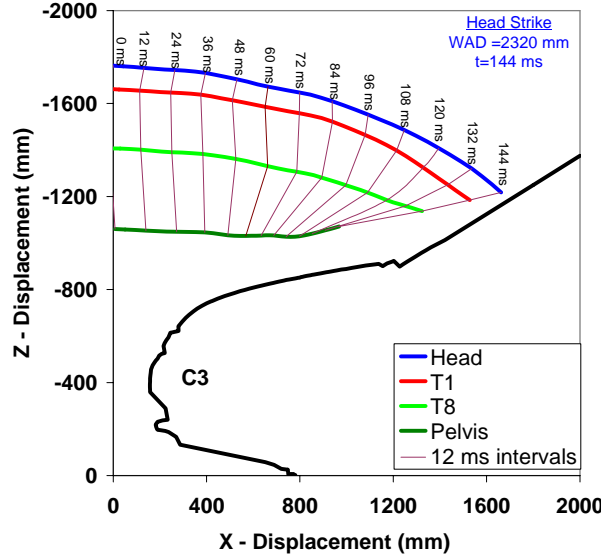


Figure 10c. Vehicle coordinate system trajectories for test C-3.

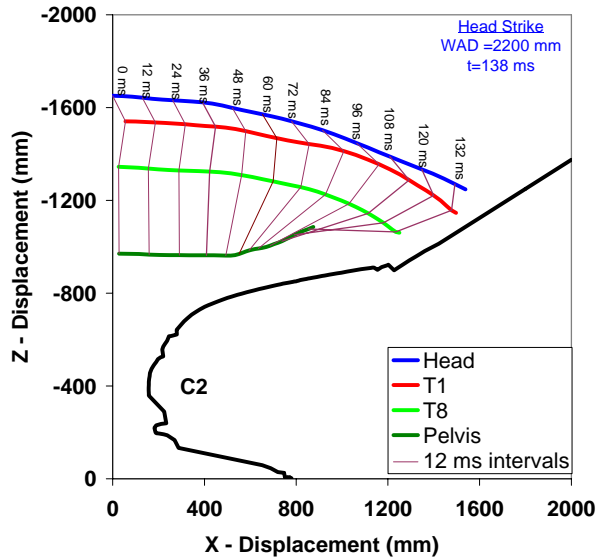


Figure 10b. Vehicle coordinate system trajectories for test C-2.

Recognizing that PMHS body-segment lengths vary slightly from PMHS to PMHS, and the lengths of the Polar-II body segments are also slightly different than those of the PMHS (Table 4), it was determined that individual scale factors should be used to scale trajectory data from each body region. Thus twelve individual scale factors were calculated to account for the head CG, T1, T8 and pelvis trajectories for all three PMHS tested. None of the dummy trajectory data were scaled.

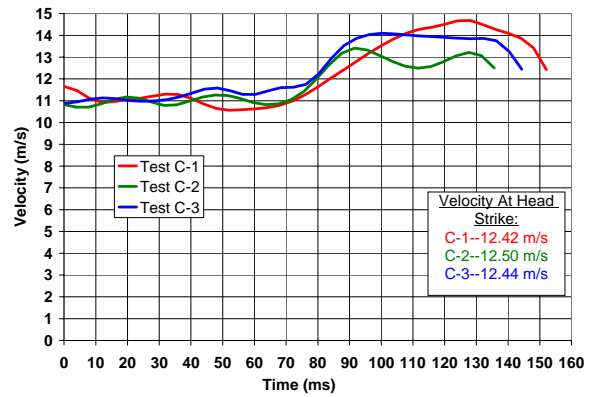


Figure 11. Head resultant velocity from the PMHS tests. Note that each signal is plotted from t=0 until the time of head strike for each particular test.

The distances between each body segment’s photo target and the origin of vehicle coordinate system in the z direction, $s_{z,c}$, were averaged for all of the dummy tests (Table 4). Using the average values, $s_{z,d}$, and the same measurements, from the PMHS tests, $s_{z,c}$, twelve scale factors were developed to scale each of the four trajectories in each test (Table 4). An example calculation to obtain the T8 scale factor in test 002, $\lambda_{002,T8}$, is given in Equation 4.

$$\lambda_{002,C-2}^{T8} = \frac{s_{z,d}^{T8}}{s_{z,c}^{T8,C-2}} = 1.0027 \quad (4).$$

Table 4. Initial vertical distance of each body segment's photo target and PMHS scale factors. Only summary data of dummy target heights are provided due to their similarity. Vertical distances appear as negative numbers because positive z is defined in the downward direction. All values are in mm.

	Photo Target Initial Height From Ground Level						Height Scale Factors					
	Dummy Mean	Dummy Range	Test C-1	Test C-2	Test C-3	PMHS Mean	PMHS Range	Test C-1	Test C-2	Test C-3	Mean	Range
Head CG	-1705	4	-1811	-1652	-1763	-1742	159	0.9415	1.0321	0.9672	0.9802	0.091
Top of Thorax	-1479	13	-1670	-1541	-1663	-1625	129	0.8853	0.9596	0.8893	0.9114	0.074
Thorax CG	-1349	15	-1419	-1345	-1408	-1391	74	0.9505	1.0027	0.9580	0.9704	0.052
Pelvis CG	-1042	11	-1073	-970	-1060	-1035	103	0.9707	1.0743	0.9826	1.0092	0.104

-All measurements are in mm.

In Equation 4,

- $S_{z,d}^{T8}$ is the average of the s_z values for the thorax CG from the three dummy tests, in mm, and
- $S_{z,c}^{T8,C-2}$ is the s_z value, in mm, for T8 in test C-2.

The filtered surrogate trajectory data, $x_{i,f}$ and $z_{i,f}$ (Equation 1) were then multiplied by their respective scale factors to obtain the scaled frame coordinate system trajectories $x_{i,f}^*$ and $z_{i,f}^*$. It is important to note that all scaled values are indicated in this study with an asterisk.

The scaled trajectories, $x_{i,f}^*$ and $z_{i,f}^*$, were then converted to the vehicle coordinate system (to obtain x_i^* and z_i^*) using Equation 5.

$$\begin{aligned} x_i^* &= s_x \lambda_L + (x_{i,f}^* - v_{x,i,f}^*) - (x_{0,f}^* - v_{x,0,f}^*) \\ z_i^* &= s_z \lambda_L - (z_{i,f}^* - v_{z,i,f}^*) + (z_{0,f}^* - v_{z,0,f}^*) \end{aligned} \quad (5)$$

Since the trajectory of each body region is defined with two parametric trajectory signals, $x(t)$ and $z(t)$, if the positions (dependant variable) are scaled, time (independent variable) must be scaled as well. Since a different scale factor is used to scale the positions of each body region, a different scaled time at frame i , t_i^* , had to be calculated for each body region and each test. When using a length scale factor, as in this case, time scales the same as length, so t_i was multiplied by each of the scale factors to obtain each of the t_i^* signals.

Scaled head velocities are calculated using both scaled position data and scaled time data by again employing the ISO methodology (ISO, 2004) (Equation 6).

$$\begin{aligned} V_{x,i}^* &= \frac{x_{i+1}^* - x_{i-1}^*}{t_{i+1}^* - t_{i-1}^*} \\ V_{z,i}^* &= \frac{z_{i+1}^* - z_{i-1}^*}{t_{i+1}^* - t_{i-1}^*} \end{aligned} \quad (6)$$

In Equation 6,

- $V_{x,i}^*$ and $V_{z,i}^*$ are each photo target's scaled component velocity, in m/s, in the x and z directions at frame i .

The resultant of the scaled head velocity is computed by computing the magnitude of the scaled velocity vector defined by the parametric components in Equation 6.

Corridor Development

Average Curves Since this study was only concerned with examining the trajectory data from initial bumper contact ($t=0$) to head strike, and the time data were scaled, the time of head strike had to be scaled as well. Given that the time of head strike had already been rounded to the nearest analysis frame, the time of the head strike frame was scaled. Finally, the scaled time at head strike, t_{hs}^* , is rounded to the nearest analysis frame (Table 5).

When each time signal was scaled, the sampling frequency changed from 250 Hz, to the inverse of the scale factor, λ^{-1} , multiplied by 250 Hz. Since one scale factor was developed for each body region in each test, each scaled time signal had a different sampling frequency. To facilitate averaging and corridor development, all of the scaled trajectory and velocity data were re-sampled, by interpolation at 250 Hz, the frame at $t=0$ to $t=t_{hs,c}^*$, where $t_{hs,c}^*$ is the lowest time, t_{hs}^* , for each body region (Table 5).

Table 5. Un-scaled and scaled head strike frame times for each body segment trajectory in each PMHS test. The earliest scaled time at head strike for each body region is also given. All times are in ms.

		Scaled Head Strike Frame Time t_{hs}^*			$t_{hs,c}^*$
		001	002	003	
Scaled	Un-scaled	152	136	144	-
	Head	144	140	140	140
	T1	136	132	128	128
	T8	144	136	140	136
	Pelvis	148	144	140	140

-All times are given in ms.

The average scaled PMHS trajectory was computed by averaging values of each trajectory signal at each 4 ms time interval. Averaged scaled trajectories were computed for the head, T1, T8 and pelvis. The resultant head velocities from each test were also averaged to create an average scaled resultant velocity.

Each body segment average trajectory was fit to a third order polynomial with parameters α , β , γ , and δ (Table 6 and Equation 7).

$$\overline{z}_i^* = \alpha \overline{x}_i^{*3} + \beta \overline{x}_i^{*2} + \gamma \overline{x}_i^* + \delta \quad (7)$$

In Equation 7,

- \overline{x}_i^* , and \overline{z}_i^* , are the average scaled x and z components of each body segment's trajectory, in mm.

Table 6. Third-order polynomial parameters for each average scaled PMHS body segment trajectory.

	Head	T1	T8	Pelvis
α	-1.11461E-08	9.11329E-08	6.64334E-08	-3.63583E-07
β	1.88378E-04	-1.67628E-05	5.95507E-05	3.51434E-04
γ	1.89965E-03	7.69504E-02	1.86501E-02	-5.59884E-02
δ	-1.70050E+03	-1.48419E+03	-1.34781E+03	-1.03857E+03
R^2	0.9997	0.9930	0.9997	0.9765

The average scaled resultant head velocity curve has too complex curvature to be accurately modeled by a third (or higher) order polynomial. Thus the average and standard deviation data were re-sampled with the minimum number of points necessary to model the complexity of the signal's curvature (Table 7). Average scaled head velocity data are given from $t=0$ to $t=t_{hs,c}^*$, where $t_{hs,c}^*$ is the lowest time, t_{hs}^* for the

head (Table 5). The standard deviation data given in Table 7 are calculated by taking the square root of the bias-corrected variance (this contains the "n-1" correction term in the denominator of the definition).

Corridors Typically response corridors based on PMHS data are developed by incorporating the standard deviation of the data into the calculation of the upper and lower corridor bounds (Lessley *et al.* 2004, Viano and Davidsson 2002, and Maltese *et al.* 2002). However, due to similarity between the PMHS trajectories (after scaling) and the number of data sets (only 3), boxed-standard deviation corridors for PMHS body segment trajectories were determined to be too narrow for dummy or computational model development or validation. Even standard deviation corridors with a two-standard deviation width were too narrow (Figure 12).

Table 7. Tabulated average and standard deviation of the scaled average PMHS head velocity signal.

Time ms	Head Velocity m/s	Standard Deviation m/s	Time ms	Head Velocity m/s	Standard Deviation m/s
0	11.34	0.931	77	11.97	0.825
7	11.20	0.766	84	12.95	0.863
14	11.24	0.556	91	13.67	0.729
21	11.33	0.491	98	13.96	0.829
28	11.30	0.664	105	13.93	1.162
35	11.29	0.745	112	13.85	1.441
42	11.36	0.595	119	13.93	1.516
49	11.34	0.492	126	13.94	1.200
56	11.23	0.416	133	13.84	0.903
63	11.27	0.638	140	12.91	0.869
			70	11.44	0.753

Because kinematic corridors based on the standard deviation of the data are too narrow, corridors needed to be developed for PMHS body segment trajectories using a different methodology. The corridors would ideally begin very narrow (because the scaling procedure forces the origin of all trajectories for each body segment to the same point), and gradually grow wider to account for variability in the data as the length of the trajectory grows.

Thus, kinematic response corridors were calculated for the head, T1, T8 and pelvis trajectories using the average trajectories and the path length of each trajectory (Equation 8).

$$S_i = \sum_{j=1}^i \sqrt{\left(\overline{x}_j^* - \overline{x}_{j-1}^*\right)^2 + \left(\overline{z}_j^* - \overline{z}_{j-1}^*\right)^2} \quad (8)$$

In Equation 8,

- S_i is the total path length of the trajectory measured up to frame i , in mm.

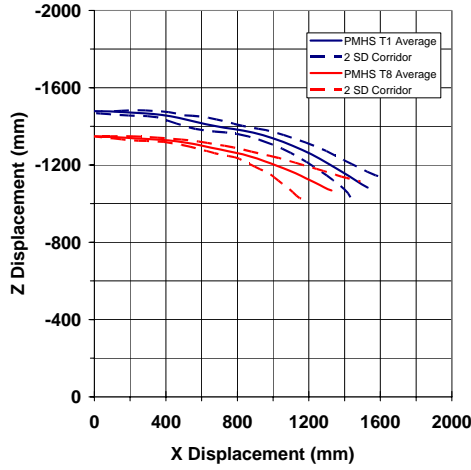


Figure 12. Averaged scaled T1 and T8 trajectory data with boxed-standard deviation corridors using a two-standard deviation width.

Boxed corridors were then developed using the path length. Boxed-corridors can be developed by creating a square around each data point in the curve, with edges aligned with the coordinate axes, where the length of the square is equal to $2k$. For the current study, k is some percentage of the trajectory's path length. Two pairs of parametric trajectory signals were calculated to determine the path of the corner's of the path length square. The four signals were calculated using Equation 9.

$$\begin{aligned}
 C_{x,i}^+ &= x_i + kS_i \\
 C_{x,i}^- &= x_i - kS_i \\
 C_{z,i}^+ &= z_i + kS_i \\
 C_{z,i}^- &= z_i - kS_i
 \end{aligned} \quad (9)$$

In Equation 9, $C_{x,i}^+$ gives the x component of the signal formed by adding the x component of the average parametric body segment trajectory at frame i to k percent of the path length at frame i . $C_{x,i}^-$, $C_{z,i}^+$, $C_{z,i}^-$ provide similar signals. It is important to note that the values calculated using Equation 8 and Equation 9 are calculated using the values of the trajectories obtained from the third order polynomial equations (Equation 7) defined by the parameters in Table 6.

By combining the x and z components of the two pairs of parametric trajectory signals in Equation 9, the trajectory of each path length square's corners can be plotted. Since the path length square is aligned with respect to the coordinate frame and the trajectory signals show more x direction displacement than z direction displacement, the trajectory of two of the path length square's corners will be above the average body segment trajectory and two of the corners' trajectories will be below the average trajectory. The upper bound for each body-segment corridor was chosen to be the trajectory of the path length square's corner that remained farthest above the average curve for the longest time. The lower bound was chosen to be the trajectory of the path length square's corner that remained farthest below the average curve for the longest time. Due to the downward concavity of the average trajectory signals (with $+z$ pointing down), the kinematic response corridors for the head CG, T1 (or top of thorax) and T8 (or thorax CG) trajectories were developed by plotting $C_{x,i}^+$ vs. $C_{z,i}^-$ (for the upper bound) and $C_{x,i}^-$ vs. $C_{z,i}^+$ (for the lower bound). Since the pelvis average scaled trajectory is concave upward, the upper bound of the pelvis corridor was developed by plotting $C_{x,i}^+$ vs. $C_{z,i}^+$, and the lower bound was developed by plotting $C_{x,i}^-$ vs. $C_{z,i}^-$. Any value of k can be used to develop corridors of varying width for each body segment's trajectory. Figure 13 presents each of the scaled average body segment trajectories (fit to third order polynomials) plotted with three sets of corridors for $k=4\%$, $k=8\%$ and $k=12\%$.

Kinematic response corridors (Figure 14) were also developed for scaled head velocity by incorporating the standard deviation (Table 7) because it did not create a corridor that was too narrow for dummy validation. The corridor boundaries for the head velocity corridor are determined by adding m standard deviations to (upper bound), or subtracting m standard deviations from (lower bound), the average scaled PMHS head resultant velocity at each time step. Figure 14 provides the averaged scaled PMHS head resultant velocity curve and corridor boundaries for $m=0.5$, $m=1.0$ and $m=1.5$ standard deviation corridors.

DISCUSSION

The trajectory analysis discussed in the "Data Manipulation" portion of the "Kinematics Measurement" section was performed for both the PMHS tests and the dummy tests. Dummy trajectory signals, as calculated in Equation 2 and Equation 3, provide evidence that the Polar-II can produce a repeatable response in a full-scale pedestrian impact

tests (Figures 15 and 16). Plotting the average PMHS trajectory signal with the dummy signals provides a basis for comparison of the dummy body segment trajectories and PMHS body segment trajectories (Figure 15). The Polar-II was shown to generally fall within 10% path length corridors, so the 10% path length corridors are included in Figure 15.

In comparison of dummy and PMHS trajectories, one interesting feature is that PMHS trajectories and dummy trajectories are not the same length. Despite the scaling procedure, PMHS trajectories are still significantly longer, typically in the x -direction, than dummy trajectories. This is also evident in that head strike in the PMHS tests typically occurred at a much larger WAD (2410, 2200 and 2320 mm) than in the dummy tests (1970, 1980 and 1990 mm). Additionally, the time of head strike in the PMHS tests is, on average, greater than the time of head strike in the dummy tests (Table 3). These results suggest that PMHS specimens traversed longer distances in the $+x$ direction than the dummy did between initial vehicle contact and head strike. Further examination of the video data suggests that this is, at least partially, due to the fact that the PMHS slides farther up the hood than the dummy does prior to head strike.

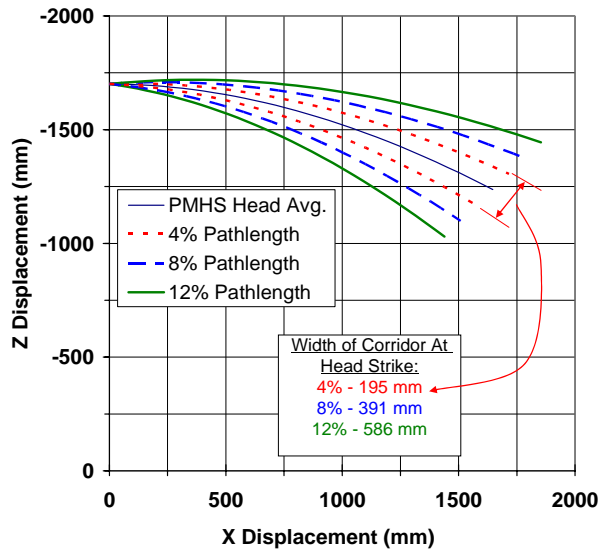


Figure 13a. Scaled average PMHS head trajectory (from the third order polynomial with parameters given in Table 6) with 4%, 8% and 12% path length corridors and corridor width at head strike.

Two factors seem to influence the amount of sliding that occurs in each surrogate. Firstly, it was noted that there was a significantly different damage pattern on the hood leading edge of the vehicle after a dummy test than after a PMHS test. Sliding up the hood by pedestrian surrogates is promoted by the smooth sloping shape of the hood. One potential

explanation for less sliding with the dummy is that either the mass, mass distribution, or stiffness of the dummy thigh and/or pelvis are not totally biofidelic. Thus a different damage pattern could be caused to the lower edge of the hood, changing its smooth shape, and restricting sliding. Secondly, the PMHS and the dummy wore different clothing during the tests. It is further hypothesized that differences in the frictional characteristics of the standard dummy shorts, and the cotton/elastic pants worn by the PMHS.

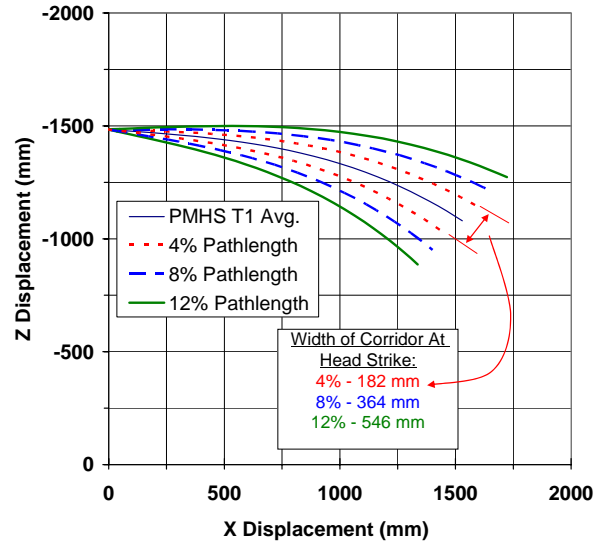


Figure 13b. Scaled average PMHS T1 trajectory (from the third order polynomial with parameters given in Table 6) with 4%, 8% and 12% path length corridors and corridor width at head strike.

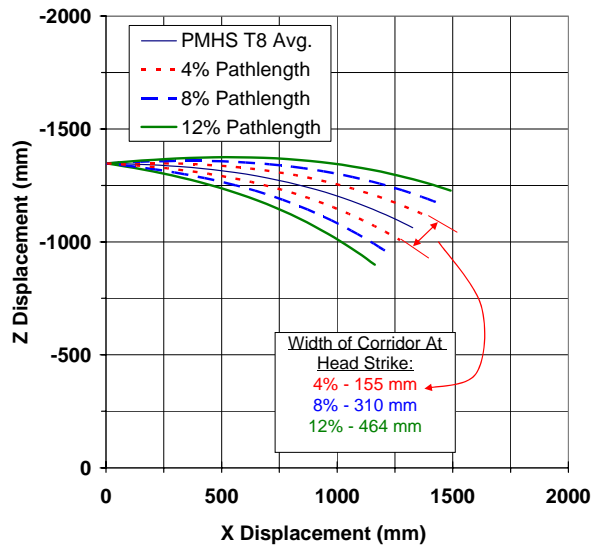


Figure 13c. Scaled average PMHS T8 trajectory (from the third order polynomial with parameters given in Table 6) with 4%, 8% and 12% path length corridors and corridor width at head strike.

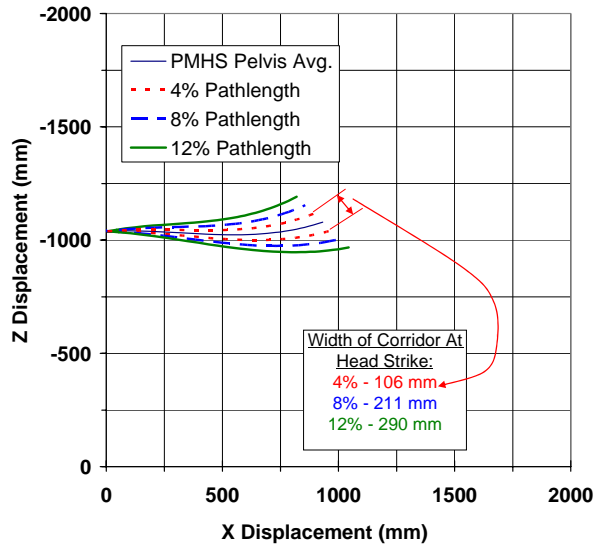


Figure 13d. Scaled average PMHS pelvis trajectory (from the third order polynomial with parameters given in Table 6) with 4%, 8% and 12% path length corridors and corridor width at head strike.

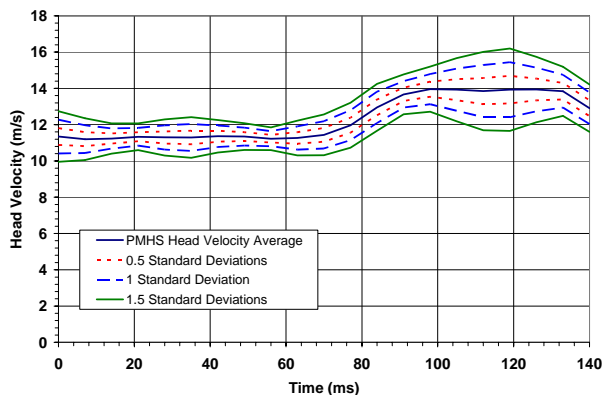


Figure 14. Scaled average PMHS head resultant velocity time history with 0.5, 1.0 and 1.5 standard deviation corridors.

Greater sliding in the PMHS tests causes increased length of the body segment trajectories, later head strike times, and longer WADs to head strike than in the dummy tests. More testing is necessary to determine the all of the factors that contribute to sliding.

An additional reason for differences in trajectory length and WAD to head strike is that is that the PMHS head starts farther from the ground level at $t=0$ than the dummy. Although the statures of the PMHS, as measured post-mortem, were between 170 cm and 175 cm, when the PMHS were hoisted over the pedestrian sled and positioned, their heights had increased to 178 cm to 187 cm. The dummy's pre-test stature measured

only 173-174 cm. The change in PMHS stature due to supporting the PMHS by the upper body (5% to 8%) is due to stretching of the spine under the tension caused by the PMHS weight.

It was impossible to support any significant portion of the PMHS weight by the PMHS lower extremities. Lowering the release mechanism only caused an increase in flexion at the knee and hip joints in the PMHS, rather than increasing the load supported by the lower extremities. Artificially stiffening the knee and hip joints of the PMHS could have permitted a small amount of the upper body weight to be supported by the lower extremities. However, artificial joint stiffening was not performed because it was determined that any joint stiffening would ultimately affect the joint stiffness and range of motion. Thus, no adjustment for the stretched stature of the PMHS could be made by attempting to get the PMHS to support its own weight.

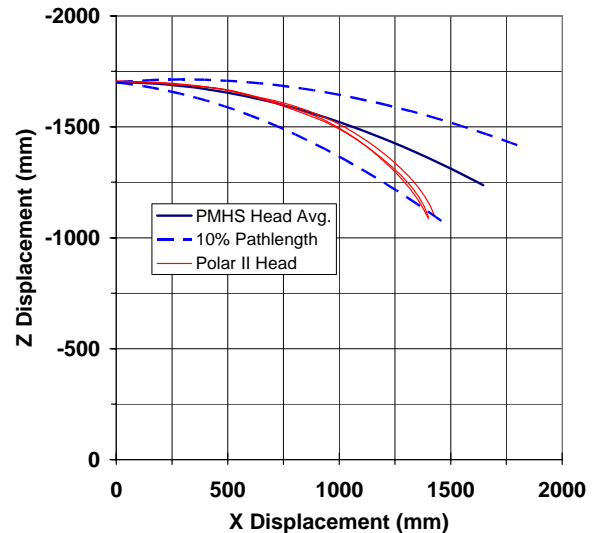


Figure 15a. Dummy head trajectories with the average scaled PMHS head trajectory and 10% path length corridors.

Since it was not possible to get the PMHS lower extremities to support any of the upper body weight, some differences in pre-test position between the dummy and the PMHS arose (Figure 5). Most notably, not as much anterior-posterior separation between the knee joints was possible in the PMHS tests as used in the dummy tests. Another difference in position between the dummy and the PMHS can be seen in the angle the dummy's spine makes with respect to the ground (lateral picture, Figure 5a). The angle of the spine in the dummy tests was produced as a result of a limited range of motion of the dummy hip in extension. The range of motion was limited due to the orientation

of the hip and pelvis flesh (without the flesh the range of motion is greater). The limited range of motion required the dummy pelvis to be pushed posteriorly so that the dummy's feet could be placed on the pedestrian sled foot plates. This alignment produces a forward-tilt in the spine.

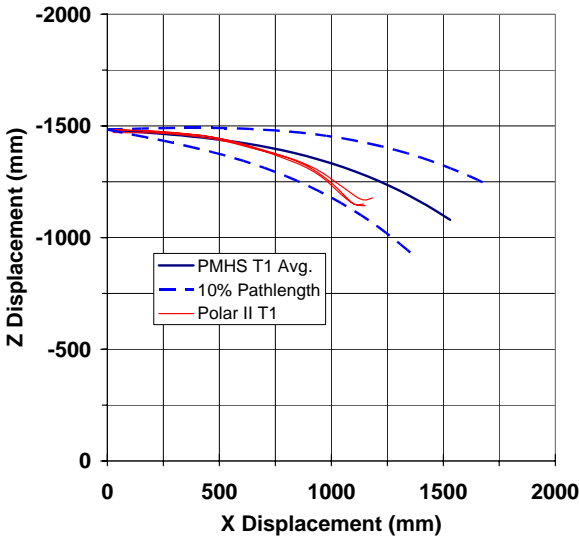


Figure 15b. Dummy top of thorax (T1) trajectories with the average scaled PMHS T1 trajectory and 10% path length corridors.

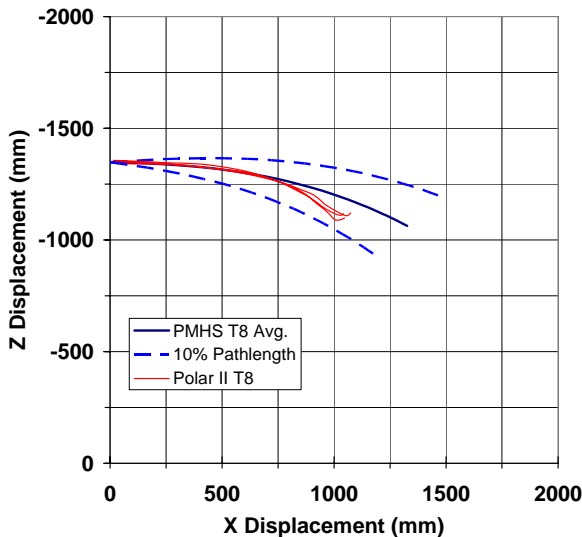


Figure 15c. Dummy thorax CG (T8) trajectories with the average scaled PMHS T8 trajectory and 10% path length corridors.

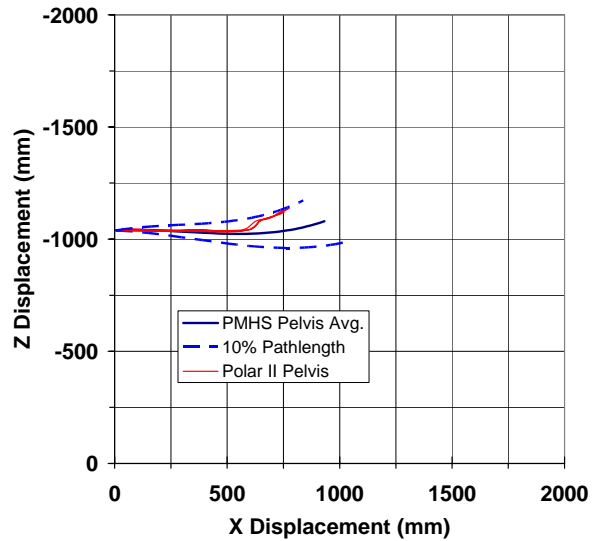


Figure 15d. Dummy pelvis trajectories with the average scaled PMHS pelvis trajectory and 10% path length corridors.

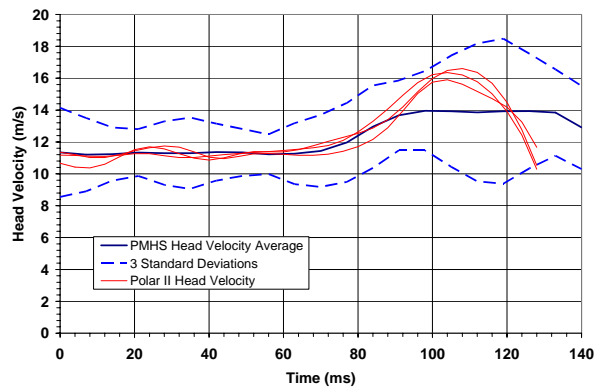


Figure 16. Dummy head resultant velocity time histories with the average scaled PMHS resultant velocity and 3-standard-deviation corridors.

The effect on surrogate kinematics as a result of differences in position and differences in height is unknown. More experiments are necessary to assess the affect of differences in height and differences in pre-test orientation on surrogate response.

Despite differences between the response of the PMHS and the dummy, overall PMHS kinematics were generally replicated by the dummy. Dummy trajectories generally fit within 10% path length corridors (Figure 15). Despite the fact that the PMHS trajectories are typically longer, there is a significant difference in the shape of the head trajectory for the dummy and the PMHS.

Although sliding potentially contributes to the difference in shape of the dummy and PMHS head

trajectories, another factor may also contribute to this difference. Without muscle tension in the PMHS, the PMHS neck has very little lateral bending stiffness. The dummy's neck however is designed to replicate the lateral bending stiffness of a living human. This difference is most evident in comparing the high speed video images from the dummy and PMHS tests shown in Figure 6. At 100 and 120 ms, the PMHS neck, due to inertial loading by the head, is under so much bending that it is in contact with the PMHS left shoulder (Figure 6b). However, in the dummy tests, at 100 and 120 ms, the dummy's neck displays much less bending and the closer to being equidistant from each shoulder (Figure 6a).

Differences in head trajectory between the dummy and PMHS are amplified in the resultant head velocity signals. Dummy head velocity is so different from PMHS resultant head velocity signals that dummy resultant head velocity signals barely fit within a three-standard deviation PMHS corridor. The dummy resultant head velocity signals begin to deviate from the scaled average PMHS head velocity around 90 ms. Further analysis of the video data suggests that inertial loading by the head begins to overcome the low stiffness of the PMHS neck around 90 ms. At 80 ms, the PMHS and dummy heads appear to be in a similar place with respect to the shoulders, but at 100 ms, the PMHS neck is under enough lateral bending that the PMHS head is touching the left shoulder (Figure 6). Thus differences in the resultant head velocity between the PMHS and dummy can be at least partially attributed to differences in surrogate neck stiffness.

Since biofidelic representation of living human pedestrians is the ultimate goal in surrogate development, this is an instance when FE modeling could be used to validate the head/neck response of the dummy in a full-scale pedestrian impact test. The motion of T1 could be used as an input to an FE model that has a validated neck muscle model to determine the corresponding head motion.

CONCLUSION

Three full-scale pedestrian impact tests with PMHS were performed with a late-model small sedan that struck the PMHS at 40 km/h. Three replicate tests were performed with the Polar-II dummy. The kinematics of the Polar-II and PMHS were analyzed by extracting planar body segment parametric trajectory data from high speed video images. A methodology and the necessary data are provided to develop kinematic response corridors for PMHS head, T1, T8 and pelvis trajectories. Trajectory corridors can be calculated based on any k percent of the path length of the trajectory. The necessary data are also provided to produce the average and standard deviation corridors

for the scaled resultant head velocity measured in the PMHS tests.

Overall, the dummy generally replicated the complex PMHS kinematics and demonstrated good overall biofidelity. Specifically, dummy head, top of thorax, thorax CG and pelvis CG trajectories generally fall within 10% path length corridors. Greater sliding by the PMHS, and lack of neck muscle tension in the PMHS have been identified as potential causes for differences in the length and shape of body segment trajectories. More testing is necessary to assess the effects differences in pre-test orientation, surrogate stature, and clothing will have on surrogate response.

REFERENCES

- [1] Akiyama A, Okamoto M, Rangarajan N. (2001) Development and application of the new pedestrian dummy. Paper 463, 17th Conference on the Enhanced Safety of Vehicles, Amsterdam, The Netherlands.
- [2] Akiyama A, Yoshida S, Matsuhashi T, Moss S, Salloum M, Ishikawa H, Konosu A. (1999a) Development of human-like pedestrian dummy. Paper 9934546, Japanese Society of Automotive Engineers, Chiyoda-Ku, Tokyo, Japan.
- [3] Akiyama A, Yoshida S, Matsuhashi T, Rangarajan N, Shams T, Ishikawa H, Konosu A. (1999b) Development of simulation model and pedestrian dummy. Paper 1999-01-0082, Society of Automotive Engineers, Warrendale, PA.
- [4] Artis M, McDonald J, White R, Huang TJ, Shams T, Rangarajan N, Akiyama A, Okamoto R, Yoshizawa R, Ishikawa H. (2000) Development of a new biofidelic leg for use with a pedestrian dummy. Proceedings of the 2000 International Conference on the Biomechanics of Impacts (IRCOBI), Montpellier, France.
- [5] Community Road Accident Database (CARE). EUROPA, European Commission, Transport. http://europa.eu.int/comm/transport/care/statistics/most_recent/detailed_breakdown/index_en.htm. 2002. (accessed 15 Apr 2004.)
- [6] Crandall J. (1994) The Preservation of Human Surrogates for Biomechanical Studies. PhD Dissertation released by the University of Virginia Department of Mech and Aero Engineering.
- [7] Huang TJ, McDonald J, Artis M, Rangarajan N, Shams T, White R, Beach D, Campbell R, Akiyama A, Yoshida S, Ishikawa H, Konosu A. (1999) Development of a biofidelic dummy for car-pedestrian accident studies. 1999 International Conference on the Biomechanics of Impacts (IRCOBI), Stiges, Spain.

- [8] Ishikawa H, Kajzer J, Schroeder G. (1993). Computer simulation of the impact response of the human body in car pedestrian crashes. Paper 933129, Proc. 37th Stapp Car Crash Conference, 235-248.
- [9] ISO TC 22/SC 22/WG 22. Motorcycles—test and analysis procedures for research evaluation of rider crash protective devices fitted to motorcycles—Part 4: Variables to be measured, instrumentation, and measurement procedures. ISO/DIS 13232-4, August 31, 2004, Copyright ISO, 2004.
- [10] ISO TC 22/SC 22/WG 22. Motorcycles—Test and analysis procedures for research evaluation of rider crash protective devices fitted to motorcycles—Part 5: Injury indices and risk/benefit analysis. ISO/DIS 13232-4, September 7, 2004, Copyright ISO, 2004.
- [11] Kam C, Kerrigan J, Meissner M, Drinkwater C, Murphy D, Bolton J, Arregui C, Kendall R, Ivarsson J, Crandall J, Deng B, Wang JT, Kerkeling C, Hahn W. (2005) Design of a full-scale impact system for analysis of vehicle pedestrian collisions. Paper 2005-01-1875, Society of Automotive Engineers, Warrendale, PA.
- [12] Lessley D, Crandall J, Shaw G, Kent R, Funk J. (2004) A normalization technique for developing corridors from individual subject responses. Paper 2004-01-0288, Society of Automotive Engineers, Warrendale, PA.
- [13] Maltese M, Eppinger R, Rhule H, Donnelly B, Pintar F, Yoganandan N. (2002) Response corridors of human surrogates in lateral impacts. Paper 2002-22-0017, Society of Automotive Engineers, Warrendale, PA.
- [14] Okamoto Y, Akiyama A, Okamoto M, Kikuchi Y. (2001) A study of the upper leg component tests compared with pedestrian dummy tests. Paper 380, 17th Conference on the Enhanced Safety of Vehicles (ESV), Amsterdam, The Netherlands.
- [15] Robbins DH. Anthropometric Specifications for Mid-Sized Male Dummy, Volume 2. University of Michigan Transportation Research Institute (UMTRI) report number UMTRI-83-53-2. December 1983.
- [16] National Highway Traffic Safety Administration. (2003) Traffic Safety Facts 2003-Pedestrians, DOT HS 809 769, 2003.
- [17] National Police Agency (Japan). Traffic Accidents Situation 2003. Fatalities by Age Group and Road User Type. <http://www.npa.go.jp/english/index.htm>. 2003. (Accessed 12 Apr. 2004.)
- [18] Viano D, Davidsson J. (2002) Neck displacements of volunteers, BioRID P3 and Hybrid III in rear impacts: implications to whiplash assessment by a neck displacement criterion (NDC). *Traffic Injury Prevention* 3: 105-116.
- [19] World Bank (2001) Road Safety. <http://www.worldbank.org/transport/roads/safety.htm> (Accessed 12 Apr. 2004).

DEVELOPMENT OF PERFORMANCE SPECIFICATIONS FOR A PEDESTRIAN RESEARCH DUMMY

Jeff Crandall

K. Wiley

Doug Longhitano

A. Akiyama

SAE Pedestrian Dummy Task Group

Paper 05-0389

ABSTRACT

Existing test procedures assessing vehicle interactions with a pedestrian have generally been limited to subsystem impactors. The complex kinematics of vehicle-pedestrian impacts necessitates test surrogates that possess whole-body response capabilities. This paper reports on the activities of an international task group working to develop a recommended practice for pedestrian dummy performance. The objective of the task group was to develop a performance standard for a research dummy based on existing technology. Potential applications include the study of pedestrian kinematics, injury prediction, and the evaluation of countermeasures including active systems. Specifications focus on the 50th percentile male for primarily lateral impacts in the range of 30 km/h to 50 km/h. Development of the specifications included a detailed review of the literature and evaluation of existing dummies including the Hybrid III and the POLAR II. Based on these studies, biofidelity priority was given to whole body kinematics, as well as head, knee, leg, and thoracic impact response. Biofidelity requirements for whole-body kinematics were developed from cadaveric impacts with a late model vehicle. The specification also includes component response corridors for the head, leg, knee, and chest. In addition to the biofidelity evaluation, testing at facilities around the world was performed to evaluate durability, usability, and repeatability of existing dummy technology.

INTRODUCTION

Worldwide, pedestrian crashes constitute the most frequent cause of traffic-related fatalities. Improving vehicle design to make automobiles less aggressive to pedestrians during impact is an essential component of reducing the frequency and the severity of pedestrian injuries. Assessing the level of protection offered by existing and future vehicles will likely be accomplished by a multi-dimensional evaluation including full-scale tests, subsystem tests, and computer modeling.

Currently, the primary evaluation tool for assessing potential pedestrian protection is subsystem test procedures. Through an evolution of procedures within the European Enhanced Vehicle-Safety Committee (EEVC) Working Groups 10 and 17, experimental test devices have been developed that represent the head, thigh-pelvis, and lower extremity (EEVC 2002). Pedestrian protection test procedures have also been discussed or developed in ISO and IHRA activities with the resulting procedures similar to those of the EEVC. In Europe and Japan, pedestrian protection regulations will be introduced based on the EEVC procedures and IHRA activities. Given the complexity of pedestrian kinematics during vehicle impact, subsystem test procedures alone, however, are likely insufficient to evaluate the comprehensive level of protection potentially afforded by vehicle countermeasures. The interrelationship of response between successive contacts of body regions is strongly determined by the pedestrian and vehicular geometry, the impact speed, the orientation of the pedestrian, and the response of previously contacted structures. In addition, subsystem tests are not effective for evaluating active safety systems such as pedestrian airbags or pop-up hood systems. These countermeasures usually include sensors that detect pedestrian contact with the vehicle that cannot be evaluated by subsystem testing. To study and assess the vast array of vehicle-pedestrian interactions, test surrogates that possess whole-body response capabilities, such as a pedestrian dummy, are necessary. Historically, testing with full-scale dummies has been hindered by both biofidelity and durability of the anthropometric test devices. Some of the problems encountered include propensity to damage dummy components, difficulty in assessing phases of impact, and uncertainty of repeatability (Harris, 1989). Recently, attempts have been made to develop improved pedestrian dummies including modifications to the H-III (Hattori et al., 2000), a modified side impact dummy (Frederikson 2001), and the Polar II (Huang et al., 1999; Akiyama et al., 2001). However, these dummies were independently designed and used primarily by the developing organizations without independent assessment or

review by a broader international community working on pedestrian safety.

OBJECTIVES

The SAE Pedestrian Dummy Task Group (SAE PDTG) was established to develop performance, as opposed to design, specifications for pedestrian research dummies based on existing dummy technology. While the objective of the group was not to develop or specify a physical device, the task group realized it was necessary to have a physical representation of such a dummy in order to assess the feasibility of meeting the dummy performance specifications using existing technologies.

Terms of Reference

The performance specification was developed based on several expected uses including the design of countermeasures, the evaluation of active systems (e.g., pop-up hoods and airbags), the validation of computer simulations, the study of pedestrian kinematics, the reconstruction of impacts including crash reconstruction of pedestrian kinematics, the refinement of component test parameters and procedures, and the prediction of injury probabilities for given vehicle, crash, and countermeasure combinations. In terms of requisite biofidelity for the dummy, whole-body kinematics were considered the foremost priority for the anticipated dummy applications.

While it is recognized that collisions involve pedestrians of all sizes, it was proposed that performance specifications for a 50th percentile adult male dummy be developed as a first step. This approach stems from the greater knowledge of biomechanics and existing dummy technologies for the mid-size male relative to other adult sizes and children. While not the initial objective, it was envisioned that additional performance specifications for other sizes of pedestrian dummies would be developed in the future based on accepted scaling procedures. The resulting pedestrian research dummy performance specifications for existing technology were based on studies of the following items:

1. An understanding of the frequency and severity of pedestrian injuries in order to properly prioritize instrumentation requirements
2. Anthropometry requirements including requirements for size, joint locations, mass, and mass distribution

3. Biomechanical response requirements for essential body regions such as the head, thorax, and lower extremities
4. Instrumentation compatibility to facilitate the measurement of engineering parameters known to relate causally to injury
5. Requirements for dummy durability, repeatability, and reproducibility
6. Functionality requirements including ease of use in a crash laboratory environment
7. A survey and evaluation of existing dummy and sensor technologies with particular emphasis on dummies currently used in pedestrian research programs
8. Whole-body kinematics observed in full scale test vehicle with post-mortem human surrogates

A brief overview of the studies conducted by the SAE PDTG is included in this paper.

Body Region Priorities

While numerous researchers have evaluated the frequency and severity of pedestrian injuries, there exists little consistency among the studies in terms of the inclusion criteria. Variations exist for the vehicle types, impact velocity ranges, body region breakdowns, injury coding schemes, and pedestrian demographics (e.g., age, gender, size). In order to determine body region priorities for a variety of performance specifications including instrumentation compatibility, component biofidelity, and whole body kinematics, a detailed review of available field injury studies was undertaken by the task group. The study simultaneously evaluated injury frequency, injury severity, injury cost, injury disability probabilities, and changing trends in the vehicle fleet. Given the lack of uniformity among studies, no quantitative assessment of the archival literature could be conducted. Therefore, a group of experts reviewed the available studies and somewhat subjectively prioritized the body regions (1 = most important, 10 = least important) based on such factors as the frequency of injury to the body region, the societal cost associated with the injury, and the probability of disability. The results of the rankings are shown in Figure 1. For the most part, the review confirmed well-known pedestrian injury trends (e.g., head injuries were the most frequent severe injuries) but perhaps lesser known observations (e.g., chest injuries moderately frequent and are associated with high injury cost) played essential roles in determining the body region priorities and instrumentation. While numerous studies were used to characterize the

lower limb as the most frequently injured body region, an examination of the injuries within regions of the lower limb identified the leg as the most frequently injured area and the knee as the most frequently injured lower limb joint. While historically the thigh was a prominent region of injury, recent investigations have shown diminished frequency (Snedeker et al., 2003) with late model cars.

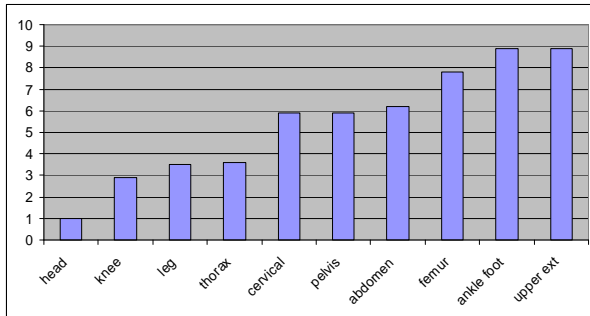


Figure 1. Body region rankings based on injury frequency, severity, cost, and disability.

METHODOLOGY AND RESULTS

Previous studies and publications were reviewed to identify response and physical parameters considered necessary for developing performance specifications for a pedestrian dummy.

Anthropometry

A target set of anthropometric specifications was determined to ensure that dummies complying with the document are, in general, representative of the 50th percentile adult male. The geometric, mass, and mass distribution specifications were defined with the goal of differentiating between parameters considered to be critical for pedestrian injury studies (e.g., overall standing height and knee height) and those considered to be non-critical parameters (e.g., elbow height). The critical parameters require mandatory compliance while the non-critical factors are recommended for consideration in the design of dummies. This approach should result in dummies that are anthropometrically similar to one another, thereby facilitating the comparison of data collected with different dummies, while still not being overly design restrictive.

Defining the human anthropometry targets was complicated by the results of human studies being dependent upon the sample size and the specific subjects measured and by the fact that not all human

studies contained all of the parameters needed to define a dummy (e.g., some studies with detailed dimensional data contained very limited mass distribution data). In addition, human studies with body segment data tended to use different body partition definitions making it difficult to make direct comparisons. Finally, human anthropometry data are dependent on the era and geographic location in which the data are collected. Thus, newer databases and those that included inherent geographic diversity were considered the most representative.

For the performance requirements, four primary references were used as the basis for the dummy specifications. The U.S. CAESAR data base is a recent study based on a large sample size and because of the diverse ethnicity of the U.S. was considered representative of the world population (Harrison and Robinette, 2002). The CAESAR data base provided a variety of joint locations, and three body region shape information such as circumferences etc. Other than overall mass, the CAESAR data set does not contain any body segment mass or c.g. data. The AMVO data base was used as a second source for body segment mass information.

The ManneQuin Pro V8.0 software, which is based on the 1988 Natick US Army anthropometric data base provided a complete set of parameters including overall height, joint locations, body segment masses, and body segment c.g. locations. In addition, because the software generates CAD models of the skeleton, the model could be used to identify the location of specific joints such as the C7/T1 interface. This data set could have been used as the sole source of information for this document, however the data is nearly 20 years old, and is based on a survey of U.S. Army personnel which may not be as representative of the population as a whole.

The PMHS study by Dempster (1955) provided body segment c.g. locations as a percentage of body segment length. The Dempster c.g. percentiles were combined with body segment lengths from CAESAR (or the Army data when the length was not available from CAESAR) to provide a second source for body segment c.g. locations.

A summary of the Army and AMVO mass data is found in Table 1. A summary of body region dimension data from CAESAR and the Army study are shown in Table 2. and target values for joint locations from CAESAR are shown in Table 3.

Table 1
Summary of body segment mass specifications

Body Segment	Database	
	Army data from ManneQuin Pro V8.0	AMVO
	Mass per dummy (kg)	Mass per dummy (kg)
Head	4.4	4.1
Neck	1.1	1.0
Upper Torso	21.5	23.7
Lower Torso	13.5	13.4
Upper arms (2)	4.0	3.5
Lower arms (2)	2.9	
Lower arms/hands (2)		4.0
Hands (2)	1.1	
Thighs (2)	19.6	17.2
Legs (2)	7.9	7.2
Feet (2)	2.0	2.0
Total	78.0	76.1

Table 2
Summary of body segment dimensions

Body Segment Dimensions	Target Value (mm)
Head Height	240
Head Breadth	154
Head Circumference	576
Head Length	200
Circumference at interscye	1008
Interscye distance	394
Hip circumference	1018
Bi-trochanteric breadth	361
Thigh Circumference	591

Table 3
Summary of joint locations

Dummy Whole Body Heights	Target Value (mm)
Top of Head	1757
T1	1519
H-Point	940
Knee	492
Ankle	73
Shoulder	1428
Elbow	1110
Wrist	851

Kinematic Response

Given the priority of whole-body kinematic biofidelity, it was considered essential to evaluate dummies under vehicle impact conditions. Kinematic response corridors based on cadaver tests were considered the most appropriate performance evaluation tool for pedestrian dummies evaluated under the same impact conditions. Since most published cadaver studies did not include the requisite combination of a late model vehicle, an identifiable vehicle model to reproduce the tests at other institutions, and multiple tests to facilitate kinematic corridors, the decision was made to focus on recent cadaver tests conducted by Kerrigan et al. (2005) with a small four-door sedan produced for sale in the US or Canadian market. While the suspension and wheels were removed to facilitate attachment to a sled system, the remainder of the vehicle fore of the b-pillar was maintained as was the total vehicle weight of $1175 \text{ kg} \pm 25 \text{ kg}$. The test impact velocity was $40 \pm 2 \text{ km/h}$ with no vehicle braking occurring until the pedestrian had ceased to be in contact with the vehicle. The pedestrian was oriented laterally with respect to the vehicle in a relatively upright mid-gait posture. The details and rationale behind the initial pedestrian orientation and impact conditions for these tests is described in Kam et al. (2005).

For assessment of pedestrian kinematics, high speed video was taken from an off board camera on the driver's side of the vehicle during the tests (Kerrigan et al., 2005). Photo targets were mounted to the cadaver head, 1st thoracic vertebra, and sacrum center. The motion of each body segment was measured by recording the location of each photo target at 4 ms intervals. The point of head strike, determined by visual examination of the video data and confirmed by head mounted accelerometers, was designated as the end of the interval of interest for computing kinematic trajectory data. Body segment velocities were calculated by differentiating the trajectory data. Since length of individual cadaveric body segments could vary, it was determined that an individual scale factor for each body segment of each cadaver was optimal for developing normalized trajectories. Corridors were developed using either the standard deviation of the recorded cadaver time-histories (e.g., head velocity) or the percentage of the pathlength traversed by the specific body region (Kerrigan et al., 2005). For pathlength corridors, it was felt that the responses shall fall within 10% and should fall within 5% corridors.

Component Response Characteristics

While the performance standard has been developed primarily for lateral pedestrian impact scenarios, it was decided that more proximal body structures (i.e., the chest and head) should have certain level of multidirectional response biofidelity. Multidirectional response is necessary to account for rotation of the pedestrian during the impact event. This rotational phenomenon is dependent upon initial orientation of the pedestrian and is described in detail by Meissner et.al. (2004). Lateral and frontal component response corridors were selected to ensure the biofidelic response characteristic of the head and thorax.

Head

Given that most existing pedestrian dummies use heads from existing frontal or side impact dummies, the decision was made to use well-established head response corridors already existing in certification, calibration, or biofidelity assessment procedures.

Frontal

The head drop test requirement for the Hybrid III (HIII) frontal dummy (FMVSS Part 572-F) was used as the biofidelity requirement for forehead impacts (Figure 2a). This requirement is based on cadaver drop tests by Hodgson and Thomas (1971). The mean peak resultant acceleration value of six forehead drop test was 250 g at 2.71 m/s, which corresponds to a free fall height of 376 mm. The requirement sets an allowable variation from the mean value of 10% (25g) (NHTSA, 2004).

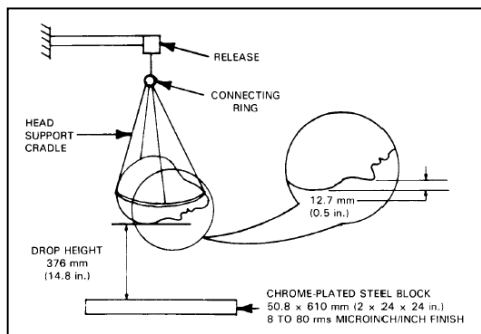


Figure 2a. Frontal head drop test.

Lateral

The head drop test requirement for the SID/HIII(FMVSS Part 572-M) was used as the biofidelity requirement for lateral head impacts (Figure 2b). This requirement was originally developed for the BioSID dummy and was also based on cadaver drop tests by Hodgson and Thomas (1975). The requirement requires the peak resultant

acceleration measured at the head c.g. to lie between 100 g to 150 g when dropped from a height of 200mm onto a rigid surface (NHTSA, 2004).

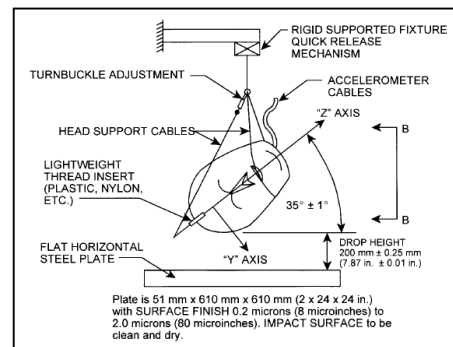


Figure 2b. Lateral head drop test.

Chest

Given that most existing pedestrian dummies used torsos from existing frontal or side impact dummies, the decision was made to use well-established chest response corridors already existing in certification, calibration, or biofidelity assessment procedures.

Frontal

For frontal response, it was decided the thoracic requirement should match the frontal pendulum requirement prescribed by Kroell (1976) for a 4.3 m/s frontal pendulum impact to the sternum.

Lateral

For lateral response, the thorax of the dummy should meet the lateral response requirements defined by ISO-9790 (ISO, 1999). This is a 4.3 m/s pendulum impact to the lateral aspect of the chest.

Lower Extremity

Unlike the more proximal body regions which experience significant rotations during the impact event, the lower limbs do not experience a significant non-lateral bending component when a pedestrian is initially struck by a laterally impacting vehicle. An assessment of pedestrian knee injury patterns (Teresinski, 2003; Bhalla et al., 2003) suggested that valgus bending was the most common failure loading mode for the knee. Pedestrian leg fractures due to bumper contact were attributed primarily to bending with shear loading of secondary importance (Teresinski, 2003). Thus, biofidelity curves were limited to valgus bending of the knee and latero-medial three-point bending of the leg.

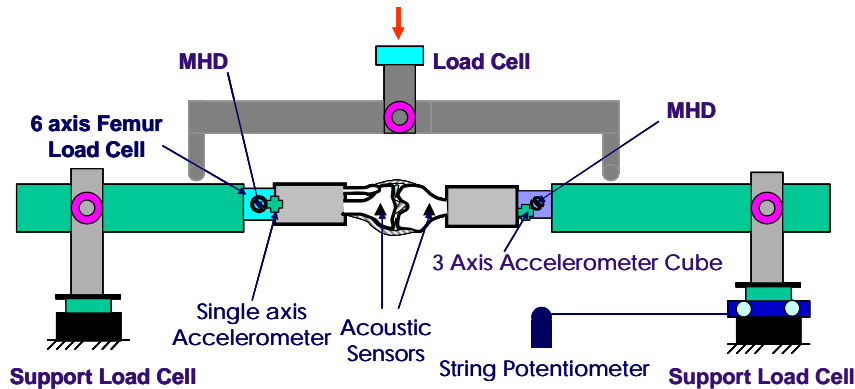


Figure 3. Schematic of the test set-up used by Bose et al. (2004) in symmetric valgus 4-point bending testing of intact human knee specimens.

Knee

The methodology and results of Bose et al. (2004) were chosen for symmetric valgus four-point bending of the knee (Figure 3). The angular velocity of the leg relative to thigh was approximately 1000°/s, determined to be a reasonable knee valgus bending rate for vehicle impacts in the range of 30 km/h to 50 km/h. Actuator and support load cells recorded the forces and moments applied to the knee specimen. Shear loads and valgus bending moments were also recorded adjacent to the knee structure using a multi-axis load cell. These forces were transferred to the knee joint using rigid body assumptions, recorded angular and linear accelerations of the segment between the load cell and knee, and inertial attributes of the segment. Ivarsson et al. (2004) scaled the inertially compensated moment-deflection responses provided by Bose et al. (2004) to the size of a 50th percentile male knee based on anthropometric femur, tibia, and patella data. A corridor was then developed around the characteristic average response using standard deviation calculations for both the independent variable (angle) and dependent variable (moment) as shown in (Figure 4).

Leg

Biofidelity requirements for leg response focused on three-point bending tests that would generate tibial bending strain rates characteristic of bumper impacts at 40 km/h. Kerrigan et al. (2003, 2004) subjected intact cadaver leg specimens to latero-medial three-point bending to failure at an approximate deflection rate of 1.5 m/s. The specimens were simply supported at a given specified distance from the proximal and distal ends such that the leg was loaded at mid-span (symmetric 3-point bending). The contact force between the impactor and specimen was

determined as the sum of the normal forces measured by the three-axis load cells at the right and left supports, respectively. The maximum bending moment acting on the specimen (right under the impactor) was determined at each instant in time during loading as the average of what was calculated from the right and left side support load cell signals. Specimen deflection was determined from the impactor displacement with zero deflection defined as initial contact between the impactor and specimen. The force-deflection and moment-deflection curves from each test were geometrically scaled to the size of a 50th percentile adult male thigh and leg. Ivarsson et al. (2004) developed response corridors of dynamic latero-medial loading for the 50th percentile male leg (Figure 5).

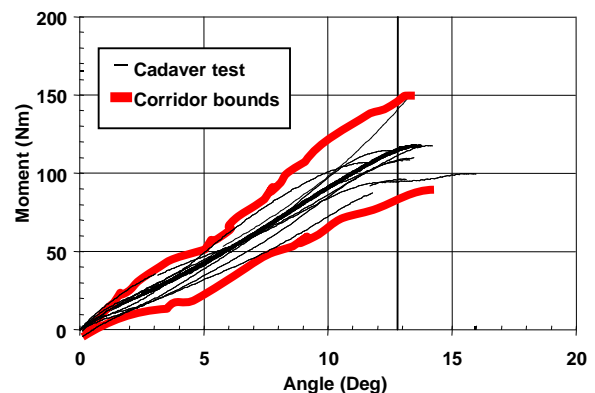


Figure 4. Moment-angle response corridor for the 50th percentile male knee subjected to dynamic 4-point valgus bending.

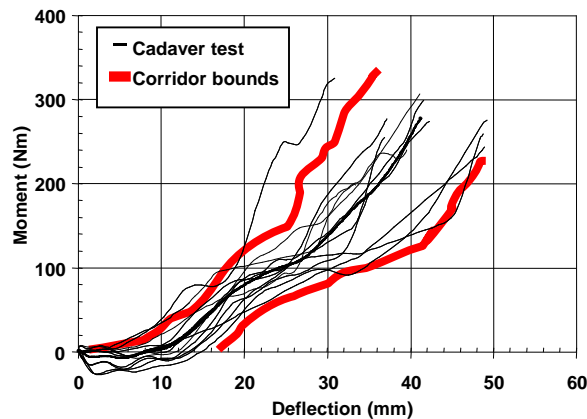


Figure 5. Moment-deflection corridor for dynamic latero-medial loading of the leg at mid-span.

While moment-angle responses were originally envisioned, inertial effects introduced complex bending modes with localized changes in deflection. Therefore, the decision was made to report a moment-deformation corridor for the mid-span position.

EVALUATION OF EXISTING TECHNOLOGY

Early in development of the pedestrian dummy recommended practice it was decided that there should be a focus on creating a practice that could be achieved using existing technology. To this end an extensive evaluation program was conducted to understand the capabilities and limitation of existing pedestrian dummy technology. These results were then used to help determine which requirements would be critical (must or shall) and which would be non-critical (recommended or should).

Test Programs

The PDTG sought involvement and participation by interested parties in the test and evaluation program for existing technology. It was requested that anyone wishing to evaluate an existing pedestrian dummy technology bring that device to the PDTG. The PDTG also solicited third party evaluations of the dummies under consideration. Two devices were submitted for evaluation, the modified Hybrid III and the Honda Polar-II, although only the latter was extensively evaluated based on interest level of the participating parties.

Five organizations participated in testing and evaluating the existing technology; DaimlerChrysler (Germany), PSA-Citroen Peugeot (France), Autoliv

(Sweden), Nissan (Japan) and University of Virginia (USA). A summary of their test programs and brief synopsis of their finding is included here. Detailed summaries for each test series can be found in the documentation of the PDTG Test and Evaluation subgroup. Several organizations also contributed reports and data from pedestrian dummy testing that was not directly part of the PDTG activity.

DaimlerChrysler

The first program to test existing pedestrian dummy technology within the PDTG was conducted by DaimlerChrysler in Germany. Originally 13 tests with the Honda Polar-II were planned, but due to dummy damage and schedule delays, the test series was reduced to 8 tests (Table 4), two of which were discounted due to severe damage at 40 km/h. All tests were conducted between 30 km/h and 40 km/h in a lateral impact stance using a Mercedes E-Class vehicle. These tests showed the importance of initial positioning for achieving consistent results as well as demonstrating the influence of arm position on pedestrian kinematics.

**Table 4
DaimlerChrysler Test Matrix**

Arm Configuration	Speed	Comments
taped to torso	30 km/h	
bound in front	30 km/h	
bound to sides	30 km/h	
bound in front	40 km/h	Not analyzed – Severe damage
bound in front	40 km/h	Not analyzed – Severe damage
bound in front	35 km/h	
bound in front	35 km/h	
bound in front	35 km/h	

PSA Peugeot Citroen

Originally seven tests with the Polar-II were planned with five vehicles at PSA in France, but upon arrival the dummy was in poor condition and required substantive repair before testing could begin. As a result of the delayed schedule only four tests were conducted as shown in Table 5. Each of these tests was conducted at 40 km/h in a lateral stance with a different vehicle type for each test. These vehicles ranged from a small car to an MPV or van. This series helps to demonstrate the usefulness of pedestrian dummies in understanding kinematic impact differences between different vehicle types

**Table 5
PSA Test Matrix**

Vehicle Category	Vehicle Model	Speed
Small Car	Citroen C3	40 km/h
Small Family Car	Peugeot 307	40 km/h
Large Family Car	Peugeot 407	40 km/h
Van/MPV	Peugeot 807 (Citroen C8)	40 km/h

Autoliv

Six tests were conducted with the Polar-II dummy at Autoliv in Sweden to assess the usefulness of pedestrian dummies in the development of active pedestrian protection systems such as pop-up hood and pedestrian windshield airbags (Table 6). These tests include one reference test, three active hood tests, and two airbag tests. All tests were conducted at 40 km/h in a right side lateral impact configuration with the hand tied in front and the impact leg rearward. The vehicle tested was modeled after the Saab 9-5 large sedan.

It was determined that due to the wrap around distance of the 50th percentile dummy, not all desired impact locations could be contacted without modification of the test setup. In order to impact the desired head impact locations the ground level of the dummy was adjusted relative to the vehicle. For impacts to the hood structures the vehicle was raised and for contacts to the windshield area the dummy was raised.

**Table 6
Autoliv Test Matrix**

Purpose	Impact Location	Vertical Position
Reference Test	Hood Centerline	-95 mm
Active Hood	Hood Centerline	-95 mm
Active Hood	Above Lifter	-180 mm
Active Hood – Late Trigger	Above Lifter	-180 mm
Scuttle Bag + Active Hood	Low Windscreen Centerline	+45 mm
A-Pillar Bag + Active Hood	A-Pillar	+45 mm

Nissan

A series of 16 tests were performed by Nissan Motor Company in Japan to evaluate the Polar-II and standing Hybrid-III dummies in pedestrian and bicyclist impact scenarios. These tests looked at repeatability, variation in impact speed, variation in hand position and variation in leg position for the standing pedestrian in a lateral impact. In addition to a typical pedestrian test configuration, bicyclist tests were conducted with each dummy in front and lateral impact scenarios.

UVa

In addition to the full-scale cadaveric pedestrian tests used to create the biofidelity corridors for whole-body trajectory, the University of Virginia conducted a series of tests with the Polar II at 40 km/h. These tests were intended to replicate the cadaver test configuration and help to assess the ability of existing technology to satisfy the proposed corridors. This testing is explained in further in the section detailing whole body kinematics.

Non-PDTG Activities: VRTC, U of Adelaide

Several organizations which performed pedestrian dummy testing outside of the PDTG activity choose to participate in the task group by providing feedback, reports, and data from their testing. These organizations include the NHTSA Vehicle Research and Test Center (VRTC) in the United States and the University of Adelaide in Australia. Both of these organizations did testing to reconstruct real world crashes using the Polar-II. These two series help to demonstrate the usefulness of pedestrian dummy technology in the investigation and reconstruction of real world pedestrian crashes. They also help provide insight into the usability and durability of existing pedestrian dummies.

Durability

Given the potentially severe interaction between a pedestrian and the exterior of the vehicle or ground, it is important that a pedestrian dummy have a reasonable level of durability. For the purpose of the PDTG, it was decided that a pedestrian dummy should be able to demonstrate durability at a speed of 50 km/h, 10 km/h greater than the target impact velocity for biofidelity assessment. Testing conducted by several organizations looked at the durability performance of the Polar-II as an example of existing technology. Damage was noted in several test series dependent upon vehicle model and impact configuration.

In the first test series, conducted at DaimlerChrysler, their test engineers concluded 40 km/h impacts were too severe for the Polar-II and

evaluation was limited to 35 km/h for the remainder of their test series. In these 40 km/h tests the dummy sustained broken tibia components as well as damage to some sensors and data acquisition unit components from both vehicle and ground contact. PSA found the dummy to be in poor condition upon initial inspection and made extensive repairs before beginning their test series. In their four tests at 40 km/h they found that overall durability of the dummy was good, but some improvements were needed for the wiring layout to avoid sensor cable damage. Nissan also found some concern for the routing of sensor wires and encountered shoulder damage when the dummy's hands were tied behind its back. Tests at Autoliv and the University of Virginia found little concern for durability of the dummy in 40 km/h impacts. Tests conducted by other organizations also identified some minor durability concerns at 40 km/h, but generally found the damage was acceptable for the severity of impact that was experienced. In addition to the test series described, Honda R&D conducted a test at 50 km/h to confirm the whole body durability requirement prescribed in the standard. In this test there was minimal damage to the dummy and therefore it was concluded that a 50 km/h impact with a small passenger car is an achievable requirement for a pedestrian dummy.

Usability

In terms of usability, or ease of use, there was a general consensus that existing pedestrian dummies such as the Polar-II are generally easy to use with a few key exceptions. Most significant is dummy positioning. Since the Polar-II dummy cannot support its own weight in a standing position, the dummy needs to be suspended which can make it difficult to achieve a consistent initial position. Considering the importance of initial position for dummy kinematics, it was determined that the standard should include extensive positioning guidelines for the whole body kinematic test requirements. Other usability items that came up were related to the data acquisition system damage and repair of damaged dummy components. Most of the data acquisition concerns were related to integration for use in individual test labs and damaged cabling during testing. Regarding the repair of dummy components the most significant issue was the availability of replacement parts. Since the Polar-II is still a prototype device, spare parts are not always available and lead times can be long.

TEST RESULTS/REPEATABILITY

Repeatability performance of the Polar-II was evaluated in test series conducted by both the University of Virginia and DaimlerChrysler. In each of these series, one vehicle model was used for multiple tests.

During the course of the biofidelity evaluation at UVA, a series of three dummy tests was conducted with the Polar-II positioned in same initial orientation to assess the kinematic response biofidelity. Film analysis of the three tests showed that very consistent results were obtained for the head, T1, and pelvis trajectories. The head trajectory response graph is shown in Figure 6 as an example. Figure 7 and 8 demonstrate repeatability of sensor responses during repeated tests at the same impact conditions.

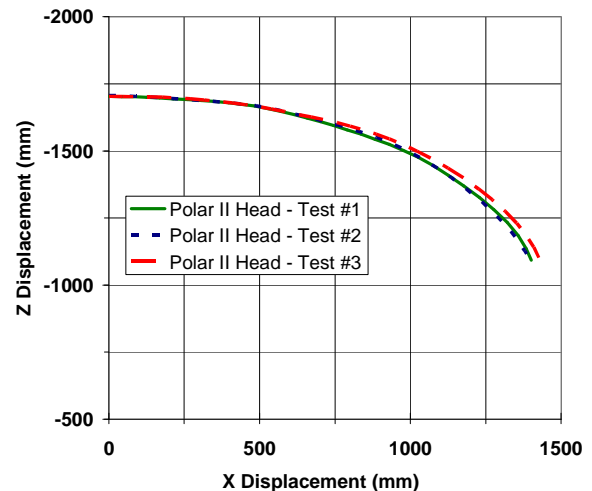


Figure 6. Polar-II head trajectory response repeatability from UVA testing

For the three tests with varied arm positions, the results of these two test series indicate that achieving a repeatable whole body trajectory is a reasonable response target for existing pedestrian dummy technology. The response, however, is dependent upon initial positioning of the dummy and can be greatly varied by changes in arm position, leg position, and orientation. Figure 9 depicts the tests conducted with variation only in the position of the upper extremities. The results indicate the sensitivity of proximal responses (e.g., the head) to more distal contacts, in this case the upper extremities. While interaction of this type would likely occur in actual pedestrian contacts with the same impact conditions, repeatability of results will require standardized procedures. Therefore, the pedestrian dummy

standard will include detailed test procedures and positioning data.

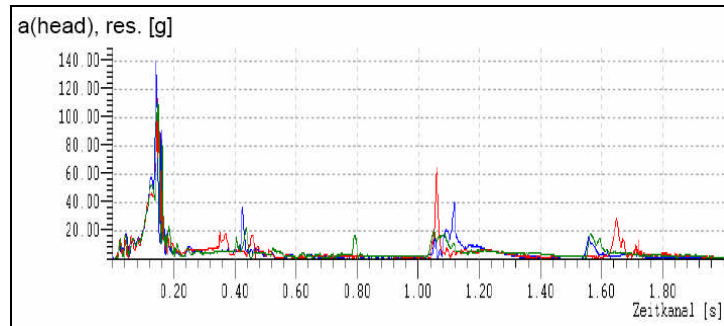


Figure 7. Polar-II head acceleration response repeatability testing at 35 km/h. (Courtesy of DaimlerChrysler).

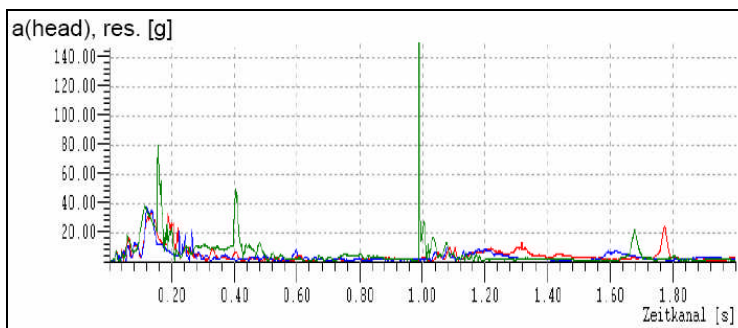


Figure 8. Polar-II head acceleration response variation with arm position changes at 30 km/h. (Courtesy of DaimlerChrysler).

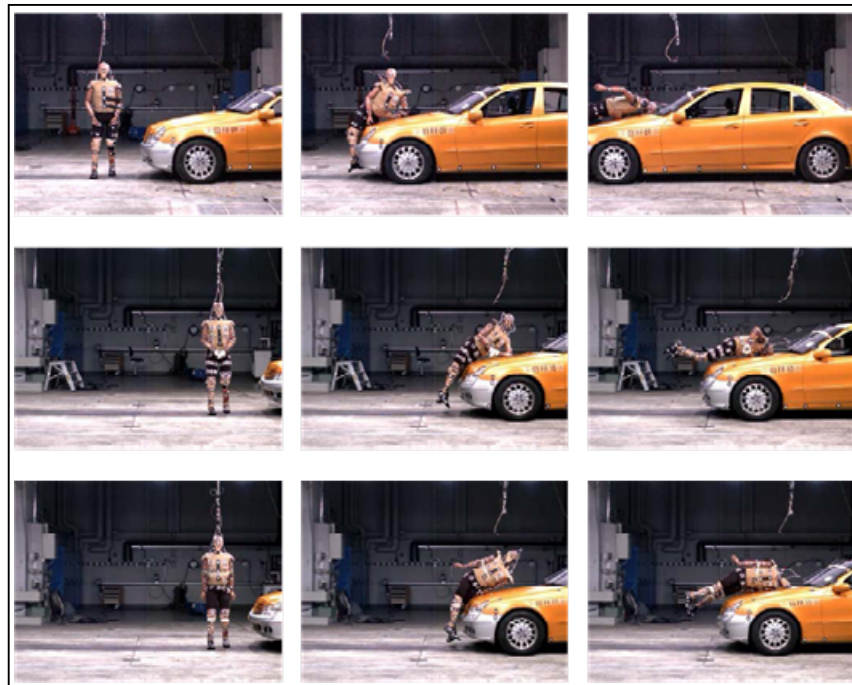


Figure 9. Polar-II whole body kinematic response variation with arm position changes at 30 km/h. (Courtesy of DaimlerChrysler).

Anthropometry

The ability of existing pedestrian dummy technologies to comply with the proposed anthropometry targets was evaluated by comparing Polar II measurements with the proposed targets. Tables 7 and 8 show the proposed target values, the Polar II measurements, and the percentage deviations.

Table 7
Comparison of body segment dimensional targets and the Polar II

Body Segment Dimensions	Target Value (mm)	Polar II (mm)	% Deviation
Head Height	240	237	1.3%
Head Breadth	154	157	-1.9%
Head Circumference	576	586	-1.7%
Head Length	200	200	0.0%
Circumference at interscye	1008	1005	0.3%
Interscye distance	394	356	10.7%
Hip circumference	1018	1038	-1.9%
Bi-trochanteric breadth	361	378	-4.5%
Thigh Circumference	591	548	7.8%

Table 8
Comparison of dummy height targets and the Polar II

Dummy Whole Body Heights	Target Value (mm)	Polar II (mm)	% Deviation
Top of Head	1757	1750	0.4%
T1	1519	1439	5.6%
H-Point	940	906	3.8%
Knee	492	489	0.6%
Ankle	73	65	12.3%
Shoulder	1428	1426	0.1%
Elbow	1110	1130	-1.8%
Wrist	851	864	-1.5%

Kinematic Response

In an effort to assess whole-body response of existing dummy designs, the Polar-II dummy was evaluated in impact conditions comparable to those used to develop the cadaver kinematic corridors (Kerrigan et al., 2005). Specifically, the pedestrian dummy was oriented to approximate the pre-impact body orientation of the cadavers. All vehicle conditions including impact speed were maintained. To facilitate body region specific response comparisons with the cadaver corridors, photo targets were affixed to the head c.g., upper spine, chest c.g., and pelvis c.g. Identical film analysis procedures were employed for the cadavers and dummies. The resulting Polar-II responses were compared with the cadaver corridors and the resulting responses are shown in Figures 10-13. Using 10% path length definitions of corridor width, all Polar-II responses with the exception of head velocity-time histories were contained in the PMHS corridor bounds. Using the standard deviation

corridor for head velocity, however, the head velocity-time history did not fall within the corridor. This suggests that existing technology does comply with the majority of standard requirements although additional refinements may be necessary to satisfy all corridors.

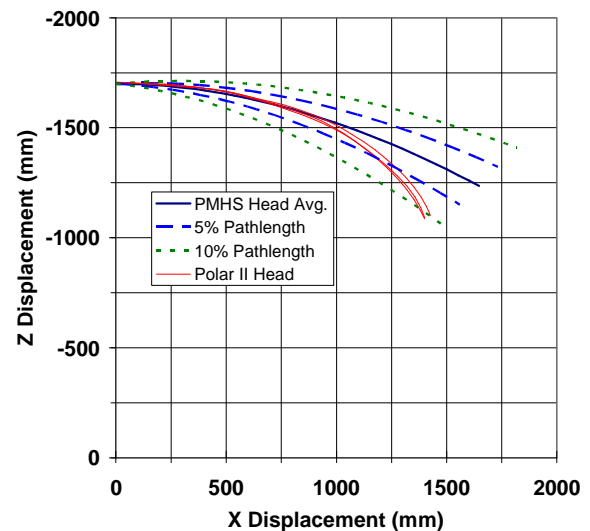


Figure 10. Polar II head response relative to cadaver corridors.

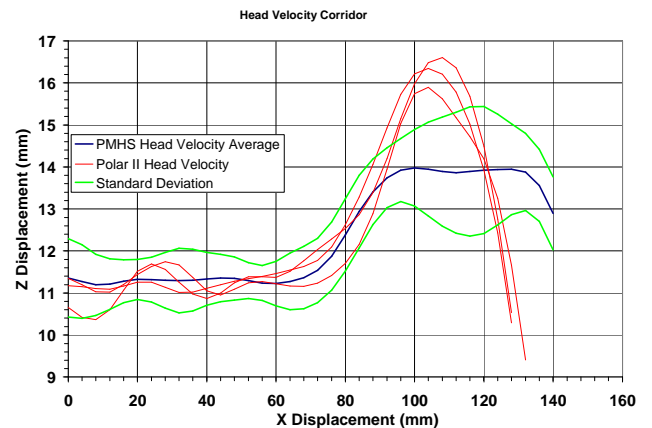


Figure 11. Polar II head velocity response relative to one standard deviation cadaver corridor.

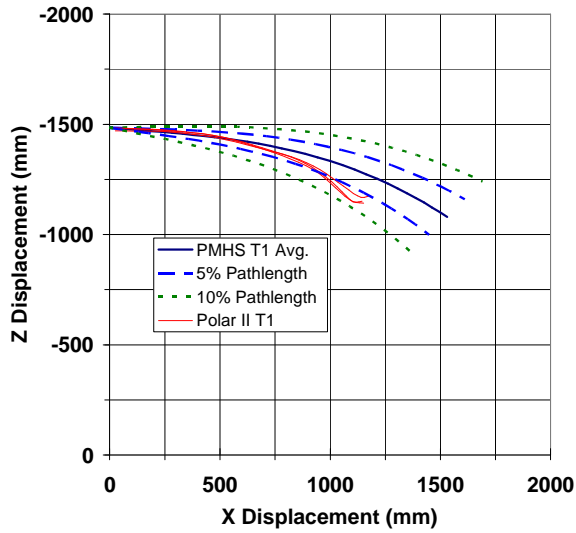


Figure 12. Polar II T1 response relative to PMHS corridors.

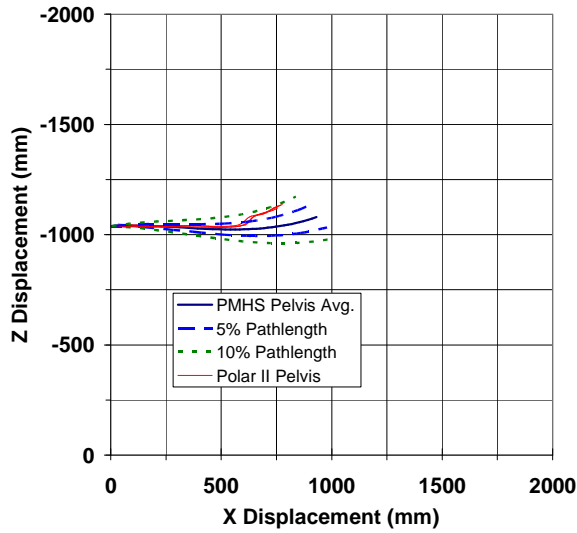


Figure 13. Polar II pelvis response relative to PMHS corridors.

The 5% corridors have also been included in the recommended practice to provide future design targets for refinement of the dummy components. In terms of satisfying the pathlength requirements, the PDTG envisions requiring (i.e., shall) compliance at the 10% corridor level while recommending (i.e., should) compliance at the 5% level.

Component Response

Head

The Hybrid III head is used for both the Hybrid III and Polar II pedestrian designs. Therefore, five frontal drop tests of the Hybrid III head were conducted in accordance with the required test procedure. Little variability was observed with minimum and maximum values of resultant head acceleration of 267 g and 270 g respectively. In addition, all resultant accelerations were within the required corridor of 225 to 275 g.

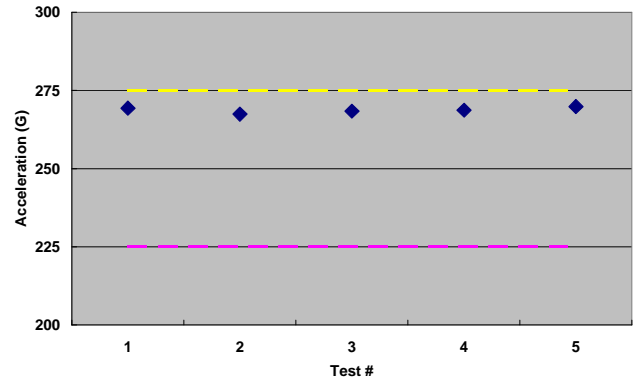


Figure 14. Frontal drop tests acceleration results and corridors.

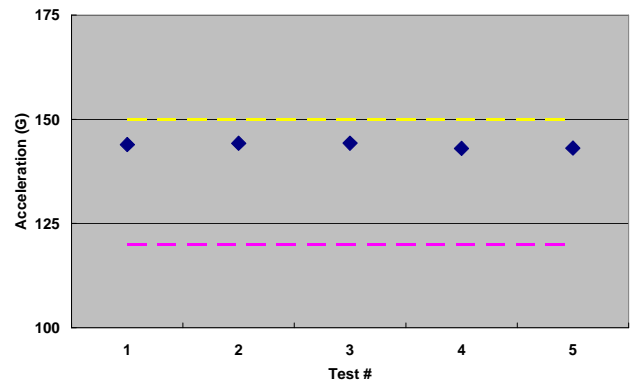


Figure 15. Lateral drop tests acceleration results and corridors.

Chest

Five 4.3 m/s pendulum tests were conducted to evaluate the Polar-II for the proposed lateral thoracic biofidelity requirement. A very repeatable response was observed in the five tests and it was demonstrated that the corridor can be achieved using

current technology (Figure 16). This dummy is not configured to measure lateral spine acceleration at T1, so the ISO-9790 lateral spine acceleration-time corridor was not evaluated.

Frontal pendulum tests were not conducted using the Polar-II because this dummy is not currently instrumented to measure anterior-posterior chest deflection. However, as the Polar-II's rib structure is a modified version of the Thor dummy it is postulated that there will be some acceptable level of biofidelity in this mode.

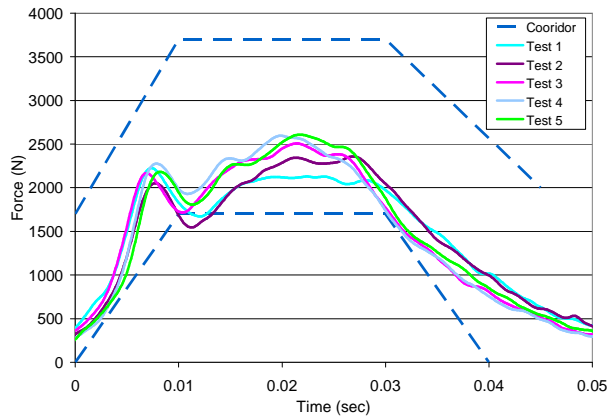


Figure 16. Lateral thoracic response biofidelity of Polar-II.

Lower Extremity

The Polar II lower extremity was evaluated using procedures identical to those of the PMHS tests used to develop the biofidelity corridors. A more detailed discussion of these tests can be found in Takahashi et al. (2005).

Knee

Three dynamic four-point bending tests of the Polar-II knee were conducted. Test results show that the moment-angle characteristics of the Polar knee are within the corridor established from PMHS test results.

Leg

Three replicate dynamic three-point bending tests were conducted with the Polar-II tibia. Moment-deflection and moment-angle characteristics were compared with corridors made from PMHS test results. Both characteristics almost fall within the corridors. These results show that the Polar tibia satisfies the biofidelity requirements for the leg.

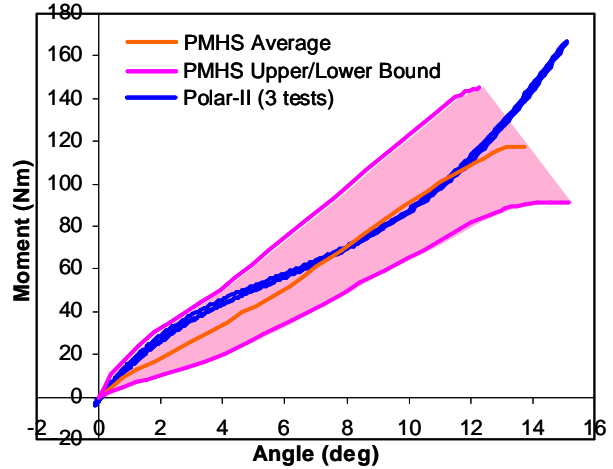


Figure 17. Moment-angle characteristics of Polar-II knee and corridors for corresponding cadaver tests.

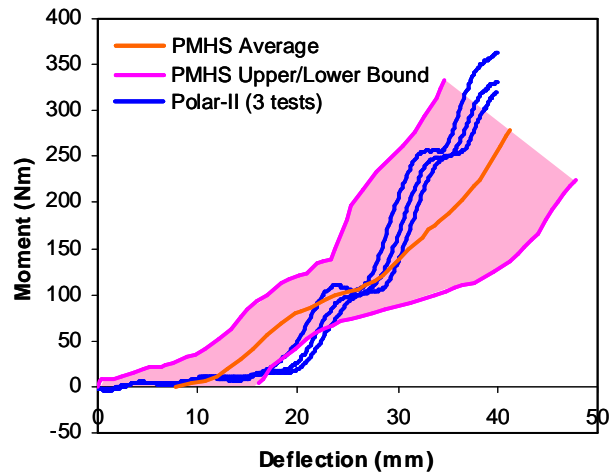


Figure 18. Moment-deflection characteristics of Polar-II leg and corridors for corresponding cadaver tests.

CONCLUSIONS

The SAE PDTG has developed a performance standard for specification of minimum anthropometric, kinematic, and response requirements of a pedestrian dummy. Existing hardware has been shown to be capable of achieving the majority of requirements at both a global (i.e., whole body kinematics) and component level (i.e., specific body region biofidelity). The goal of the SAE PDTG is to have the standard completed by

June 2005. Therefore, while the intent of the PDTG in specifying performance targets will remain unchanged, many of the precise tolerances on these requirements should be considered preliminary.

DEFINITIONS

PMHS – post-mortem human subject
PDTG – Pedestrian Dummy Task Group
SAE – Society of Automotive Engineers
NHTSA – National Highway Traffic Safety Administration
VRTC – Vehicle Research and Test Center
UVA – University of Virginia
PSA – Citroen Peugeot

ACKNOWLEDGEMENTS

We would like to thank the organizations who have been actively involved in the PDTG activities for their generous contributions. In particular we thank DaimlerChrysler, PSA-Citroen Peugeot, Nissan, Autoliv, and the University of Virginia for their test and evaluation programs. We also thank GESAC, DTS, and FTSS-Europe for their technical support and TRW and TNO for simulation support. Finally we thank Honda R&D for making the Polar-II available for industry wide evaluation.

REFERENCES

Akiyama, A., Okamoto, M., Rangarajan, N., Development and Application of the New Pedestrian Dummy, Paper 463, 17th ESV, Amsterdam, Netherlands, 2001.

Bhalla, K.; Bose, D.; Madeley, J.; Kerrigan, J.; Crandall, J.; Longhitano, D.; Takahashi, Y.; "Evaluation of the Response of the Mechanical Pedestrian Knee Joint Impactors in Bending and Shear Loading," Paper Number 429, 18th International Technical Conference on the Enhanced Safety of Vehicles, Nagoya, Japan, May, 2003.

Bose, D., Bhalla, K., Rooij, L., Millington, S., and Crandall, J., 2004, "Response of the knee joint to the pedestrian impact loading environment," Society of Automotive Engineers, 2004-01-1608, Warrendale, PA, March, 2004.

Dempster, W. T., Space requirements of the seated operator. Technical Report USAF, WADC TR-55-159

(AD 87 892), Wright Air Development Center, Wright-Patterson Air Force Base, Ohio, 1955.

European Enhanced Vehicle-Safety Committee, "EEVC Working Group 17 Report – Improved Test Methods to Evaluate Pedestrian Protection Afforded by Passenger Cars" www.eevc.org, 2002.

Frederiksson, R., Haland, Y., Yang, Evaluation of a New Pedestrian Head Injury Protection System with a Sensor in the Bumper and Lifting of the Bonnet's Rear Part, Paper 131, 17th ESV, Amsterdam, Netherlands, 2001.

Harris, J. A study of test methods to evaluate pedestrian protection for cars. European Experimental Vehicles Committee. The 12th International Technical Conference on Experimental Safety Vehicles, 1989.

Harrison C. and Robinette, K. "CAESAR: Summary Statistics for the Adult Population (Ages 18-65) of the United States of America," AFRL-HE-WP-TR-2002-0170; United States Air Force Research Laboratory, Wright-Patterson AFB, Ohio, 2002.

Hattori, K., Hayashi, S., Sakuma, S., Study for evaluation method of pedestrian injury on simulated pedestrian accidents, Paper 20005406, JSAE, Yokohama, Japan, 2000.

Hodgson, V. R. and Thomas, L. M., "Breaking Strength of the Human Skull versus Impact Surface Curvature," NHTSA Report No. DOT-HS-800-583, June 1971; partial results published as "Comparison of Head Acceleration Injury Indices in Cadaver Skull Fractures," Paper 710854, Proceeding of Fifteenth Stapp Car Crash Conference, P-39, New York; Society of Automotive Engineers, Inc., 1971.

Hodgson, V. R. and Thomas, L. M., 1975, "Head Impact Response," Vehicle Research Institute Report-VRI 7.2, Society of Automotive Engineers, 1975.

Huang, T. J., McDonald, J., Artis, M., Rangarajan, N., Shams, White, R., Beach, D., Campbell, R., Akiyama, A., Yoshida, S., Ishikawa, H., Konosu, A., Development of a Biofidelic Dummy for Car-pedestrian Accident Studies, IRCOBI, Sitges, Spain, 1999.

ISO/TC22/SC12 Road vehicles – Anthropomorphic side impact dummy – Lateral impact response requirements to assess the biofidelity of the dummy. Reference number ISO/TR 9790:1999.

ISO TC 22/SC 22/WG 22. "Motorcycles — Test and analysis procedures for research evaluation of rider crash protective devices fitted to motorcycles — Part 4: Variables to be measured, instrumentation, and measurement procedures". ISO/DIS 13232-4, August 31, 2004, Copyright ISO, 2004.

ISO TC 22/SC 22/WG 22. "Motorcycles — Test and analysis procedures for research evaluation of rider crash protective devices fitted to motorcycles — Part 5: Injury indices and risk/benefit analysis". ISO/DIS 13232-4, September 7, 2004, Copyright ISO, 2004.

Ivarsson, J., Lessley, D., Bhalla, K., Kerrigan, J., Crandall, J., and Kent, R., "Dynamic response corridors and injury thresholds for the pedestrian lower extremities," 2004 IRCOBI Conference on the Biomechanics of Impacts, Graz, Austria.

Kam C, Kerrigan J, Meissner M, Drinkwater C, Murphy D, Bolton J, Arregui C, Kendall R, Ivarsson J, Crandall J, Deng B, Wang JT, Kerkeling C, Hahn W. (2005) Design of a full-scale impact system for analysis of vehicle pedestrian collisions. Paper 2005-01-1875, Society of Automotive Engineers, Warrendale, PA.

Kerrigan, J., Bhalla, K., Funk, J., Madeley, N., Crandall, J., "Experiments for Establishing Pedestrian-Impact Lower Limb Injury Criteria ", SAE Paper 2003-01-0895, Warrendale, PA, 2003.

Kerrigan J, Drinkwater DC, Kam CY, Murphy D, Ivarsson BJ, Crandall J, Patrie J. "Tolerance of the human leg and thigh in dynamic latero-medial bending." International Journal of Crashworthiness, 9(6): 607 – 623, 2004.

Kerrigan, J. R.; Drinkwater, C.; Kam, C.; Murphy, D.; Crandall, J. R.; "Kinematic Corridors comparing the Polar II with Cadavers in Pedestrian Impact Tests," Paper 05-0394, ESV 2005, Washington, D.C., June 2005

Kroell, C., Schneider, D., Nahum, A., (1971) "Impact Tolerance and Response of the Human Thorax." Proceedings of the 15th Stapp Car Crash Conference, SAE Paper 710851.

Kroell, C., Schneider, D., Nahum, A., (1974) "Impact Tolerance and Response of the Human Thorax II." Proceedings of the 18th Stapp Car Crash Conference, SAE Paper 741187.

Kroell, C (1976) "Thoracic Response to Blunt Frontal Loading." Society of Automotive Engineers, Warrendale, PA.

Lessley, D. R., Crandall, J. R., Shaw, C. G., Kent, R. W., Funk, J. R., "A Normalization Technique for Developing Corridors for Individual Subject Force-Deflection Responses," Society of Automotive Engineers, 2004-01-0288, Warrendale, PA, March, 2004.

ManneQuinPRO V8.0 Software Program as used and displayed by Natick US Army Database. (1988) Anthropometric database for creating mannequins and the Highway Safety Research Institute database for creating child mannequins.

Meissner, M., Van Rooij, L., Bhalla, K., Crandall, J. R., Longhitano, D. C., Takahashi, Y., Dokko, Y., "A Multi-body Computational Study of the Kinematic and Injury Response of a Pedestrian with Variable Stance upon Impact with a Vehicle," Society of Automotive Engineers, 2004-01-1607, Warrendale, PA, March, 2004.

NHTSA (2004) "Anthropomorphic Test Devices" 49 CFR Ch. V Pt. 572; Code of Federal Regulations, National Archive and Records Administration, Washington.

Snedeker, J., Muser, M., Walz, F., Assessment of Pelvis and Upper Leg Injury Risk in Car-Pedestrian Collisions: Comparison of Accident Statistics, Impactor Tests and Human Body Finite Element Model, 47th Stapp, San Diego, CA, USA, October 2003.

Takahashi, Y.; Kikuchi, Y.; Okamoto, M.; Akiyama, A.; Ivarsson, J.; Bose, D.; Subit, D.; Shin, J. H.; Crandall, J.; "Biofidelity Evaluation for the Knee and Leg of the Polar Pedestrian Dummy," Paper Number 05-0280, ESV 2005, Washington, D.C., June 2005.

Teresinski, G. and Madro, M., A Comparison of Mechanisms of Ankle, Knee, Pelvis and Neck Injuries in Pedestrians and in Cyclists According to the Direction of Impact and Type of Vehicle, IRCOBI, Lisbon, Portugal, 2003.

THE NEXT STEPS FOR PEDESTRIAN PROTECTION TEST METHODS

Graham J L Lawrence

TRL Limited

United Kingdom

with contributions from EEVC WG17 members

Paper 05-0379

ABSTRACT

In most countries pedestrians and other vulnerable road users form a significant proportion of all road user casualties. Research has shown that measures to improve car design, to mitigate pedestrian injuries in collisions, can be very effective in reducing the number of fatalities and serious injuries. Therefore EEVC Pedestrian Working Groups (WGs 7, 10 and 17) have worked since the 1980's to produce test methods and criteria. Recently the European Parliament and Council approved a Directive, which reflects the EEVC WG17 test methods (in two stages), to require new cars to provide pedestrian protection.

Most test tools and procedures can be improved, as can be seen for example by the ongoing process of developing new and improved vehicle occupant dummies and their associated test procedures. The IHRA Pedestrian Safety Working Group (with input from EEVC WG17) and others are all contributing to this process by building on, and expanding the current test methods.

This paper discusses the way forward for the next generation of pedestrian test methods. It includes discussion of the options to increase the number of vehicle types and protected areas and to protect at higher speeds. Possible improvements to the test methods and tools, such as adding an upper body mass and flexible bones to the legform impactor, refining the impact conditions, and testing with a combination of dummy and subsystem tests, are also discussed.

INTRODUCTION

Pedestrians and pedal cyclists form a significant proportion of all road user casualties in most countries. There are two complementary ways of improving this situation: by preventing or reducing the severity of the collision and by making vehicles less injurious to pedestrians in accidents; ideally both of these should be used together. The EEVC Pedestrian Working Groups WGs 7, 10 and 17 have been working since the 1980's on the second of these two measures and have produced test methods and criteria suitable for developing and testing safer vehicles. Recently the European Parliament and Council approved a Directive (with two stages), which reflects the EEVC WG17 test

methods, to require new cars to provide protection for pedestrians (vulnerable road users).

Most test tools and procedures can be improved, as can be seen by the ongoing process of developing new and improved vehicle occupant dummies and their associated test procedures, for example the THOR and World SID dummies. For pedestrian protection the IHRA Pedestrian Safety Working Group (IHRA PSWG) and others are all contributing to this process by building on and expanding the current test methods.

Following completion of their primary task of developing pedestrian test methods, EEVC WG17's new mandate includes providing a contribution to the work of the IHRA PSWG. Although WG17's mandate does not include a comprehensive programme of improving and expanding their test methods they are well placed to provide some guidance on the options and best ways that this could be achieved.

This paper discusses the way forward for the next generation of pedestrian test tools and methods.

OPTIONS FOR ASSESSING OR REQUIRING PROTECTION

The pedestrian protection provided by a vehicle can be assessed by using suitable test methods and appropriate injury risk curves for the injury parameters recorded by the test tools. If these are combined with suitable protection performance criteria, then it can be used in a regulation to require minimum standards of pedestrian protection as is the case with the EU Directive. It should be noted that the tests methods developed by WG10 and later refined by WG17 were, at the request of the European Commission, developed to be suitable for use in a regulation to require manufacturers to make vehicles with pedestrian protection.

Types of Test

Physical dummies. Test methods making use of physical pedestrian dummies might initially appear to be the most obvious test tool for assessing a car's pedestrian protection. Provided that the pedestrian dummy or dummies used have appropriate properties such as joints, etc. and instrumentation then every contact likely to cause serious or fatal injuries can be assessed from

bumper contact through to head impact. Stature is the most important variable for head impact location in real life. Therefore, if the test method is intended to assess the whole area of a car that could be involved in a head impact, then a family of pedestrian dummies of different statures would be required. For the head impact area, as well as having to test each vehicle with this family of dummies, a number of tests would be required with each dummy at increments across the width of the car. In addition a pedestrian's stance and direction of motion will influence the nature and severity of each stage of the accident. For example in one case the shoulder might make first contact reducing the severity of the head impact but in a second case the kinematics might be such that shoulder contact is minimal giving a more severe head impact. However, some form of worst case setting of the dummies stance might overcome the need to reproduce this range in full. Nevertheless, even if it was decided that only one stance was necessary a dummy based test method require that a suitable family of dummies be developed and it would need a very large and expensive test matrix to be carried out for each car model to assess the protection provided.

Sub-system tests. As discussed above, test methods using impacts between the physical car and a pedestrian dummy have a number of disadvantages for use in a regulatory type test. Sub-systems tests have the following advantages over testing with dummy tests:

- They can easily be used to test the whole area likely to strike pedestrians.
- They can be aimed accurately at selected danger points.
- They give good repeatability.
- The tests cost less to perform.
- The test requirements are simpler to design and to model mathematically.
- They can be more easily used in component development.
- The test severity can be adjusted (e.g. by energy cap) to take account of practical design limitations.

On the other hand, although sub-system tests solve many of the problems of a regulatory test based on physical dummies, they also introduce their own problems:

- They are a simplification of the real situation.
- Appropriate test conditions and test areas must be provided for each sub-system test.
- The test conditions, test areas and any associated mark-up rules, look-up graphs or tables may become inappropriate with time, if vehicle styling goes outside the range considered or anticipated by their authors.

Mathematical modelling of pedestrian (or impactors) and car. There are at least six potential or already established uses for mathematical modelling for pedestrian protection:

1. To determine generic sub-system tests' impact conditions; these can be expressed with in a test method in look-up graphs or tables.
2. Interactively within a test method to determine impact conditions appropriate for the specific vehicle under test; this should be for both the shape and stiffness of the vehicle under test (not just shape as both will influence subsequent contacts).
3. As a completely virtual vehicle and pedestrian test approval tool.
4. To serve as a vehicle design and development tool for new models for:
 - a. pre-development and concept studies
 - b. definition of design guidelines and styling fix points
 - c. determining and refining the energy absorption performance of the vehicle body parts in the pedestrian impact area.
5. To examine the effects of measures to meet the test requirements under a wider range of accident situations to identify and rectify any inadvertent negative effects.
6. To determine whether deployable protection devices work as intended, e.g. for a pop-up bonnet system the kinematics and timings for a range of vehicle impact speeds, pedestrian statures and motion.

For point one above, this has the advantage that the experts developing the test method would be best placed to determine whether the simulation results are appropriate. It is important to reflect in the vehicle model the level of pedestrian protection likely to be found in the real vehicles that the method is intended for. For example the EEVC test methods were developed for approving vehicles with pedestrian protection and therefore the simulated car used to determine the bonnet leading edge test energies used a family of generic cars that had a pedestrian friendly bumper and bonnet leading edge. If instead the sub-system test results were intended for comparing with the real life bonnet leading edge injuries found with current cars, then the car model would need to represent a car with current levels of pedestrian protection. This is because, for example, a more violent bumper impact might reduce the severity of the bonnet leading edge impact.

Point two, above, might be achieved with a relatively simple pedestrian and car model as it will only have to produce realistic kinematics. Point 3 would require sophisticated finite element models of the pedestrian (or the pedestrian sub-system impactor) and of the car being assessed. Both the software and a protocol for these two uses would

need to be included in the test method to give consistent results. Alternatively, a series of validation corridors for both the pedestrian and car model could be provided against which the performance of any proposed or improved model could be judged. Provided that these validation corridors were appropriate a score system could be used to accept or reject proposed models.

For point four both the models and the levels of validation of them would be chosen by the manufacturer and they could balance their confidence in the simulation results with an appropriate level of physical testing of materials, components and prototype vehicles.

Point five might again be at the manufacturers' discretion to cover their 'due care' responsibilities to identify and rectify solutions that pass the test but might be dangerous in real life (unsatisfactory solutions that the test methods or test tools are insensitive to).

For point six, both the validation of the pedestrian and vehicle models and the range of impact situations (vehicle speed, pedestrian stature, etc.) simulated would have to be sufficient to satisfy the approval authorities that the system will work as intended.

Combination of test methods. Features of the three main types of test listed above can be used in combination to find a 'best' test method solution. One example is the EEVC upper legform to bonnet leading edge sub-systems test. The upper legform to bonnet leading edge sub-system test is designed to assess the aggressiveness of the bonnet leading edge in car to pedestrian impacts, which is highly dependent on the vehicle shape. This is because the impact velocity and effective mass of the parts of the pedestrian (typically thigh and / or pelvis) impacted by the bonnet leading edge vary with vehicle shape. Therefore, for this test the impact conditions were derived from a combination of tests between physical pedestrian dummies and instrumented car(s) and results of mathematical simulations of pedestrian and car. These results, in the form of look-up graphs, are included in the test method and are used to select the impact conditions appropriate for the shape of the car under test. This method has the advantage that the experts developing the test make an informed judgment on the best data to use; avoiding the need to use mathematical modelling or testing with a physical pedestrian dummy interactively within the test method. A proposal to update the energy look-up graph was recently made, based on the results of simulations using a more biofidelic pedestrian model and an improved pedestrian friendly family of car shapes (Lawrence *et al.*, 2004). The pedestrian and car models can be seen in Figure 1 and Figure 2 respectively and the updated energy look-up graph can be seen in Figure 3.

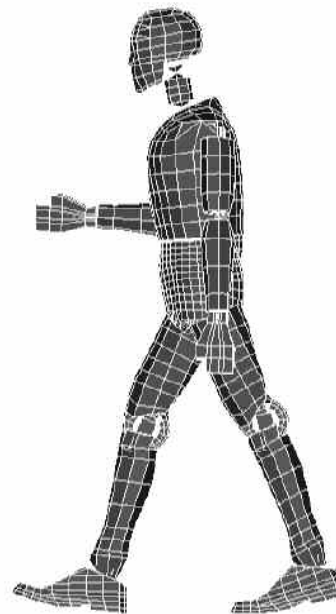


Figure 1. The finite element biofidelic pedestrian model.

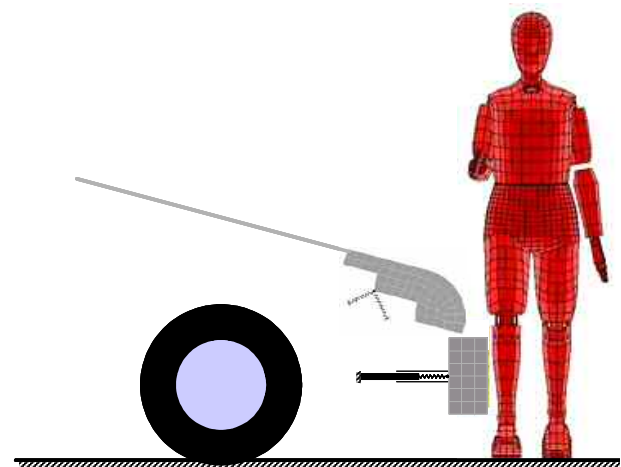


Figure 2. The adjustable-shape pedestrian friendly car and pedestrian models.

Recently the IHRA Pedestrian Safety Working Group have adopted a similar method for their head test procedure where the results of mathematical modelling of impacts between pedestrian and a range of car shapes have been used to produce look-up tables for the headform test conditions (velocity and angle) depending on the shape of the car under test.

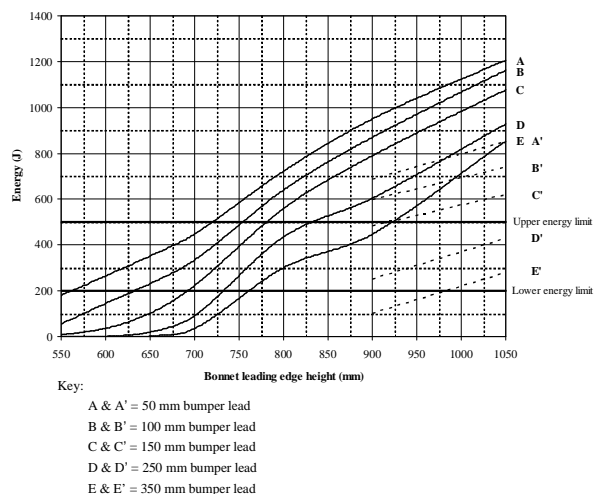


Figure 3. Upper legform impact energy curves for use with a straight edge at 40° to the vertical (proposed for use in phase two of the EU Directive).

However, other combinations might be considered. One option might be to use a physical pedestrian dummy to test the bumper and bonnet leading edge and a sub-system headform test method for the bonnet top, windscreen and windscreen frame. Alternatively, a more complex sub-systems impactor might be developed to test both the bumper and bonnet leading edge in one test. This might consist of a leg or legs and a simplified hip and upper body mass. With suitable instrumentation on the leg (tibia and femur), knee and hip this might be used to assess all vehicles except those with very high bonnet leading edges. However, one advantage of a sub-systems test approach is that the impactor can be repeatably propelled into the car. Any increase in the weight, number of impactor components and number of joints would make the task of impactor propulsion increasingly difficult. Nevertheless, such a combination impactor should have the advantage of responding to the actual shape and stiffness of the vehicle under test.

Scope of Tests

The potential for regulatory pedestrian protection measures to reduce the number of pedestrian and vulnerable road user casualties will be dependent on the proportion of accident situations (vehicle types, protected areas and speeds) where effective protection is provided. This in turn is dependent, amongst others things, on the:

- Number of vehicle types required to provide protection
- Number of accident scenarios covered
- Level of protection required

- Speed range in which the protection is effective

Obviously as the above are increased the larger the proportion of casualties that can be saved. However, to be both feasible and cost effective some limitations are likely to be required. Vehicle types most frequently involved in pedestrian accidents can be found from accident data. Figure 4 shows the distribution of pedestrian casualties in Great Britain by type of vehicle.

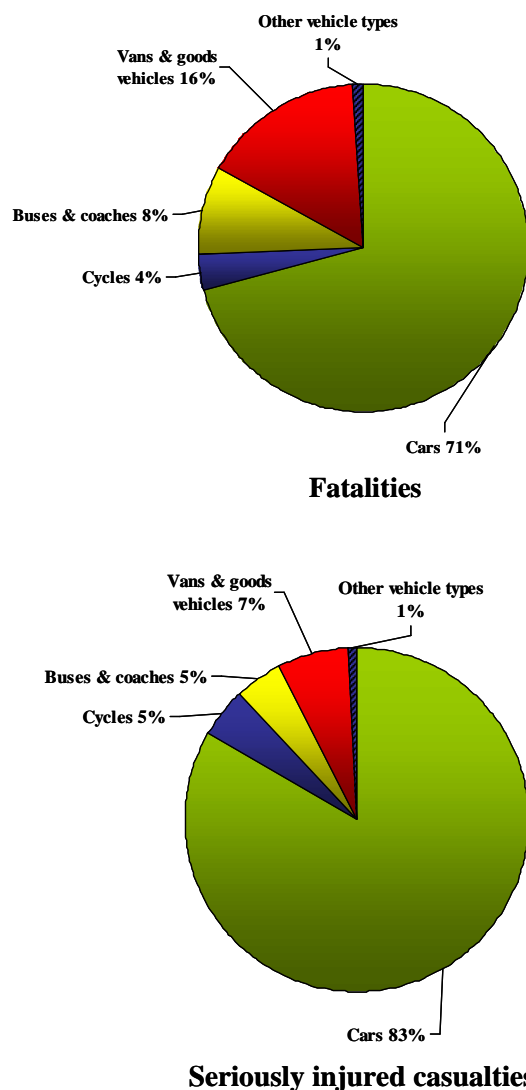


Figure 4. Proportions of vehicles involved in fatal and serious pedestrian accidents in Great Britain (1997-2001)

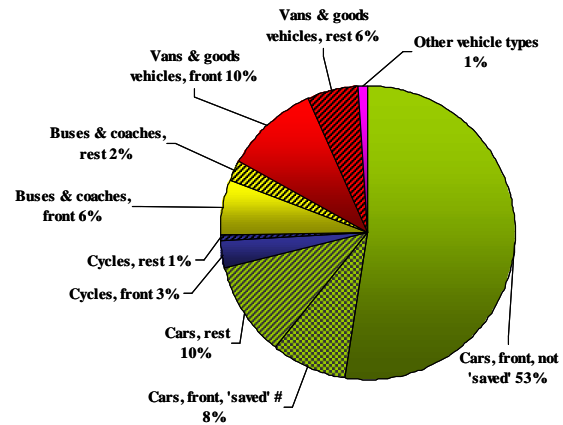
An analysis such as this can be used to help focus protection efforts on the vehicle types with the most potential to reduce the number of casualties; however, the number of vehicles within each sub-division of the fleet would influence the costs. For highly motorised countries the distribution shown in Figure 4 may be appropriate, but for less highly motorised countries the

distribution might be very different so that the vehicles types covered by a test method should ideally be tailored to the countries for which it is intended. From the Figure 4 it can be seen from GB accident data that the car should have the first priority in terms of reducing casualties, however, including other vehicle types would further increase the potential savings. Ideally a detailed break-down of accident data for each country covered by the test methods, should be used to identify which vehicle categories it would be most effective to target.

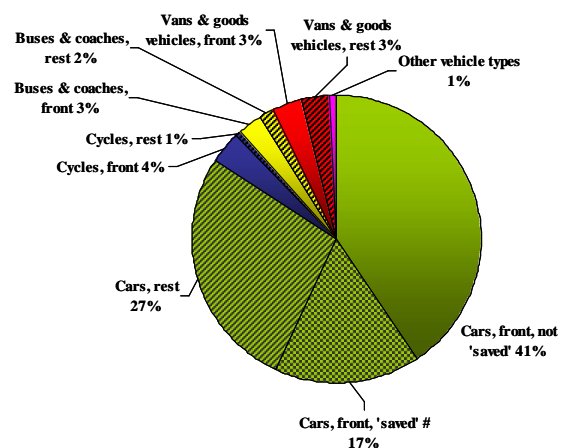
The accident scenarios covered. Test methods, tools and protection criteria can be developed for a number of accident scenarios to require protection on the vehicle including:

- restricted front - with some restrictions or exemptions based on feasibility or cost concerns. Note that the mandate for the EEVC test methods deliberately excluded the 'A' pillars due to feasibility concerns, however, new technology such as air bags may soon make protection in this area practical
- whole front – including the windscreen, dashboard top (can be hit by going through the windscreen) and the windscreen frame, including the 'A' pillars
- side-swipe, which often results in direct contact between the head and the 'A' pillar
- rear – reversing, running over, crushing against walls or pedestrian or cyclist running into the rear of the vehicle

A detailed break-down of accident data could be used to identify which vehicle types and accident scenarios it would be most effective to target for improved test methods. Fortunately the EU pedestrian protection Directive is expected to have significant benefits and these should be taken into account when trying to decide future priorities. As previously noted, ideally, the accident data used should be for the countries covered by the test methods. Nevertheless an indication of the vehicle types and accident scenarios to be targeted can be obtained from the analysis of accident data from Great Britain illustrated in Figure 5. Also included are the estimated savings that will ultimately result from the protection provided by Phase Two of the EU Directive.



Fatalities



Seriously injured casualties

#TRL estimate of the proportion of current casualties that could be prevented if all cars meet the EEVC WG17 2002 requirements

Figure 5. Proportions of vehicles involved and impact directions in fatal and serious pedestrian accidents in Great Britain (1997-2001).

Protection criteria along with appropriate test methods and tools can be applied to each test area to:

- save a specific proportion of the population taking into account the normal variation in strength found in the population. The EEVC protection criteria are intended to save about 80 percent of the population at the test speed (note that different criteria may be used in phase two of the Directive). Reducing the injury risk would increase savings but would make protection more difficult and expensive, increasing it would have the reverse effect, for example see in Figure 6 the injury risk curve used by EEVC WG17 to select their head injury protection criterion.
- save the more frail or elderly population
- save specific life threatening injuries

- save disabling injury or those that reduce quality of life
- require protection for different pedestrian body regions contacting the same area due to a combination of variation in pedestrian stature and / or vehicle size. For example: child femur to normal bumper, adult femur to high bumper and child pelvis, abdomen, chest or head to bonnet leading edge

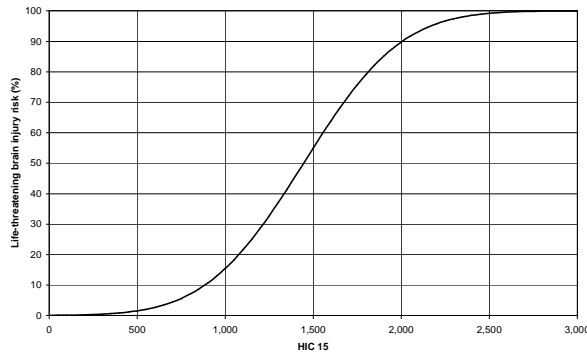


Figure 6. Example of injury risk curve for life-threatening brain injury, derived from Mertz, 1993.

Protection speed can be selected to save the desired proportion of accident casualties using data found in detailed accident studies. It should be noted that this protection or vehicle speed is not necessarily the same as the sub-system test speed, as pedestrian kinematics can cause body parts to impact at higher or lower speeds than the initial vehicle speed. The cumulative impact speed distributions found from the IHRA pedestrian accident dataset can be seen in Figure 7. The number of casualties that could potentially be saved by a selected protection speed is dependent on a number of factors including the proportion of injuries caused by the tested areas, the injury risk chosen for the protection criteria and the degree of bottoming out of vehicle deformation at speeds in excess of that used in the test. Nevertheless, it is likely that the simplified assumption that all current injuries caused by parts of the car that will be protected in future will be saved in accidents up to or slightly in excess of the protection speed will produce a reasonable estimate of the potential savings in casualties. Using this assumption the potential injury reduction can be estimated from the IHRA pedestrian accident dataset or similar accident data for cars without pedestrian protection.

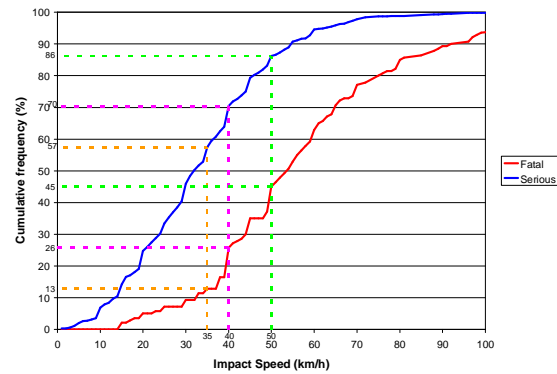


Figure 7. Cumulative impact speed distribution, from the IHRA pedestrian accident dataset, by casualty severity, with values for specific vehicle speeds

IMPROVEMENTS TO TEST METHODS AND TOOLS.

For regulatory use it is important that the test methods and tools are simple, accurate, repeatable and robust. To achieve this normally requires some simplification and compromise in reproducing the accident conditions in both the test method(s) and tool(s). Ideally when these test methods and the chosen protection criteria are applied to vehicles this simplification and compromise will result in the overall improvement in safety intended. However, if inappropriate, they will fail to provide the protection intended. A further problem for test methods is that the design, technology and styling of vehicles are constantly changing. Therefore it is important that the test methods are insensitive to such changes or that they are regularly reviewed.

Considerable effort has been expended by the EEVC experts in developing the current test methods and tools. Therefore in future it may be better to capitalise on this existing knowledge by refining and improving these test methods and tools rather than developing alternatives.

In real life each pedestrian accident is unique in some way so that there are an almost infinite number of real accident situations. Therefore for a regulatory test some simplifications and reduction in scope are necessary. To provide the best cost to benefit ratio care must be taken to make sure that these simplifications and reduction in scope are reasonable, whilst providing the best savings; this optimum compromise is referred to as a 'reasonable worst case' in this paper. These simplifications can take a number of forms, from limiting the protection speed, selecting protection criteria to protect all but the weakest and focusing on vehicle types and vehicle parts most frequently involved.

Sub-Systems Tests

Sub-systems tests are intended to produce a simplified representation of each phase of a pedestrian accident. Not only does this method of an individual test for each contact produce a simple and repeatable procedure, but it also has the advantage that they can be used to represent a whole range of accident situations, with a limited number of tests and tools. For example, two headform procedures can be used to test the whole bonnet top area. Provided that the test method represents an appropriate 'reasonable worst case' then measures to meet the test requirements will provide effective protection in a large number of real life accident scenarios, including a range of pedestrian statures, pedestrian crossing speeds and directions, vehicle speeds, directions of travel and vehicle types that would require an unfeasibly large programme of tests were the vehicle to be tested with a family of pedestrian dummies.

Improvements to sub-systems test may well come from:

- Improved understanding of accident scenario and injury mechanisms, to select more appropriate 'reasonable worst case' test conditions and worst case injury types, for representation in the test methods. For example for the bumper, there are a number of potential injury mechanisms depending on the pedestrian's stature and the shape and stiffness of the vehicle. The injuries caused by the bumper are typically to the tibia and knee for the adult, and for the child they can also include the femur and pelvis. An improved understanding could confirm or adjust the current EEVC conclusion that the adult leg is more vulnerable to injury than the child leg, from the bumper, which was their rationale to simplify the test by just having an adult test tool.
- Improved understanding of the impact conditions at each main point of contact which might be found from accident data, Post Mortem Human Surrogate (PMHS) tests and computer simulations.
- Taking into account the effect of saving initial injuries on subsequent impacts. For example protection measures that save tibia fractures and knee joint injuries could influence the nature and severity of subsequent injuries such as the head impact. (As this cannot be found from analysing accidents for current cars, computer simulation would probably be the most suitable method. It was for this reason that a pedestrian friendly bumper was included in the simulated car shapes

used to derive the EEVC upper legform test energies.)

- Taking advantage of areas where higher protection is considered feasible by specifying lower injury risk protection criteria to protect more of the population, and / or by protecting at a higher speed. These can revert to lower levels where protection is more difficult.
- New and improved biomechanical data for both injury risk and impactor properties (including those derived from mathematically models or from accident reconstructions for properties difficult to measure directly or where live characteristics such muscle tension, blood pressure, etc. are deemed important).
- Sensitivity analysis - to find limitations of current tools and identify what type of improvements are needed. For example, would the legform impactor be improved by the addition of an upper body mass for high bumpers and would it encourage more appropriate protection measures if it had flexible bones?
- Expanded test area and / or vehicle types and protection of more pedestrian body parts. These might include child femur and pelvis and adult and child abdomen and chest.
- Work by others – IHRA, ISO, JARI, etc.
- Feedback from the performance of new cars that meet the requirements of phase one or phase two of the EU Directive in real life pedestrian accidents to identify any remaining problem areas. The results of good and poor monitoring test results could be used for example to see if they result in different injury patterns.

Combined 'Dummy' and Sub-Systems Tests

One of the advantages of using a pedestrian dummy or dummies in a test method is that they can take account of both the shape and stiffness of the car under test, within their biomechanical and instrumentation limits, as the impact progresses. Therefore, they are more likely to be insensitive to changes likely to occur over time in vehicle styling, engineering and body construction. However, as discussed previously, for the head contact a dummy based test method would require an unfeasibly large programme of tests where the vehicle was tested with a family of pedestrian dummies. A further disadvantage of testing with dummies is that, unlike sub-system impactors, it is probably not feasible to propel them into the car in a realistic and repeatable fashion. Nevertheless, it is possible that some combination of dummy and sub-system testing could be devised to take advantage of the

benefits of these two methods whilst avoiding their disadvantages. This might involve testing the bumper and bonnet leading edge with an adult dummy and possibly with a second smaller dummy to represent the most at risk smaller stature, combined with a child and adult headform sub-system test. A further simplification of this idea might be to use an impactor that represents a cut-down dummy, with a simple mass representing the torso of the pedestrian with instrumented pelvis and with a single instrumented leg attached. It might be feasible to propel a cut-down dummy into a stationary car, thus overcoming a further disadvantage of testing with dummies.

DISCUSSION AND RECOMMENDATIONS

Physical pedestrian dummies might initially appear to be the most obvious test tool for assessing a car's pedestrian protection. However, real life pedestrian accidents have a large number of variables which can make dummies less appropriate. In addition pedestrian dummies are likely to give poor repeatability and reproducibility because they are subjected to far more violent impact situations with larger motions than occupant dummies. Therefore they will be more sensitive to differences in the interactions of the many components that make up a complete dummy. Any inadvertent variations in setting the initial conditions, such as the dummy's stance, will as the impact progresses have an increasing influence on the impact severity and position on the car of dummy body parts.

It can be concluded that it would be very difficult to produce a suitable family of dummies to test the whole area of a vehicle that could be involved in a head impact in real life. Amongst other problems each stature would have to meet different biomechanical requirements to reproduce real life. For example, for good head impact kinematics, the correct flexibility of the torso and neck will be more important for a child hit high on the body by the front of the vehicle whereas for an adult, the legs and hips might be more important. In addition, using a family of dummies to test the whole area of a vehicle that could be involved in real life accidents would require a test programme of unacceptable size. Therefore it is reasonable to conclude that a test method to test all the areas of a vehicle likely to injure pedestrians in real life, based on physical dummies, would not be feasible. However, dummies will continue to be very useful for research and for testing the performance of deployable protection measures such as pop-up bonnets.

Dummies have the advantage that they can respond to both the shape and stiffness of the vehicle under test as the impact progresses. In this way, provided that they are sufficiently biofidelic,

impacts with the bumper will correctly affect the nature of the subsequent impacts with the bonnet leading edge and following that with the bonnet top or windscreen. However, if it is required to test in a realistic way a vehicle that would cause injuries in the initial stage of the contact, then the biofidelity requirements for the dummy would have to include frangible bones and joints, etc. This is because it is very likely that injuries such as a broken tibia or femur would influence the kinematics and impact conditions of subsequent contacts. Obviously this would not be necessary if used to test vehicles with adequate pedestrian protection.

For pedestrian protection, sub-systems test methods offer many advantages over dummies. However, by their nature, the impactors are a simplification of real life and their impact conditions must be specified, unlike in a pedestrian accident where the nature and severity of the individual contacts are a function of the accident circumstances and the shape and stiffness of the car involved. Therefore great care should be taken to ensure that the simplifications and impact conditions are appropriate when developing sub-system test methods. To provide protection to the selected proportion of the pedestrian population requires appropriate protection criteria to achieve the intended injury risk and impact conditions for the selected 'reasonable worst case'. The IHRA Pedestrian Safety Group have, for example, carried out a programme of mathematical simulations to find the head impact velocity for a range of vehicle shapes. However, the IHRA study produced a wide range of results for the same nominal impact situation, because they used three different models which introduced different types of variation. If it is assumed that these variations reflect real life, then taking an average of these values would provide protection in only about 50 percent of real accidents at the intended protection accident speed. This demonstrates the need to select a 'reasonable worst case' and carry this through every aspect of developing sub-systems tests (it is for this reason that IHRA also give the standard deviation of their results).

Care should be taken when using injury trends from current cars to set priorities for reducing specific injury types, because such targeted protection could just result in transferring injuries to another part of the body. For example, early work on pedestrian bumpers, where only the stiffness and not the shape was modified, were found to save lower leg fractures at the expense of increasing knee joint injuries. Knee joint injuries are more likely to result in disablement. It is for this reason that the EEVC legform impactor and protection criteria are intended to protect against both lower leg fractures and knee joint injuries, despite the fact that injury trends for current cars

would give first priority to preventing lower leg fractures.

Another disadvantage of sub-system test methods is that they do not automatically take account of the shape and stiffness of the car under test. Instead the impact conditions for each impactor have to be specified in the sub-system test method. These impact conditions can be found from the results of real or simulated pedestrian impacts using a range of car shapes. If the test methods are intended to be used to approve pedestrian safe cars, then the cars used to derive the sub-system test impact conditions must also be pedestrian friendly, as with the EEVC test methods. If this is done then the impact conditions will only become inappropriate if significant changes are made to vehicle shape, styling, engineering and body construction methods in the future.

The possibility of using a cut-down pedestrian dummy or a legform impactor combined with an upper body mass has been mentioned previously. Currently the IHRA Pedestrian Safety Working Group are carrying out research to see if and when a legform impactor needs an upper body mass for testing high bumpers. They are also producing a specification for a legform impactor with flexible leg bones. JARI has already developed a prototype flexible legform which is likely to meet or be able to be made to meet this specification. If this or a similar impactor were to be combined with a suitable upper body mass and instrumentation then it might be suitable for testing both the bumper and bonnet leading edge. Such an arrangement would have the advantage of automatically adjusting to the shape and stiffness of the car under test. However, adding a suitable upper body mass with appropriate instrumentation will be a complex task requiring further research and development effort.

Clearly the flexible 'bones' in the JARI legform have the potential to significantly improve the biofidelity, however, they increase the complexity of the tool and may well have negative implications for robustness or accuracy. The suitability of the JARI prototype legform for use as a regulatory tool in terms of repeatability, robustness and instrumentation accuracy has yet to be assessed.

Many of the options to improve the current sub-system test methods have been discussed; of these it is thought best to concentrate on improving the current test tools and methods to make them more biofidelic and realistic, and on developing new test methods and test tools for other parts of the vehicle or other parts of the pedestrian's body. However, if they are intended to be ultimately used in a regulation then these improvements should not be at the expense of repeatability, accuracy of measuring injury risk and robustness of the method and test tools.

Mathematical simulation of the human and the car have a lot to offer in developing pedestrian test

methods and cars to meet them. In the EEVC pedestrian test methods, mathematical simulation has been used by appropriate experts to derive impact conditions for the sub-system tests in the form of test conditions and look-up graphs. In the future, a more direct inclusion of mathematical models in regulations is thought to be valuable. In a first instance this could be to derive vehicle specific test conditions. However, WG 17 has concerns about the feasibility of specifying the necessary expertise needed for this kind of modelling within a robust procedure.

It is the view of WG17 that the current standards of simulation and data for validating the models are not yet suitable for virtual approval methods to replace physical testing.

The potential for pedestrian protection measures to reduce the number of pedestrian and vulnerable road user casualties can be improved by widening the scope or increasing the level of protection required. It can be seen from the data in Figure 5 that casualties not saved by the EU Directive, in impacts involving the front of cars, form the largest remaining group of vulnerable road user casualties in GB.

It is important that improved test methods be targeted not only at the largest group of casualties but also take into account the costs and feasibility of providing protection. It might be argued that because the EU Directive has already made the 'easy savings' for the car front it would be more effective to target a new vehicle type. Although there is some truth in this argument there is some scope to further improve the car front by providing protection on the windscreen frame and, for vehicles with very short bonnets, on the roof. It can also be seen from this Figure that accidents where the first contact is to the side or the rear are relatively small in number compared with those where the first contact is to the front. Because of this, including these accident scenarios should probably be given a lower priority. Nevertheless, many of the pedestrians struck first by the side of the vehicle are likely to receive serious injuries from the 'A' pillars or upper windscreen frame, in a frontal direction, as they fall or bend over the vehicle. Therefore frontal protection to the windscreen frame may also provide protection for many of these cases. Although it is currently thought not to be feasible to provide significant protection on the 'A' pillars, protection on the upper windscreen frame and adjacent glass and on the roof of short bonneted vehicles is likely to be feasible and this might provide further worthwhile savings in casualties. Protection measures for 'A' pillars are under development (air-bags), although reliable pedestrian pre-impact sensor trigger systems for such devices are thought to be some years away. However, the availability of a suitable method for testing 'A' pillars would help the

development of 'A' pillar airbags and possibly the provision of low speed protection through 'A' pillars having some local deformation capability. The data in Figure 5 also suggest that it would be worthwhile to develop test methods for the fronts of buses, coaches and goods vehicles, and it is suggested that this should be the next priority.

Increasing the standard of protection required to protect a larger proportion of the population would obviously increase the potential savings. The current injury risks in the EEVC protection criteria are already low, so the benefits would be comparatively low. A typical injury risk curve is given in Figure 6, and it can be seen that it flattens out at low injury risks; therefore the protection required would have to be increased significantly with associated feasibility and cost issues. Therefore it is recommended that protection measures be kept at an injury risk of about 20 percent, because reducing them further would give little benefit at high cost. Preventing life threatening injuries is obviously the first priority when selecting protection criteria, but quality of life is also important. Therefore, priority should also be given to preventing injuries that are detrimental to quality of life, such as injuries to joints likely to result in diminished mobility, or injuries likely to result in mental impairment.

It can be seen from Figure 7 that the potential savings from pedestrian protection measures increase disproportionately with increased vehicle impact speed; therefore ideally a high test speed would appear attractive. However, the crush depth in the vehicle required to provide protection also increases disproportionately with speed. There will be practical limits on the depth of crush that it is feasible to provide in a vehicle. Although the rules of physics can be used to estimate the crush depths required to meet the protection criteria at any selected test speed, it is very difficult if not impossible to obtain consensus on what is the highest speed at which it is feasible to provide protection. This is because the judgment depends on the perceived practical limits of the materials and construction methods used to make vehicles and what costs and functional and aesthetic compromises are deemed acceptable, by vehicle manufacturers and ultimately by society. However, new technologies such as airbags and pop-up bonnets, which provide extra crush depth by deploying during or just before pedestrian impact, may increase the 'feasible' speed. Ultimately, the speed selected for protection measures is a choice for society or their political representatives, however, it must remain within what is practical to provide in terms of vehicle crush depth. It is recommended that the approach of the IHRA group is adopted for this, where impact conditions for a range of speeds up to 50 km/h are being provided,

so that the final decision can be made by the appropriate authorities.

CONCLUSIONS

1. Testing with physical pedestrian dummies might initially appear to be the most obvious test tool for assessing a car's pedestrian protection, but there are a number of good reasons why this would be an impractical method when the wide range of variables that occur in real life accidents are taken into account. However, dummies will continue to be very useful for research and for testing the performance of deployable protection measures such as pop-up bonnets.
2. For pedestrian protection, sub-systems test methods offer many advantages over dummies. However, great care should be taken to ensure that the simplifications in the test methods and tools are appropriate.
3. The possibility of using a cut-down pedestrian dummy or a legform impactor combined with an upper body mass for assessing the bumper and bonnet leading edge in one test or for testing vehicles with high bumpers has been discussed. It is thought that this method offers some advantages, provided that it is found to be feasible to propel such a large impactor.
4. One of the disadvantages of sub-system test methods is that the impact conditions for each impactor have to be specified in the test method. These impact conditions can be obtained from the results of real or simulated pedestrian impacts using appropriate vehicles. Therefore if the test methods are intended to be used to approve pedestrian safe cars, then the cars used to derive the sub-system test impact conditions must also be pedestrian friendly, as with the EEVC test methods.
5. It is recommended that future research be concentrated on improving the current test tools and methods to make them more biofidelic and realistic, and on developing new test methods and test tools for other parts of the vehicle and other areas of the pedestrian's body.
6. To provide protection to the selected proportion of pedestrian accidents requires impact conditions that represent the selected range of accident scenarios or the worst case within that range as well as appropriate protection criteria.
7. Considerable effort has been expended by the EEVC experts in developing the current test methods and tools. Therefore in future it may

- be better to capitalise on this existing knowledge by refining and improving these methods and tools rather than developing alternatives.
8. Care should be taken when using injury trends from current cars to set priorities for protection to reduce specific injury types, because such targeted protection could result in transferring injuries to another part of the body.
 9. Mathematical simulation of the human and the car have a lot to offer in developing pedestrian test methods and cars.
 10. Mathematical simulations have been used by experts to specify impact conditions for the EEVC sub-system tests. In the future, a more direct inclusion of mathematical models in regulations is thought to be valuable. However, WG 17 has concerns about the feasibility of specifying the necessary expertise needed for this kind of modelling within a robust procedure.
 11. It is the view of WG17 that the current standards of simulation and data for validating the models are not yet suitable for virtual approval methods to replace physical testing.
 12. There is some scope to further improve the car front by providing protection on the windscreen frame and, for vehicles with very short bonnets, on the roof.
 13. The availability of a suitable method for testing 'A' pillars would help the development of 'A' pillar airbags and possibly the provision of low speed protection through 'A' pillars having local deformation capability.
 14. It would be worthwhile to develop test methods for the fronts of buses, coaches and goods vehicles, and it is suggested that this should be the next priority.
 15. The potential savings from pedestrian protection measures increase disproportionately with test speeds in excess of those currently being considered; however, the crush depth required to provide protection also increases disproportionately with speed. It is recommended that impact conditions for a range of speeds are provided in any new test methods, so that the final decision can be made by the appropriate authorities. However, the speed ultimately selected must remain within what is feasible to provide in terms of vehicle crush depth.
 16. It is recommended that protection measures be kept at an injury risk of about 20 percent, because reducing them further would give little benefit at high cost. Preventing life threatening injuries is the first priority but priority should also be given to preventing injuries that are detrimental to quality of life, such as injuries likely to result in diminished mobility or mental impairment.

REFERENCES

Lawrence G J L, Hardy B J, Carroll J A, Donaldson W M S, Visvikis C and Peel D A (2004). *A study on the feasibility of measures relating to the protection of pedestrians and other vulnerable road users – Final report.* TRL Project Report available from the European Commission: http://www.europa.eu.int/comm/enterprise/automotive/pagesbackground/pedestrianprotection/pedestrian_protection_study.pdf.

Mertz H J (1993). *Anthropomorphic test devices.* In: *Accidental Injury - Biomechanics and Prevention.* (Eds A M Nahum and J W Melvin.) New York: Springer-Verlag. pp 66-84.

RESEARCH AND RULE-MAKING ACTIVITIES ON PEDESTRIAN PROTECTION IN KOREA

Younghan Youn

Korea University of Technology and Education

Siwoo Kim

Korea Automotive Testing and Research Institute

Cheol Oh

Korea Transport Institute

Moonkyun Shin

Hanyang University

Chungho Lee

Ministry of Construction and Transportation

Paper Number 05-0117

ABSTRACT

Pedestrian safety is one of the most demanding topics in vehicle safety in Korea. Although the total numbers of deaths and injuries have continuously decreased year by year, the pedestrian is still a major source of traffic victims. Among 240,832 cases (total traffic accidents), 37% (89,443) was pedestrian involved accidents in 2003. Last year, 50% (3,594 fatalities) of all traffic accidents that related fatality (total 7,212) was vehicle-pedestrian type accident in Korea. Among them, numbers of deaths in pedestrian age under 6 were 142 with 13,528 injured children.

In 1999, Korean government, Ministry of Construction and Transportation, launched a research project to develop a proper solution on pedestrian protections from vehicle related accidents. The project also included the evaluations of current existing test methods, i.e. EEVC type test and IHRA type test, and the possibility of harmonization with these test methods.

The main objective of the presented method is to develop the adequate dynamic test procedure and injury assessment criteria. The current all existing passenger vehicles of the front shape were measured and categorized into three groups according to IHRA recommendation, and the effect of vehicle shape on pedestrian kinematics was investigated to define the head impact speed, head impact angle and WAD with the various impact speeds and walking postures as the test procedures. In this paper, JARI pedestrian

computer model, TNO MADYMO computer model and FEM H-model were used to configure and compare the pedestrian dynamic behaviors during the various impact events. With head impact tests and simulations, the design feasibility, lead times for auto industry and suitable injury criteria were investigated.

Based on the research, Korean government will extend the KNCAP on new vehicle's pedestrian impact test to evaluate how vehicle front structure is pedestrian friendly. With careful study on the results of NCAP, after that pedestrian regulation will come into effect within 2 or 3 years later.

ASSESSMENT OF PEDESTRIAN RELATED TRAFFIC ACCIDENTS IN KOREA

Late 80's when Korea rapidly increases of use the automotive as a personal transportation means, the traffic related accidents were inevitable. Early '90, over the 13,000 valuable lives killed by the vehicle related accidents. Until 1997, the number of persons killed each year in the traffic accidents is about 10,000 and more than 300,000 peoples were injured though it has shown a decreasing trend. Casualties who were involved with vehicle to pedestrian related accidents were approximately up to 50% of the total traffic related death in 2003 and unfortunately the rate is still increasing year after year.

Based on the police reports, total traffic accident fatality was 7,212 and vehicle to pedestrian type accident's fatality was 3,595 including fatality of

occupants on vehicles. In terms of pure pedestrian, the death was 2,896. It is 40.2% of all traffic accident fatality. The injured pedestrian was 53,069 while total traffic injured person was 376,503. The pedestrian injured rate was 14.1%. The main reason why the fatality is so higher than injured rate is that the pedestrian is relatively weak compared with the stiffness of vehicle outer structure surfaces. In order to reduce the number of victims from traffic accidents, the Ministry of Construction and Transportation (MOCT) has been investigated adoption of regulation for pedestrian protections from vehicles. During last 3 years of research works, studied characteristics of domestic environments of pedestrian along with pedestrian related traffic

accidents investigations.

Trends of Traffic Accidents Patterns

Since 1990, 48% of all accumulated police reported fatality accident data (1990-2003) was a vehicle-pedestrian crash type accident as shown in Table 1 and Fig. 1. Each year's data is shown in Fig. 2. This is the largest accident type cause the death during the accidents. The total reported data exceed 3 million accidents. In fatality, the second accident type was a vehicle-pedestrian accident. It was about 36% of total accidents while the total case of accidents is the largest. The remaining 4% of total accidents was vehicle only involved accident and vehicle only accident's fatality is about 15%.

Table 1. Trends of Traffic Accidents Periods of 1990 – 2003 in Korea

	Vehicle-vehicle		Vehicle-person		Vehicle only		Vehicle-train		Total	
	Accidents	Deaths	Accidents	Deaths	Accidents	Deaths	Accidents	Deaths	Accidents	Deaths
1990	110,513	4,442	133,282	6,441	11,395	1,376	113	66	255,303	12,325
1991	118,897	4,805	136,941	6,952	10,036	1,609	90	63	265,964	13,429
1992	125,006	4,455	122,951	5,802	91,39	1,321	98	62	257,194	11,640
1993	133,587	3,947	117,431	5,241	97,98	1,159	105	55	260,921	10,402
1994	149,899	4,204	105,261	4,641	10,859	1,194	88	48	266,107	10,087
1995	146,783	4,315	91,395	4,564	10,603	1,378	84	66	248,865	10,323
1996	166,677	5,390	87,292	5,070	11,037	2,160	46	33	265,052	12,653
1997	162,085	4,981	74,144	4,458	10,192	2,134	31	30	246,452	11,603
1998	158,732	3,593	70,631	3,495	10,318	1,949	40	20	239,721	9,057
1999	190,437	3,788	74,527	3,692	10,943	1,855	31	18	275,938	9,353
2000	206,971	4,208	72,932	3,890	10,569	2,135	9	3	290,481	10,236
2001	185,207	3,258	65,898	3,243	9,466	1,590	8	6	260,579	8,097
2002	164,334	2,808	59,271	3,201	7,411	1,207	10	6	231,026	7,222
2003	141,841	2,197	89,443	3,595	9,531	1,416	17	4	240,832	7,212

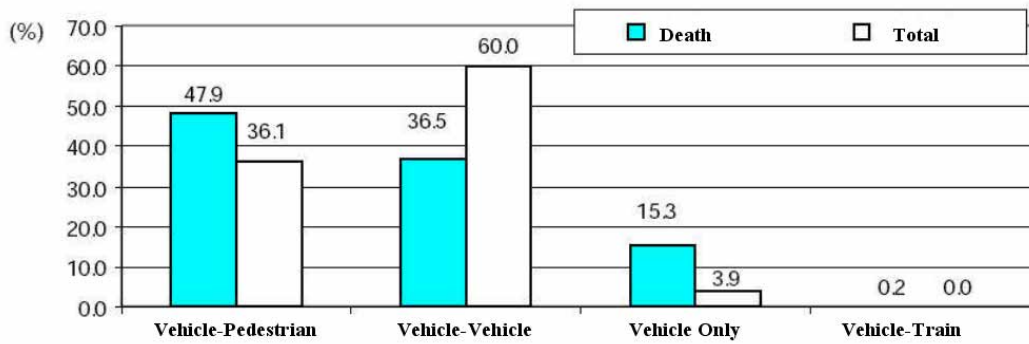


Figure 1. Accumulated accident type distribution of fatalities in Korea

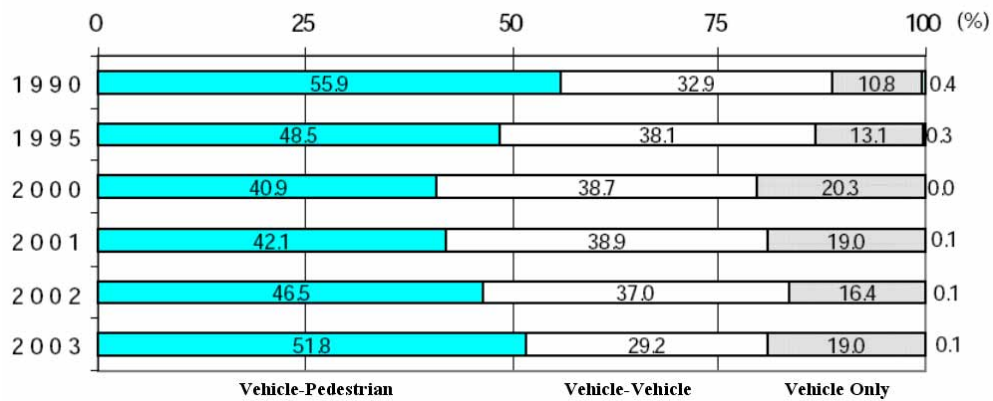


Figure 2. Accident type distribution of fatalities in Korea

Pedestrian Accident Patterns by Age Group

As shown in Table 2, 44.6% of pedestrian death is over 61 years and older people. Their total death is 1,291. Among them, 724 deaths are over 71 years and older elderly peoples. The statistics of casualties standardized by population distribution by age or those of fatalities by age indicate that the rate of meeting with accidents or being killed in such accidents increases among pedestrians at age 61 and over. Fatality of child (less than 14 years old) is 9.5% (274 death). However in terms of injured case, 24.8% (13,181 injured child) of all pedestrian injured cases is less than 14 years old child. Elderly people's injured rates are less than 10% (61-70 years old: 9.8%, over 71 years and older: 6.6%). It may be due to the different

characteristics of biomechanics behaviors during crash.

As shown in Figure 3, pedestrian casualty (both death and injured) per 10,000 populations, injured over 61 years and older is the largest group with 158.6 persons. The ratio is more than 2 times of those of 20 years old age group. Fatality ration of elder people is 24.3 persons per 10,000 populations while 21 – 30 years old group's ration is less than 1.8 persons. This indicates killed rate of elder pedestrian is more than 13 times of those of 21 – 30 years old group. This indicates that, the more elderly peoples in near future, the more pedestrians are likely to meet with accidents.

Table 2. Pedestrian fatality and injury by age group in 2003

	Total	14 less	15-20	21-30	31-40	41-50	51-60	61-70	71 over	N/A
Death	2,896	274 (9.5%)	54 (1.9%)	141 (4.9%)	279 (9.6%)	429 (14.8%)	400 (13.8%)	567 (19.6%)	724 (25.0%)	28 (1.0%)
Injured	53,069	13,181 (24.8%)	3,528 (6.6%)	6,768 (12.8%)	6,729 (12.7%)	7,850 (14.8%)	5,618 (10.6%)	5,202 (9.8%)	3,527 (6.6%)	666 (1.3%)

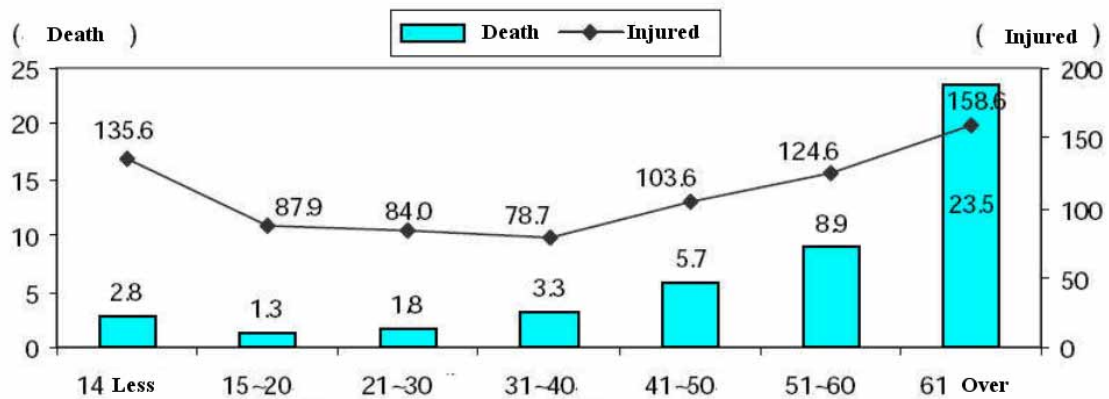


Fig. 3. Age group pedestrian death and injured rates per 10,000 populations in 2003

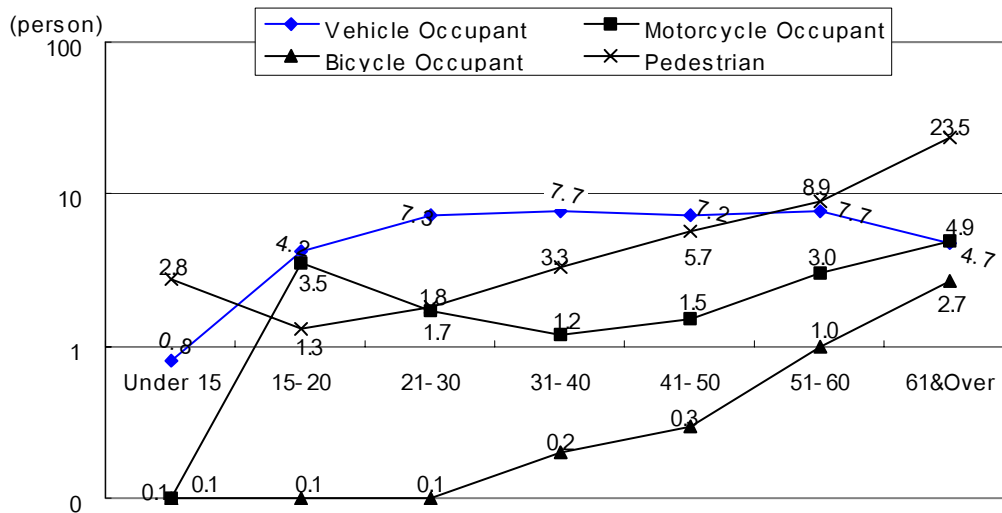


Fig. 4. Age group accident type death rate per 10,000 populations in 2003

Figure 5 show that the percentage of injured parts of traffic accidents involved persons who had experienced at least hospitalized 2 or 3 days. Up to serious injured cases, the incidence of injury is the most frequently observed in the

lower leg and necks, followed by head.

In the fatal accidents, injury to the head is the major cause of death (64%), followed by lower legs (11%) and neck (9%). The body of injured occupant in the vehicle is shown in Figure 5.

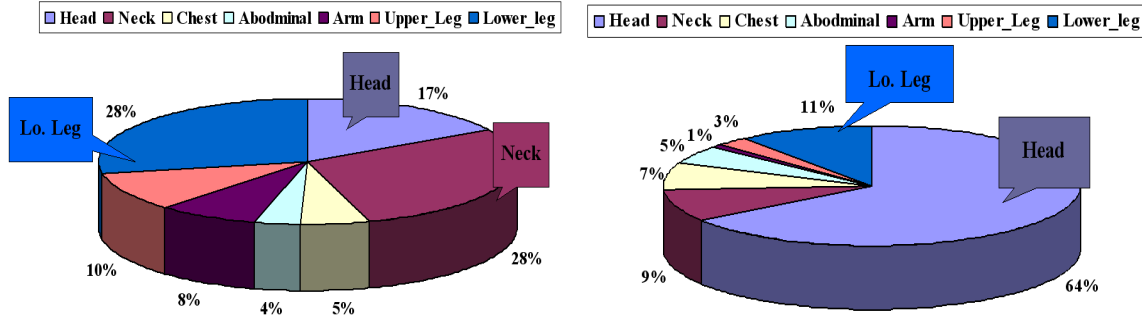


Fig. 5. Injured body parts and Fatality caused main severely injured body parts in pedestrian

RESEARCH AND RULE MAKING ACTIVITIES

This accidents data analysis indicates that significant improvement of vehicle safety performances are needed to protect the pedestrians during the accidents. In order to reduce number of fatalities, especially from the vehicle, the Ministry of Construction and Transportation (MOCT) has been seriously considered adoption of pedestrian protection regulations. Recently MOCT of Korea launched special task team for pedestrian researches. This research group studied the patterns of Korean pedestrian accident, and injury as well as survey of existing test methods for feasibilities and international harmonization as shown in Figure 7.

Pedestrian Kinematics During Vehicle Impacts

Figure 7 shows two pedestrian models currently used for the simulation study. These are JARI, and TNO pedestrian models that already validated by TNO and IHRA (JARI) with comparing results from their computer simulations and published PMHS (Post Mortem Human Subject) tests.

According to IHRS recommended simulation procedures, a parameter study was conducted to understand the influence of pedestrian size, waling position, vehicle shape, vehicle stiffness, and vehicle impact speed onto the pedestrian impact condition such as head impact velocity, head impact angle, and head impact location (Wrap Around Distance: WAD). IHRA's three walking position WP1, WP2, and WP3 were used for the parameter study as well as a standing position with 40kph vehicle impact speed.

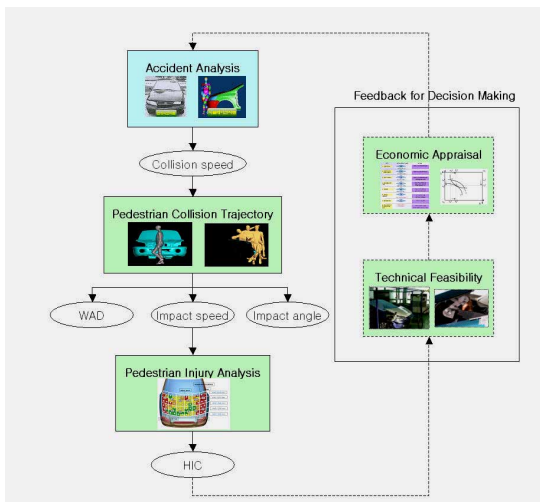


Fig. 7. Scheme of research procedures

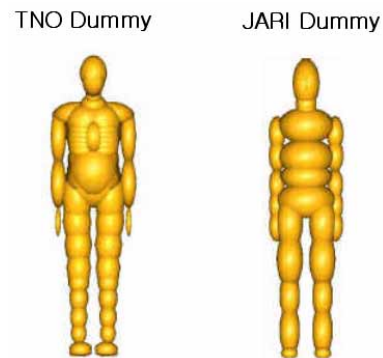


Fig. 7. Pedestrian Models (AM50)

Two different vehicle stiffness, IHRA's hard and friendly, was used, and the definition of the head impact velocity and the head impact angle and the definition of the head impact velocity and the head impact angle are illustrated in Figure 8.

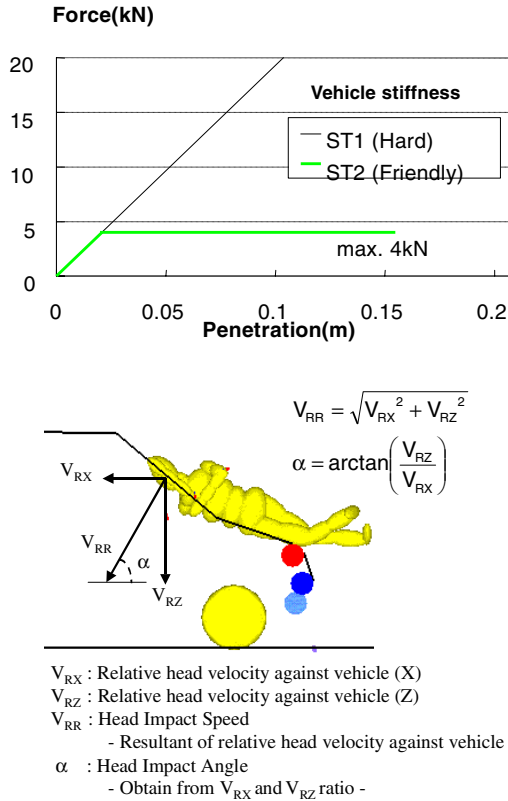


Fig. 8. Pedestrian simulation conditions

Vehicle Shapes in Different Categories

Based on the IHRA and WP29 W/G studies, front shape of passenger car was investigated and categorized into three groups, Sedan, SUV and 1-Box, so that the effect of vehicle front shape on the pedestrian impact was studied with computer simulations focusing on the head impact velocity, head impact angle, WAD (Wrap Around Distance) and head effective mass.

Figure 8 shows the car front shape corridors for the three groups obtained from current Korean production cars with overplots of IHRA's results. The measured corridors of domestic vehicles are fall into the results of IHRA measures. However the hood angle of one 1-BOX vehicle is less than 30

degree. This means that even though intended design and purpose of vehicle was 1-BOX vehicle, the test procedure will be followed by SUV vehicle category. It will mislead the government's pedestrian protection policy and the level of protections.

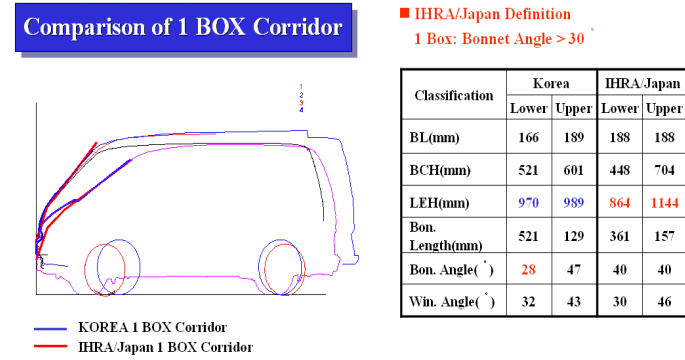
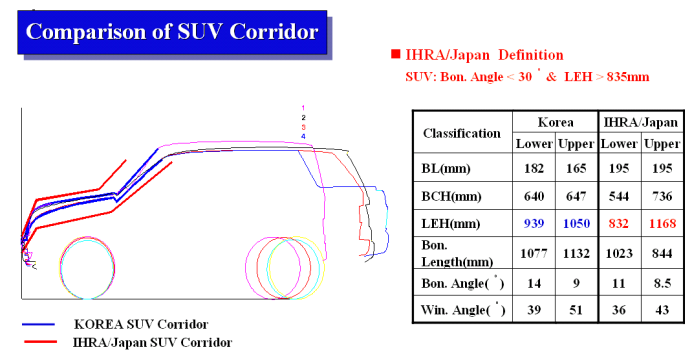
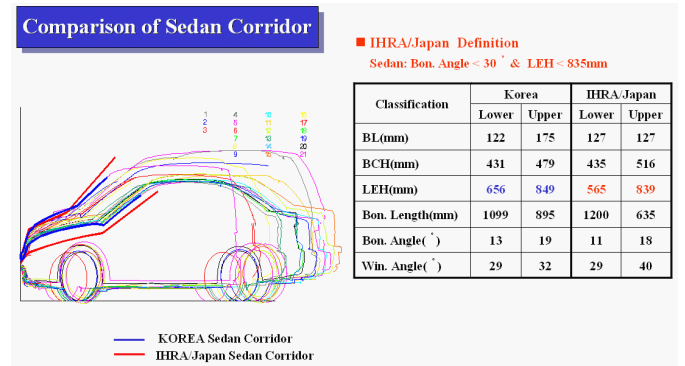


Fig. 8. Three vehicle categories 2-D front shape corridors from domestic vehicles

Pedestrian Trajectory Simulation Results

As shown in Figure 9, it is clear that the pedestrian size and the vehicle category affects to the head impact condition, especially for the head impact location, angle, and head velocity.

Compared with JARI and TNO model, however the simulations were influenced by pedestrian-vehicle contact locations, contact characteristics, and upper arms interference with vehicle and body parts of dummy.

In general, the head contact locations, WAD are similar, but impact velocity and angle are shown some discrepancy for adult pedestrian model. In 6 years old child model case, JARI and TNO model show the consistent results both in speeds and angles. This is due to the relatively small body that contact with striking vehicle with initial stage of crash.

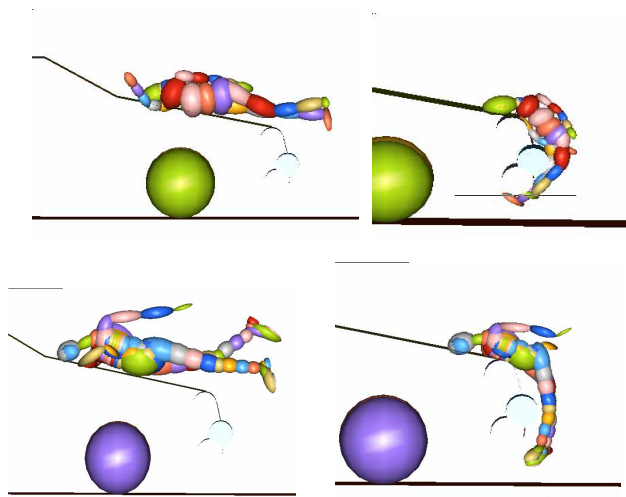


Fig. 9. Sedan type vehicle simulation results with JARI and TNO models(A50 and 6Y)

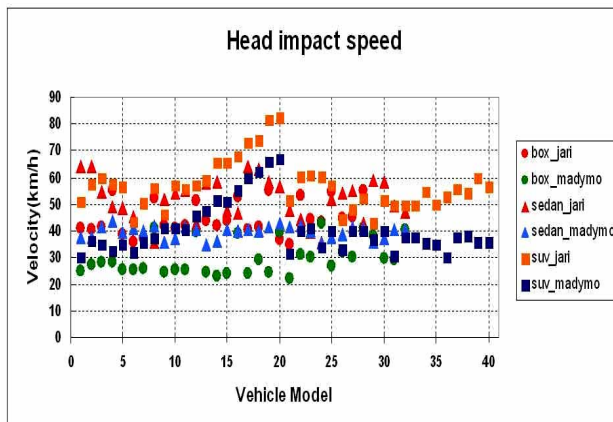


Fig. 10. Results of head impact speeds with JARI and TNO models(A50)

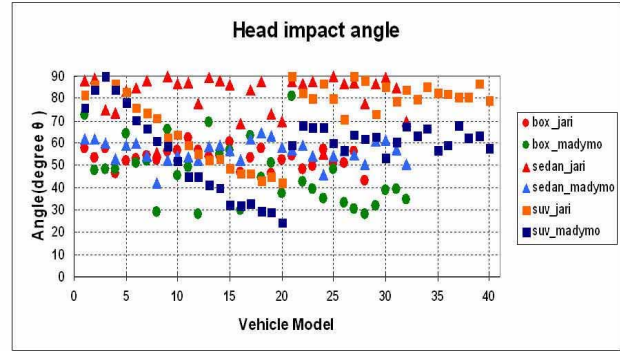


Fig. 11. Results of Head impact angle with JARI and TNO models(A50)

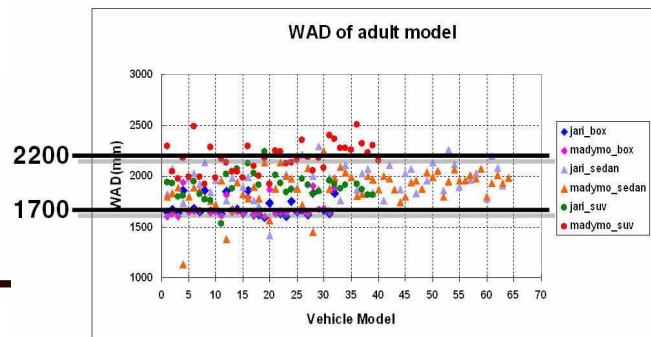


Fig. 12. Results of head impact WAD with JARI and TNO models(A50)

Evaluation of Existing Head Impact Test methods with Simple Hood Structure Model

The EEVC performed several studies and proposed various recommendations on test methods to assess pedestrian protection. The test methods should be based on sub-system tests, essentially to the bumper, bonnet leading edge and bonnet top surface. The test methods should be considered to evaluate the performance of each part of the vehicle structure with respect to both child and adult pedestrians, at car to pedestrian impact speed of 40 km/h with fixed impact angle for all applicable vehicles. (adult: 60 ° with 4.8 kg mass, child: 50 ° with 2.5 kg mass)

However, according to finds from IHRA study, Japan announced their new pedestrian regulation for head protection in both adult and child. IHRA

approach is quite different that based on the observations from real world accidents. The starting point is different frontal shapes must influence the kinematics of occupant which leads specific head impact velocities and impact angles.

Japan's regulation based on the IHRA's results is same impact speed both child (mass: 3.5kg) and adult(mass:4.5kg) with 32kph. But the different vehicle categories have different head impact speeds. 65 ° / 90 ° / 50 ° (sedan/SUV/1-BOX) for adult, and 65 ° / 60 ° / 25 ° (sedan/SUV/1-BOX) for child.

UNECE/WP29 is under discussion for harmonization between EEVC and IHRA test method and injury criteria.

Meanwhile, NHTSA proposed the most sever head impact conditions. To maximum protections, the impact angle should be perpendicular to the bonnet surface that leads the maximum penetration of head into the bonnet surface.

evaluated using computer simulation with a hood of common passenger vehicle. To eliminate the interference of engine block structure, only hood was modeled with proper boundary conditions. As shown in Figure 13, 2.5kg or 3.5kg child head form was impacted center of hood with three different test conditions (EEC, IHRA and NHTSA)

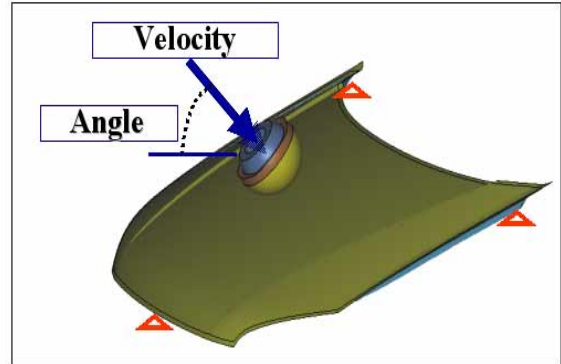


Fig. 13. Child head form impact model

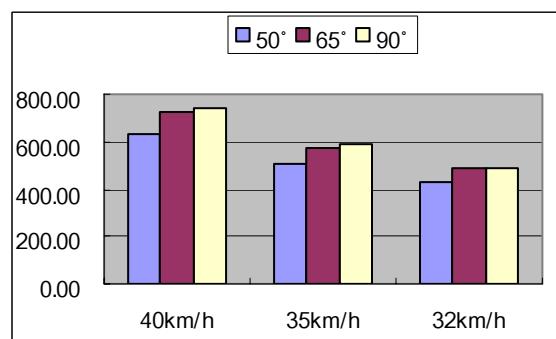
In our study, three different test methods were

Table 3 Comparison with three different child head impact test methods

	40km/h		35km/h		32km/h	
	2.5kg	3.5kg	2.5kg	3.5kg	2.5kg	3.5kg
50°	1.00	0.79	0.77	0.63	0.64	0.53
65°	1.14	0.90	0.90	0.72	0.75	0.60
90°	1.18	0.92	0.91	0.73	0.77	0.61



a) 2.5kg



b) 3.5kg

Fig. 14. HIC of Child head form impact simulations

ECONOMIC APPRAISALS AND FUTURE PLANS

During the research, it must be make sure that the establishment of rule-making activities achieved proper number of lifesaving effects assuming that it is introduced and that all the vehicles concerned are replaced with vehicles complying to the regulation. Target Population is estimated for each of the age groups as following variables.

- Pedestrian head injury ratio (P_{ha})
- Death ratio of the head injury accidents (P_{dhk})
- Ratio of the pedestrian accidents under 40kph [PVd40]
- Ratio of injury over HIC 1000 [$H_{1000,d}$]

Benefits are estimated using target population and social costs for the life savings and incident injury reduction. Social costs [C_{da}] are estimated using accident compensation cost for the car insurance. The benefits are calculated by the following equation.

$$B_{da} = C_{da} \cdot D_p \cdot p_{ha} \cdot p_{dha} \cdot p_{v_{d,40}} \cdot H_{1000,d}$$

The estimate used the traffic statistics of 1999 and took into account passenger cars with 3500 kg

or less in gross vehicle weight (the weight range of trucks being different from that of the regulation). The injury reference value was set to HIC 1,000.

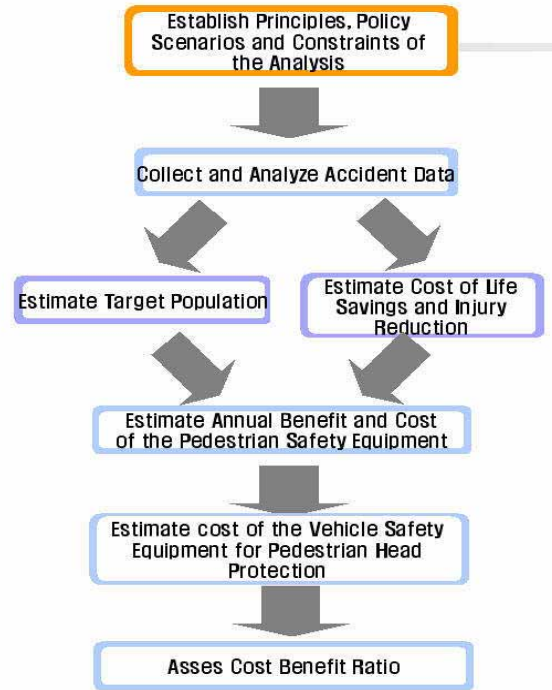


Fig. 15. Scheme of economic appraisals

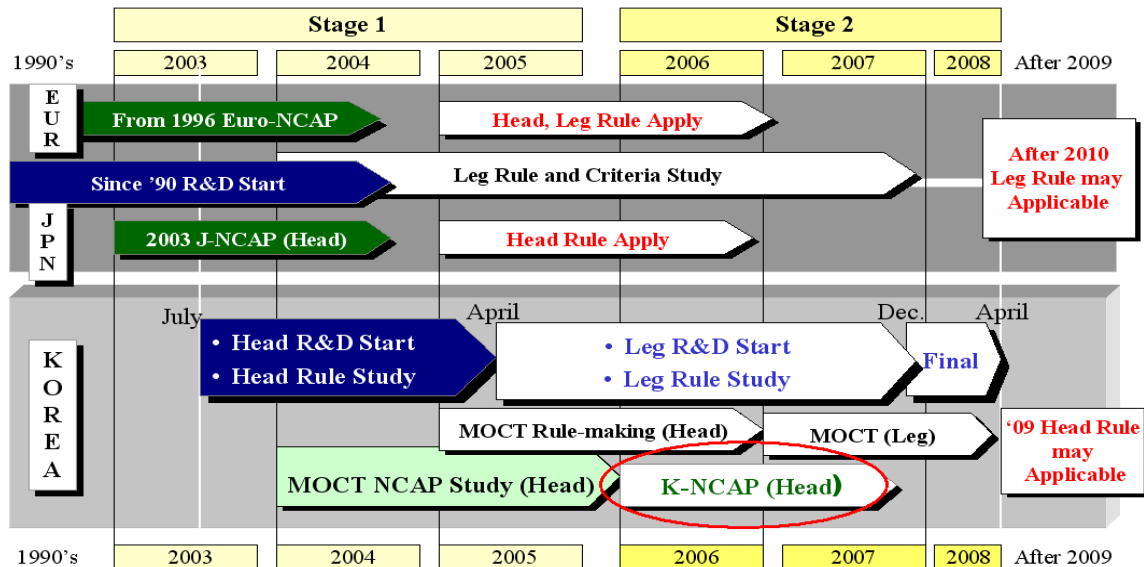


Fig. 16. Milestone of pedestrian protection rule-making activities

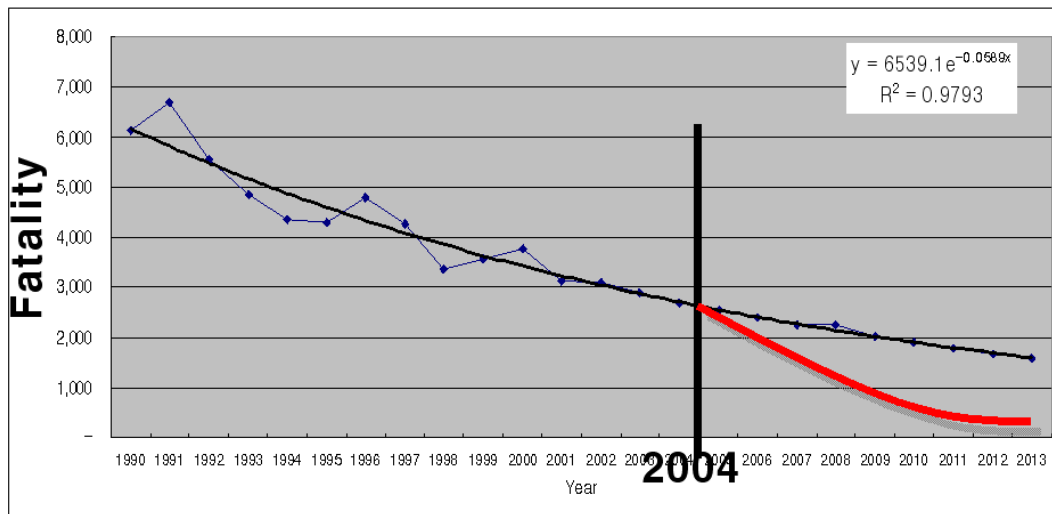


Fig. 17. Expected reduction of pedestrian related fatalities with enhanced rule-making activities

As a member of both on 1958 and 1998 agreements, Korea will continuously work for international harmonization. An informal group, GRSP/PS was organized under ECE/WP29/GRSP for establishing a Global Technical Regulation for pedestrian safety. According to its Terms of Reference, the informal group plans to finalize its written justification by the middle of 2005 and its complete and detailed recommendation by 2005 for a head protection regulation and a leg protection regulation.

Accordingly, Japan plans, respecting the discussion to be held in this Informal Group to the maximum, to introduce also a regulation for leg protection, while working for the harmonization of head protection regulations.

REFERENCES

[1] Isenberg, R.A., Walz, M., Chidester, C., Kaufman, R.; "Pedestrian Crash Data Study-An Interim Evaluation," Fifteenth International Technical Conference on the Enhanced Safety of Vehicles, Paper No. 96-S9-O-06, 1996.

[2] Isenberg, R.A., Chidester, C., Mavros, S.; "Update on the Pedestrian Crash Data Study," Sixteenth International Technical Conference on the Enhanced Safety of Vehicles, Paper No. 98-S6-O-05, 1998.

[3] Yoshiyuki Mizuno; "Summary of IHRA Pedestrian Safety WG Activities (2003) – Proposed Test Methods to Evaluate Pedestrian Protection Offered by Passenger Cars," 18h International Technical Conference on the Experimental Safety of Vehicles, 2003

[4] Commission of the European Communities; "Frontal Surfaces in the Event of Impact With a Vulnerable Road User," Ad-hoc Working Group ERGA Safety, document ERGA S/60, Brussels.

[5] Kajzer, J., Aldman, B., Mellander, H., Planath, I. and Jonasson K.; "Bumper System Evaluation Using an Experimental Pedestrian Dummy," 12th International Technical Conference on the Experimental Safety of Vehicles, 1989.

[6] Kallieris, D. and Schmidt, G.; "New Aspect of Pedestrian Protection Loading and Injury Pattern in Simulated Pedestrian Accidents," 32nd Stapp Car Crash Conference, SAE 881725, 1988.

[7] Akiyama, A., et al.; "Development of a Simulation 1999-01-0082.

[8] Lawrence, G. J, B. J. Hardy and R. W. Lowne; "Cost and benefits of the EEVC pedestrian impact requirements," Project Report 19, Crowthorne, UK TRL Limited, 1993

J-MLIT RESEARCH ONTO APEDESTRIAN LOWER EXTREMEITY PROTECTION - Evaluation Tests for Pedestrian Legform Impactors -

Masao Notsu

Ministry of Land, Infrastructure and Transport of Japan (J-MLIT)

Toshiyuki Nishimoto

National Traffic Safety and Environment Laboratory (NTSEL)

Atsuhiko Konosu, Hirotoshi Ishikawa

Japan Automobile Research Institute (JARI)

Paper Number 05-0193

ABSTRACT

As for a Global Technical Regulation (GTR) legform impactor, which is discussed at the United Nations ECE/WP29/GRSP, a flexible pedestrian legform impactor (Flex-PLI) and a rigid legform impactor (TRL-LFI) is proposed. However, as for the Flex-PLI, evaluation test for its repeatability and reproducibility has not been confirmed. Besides, its advantage over the TRL-LFI must be demonstrated in full-scale vehicle tests.

In this research, several kinds of loading tests were conducted to the Flex-PLI, and its favorable repeatability and reproducibility was confirmed. Besides, vehicle tests were performed using the Flex-PLI and the TRL-LFI, and the Flex-PLI demonstrated its higher biofidelity and load measurability in full-scale vehicle tests.

INTRODUCTION

The Ministry of Land, Infrastructure and Transport of Japan (J-MLIT) has been studied for a domestic regulation aimed at moderating the injury severity of pedestrians in the event of a collision with a motor vehicle. As a result the Japanese Pedestrian Head Protection Regulation was issued in April 2004. This regulation requires vehicles to have a pedestrian head protective structure, and applicable to new-model vehicles which is put on a sale in September 2005 onwards.

To further advance the pedestrian protection performance of vehicles, J-MLIT is participating in the activity to develop the Global Technical Regulation (GTR) on the pedestrian head and lower extremity protection in view of adopting it into Japanese legislation. That is currently in the drafting stage at the United Nations ECE/WP29/GRSP. However, as for the GTR for the lower extremity protection, two different legform impactors - a rigid legform impactor (TRL-LFI) [1] and a flexible pedestrian legform impactor (Flex-PLI) [2] - have been proposed.

Figure 1 shows the overall design of TRL-LFI. Because

of the TRL-LFI employs rigid units in the place of human bones, this legform impactor cannot reproduce the bending responses of human bones under impacts. The knee of TRL-LFI also differs from the human knee in consisting of metallic bending plates and shear springs instead of the ligament restraint structure of the human knee. The TRL-LFI is therefore considered to exhibit a low biofidelity in both structure and deformation characteristics [3][4].

Figure 2 shows the overall design of Flex-PLI. This legform impactor incorporates bendable units to simulate the human lower extremity bones bending, so that the biofidelity of Flex-PLI is considered as high [2]. In addition its knee structure was developed to equate the human ligament restraint structure and exhibits deformation characteristics equivalent with those of the human knee under impacts [2].

The measurement items of TRL-LFI are listed in Figure 3. This legform impactor has three measurement items around its knee, but no other items are present anywhere in the lower extremity structure.

On the other hand, as shown in Figure 4, the Flex-PLI has a total of 15 measurement items enabling load measurement in most of the lower extremity portions.

From the above comparisons, it can be stated that the Flex-PLI is more suitable for the formulation of an appropriate pedestrian lower extremity protection regulation because of its higher biofidelity and more detailed measurability in extensive portions of the lower extremity. However, to utilize Flex-PLI in actual regulation enforcement, its repeatability and reproducibility must be verified. Besides, its advantage over the TRL-LFI must be demonstrated in full-scale vehicle tests.

The present study was conducted sectional loading test and vehicle test using a Flex-PLI (ver. 2003) unit in order to verify its repeatability and reproducibility. Additionally, a vehicle test employing a Flex-PLI and a TRL-LFI was carried out to verify the advantage of Flex-PLI over TRL-LFI.

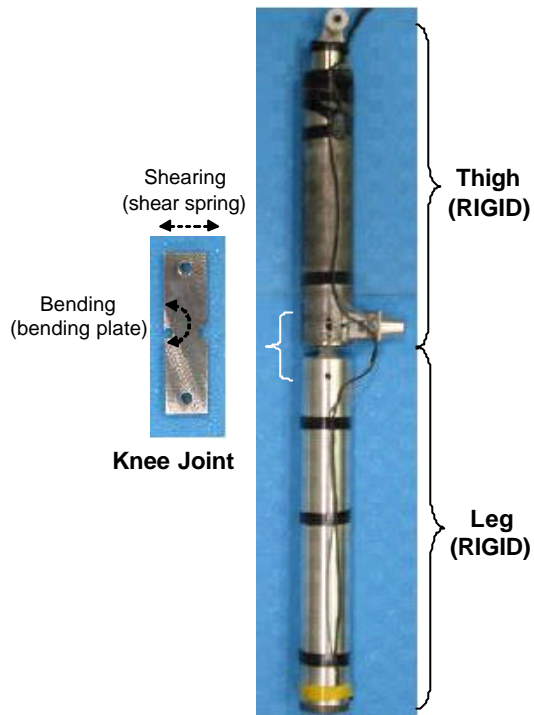


Figure 1. Overall design of TRL-LFI.

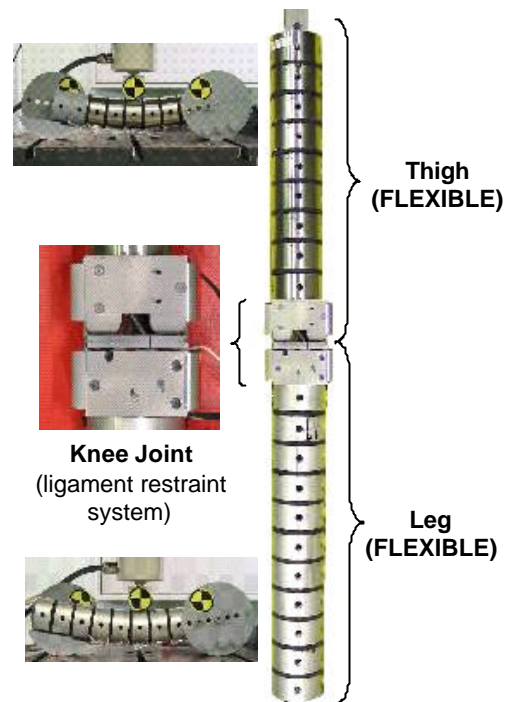


Figure 2. Overall design of FlexPLI.

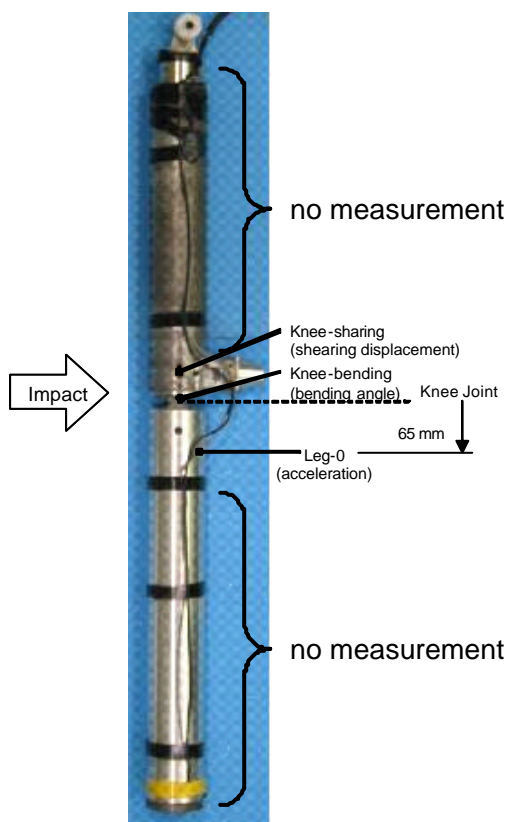


Figure 3. Measurement items of TRL-LFI.

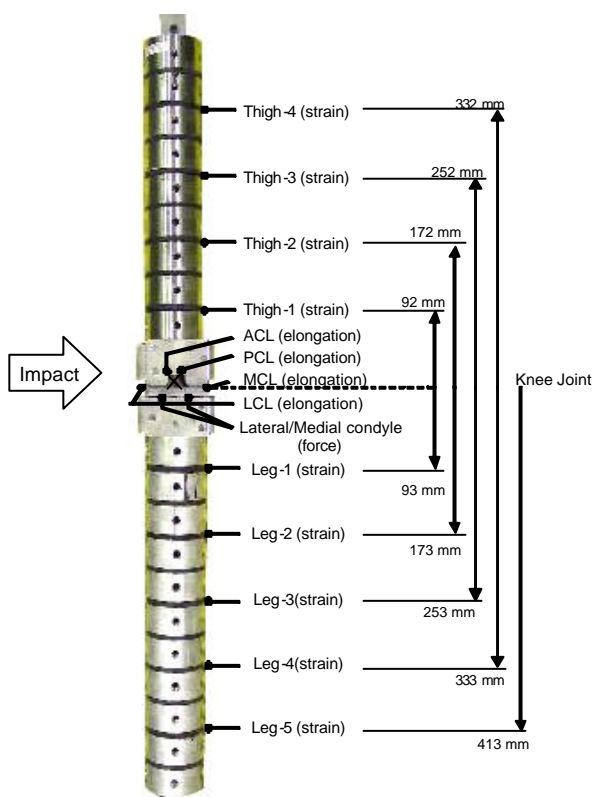


Figure 4. Measurement items of FlexPLI.

METHODOLOGY

Sectional Loading Test

The methodologies of the sectional loading tests are summarized in Figures 5 to 7. The thighs (Products Nos. 1, 3, 4), legs (Products Nos. 2, 4, 6), and knees (Products Nos. 2, 4, 5) of Flex-PLI for the tests were randomly selected.

Vehicle Test

The setup of the vehicle test is shown in Figure 8. This vehicle test was conducted to utilize the subsystem test method [1] which is propelling the legform impactor to the vehicle.

As shown in Figure 9, a sedan was used as the test vehicle. The impact point was located 200 mm to the left of the vehicle's center line as seen from the driver's seat. The test vehicle and the horizontal position of the impact point were selected randomly.

The legform impactor propulsion system, compressed gas type, is shown in Figure 10. In this vehicle test, Flex-PLI and TRL-LFI were each collided into the test vehicle at an initial impact speed of 11.1 m/s using the propulsion system.

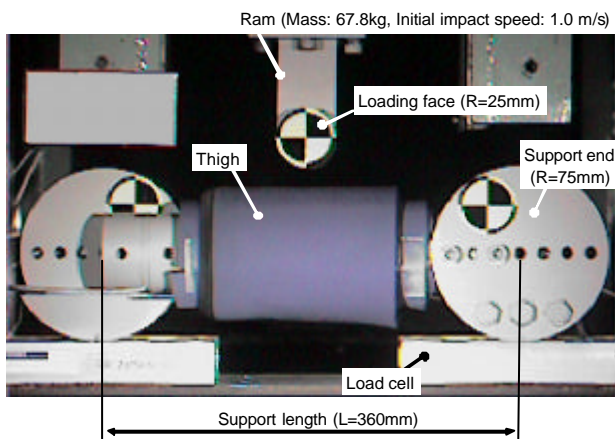


Figure 5. Sectional loading test set up for thigh (Flex-PLI).

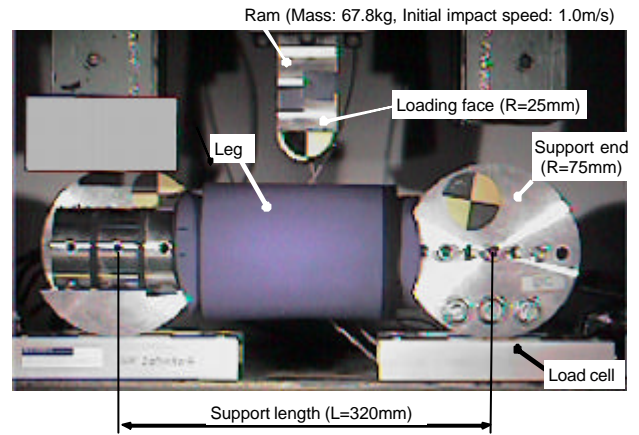


Figure 6. Sectional loading test set up for leg (Flex-PLI).

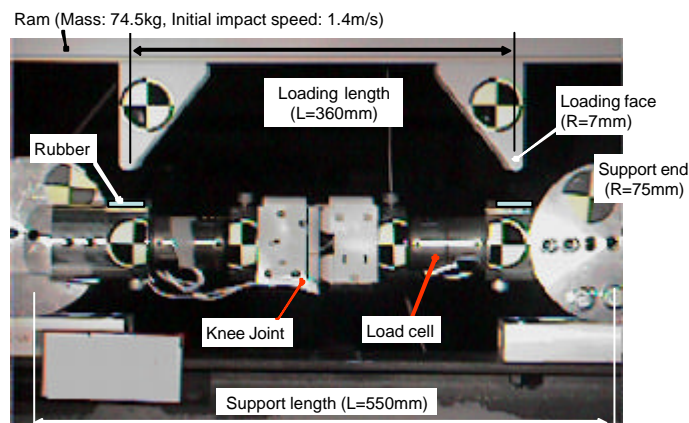


Figure 7. Sectional loading test set up for knee (Flex-PLI).



Figure 8. Vehicle test set-up. (subsystem test).

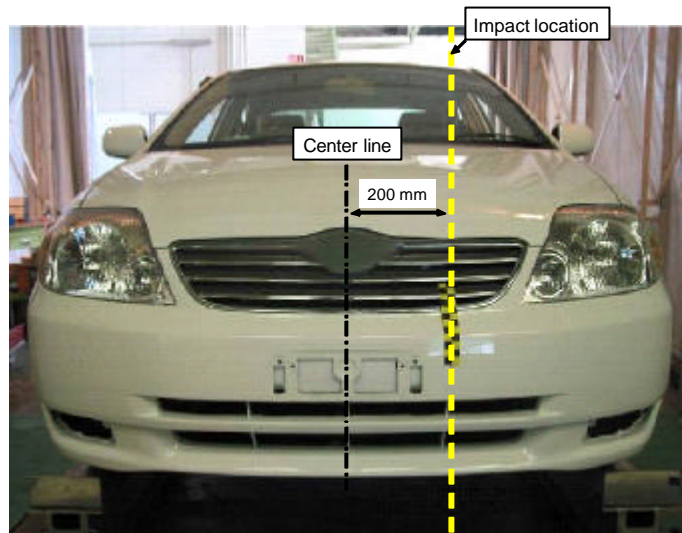


Figure 9. Test vehicle and impact location.

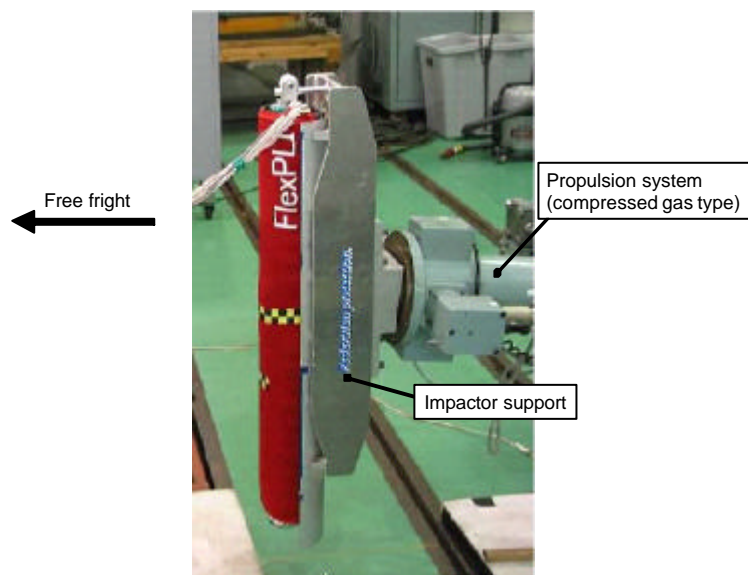


Figure 10. Legform impactor propulsion system.

RESULTS

Sectional Loading Test

The deflection characteristics of the thigh and leg of Flex-PLI against repeated loading are reported in Figures 11 and 12. Both the responses of the thigh and leg remained highly constant throughout more than 20 times of loading.

Results on the reproducibility of the thigh, leg and knee of the Flex-PLI are described in Figure 13 to 15. Each of these Flex-PLI sections exhibited highly uniform load responses among the three discrete units tested.

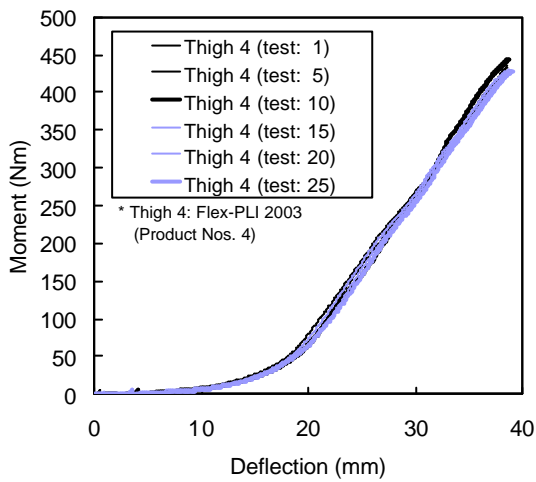


Figure 11. Repeatability test results for thigh (Flex-PLI).

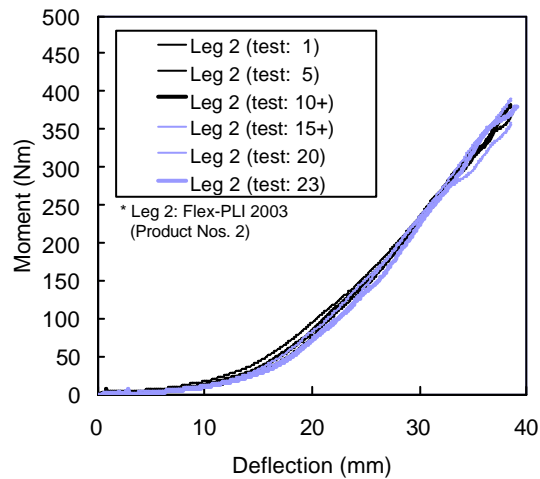


Figure 12. Repeatability test results for leg (Flex-PLI).

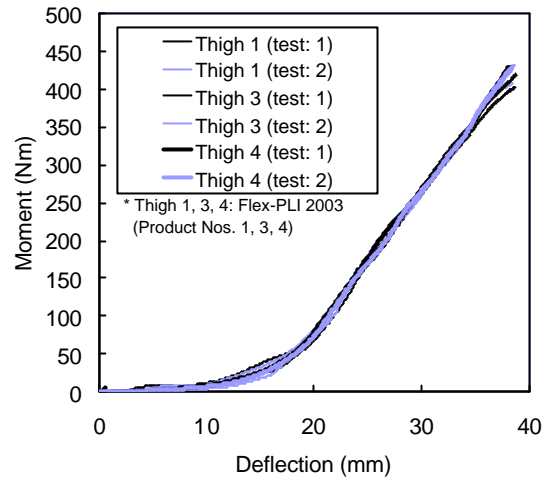


Figure 13. Reproducibility test results for thigh (Flex-PLI).

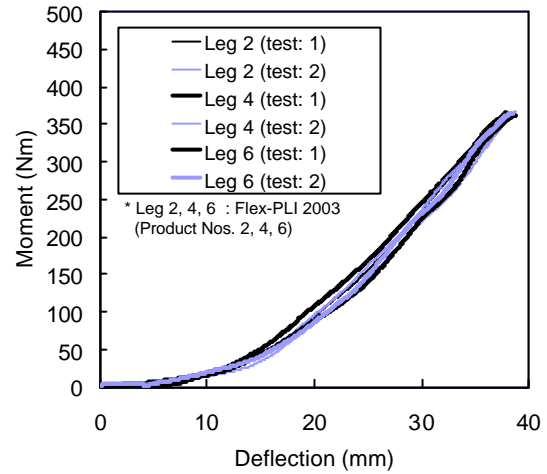


Figure 14. Reproducibility test results for leg (Flex-PLI).

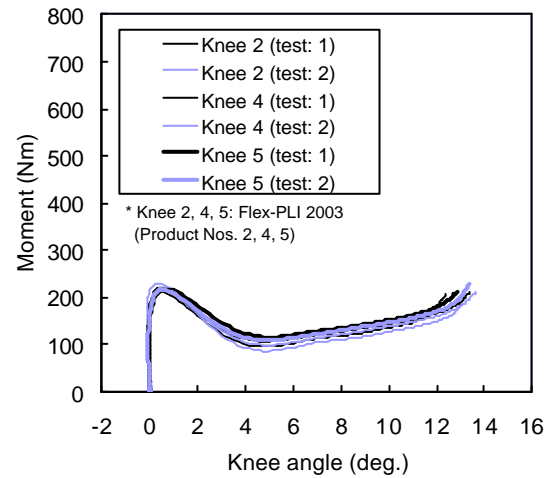


Figure 15. Reproducibility test results for knee (Flex-PLI).

Vehicle Test

The behaviors of Flex-PLI and TRL-LFI observed in the vehicle test are illustrated in Figure 16. The time-sequence photos clearly show that all the sections of Flex-PLI bend in a collision with a vehicle, while the TRL-LFI bends only at its knee under an impact.

The impact waveforms measured by Flex-PLI and TRL-LFI are given in Figures 17 and 18. The Flex-PLI allows measurement of load conditions in detail

throughout the lower extremity, but the TRL-LFI measures load conditions only around the knee.

The results of the vehicle test on the repeatability of Flex-PLI are reported in Figure 19. The Flex-PLI exhibited an excellent stability of responses to repeated collisions with the test vehicle.

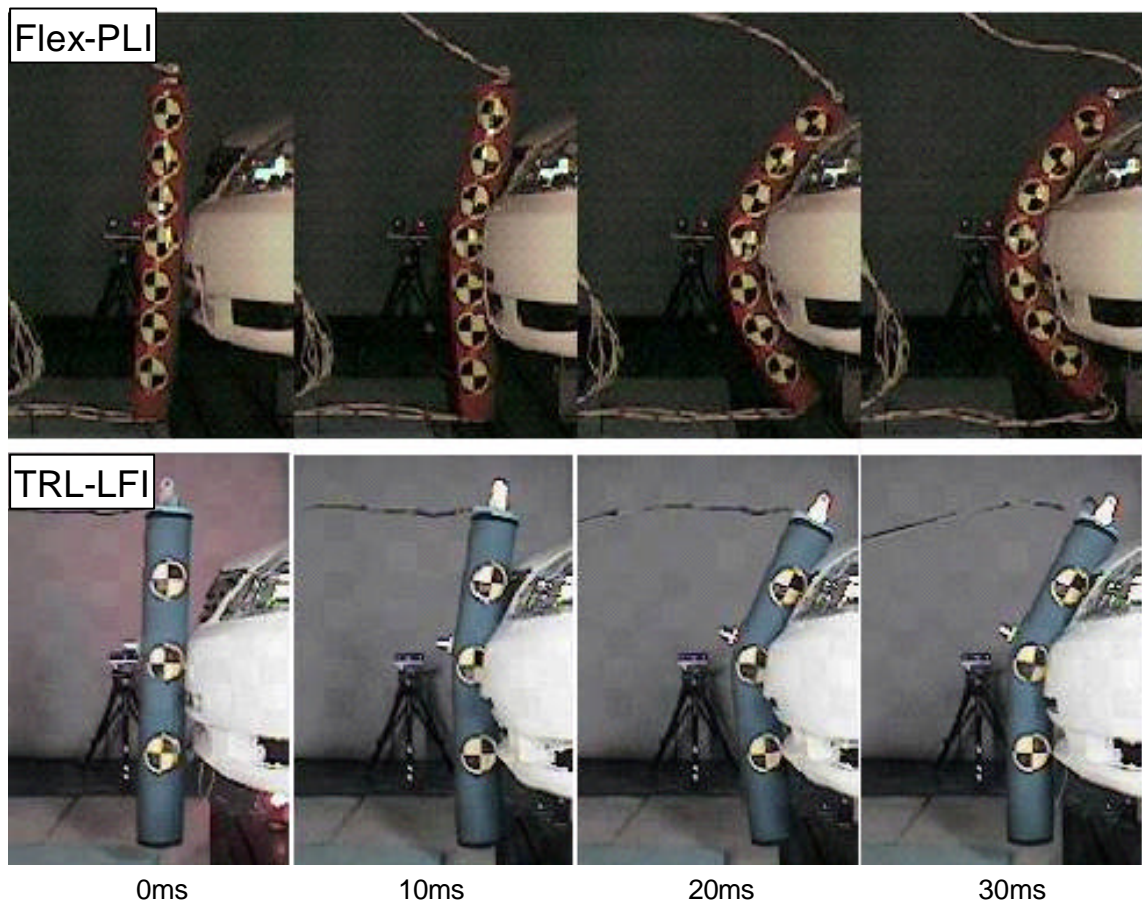


Figure 16. Vehicle test results (Kinematics).

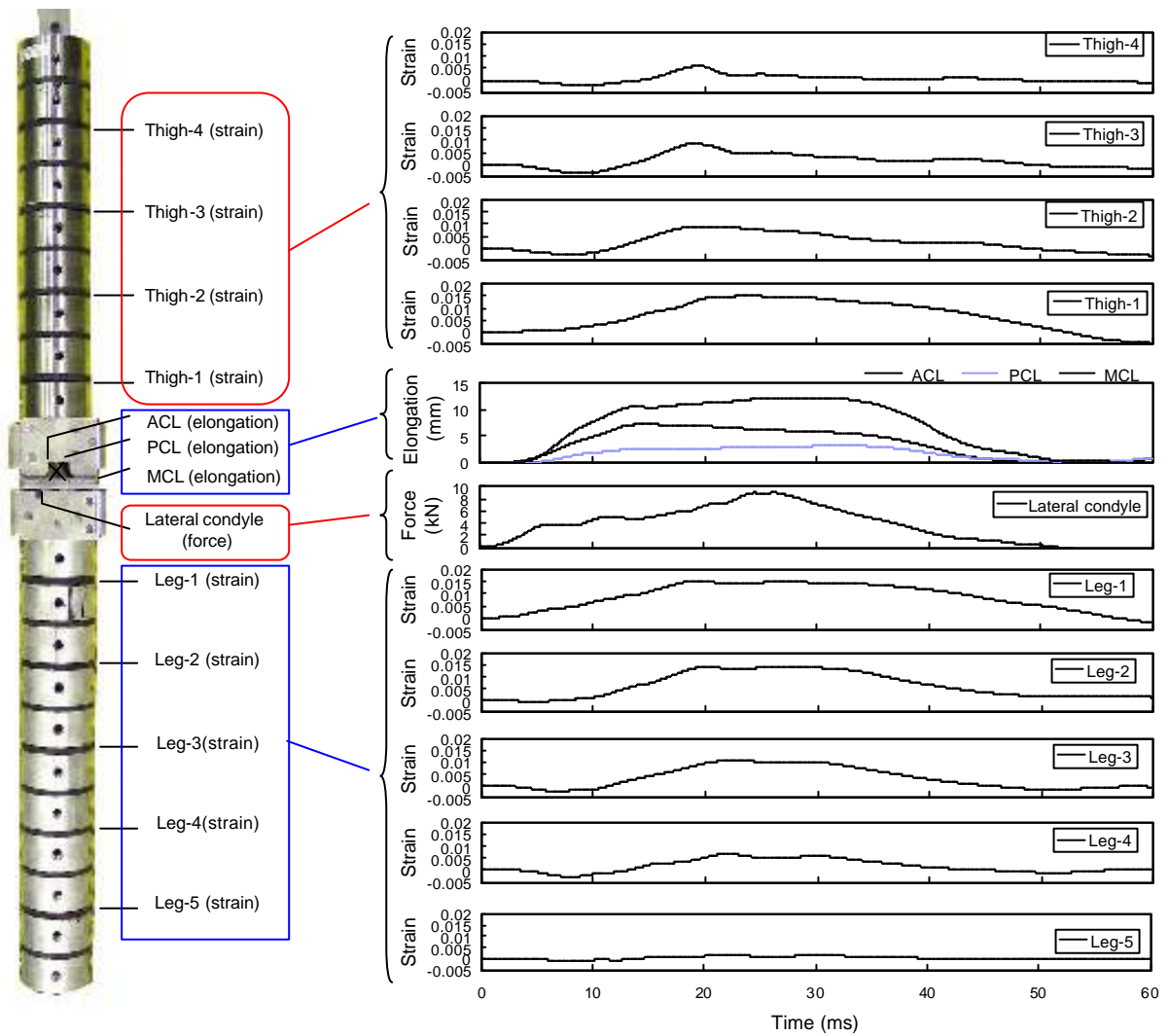


Figure 17. Vehicle test results (FlexPLI waveforms).

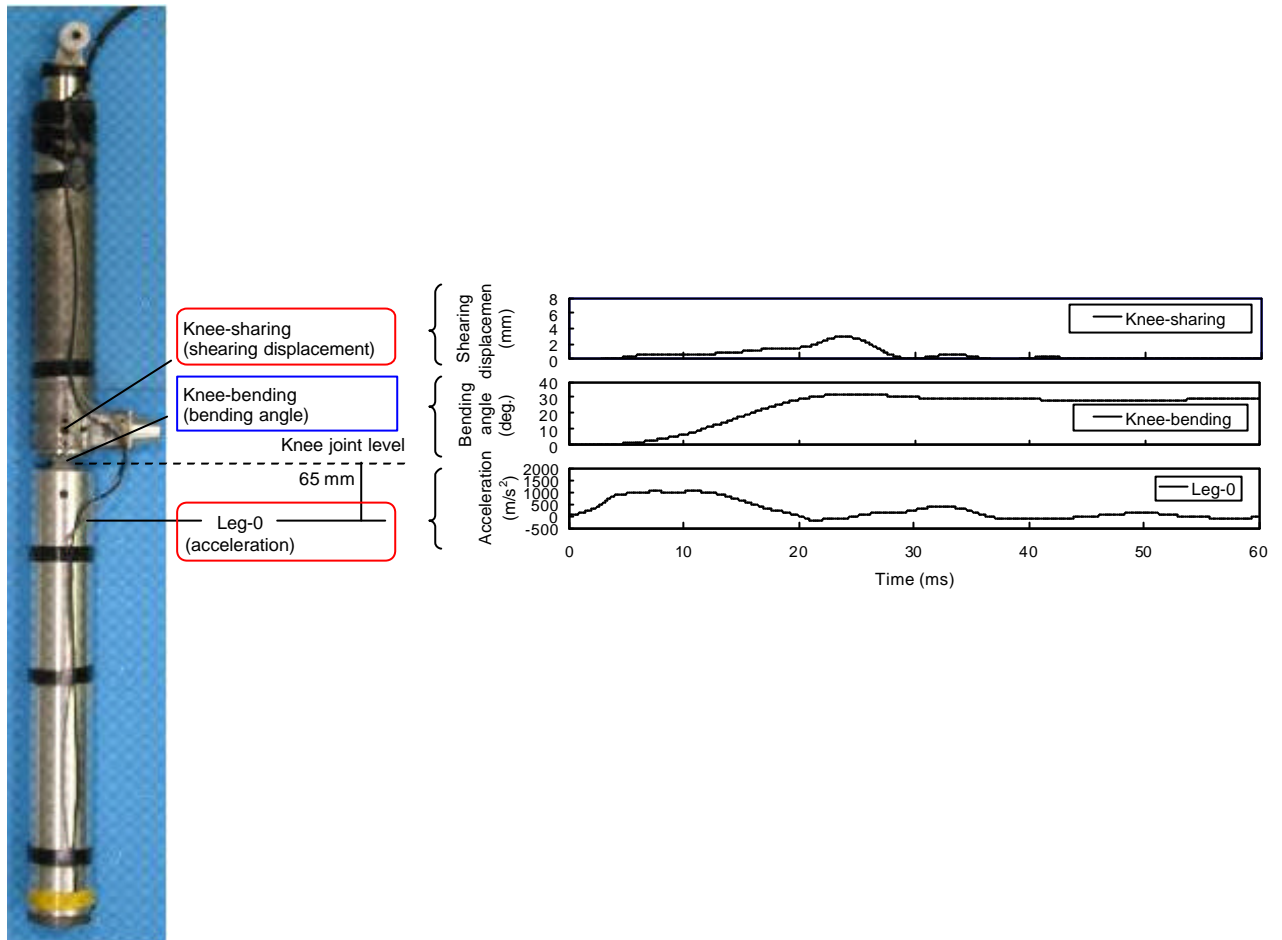
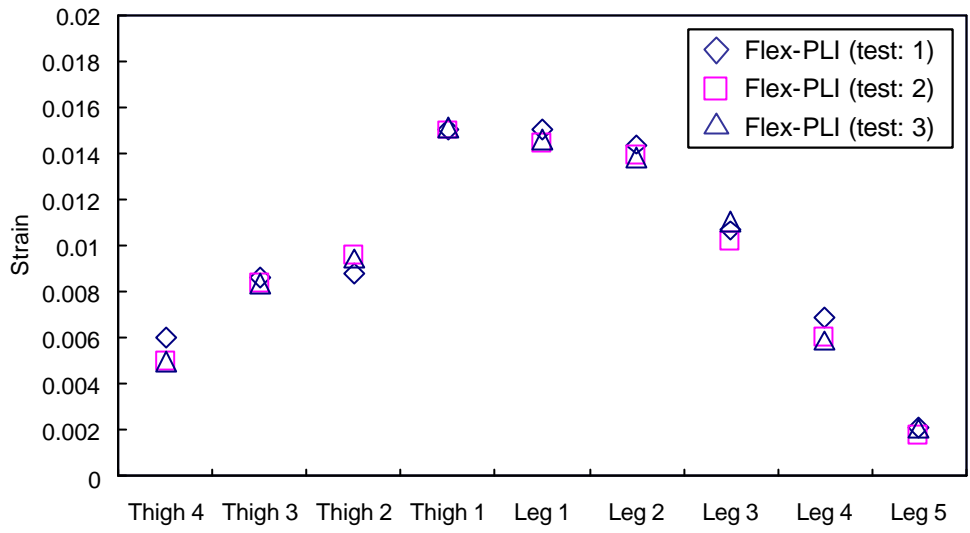
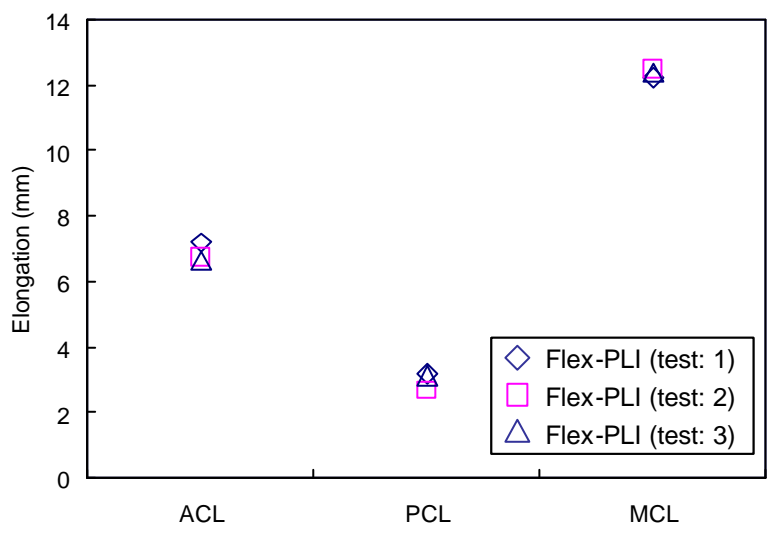


Figure 18. Vehicle test results (TRL-LFI waveforms).



a). Thigh and leg strains



b). Knee ligament elongations

Figure 19. Vehicle test results (Repeatability test, maximum values).

DISCUSSION

In the present study a sectional loading tests were first conducted on the thigh, leg and knee sections of the Flex-PLI. The results confirmed that all the lower extremity sections of Flex-PLI have favorable repeatability and reproducibility characteristics.

The next , a vehicle test was performed to compare the Flex-PLI and the TRL-LFI in collisions with a vehicle. The results indicated: 1) the Flex- PLI responds with a higher biofidelity in a collision as compared to the TRL-LFI, 2) the Flex-PLI enables measurement in greater detail than does the TRL-LFI, and 3) the Flex-PLI demonstrates an excellent repeatability in vehicle tests.

It is therefore hoped that laboratories in many countries will conduct verification tests on Flex-PLI so that a GTR for pedestrian lower extremity protection can be formulated assuming the use of Flex-PLI legform impactor.

CONCLUSIONS

- In the sectional test of the present study, it was confirmed that the thigh, leg and knee of Flex-PLI all exhibit a favorable repeatability and reproducibility.
- In the vehicle test comparing the behavior of Flex-PLI and TRL-LFI, it was verified that the Flex-PLI has a higher biofidelity and enables measurement in greater detail.
- In the vehicle test on Flex-PLI, an excellent stability of responses to repeated loading was confirmed.
- It is hoped that laboratories in many countries will conduct verification tests on Flex-PLI so that a GTR pedestrian lower extremity protection can be formulated assuming the use of Flex-PLI legform impactor

REFERNECES

[1] EEVC Working Group 17 Report: Improved test methods to evaluate pedestrian protection afforded by passenger cars (1998) European Enhanced Vehicle Safety Committee.

[2] Konosu, A., Tanahashi, M. (2003) Development of a biofidelic pedestrian legform impactor: Introduction of JAMA-JARI legform impactor ver. 2002, Proc. 18th International Technical Conference on the Enhanced Safety of Vehicle, Paper No. 378.

[3] Matsui, Y., Ishikawa, H., Sasaki, A., Kajzer, J.,

Schroeder, G. (1999) Impact response and biofidelity of pedestrian legform impactors, Proc. Inernational Conference on the Biomechanics of Impact, pp. 343-354.

[4] Bhalla, K.S., Bose, D., Madeley, N.J., Kerrigan, J., Crandall, J., Longhitano, D., Takahashi, Y. (2003) Evaluation of the response of mechanical pedestrian knee joint impactors in bending and shear loading, Proc. 18th International Technical Conference on the Enhanced Safety of Vehicle, Paper No. 429.

DEVELOPMENT AND FULL-SCALE DUMMY TESTS OF A POP-UP HOOD SYSTEM FOR PEDESTRIAN PROTECTION

Kaoru Nagatomi
Ken Hanayama
Tatsuya Ishizaki
Sakae Sasaki
Kazuo Matsuda
Honda R&D Co., Ltd.
JAPAN
Paper number 05-0113

ABSTRACT

A pop-up hood system has been developed to reduce the severity of head injuries to pedestrians in pedestrian-to-automobile accidents.

The system employs sensors located on the bumper to detect impact with a pedestrian. If an impact occurs, a signal is sent to an actuator to raise the rear portion of the engine hood approximately 100mm. This provides a space between the engine and other hard components and the hood, resulting in reduced pedestrian head injuries.

Previous studies have mainly employed headform impactors to evaluate the head injury criteria (HIC) values for pop-up hoods.

This report describes studies of the effect of the pop-up hood on injury parameters and kinematics using the POLAR pedestrian dummy. The effectiveness of the pop-up hood system was confirmed by the significant reduction of HIC values in impact tests using the POLAR dummy.

INTRODUCTION

There are approximately 2,300 pedestrian fatalities annually in Japan, accounting for roughly 30% of all traffic fatalities. (1) In the EU this figure is approximately 7,000 fatalities (20%) (2), and in the USA approximately 4,700 fatalities (11%) (3).

The most frequent area of injury, in pedestrian fatalities, is the head in approximately 60% of the cases (2), and the vehicle area causing these injuries most often is the hood. (4) To reduce the number of pedestrian fatalities, countermeasures can be taken to help reduce the severity of head injuries caused by the pedestrian's head impacting the hood.

As means of helping reduce pedestrian head injuries, Honda has adopted impact-absorbing structures in the hood, link type hinges, pyro-actuators and sensors in the front bumper.

Honda has developed a pop-up hood that provides a space in the engine bay by lifting up the hood at the time of collision, thereby helping reduce the severity of a pedestrian's head impact with the hood.

Previous studies of pop-up hoods have reported

Head Injury Criteria (HIC) evaluations according to tests using headform impactors. (5)

The purpose of this paper is to evaluate the effect of the hood pop-up action on dummy kinematics and on HIC, using pedestrian dummies (6).

The research includes the following:

1) Calculations of contact time of the pedestrian's head with the hood using a computer simulation

2) Setting the device operation time

3) The pop-up hood system

4) Test confirmation of the deployment time

5) Confirmation of dummy kinematics and injury values, through pedestrian dummy tests

CALCULATIONS OF CONTACT TIME OF THE PEDESTRIAN'S HEAD ON THE HOOD

Figure 1 shows the simulation model. Each part of the dummy model body is expressed as ellipsoid elements. (7) The dummies used were C6Y, AF05, and AM50. The dummies represent pedestrians impacted from the side while crossing a road. The hood edge height in this vehicle model was approximately 670mm.

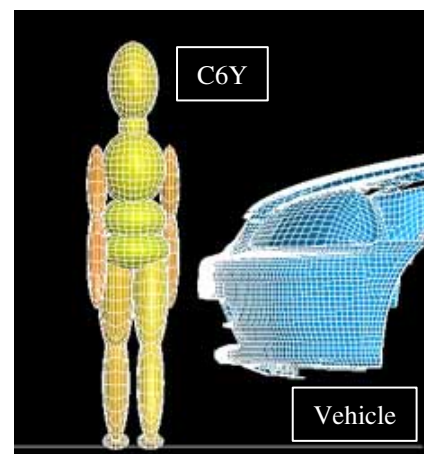


Figure 1. Simulation model of dummy crash.

The impact speed was set at 40km/h, and the location of the impact was the center of the vehicle.

The height of each dummy model and the time to collision of the head with the hood, obtained through the simulations, are given in Table 1.

The shorter the height, the shorter the head contact time with the hood. With C6Y, the contact time was 63ms under this simulation condition.

Table 1.
Dummy's height and head contact time.

	C6Y	AF05	AM50
Height	1.15m	1.52m	1.77m
Head contact time	63m s	97m s	140m s

SETTING THE DEVICE OPERATION TIME

Based on the results of C6Y's simulation, the target device operation time was set at 60ms or less in this study so that the device completes its operation faster than the time between the pedestrian's leg contacting the bumper and the pedestrian's head contacting the hood.

POP-UP HOOD SYSTEM

As shown in Figure 2, the pop-up hood is composed of a sensing system and hood lifting elements.

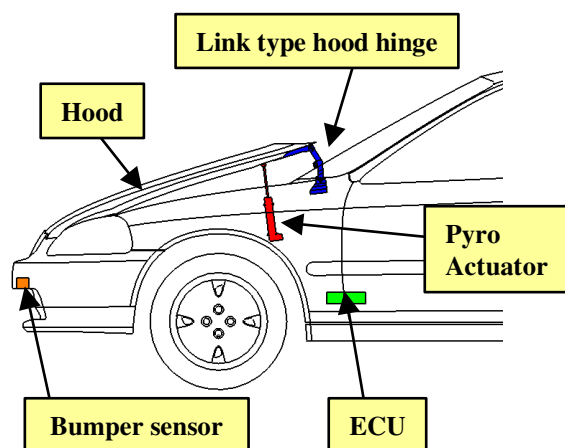


Figure 2. Pop-up hood system.

Sensing System

As shown in Figure 3, sensors are located on the structure in front of the bumper beam, in areas that deform due to collisions with pedestrians.

Accelerometers are used for the bumper sensors. Bumper sensors detect collisions with an object of a weight equivalent to that of a pedestrian.

The ECU located inside the cabin judges the need for device operation, according to collision signals from the bumper sensors, and vehicle speed information.

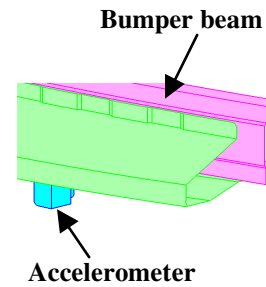


Figure 3. Sensing system.

Hood Lifting Elements

As shown in Figure 2, the hood lifting elements are actuators, hood hinges, and the hood. A pyro-actuator has been adopted so that the hood lifts rapidly. The actuator is composed of a micro gas generator and a shaft, as shown in Figure 4.

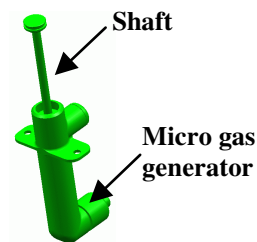


Figure 4. Pyro-Actuator.

The hood hinge adopted is a link type hinge, as shown in Figure 5. The link hinge is composed of an upper bracket, lower bracket, arm A, arm B, three pivots, and a pin.

According to an ignition signal from the ECU, gas from the micro gas generator raises the shaft. The shaft shears the hood hinge pin, lifting the rear portion of the hood approximately 100mm, thereby providing a space between the hood and the hard components under the hood, such as the engine.

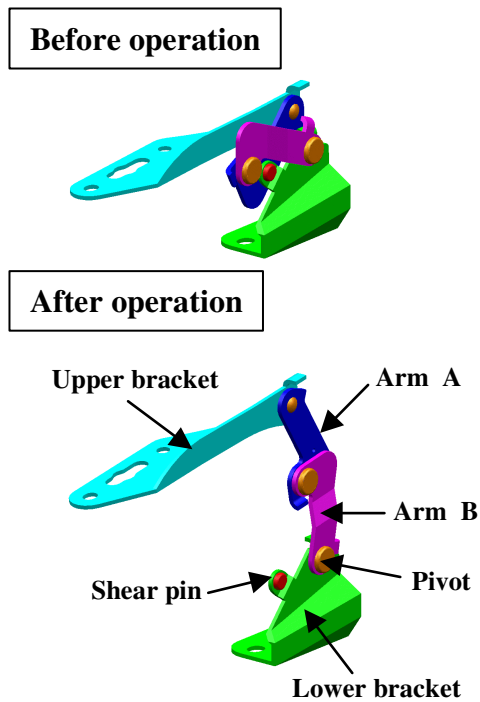


Figure 5. Hood hinge of link type.

TEST CONFIRMATION OF THE DEPLOYMENT TIME

The setup for the hood lift operation testing is given in Figure 6. The actuators were placed near the hood hinges, one each on the left and right sides. The actuators were operated by an ignition signal, and the time until the hood has been lifted 100mm was measured.



Figure 6. Setup for hood lift operation testing.

As the target device operation time was equal or less than 60ms, as noted above, the target deployment time was set at 30ms or less in this study, excluding the sensing time.

Figure 7 gives the test results. With the adoption of the pyro-actuators, a hood lift time of no more than 30ms was confirmed.

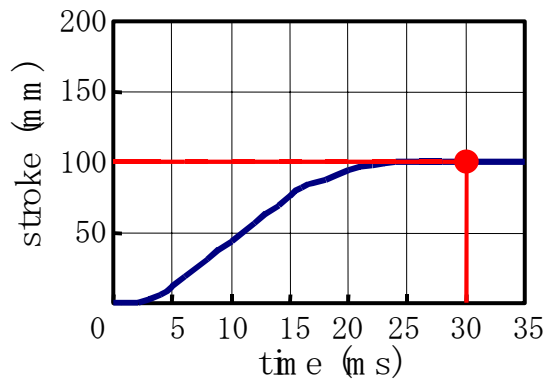


Figure 7. Results of hood lift operation testing.

CONFIRMATION OF DUMMY KINEMATICS AND INJURY VALUES, THROUGH PEDESTRIAN DUMMY TESTS

In order to confirm the effect of the hood lift operation on dummy kinematics and on injury values, impact tests were performed using a pedestrian dummy. The test conditions and setup are shown in Figure 8.



Figure 8. Setup of Pedestrian dummy test.

Tests were conducted both with and without operation of the hood lift device. The pedestrian dummies were set to receive a collision impact from the side. The dummy's arms were in front, and both wrists were tied together with rope. High-speed digital cameras were set in order to record the kinematics of the dummies during the collisions. The impact speed was 40km/h, and the impact location was the center of the vehicle.

Figure 9 shows the test results of the dummies' head and chest trajectories, both with and without the hood lift device operation.

Large differences in head and chest trajectories against the vehicle were not seen when comparing results with and without hood lift device operation. The hood lift actuator operated approximately 15ms

after collision, and the time until the hood to be completely lifted was approximately 45ms.

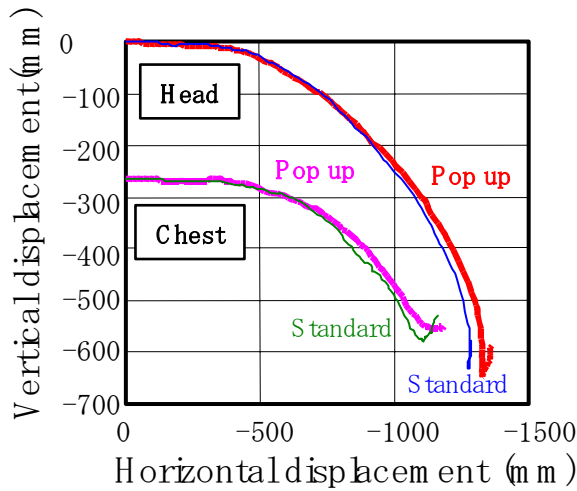


Figure 9. Head and chest trajectories with pop up hood compared to standard hood.

Figure 10 shows the dummy’s resultant head speed against the vehicle, both with and without the hood lift device operation. The head speed rises from approximately 70ms, when the head starts to swing. The resultant head speed starts to lower from approximately 120ms when the shoulder and hood contact. The time of head contact with the hood was approximately 130ms.

It was confirmed that this system supports the hood up during the dummy’s torso impacts the vehicle, until its head impacts with the hood.

Large difference in head speed against the vehicle was not seen when comparing results with and without hood lift device operation.

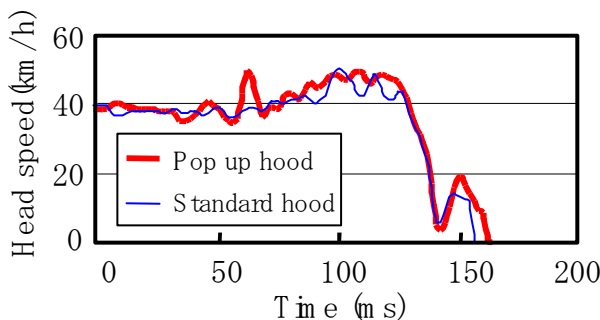


Figure 10. Head resultant speed.

Table 2 gives the wrap around distance (WAD), the speed at which the head impacts the hood, and the HIC value, both with and without the hood lift device operation.

Table2. Test results of pedestrian dummy impact with pop up hood compared to standard hood.

	WAD	Head impact speed	HIC
Pop up hood	1910mm	34km/h	926
Standard hood	1910mm	35km/h	1353

Comparing the test results with the hood lift device operation and without its operation, the wrap around distance was the same. At the moment of head-hood contact, there were no great differences in head impact speeds.

There was an approximately 30% reduction in HIC values with the use of the pop-up hood system.

It is believed that increasing the space between the hood and the hard components under the hood, by lifting the hood, helps reduce the severity of the head contact with the hard components under the hood, thereby reducing HIC values.

CONCLUSIONS

C6Y’s head contact time with the hood was determined through simulation, and a target device operation time was set at 60ms or less.

Giving due consideration to the sensing time, the target deployment time was set at 30ms or less in this study.

A pop-up hood system was developed, composed of bumper sensors, link type hinges, and pyro-actuators. The device operation was confirmed through tests.

Furthermore, pedestrian dummy tests were conducted, confirming the effect of the hood lift operation on dummy kinematics and on injury values.

The findings are as follows:

- 1) The hood lift time was within the targeted time of 30ms. With the adoption of pyro-actuators, a rapid operation speed was actualized.
- 2) Comparing the test results with and without the hood lift device operation, there were no great differences in dummy trajectory, or in head impact speed. And the wrap around distance was the same.

3) The effect of the pop-up hood system was a HIC reduction of approximately 30%, and this was confirmed through pedestrian dummy tests.

REFERENCES

- (1) Institute for Traffic Accident Research and Data Analysis
Annual Traffic Accident Report 2004
(In Japanese)
- (2) ETSC
Safety of Pedestrian and Cyclists in Urban Areas
European Transport Safety Council 1999
- (3) NHTSA
Fatality Analysis Reporting System 2003
- (4) Y.Foret-Bruno, et al.
Injury Pattern of Pedestrians Hit by Cars of Recent Design
16th ESV Conference 1998
- (5) R. Fredriksson, et.al.
Evaluation of a New Pedestrian Head Injury Protection System with a Sensor in the Bumper and Lifting of the Bonnet's Rear Part
17th ESV Conference 2001
- (6) A. Akiyama, et.al.
Development and Application of the New Pedestrian Dummy
17th ESV Conference 2001
- (7) S.Yoshida, et al.
Simulation of Car-Pedestrian Accident for Evaluate Car Structure
16th ESV Conference 1998

PEDESTRIAN PROTECTION BASED ON COMBINED SENSOR SYSTEMS

Dr. Jan Tilp, Dr. Ralf Walther, Dr. Soenke Carstens-Behrens, Claudia Zehder, Dr. Christian Zott

Robert Bosch GmbH, Stuttgart, Germany

Dr. Thomas Fischer, Mirko Ruhs, Thorsten Sohnke, Oliver Wieland

Robert Bosch GmbH, Frankfurt, Germany

Andreas Busse, Frank Suhling

Robert Bosch GmbH, Hildesheim, Germany

Paper Number 05-0156

ABSTRACT

Pedestrian protection has come up to an important issue. The European Community (EC) has released a draft law, which mandates manufacturers to increase pedestrian safety. This law consists of two phases, beginning in 2005 and 2010 respectively.

To face up with present and future challenges, the Bosch roadmap of Electronic Pedestrian Protection (EPP) provides three sensor system generations: a contact sensor system (EPP1), a system combining contact sensors and ultrasonic sensors (EPP2) and a system combining ultrasonic sensors and video sensors (EPP3). In this paper, we focus on EPP2 and EPP3.

EPP2 uses synergy effects with ultrasonic systems (e.g. the parking aid) that are well-established on the market, in order to enhance the classification performance. In the EPP2 system, the ultrasonic sensor subsystem generates a feature vector which carries ultrasonic as well as geometric properties. This feature vector is combined with that of the contact sensor subsystem, which gives information about the mechanical object properties “stiffness” and “impact energy” of the object. The combination of the feature vectors leads to an improved and robust classification, allowing the use of an irreversible actuator.

In the EPP3 system, the video subsystem accomplishes pedestrian recognition in a mid-range ahead of the car and, if necessary, initiates a driver warning (acoustic, optical). Video-based pedestrian recognition is achieved by contour analysis, while tracking of pedestrians is carried out by applying an extended Kalman filter to active-shape representations of pedestrian contours. Any time the video subsystem predicts a pedestrian to enter the ultrasonic field-of-view, information concerning direction of movement and velocity of the respective pedestrian plus an estimate of the time-to-impact is

transferred from the video subsystem to the ultrasonic subsystem. The main task of the ultrasonic subsystem is to verify or reject the hypothesis of pedestrian presence delivered by the video subsystem.

INTRODUCTION

The year-2000 White Paper of the European Commission [1] states the target of halving the number of traffic fatalities on European roads until the year 2010. In November 2003, a European directive envisioning the protection of pedestrians and other vulnerable road users was passed [2]. This directive is made up of two phases becoming effective in 2005 and 2010 respectively. Models of new car platforms will then be type-approved only if they pass defined component tests with headform- and legform-impactors.

For several car types, the requirements can be fulfilled with passive solutions (e.g. energy-absorbing structures at a car’s front end). However, there are many models where active systems containing a sensing unit as well as an actuator element (e.g. an active hood – also called pop-up bonnet) are necessary.

Active protection systems based on contact sensors are able to fulfil the use-case tests that are defined by legislation. Nevertheless, the discrimination of use and misuse cases represents a challenge due to the real-world diversity of human beings and “misuse” objects (e.g. animals or pillars) occurring in the surroundings of road traffic. Even though this aspect is not encompassed by the EC directive, it is of prime importance with respect to customer satisfaction. Therefore, it is reasonable to think of systems containing remote-type sensors.

According to Figure 1, the Bosch roadmap of Electronic Pedestrian Protection (EPP) provides – besides the contact sensor system (EPP1), which

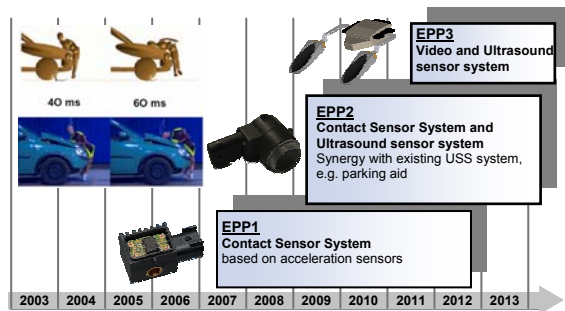


Figure 1: Bosch Electronic Pedestrian Protection roadmap.

will enter the market in 2007 – two further generations of interlocking sensor systems: a system combining contact sensors and ultrasonic sensors (EPP2) and a system combining ultrasonic sensors and video sensors (EPP3). In this paper, the focus lies on the latter two of these EPP system generations.

ELECTR. PREDESTRIAN PROTECTION 2

Motivation

Figure 2 shows a sketch of the EPP2 system. This system is composed of two subsystems: a contact sensor system (EPP1) and an ultrasound sensor system. In order to gain synergies by use of an existing ultrasound sensor system, the ultrasound sensors can also be used for e.g. a parking aid system.

The combination of the contact sensor system with an ultrasound sensor system leads to three main benefits:

- A) The object features obtained from the ultrasound sensor system are based on the reflection behaviour of the object and are thus in general independent from the mechanical object features “effective mass” and “stiffness” obtained by EPP1. These additional object features lead to an improvement of the object classification.
- B) The measured relative velocity v_{rel} is a beneficial information for the EPP1 algorithm: The use of the relative velocity instead of the vehicle velocity improves the estimation of the relative mass of the object.
- C) The estimated time-to-impact can be used for a faster safing functionality of the contact sensor system – in particular in the case of slow objects with a low acceleration signal.

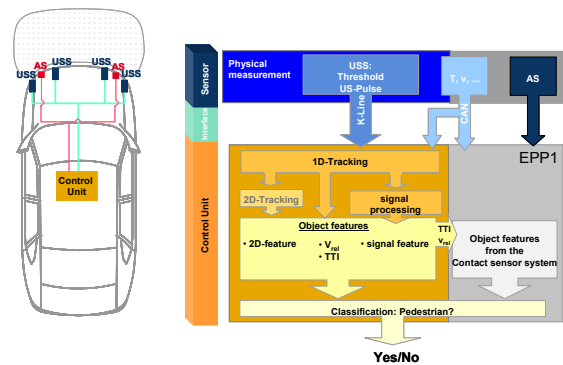


Figure 2: Sketch of the EPP2 system.

Contact Sensor Subsystem

The contact sensor subsystem EPP1 is based on acceleration sensors, which are placed in the bumper cover. This allows to measure the object impact in a very early stage of the collision (within 10-15ms after the first contact). From the acceleration signals mechanical object features – the effective momentum as well as the object stiffness – are inferred. Additionally, EPP1 uses the velocity information of the vehicle in order to estimate the effective mass of the object from the effective momentum.

Ultrasound Sensor Subsystem

In order to gain synergy with an existing ultrasound sensor system, we use standard Bosch generation-4 ultrasound sensors (USS4), which are in the market for e.g. the parking aid system. The sensors are located at the positions driven by the parking aid requirements. The USS4 provides a digital signal, which is obtained from the received analogue ultrasound echo by comparison with a threshold. The USS4 has a detection range of about 0.25m to 3m (related to a 7cm-tube).

The ultrasound sensors operate synchronized in parallel mode at which the time between two transmitted pulses is chosen stochastically. This so-called “stochastic coding” enables to use shorter cycle times down to 20ms even for large detection ranges and improves the robustness regarding external ultrasound systems [3]. Furthermore, the robustness regarding electromagnetic compatibility and ultrasound of other ultrasound systems is improved. Finally, this method allows to assign the received pulse to a transmitting and receiving sensor, i.e. to split-up the signal into direct and cross echoes for each sensor (see Figure 3).

The algorithm consists of three modules: a module for the estimation of the mechanical object features,

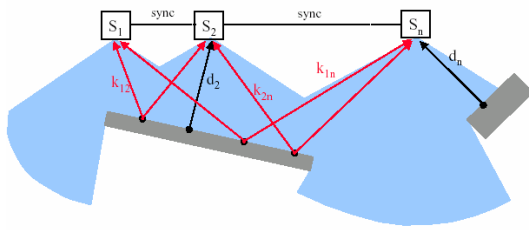


Figure 3: For a set of n ultrasound sensors s_1, \dots, s_n , direct echoes (d_1, d_n) and cross echoes (k_{12}, k_{2n}, k_{3n}) are measured. The stochastic coding enables an assignment of the measured echoes to a transmitting and receiving sensor, i.e. to a direct echo d_{ii} or cross echo k_{ij} .

a module for the estimation of the ultrasound object features, and a module for the fusion of both subsystems (see also Figure 2).

The module for the estimation of the mechanical object features is mainly given by the EPP1 algorithm. For a detailed discussion of the contact sensor system and the corresponding algorithm be referred to [4].

The module for the estimation of the ultrasound object features is based on tracking algorithms, in consideration of the stochastic coding, which provides a list of radial distances and velocities for each channel

The module for the estimation of the ultrasound object features is based on a stochastic coding algorithm which provides a list of one-dimensional object tracks for each channel, i.e., direct echoes d_{ii} and cross echoes k_{ij} (cf. Fig. 5). On basis of these object tracks ultrasonic object features as well as the variation of these features are estimated. Thus, for every object track a feature vector is obtained, which corresponds to the ultrasound properties of the concerning object.

The third module uses both the feature vector of the contact sensor subsystem and the feature vector of the ultrasound sensor subsystem. Using the estimated time-to-impact of the object, the ultrasound feature vector is assigned to the related impact feature vector. Based on these two feature vectors a classification of the object is performed.

Due to the fact that the one feature vector is correlated to the mechanical properties like stiffness and effective mass and the other feature vector is correlated to the ultrasound scattering behaviour – which is in general independent from

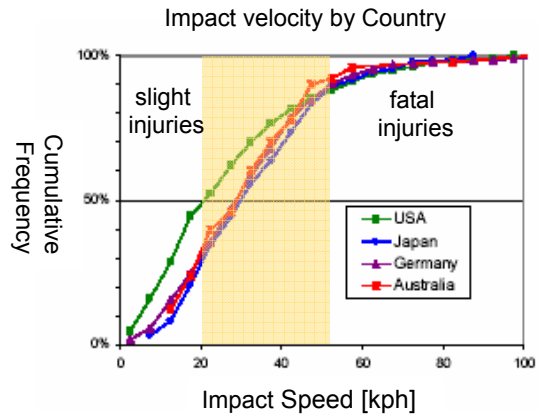


Figure 4: Cumulative frequency of accidents in dependency on impact speed. In the range of 20-50 kph (shaded area) most of all severe injuries occur.

system in order to calculate the effective mass from the measured effective momentum. This leads to an improved classification in cases where the velocity of the object is large and thus cannot be neglected by the calculation of the effective mass. The time-to-impact is needed in order to assign the right object track – and the right relative velocity – to the impact signal of the contact sensor subsystem. Moreover, the knowledge of the time-to-impact allows to reduce the thresholds of the safing path of the contact sensor algorithm. This leads to shorter decision times, in particular in cases where the object is slow and the signal as well as the safing signal is small.

Velocity range

EPP2 is designed for a velocity range of 20 – 50 kph. This velocity range is founded on statistical investigations, which show that at velocities lower than 20 kph slight injuries occur and an activation of protection systems is not necessary. For velocities faster than 50 kph, the impact energy is that large that an activated protection system does not significantly increase the chance of survival. Nevertheless, a velocity range of 20 – 50 kph covers a very large amount of accidents resulting in severe injuries (cf. Figure 4). In order to investigate the influence of the velocity on the performance of the ultrasonic system, collision tests with a test car and a cube at velocities from $v = 10 - 40\text{kph}$ were performed. The results shown in Figure 5 demonstrate the functionality of the system in the required velocity range.

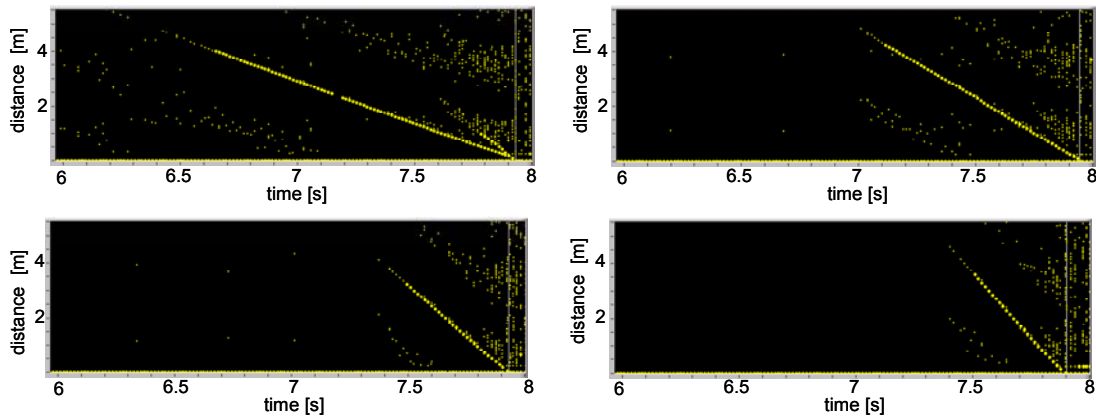


Figure 5: Object tracks for velocities from 10kph (upper left) to 40kph (lower right). Even at 40 kph the cube was detected at 3.5 m and a stable object track was obtained. Note: for lower velocities the object was detected at a distance of 4 m.

ELECTR. PEDESTRIAN PROTECTION 3

Motivation

Stricter pedestrian protection requirements – as are currently under discussion for phase 2 of the EU legislation [1] – may necessitate to initiate an actuator deployment prior to the impact (e.g. the extended lifting of an active hood in order to provide sufficient deformation space between the deformable hood and non-deformable aggregates beneath it).

Video technology has a significantly longer detection range in comparison to stand-alone ultrasound systems and possesses a high potential with respect to the classification of pedestrians and other vulnerable road users [5,6]. Since video sensors for traffic applications are commonly mounted behind the front window, a video-based observation of entire pedestrian contours is feasible for distances greater than approximately 4 meters ahead of the front bumper. However, to have an enlarged detection range also covering small distances ahead of the car, a combined approach to pedestrian detection made up of video and ultrasound sensors is proposed.

System task

The task is to reliably detect impending collisions with pedestrians, to give a warning (acoustical, optical) and, if necessary, to trigger an actuator (e.g., an active hood) as early as possible before a contact of a pedestrian with the car front occurs.

Video subsystem

In our combined approach, video technology carries out the detection of objects, the classification of

detected objects with respect to the classes “pedestrian” and “non-pedestrian” as well as the tracking of pedestrians.

Video-based pedestrian detection and classification is achieved by contour analysis [7], while the tracking of pedestrians is carried out by applying an extended Kalman filter [8] to active shape representations of pedestrian contours [9].

Any time the video subsystem predicts a pedestrian to enter the ultrasonic field-of-view, information concerning direction of movement and velocity of the respective pedestrian plus an estimate of the time-to-impact is transferred from the video subsystem to the ultrasonic subsystem.

Ultrasound subsystem

The ultrasound subsystem provides for a verification of the pedestrian data received by the video subsystem. Moreover, it predicts collision parameters – in particular the time to impact, the closing velocity (i.e., the velocity of the pedestrian relative to that of the car at the beginning of the collision) – and triggers the actuator(s) – see Fig. 6.

System prototype

As shown in Figure 3, we have equipped a test vehicle with a stereo-video subsystem and a four-channel ultrasound subsystem.

The cameras of the video subsystem contain high-dynamic-range CMOS imagers with a resolution of 512x256 pixels. Video-based pedestrian recognition is accomplished in a range of up to 25 m ahead of the bumper at aperture angles of 50° horizontally and 35° vertically.

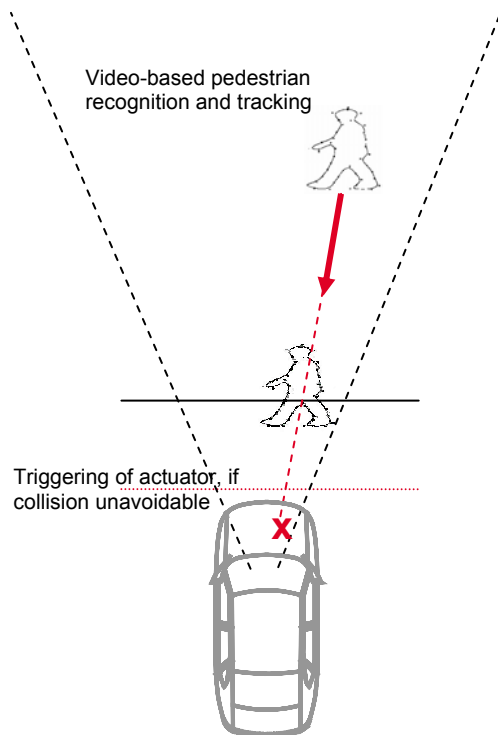


Figure 6: Basic principle of electronic pedestrian protection using video and ultrasound sensors.

Predictive information is transferred via CAN bus from the video subsystem to the ultrasonic subsystem. For details concerning the ultrasound system part, refer to the section above discussing the EPP2 system.

In comparison to EPP2, EPP3 provides a significant gain with respect to the forewarn time. According to our experiments, for a closing velocity of 30 kph, a final decision concerning the triggering of an actuator can be taken 150-200ms (i.e., 1-2m) before the actual beginning of a collision.

First preliminary test results confirm the feasibility of the chosen system approach. However, possible solutions regarding the handling of night-time situations, of partly occluded pedestrians and of groups of pedestrians have to be investigated in more detail.

Envisioned time of market introduction

Referring to the EPP roadmap in Figure 1, three key reasons can be given for a market introduction of EPP3 in the next decade:

a) *Legislation:*

Stricter protection criteria are to be expected in the European Union from quarter 4 of the year 2010 when phase 2 of the EC directive will become effective.

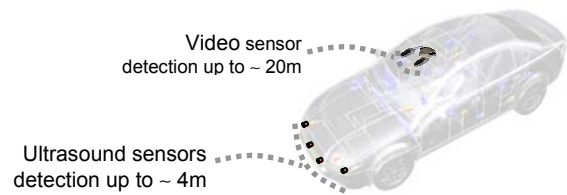


Figure 7: Positioning of video and ultrasound sensors in the EPP3 prototype.

b) *Technological and functional maturity:*

Video-based safety applications are yet to be introduced to the market. According to press announcements of several car manufacturers and suppliers, this will be done within the next five years.

c) *Price / Costs:*

Customers are price-sensitive. This is of particular importance for pedestrian protection systems, as these do not involve a direct benefit for the buyer and driver of a car. Price and cost degradation without sacrificing performance are expected to be sufficient in approximately five years. Synergies between safety and driver assistance will support the required degradation process.

CONCLUSIONS

On the basis of system prototypes set up in test cars, we could demonstrate the feasibility of combined sensor systems for the task of electronic pedestrian protection.

By use of sensor system fusion, the pedestrian-recognition performance can be increased and plausibility can be guaranteed.

However, due to current technological limitations and complexity of real-world scenarios, it will take approximately three to five years time until first system generations based on remote sensors appear on the market.

REFERENCES

- [1] White Paper "European transport policy for 2010: time to decide", European Commission, 2000.
- [2] Directive 2003/102/EC of the European Parliament and of the Council, 11/2003.
- [3] B. Wirmitzer et al.: "Interference Cancellation in Ultrasonic Sensor Arrays by Stochastic Coding and

- Adaptive Filtering”, IEEE International Conference on Intelligent Vehicles, 1998.
- [4] U. Groeger et al.: “Active Pedestrian Protection – System Development”, Paper #04B-106, SAE World Congress, 2003.
- [5] D. Gavrilă: “Sensor-based Pedestrian Protection”, IEEE Intelligent Systems, Vol. 16, No. 6, 2001.
- [6] D. Gavrilă et al.: “Vision-based pedestrian detection: the PROTECTOR system”, Proc. IEEE Intelligent Vehicles Symposium, pp. 14-17, 2004.
- [7] D. Gavrilă and J. Giebel: “Shape-based pedestrian detection and tracking”, Proc. IEEE Intelligent Vehicles Symposium, Vol. 1, pp. 8-14, 2002.
- [8] G. Welch and G. Bishop: „An Introduction to the Kalman filter“, TR 95-041, Technical Report, Department of Computer Science, University of North Carolina, Chapel Hill, 2003.
- [9] A. Blake and M. Isard, “Active Contours”, Springer, 1998.

PEDESTRIAN MEASURES FOR THE OPEL ZAFIRA II

Thomas Wanke

Dr Grace Thompson

Christoph Kerkeling

International Technical Development Center

Adam Opel AG

D-65423 Ruesselsheim

Germany

Paper Number 05-0237

ABSTRACT

In Europe & Japan, new legislation will come into effect from autumn 2005, which aims to reduce the number of pedestrian fatalities and serious injuries .

These pedestrian protection legal requirements are a new challenge for the automotive industry, deeply influencing front end styling, package, design & the complete development process. In the pedestrian tests for Type Approval, free-flying head, upper & lower leg impactors will be propelled against the vehicle front end. The vehicle must absorb these low impact energies by means of a “pedestrian-friendly soft nose”, to ensure acceptable injury values. The size & shape of the pedestrian protection test impact areas are largely determined by the exterior styling theme.

When satisfying pedestrian protection, other vehicle requirements, e.g. insurance classification, panel dent resistance of diverse panels, high speed crash and hood slam tests must also be fulfilled. During vehicle development, all these loadcases must be balanced to produce the best possible vehicle.

The new Opel ZAFIRA II is General Motors’ first car worldwide which will provide a “soft-nose design” to comply with the new legal requirements in Japan and Europe Phase 1. The ZAFIRA will be launched in spring 2005.

In the new ZAFIRA II, specially developed passive deformation elements absorb impactor energies. Other components may collapse to decrease stiffness and increase deformation space. The light-weight thin steel hood is designed to ensure decreased acceleration values for the head impactors together with homogenous hood stiffness. In the lower bumper fascia area, a spoiler improves the lower leg impactor kinematics by reducing knee bending.

This presentation shows the Opel ZAFIRA’s pedestrian protection measures and reports on Opel’s experience gained in making a car more pedestrian-friendly.

INTRODUCTION

Major changes to current vehicle fronts are required to satisfy the proposed (and differing) legal requirements in Europe, Japan and possibly other countries, as well as to achieve a good Euro NCAP pedestrian rating. The aim of the legislation is to further improve pedestrian protection.

The Opel ZAFIRA II

The Opel ZAFIRA is a mass production family car in the minivan segment, see Figures 1a and 1b. It is a seven-seater with a highly flexible interior and seat system

This is a very important vehicle in the General Motors Europe / Opel product portfolio and is one of the top selling vehicles in Europe in its class. Therefore, it is a significant step for the ZAFIRA II to be made compliant with Japan and EU Phase 1 pedestrian regulations.



Figure 1a. The new Opel ZAFIRA II: a seven seater with a highly flexible seat concept.



Figure 1b. The new Opel ZAFIRA II

The ZAFIRA II is the first vehicle for Opel, and indeed for General Motors, to be compliant with the EU Phase 1 pedestrian protection requirements. Hence, its development was a considerable challenge for the General Motors Europe International Technical Development Center.

This paper will discuss the challenges and the solutions in some technical detail.

1. Main Legal Requirements and Consumer Tests

The forthcoming legal and Euro NCAP requirements define impacts by free-flying pedestrian impactors – heads of various sizes, lower leg, upper leg – against the vehicle front.

1.1 Head Impact Definition

The HIC (Head Injury Criterion) is the only criterion for legal and consumer head impact tests, see equation (1):

$$HIC := \max \left\{ \left[\frac{1}{t_2 - t_1} \int_{t_1}^{t_2} a(t) dt \right]^{2.5} (t_2 - t_1) \right\} \quad (1).$$

The EU and Japan have different head impactors and impact speeds. For both the EU and Japanese Phase 1 legal requirements, directives 2003/102/EC [1] and TRIAS63 [2] respectively, the pass criteria for head impact are as follows:

- HIC < 1000 for 2/3 of the impact area
- HIC < 2000 for 1/3 of the impact area

In addition, the EU Type approval includes adult head impact tests against the windscreen, which are for monitoring purposes. The EuroNCAP (European consumer) tests [3] for adult head are for impacts against the hood and other components e.g. windscreen, A-pillars, fenders.

1.2 Remaining Impact Definitions

In addition to the above head impactor tests, the EU Type Approval and EuroNCAP each specify impactor tests for the lower leg and the upper leg, with the upper leg Type Approval tests being for monitoring purposes. There are no upper or lower leg tests for Japan.

1.3 Summary of EU and Japan Legal Regulations

The definitions of the aforementioned EU and Japanese Type Approval tests are summarised in Figures 2 and 3:

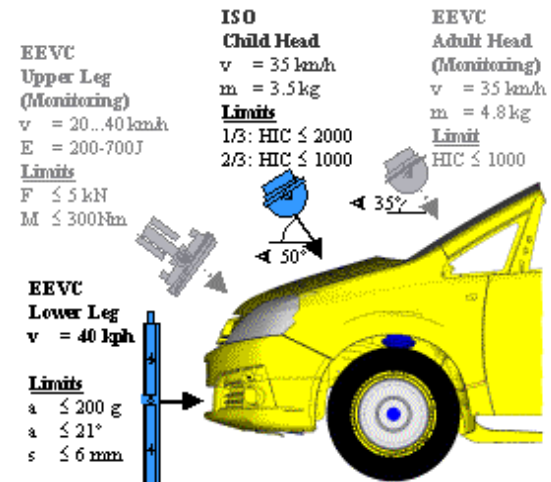


Figure 2. Main EU Legal Requirements



Figure 3. Main Japanese Legal Requirements

1.4 Summary of Euro NCAP Pedestrian Tests

The definitions of the Euro NCAP (European consumer) tests, together with the upper and lower limits for zero-maximum points, are summarised in Figure 4:

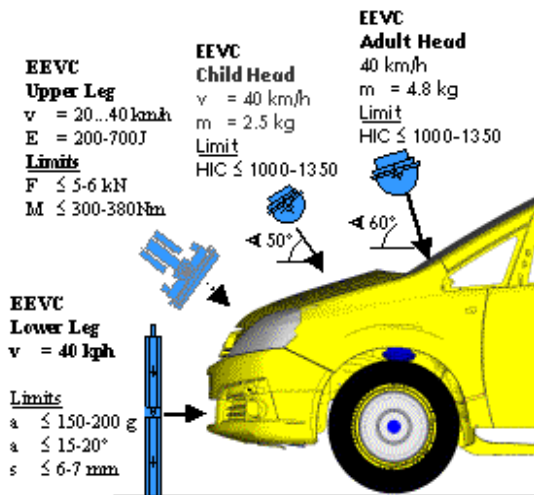


Figure 4. Euro NCAP Tests

2. Difficulties and Aims

Pedestrian protection basically requires the following principals:

1. Making available sufficient deformation space, so that the kinetic energy of the impactor or pedestrian can be absorbed
2. Making the vehicle structure in these deformation zones softer so that the necessary deformation can occur

The following pedestrian loadcases were considered for the ZAFIRA II development:

- 3.5 kg ISO Child Head @ 35 kph (EU Legal Phase 1)
- 4.8 kg Adult Head @ 35 kph (Monitoring EU Legal Phase 1)
- Lower Leg @ 40 kph (EU Legal Phase 1 and Euro NCAP)
- Upper Leg @ 700 J (Monitoring EU Legal Phase 1)
- 2.5 kg Child Head @ 40 kph (Euro NCAP)
- 4.8 kg Adult Head @ 40 kph (Euro NCAP)
- 3.5 kg Japan Child Head @ 32 kph (Japan Legal Phase 1)
- 4.5 kg Japan Adult Head @ 32 kph (Japan Legal Phase 1)

In developing pedestrian protection, it is necessary to frequently check that other vehicle loadcases and requirements are fulfilled, including:

- Low speed insurance classification test (soft nose design can lead to higher damage, hence higher repair costs)
- ODB crash (hinge integrity)

- Hood stiffness (torsion, bending, ..)
- Hood dent resistance
- Hood slam durability
- Hood flutter under aerodynamic loading
- Hood hinge stiffness (lateral stiffness, hood opening and gas spring load)
- Hood bumpstop bracket stiffness/ strength
- Fender brackets stiffness/ strength
- Fender stiffness

Vehicle development always requires optimizing and balancing a wide range of requirements to obtain the best possible vehicle. However, this balance is more difficult for vehicles which are pedestrian compliant.

3. Development Timing and Process

In the lean General Motors Europe development process, “Structure Car” prototypes (to check the basic car structure for performance) have been rendered unnecessary because of current simulation capabilities. However, since pedestrian protection is a new requirement, it was decided to build a prototype front end buck, the “Architectural Mule Upgrade”, to examine the new ZAFIRA II properties, styling, package and design.

Therefore, in an early project phase, the CAE team was able to use test results to check the effectiveness of the pedestrian protection measures and concepts and to verify the previously non-validated pedestrian CAE models. This hardware phase reduced development risks and avoided high costs for late changes .

The development timing for the ZAFIRA II is shown in Figure 5 below:

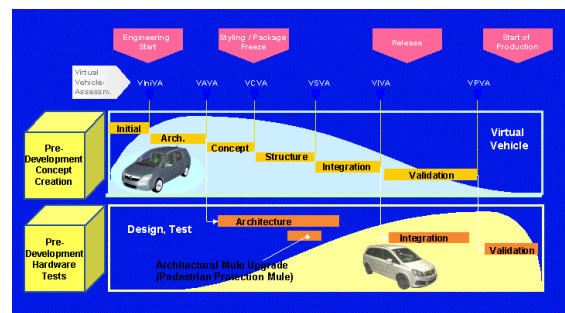


Figure 5. Development Timing

The development process was mainly CAE-driven, with multi-disciplinary teams to manage challenges and cross-functional interfaces.

4. Influence on Front End Styling and Package

The requirements for pedestrian protection had a considerable influence on the ZAFIRA II front end styling, front end package and body structure design, see Figure 6:

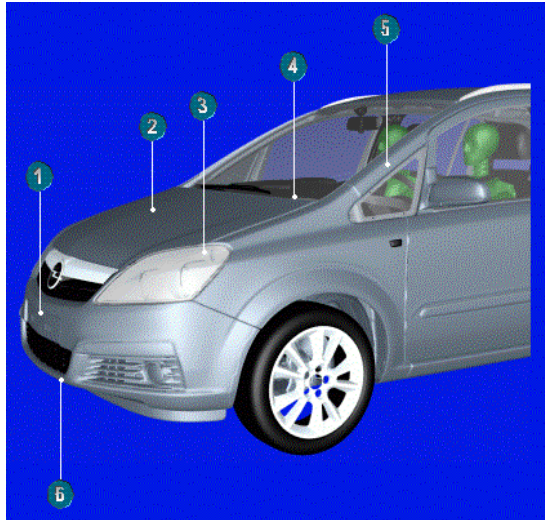


Figure 6. Front End Styling Influence

The styling of the ZAFIRA II shows several changes and optimizations, which were necessary to make the car compliant with EU Phase 1:

1. Increased bumper overhang to implement deformation elements in front of bumper beam
2. Increased hood height to ensure deformation space
3. Optimized headlight styling
4. Optimized windscreen front edge sweep to implement new cowl system for pedestrian protection
5. Cab-forward windscreen and A-Pillar position to stylistically compensate for increased hood height and increased bumper overhang
6. Moved forward lower bumper fascia area to control lower leg kinematics

5 Lower Leg Design in Opel ZAFIRA II

5.1 Design Overview

The main requirements for pedestrian lower leg protection are to minimize the knee bending angle and the tibia acceleration of the lower leg. If the lower leg acceleration and bending requirements are satisfied then, in practice, so is the shear displacement.

There were two key elements implemented in the Opel ZAFIRA II for pedestrian protection:

- Energy-absorbing components
- A system to control the leg kinematics

The following measures have been developed for lower leg protection, see Figure 7 and the associated list below:

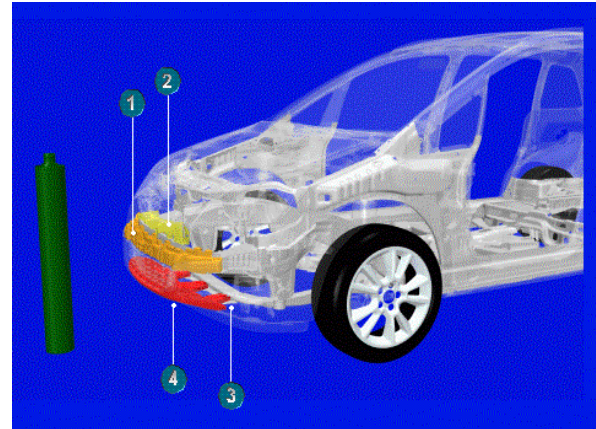


Figure 7. Lower Leg Impact Design

1. Optimized low-density pedestrian protection foam in front of a stiff aluminium bumper crossmember to absorb the impact energy, together with sufficient deformation space to avoid the impactor hitting the stiff, aluminium bumper crossmember or the foam bottoming out.
2. Optimized and elongated upper bumper support to stabilize the bumper fascia and to avoid the support being pushed backwards with bottoming out.
3. Interface bracket to firmly mount the Lower Bumper Stiffener to the front axle tube.
4. Optimized, ribbed, plastic lower bumper stiffener, firmly mounted to the chassis and bumper fascia, to control the leg kinematics by reducing knee bending.

Figures 8 and 9 illustrate the lower leg kinematics and performance:

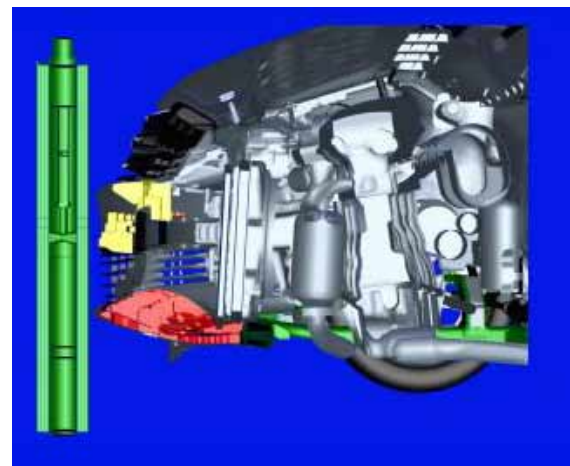


Figure 8a. Lower Leg Kinematics in Opel ZAFIRA II: Section through Center Line at Time = 0

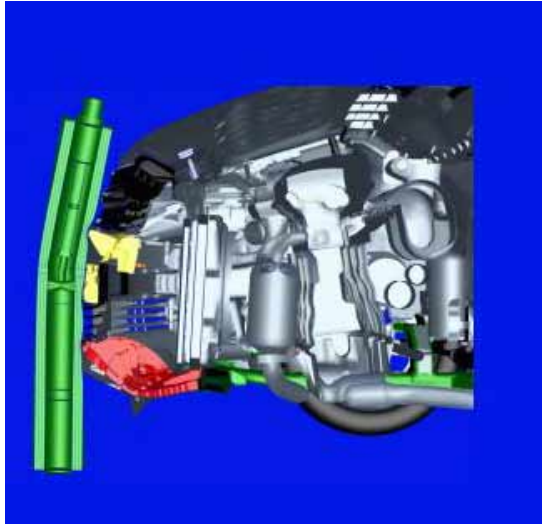


Figure 8b. Lower Leg Kinematics: Section through Center Line at Time = Rebound

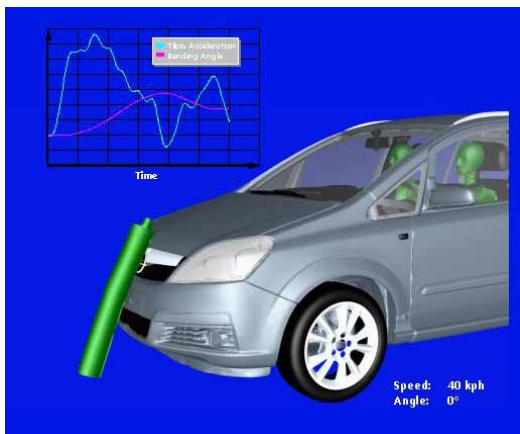


Figure 9. Lower Leg Kinematics, Acceleration and Knee Bending for the Opel ZAFIRA II

5.2 Benefits:

- Enables compliance with EU Phase 1 requirements (in advance of this law coming into effect)
- Optimized energy absorption capabilities
- Controlled lower leg kinematics
- Minimised knee bending angles
- Minimised tibia accelerations
- Minimised shear deformations in knee

6. Head Impact Design in Opel ZAFIRA II

6.1 Design Overview

To achieve the desired pedestrian head impact performance required considerable changes to the previous ZAFIRA I hood and the associated components. The main principles of the head protection design were:

- Optimized energy absorption capabilities

- Deformation space provided by optimized engine bay package and diverse deformable systems

The main elements of this design for head impact are illustrated in Figure 10 and listed below:

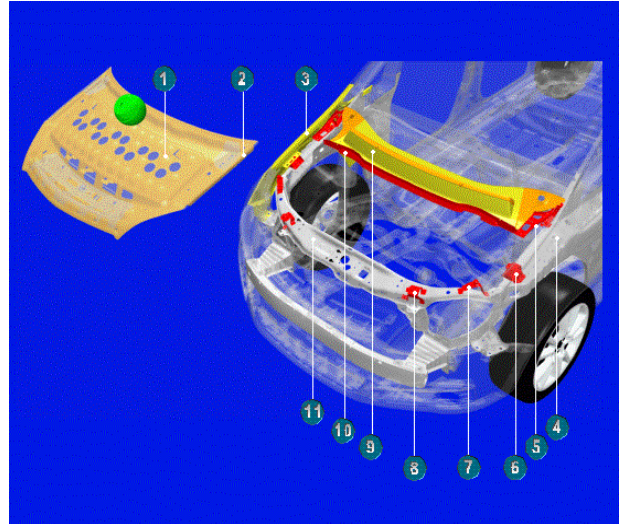


Figure 10. Overview ZAFIRA II Design for Pedestrian Head Impact

1. Thin steel hood with homogeneous, optimized “muffin tin” design for the hood inner panel
2. Cut-out hood flange
3. Thin steel fender with optimized cut out design
4. Lowered brace wheelhouse
5. Deformable hood hinge with cranked beam integrated fender bracket rear
6. Deformable fender bracket front
7. Deformable bumpstop bracket outer
8. Deformable bumpstop bracket inner
9. Deformable multi-part plastic cowl system
10. Plastic service panel with planned fracture points under pedestrian impact loading
11. Lowered front upper and front side

6.2 Benefits:

- Enabled fulfillment of EU Phase 1 and Japan requirements (in advance of these laws coming into effect)
- Sufficient deformation space available to enable absorption of impact energy
- Avoidance of hard points which could worsen head impact injuries.
- Minimised head accelerations
- Minimised HIC values

This performance is illustrated in Figure 11:

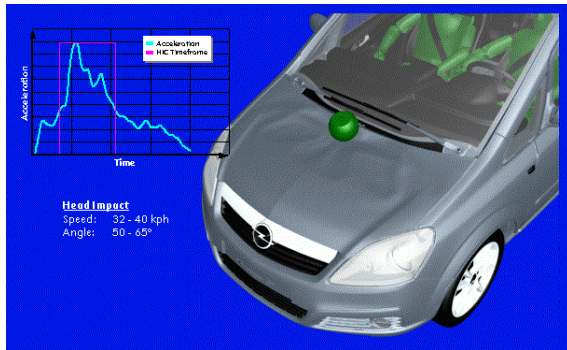


Figure 11. Head Impact Performance for Opel ZAFIRA II

6.3 Hood Design

The ZAFIRA II has steel inner and outer hood panels, which are of lower gages than the ZAFIRA I, to enable softer deformation behaviour under head impact. The hood was designed to have homogeneous stiffness for more uniform head impact characteristics, with an optimized “muffin tin” design for the hood inner panel.

This new concept has a further advantage: in addition to the benefits for pedestrian protection, the ZAFIRA II hood has lower mass than the ZAFIRA I, due to the thin steel design. This is summarised in Figure 12 and Table 1 below:

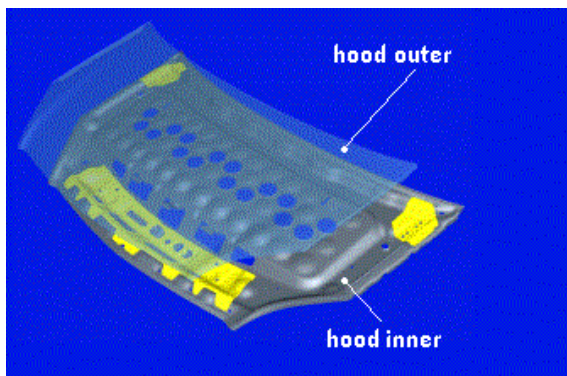


Figure 12. ZAFIRA II Hood

	ZAFIRA I	ZAFIRA II	ZAFIRA II Mass Saving
Hood outer panel gage	0.8 mm	0.6 mm	26 %
Hood outer panel gage	0.7 mm	0.5 mm	18 %

Table 1. Mass saving for ZAFIRA II Hood compared to ZAFIRA I

Some aspects of the pedestrian measures in the new ZAFIRA II will be discussed in more detail below:

6.4 Hinge Design

The hinge area is of particular interest when designing for head protection, because of the high stiffness in this region. The hinge area was part of

the 1/3 zone with HIC < 2000, as it was not feasible to reduce the HIC to 1000 in this area.

The new hinge design for the ZAFIRA II is shown in Figure 13 and summarised below:

1. The body-side hinge part deforms easily in planned folding, absorbs energy and reduces the impactor’s acceleration.
2. The cranked beam integrated fender bracket at the rear deforms downwards, absorbs energy and softens the fender behaviour to reduce the impactor’s acceleration.
3. The hood-side hinge part bends slightly and transfers vertical loads into the pivot point.

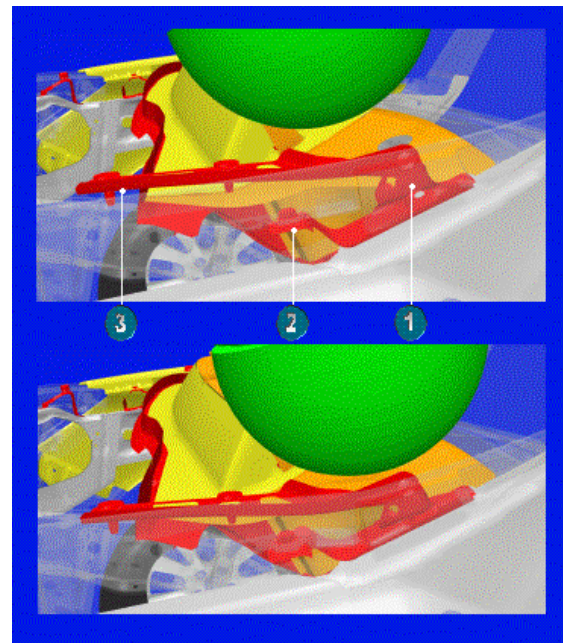


Figure 13. ZAFIRA II Hinge

The development of the hinge design involved balancing different requirements:

- Pedestrian protection for head impact (structure must collapse, with low vertical stiffness)
- Hinge lateral stiffness
- Fender stiffness (vertical and lateral stiffness targets, with no plastic deformations allowed)
- High speed front impact (hinge integrity must be maintained to prevent hood intrusion into the windscreen)
- Insurance test (minimal hood translation, rotation and plastic deformation)
- Hood opening (end stop to prevent the hood opening too wide)
- Body shop assembly (tolerance balance, height adjustability)

To optimize the hinge for pedestrian head impact, while still satisfying the other requirements, the following measures were developed, see Figure 14:

1. Increased material thickness to improve lateral hinge stiffness.
2. Turned edge on hood-side hinge part to increase buckling strength in low-speed insurance classification test (less hood rotation and translation).
3. Turned edge on body-side hinge part to increase buckling strength in insurance test (less hood rotation and translation).
4. End stop to prevent the hood being opened too wide.
5. Fold initiator for easy deformation in head impact loadcase.
6. Cranked beam integrated fender bracket rear to deform downwards in head impact loading.

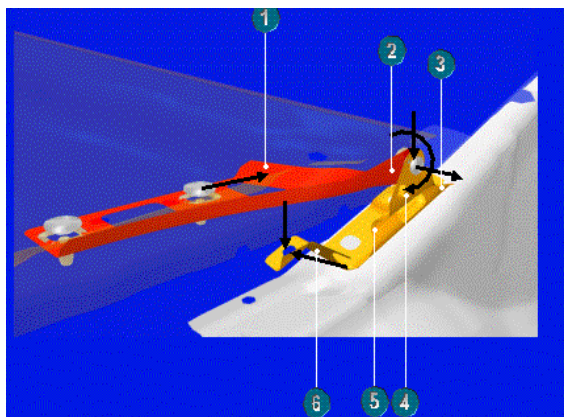


Figure 14. The ZAFIRA Hinge Optimized for Pedestrian Head Impact

6.5 Fender and Bumpstop Design

The fender and bumpstops are also usually difficult areas for pedestrian head protection, because of their high local stiffnesses. The ZAFIRA II has energy-absorbing brackets in this region which were optimized for head impact and other requirements.

The main design measures for the ZAFIRA II system are listed below and illustrated in Figure 15:

1. The fender brackets deform downwards, absorb energy and enable reduced head accelerations (see rear fender bracket in Figure 13 and front bracket in Figure 15).
2. The bumpstop brackets also deform to absorb impact energy and reduce head accelerations.
3. The fender (blended out of the picture) is made of thinner steel than in ZAFIRA I, to help reduce the stiffness in the region, but it remains sufficiently stiff to withstand normal service requirements.

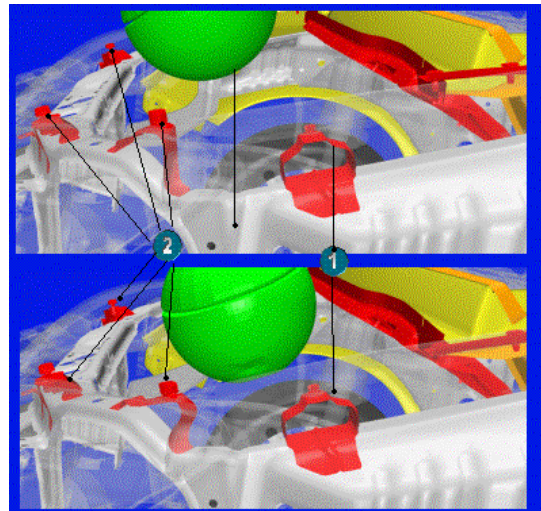


Figure 15. The ZAFIRA II Fender and Bumpstop Brackets

Impact on Insurance Classification/ Repair Costs

7.1 Overview of Insurance / Repair Costs

When developing pedestrian protection measures, other loadcases must always be considered, in particular the low-speed insurance classification test. The main reason for this is the inclusion of a deep, low density foam (30 g/l) positioned in front of the aluminium bumper crossmember, laterally across the vehicle, see Figure 16 :

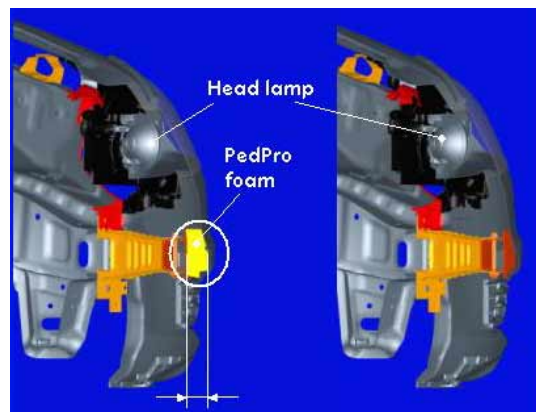


Figure 16. Vehicle front, with and without pedestrian leg impact protection: positioning of low-speed energy absorption system in relation to key components

For styling reasons, the vehicle cannot simply be elongated, by putting the pedestrian foam in front of the low-speed energy absorption system. Therefore, in the ZAFIRA II, the headlights, hood, etc have been moved forward to achieve a stylish and dynamic appearance. These components are much further forward than usual with respect to the low speed-energy absorption system and hence the risk of their being damaged is much higher.

Additionally, the pedestrian foam reduces the efficiency of the low speed energy absorption system, so that in the insurance test, the barrier intrusion is higher. Hence, without further measures, the vehicle damage and the repair costs would increase, which would worsen the insurance classification.

To compensate for the effects of pedestrian protection, several measures were implemented in the Opel ZAFIRA II, some of which are shown in Figure 17 and listed below:

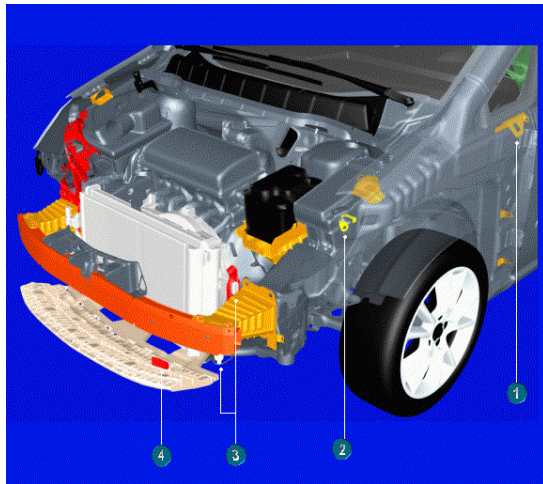


Figure 17. Front End Design to Compensate for Pedestrian Protection

1. Shear-stiff fender bracket to avoid the fender being pushed into the front door
2. Capture bracket to prevent the headlight being pushed outwards into the fender
3. Bolted upper and lower radiator brackets with load limiter
4. “Pushing bracket” for Lower Bumper Stiffener to improve radiator kinematics
5. Hood hinge measures (see section 6.4 and Figure 13) to decrease hood rotation and translation, hence avoiding paint damage to the fender on the non-impacted side

7.2 Benefits:

- Low front end damage
- Minimised effect of pedestrian protection on insurance classification
- Reduced risk of radiator leakage
- Reduced spare part and labour costs
- Simplified repair after crash
- Improved insurance classification

The performance of the ZAFIRA II in the front insurance test is illustrated in Figure 18:

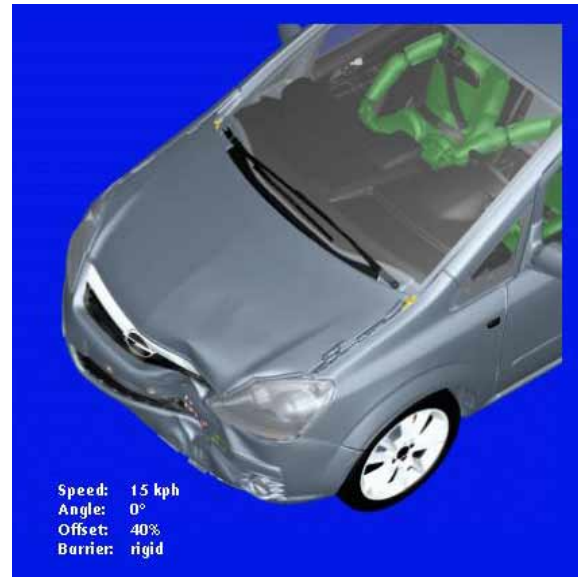


Figure 18. Insurance Test Front Impact Performance of the Opel ZAFIRA II

8. Influence on Hood and Fender Stiffness

8.1 Stiffness in Upper Fender Region

The soft fender attachments meant that the vehicle had to be further developed for additional loadcases, which conventional vehicles (without these advanced pedestrian protection measures) would automatically fulfill.

For example, during production assembly and later during servicing or repairs, a mechanic would probably lean on the fender when working on the engine compartment, see Figure 19. Additionally, anybody might lean against the fender or push the vehicle from the fender. Under these loadings, no unacceptable elastic or plastic deformations should occur.



Figure 19. The Opel ZAFIRA II Fender: expected loading under maintenance / repair work

Accordingly, the geometry and dimensions of the fender brackets were balanced and optimized between these loadcases and the pedestrian protection requirements.

It should be noted that this fender region could only satisfy $HIC < 2000$, not $HIC < 1000$.

Among other measures, this balance was achieved by making use of the material properties of mild steel: The low yield point of the mild steel fender brackets enables higher material thicknesses and therefore higher elastic stiffnesses for the linear elastic loadcases, while the brackets readily deform plastically under pedestrian head impact.

8.2 Hood Stiffness

The thin steel hood caused problems with the buckling and polishing strength of the hood outer panel. In particular, it was necessary to ensure that the front surface of the hood, where someone might press to close the hood, did not buckle under this type of loading.

To prevent such buckling and to support / stiffen this hood front area, the following measures were implemented, see Figure 20 and the list below:

1. Three tabs were formed on the hood inner panel and bonded to the hood outer
2. A small adhesive strip, applied by robot, was added to the undersurface of the hood outer panel.

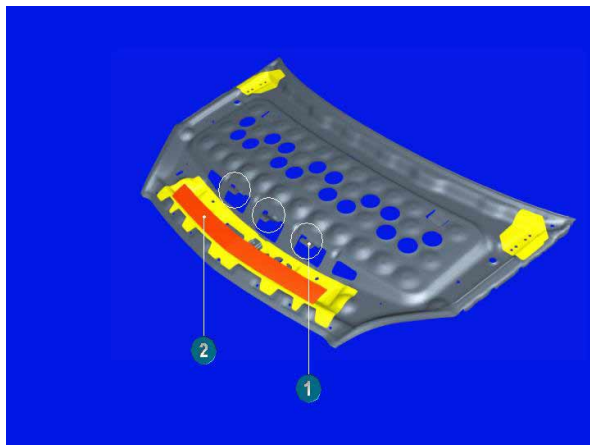


Figure 20. Thin steel hood of the Opel ZAFIRA II

With these measures, a balance was found to ensure good pedestrian protection performance and to allow weight reduction. The area-specific mass (the ratio of mass to area) of the hood was improved by 11% compared to the ZAFIRA I.

8.3 Hood Bumpstop Brackets

The bumpstop brackets were dimensioned to achieve the following requirements:

- Deformation under pedestrian head impact
- Compliance with fatigue and durability targets
- No plastic deformation with the hood slam test, see Figure 21:

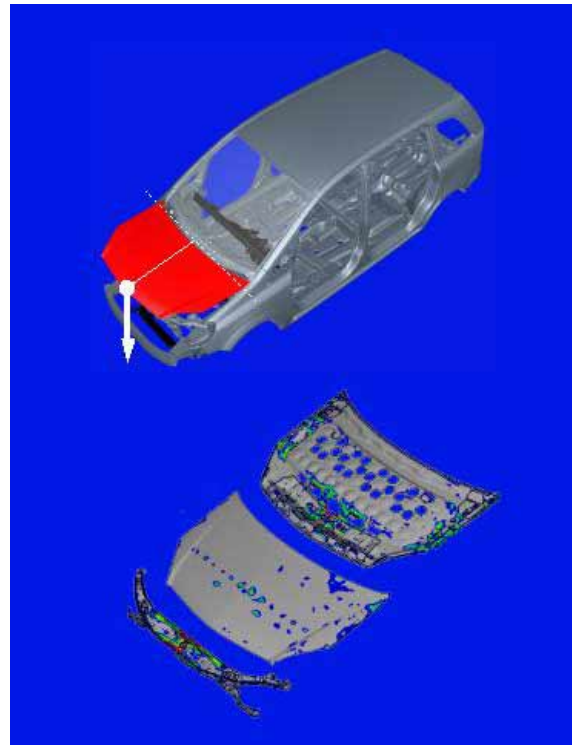


Figure 21. Hood Slam Test Performance

8.4 Hood Flutter

At high speeds, high aerodynamic loads are produced on the thin steel hood structure which may cause the hood trailing edge to flutter. To prevent this flutter, the entire rearmost “muffin tin” row of the hood inner panel was bonded to the outer panel.

9. CAE and Test Activities

Pedestrian protection measures for the new Opel ZAFIRA II were developed and optimized by means of detailed CAE modelling and then verified by an extensive test program at different stages.

9.1 CAE Challenges

Pedestrian CAE has particular difficulties compared to CAE for “standard crash”, i.e. impact with a barrier or another vehicle:

- Since the kinetic energy is only about 1% of that in a typical barrier impact, the degree of CAE accuracy and refinement required is even higher than that for standard crash.
- The accuracy required for head impact simulation is even higher for two reasons caused by the HIC definition: the acceleration

is raised to the power of 2.5 and the HIC time window is very sensitive to the curve form.

- Pedestrian injury is often heavily influenced by either very small components, e.g. screw heads, or components made from plastic or rubber, e.g. cowl, headlights, hoses. Such components, which do not play a significant role in standard crash, are therefore not normally present in their CAE models, or are not modelled in such detail.
- It is very difficult to obtain adequate material data for important non-metallic materials, particularly plastics, which are often anisotropic, heavily strain rate-dependent and susceptible to fracture.
- Material fracture of plastic components, e.g. cowl, headlights, may significantly affect local behaviour. However, such fracture is difficult to predict reliably and simulate, even when suitable material test data is available, since the material laws and algorithms in the commercial crash codes are not fully adequate for this.
- Pre-stressing of critical components, e.g. of the hood outer, may affect behaviour and this is also very difficult to simulate, particularly when performing a large number of simulations under time pressure, as is the case during vehicle development.
- The behaviour of some components, such as hood and fender, are particularly influenced by the forming process, which should be included within the CAE modelling.

9.2 Test Challenges

As with CAE, pedestrian impact brings additional problems compared to standard crash. Test variability (most importantly, the injury values), particularly for leg impact, is higher than for standard crash, since there are a large number of sensitive parameters – all interacting - which can significantly affect the behaviour:

- Variables within the impactor itself, such as the knee ligament and the foam “flesh” characteristics for the leg impactor and the rubber skin for the head impactors.
- Allowed tolerances within the test setup, for positioning, speed, angles etc.
- Thickness, geometry and material tolerances for prototype parts together with hand-built test bucks during the vehicle development further increase the variability, particularly since prototype materials can be very different to production ones.

9.3 CAE and Testing during Development

Pedestrian simulation requires a sophisticated integrated model, i.e. detailed modeling of both the pedestrian impactor and the vehicle, together with the complex vehicle / impactor interaction. Thus,

the FE model must contain both the pedestrian impactor and the relevant parts of the vehicle front.

The ZAFIRA II pedestrian protection CAE model consisted of the complete vehicle front, containing all components from bumper to A-pillars and windscreen, including the relevant engine bay components and structure.

Model details for pedestrian CAE:

- Approximately 450,000 elements for the vehicle front
- All components within the expected deformation zone were modelled accurately, meshed exactly on the CAD data, with full geometric, material and kinematic properties
- Key components were modelled in particular detail, with 2-5 mm element length and strain-rate dependent material properties, e.g. the complete hood, hinge, lock, bumpstops, upper fender, fender brackets, cowl, service panel, wiper system, headlights, lower bumper stiffener, bumper fascia, bumper foam.
- Data was obtained from dynamic material tests for important plastic components, such as the fascia, grill, lower bumper stiffener, headlights etc.

This vehicle pedestrian CAE model, with the most important components highlighted, is shown in Figure 22:

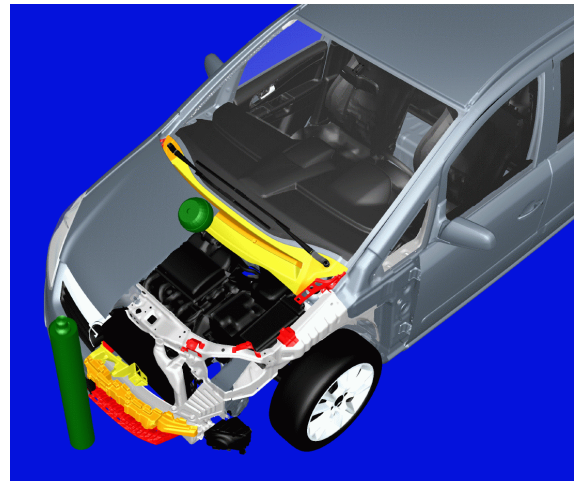


Figure 22. The ZAFIRA CAE Model for Pedestrian Simulation: section through center line. Key components are shown as red.

A large number of different impactor positions were simulated to predict injury values for the legal and EuroNCAP head and lower leg impacts, as well as to develop optimisation measures.

Figure 23 illustrates the number of impact positions for the different pedestrian loadcases:

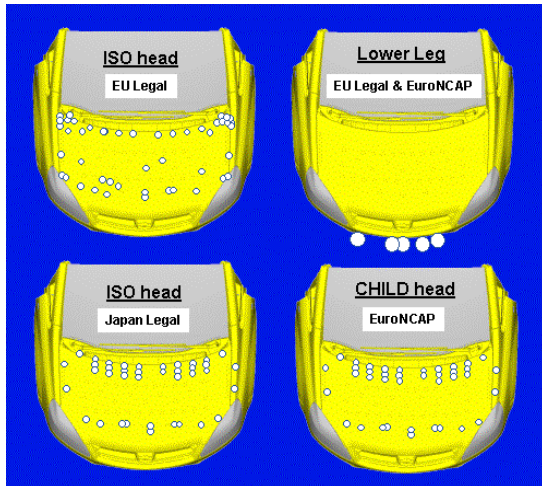


Figure 23. The ZAFIRA II Pedestrian Impact – Key Points (White) Investigated by CAE

The very large number of impact positions necessary to determine the legal and Euro NCAP status at each stage placed very heavy demands on CAE manpower and CPU, as well as on the team performing the hardware tests. The creation of CAD data for all the different impact areas also required considerable CAD experience and detailed understanding of the complex impact area definitions for the different requirements.

Pedestrian CAE validation is difficult and critical hardware tests must be repeated to obtain reliable results.

Therefore, extensive hardware concept confirmation at a number of stages is vital for pedestrian protection development. The critical impact positions for the ZAFIRA II were later validated by hardware tests at 3 stages:

1. Pre-concept studies
2. Architectural Mule Upgrade (to check basic concepts and architecture for pedestrian protection)
3. Integration Car (to confirm production-near concepts)
4. Validation Car (final confirmation before production car and also for Type Approval)

Opel has installed a sophisticated setup including the BIA pedestrian testing equipment, to perform all legal and NCAP pedestrian tests in-house at Ruesselsheim, Germany.

SUMMARY / LESSONS LEARNED DURING ZAFIRA II DEVELOPMENT

The ZAFIRA II has achieved pedestrian compliance in advance of future legislation, while achieving a dynamic vehicle styling. With this, its first vehicle to be compliant with pedestrian Phase 1, General Motors Europe has taken an important

step in pedestrian protection and gained considerable knowledge for future vehicle development:

- There are considerable difficulties in the integration of pedestrian protection into a vehicle without sacrificing other normal in-service requirements.
- Pedestrian protection has a significant effect on other loadcases e.g. low-speed insurance, fender stiffness, hinge stiffness, hood slam etc.
- Pedestrian development affects most areas of vehicle development. Hence, an experienced multi-disciplinary team, drawing from many departments, such as the ZAFIRA development team at Opel ITDC, is essential. Of particular importance is the close cooperation between simulation, test, design and styling. Pedestrian protection is very sensitive to styling and package changes.
- The CAE confidence level is insufficient to reliably predict results at all the necessary impact positions. However, CAE is an essential tool in developing pedestrian measures, enabling the development team to understand and analyse the vehicle structural behaviour in detail.
- CAE front-loading avoids late and costly design change.
- Non-metallic materials play a significant role in pedestrian impact behaviour and it is very difficult to obtain sufficient data for CAE, e.g. anisotropic, strain-rate dependent stress-strain curves for plastics, with fracture criteria.
- Significant pedestrian development without hardware is currently impossible. Due to test variability and CAE limitations, extensive hardware tests (requiring expensive prototype builds) are necessary for concept confirmation, or to indicate non-compliant areas well before starting the production tooling.
- There is often high test variability for pedestrian impact tests; hence tests at critical impact positions must be repeated at least once for reliable results.
- The selection of impact positions must be made separately for the different pedestrian impactors and speeds and must also be updated after each relevant styling or package change. The creation of CAD data for the different impact areas, especially for head impact, is very complicated, requiring detailed knowledge of the different impact area definitions and extensive checking.
- The large number of impact positions and the different pedestrian loadcases for the EU, Japan and Euro NCAP created a tremendous additional volume of work for the CAE and test engineers, which required very substantial

manpower, CPU and hardware resources to complete.

- With simulation front-loading, the ZAFIRA II has been successfully developed to comply with Japan and EU Phase 1 pedestrian requirements, in advance of legislation coming into effect.

REFERENCES

- [1] European Directive 2003/102/EC
- [2] Japanese Directive TRIAS63
- [3] EuroNCAP Protocol

DISCLAIMER

This presentation is solely provided for the purpose of scientific discussion of the main tasks and concepts in order to implement national and international legal requirements related to pedestrian protection efforts in automotive engineering. This presentation explicitly does not cover all and any engineering and design issues around Pedestrian Protection efforts; it is not to be construed to being an engineering manual, to provide any specific or ultimate solution nor to represent a certain engineering decision by Adam Opel AG., its subsidiaries and affiliates and / or any reasons for such decisions.

INTRODUCTION OF PEDESTRIAN HEAD PROTECTION PERFORMANCE TEST IN J-NCAP

Yuji Ono

National Agency for Automotive Safety and Victims' Aid

Yukikazu komiyama

Ministry of Land, Infrastructure and Transport

Kunio Yamazaki

Japan Automobile Research Institute

Japan

Paper Number 05-0307

Abstract

In Japan, pedestrian accidents account for about 30% of traffic accident mortality. Head injuries are 60% of the cause of death in pedestrian accidents. Therefore, the pedestrian head protection performance test using adult and child head impactors has been conducted in J-NCAP since 2003.

The testing method was created based on the Japanese laws and regulations and proposals made by IHRA pedestrian WG. However, taking into consideration the distribution of the head impact positions for vehicles in the accident data, the impact area was extended to the windshield section (windshield, A-pillar, roof front edge, etc.). In addition, in order to cover a larger number of accidents, the impact velocity of the head impactor was set at 35 km/h, approximately 10% higher than the legal requirement.

The evaluation method was created based on the Euro-NCAP method. In order to more minutely evaluate the vehicle safety performance, the number of areas was increased in comparison with that used in Euro-NCAP. Moreover, in order to clearly evaluate the difference in the vehicle safety performance, a sliding scale was adopted to convert the injury values ranging from HIC650 to HIC2000 to the score. A vehicle is evaluated according to a 5-stage evaluation system from the total score of all the areas. In the 5-stage evaluation system, each stage was determined based on the AIS4 injury probability.

In 2003, 19 vehicles were tested, and 4 vehicles were tested in the first half of 2004. The distribution of the evaluation results classified as levels 1 to 5 (the higher the level, the better the pedestrian protection performance) indicated that 7 vehicles were at level 3, 13 vehicles were at level 2, 1 vehicle was at level 1, and none for levels 4 and 5. In general, the HIC value was higher in the section close to the side of the vehicle and the window frame.

Analysis of Pedestrian Accidents

In order to understand the actual situation of pedestrian accidents in Japan, the accident data was analyzed.

Occurrence of Pedestrian Accidents

Figure 1 shows the distribution of the number of casualties and fatalities from automotive accidents that occurred during 2001 in Japan^[1].

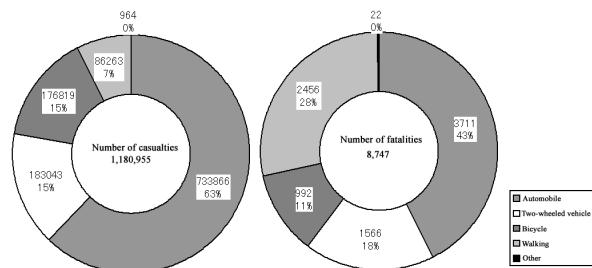


Figure 1 Number of casualties and fatalities from automotive accidents (ITARDA: 2001 Statistical Yearbook on Traffic Accidents)

Pedestrian accidents account for 7% of the total in terms of casualties, which are comparatively minor. However, in terms of fatalities, they occupy nearly 30% of the total or more than 2,400 persons only next to the fatalities while riding in vehicles.

Figure 2 shows the mortality (number of fatalities/number of casualties) by state.

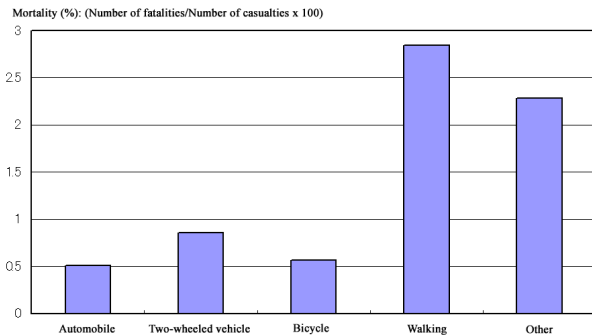


Figure 2 Mortality by state (ITARDA: The 2001 Statistical Yearbook on the Traffic Accidents)

The mortality of pedestrians is the highest at nearly 3%, or about 6 times as high as the counterpart for while riding in the vehicle.

Therefore, judging from the fatalities and the mortality, we can understand that we need protective measures for pedestrian accidents.

Table 1 indicates the distribution of the types of vehicles involved in the pedestrian accidents.

	Death		Serious injuries		Minor injuries		
	(persons)	(%)	(persons)	(%)	(persons)	(%)	
Large passenger vehicle	Bus	12	0.6	37	0.4	264	0.5
	Microbus	5	0.3	19	0.2	100	0.2
Ordinary passenger vehicle	1Box	116	6.2	561	5.6	3023	5.8
	Sedan	745	40.0	4576	45.6	24680	47.6
	RV	87	4.7	322	3.2	1567	3.0
Light vehicle	Sedan	125	6.7	920	9.2	4422	8.5
	Others	18	1.0	157	1.6	749	1.4
Trailer	17t<	7	0.4	16	0.2	37	0.1
	7t<×≤17t	0	0.0	3	0.0	3	0.0
	≤7t	0	0.0	3	0.0	6	0.0
Dump truck	8t≤	26	1.4	57	0.6	100	0.2
	<8t	17	0.9	49	0.5	118	0.2
Truck mixer	8t≤	5	0.3	9	0.1	17	0.0
	<8t	1	0.1	4	0.0	14	0.0
TanTruck	8t≤	2	0.1	7	0.1	11	0.0
	<8t	3	0.2	7	0.1	9	0.0
Truck	20t≤	30	1.6	43	0.4	85	0.2
	8t≤×<20t	46	2.5	80	0.8	152	0.3
	7t≤×<8t	74	4.0	134	1.3	446	0.9
	3.5t×<×<7t	68	3.7	264	2.6	1293	2.5
	2.8t×<×≤3.5t	46	2.5	147	1.5	628	1.2
	≤2.8t	68	3.7	267	2.7	1466	2.9
Light van	4t	23	1.2	239	2.4	1352	2.6
	Others	42	2.3	239	2.4	1352	2.6
Light truck	Light van	49	2.6	329	3.3	1538	3.0
	Others	181	9.7	780	7.8	3907	7.3
Motorcycle	Motor bicycle	23	1.2	587	5.8	4220	8.1
	Motorcycle	57	3.1	400	4.0	1506	2.9
Others		8	0.4	19	0.2	147	0.3
Total		1861	100.0	10036	100.0	51800	100.0

Table 1 Distribution of vehicle types involved in accidents

The state of the distribution shows that most accidents were caused by sedans of standard size accounting for 40% of the total vehicles. When vehicle types (in bold font) subject to the test method under the Japanese regulations are included, they account for 77%.

Analysis of Types of Injuries

Figure 3 shows the regions of injury by the level of pedestrian injuries cited from the general data held by ITARDA for 1993 to 2000^[2].

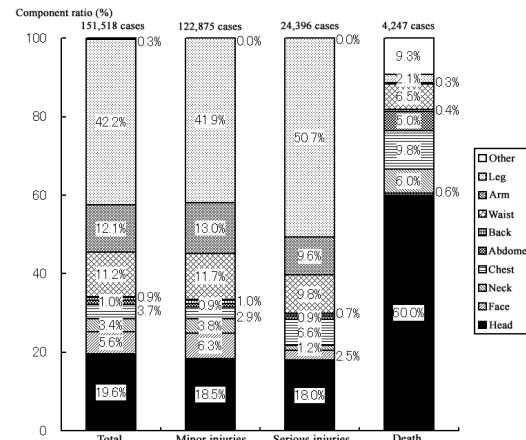


Figure 3 Pedestrian regions of injuries (ITARDA: The 2001 Statistical Yearbook on the Traffic Accidents)

Legs have the highest ratio for serious injuries, accounting for over 50% of the total regions of injuries. On the other hand, in the case of fatalities, the legs hold a small ratio while heads occupy 60%. Compared with the fatalities, serious injuries involve a greater number of cases. Therefore, to take measures for a number of serious injuries, it is necessary to reduce injury to the legs. Conversely, we find that a reduction of head injuries is necessary as the measures for reducing fatalities, which have fewer cases but of a more serious level of injuries.

Figure 4 shows the cumulative percentage of the vehicle impact velocity involving the pedestrians' death and serious injuries cited from the ITARDA data of accident cases for 1993 to 2001. The data covers only those subject vehicles, excluding large trucks, whose impact velocity at the accident could be estimated.

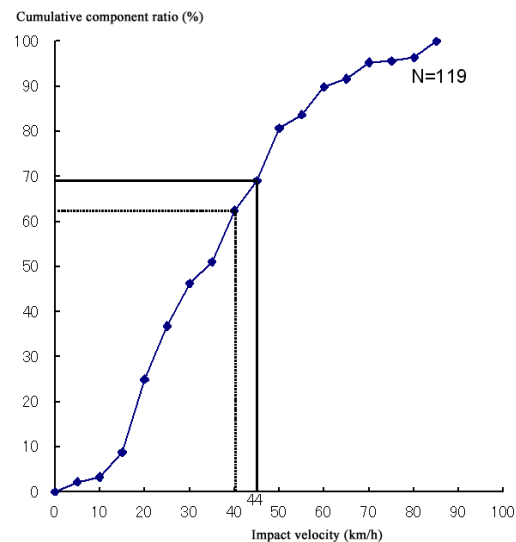


Figure 4 Cumulative percentage of vehicle impact velocity involving death and serious injuries of pedestrians

The Japanese legal test method sets the impact conditions by setting the vehicle impact velocity at 40 km/h. The figure shows that approximately more than 60% of the traffic accidents occurred at this velocity. If the impact velocity is raised by 10% to 44 km/h, the coverage ratio of the accidents rises to 70% approximately.

Analysis of Head Impact Position

Figure 5 shows the pedestrian head impact positions at different impact velocities of the vehicles causing the accidents. The velocity range was classified into 3 levels of under 30 km/h, 30 to 50 km/h, and over 50 km/h in consideration of the vehicle impact velocity (40 km/h) expected in the head impact test.

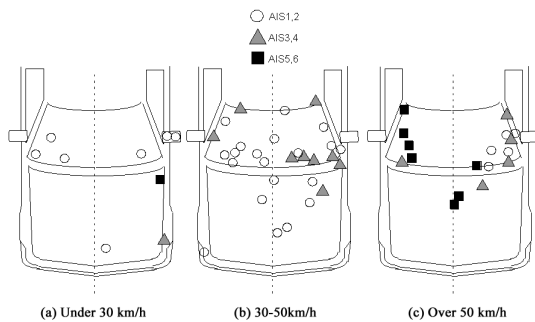


Figure 5 Head impact position for bonnet type vehicles

In the case of a vehicle impact velocity of under 30 km/h, minor injuries of AIS1 or 2 frequently occur except in the vicinity of the edge of the bonnet where injuries of AIS3 and over occur.

In the case of a vehicle impact velocity of 30 to 50 km/h, injuries of over AIS3 tend to occur at the edge of the bonnet, near the strut tower, and in the vicinity of the window frame and A-pillar.

In the case of the vehicle impact velocity of over 50 km/h, the percentage occupied by minor injuries of AIS1 or 2 drops and the higher level of injuries tend to occur near the center of the bonnet and at the windshield.

Setting of Test Method

The test method was set based on the actual condition of Japanese traffic accidents and the examination results of related matters domestic and overseas. As shown in Figure 3, Japanese data on the pedestrian accidents indicates the head as the top region of injuries causing the pedestrians' fatalities, while serious injuries mostly occurring to the leg region. On the other hand, regarding the discussion on the test method for the head, examinations have been almost completed with IHRA and the Japanese test method based on it. Regarding the leg region, however, discussion still goes on.

Under the circumstances, while the J-NCAP pedestrian

protection performance test is intended to reduce injuries of both the head and leg regions, it has been decided to conduct tests on the head for the time being since this region has acquired consensus domestically and overseas.

In the current test method, specifications for the impactors (165 mm in diameter and 3.5 kg in weight for a child and 165 mm and 4.5 kg for an adult), child and adult ranges of impact (WAD 1000 to 1700 mm for child, and WAD 1700 to 2100 mm for adult), setting procedures for impact area, etc. were determined based on the test method described in the Japanese regulations. The following modifications were made, however, to understand the vehicle safety performance more in detail and clarify the performance difference among the vehicles.

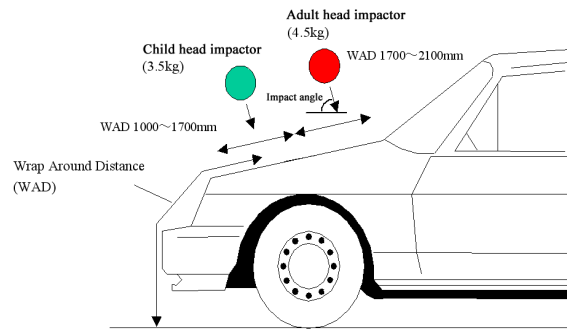


Figure 6 Test method under Japanese regulations

Impact Area

As it is thought effective to improve the head protection performance of the vehicle in these positions, J-NCAP specifies the impact range to be between WAD1000 to 2100 in principle and includes the windshield and window frame in the impact area, which was excluded by the Japanese legal test method. In addition, it made the following examinations of the impact area according to this precondition.

Examination of Rear Edge of Impact Area

The rear edge of the impact area shall be WAD 2100 mm.

The rear section was not included in the impact area because no injury cases were reported as caused by the roof although the accident data has some cases of injuries by the roof edge. Incidentally, Euro-NCAP^[4] and other test methods call for no roof test, and there exists no impact condition to which an international consensus has been obtained.

The boundary between the roof and windshield is defined as the line in the latitudinal direction of the vehicle consisting of the contact points between the line inclined at 75° rearward from the vertical line and the top of the window frame in the vertical section parallel to the longitudinal axis of the vehicle.

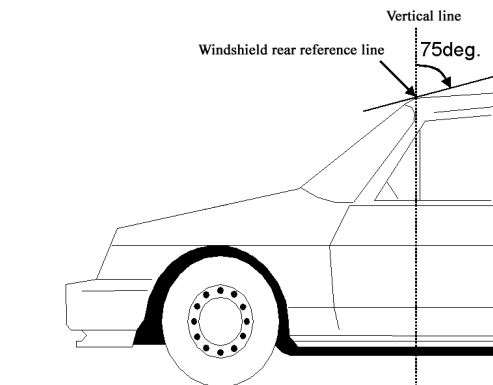


Figure 7 Boundary between roof and windshield

Examination in vertical direction

In a vehicle having an almost flat-formed front, WAD and the pedestrian height roughly coincide, but it is thought that pedestrians having a height of 2100 mm are rare. Moreover, if impacted by such a vehicle, it is hard to think that the head impact position shifts upward. Therefore, it was necessary to examine a limitation in the direction of height. Accordingly, it was decided to make the vehicle height of 1900 mm as the rear edge of the impact area as adopted by IHRA.

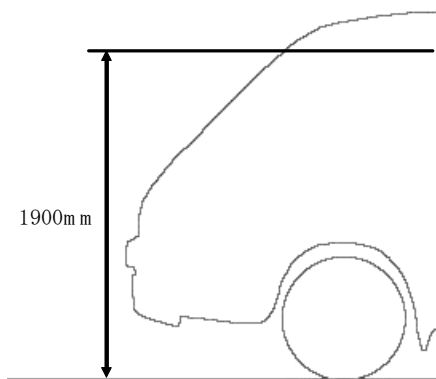


Figure 8 Limitation of height of impact area

Examination of Leading Edge of Impact Area

It is decided to make the front edge of the impact area to be WAD1000 mm. In addition, the same method will be used for setting the bonnet leading edge reference line as defined by the test method under the Japanese laws and regulations.

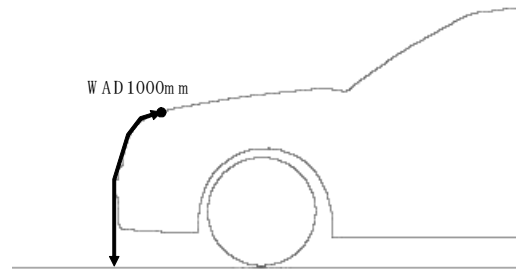


Figure 9 Leading Edge of Impact Area

Examination of Leading Edge of Impact Area

Regarding the evaluation of the sides around the bonnet, if impact is given to a sharply slanted section such as the fender, the impactor may show a sharp behaviour in the latitudinal direction that is impossible with a human body, possibly preventing proper evaluation. Moreover, it is likely that the impactor would be damaged after rebounding. In this respect, the longitudinal line (bonnet side reference line, Figure 10) along which the fender inclines inward at 45° is defined. The line entering inward from this line by half of the diameter of the impactor (82.5 mm) will be the side edge of the impact area (Figure 11). Regarding the surrounding of the windshield, the A-pillar is included in the impact range.

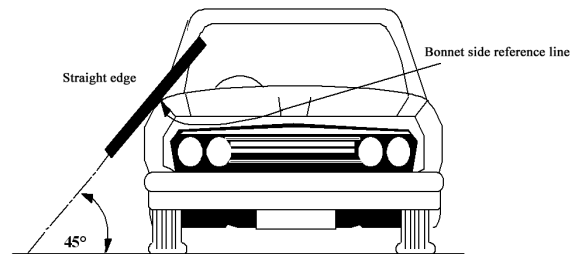


Figure 10 Bonnet side reference line

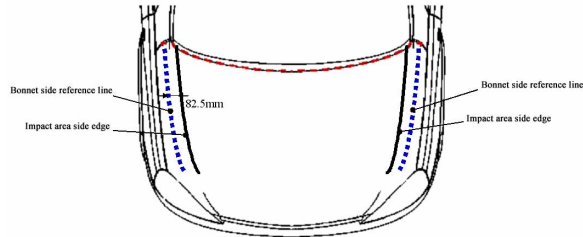


Figure 11 Bonnet impact area side edge

Impact Speed and Angle

Regarding the impact conditions, the vehicle impact velocity was set to 44 km/h, 10% higher than the Japanese legal test method requirement. This velocity setting raises the coverage ratio to approx. 70% (Figure 4) in the accidents causing fatalities and serious injuries of pedestrians.

Tables 2 and 3 outline the recommended impact conditions for adult and child impactors by IHRA. We have set the impact condition as follows based on this data:

Shape Corridor	Car impact speed 30km/h					
	Head impact velocity (km/h)			Head impact angle (deg.)		
	Bonnet	Windshield	BLE/Grid	Bonnet	Windshield	BLE/Grid
Sedan +	21.6 +/- 3.0	nc	nc	65.1 +/- 0.8	nc	nc
SUV	21.3 +/- 1.2	nc	21.3 +/- 6.0	55.6 +/- 5.5	nc	26.0 +/- 7.5
One box	20.1 +/- 0.6	nc	21.9 +/- 5.1	47.5 +/- 2.8	nc	20.3 +/- 8.0

Shape Corridor	Car impact speed 40km/h					
	Head impact velocity (km/h)			Head impact angle (deg.)		
	Bonnet	Windshield	BLE/Grid	Bonnet	Windshield	BLE/Grid
Sedan +	30.0 +/- 4.0	nc	nc	66.0 +/- 6.3	nc	nc
SUV	27.2 +/- 1.6	nc	32.0 +/- 3.6	59.2 +/- 2.6	nc	22.5 +/- 4.2
One box	27.6 +/- 0.8	nc	33.2 +/- 3.2	49.8 +/- 1.8	nc	17.4 +/- 6.1

Shape Corridor	Car impact speed 50km/h					
	Head impact velocity (km/h)			Head impact angle (deg.)		
	Bonnet	Windshield	BLE/Grid	Bonnet	Windshield	BLE/Grid
Sedan +	38.5 +/- 5.0	nc	nc	65.2 +/- 6.5	nc	nc
SUV	34.0 +/- 1.5	nc	44.5 +/- 1.0	61.9 +/- 3.8	nc	18.1 +/- 3.8
One box	36.0 +/- 0.5	nc	46.5 +/- 2.0	47.4 +/- 2.1	nc	14.8 +/- 3.6

nc: No contact, ^{CH} Child headform impact test conditions, ^{HL} Linear interpretation to be used to determine impact conditions for in-between speeds if required.

Table 2 Impact conditions for child impactor

Shape Corridor	Car impact speed 30km/h					
	Head impact velocity (km/h)			Head impact angle (deg.)		
	Bonnet	Windshield	BLE/Grid	Bonnet	Windshield	BLE/Grid
Sedan +	23.7 +/- 6.0	27.3 +/- 5.4	nc	73.3 +/- 5.6	48.8 +/- 9.9	nc
SUV	26.4 +/- 3.6	nc	nc	73.8 +/- 21.5	nc	nc
One box	nc	20.4 +/- 3.6	nc	nc	55.1 +/- 10.4	nc

Shape Corridor	Car impact speed 40km/h					
	Head impact velocity (km/h)			Head impact angle (deg.)		
	Bonnet	Windshield	BLE/Grid	Bonnet	Windshield	BLE/Grid
Sedan +	30.4 +/- 7.2	35.2 +/- 6.8	nc	66.0 +/- 14.0	38.4 +/- 10.9	nc
SUV	30.8 +/- 8.8	nc	nc	76.7 +/- 22.2	nc	nc
One box	nc	29.6 +/- 3.2	nc	nc	47.3 +/- 9.6	nc

Shape Corridor	Car impact speed 50km/h					
	Head impact velocity (km/h)			Head impact angle (deg.)		
	Bonnet	Windshield	BLE/Grid	Bonnet	Windshield	BLE/Grid
Sedan +	37.5 +/- 9.5	46.5 +/- 11.0	nc	56.8 +/- 11.5	33.5 +/- 11.3	nc
SUV	39.5 +/- 11.0	nc	nc	73.5 +/- 25.2	nc	nc
One box	nc	43.0 +/- 6.0	nc	nc	38.4 +/- 12.3	nc

nc: No contact, ^{AA} Adult headform impact test conditions, ^{HL} Linear interpretation to be used to determine impact conditions for in-between speeds if required.

Table 3 Impact conditions for adult impactor

Test Conditions for Bonnet

Observation of the head impact velocity data at the vehicle impact velocities of 40 km/h and 50 km/h in Tables 2 and 3 indicates a tendency where the head impact velocities tend to be 80% or slightly less of the

vehicle impact velocity. Therefore, if the vehicle impact velocity is set at 44 km/h, the desirable head impact velocity would be 35 km/h being approximately 80% of the vehicle impact velocity.

Moreover, when the head impact angles are observed at vehicle impact velocities of 40 km/h and 50 km/h, no major difference is observed except with the adults for sedans. Even in the case of the adults for sedans, the impact angle is presumed to be between 62 and 63°. Consequently, the head impact angle should desirably be tested under the same impact conditions as the legal Japanese test method.

Test Conditions for Windshield And Wind Frame

IHRA defines no boundary between the bonnet and windshield. In the case where the head of a pedestrian comes into contact with the vicinity of the lower edge of the windshield, the impact may be similar to contact with the bonnet. Therefore, the impact conditions for the bonnet will be applied to the impact that is made to the lower edge of the windshield.

Regarding the area from the center of the windshield to the upper edge, impact conditions will be set based on the recommended impact conditions for the adult. The estimated head impact velocity at the vehicle collision speed of 44 km/h will be 34 to 40 km/h according to the data for the head impact velocity to the windshield of the vehicle having impact velocities of 40 km/h to 50 km/h in Table 3. This head impact velocity tends to be slightly higher than the impact velocity to the bonnet. However, considering that the velocity range is great as a whole under the recommended impact conditions of IHRA, and that it is difficult to take measures for the sides of the vehicle with the window frames, a desirable impact velocity would be 35 km/h the same as for the bonnet.

The impact angle will be the rounded off value of the angle specified in the impact conditions recommended by IHRA. The same angle of 40° as sedans will be specified for SUVs since no data is available for the latter.

With some of small vehicles, the windshield and window frame may be the range in which a child impactor is used. Under the current state, no data is available for IHRA-recommended impact conditions for the vicinity of the windshield for a child as in Table 2. However, a child which collides with the windshield or window frame may be considered to have a height comparatively close to that of an adult. In this respect, the test will be conducted using the adult impact conditions for the time being.

The above statements are summarized into the test conditions as outlined in Table 4.

		Evaluation area using head impactor for child		Evaluation area using head impactor for adult	
Impactor		165mm/3.5kg		165mm/4.5kg	
WAD		1000-1350mm		1700-2100mm	
Impact velocity (km/h)	Bonnet	Sedan	35		
		SUV			
		1BOX			
	Windshield	Sedan			
		SUV			
		1BOX			
Impact angle (deg.)	Bonnet	Sedan	65	65	
		SUV	60	90	
		1BOX	25	80	
	Windshield	Sedan	40		
		SUV	40		
		1BOX	45		
Classification	Definition				
Sedan	Vehicles with bonnet leading edge height of under 635 mm				
SUV	Vehicles with bonnet leading edge height of over 635 mm				
1BOX	Vehicles having a bonnet angle of over 30 deg.				

Table 4 Impact conditions

Evaluation Method

On making evaluation, it has been decided to calculate the total scores by dividing the impact area for multiple tests to more closely understand the pedestrian protection performance of the vehicles. At the same time, to clarify the relationship between the scores and the injury probability, injury values obtained from the tests (HIC) are converted into scores representing the safety performance by using the evaluation functions associated with the injury probability.

Division of Impact Area

Euro-NCAP^[5] divided the impact area and evaluated each divided areas. Scores for those divided area are aggregated and evaluated as a vehicle. The aim is to find the distribution of pedestrian protection performance of a vehicle by incorporating the concept of area, without having the pedestrian protection performance of the vehicle represented by a single point.

The more divided the area, the more accurately understood the distribution of the pedestrian protection performance of the vehicle. Excessive division, however, may lead to a sharp and impractical increase of test frequency, requiring longer time and more expense in evaluation. Therefore, it is required to develop a division method that enables an efficient testing operation while closely understanding the pedestrian safety performance of the vehicles. From this respect, J-NCAP has decided to divide the impact area using the following method:

Longitudinal Direction

Regarding the longitudinal direction, the longitudinal ratio of WAD will be approximately 2:1 in the evaluation areas using a child impactor and an adult impactor. Accordingly, the evaluation area using the child impactor has been divided into two portions.

In other words, three areas are set up with an evaluation area using an adult compactor (Area I), a rear part of an evaluation area using a child impactor divided into two parts (Area II), and the forward part (Area III).

Latitudinal Direction

The impact areas of Area I and Area II are each divided into 6 portions in the latitudinal direction of the vehicle. As to Area III, the latitudinal division is made into 3 portions because of fewer impact positions of high injury value due to the structures inside the engine compartment, and the forward section of the bonnet having the possibility of occupying a smaller area than the rear section due to the position of the bonnet leading edge.

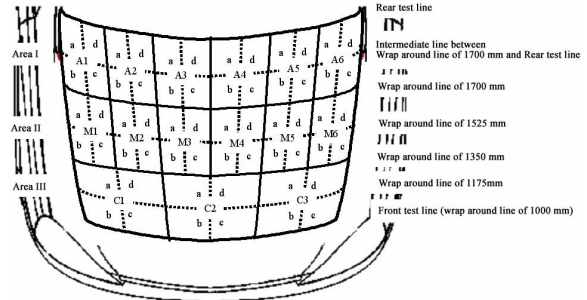


Figure 12 Area division method by J-NCAP

Subdivision of Divided Areas

The divided areas are subdivided according to the following procedure for use for evaluation:

- Regarding the area totally divided into 15, the secretariat selects one place where the HIC value is seemingly the highest. An impact is applied to this position and the subsequent injury value is used as the representative value with which to evaluate the area.
- As may be desired by a manufacturer, each divided area may be further divided into 4 areas, and the test can be conducted with the impact positions other than the subdivided areas that fall under the positions already tested. At this time, the manufacturer selects 1 to 3 areas for subdivision out of the remaining areas for subdivision. The secretariat selects an impact position seemingly having the highest injury value out of the areas for subdivision as selected by the manufacturer.
- Scores of the divided areas are evaluated using the weighted average of the scores from 2 areas. The weight varies according to the number of areas for subdivision specified by the manufacturer as the area desired for the test.

1) In the case where the manufacturer selects all of the remaining 3 areas for subdivision

$$\text{Score of divided area} = (1/4) \times (\text{score of main test}) + (3/4) \times (\text{score of requested test})$$

2) In the case where the manufacturer selects 2 areas out of the remaining 3 areas for subdivision

$$\text{Score of divided area} = (2/4) \times (\text{score of main test}) + (2/4) \times (\text{score of requested test})$$

3) In the case where the manufacturer selects 1 area out of the remaining 3 areas for subdivision

$$\text{Score of divided area} = (3/4) \times (\text{score of main test}) +$$

(1/4) + (score of requested test)

Evaluation Function

To make the conversion from test injury value (HIC) to a score, an evaluation function is used. For the evaluation function, a sliding scale will be used after making linear approximation based on the risk curve (relations between the injury value and the injury probability). Regarding the scope of evaluation, a wide range of evaluation will be specified to prompt improvement of the pedestrian protection measures on the part of the manufacturer.

At J-NCAP, the evaluation function is also used to convert the injury value to a score in the general evaluation of impact safety related to the passenger protection. In the case of passenger protection, the head injury value does not necessarily rise remarkably thanks to the airbag, seat belt and other safety devices, hence the upper limit is set at HIC1000. On the other hand, in the case of the protection of pedestrians, it is difficult to reduce the injury value compared with the passengers under the present level of technologies due to the absence of having an airbag and other safety devices. Therefore, a wide evaluation range has to be set.

As a result, based on the pedestrian protection performance of the present vehicles, it is decided to use for evaluation a sliding scale between injury probability of 5% (HIC650) and 90% (HIC2000) from the risk curve^[6] of the injury value (HIC) to conduct evaluation in a wider range (Figure 13). The evaluation range will be reviewed at a stage when the manufacturers have improved their measures for pedestrian protection.

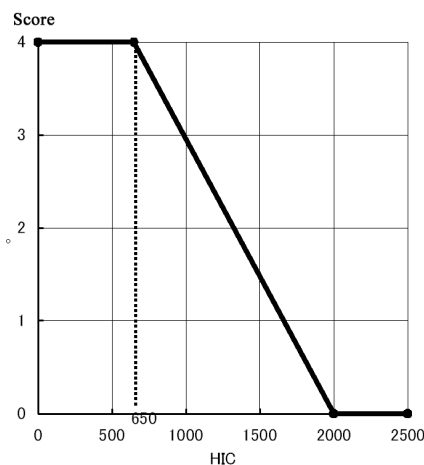


Figure 13 Sliding Scale

Evaluation of Windshield and Window Frame

When testing the windshield and window frame portions, the windshield needs to be replaced each time.

Considering the time needed for fitting the windshield, the testing period is prolonged to a large extent. The injury value of the windshield is expected to be sufficiently lower unless interfering with the window frame and/or instrument panel. On the other hand, the injury value of the window frame is expected to exceed the upper limit (HIC2000) in most cases. Therefore, unnecessary tests are omitted for the evaluation of the windshield and window frame according to the following examination results.

Examination of Influence of Window Frame

Using three types of vehicles (Sedan A, Sedan B and Light vehicle), relationship between the distance from the window frame (A-pillar, roof and instrument panel upper end) and HIC on four types of windshields (one type being of thin glass) is examined (Figure 14-16). As a result, it was found that, except for the instrument panel upper end where contact occurs, the HIC becomes under 650 given a distance of more than the radius of the impactor from the window frame. Accordingly, regarding the side and upper portions of the windshield, a full mark (automatic rating) is given without conducting a test at the positions away from the A-pillar and the roof by 82.5 mm or more.

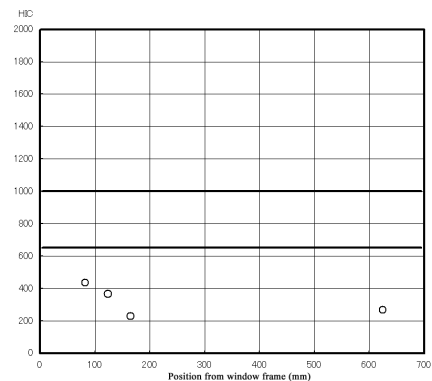


Figure 14 Distance from the window frame and HIC (Sedan A, A-pillar and adult impactor)

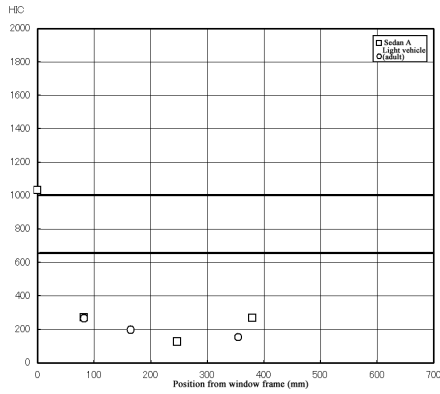


Figure 15 Distance from the window frame and HIC (Roof, adult impactor)

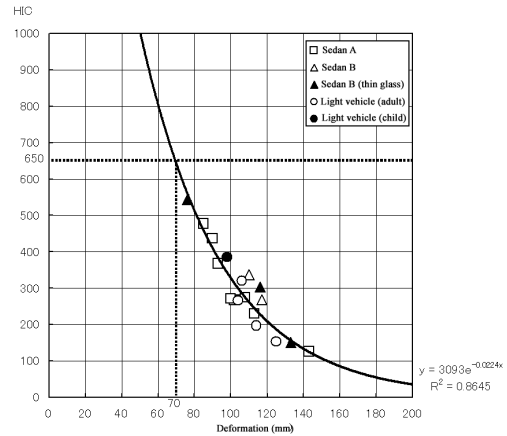


Figure 17 Dynamic deformation of impactor and HIC

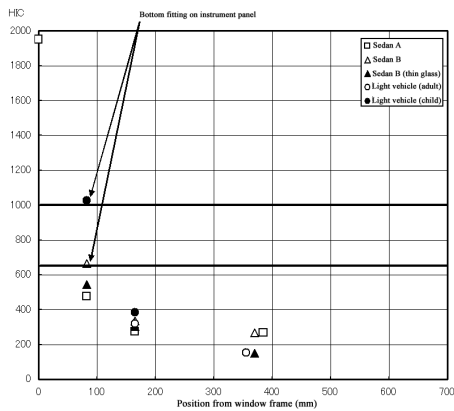


Figure 16 Distance from the window frame and HIC (Instrument panel upper end)

When the above is summarized, the automatic rating area will be as shown in Figure. 18.

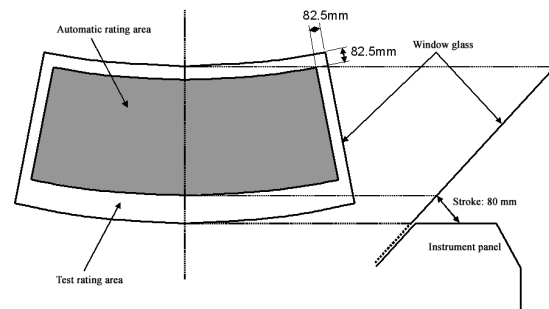


Figure 18 Automatic rating area

Examination of Influence of Contact with Instrument Panel

From the test result of the examination of the influence of the window frame, the relation between the dynamic deformation amount of the impactor and HIC was examined (Figure 17). As a result, regarding the lower portion of the windshield, it is estimated that the HIC will be less than 650 given a stroke of over 70 mm from the windshield to the instrument panel upper end. Accordingly, regarding the lower side of the windshield, taking into consideration the standard data deviation of 6.3 mm, full marks are given without conducting a test at the positions where the distance from the windshield and the instrument panel is more than 80 mm.

In addition, if evaluation is made on the windshield and window frame by 15-divided areas, the influence from the A-pillar becomes greater, tending to rate the safety performance of vehicles lower than it actually is. In this respect, it has been decided to evaluate the area near the connecting section of the windshield and window frame with the area ratio.

Ranking

The general average score is calculated on the divided areas for ranking. Calculation steps are as follows (Figure 19).

- (a) The HIC value of respective impact positions is converted to the score using the sliding scale.
- (b) The score for the impact position is weighted for each divided area to obtain the score for the divided areas.
- (c) The average score is obtained for the divided areas in Areas I, II and III to obtain the area scores.
- (d) The average score is obtained for Area I to III to calculate the general average score.

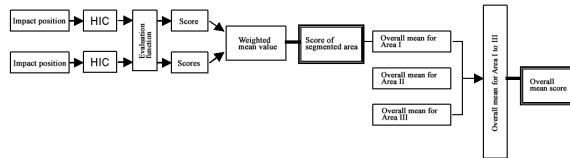


Figure 19 Calculation steps of overall average score

To give ranking, overall average scores are converted to HIC using the sliding scale. Vehicles are classified into 5 levels according to their safety performance. The method of classification is set to rank each vehicle at a different level as the injury probability drops by about 10% from the standard level of HIC1436 where the head injury probability is approximately 50% (Figure 20).

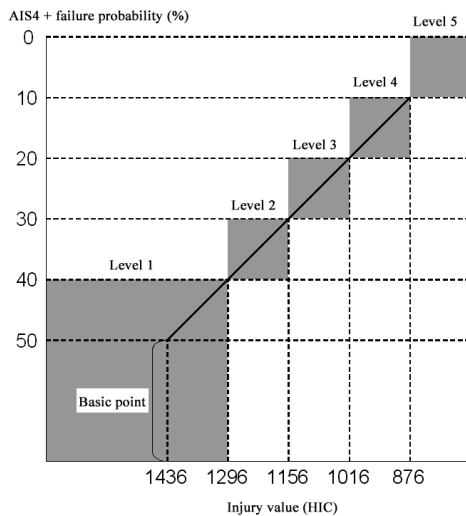


Figure 20 Ranking

Test Results

Figure 21 shows the state of the pedestrian head protection performance test by J-NCAP. In 2003, a total of 19 vehicles were tested including 9 units of passenger vehicles, 4 1Box/Mini Van vehicles, 4 light vehicles and 2 commercial vehicles (vehicle types were by the J-NCAP classification different from the vehicle classification for the pedestrian protection performance test). In addition, a test was conducted with 4 vehicles including 2 passenger vehicles and 2 1Box/Mini van vehicles in the first half of 2004. The evaluation results were distributed with 7 vehicles to Level 3, 13 vehicles to Level 2 and 3 vehicles to Level 1 and none for Levels 4 and 5 (Figure 22).

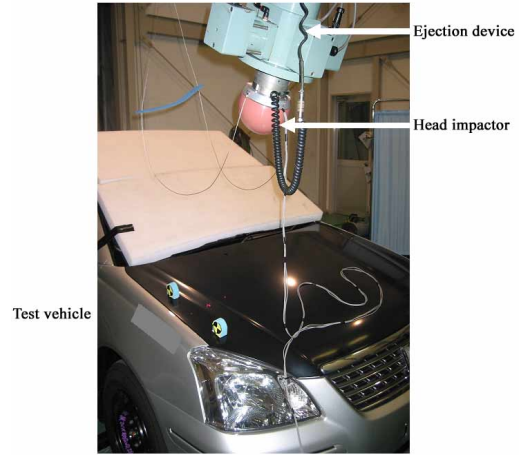


Figure 21 Testing state

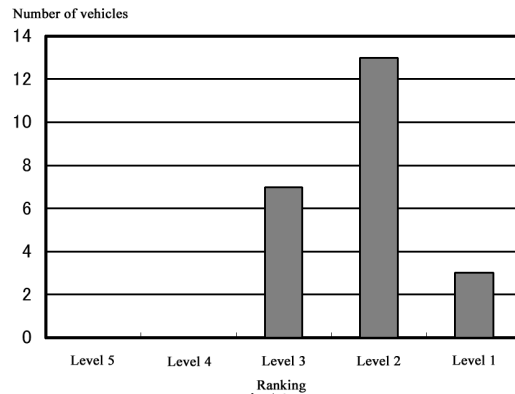


Figure 22 Distribution of vehicle levels (fiscal 2003 and first half of 2004, J-NCAP pedestrian protection performance test)

Figure 23 shows the state of distribution of injury values in the tests conducted during 2003 and the first half of 2004. A total of 283 impact positions were involved, of which the injury value reads HIC650 or under at 56 positions and HIC2000 or over at 26 positions. The reading of the remaining 201 positions was between the upper and lower limits of HIC values. The mean HIC value was 1204.1.

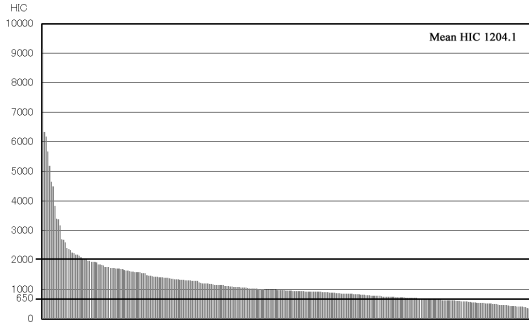


Figure 23 Distribution of HIC (2003 and first half of 2004, J-NCAP pedestrian protection performance test)

Figure 24 shows the impact positions where the HIC reading exceeded 2000 in the tests conducted during 2003 and 2004. It shows that the impact positions are mostly on the fender, lower end of the window glass, and the rear end of the bonnet. The A-pillar may be considered as another impact position where the HIC rises. It is evaluated as (zero (0) score) without a test unless specifically desired, hence no indication on the graph.

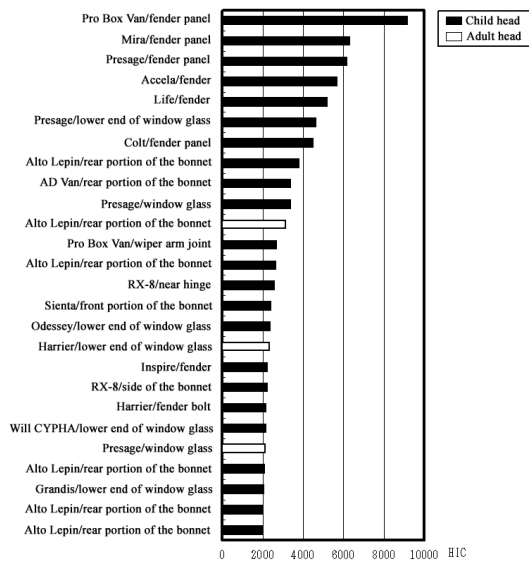


Figure 24 Impact positions where HIC reading exceeded 2000 (2003 and first half of 2004, J-NCAP pedestrian protection performance test)

Conclusions

In Japan, pedestrian accidents account for 30 percent of traffic accident fatalities and head injuries account for 60 percent of the injury regions in pedestrian fatalities. In view of these facts, J-NCAP has introduced a pedestrian head protection performance test. The test method has been set up based on the test method under the Japanese laws and regulations and the IHRA test method. In consideration of the distribution of head impact positions in actual accidents,

subject area for evaluations has been extended to include the windshield, simultaneously setting the impact velocity 10 percent higher to understand differences in the safety performance among the vehicles.

Regarding the evaluation method, the Euro-NCAP evaluation method was used to grasp the pedestrian protection performance of the vehicles in detail. Accordingly, the impact area is divided and the total score is calculated based on the scores from multiple tests. Moreover, to clearly evaluate the safety performance of the vehicles, a sliding scale is adopted to convert HIC650 to HIC2000 into the scores. The ranking of vehicles is given by a 5-level evaluation system based on the head injury probability. During 2003, 19 vehicles were tested followed by 4 vehicles during the first half of 2004. Evaluation results were distributed with 7 vehicles to Level 3, 13 vehicles to Level 2 and 3 vehicles to Level 1 and none to Levels 4 and 5. In general, higher HIC values were observed in the portions close to the side and the window frame of the vehicles.

References

- [1] "A year book of accident statistics of Japan 2001", ITARDA
- [2] "Traffic Accident Investigation Report 2001", ITARDA
- [3] "IHRA/PS/200", IHRA
- [4] "European New Car Assessment Programme – Pedestrian Testing Protocol Version 4.0", January 2003.
- [5] "European New Car Assessment Programme – Assessment Protocol and Biomechanical Limits Version 4.0", January 2003.
- [6] Mertz et al., "Injury Risk Curves for Children and Adults in Frontal and Rear Collisions", SAE Paper No. 983318.

A Survey on the Biofidelity of the Knee Bending Angle of the TRL Lower Leg Impactor

Tsuyoshi Yasuki
Toyota Motor Corporation
Japan
Paper Number 05-0101

ABSTRACT

This paper describes the biofidelity of the TRL lower leg impactor (here after referred to as “The Impactor”). The knee-bending angle biofidelity of The Impactor is compared with the THUMS (Total Human Model for Safety) FEM human body model. Detailed sedan and SUV FEM models were generated and were correlated with test results. FEM results show The Impactor’s knee-bending angles correlate well with test results.

When the tibia deflection of The Impactor is small, The Impactor has a larger knee-bending angle than the THUMS model in a finite element (FE) analysis of the pedestrian impacted by a sedan. When the tibia deflection of the THUMS is small, The Impactor has a similar knee-bending angle to the THUMS model in FE analysis of a pedestrian impacted by an SUV.

Movement of The Impactor coincides with the THUMS model in an FE analysis of the pedestrian impacted by a sedan until the medial collateral ligaments ruptured. Movement of The Impactor does not coincide with the THUMS model in FE analysis of a pedestrian impacted by an SUV with a bumper height 520 mm. If the bumper height of the SUV is less than 420 mm, movement of The Impactor is similar to that in the THUMS model.

Biofidelity of the knee-bending angle of The Impactor is not sufficient if compared with the THUMS model. Deflection of the tibia should be taken into account to improve biofidelity of The Impactor’s knee-bending angle.

INTRODUCTION

Rupture of pedestrian knee ligaments are sometimes observed in car to pedestrian accidents. The Impactor is one tool to evaluate the rupture of these knee ligaments. The Impactor measures the knee-bending angle in order to estimate the rupture of knee ligaments. Biofidelity of the knee-bending angle is crucial in order for The Impactor to precisely evaluate the possibility of knee ligament rupture. A comparison of the knee-bending angle of The Impactor with the knee-bending angle of a human would be effective in realizing the difference in behavior

between The Impactor and a human leg. An FE model of the lower leg impactor and an FE human body model can be utilized to compare these knee-bending angles.

FE MODELS

Four FE models were generated to evaluate the knee-bending angle of a pedestrian as follows:

Case 1: Sedan and The Impactor (Figure 1),

Case 2: Sedan and THUMS (Figure 2),

Case 3: SUV and The Impactor (Figure 3),

Case 4: SUV and THUMS (Figure 4).

The author developed The Impactor FE model. The human FE model is the Total Human Model for Safety developed by the Toyota Central Research and Development Laboratory and Toyota Motor Corporation (Figure 5). THUMS is the same size as an AM50 percentile size.

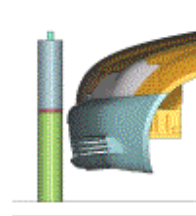


Figure 1. Sedan and The Impactor

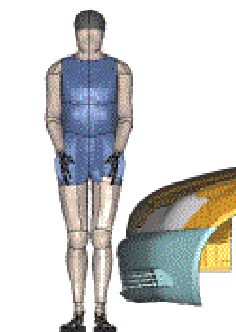


Figure 2. Sedan and THUMS

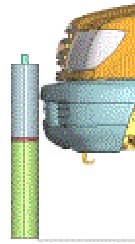


Figure 3. SUV and The Impactor

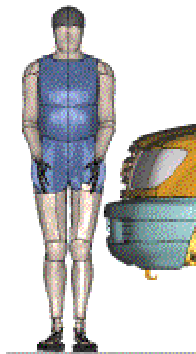


Figure 4. SUV and THUMS

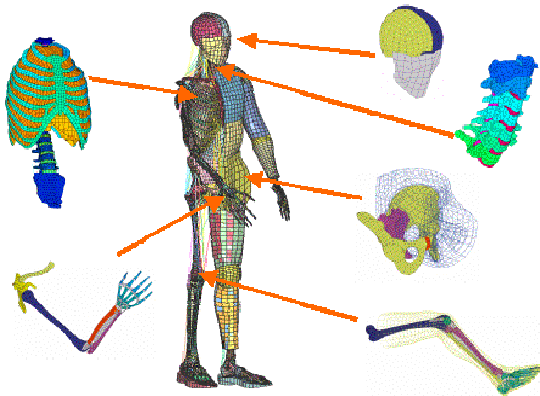


Figure 5. THUMS

MODEL VALIDATION

The THUMS pedestrian model was validated with test results with post mortem human subjects^(1,2).

Two tests were conducted in order to evaluate the accuracy of the knee-bending angle of case 1 and 3. The test conditions are similar to the EuroNCAP procedure⁽³⁾. Both validations show good correlations of acceleration and knee-bending angle with the tests (Figure 6,7,8,9).

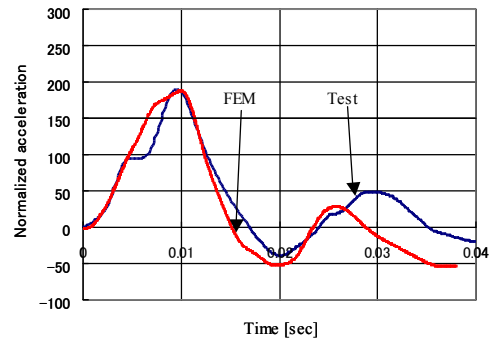


Figure 6. Comparison of acceleration in case 1

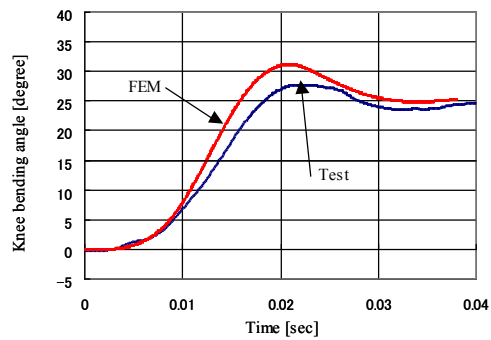


Figure 7. Comparison of knee-bending angle in case 1

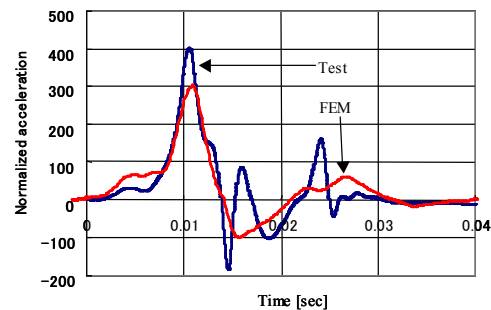


Figure 8. Comparison of acceleration in case 3

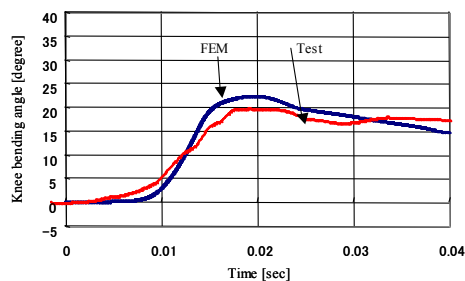


Figure 9. Comparison of knee-bending angle in case 3

KNEE-BENDING ANGLE

Knee-bending angles calculated for case 1 and case 2 are shown in Figure 10. The knee-bending angle of The Impactor coincides with THUMS from 0 sec to 0.01 sec. The knee-bending angle of The Impactor is greater than THUMS from 0.01 sec to 0.033 sec.

The MCL of THUMS model was ruptured at 0.028 sec, while the maximum knee-bending angle of The Impactor occurs at 0.20 sec.

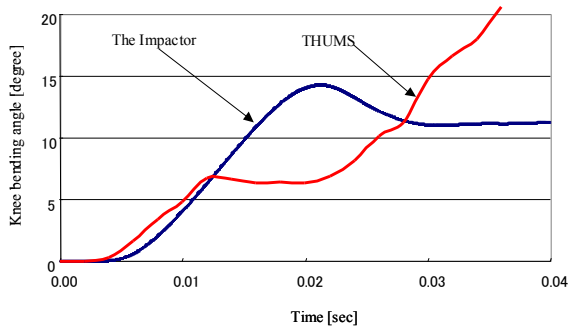


Figure 10. Knee-bending angles of THUMS model and The Impactor.

The knee-bending angle calculated for case 3 and case 4 are shown in Figure 11. The knee-bending angle of The Impactor coincides with THUMS from 0 sec to 0.02 sec.

The MCL of the THUMS model was ruptured at 0.012 sec, while the knee-bending angle of The Impactor increased to 15 degrees at 0.013 sec.

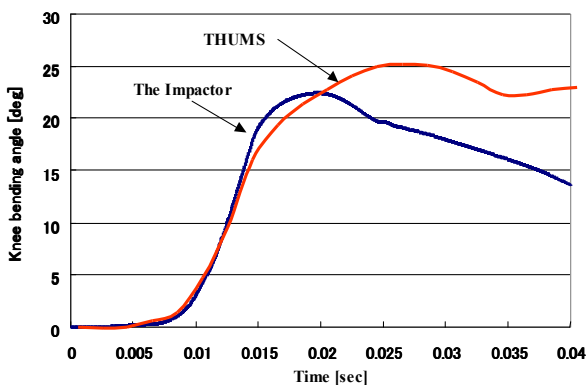


Figure 11. Knee-bending angle in cases 3 and 4

DISCUSSION

SEDAN VS. THUMS AND IMPACTOR

THUMS and The Impactor movements observed relative to fixed coordinates on the vehicle in cases 1 and 2 are shown in Figure 12.

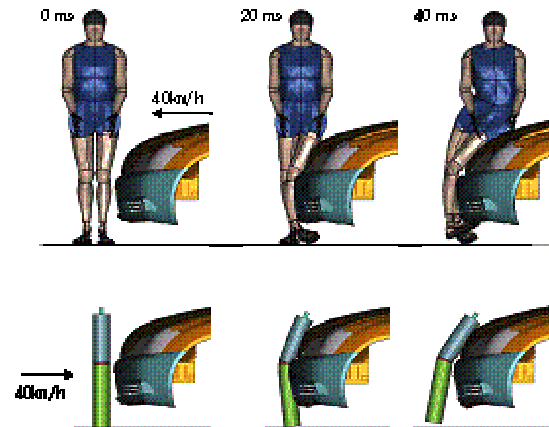


Figure 12. Movements of THUMS and The Impactor vs. Sedan

Movements of The Impactor are similar to THUMS at 0.02 sec, but the bumper fascia bends the tibia of THUMS. The tibia of The Impactor is already rebounding from the bumper fascia while THUMS is still contacting the bumper fascia at 0.04 sec.

The tibia bending-angle and knee-bending angle of THUMS are shown in Figures 13 and 14. The knee-bending angle difference between THUMS and The Impactor increases as the THUMBS tibia bending-angle increases. These Figures indicate the tibia-bending deflection should be engaged in evaluating the knee-bending angle of the pedestrian.

The main reasons that The Impactor has a smaller tibia-bending angle than THUMS are as follows:

- THUMS has a fibula and a tibia, which are the same as a human leg, while The Impactor has one bone structure representing both the fibula and the tibia (Figure 15).
- The THUMS tibia has similar bending stiffness to that of post mortem human subject tests, while The Impactor has a much stiffer bending stiffness than post mortem human subject tests (Figure 16).

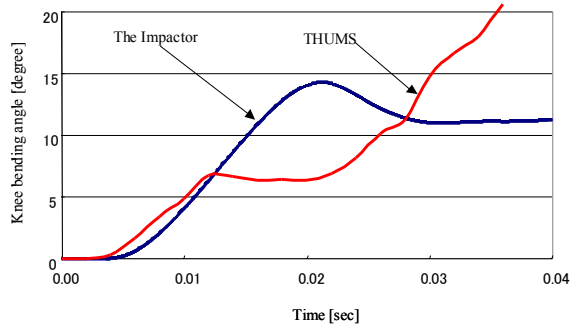


Figure 13. Knee-bending angle of THUMS and The Impactor in cases 1 and 2

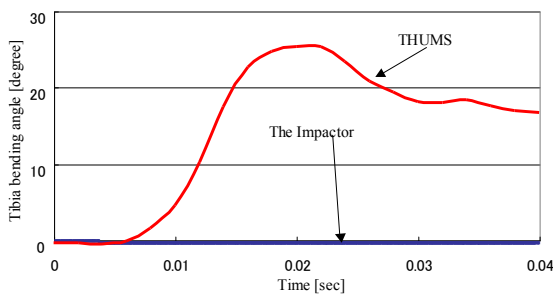


Figure 14. Tibia-bending angle of THUMS in case 2

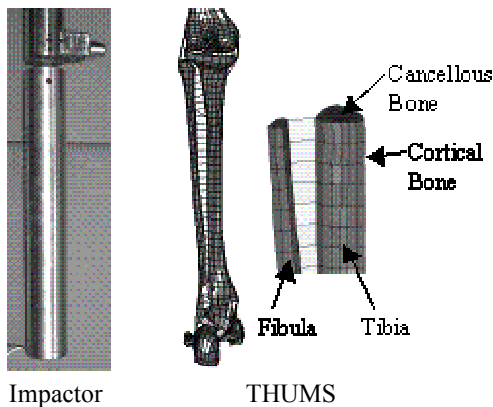


Figure 15. Comparison of fibula and tibia

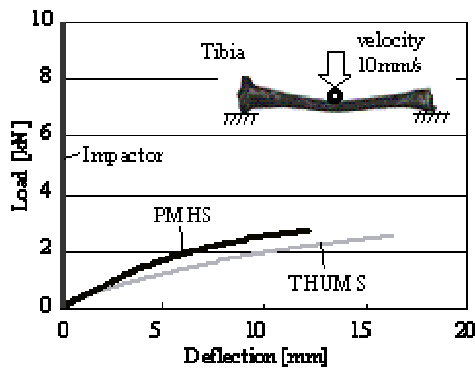


Figure 16. Force displacement relationship of tibia resulting from a 3-points bending test^(1,2)

SUV VS. THUMS AND IMPACTOR

THUMS and The Impactor movements observed from fixed coordinates on the vehicle in cases 3 and 4 are shown in Figure 17. The Impactor movements are similar to THUMS at 0.02 sec. The THUMS tibia did not bend because the tibia does not come in contact with the bumper fascia. The Impactor's femur is already rebounding from the bumper fascia while the THUMS femur is still contacting the bumper fascia at 0.04 sec.

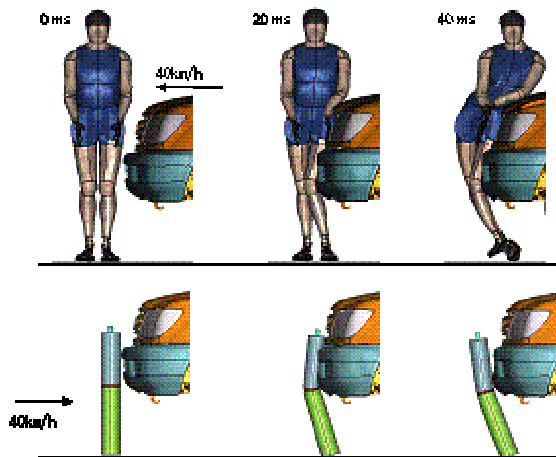


Figure 17. Movements of THUMS and The Impactor vs. SUV

The main reasons for The Impactor's femur rebounding at 0.04 sec are assumed as follows:

- THUMS has a similar femur bending stiffness to post mortem human subject tests, while The Impactor has much stiffer bending stiffness compared to post mortem human subject tests (Figure 18).
- THUMS has a knee structure similar to a human's knee. The knee-bending moment of THUMS is generated by elongation of ligaments, while the knee-bending moment of The Impactor is generated by plastic bending of a single steal plate (Figure 19). The knee-bending moment of THUMS is similar to post mortem human subject tests, while the knee bending moment of The Impactor is stiffer than post mortem human subject tests (Figure 20).

The author estimates that excessive bending stiffness of The Impactor's femur and knee-bending moment may affect rebounding of The Impactor's femur at 0.04sec. Also, the author estimates that bumper height may affect the rebounding of The Impactor's femur at 0.04sec.

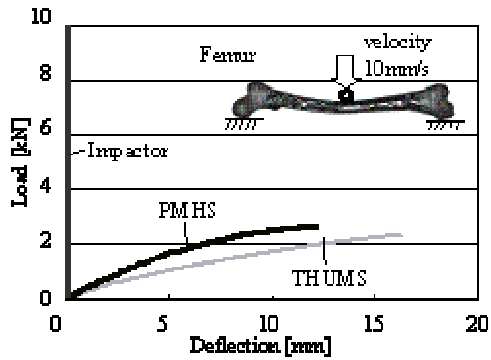


Figure 18. Force displacement relationship of femur 3-points bending tests^(1,2)

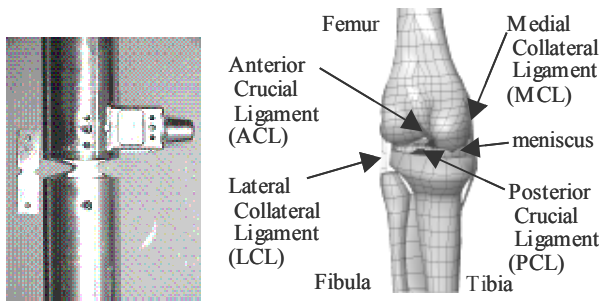


Figure 19. Comparison of knee structure

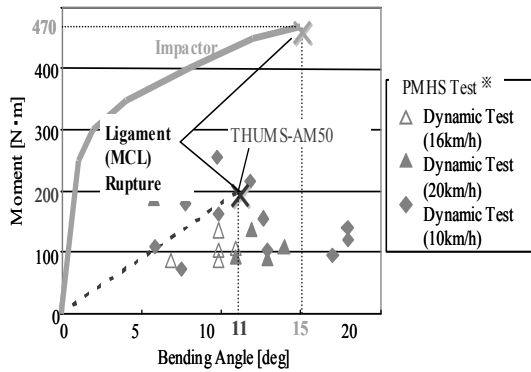


Figure 20. Moment bending angle relationship of knee^(4,5,6)

BUMPER HEIGHT EFFECT

Lower bumper height (LBH) is defined as indicated in Figure . 21. LBH of the FE model for cases 3 and 4 is 520 mm. LBH of the FE model for case 3 was reduced to 420 mm, 320 mm and 220 mm.

The Impactor movements are shown in Figure 22. When the LBH is reduced to 420 mm, 320 mm and 220 mm, The Impactor's femur does not rebound at 0.04 sec. The LBH of 520 mm is too high to avoid rebounding of The Impactor's femur at 0.04[sec].

An LBH upper limit for testing should be applied to The Impactor, as long as The Impactor has no pelvic mass.

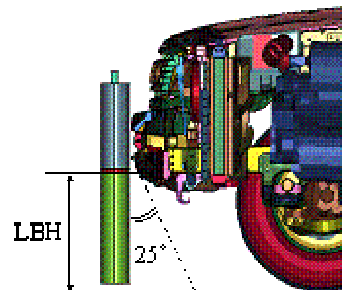


Figure 21. Definition of lower bumper height

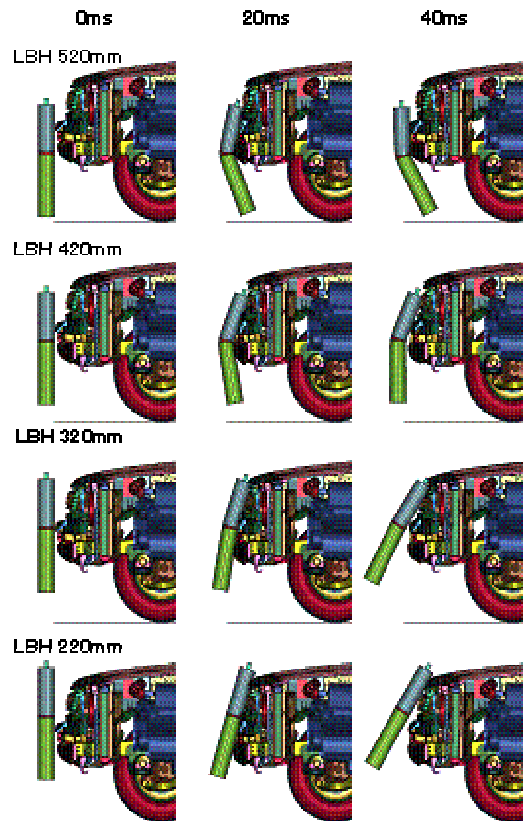


Figure 22. Impactor Movement at different LBHs

CONCLUSION

The knee-bending angle of the TRL lower leg impactor FE model was compared with the THUMS model.

The TRL lower leg impactor indicated more knee-bending angle than THUMS due to less bending deflection of the tibia in collisions with a sedan type vehicle. The tibia bending stiffness of the TRL lower leg impactor should be improved to better simulate similar knee-bending angle to that of THUMS.

The TRL lower leg impactor indicated a similar knee-bending angle to THUMS in a collision with an SUV type vehicle. However, rebounding of the TRL lower leg femur was observed. Lower bumper height for testing with the TRL lower leg impactor should be limited to avoid rebounding of the TRL lower leg impactor femur.

ACKNOWLEDGEMENT

The author appreciates Mr. Yasuo Yamame of Toyota Communication Systems, Mr. Kazuo Miki, Mr. Masakazu Iwamoto of Toyota Central Research and Development Laboratory for suggestions and their reviews for completion of this technical paper.

REFERENCES

- [1]Maeno T., Hasegawa J., .Development of a Finite Element Model of the Total Human Model for Safety (THUMS) and Application to Car-Pedestrian Impacts, ESV2001, paper NO. 494.
- [2] Iwamoto M., Tamura A., Furusu K., Kato C., Miki K., Hasegawa J., Yang K., .Development of a Finite Element Model of the Human Lower Extremity for Analyses of Automotive Crash Injuries, SAE Paper 2000-01-0621, 2000.
- [3]Euro-NCAP. EURO-NCAP's Pedestrian Impact Tests, <http://www.euroncap.com>.
- [4] Kajzer J., Cavallero C., Bonnoit J., Morjane A., Ghanouchi S.Response of the Knee Joint in Lateral Impact, Effect of Bending Moment, Proceeding of the 1993 International IRCOBI Conference on the Biomechanics of impact, p.105-116 (1993).
- [5]Levine R.S., Begeman P.C., King A.I..An Analysis of the Protection of Lateral Knee Bracing in Full Extension Using a Cadaver Simulation of Lateral Knee Impact, American Academic of Orthopedic Surgical,(1984) .

[6] Ramet, M., Bouqut R., Bermond F., Caire Y., Bouallegue M., Shearing and Bending Human Knee Joint Tests in Quasi-Static Lateral Load, Proceedings of the 1995 IRCOBI Conference on the Biomechanics of Impacts, p.93-105, (1995) .

MATHEMATICAL SIMULATIONS OF REAL-WORLD PEDESTRIAN-VEHICLE COLLISIONS

Astrid Linder

Clay Douglas

Anthony Clark

Brian Fildes

Monash University Accident Research Centre
(MUARC), Australia

Jikuang Yang

Chalmers University of Technology, Sweden

Dietmar Otte

Medical University of Hanover, Germany

Paper No. 05-285

ABSTRACT

Pedestrian-vehicle crashes result in a substantial number of pedestrian fatalities and injuries worldwide. Computer models are powerful tools in understanding how the severity of injuries could have been reduced in the crash. Pedestrian real-world cases serve as an important source of information to evaluate the dynamic performance of pedestrian models and their ability to reconstruct injury-causing events.

The objective of this study was to evaluate the ability of a mathematical pedestrian model to assess the severity of an impact using real-world data. The dynamic performance of the pedestrian model was evaluated by the reconstruction of six real-world pedestrian collisions, which occurred during 1995-2003 in the surroundings of Hanover, Germany. The impact severities were 32-59km/h. Each case contained information about the pre-crash, crash, and post-crash events. This information included hospital reports and detailed description of damages to the vehicle, pedestrian injuries, and the crash environment collected at the scene. The evaluation focused on head injuries since these are the most common cause of severe injuries and fatalities of pedestrians involved in passenger vehicle-pedestrian crashes.

The results showed that the model produced injury measures and readings of the magnitude expected for the highest severity head injuries sustained by the pedestrian in the reconstructed case. Furthermore it highlights the usability of mathematical pedestrian models in evaluating the severity of a vehicle-pedestrian collision.

INTRODUCTION

Road crashes result in a substantial number of pedestrian fatalities and injuries worldwide. Statistics from 35 European countries have shown that pedestrian fatalities represented on average 25% of road users killed throughout Europe (ECMT, 2003). In Japan, pedestrian fatalities accounted for 28% of the road toll (ECMT, 2003), while in Australia approximately 16% of road fatalities were pedestrians (ATSB, 2003). Pedestrian fatalities as a proportion of road fatalities were estimated at 13% in the USA and were as high as 40-50% of the annual road toll in India and Thailand (Mohan and Tiwari, 2000). Head injuries are the most common cause of pedestrian fatalities. Injuries to the chest, spine, abdomen and the lower extremities are also commonly sustained (Anderson and McLean, 2001, Fildes et al., 2004).

Computer simulations provide a powerful tool for studying the loading to the pedestrian in a crash. For the study of overall human kinematics in a crash, computer models based on rigid bodies connected to each other by joints are time efficient. The dynamic and kinematic response of computer models is validated towards biological test results. However, it is important to include evaluation towards real-world cases as part of this process in order to determine the models ability to assess the impact severity in a wide range of scenarios.

The aim of this study was to evaluate the ability of a mathematical pedestrian model to assess the severity of an impact by reconstruction of six real-world passenger vehicle-pedestrian collisions.

MATERIALS AND METHODS

Six real-world vehicle-pedestrian crashes were reconstructed using PC-Crash and MADYMO. The data about the collision and the injuries were compiled from on-site collected data and hospital records coded using AIS (AAAM, 1990) when available. The on-site inspection provided detailed information about the site and circumstances for the crash, such as skid marks and resting positions, in addition to detailed documentation of the damages to the vehicle.

Real-World Cases

The real-world cases were collected around the area of Hanover, Germany in an area with a radius of approximately 70km. An inspection team consisting of 4 members perform an investigation of the collision. Two team members go to the scene, one team member follows the injured person and the 4th team member is the coordinator. The police or fire brigade alert the team and the team normally arrived 30min after the collision.

Case 1 (ID 030816)

A male pedestrian was hit with an estimated impact velocity of 45-50km/h by a VW Golf in an intersection. The intersection consisted of three lanes for forward traffic and one lane for left turning traffic. Vehicles were stationary in the inner forward running lane and the case vehicle was in the forward running lane next to the left turning lane (Figure 1). The driver of the case vehicle saw from a distance the light change from red to green and entered the intersection at a travel speed of 45-50km/h. A pedestrian was walking quickly across the intersection, hidden from the case vehicle by the stationary vehicle. The pedestrian was hit by the right front of the case vehicle, which started to brake at impact.

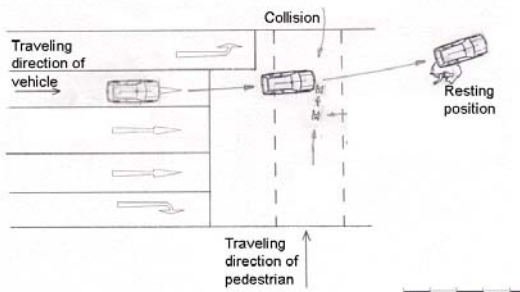


Figure 1. The intersection in Case 1 where a VW Golf struck a pedestrian. The pedestrian was hidden from the view of the driver in the case vehicle by stationary vehicles in the forward running lanes.

The impacting vehicle was a 2000 2-door VW Golf. Marks on the vehicle showed that the pedestrian struck the front right quarter panel, the right side of the windshield and the right side of the roof adjacent to the windshield (Figure 2). The pedestrian was thrown 9.4m from where the impact occurred. The range of thrown distance was estimated to be ± 1 m.



Figure 2. The impact locations of the male pedestrian on the front right quarter panel, windshield and roof on the VW Golf in Case 1.

The pedestrian was a 68-year-old male, 175cm and 85kg. He sustained MAIS 3 injuries. All the injuries were: multiple left side rib fractures AIS 3, left tibia fracture AIS 2, concussion AIS 2, open fracture of nose bone AIS 1.

Case 2 (ID 030945)

Two pedestrians, one male and one female (denoted Case 2a and 2b), were hit with an estimated impact velocity of 43-49km by a BMW when they appeared suddenly from between parked cars in the dark. The male pedestrian was hit by the left front and the female pedestrian was hit by the centre of the case vehicle (Figure 3).

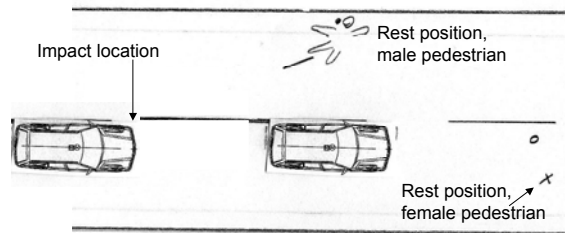


Figure 3. The road where a BMW struck two pedestrians. The pedestrians appeared suddenly from between parked cars and attempted to cross the street in Case 2.

The male pedestrian impacted the left a-pillar; the front left side of the hood and the area above the left side of the head-lamp (Figure 4). The male pedestrian was thrown 8.5m from where the impact occurred. The range of thrown distance was estimated to be ± 1 m. The female pedestrian hit the centre of the hood (Figure 4) and was thrown approximately 15m from where the impact occurred. The female pedestrian rose immediately after having landed on the ground and there were no marks that could further verify the orientation of the pedestrian in her rest position. The range of thrown distance was estimated to be ± 2 m.



Figure 4. The impact locations of the male pedestrian on the BMW in Case 2.

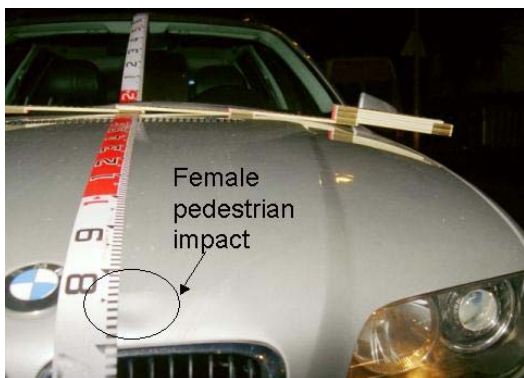


Figure 5. The impact locations of the female pedestrian on the BMW in Case 2.

The striking vehicle was a 1999 BMW 3 Series Touring Wagon. The more severely injured pedestrian in Case 2 was a 48-year-old male (denoted Case 2a). He sustained MAIS 4 injuries. All the injuries were: head haematoma and oedema AIS 4, subarachnoidal bleeding and fractured base of the skull AIS 3 and skull and fractures to the orbit AIS 2. The other pedestrian in Case 2 was a 23-year-old female (denoted Case 2b). She sustained MAIS 1 injuries. All the injuries were: haematoma

of pelvis and lower leg and distortion of cervical spine AIS 1.

Case 3 (ID 17028)

A male pedestrian was hit by a VW Passat with an estimated impact velocity of 59km/h. The case vehicle was driving in the right lane and the traffic light showed a green light for the vehicle. The pedestrian started crossing the street and was hit by the right front of the vehicle (Figure 6). The case vehicle started to brake at impact.

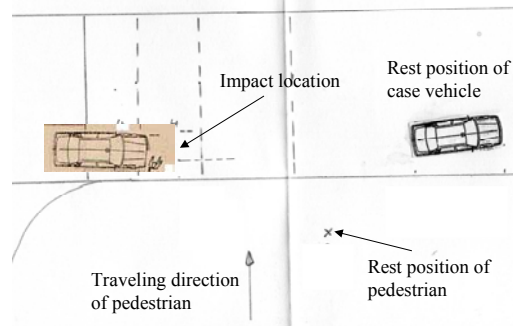


Figure 6. The road where a VW Passat struck a male pedestrian in Case 3. The pedestrian walked out despite having a red light in an attempt to cross the street.

The male pedestrian was hit by the right side of the windscreen, the front right side of the hood and the on the right side of the bumper (Figure 6). The male pedestrian was thrown 10.3m from where the impact with the vehicle occurred. The range of thrown distance was estimated to be ± 1 m.



Figure 7. The impact locations of the pedestrian on the VW Passat in Case 3.

The striking vehicle was a 1987 to 1995 VW Passat. The pedestrian was a 35 years old male, 172cm and 70kg. He sustained MAIS 3 injuries. All the injuries were: haematoma frontal thorax and lacerations right

forehead AIS 1, fracture right tibia AIS 3 and fracture right fibula AIS 2.

Case 4 (ID 17910)

A female pedestrian was hit by a VW Caravelle with an estimated impact velocity of 32-35km/h. The case vehicle was driving along the road and the pedestrian started crossing the street and was hit by the left front of the vehicle (Figure 8). The case vehicle started to brake prior to impact.

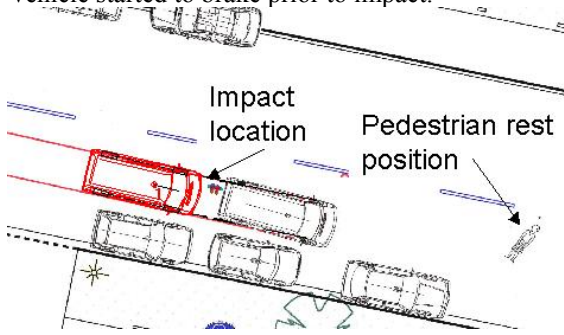


Figure 8. The road where a VW Caravelle struck a female pedestrian in Case 4. The pedestrian walked out in an attempt to cross the street.

Marks on the vehicle showed that the female pedestrian hit the left side of the front (Figure 9). The female pedestrian was thrown approximately 12.5m from where the impact occurred. The pedestrian rose immediately after having landed on the ground and there were no marks that could further verify the orientation of the pedestrian in her rest position. The range of thrown distance was estimated to be ± 2m.



Figure 9. The impact locations of the female pedestrian on the VW Caravelle in Case 4.

The striking vehicle was a 1998 VW Caravelle. The pedestrian was a 77-year-old female. The pedestrian sustained no recorded injuries.

Case 5 (ID 30010020)

A male pedestrian was hit by a Ford Mondeo with an estimated impact velocity of 40-45km/h. The pedestrian crossed the street at night and was struck by the case vehicle (Figure 10).

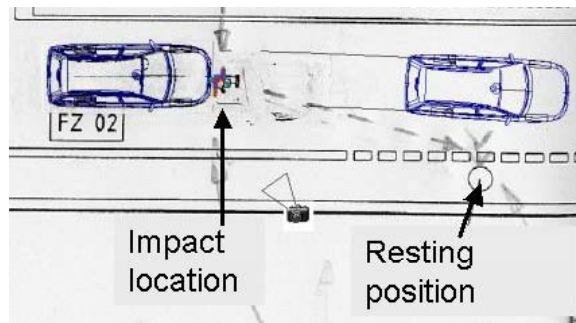


Figure 10. The road where a Ford Mondeo struck a male pedestrian in Case 5. The pedestrian attempted to cross the street.

Marks on the vehicle showed contact with the pedestrian at the windshield and the hood. The pedestrian was struck by the centre front of the vehicle, slid to the right along the hood and hit the head on the windshield (Figure 11). The male pedestrian was thrown 7.8m from where the impact occurred. The range of thrown distance was estimated to be ± 2m. According to a witness the pedestrian was seen to run across the street.



Figure 11. The impact locations of the male pedestrian on the Ford Mondeo in Case 5.

The striking vehicle was a 1998 Ford Mondeo. The pedestrian was a 19-year-old male, 182cm, 72kg. The pedestrian sustained deep lacerations forehead, nose and right ear, lacerations to the fingers on the left and right hand and ligament rupture to the right knee.

Case 6 (ID 17946)

A female pedestrian was hit by a Mercedes with an estimated impact velocity of 43km/h. After having reached the middle of the road the pedestrian turned back (Figure 12). The case vehicle braked and struck the pedestrian with the left front. The information about the rest position of the pedestrian was that she ended up within the area where glass splinters from the windshield were found.

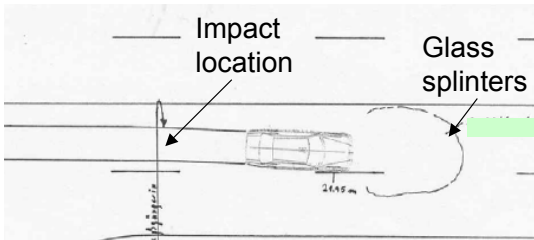


Figure 12. The road where a Mercedes struck a female pedestrian in Case 6. The pedestrian turned back after having reached the middle of the road.

Marks on the vehicle showed that the female pedestrian hit the left side of the windshield (Figure 8). The female pedestrian was thrown approximately 9-14m from where the impact occurred.



Figure 13. The impact location of the female pedestrian on the Mercedes in Case 6.

The striking vehicle was a 1988-9 Mercedes 200E. The pedestrian was a 45 years old female, 170cm and 70kg. She sustained MAIS 2 injuries. All the injuries were: concussion AIS 2, laceration right forehead and nose, haematoma right side of right knee AIS 1.

Reconstruction of Pedestrian Collisions

For some cases the range of the impact velocity was estimated based on thrown distance and braking distance. The pedestrian collisions were then firstly reconstructed with PC-Crash to verify the estimation of impact velocities. Secondly, the collision was reconstructed in MADYMO 5.4.1 (TNO, 1999), using EASI-CRASH and the pedestrian model by Yang et al. (2000).

In the MADYMO simulations, an impact velocity that generated the best match with the thrown distance measured at the scene was used. In the cases where the pedestrian was not regarded as stationary it was given a velocity perpendicular to the vehicle. The velocity of the pedestrian was chosen within the ranges obtained as follows: A healthy male in his 20s performed tests on a treadmill. From these tests, running was established to be $\geq 3\text{m/s}$ and fast walking was established as 1.5 - 3m/s. All cases were initially reconstructed with the 50th percentile male model. In Case 2 where the height and weight of the pedestrians were unknown additional simulations with the 5th percentile female and the 95th male model were performed.

For the MADYMO simulations the position of the pedestrian prior to impact was estimated from the photos of the damaged vehicle. The orientation of the pedestrian prior to the impact was thus estimated individually for all cases. For each case approximately 20 simulations were run to tune the positioning and the velocity of the pedestrian, in the aim of matching the thrown distance, braking distance and impact locations on the vehicle and the ground to the real-world cases.

The reconstruction of the real-world cases in MADYMO is schematically illustrated in Figure 14. The figure shows the flow of data and the loop of iterations of the MADYMO simulations.

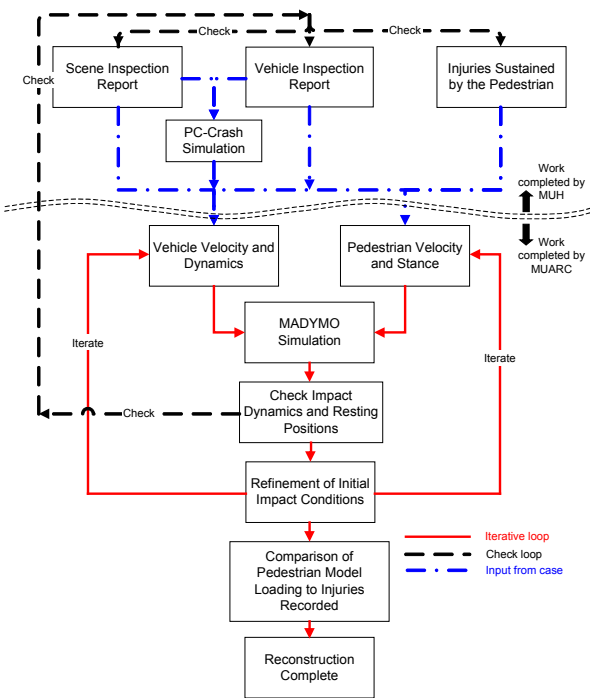


Figure 14. A schematic illustration showing the reconstruction of the real-world cases in MADYMO, the flow of data and the loop of iterations of the simulations.

Mathematical models of the vehicles' structure were constructed using dimensioned drawings obtained from the web page of 3dcenter.ru. These were cross referenced against measurements taken from a vehicle of the same make, year and model as in the cases using straight-edges, tape measures and rulers with particular focus on the pedestrian impact point locations. The force-penetration curves used for the MADYMO vehicle models were approximated from van Rooij et al. (2003) and Mizuno and Kajzer (2000). For the windshield the centre force-penetration curve (Mizuno and Kajzer, 2000) was used. The roof was given a force-penetration loading curve obtained from the average between the hood and hood edge of van Rooij et al. (2003). The hood edge and the quarter panel were given midsection hood edge force-penetration loading curve of van Rooij et al. (2003). The door was given midsection door force-penetration loading curve and the upper and lower bumper the midsection bumper force-penetration loading curve of van Rooij et al. (2003). The a-pillar was given the force-penetration loading curve of the a-pillar as in van Rooij et al. (2003).

The contact interactions between the vehicle and the pedestrian were defined as 'ellipsoid-ellipsoid' using the 'evaluations' keyword where necessary to avoid multiple contact interactions. A friction coefficient

was applied to the pedestrian to vehicle contact (0.3) and the pedestrian to ground contact (0.7), as well as a small amount of damping. Where applicable the vehicle was subjected to deceleration and nose-dive due to braking. The amount of braking was chosen so that the final position of the case vehicle being simulated matched as close as possible to that of the case. A 50mm nose-dive and 2 degrees rotation around the front was applied to the models when braking prior to impact was present.

MADYMO Vehicle Model and pedestrian position Case 1

The VW Golf was generated using 15 ellipsoids. The front-right quarter panel, a-pillar and roofline of the vehicle were modelled in detail. Impact velocity of 11.8m/s, braking prior to impact and a braking distance of 13.3m were applied. The pedestrian's initial posture was in a walking stance with the left leg slightly in front of the right. The pedestrian was given an initial velocity of 3m/s.

MADYMO Vehicle Model and pedestrian position Case 2

The BMW was generated using 22 ellipsoids. As a result of the multiple pedestrian impact condition, the curvature of the front of the vehicle was constructed using 3 sections of ellipsoids. As the male pedestrian struck the right hand edge of the vehicle, it was necessary to include an a-pillar, side guard and a door to represent the vehicle being struck. Impact velocity of 12.7m/s and a braking distance of 10.1m were applied. The male pedestrian's initial posture was in a walking stance with the left leg slightly in front of the right. The female pedestrian's initial posture was facing towards the vehicle, right leg slightly in front of the left and using her arms to protect herself from the impact. Both pedestrians were given an initial velocity of 1.5m/s.

MADYMO Vehicle Model and pedestrian position Case 3

The 1993 VW Passat was generated using 11 ellipsoids. The front-right quarter panel was modelled in detail. Impact velocity of 12.7m/s, braking prior to impact and a braking distance of 18.6m were applied. The pedestrian's initial posture was in a walking stance with the right leg in front of the left. The pedestrian was given an initial velocity of 2m/s.

MADYMO Vehicle Model and pedestrian position Case 4

The VW Caravelle was generated using 11 ellipsoids. Impact velocity of 9.5m/s, braking prior to impact and a braking distance of 5.5m were applied. The pedestrian's initial posture was in a walking stance with the left leg slightly in front of the right. The pedestrian was given no initial velocity as it was deemed to be small.

MADYMO Vehicle Model and pedestrian position Case 5

The 1998 Ford Mondeo was generated using 9 ellipsoids. Impact velocity of 9.7m/s, braking prior to impact and a braking distance of 10.4m were applied. The pedestrian's initial posture was in a running stance with the left leg in front of the right. The pedestrian was given an initial velocity of 2m/s.

MADYMO Vehicle Model and pedestrian position Case 6

The 1988-9 Mercedes 200E was generated using 12 ellipsoids. Impact velocity of 12m/s, braking prior to impact and a braking distance of 8.8m were applied. The initial posture of the pedestrian was in a walking stance, turned slightly towards the vehicle with the left leg in front of the right. The pedestrian was given an initial velocity of 1m/s to simulate this walking motion.

RESULTS

The results showed that the kinematics of the pedestrian model in the MADYMO simulations were comparable with that in the real-world cases in terms of impact location, resting position and throw distance. An increased 3ms linear acceleration and HIC₁₅ corresponded to an increased severity of the collision in terms of MAIS head injuries for MAIS 2+. This applied to three out of the four cases and for the exception case an unusual initial posture made this impact less severe in terms of injuries compared to what the output from the simulation indicated. Furthermore, both the 3ms linear head acceleration and HIC₁₅ showed the highest values for the case where the highest severity of head injuries occurred.

Case 1

Figure 15 shows photos of the impacted vehicle and images from the simulations of Case 1 where the male pedestrian impacted the side of the vehicle. The simulated throw distance was 9.8m forward of the vehicle with the impact velocity of 45km/h. Head impact occurred at similar spot on the vehicle as in the real-world case.



Figure 15. Photos of the impacted VW Golf and images from the simulation of the male pedestrian hit by the vehicle with an impact velocity of 45km/h, Case 1.

Case 2

Figure 16 shows photos of the impacted vehicle and images from the simulations of the male pedestrian Case 2a (simulated with the 95th percentile male model) impacting the front left side of the vehicle. The simulated throw distance was 9.3m from the vehicle and the impact velocity used in the simulation was 46km/h. Head impact occurred at similar spot on the a-pillar as in the real-world case.



Figure 16. Photos of the impacted BMW and images from the simulation of the male pedestrian hit by the vehicle with an impact velocity of 46km/h, Case 2a.

Figure 17 shows photos of the impacted vehicle and images from the simulation of the female pedestrian Case 2b (simulated with the 5th percentile female model) impacting the centre of the vehicle. The female pedestrian showed no sign of head impact, neither from marks on the vehicle nor from injuries. The simulated throw distance was 14.7m from the vehicle and the impact velocity used in the simulation was 46km/h.



Figure 17. Photos of the impacted BMW and images from the simulation of the female pedestrian hit by the vehicle with an impact velocity of 46km/h, Case 2b.

Case 3

Figure 18 shows a photo of the impacted vehicle and images from the simulation of Case 3 where the male pedestrian impacted the front right hand side of the vehicle. The simulated throw distance was 10.3m from the vehicle and the impact velocity used in the simulation was 46km/h. Head impact occurred at similar spot on the windshield as in the real-world case.

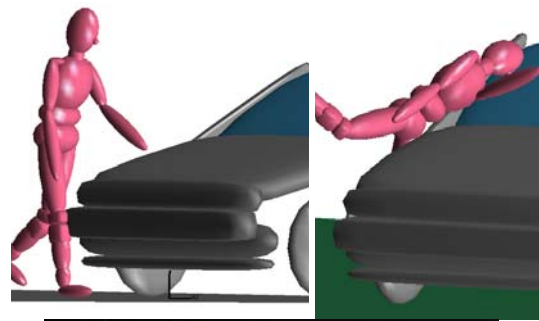


Figure 18. A photo of the impacted VW Passat and images from the simulation of the male pedestrian hit by the vehicle with an impact velocity of 47km/h, Case 3.

Case 4

Figure 19 shows a photo of the impacted vehicle and images from the simulation of Case 4 where the female pedestrian impacted the front side of the vehicle. The simulated throw distance was 12m from the vehicle and the impact velocity used in the simulation was 34km/h. The impact occurred at similar spot on the hood as in the real-world case.

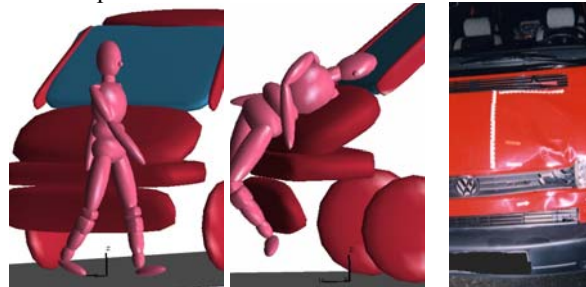


Figure 19. A photo of the impacted VW Caravelle and images from the simulation of the female pedestrian hit by the vehicle with an impact velocity of 34km/h, Case 4.

Case 5

Figure 20 shows photos of the impacted vehicle and images from the simulation of Case 5 where the male pedestrian was impacted while running across the road. The simulated throw distance was 8.2m, with an impact velocity of 35km/h. Head impact occurred at similar spot on the windshield as in the real-world case.



Figure 20. Photos of the impacted vehicle and images from the simulation of the male pedestrian struck by a Ford Mondeo with an impact velocity of 35km/h, Case 5.

Case 6

Figure 21 shows photos of the impacted vehicle and images from the simulation of Case 6 where the male pedestrian impacted the front of the vehicle. The simulated throw distance was 10.1m from the vehicle and the impact velocity used in the simulation was 36km/h. Head impact occurred at similar spot on the windshield as in the real-world case.



Figure 21. Photos of the impacted vehicle and images from the simulation of the female pedestrian struck by a Mercedes with an impact velocity of 36km/h, Case 6.

Figure 22 shows the thrown distance from the real-world cases and those generated in the simulations of the cases. The impact velocities used in the simulations are shown in Figure 23 together with the calculated range of the impact velocity based on thrown and braking distance and velocities used in the PC-Crash simulations.

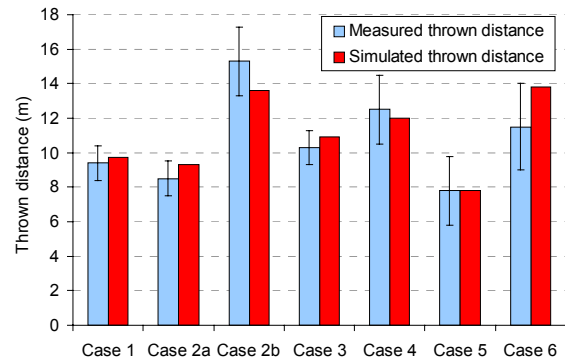


Figure 22. The thrown distance measured at the crash scene and from the simulation of the six cases. The bars on the measured data represent the range of thrown distances.

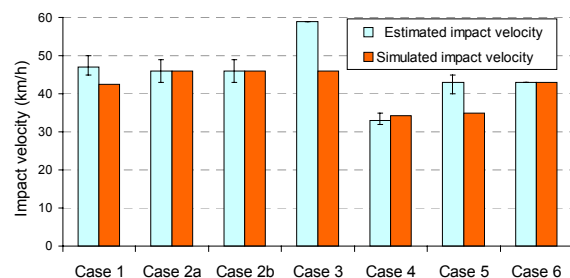


Figure 23. The impact velocity estimated from the crash scene data and the impact velocity in the simulation of the six cases. The bars on the estimated data represent the calculated range of impact velocities based on thrown distance and braking distance.

The HIC 15 and 3ms head linear and rotational acceleration from the simulations of the six cases is shown in Figures 24-26.

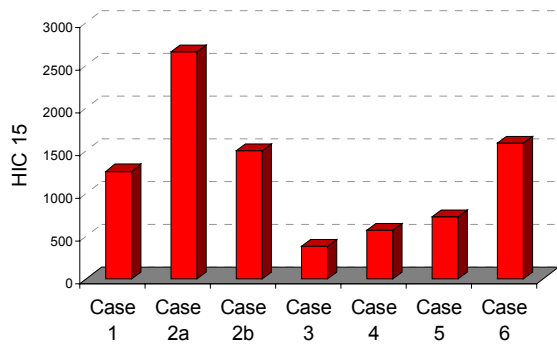


Figure 24. The HIC 15 from the simulations of the six cases.

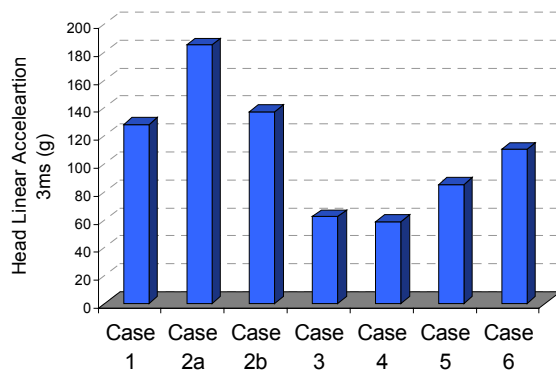


Figure 25. The 3 ms head linear acceleration from the simulations of the six cases.

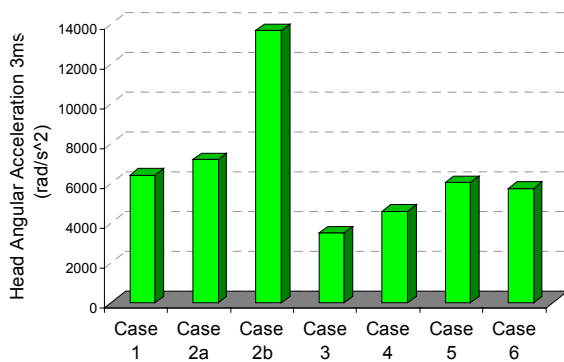


Figure 26. The 3ms head angular acceleration from the simulations of the six cases.

DISCUSSIONS

Through simulating six real-world pedestrian vehicle crashes, it was observed that in general, the kinematics of the pedestrian model of Yang et al. (2000) corresponded well with crash scene data in terms of impact location, thrown distance and resting position. Even though the model was used for various impact conditions in terms of pedestrian posture, orientation and velocity prior to impact,

the pedestrian model was able to generate a close match to the on-scene collected data. Also head loading was compared to the real-world injury outcome without any internal modifications of the model needed.

The head injuries MAIS from the six cases is shown in Figure 27. The simulation of the case with the highest MAIS head injury, MAIS 4, produced a HIC 15 of 2660. A HIC of 2660 correspond to 85% risk of skull fracture according to the relation determined by Hertz (1993) and in this case the pedestrian sustained skull fractures.

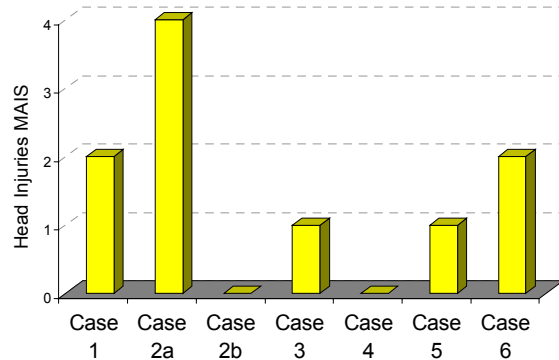


Figure 27. The head injuries MAIS from the six real-world cases.

Of the dynamic responses investigated, it was found that both 3ms Linear Head Acceleration and HIC₁₅ displayed the same trend as did the severity of head injuries. An increase in either of these parameters corresponded with an increased severity of the collision, with respect to MAIS 2+ head injuries (Figures 24, 25 and 27). The exception being case 2b, where the pedestrian had an unusual initial posture, due to her awareness of the approaching vehicle. This consequently led to her having a very different kinematic response to the other cases. Specifically, for this case, the pedestrian managed to avoid any noticeable head contact with the vehicle. This event was unable to be replicated through simulations.

It was also observed that both 3ms Linear Head Acceleration and HIC₁₅ showed the lowest values for cases 3, 4 and 5. For these cases, head impact severity was limited to AIS 0 or 1. For Case 4, an AIS 0 was estimated as no official injuries were recorded as the pedestrian had left the hospital prior to meeting with the investigation team. If the pedestrian in this case sustained any head injuries it was most likely a low AIS head injury.

The thrown distances observed in the MADYMO simulations were shown to be within the range given from the real-world cases (Figure 22). To generate the match between simulated and measured thrown distance, in combination with vehicle impact location and braking distance, the impact velocities were in some cases somewhat lower than those estimated from the crash scene data (Figure 23).

All cases were initially simulated using the 50th percentile male pedestrian model. For Cases 1,3,5 and 6 the height and weight of the pedestrian was similar to that of the 50th percentile male model. Whereas the height and weight of the pedestrians in Case 2 and 4 were unknown. In Case 4 a reasonable match between simulated, measured and estimated values of kinematics, impact locations and rest positions were obtained using the 50th percentile male model. However this was not the situation for Case 2, thus models other than the 50th percentile male were necessary to be used. For both pedestrians in Case 2, the 50th percentile male was not able to generate the kinematics, impact locations and rest positions expected from the crash scene data. In the case of the male, the 50th percentile male model predicted a lower impact location on the a-pillar to what occurred in Figure 4. For the female's impact, the 50th percentile male model struck his head on the windshield. This is thought to be unlikely, as if this was the case, windshield damage would be expected. This led to the choice of using the 5th percentile female and 95th percentile male models for the female and male in this case. When simulating the case with the large male and the small female pedestrian models, the impact locations, thrown distance and kinematics were closer to that observed in the real-world case. The head impact location from the simulations with the various models is shown in Figures 28-29.

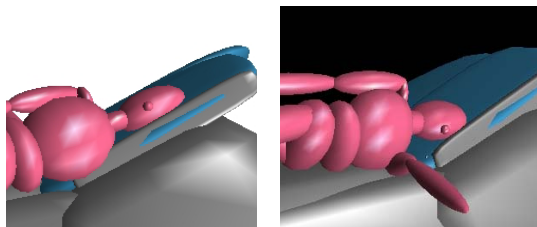


Figure 28. The simulation of the 95th percentile (left) and the 50th percentile (right) male pedestrian model impacting the BMW with the simulated impact velocity of 46 km/h, Case 2a.

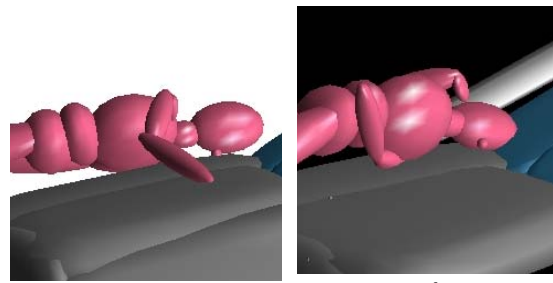


Figure 29. The simulation of the 5th percentile (left) female and the 50th percentile (right) male pedestrian model impacting the BMW with the simulated impact velocity of 46km/h, Case 2a.

In Case 2 there were remarkable differences between the injury outcomes for the two pedestrians. The male pedestrian struck the a-pillar and suffered severe head injuries, whereas the female pedestrian only sustained minor injuries. The pedestrians were struck by the same vehicle and by the same impact velocity. This case highlights the importance of preventing pedestrians from hitting high stiffness structures and the large difference that can occur for a given impact velocity.

The stiffness of various vehicles parts was generated from component tests at 40 km/h (van Rooij et al., 2003 and Mizuno and Kajzer 2000). The range of impact velocities used in these simulations was 40 ± 6 km/h. The simulations were thus carried out at a range of impact severities close to that for which the force-penetration curves were defined.

It has previously been highlighted by among others van Rooij et al. (2003) that generating a vehicle model with the correct geometry largely determines where on the vehicle various parts of body impact. In addition, localized contact stiffness characteristics have a great influence on the injury outcome. Therefore great care was taken to ensure that for each case vehicle, profiles and appropriate stiffnesses were used in the simulations. Furthermore, the initial position of the pedestrian, braking distance and impact velocity from the real-world case were important factors in the reconstruction of the real-world pedestrian collisions. These all played an important role in order to generate the match between measured and simulated thrown distance (Figure 22) and the impact locations of the pedestrian on the vehicle (Figures 15-21).

In depth analysis and reconstruction of real-world collisions are important to link simulation responses to real-world outcomes. In this study, the pedestrian model was used to identify two head loading measurements that corresponded in increased magnitude to increased severity of MAIS 2+ head injuries. Further study of higher severity head injuries sustained in real-world pedestrian-vehicle crashes may enable a stronger link to be generated between these simulated dynamic responses and actual head injury.

CONCLUSIONS

In the reconstruction of six real-world pedestrian-passenger vehicle crashes in the range of impact velocities around 40km/h it was found that an increased 3ms linear acceleration and HIC₁₅ corresponded to an increased severity of the collision in terms of MAIS head injuries for MAIS 2+.

The results of this study showed that the kinematics of the pedestrian model in the MADYMO simulations of the six real-world cases were comparable with that in corresponding collisions in terms of impact location and throw distance.

ACKNOWLEDGEMENT

The authors would like to thank Holden Ltd for financial support for the study. We are also grateful for the support from Mr Joachim Nehmzow who patiently has provided details about the real-world cases and performed the PC-Crash simulations.

REFERENCES

- AAAM. (1990) The Abbreviated Injury Scale – 1990 Revision. American Association for Automotive Medicine, Des Plaines IL.
- Anderson R.W.G and McLean A.J. (2001) Vehicle design and speed and pedestrian injury: Australia's involvement in the International Harmonised Research Activities pedestrian expert group, *In Proceedings of the Road Safety Research, Policing and Education Conference*, Melbourne, Australia.
- ATSB (2003). Website: www.atsb.gov.au 17/09/03.
- ECMT (2003) Statistical report on road accidents, ISBN 92-821-0299-8.
- Fildes, B., Gabler, C.H., Otte, D., Linder, A., Sparke, L. (2004) Pedestrian Impact Priorities Using Real-World Crash Data and Harm, *In*

Proceedings of the International IRCOBI Conference on the Biomechanics of Impacts. Graz, Austria.

Hertz (1993) A note on the head injury criterion (HIC) as a predictor of the risk of skull fracture, *In Proceedings of the 37th AAAM Conference*, San Antonio, Texas, USA.

Mohan D. and Tiwari G. (2000) Road safety in less motorized countries – relevance of international vehicle and highway standards, *In Proceedings of the International Conference on Vehicle Safety, IMechE*, London, UK, Paper No C567/008/2000, pp 155-166.

Mizuno, K., Kajzer, J. (2000) Head injuries in Vehicle-Pedestrian Impact, *SAE Paper No. 2000-01-0157*, Society of Automotive Engineers, Warrendale, PA, USA.

van Rooij, L., Bhalla, K., Meissner, M., Ivarsson, J., Crandall, J., Longhitano, D., Takahashi, Y., Dokko, Y., and Kikuchi, Y. (2003). Pedestrian crash reconstruction using multi-body modelling with geometrically detailed, validated vehicle models and advanced pedestrian injury criteria. *In Proceedings of the 17th International ESV Conference*, Nagoya, Japan. Paper 468.

TNO Automotive (1999) MADYMO User's Manual 3D Version 5.4, Delft, The Netherlands.

Yang, J.K., Lövsund, P. Cavallero C., Bonnoit J. (2000). A Human-Body 3D Mathematical Model for Simulation of Car-Pedestrian Impacts. *International Journal of Crash prevention and Injury Control*. Vol.2(2), pp 131-149.

3D Center, Website: <http://3dcenter.ru/blueprints>, 15/01/05.

COMPARISON OF SEVERAL METHODS FOR REAL PEDESTRIAN ACCIDENT RECONSTRUCTION

Jean-Philippe Depriester

Criminal Research Institute of the French National Gendarmerie
(Institut de recherche criminelle de la gendarmerie nationale - IRCGN)
France

Christophe Perrin

Thierry Serre

Sophie Chalandon

French National Institute for Transport and Safety Research (INRETS)
France

Paper Number 05 - 0333

ABSTRACT

The aim of this paper is to evaluate and compare several methods allowing the reconstruction of real accidents involving pedestrians. These different methods have various levels of complications and are commonly used in primary or secondary safety research. They can be classified into three categories corresponding to their levels of complications. The first class concerns "simple" methodologies based on an analytical or semi-analytical approach ("hand-calculi") such as Searle's model, Fall and Slide model, equations proposed by Rau et al., Simms et al., etc. The second one is more complicated and considers for example the pedestrian as a single segment as described by Wood. Finally, the last class contains the most complicated approaches and is based on three-dimensional multi-body models. Concerning this third class, this work has been based on the PC-Crash® and Madymo® softwares. We have tested all of these methods for one of the most usual real car-to-pedestrian accident configurations: frontal collision with pedestrian wrap trajectory. Data issuing from two real cases have been used. They have been provided by an in-depth multidisciplinary accident investigation (psychology, technical, medical). Reconstructions are thus based on driver and witness statements, on accurate information relating to material evidence (e.g. skid marks, car damage, pedestrian injuries, throw distance) and parameters fitted to vehicle and pedestrian (e.g. vehicle shape, pedestrian anthropometry, etc). Results have been compared in terms of quality of the reconstruction balanced by the limitation of the different methods. Evaluated elements are in particular the speed of the vehicle, the final position of the pedestrian, his kinematics, the impact points on the car and injuries (when the method allowed it).

In parallel, methodologies have also been compared qualitatively by establishing the necessary means to apply them. In this way, the potentiality of the methods, their requirements (necessary input data, into operation bringing time, computer time) have been evaluated and reported in a general matrix. It allows us to summarize advantages and disadvantages of the different methods.

INTRODUCTION

Several sorts of methods are commonly used to reconstruct a real car-to-pedestrian accident. All of them are based on a "model" which is the abstract simplified representation of the reality. These models are uncompleted and temporary results of the building up of knowledge, which we have from a reality. In agreement with this status, the models can be more or less complicated according to modelling assumptions. Level of complication is so dependant on the mathematical hypothetic-deductive system, the input and output data definition, coherence of the concepts taking into account the modelling, etc.

We took an interest in comparing some different dynamic hypothetic-deductive models (more precisely, some models of Newtonian Mechanics) used to represent a real car-to-pedestrian collision in the most usual configuration, i.e. a vehicle frontal impact with a pedestrian wrap trajectory. These models are based on the Galilean-Cartesian paradigm which does not take into account the complexity but the complication. It was therefore interesting to observe if they can propose a collision reconstruction (impact and post-impact phases) fitted to the reality, even if they split up this complex event (a priori irreducible) into simple problems which have to be treated one by one. It was relevant to determine in what propor-

tion the increase in complication of a model, as used in a secondary safety research way, can improve the findings of the forensic and the in-depth investigation fields.

Chosen models have been classified into three categories as regards their complication level:

- a first category concerning simple methodologies based on an analytical or semi-analytical approaches (hand calculi): Searle's model [13], Fall and slide model [4], equations proposed by Rau et al. [11], Toor and Araszewski [17], Simms et al. [15],
- a second one illustrated by the Wood's Single Segment Method [18] in which the pedestrian is considered as a single two-dimensional solid (a segment),
- a third one containing the most complicated approaches based on three-dimensional multi-body models of the pedestrian (used with PC-Crash® [9, 10] or Madymo® softwares).

Data issuing from two real and well-documented (by an in-depth multidisciplinary investigation) cases have been used to test these different models. The objective consists in evaluating their potentiality and their requirements in terms of input, output, time consumption, etc.

Beyond this comparison, this study provided the opportunity for fruitful, scientific and methodological exchanges between connected ways which work towards improving the road safety policy with prevention or repression (from a forensic point of view) finalities:

- in-depth multidisciplinary investigation field [5]: it is mainly orientated towards primary safety and belongs to the research field with a clinical thought process. Based on the complexity paradigm, it studies the dysfunctions of the Human-Vehicle-Environment system and also interactions between its components, from several points of view: psychology, automotive mechanics, theoretical mechanics, road infrastructure, medicine,
- biomechanics applied to the vehicle passive safety research: it tries to understand, by experimental (for example with Post Mortem Human Subject - PMHS - tests) and theoretical approaches, the relations between vehicle design and human injury mechanism (e.g. to establish the influence of front bumper design on pedestrian lower leg injuries),

- forensic kinematic road accident reconstruction work: its aim is to provide the judicial court evidence relating to the crash sequence, the collision configuration, the impact configurations and the respective behaviour and velocity of vehicles involved for each sequence.

IN-DEPTH ACCIDENT INVESTIGATION

With regard to real data, two cases of car-to-pedestrian collision with wrap pedestrian post-impact trajectory were selected. They issue from the in-depth investigation database of a research unit (department of Accident Mechanism) belonging to the French National Institute for Transport and Safety Research (INRETS), which has been carrying out multidisciplinary studies on road accident since the beginning of the 80's [6]. In these two cases the "point" of impact and the rest position of the pedestrian were known on the accident scene.

In the first one, some skid marks are related to the front track of the accident-involved vehicle. These tyre marks, the collision configuration, the final configuration and the "point" of impact classified this case as a typical pedestrian wrap trajectory as was defined by Ravani et al [12]. Moreover, the tyre marks allow to determine the vehicle impact velocity by an alternative way expressing the kinetic energy loss as a function of the length of the marks and a mean given deceleration.

In the second one, no material evidence was related to the vehicle behaviour (deceleration beginning unknown) even if this vehicle is not equipped with an Antilock Braking System (ABS) system. This case corresponds to a pedestrian wrap trajectory regarding the vehicle-pedestrian contact sub-phase, but it is not typical (cf. relative rest position of vehicle and pedestrian). It represents a configuration in which (without a vehicle Event Data Recorder or reference crash tests) the modelling of the pedestrian impact and post-impact trajectory seems to be the only solution to determine the vehicle impact velocity.

- case No 1:
A January day, at 9 a.m., the weather is dry and sunny. A Citroën Xantia® vehicle was driving along a boulevard in urban areas. In the middle of its lane, the vehicle crashed into the right side of an old man on a pedestrian crossing. It braked in emergency before impact. The pedestrian died on the spot (see figure 1).
- case No 2:
A June day, about 8 a.m., the weather is dry and sunny. A Renault Twingo® vehicle was



Figure 1. Case No 1 (some in-depth investigation data).

driving through a village. It crashed into the left side of an old woman on a pedestrian crossing. She died as the result of her injuries the next day. The vehicle driver was a priori dazzled by the sunlight. He did not see the pedestrian and didn't begin to brake before impact (see figure 2).

MODELS

Simple Models

With regard to the first above-mentioned model category, some models with a simple mathematical formalism (even if they are the results of a great amount of research) are considered. They can be classified as analytical or semi-analytical methods. Most of the analytical ones derive from fundamental mechanics equations and correspond to a modelling of a pedestrian post-impact trajectory part: airborne and

ground-pedestrian sub-phases (see figures 3 and 4). They are based on a 2D kinematics applied to the pedestrian centre of gravity. Two usual and well-known models have been chosen: "fall and Slide" [4] and Searle's "fall, bouncing, sliding" model [13] which tries to take into account pedestrian bounces on ground (see figure 4). Their respective mathematical expression (equations 1 and 2) proposes a relation between pedestrian projection speed $V_p(t_p)$, projection angle θ , a partial throw distance $D_2 + D_3$, vertical distance H_2 between projection moment t_p and first contact on ground moment t_g , gravitational acceleration g , and pedestrian friction coefficient on ground μ_p .

$$D_2 + D_3 = V_p(t_p) \sqrt{\frac{2H_2}{g}} + \frac{V_p^2(t_p)}{2\mu_p g} \quad (1)$$

$$V_p(t_v) = \frac{\sqrt{2\mu_p g [(D_2 + D_3) - \mu_p H_2]}}{\cos(\theta) + \mu_p \sin(\theta)} \quad (2)$$



Figure 2. Case No 2 (some in-depth investigation data).

The Searle's model allows us to provide a range of predicted pedestrian projection speeds for a given partial throw distance with a mathematical lower bound (equation 3) and an arbitrary upper bound (equation 4).

$$\min\{V_p(t_v)\} = \frac{\sqrt{2\mu_p g [(D_2 + D_3) - \mu_p H_2]}}{\sqrt{1 + \mu_p^2}} \quad (3)$$

$$\max\{V_p(t_v)\} = \sqrt{2\mu_p g [(D_2 + D_3) - \mu_p H_2]} \quad (4)$$

These models are suited for typical wrap trajectories, considering the total throw distance $D_t \approx D_2 + D_3$ and the vehicle impact speed V_0 equal to:

$$V_0 = \frac{1}{PE} V_p(t_p) \quad (5)$$

where PE is defined as an impact factor [4] or a projection efficiency [17]. The use of this factor is rather empirical.

Semi-analytical models can be, on one hand, based on experimental (with dummies and PMHS tests) results or real well-documented collision data. Considered as empirical, they use regression curves between vehicle impact speed and total throw distance without modelling projection processes. On the other hand, they can derive from a statistical approach which is based on a variability study (collision parameters and circumstance factors) and on an analytical study of the three trajectory phases. These statistical models correspond to a mathematical function with a simple formalism, but are result of a great modelling way effort. Both empirical

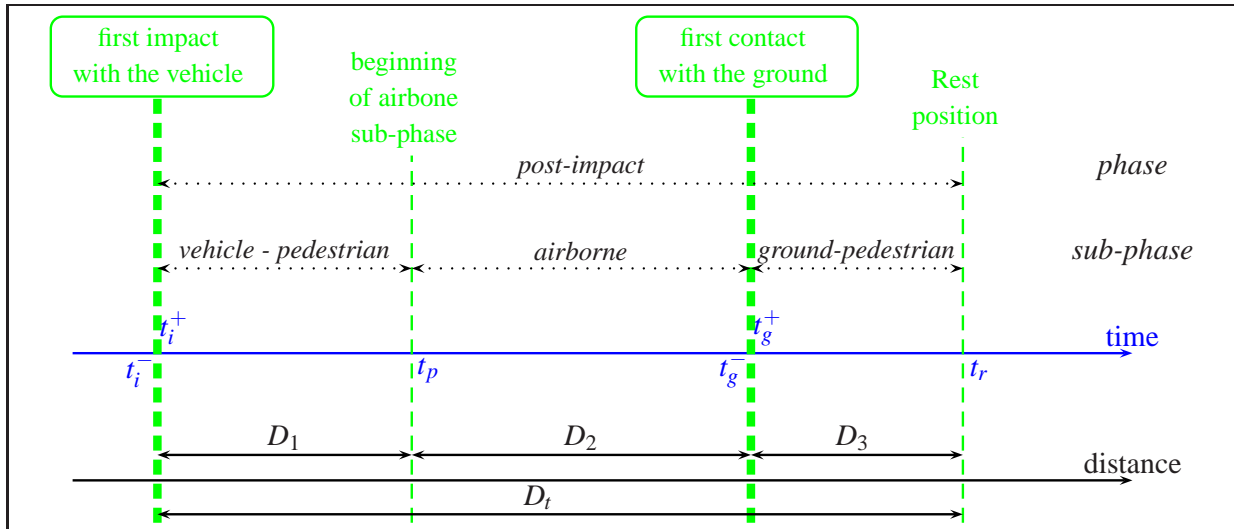


Figure 3. Schematic diagram of impact and post-impact phases corresponding to a wrap trajectory: phases, sub-phases, events, time and distance.

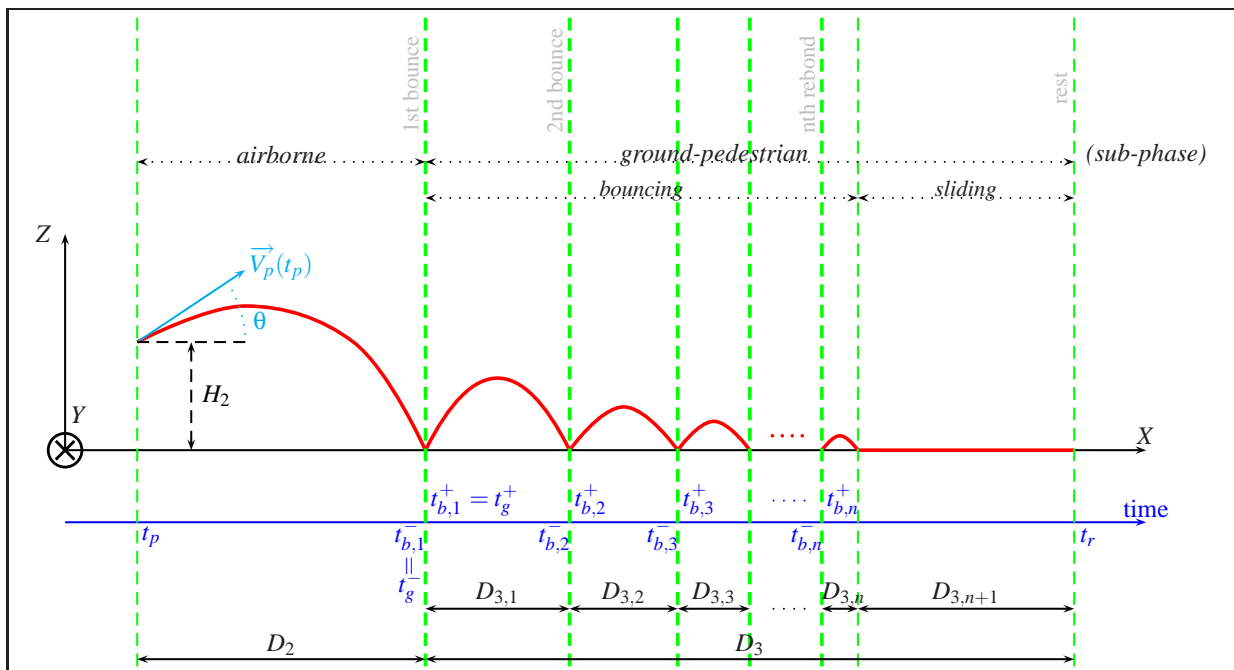


Figure 4. Schema corresponding to the pedestrian centre of gravity trajectory in Searle's model entitled "fall, bouncing and sliding" [13].

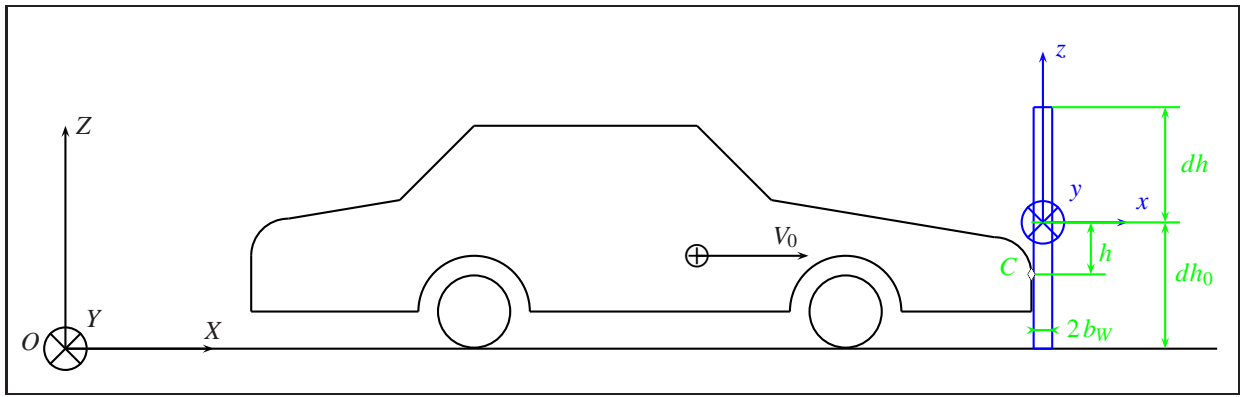


Figure 5. Schematic representation of vehicle and pedestrian segment at primary impact - illustration of some parameters used in Wood's SSM equations.

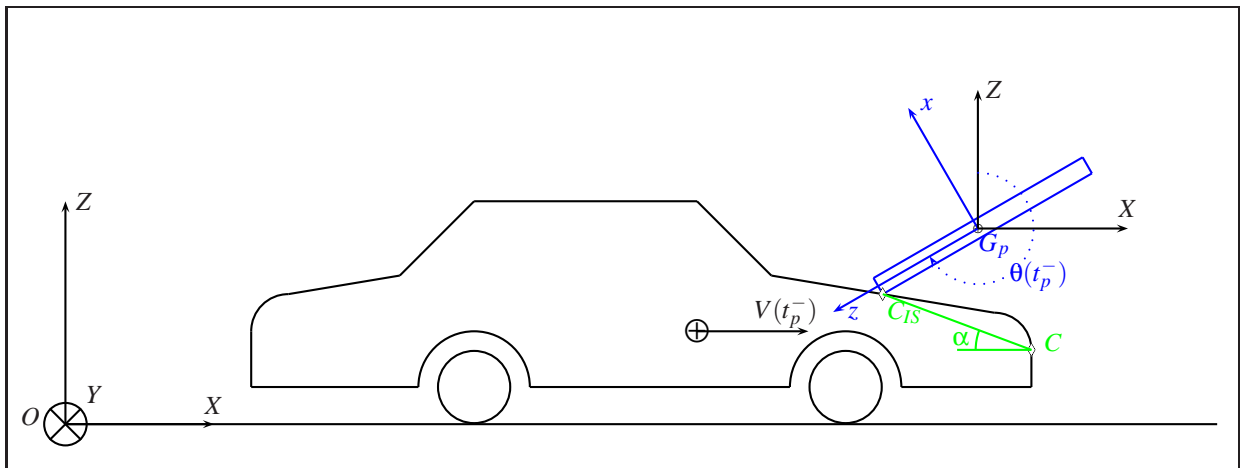


Figure 6. Schematic representation of vehicle and pedestrian segment at secondary impact - illustration of some parameters used in Wood's SSM equations.

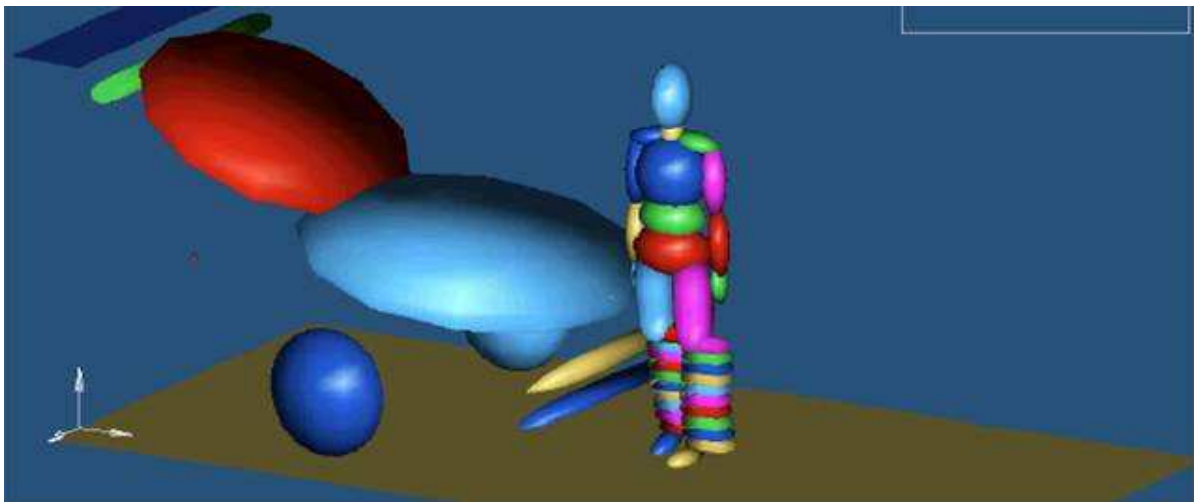


Figure 7. General view of the multibody system (Madymo).

and statistical models enable us to provide a range of value with variable degrees of certainty. Three models have been chosen: two empirical ones (cf. Rau et al. [11], (equation 6), Toor and Araszewski [17], (equation 7)) and a statistical one (cf. Simms et al. [15], (equation 8)):

$$D_t = 0.0052 V_0^2 + 0.0783 V_0 \quad (6)$$

with D_t in m and V_0 calculated in km/h (± 5 km/h).

$$V_0 = 8.25 D_t^{0.61} \quad (7)$$

with D_t in m and V_0 calculated in km/h (± 7.7 km for the 15th and 85th percentile prediction interval).

$$V_0 = \frac{m_v}{m_v + m_p} C [D_t - S_0]^D \quad (8)$$

with D_t in m, V_0 in m/s, and where C , D , S_0 are regression parameters (see [15] to chose a set of regression parameters functions of circumstances and certainty degree in order to determine lower and upper bounds) and m_v (respectively m_p) is vehicle (respectively pedestrian) mass.

Advanced Models

To illustrate the second above-mentioned model category, one model has been chosen: Wood's Single Segment Model (SSM) [18]. It is a mixed analytical formulation (equation 9) for the total post-impact trajectory. It models the vehicle-pedestrian sub-phase considering that the pedestrian could be represented by a single 2D segment (see figures 5 and 6). Then, it models the following sub-phases (airborne and ground-pedestrian) with the Searle's formula considering the pedestrian could be represented by a weighted point. It makes the assumption that there are two vehicle-pedestrian impacts: a primary impact relating to the pedestrian lower part (see figure 5) and a secondary impact relating to the pedestrian head (see figure 6).

$$D_t = \frac{V_p^2(t_p) (\cos(\theta) + \mu_p \sin(\theta))^2}{2\mu_p g} - \frac{k^2 \theta(t_p^-)}{h} + \mu_p (H_2) \quad (9)$$

with k radius of segment gyration and h vertical distance between pedestrian centre of gravity and upper contact point on the vehicle front. $V_p(t_p) \cos(\theta)$, $V_p(t_p) \sin(\theta)$, $\theta(t_p^-)$ and H_2 are functions of vehicle mass, pedestrian segment geometry, secondary impact location, vehicle braking rate, vehicle impact speed V_0 , etc. Segment angle at the beginning of secondary impact, $\theta(t_p^-)$, is more particularly a function of the following parameters:

$$\theta(t_p^-) = f(\theta(t_p^-), V_0, m_v, m_p, \alpha, h, dh, bw, g) \quad (10)$$

with α bonnet angle, dh distance between segment centre of gravity and top (head), bw segment half-width (see figures 5 and 6).

It is worth noting that this model (with a complicated formalism) was the theoretical base of some statistical models (with a simpler formalism) (e.g. Wood's Hybrid Model [19]).

Complicated Models

Concerning the third category which referred to complicated model, two softwares have been used : the PC-Crash V6.0 one and the Madymo V6.0 one. PC-Crash software is a common commercial tool to reconstruct road accidents [3]. A part of this one has been developed to take into account vehicle-pedestrian accidents with a specific pedestrian multibody model and a single body vehicle whose geometry shape is detailed [10]. This approach has been validated with dummy crash-tests and well-documented real cases [9]. The human body model chosen in this paper included 20 bodies interconnected by 19 joints. Default joint and body characteristics fitted to pedestrian mass and height are provided in the software. Eight specific measurements were used to define the front vehicle geometry. Accident configuration was fixed thanks to side pedestrian injuries and vehicle driving direction. The pedestrian position on impact was chosen standing up without speed and with both feet near each other on the ground. The simulation was iteratively used changing impact vehicle velocity and mean vehicle deceleration in order to obtain pedestrian throw distance and impact points on front vehicle measured by the in-depth investigation.

The last method concerns the pedestrian accident reconstruction using a typical multibody software which is commonly used in passive safety. The Madymo software V6.0 has been employed to develop the numerical models and to perform the simulations [16]. The whole multibody model is divided into two parts: the car and the pedestrian (see Figure 7). The human body model has been developed by the University of Chalmers (cf. Yang et al. [21]), Faurecia (cf. Glasson et al. [7]) and validated in collaboration with the Laboratory of Applied Biomechanics (see Cavallero et al. [2]). The original model represents a human body close to the 50th percentile male: 1.75 m, 78 kg. It includes 35 bodies with 35 joints and it is represented by 85 ellipsoids. Joint and body segment characteristics are based mainly on available biomechanical data (cf. Yamada [20] and Kajzer et al. [8]). The specific characteristics of this model concern its lower leg because it is predictive of fractures.

This model has already been validated qualitatively but also quantitatively in pedestrian configuration by comparison with PMHS experimental tests performed at INRETS-LBA (cf. Cavallero et al. [2]).

Concerning the real accident reconstruction, the multibody model was first adapted to the corresponding configuration of the accident: orientation of impact, anthropometry of the victim, front shape of the car. A first simulation has been performed on this starting configuration provided as being the most probable one by the in-depth investigation. Next, effects of some parameters such as car velocity or pedestrian position on impact have been numerically studied in order to find the best correlations with all indications produced by the in-depth analysis. All simulations which were not in accordance with the in-depth investigation were rejected. Finally, the configuration retained is close to the presumed real accident conditions because it reproduces in particular the same impact points on the car, the same injuries, and is according to the driver statement (cf. Serre et al. [14]).

RESULTS

Results Obtained With Simplest Models

Concerning the case No 1 (Xantia) which corresponds to a typical wrap trajectory, analytical and semi-analytical models were applied. Ranges of vehicle impact speeds were calculated for each method considering $D_t \in [16 \text{ m}, 18 \text{ m}]$ and eventual bounds (only given by Searle's method and semi-analytical ones). They are synthesized in table 1. With pa-

Table 1.
Results for case No 1 obtained with simplest methods.

method name	range of vehicle impact speeds V_0 (km/h)
fall and slide	[42,45]
Searle	[42,54]
Rau et al.	[43,57]
Toor and Araszewski	[37,56]
Simms et al.	[42,53]

parameter values $\mu_p = 0.66$ and $H_2 = 1 \text{ m}$, projection efficiency (or impact factor) was set to 1 for "fall and slide" and Searle's models. Regarding Simms et al.'s model, lower bound (respectively upper) so-called probable was chosen with regression parameters: $C = 3.2$, $D = 0.47$, $S_0 = 1.6$ (respectively $C = 3.7$, $D = 0.47$, $S_0 = 1.2$).

Concerning the case No 2 (Twingo) which does not

correspond exactly to a typical wrap trajectory, analytical methods were rejected. Considering $D_t \in [17 \text{ m}, 20 \text{ m}]$ and lower and upper bounds, semi-analytical methods were used in the same conditions as for case No 1. Ranges of vehicle speeds are summarized in table 2. According to driver statement

Table 2.
Results for case No 2 obtained with simplest methods (semi-analytical models).

method name	range of vehicle impact speeds V_0 (km/h)
Rau et al.	[45,60]
Toor and Araszewski	[38,59]
Simms et al.	[44,56]

(time-lag braking) and lack of tire marks on ground, low part of vehicle impact speed range would be selected.

Results Obtained With Wood's SSM

Wood's Single Segment Model assumes that the vehicle decelerates at impact. So it needs a vehicle coefficient friction μ_v to model the interaction between vehicles and pedestrians in terms of primary and secondary segment impacts in vehicle-pedestrian sub-phase. Therefore, Wood's SSM was only used for case No 1. For this case, angle α was varied in the range $[0.20 \text{ rad}, 0.30 \text{ rad}]$ also using different values for impact speed V_0 . Throw distances D_t calculated between 16 m and 18 m allowed us to determine solutions in terms of V_0 . Segment characteristics (location of gravity centre, radius of gyration k) were fixed using the approach recommended by Burg and Rau [1]. In this way, V_0 was determined as belonging to the range $[48 \text{ km/h}, 56 \text{ km/h}]$.

Results Obtained With Multibody Models

Use of the PC-Crash Software

With PC-Crash software, the two cases were treated using its default multibody models. Two pedestrian multibody models are included in the version 6.0 of this software. The one which was used has been validated with dummy crash-tests [9, 10] and seems to give for the two accident cases better results than the other one. The main differences are in the values of the friction coefficients between pedestrian/car and pedestrian/ground both equal to 0.6 for the model we have used and 0.4 and 0.2 for the second one.

Concerning the accident case No 1, the reconstruction results gave an impact speed of 48 km/h for

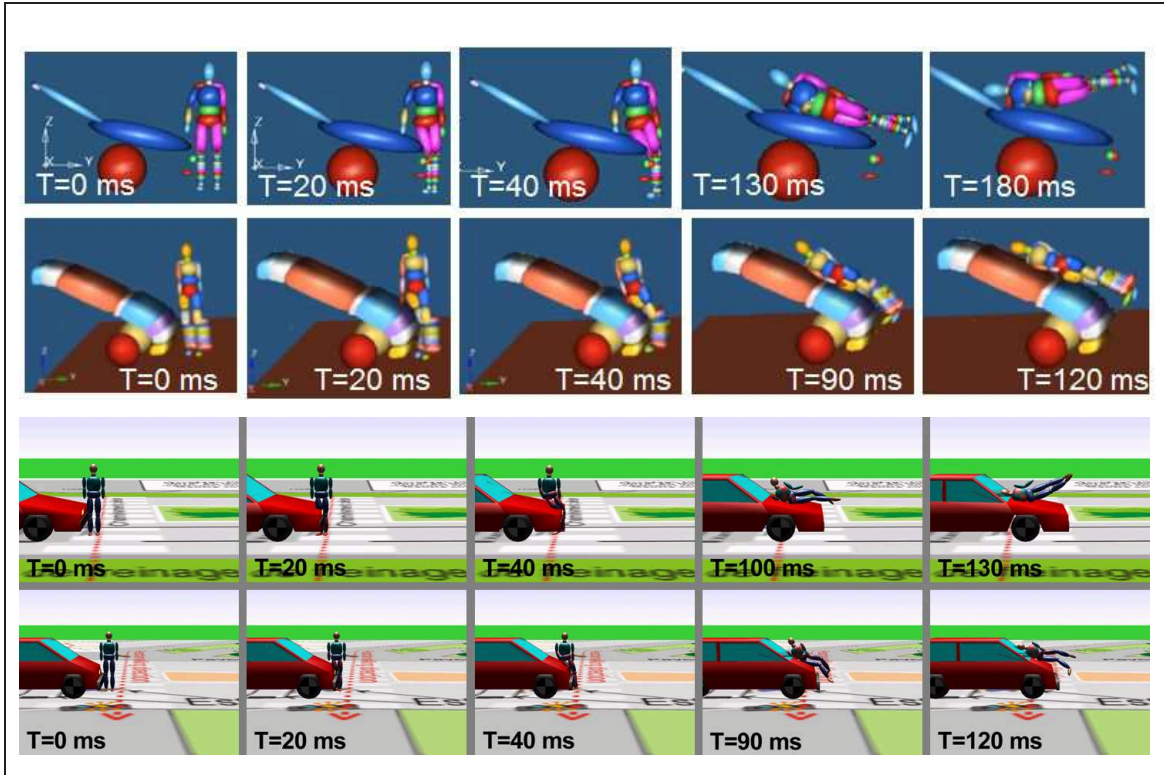


Figure 8. Multibody simulation of the two real accidents with Madymo (line 1: case No 1 (Xantia), line 2: case No 2 (Twingo)) and PC-Crash (line 3: case No 1 (Xantia), line 4: case No 2 (Twingo)).

Table 3.

synthetic table of vehicle impact speed V_0 and pedestrian throw distance D_t obtained (or used) by the different methods for real cases No 1 & 2.

method category	method name	case No 1		case No 2		comments
		V_0 (km/h)	D_t (m)	V_0 (km/h)	D_t (m)	
	in-depth investigation	55	16	[40,45]	19	V_0 evaluated or calculated, D_t measured and evaluated
simple	fall and slide	[42,45]	[16,18]	rejected		D_t input, V_0 output
	Searle	[42,54]	[16,18]	rejected		
	Rau et al.	[43,57]	[16,18]	[45,60]	[17,20]	
	Toor and Araszewski	[37,56]	[16,18]	[38,59]	[17,20]	
	Simms et al.	[42,53]	[16,18]	[44,56]	[17,20]	
advanced	Wood's SSM	[48,56]	[16,18]	rejected		iterative process to determine V_0
complicated	PC-Crash V6.0 pedestrian model	48	16	35	20	
	Madymo V6.0 + specific pedestrian model	50	17	40	18	

the car and a throw distance of 16 m for the pedestrian. The calculated pedestrian final position was quite good for the X axis (in the car way of travelling) but not so good for the Y axis (perpendicular to the car way of travelling) with a difference of 3.5 m with reality. In the simulation, the car stopped 3 m before the real rest position of the car. The calculated pedestrian impact areas on the car were coherent with car deformations (see figures 1 and 8), except for the hip impact which was too high on the car bonnet (T=40 ms). However, a relatively important penetration of the pedestrian into the car body (T=40 ms, for both cases) was observed showing the difficulty of contact modelling. During the airborne sub-phase, the pedestrian trajectory corresponded to a somersault. Such pedestrian kinematics did not square with the Madymo simulation and neither with PMHS crash-tests for this range of impact speed.

For the accident case No 2, the impact speed of the car is calculated to 35 km/h and the pedestrian throw distance to 20 m. For this case, both final positions, car and pedestrian, were in good coherence with the reality. The simulation provided impact areas on the car coherent with those observed by in-depth investigation. As in the precedent case, the calculated pedestrian trajectory corresponded also to an improbable somersault during the airborne sub-phase.

Use of the Madymo Software

With regard to the more complicated method based on the Madymo software, the accident reconstruction can be decomposed into two phases: the numerical model adaptation and the parametric study. Time consumed to perform both works is about 1 week and numerical simulations last less than 1 hour on a classical PC computer.

Model adaptation concerns the representation of the car, the pedestrian and the definition of an initial accident configuration. Input data are thus a short description of the anthropometry of the pedestrian (height and weight), geometry and mechanical characteristics of the car and an initial impact speed of the car to start the parametric study. This parametric study concerns mainly the velocity of the car, the position of the pedestrian at impact and the pitch angle during the braking phase. Output data concerns qualitative information such as injuries but also quantitative ones such as an accurate impact speed of the car, impact areas of the pedestrian with the car and the throw distance.

Concerning the case No 1 (Xantia), a first simulation was performed on the configuration provided by the in-depth investigation. Car speed was fixed to 55 km/h. Pedestrian was placed in a walking posi-

tion from the left to the right side of the car in order to be impacted on the right side of his body. The configuration retained during the parametric study was the one which reproduced closely the same impact area and the same injuries reported by the in-depth investigation. Four impacts during the simulated kinematic were observed: the lower leg on the bumper, the upper leg on the low bonnet, the shoulder on the high bonnet, the head on the windscreen (see figure 8). Compared to the real injuries, tibia fractures were observed numerically on the third superior part but not on the femur. The retained impact speed for the car was finally 50 km/h and the throwing distance 17 m.

For case No 2 (Twingo), initial car speed was fixed to 45 km/h and the pedestrian position placed in walking posture with the right leg put forwards. After the parametric study, the retained configuration provided a kinematic in accordance with the in-depth accident investigation (see figure 8). Same impact areas were found and fracture on the superior third of the lower leg was simulated. Car speed was finally found equal to 40 km/h and the throw distance close to 18 m.

DISCUSSION

In order to compare the methods in terms of quality of real accident reconstruction, their numerical results corresponding to the case No 1 and No 2 were reported on table 3.

The case No 1 corresponds to a typical wrap trajectory for which skid marks of emergency braking allow us to have a good estimation of the vehicle impact speed (55 km/h). All the methods - except the fall and slide model - provide a solution for vehicle speed on impact compatible or close to the in-depth investigation estimation.

For the case No 2, the vehicle impact speed has been chosen by in-depth investigation as equal to 40-45 km/h. These values have been evaluated from comparison of vehicle damage with those observed on a crash-test (same vehicle, impact speed 32 km/h, PMHS) performed by INRETS-LBA. This case No 2 represents a non typical wrap trajectory (no vehicle deceleration at impact or time-lag after impact) for which the analytical simple and advanced model (e.g. Searle's model) are not suited in term of sub-phase modelling. Therefore, they have not been used contrary to the others methods (semi-analytical simple models and 3D multibody model). From a theoretical point of view, this case highlights limits of the analytical methods (simple and advanced) which didn't take into account enough the contact phase.

Table 4.
Comparative matrix for the different methods.

Complication level	method name	inputs	outputs	precision preconised by author's method	operation bringing time (rough)	computer calculation time	field application
simple	fall and slide [4]	$H_2, D_1 + D_3, \mu_p, PE$	V_0	no element	few minutes	immediate	typical wrap and forward trajectory
simple	Searle [13]	$H_2, D_1 + D_3, \mu_p, PE$	$\min\{V_0\}, \max\{V_0\}$	mathematical lower bound and arbitrary upper ground	few minutes	immediate	typical wrap and forward trajectory
simple	Rau et al. [11]	D_t	V_0	± 5 km/h (corridor)	few minutes	immediate	wrap trajectory
simple	Toor and Araszewski [17]	D_t	V_0	± 7.7 km/h for the 15 th and 85 th percentile prediction interval, ± 12.2 km/h for the 5 th and 95 th one (corridor)	few minutes	immediate	wrap trajectory
simple	Simms et al. [15]	D_t, m_v, m_p , set of regression parameters	$\min\{V_0\}, \max\{V_0\}$	upper and lower bounds depending on degree of certainty (probable, normal, overall)	few minutes	immediate	wrap trajectory
advanced	Wood'SSM [18]	$V_0, m_v, m_p, \alpha, h, dh, bw, k, \mu_p, \mu_v$	V_0, D_t	see statistical models derived from it (e.g. [15])	half an hour	few seconds for one step of the iteration process	typical wrap trajectory
complicated	PC-Crash V6.0 pedestrian model [9, 10]	veh. geometry, m_v , veh. deceleration, V_0 , impact areas, veh. and ped. positions on impact, ped. height, m_p, D_t	V_0 , impact areas, veh. and ped. positions on impact, D_t , 3D kinematics and dynamics	qualitative and quantitative validation based on input/ouput parameters comparison	one day	few minutes for one step of the iteration process	frontal impact + possible use for other configurations with attention to the validation
complicated	Madymo V6.0 + specific pedestrian model [16, 21, 7]	veh. geometry, m_v , veh. deceleration, V_0 , impact areas, veh. and ped. positions on impact, ped. height, m_p, D_t , injuries	V_0 , impact areas, veh. and ped. positions on impact, D_t , 3D kinematics and dynamics, injuries	qualitative and quantitative validation based on input/ouput parameters comparison	one week	less than an hour for a step of the iteration process	frontal impact + possible use for other configurations with attention to the validation

Reconstructions performed with PC-Crash and Madymo allow us to compare also kinematics. It has been observed good accordance in the both timing of the vehicle-pedestrian sub-phases (cf. figure 8).

Concerning the comparison of the different methodologies, some criteria have been reported in a general matrix and summarized in table 4. It concerns their requirements (inputs, outputs, computer time, into operation bringing time), their precision (if it is defined by their reference authors) and their field of application (validity domain). Concerning the operation bringing time, it includes, if necessary, the time for measuring specific element such as the vehicle geometry, preparing the adaptation of the pedestrian multibody model, performing the parametric study with the simulation tool, operating results. This general matrix illustrates the relation between the complication increase of mechanical model and the improving of findings related to particular car-pedestrian collisions with a wrap trajectory.

In the first category of methods, analytical and semi-analytical models with simple formalism and very few inputs propose relations (sometimes with lower and upper bounds) between vehicle impact speed and pedestrian throw distance projection. In these relations, the pedestrian position on impact and the vehicle geometry for example are not explicitly used. They rather contribute to the formulation assumptions (e.g. definition of the collision type as a wrap trajectory) which allows us to utilize these simple methods.

In the second category, some more advanced two-dimensional methods like the Wood's SSM try to relate vehicle impact deceleration and speed on impact, throw distance and a few parameters concerning respectively pedestrian and vehicle geometry. The equations obtained in that way are solved iteratively in order to determine an accurate vehicle impact speed. Their assumptions are too simplistic to describe exactly the sub-phase where the pedestrian is in contact with the vehicle. As their equations are moreover difficult to solve, either they are used as a theoretical base for statistical methods (with simpler formalism), or the use of more complicated methods is preferred.

In the third category, the most complicated methods, i.e. the three-dimensional multibody models (used in biomechanics applied to the vehicle passive safety), allows us to relate directly: pedestrian throw distance, vehicle acceleration and velocity during the vehicle-pedestrian contact sub-phase, collision configuration, impact areas on the vehicle

front, pedestrian injuries. Their solution in the context of a real accident reconstruction implies an iterative process which is due to a parametric study. This parametric study has been done for the PC-Crash method only for the car impact speed when it has been done for more variables for the Madymo method: car speed, pitch angle of the car due to braking phase, pedestrian position on impact [14]. Validation of real accident reconstructions performed by these softwares is made mainly with the pedestrian throw distance and the location of the impact points on the car. The Madymo method can allow us to add a validation regarding pedestrian injuries with specific biomechanics models. The application of PC-Crash and Madymo methods in two simple real cases of wrap trajectory highlighted:

- the three-dimensional multibody models are the best-fitted methods to describe the complexity of these collision events,
- they are rather time consuming,
- their accurate and complete utilization is still the appanage of parameterization specialists (in vehicle design, in biomechanics, in medicine, ...) who know about or take part in their experimental validation.

The PC-Crash software uses an important number of parameters to model a pedestrian accident. Most of them are given by default with the software and the results of the accident reconstruction are very sensible to their variations. The apprehension of what they represent of the reality of these complex phenomena is often difficult. Thus the use, apparently "easy", of the PC-Crash software by non specialist users can be dangerous. The PC-Crash technical guideline should be more detailed on the definitions, descriptions, and influences of the numerous parameters needed to compute a reconstruction. The Madymo software method needs also and even more numerous parameters. But because this software is more complicated, its use is reserved to experts in the field of accident analysis and biomechanic.

From a general point of view, the increase in complication of the models corresponds so to the direct use of supplementary material data either as input data (e.g. very detailed geometrical vehicle and pedestrian description) or as validation parameters (e.g. calculated impact areas on the vehicle) which are the simulation results at a step of an iterative process. This approach is particularly pertinent for the in-depth investigation and the forensic field in order to take advantage of the most material

evidence possible by means of hypothetic-deductive models. The adequate use of the multibody models corresponds however to update, multidisciplinary and extensive knowledge with regard to input data (e.g. human body segment inertial parameters) and validity domain of different modellings (e.g. contact modelling between ellipsoids, parts of multibody model).

CONCLUSION

This work was focused on the comparison of different methods allowing real pedestrian accident reconstructions corresponding to a wrap trajectory. This kind of trajectory can be modelled in terms of vehicle impact speed and throw distance with simple formalism models. Methods with different levels of complication were tested with two sets of real data issued from in-depth investigation. They have been classified into three categories: simple, advanced and complicated. For this well-known configuration of vehicle pedestrian collision, the aim was to illustrate in what proportion the increase in complication of a model can improve results in terms of quality. Simple and advanced methods give good results but their validity domain are restrictive (wrap trajectory and forward projection). The increase in complication of the models corresponds to the direct use of supplementary material data either as input data (e.g. very detailed geometrical vehicle and pedestrian description) or as validation parameters (e.g. calculated impact areas on the vehicle). In particular the 3 dimensional multibody models initially developed for passive safety research allow us to relate most of relevant parameters (speed vehicle, impact areas, injuries, ...) of the pedestrian accident. Their applications to the reconstruction are very interesting in the in-depth investigation and forensic fields. It would enable us to achieve reconstruction of other types of collision involving pedestrian (e.g. vehicle frontal impact with fender vault post-impact trajectory, vehicle corner impact), even if there is a lack of material evidence (e.g. no skid mark for an ABS equipped vehicle). That could be possible if the multibody models could be refined and validated for these sorts of real collision configurations. This validation could be based on experimental tests (for example crash-tests using PMHS) reproducing real accident configuration instead of standard ones. Connected to the complementary vehicle primary and passive safety, and the forensic road accident reconstruction, this work would lead to the improvement of the pedestrian safety. It also could be extended to other vulnerable road users such as bicyclists.

ACKNOWLEDGEMENTS

This work is partly supported by the French Transport Ministry (DSCR) and is partly included in the framework of the APPA project (Amélioration de la Protection du Piéton lors de collision par des Automobiles).

REFERENCES

- [1] BURG and RAU. 1981. *Handbuch der Verkehrsunfallrekonstruktion*. Verlag Information Ambs GmbH.
- [2] C. CAVALLERO, D. CESARI, M. RAMET, P. BILLAULT, J. FARISSE, B. SERIAT-GAUTIER, and J. BONNOIT. 1983. Improvement of pedestrian safety: Influence of shape of passenger car-front structures upon pedestrian kinematics and injuries: Evaluation based on 50 cadaver tests. *ASME Paper*, (830624).
- [3] Dr. Steffan Datentechnik, LINZ AUSTRIA. july 1999. PC-CRASH - A simulation program for vehicle accidents - Version 6.0, 6th edition.
- [4] Jerry J. EUBANKS et Paul F. HILL. 1998. *Pedestrian Accident Reconstruction and Litigation*. Lawyers & Judges Publishing Co, Inc., second edition.
- [5] F. FERRANDEZ, T. BRENAC, Y. GIRARD, D. LECHNER, J.-L. JOURDAN, J.-E. MICHEL, and C. NACHTERGAELE. 1995. *L'étude détaillée d'accidents orientée vers la sécurité primaire*. Presses de l'Ecole Nationale des Ponts et Chaussées.
- [6] Y. GIRARD. 1993. In-depth investigation of accidents: the experience of INRETS at Salon-de-Provence. In *International congress on Safety evaluation of traffic systems: traffic conflicts and other measures, ICTCT Congress, in Salzburg*.
- [7] E. GLASSON, J. BONNOIT, C. CAVALLERO, and F. BASILE. 2000. A numerical analysis of the car front end module regarding pedestrian lower limb safety. In *Part of Vehicle Safety 2000, International Conference*, number C567/016/2000, pages 79–91. Institution of Mechanical Engineers.
- [8] Janusz KAJZER, Yasuhiro MATSUI, Hirotoishi ISHIKAWA, Günter SCHROEDER, and Ulrich BOSCH. 1999. Shearing and bending effects at the knee joint at low speed lateral loading. *ASME Paper*, (1999-01-0712).

- [9] Andreas MOSER, Heinz HOSCHOPF, Hermann STEFFAN, and Gustav KASANICKY. 2000. Validation of the PC-Crash pedestrian model. *ASME Paper*, (2000-01-0847).
- [10] Andreas MOSER, Hermann STEFFAN, and Gustav KASANICKY. 1999. The pedestrian model in PC-Crash - the introduction of a multi body system and its validation. *ASME Paper*, (1999-01-0445).
- [11] Hartmut RAU, Dietmar OTTE, and Burkhard SCHULZ. 2000. Pkw-Fußgängerkollisionen im hohen Geschwindigkeitsbereich Ergebnisse von Dummyversuchen mit Kollisionsgeschwindigkeiten zwischen 70 and 90 km/h. *Verkehrsunfall und Fahrzeugtechnik*, 12:341–350.
- [12] B. RAVANI, D. BROUGHAM, and R. T. MASON. 1981. Pedestrian post-impact kinematics and injury patterns. *ASME Paper*, (811024).
- [13] John A. SEARLE and Angela SEARLE. 1983. The trajectories of pedestrians, motorcycles, motorcyclists, etc., following a road accident. *ASME Paper*, (831622).
- [14] T. SERRE, C. PERRIN, M. BOHN, and C. CAVALLERO. 2004. Detailed investigations and reconstructions of real accidents involving vulnerable road users. In *Expert Symposium on Accident Research 2004*.
- [15] C.K. SIMMS, D.P. WOOD, and D. G. WALSH. 2004. Confidence limits for impact speed estimation from pedestrian projection distance. *International Journal of Crashworthiness*, 9(2):219–228.
- [16] TNO Automotive. 2001. *Theory manual - Madymo V6.0*.
- [17] Amrit TOOR and Michael ARASZEWSKI. 2003. Theoretical vs. empirical solutions for vehicle/pedestrian collisions. *ASME Paper*, (2003-01-0883).
- [18] D.P. WOOD. 1988. Impact and movement of pedestrians in frontal collisions with vehicles. In *Proceedings of Institution Mechanical Engineer*, volume 202 n°D2, pages 101–110.
- [19] D.P. WOOD and C.K. SIMMS. 2000. A hybrid model for pedestrian impact and projection. *International Journal of Crashworthiness*, 5(4):393–403.
- [20] YAMADA. 1970. *Strength of biological materials*. Williams & Wilkens.
- [21] J.K. YANG, Heinz LÖVSUND, C. CAVALLERO, and J. BONNOIT. 2000. A human body 3D mathematical model for simulation of car-pedestrian impacts. *Journal of Crash Prevention and Injury Control*, 2(2):131–149.

CORRELATION OF DIFFERENT IMPACT CONDITIONS TO THE INJURY SEVERITY OF PEDESTRIANS IN REAL WORLD ACCIDENTS

Jikuang Yang

Jianfeng Yao

Chalmers University of Technology, Sweden

Dietmar Otte

Hannover Medical University, Germany

Paper Number 05-0352

ABSTRACT

This study aimed to investigate the correlation of different impact conditions to the injury severity and impact biomechanics of pedestrians in real world accidents, and study the tolerance level with focus on head-brain of adults and children via in-depth analysis and reconstructions of real world accidents.

For this purpose, 188 pedestrian accident cases were selected from existing accident databases. Of which 186 cases obtained from GIDAS (German In-Depth Accident Study) documented by Accident Research Unit at Medical University Hannover in Germany, and 2 cases from Sweden. For each collected case, complete information regarding pedestrian injuries, accident cars, and crash environment was registered based on hospital clinical record and police report. In order to find the correlation of injuries observed in accident with physical parameters during a collision, reconstructions of selected 8 adult- and 12 child-pedestrian cases were conducted by using pedestrian and passenger car models. The pedestrian models were generated based on the height and weight of pedestrians involved in accidents. Each car model was built up based on the corresponding accident car. The mechanical properties of the accident cars were defined based on available data from EuroNCAP tests.

The correlations of calculated injury parameters with injury outcomes registered in the accident database were determined. Influences of impact conditions and pedestrian initial moving posture on HIC value were analyzed and discussed. Furthermore, the relative importance of the factors was determined according to their effects on various injury parameters. The difference of injury distribution and dynamic responses of pedestrians at various body sizes for adult and child were analyzed, which would provide background

knowledge to develop safety counter-measures and protection devices.

INTRODUCTION

The pedestrians are the most vulnerable road users who exposure a high risk in road traffic collisions with motor vehicles. Each year, about 1.2 million people are killed in road vehicle traffic worldwide, of which the pedestrians account for a large part of the traffic fatalities, especially in low- and middle-income countries. In high-income countries, car occupants account for a large majority of road users and the majority of road traffic deaths. Nevertheless, even there, pedestrians, cyclists and moped and motorcycle riders have a much higher risk of death per kilometer traveled [1].

The studies in Europe [2-4] indicated that the passenger cars are most commonly involved in pedestrian accidents. Figure 1 shows a distribution of vehicle type in pedestrian accidents which based on accident data from Swedish national accident database STRADA.

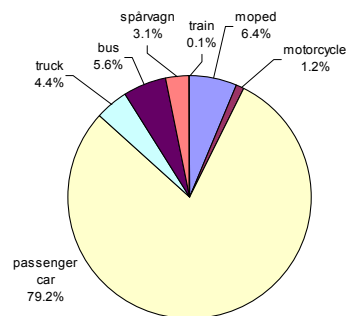


Figure 1. Involved vehicle types in pedestrian accidents based on Swedish national accident database STRADA (1999-2004).

During the past three decades significant reductions in pedestrian fatalities have been achieved in Europe [5] and the United States [6]. This tendency is mainly due to improved traffic planning in built-

up areas. Other safety program such as appropriate speed limits, drink driving control, education of young people could also contribute to the reduction of casualties. So far, there is not any statistical study to prove that injury reduction is caused by changes of car-front shape, but the findings from studies suggest that a potential benefit can be obtained from improvement of new vehicle designs which meet the EEVC requirements.

A study on pedestrian accidents is presented in this paper with focus on detailed individual case analysis via accident reconstruction using the mathematical models. The objective of the study is to determine the correlations of impact conditions and dynamic responses with the injuries and injury severity of pedestrians from accident. The results were analyzed and discussed in terms of data collection, estimating vehicle impact speeds, pedestrian moving speeds and initial posture, secondary ground impact, as well as impact biomechanics.

METHOD AND MATERIALS

Accident cases were selected from the accident database GIDAS (German In-Depth Accident Study) documented by Accident Research Unit at Medical University Hannover [7, 8]. In the district of Hannover a representative sampling of accidents is carried out by order of the German Government (Federal Highway Research Institute BAST) in co-operation with the car manufacturers. A general statistics analysis was carried out with the collected sample cases. Reconstructions were conducted using selected cases from the whole samples. The results from accident reconstructions were analyzed and discussed.

Selection of Accident Cases

For the purpose mentioned above, 188 pedestrian accident cases were selected from Hannover Medical University, of which 117 adult- and 69

child-pedestrian accident cases, and 2 cases from Sweden. For each collected case, complete information regarding pedestrian injuries (AIS1+), damage of accident cars, and crash environment was registered based on hospital clinical record and police report. The anthropometric data of pedestrian such as age, gender, height, and weight were also documented in the hospital. Accident witnesses were investigated to obtain the accident information such as pedestrian posture, impact direction etc.

The passenger cars involved in the accidents were recorded with detailed information about car makers, model, registration year, estimated impact speed. The selected cases were limited with accident car introduced to the market after 1990. The deformation pattern, contact points on the car and characteristics of special traces on the road and on the car were measured and documented in a 3D coordinate system with reference to longitudinal central line of vehicle. Pictures of impact location are documented and could be used for analysis. The final positions of the pedestrian and car were also recorded. Thus these accidents reflect the most up to date pedestrian accident characters.

Selection of Accident Cases for Reconstruction

Further screening the collected cases was carried out for reconstructions that request very detailed accident data in pre-crash, crash, and post crash phases. The requested data are summarized in Table 1. It is necessary to mention here that some information for accident reconstruction is not possible to acquire from field investigation, such as the vehicle front stiffness, and kinematics of the pedestrian collision.

In the present study, 8 adult cases and 12 child cases were selected for accident reconstructions. Two examples are described in following section.

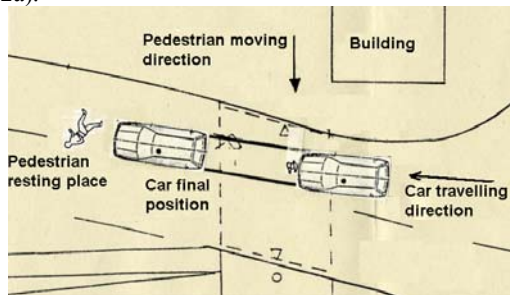
Table 1. Summary of accident data collection for reconstruction in case 1

	Pre-crash	Crash	Post crash
Vehicle	- Travel speed - Pre-crash braking - Driver maneuver	- Impact speed - Contact point	- Maker, model, year, weight - Damage (dents, scratch)
Pedestrian	- Initial posture - Moving speed - Orientation	Grass Kinematics Wrap around distance Throw distance - Landing point - Sliding distance - Resting point Ground impact mode - Body contact	- Gender, Age, Height, Weight Injuries - Injury patterns - Injury distribution - Severity - Cause of injury
Road and Environment	- Road type - Road surface - Weather condition	Ground impact	- Skid mark and other traces

Example Case 1: Adult Pedestrian Accident

Pre-crash

A passenger car-to-pedestrian accident happened in a residential area in Hannover, Germany (Figure 2a).



(a)



(b)

Figure 2. (a) Scheme of accident scene, (b) the location of head impact on windscreen and pelvis impact on hood top.

The accident car is a VW Golf III 1993 model. The car was traveling over a cross in which corner standing a building. A 70-year-old male walked fast behind the building to cross the street. Because of the building, the driver could not see the man in advance. After the driver saw the man, he braked hard but still hit the man. The impact speed was about 43 km/h.

Crash

The car hit the left leg by the right side of the bumper. The head impacted against the windscreen. The scratches and damages of the vehicle are shown in Figure 2b. The man was thrown away for about 11 m.

Post crash data

The man sustained laceration wound at the head, oedema of the brain, concussion and fracture at the left tibia.

Example Case 2: Child Pedestrian Accident

Pre-crash

A passenger car-to-child pedestrian accident occurred in a resident area in Hannover, Germany.

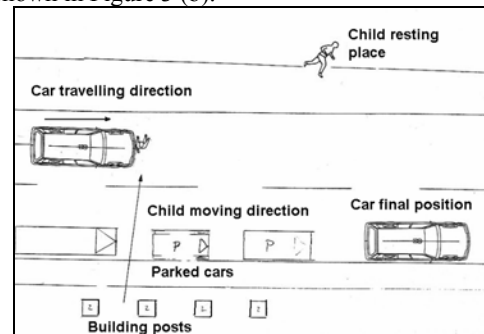
The accident car is an OPEL Omega Combi 1994 model. The car was traveling on a street where several vehicles were parking along right side (Figure 3a). A 4-year-old boy walked fast to cross the street. Because of the parked car, the driver could not see the boy in advance. After the driver saw the boy, he braked hard but still hit the boy. The impact speed was about 25 km/h.

Crash

The car hit the child by the left front part. The boy was thrown away and the throw distance was about 6 m.

Post crash data

The child sustained AIS 2 head injury, AIS 1 lower extremity injury. On the vehicle, scraps on the bumper and dents on the hood were found as shown in Figure 3 (b).



(a)



(b)

Figure 3. (a) Scheme of accident scene, (b) Scraps and dent on the accident car

Accident Reconstructions

The selected accident cases are reconstructed using pedestrian models and passenger car models. The reconstructions were carried out by using MADYMO program.

The Set-up of Reconstruction Models

The anthropometric data of the pedestrian models used in the reconstructions are summarized in Table A1 (Appendix), which based on the height and weight of pedestrians involved in accidents.

The pedestrian models were generated by GEBOD code in MADYMO program for both adults and children. The characteristics of the adult models was defined based on a validated human body model [9, 10]. The characteristics of child models were scaled from the validated adult pedestrian model.

The car models were built up based on the corresponding accident car. The geometry of the car models was obtained from the drawings of the production cars that had the same make, model and series as those involved in the accidents. The mechanical properties of the car models were defined in terms of stiffness properties acquired from Euro NCAP sub-system tests.

The impact speeds of the cars and the pedestrian moving speeds were estimated based on the accident data, considering the car braking skid marks on the road surface and the pedestrian moving postures before the impact. The friction coefficient between the wheels and road surface was defined according to road surface conditions. The diving angle of emergency braking and steering effect were also simulated. The Figures 4a and 4b show the reconstruction models for example adult and child accidents.

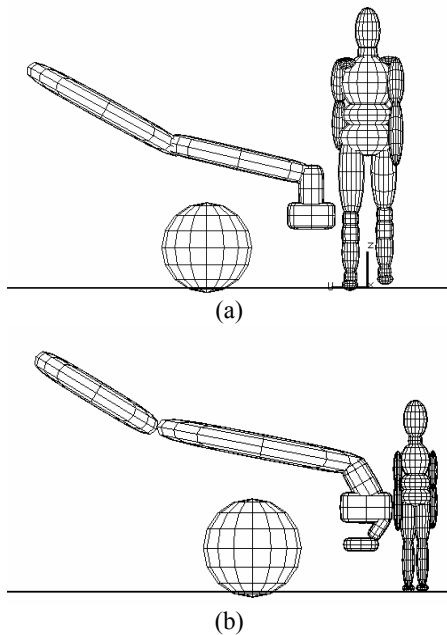


Figure 4. Simulations of (a) adult pedestrian accident, (b) child pedestrian accident.

The kinematics was simulated in reconstructions of the selected accident cases. The injury parameters in head, chest, pelvis and lower extremities were calculated to evaluate the injury severities from the accidents. The correlations of the output parameters from simulations with the injuries described in medical and accident report were analyzed. The

threshold of brain injury parameters, such as HIC was discussed based on reconstruction results.

RESULTS

General Statistic Analysis

The initial posture at the moment of impact was determined at running, fast walking, walking or standing. Figure 5 shows that half of children were running but only 2% children were standing when they were hit by the vehicle. This is remarkable comparing to the situation of adult pedestrians (7% running). The accident data also showed that 82% adults and 87% children were impacted from the lateral direction.

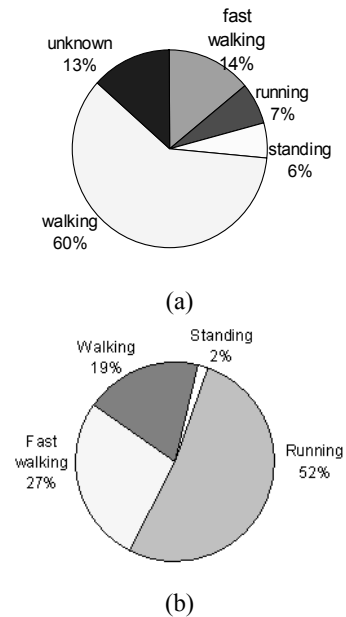


Figure 5. Pedestrian moving posture at the moment of impact: (a) adults, and (b) child.

The injury distribution of pedestrian is shown in Table 2. It was observed that the head and the lower extremities were the two most frequently injured body parts during the accidents for both adults and children, but adult lower extremities are more frequently injured than children. For AIS 2+ injuries, head injuries accounted for 30.9% for adults and 56.4% for children, respectively.

Table 2. Injury distribution by body regions

Body	AIS 2+		All injuries	
	Adult	Child	Adult	Child
Head	30.9%	56.4%	25.9%	33.1%
Neck	4.3%	0.0%	5.0%	1.8%
Thorax	12.8%	7.7%	12.0%	5.5%
U-Limbs	7.4%	12.8%	16.6%	20.9%
Abdomen	1.1%	0.0%	1.9%	3.0%
Pelvis	5.3%	0.0%	6.2%	8.6%
L-Limbs	38.3%	23.1%	32.4%	27.0%

Reconstruction Analysis

Overall kinematics of pedestrian

The contact location of head on the vehicle could be defined by the wrap-around distance (WAD) along the car-front surface. Results from accident reconstructions show that the WAD is influenced by the pedestrian height and impact speed. Table A2 (Appendix) shows the overall kinematics of pedestrians from reconstructions. The wrap around distance was close to the information collected by police.

Head impact conditions

The head impact conditions to the car front were determined for each case in terms of head resultant impact velocity relative to the car, head impact angle relative to the horizontal, head impact location, as well as timing of head impact.

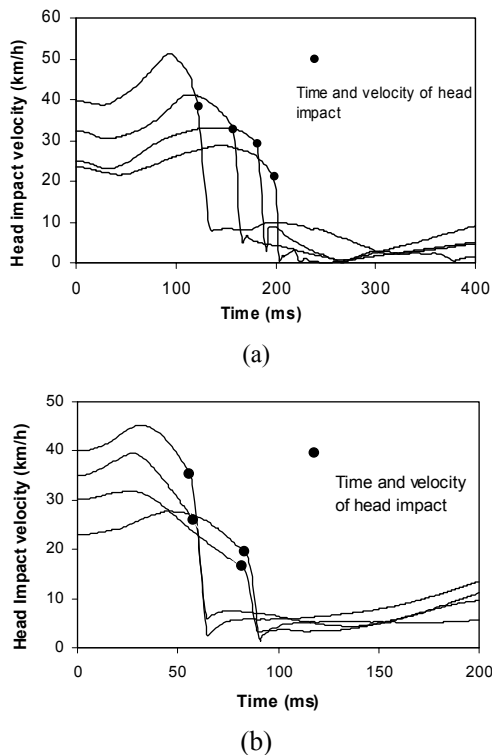


Figure 6. The time history of head resultant velocity relative to car front: (a) adult, (b) child.

Figure 6a and 6b illustrate the time history of the head resultant velocities for 4 adults with the height of around 170 cm and 4 children with the same height of 120 cm. The head impact timing varies from 123 ms to 199 ms for the adults, and from 56 ms to 83 ms for children. The results indicated that the head impact timing varied in a wide range due to vehicle speed and size of the pedestrians.

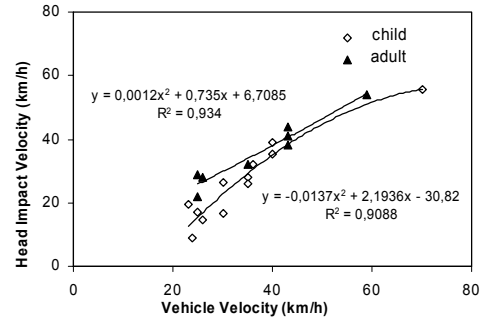


Figure 7. Relationship between head impact speed and vehicle speed

The head impact speed appears to be proportional to vehicle impact speed as shown in Figure 7. Normally, the child head impact speed is lower than the vehicle travel speed at the moment of impact.

The head impact angle could be greatly influenced by several factors such as the pedestrian height, hood edge height, hood angle and impact speed. The individual contribution of each factor to the head impact angle should be investigated using more detailed parameter studies. Figure 8 shows the relationship between head impact angle and vehicle velocity. The results showed that the head impact angle usually decreases with the increasing of vehicle impact speed for both adult and child.

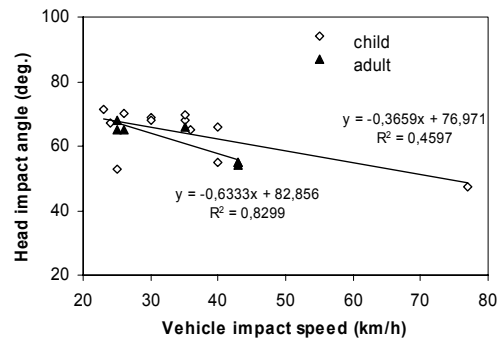


Figure 8. Relationship between the vehicle impact speed and head impact angle

Calculated injury parameters

The head injury risks were evaluated by calculating HIC as shown in Table A3 (Appendix). The relative importance of ground and vehicle in causing the head injury is investigated in terms of HIC ratio β which is defined as follows:

$$\beta_{HIC} = \frac{HIC_{car-impact}}{HIC_{ground-impact}} \quad [1]$$

Table A3 shows that during the second impact, it could be the head or other body parts that first landing on the ground. If the head first landing on

the ground, it has a high injury risk of the head caused by ground.

The relationship between head injury severity and vehicle impact speed is shown in Figure 9. A nonlinear correlation is achieved by a second-order polynomial curve.

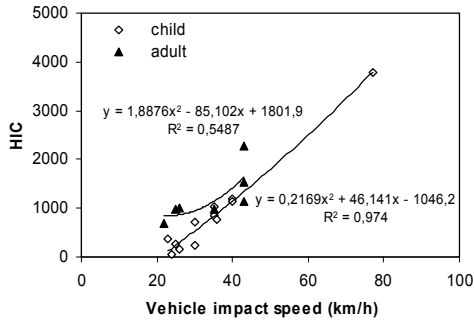


Figure 9. Correlation of vehicle impact speed and HIC

Throwing Distance

Figure 10 shows the calculated pedestrian throwing distances in accident reconstructions, which are comparable with the throwing distances registered in police report. It appears that the child throwing distances are greater than that of adult at the same impact speed.

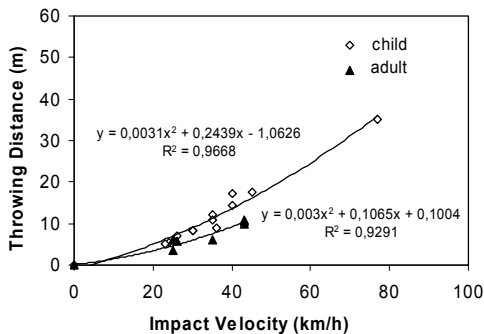


Figure 10. Throwing distance

DISCUSSION

In this study efforts have been made to find the correlation of the calculated biomechanical responses of pedestrian body segments with the corresponding injuries observed in accidents. The reliability of the findings from accident reconstructions is dependent on quality of data sources, including information about three aspects: vehicles, pedestrians, and road traffic environment.

Data sources and the basic variables

The accident data used in these studies were collected from hospital clinical record and police

report, which contributed to form national databases. This study was carried out based on the databases for acquisition of detailed information about causation and occurrence of accidents, injury patterns, causation and distribution of the injuries. The collected information forms firm background for in-depth study on impact biomechanics and injury correlations of pedestrians in vehicle collisions.

Estimating vehicle impact speeds

The vehicle impact speed is one of the most important issues to investigate the pedestrian impact responses and injury biomechanics. There are various approaches to estimate the vehicle speed at the moment of the collision. In the present study the following techniques were used to estimate the vehicle impact speeds based on available accident data.

Vehicle speed based on skid marks

Calculation of vehicle speed by using skid marks is the most common way in pedestrian collision analysis, in the case of accident vehicle skidded after an emergency braking. The length s of the skid marks can be measured in field investigations. The possible car impact speeds V_i are calculated using equation as follows:

$$V_i = \sqrt{2g\mu s} \quad [2]$$

It is necessary to point out that there could be some difference of the calculated speed from the speed in real world accident due to effect of pedestrian mass and road surface conditions.

Vehicle speed based on pedestrian throw distance

The skid marks are not always available in accident field. One of the reasons is due to the increasing use of Anti-lock Brake Systems, skid marks are less common. The pedestrian's total throw distance is another indicator of the speed of the vehicle at impact. Estimating vehicle speed by pedestrian throw distance is thus becoming more important in accident investigations. The vehicle impact speed can be estimated by simulation of the vehicle and pedestrian motions [4].

Pedestrian initial posture and moving speeds

In the real world vehicle-pedestrian accidents the initial posture of a pedestrian at an impact is varied in different motion attitude. Therefore an appropriate initial position should be investigated and defined for reconstruction of the pedestrian accidents. According to present study, the child initial posture in an accident is quite different from that of an adult.

The majority 98% of the child pedestrians are in motion during impact, either walking or running. This indicated a remarkable difference from study on initial posture of pedestrians in all age group, of which 79% in motion [11].

The impact responses and injury outcomes are significantly affected by the initial postures and the orientation of body segments. It was proposed to take into account the leg orientation for the moving posture. During the pedestrian impact the kinematics and dynamic loading of pedestrian are not the same if you have the left leg forward or the right leg forward.

The moving speed is another important variable to define in accident reconstruction. The child normal crossing speeds were established as 1.5 m/second to 2 m /second, which are recommended to be used in present study.

Secondary ground impact

In reconstruction results the HIC values were calculated in both first contact with car and second contact with road surface. It is usual that the HIC value in contact with car front is larger than that in second ground impact without head landing ground first. The reverse is the case for the second ground impact with head contact ground first. It indicated that the contact modes in secondary ground impact are complicated, which could be dependent to the vehicle front shape, impact velocity, and body size.

Impact biomechanics

It was found that the injury distribution of pedestrians varies with the body size. In general children exposure higher risk for head injuries, and adults for lower extremities.

The HIC is an important measurement of the head injury. The results show a good correlation between calculated injury parameters and the head injury severities in the accidents. However, more accident cases are needed to establish a tolerance level and a correlation of head injury risk with HIC value.

CONCLUSIONS

In car-pedestrian accidents, the pedestrians are often struck from the side by the front structure of a vehicle when crossing a street. In this study it was found that the pedestrians were hit from the side for 82% of adult cases and 87% of the child cases

It was found that the child head injuries account for 56.4% of total child pedestrian injuries, adult head injuries for 30.9% of total adult pedestrian injuries.

The head impact conditions such as impact velocity, impact timing and angle, wrap around

distance are mainly dependent on the car front shapes, impact speed and size of child pedestrian.

The head injuries caused by car front structures were usually much severe than caused by the secondary ground impact.

The impact velocity and car front structures have a significant influence on the kinematics and injury severity of child pedestrian head. By limiting the vehicle speed and improving car front design, the head injury severity of child pedestrian could be reduced.

The dynamic responses and injury parameters from accident reconstructions would provide complement knowledge to develop safety countermeasures and protection devices.

REFERENCES

- 1 World Health Organisation (2004). World Report on Road Traffic Injury Prevention, ISBN 92 4 156260 9, World Health Organisation, Geneva.
- 2 EEVC (2002): Improved Test Methods to Evaluate Pedestrian Protection Afforded by Passenger Cars. EEVC Working Group 17.
- 3 Otte, D. ; Krettek, C. ; Brunner, H.; Zwipp, H. Scientific Approach and Methodology of a New In-Depth-Investigation Study in Germany so called GIDAS, ESV-Paper Nagoya Japan 2003
- 4 Otte, D. Use of Throw Distances of Pedestrians and Bicyclists as Part of a Scientific Accident Reconstruction Method, SAE paper 626, Detroit 2004-06-30
- 5 CARE - Community database on Accidents on the Roads in Europe, 2004.
http://europa.eu.int/comm/transport/home/care/index_en.htm
- 6 FARS- National Highway Traffic Safety Administration's (NHTSA) Fatality Analysis Reporting System (FARS) Web-Based Encyclopedia, 2004.
<http://www-fars.nhtsa.dot.gov/>
- 7 D Otte, Severity and Mechanism of Head Impacts in Car to Pedestrian Accidents, Proc. Int. IRCOBI Conf. Biomechanics of Impact, 329-341, 1999.
- 8 Otte, D., Severity and Mechanism of Head Impacts in Car to Pedestrian Accidents, Proc. of Int. IRCOBI Conf. Biomechanics Impacts, 1998, pp.329-341.
- 9 Yang, J K Lövsund, P Cavallero, C and Bonnoit, J. A Human-Body 3D Mathematical Model for Simulation of Car-Pedestrian Impacts, Journal of Crash Prevention and Injury Control, 2000, 2(2):131-149.
- 10 Liu, X.J and Yang, J.K. Development of Child Pedestrian Mathematical Models and Evaluation with Accident Reconstruction, Traffic Injury Prevention, 2002, 3(4):321-329.
- 11 Yang, J.K., Ries, O., Schoenpflug, M., Brianso, C. (2003). Pedestrian Position Definition. EU-HUMOS2 project report, 2CHA-030928-E1-DB.

APPENDIX

Table A1a. Anthropometric data of adults

Case No.	1	2	3	4	5	6	7	8
Age	62	24	81	49	50	70	28	84
Height(cm)	170	155	153	168	180	175	170	150
Weight (kg)	90	50	45	70	87	85	69	55

Table A1b. Anthropometric data of children

Case No.	1	2	3	4	5	6	7	8	9	10	11	12
Age	7	9	12	4	7	6	6	6	5	6	4	8
Height(cm)	123	130	120	110	120	113	120	115	120	126	110	128
Weight (kg)	25	30.7	45	18	31	22	18	12	25	31	17	25

Table A2a. Correlation of WAD distance with adult pedestrian height

Case No.	1	2	3	4	5	6	7	8
Height (cm)	170	155	153	168	180	175	170	150
WAD _R (cm)	173	146	149	188	207	191	172	163
WAD _R /Height	1.01	0.94	0.97	1.12	1.15	1.09	1.01	1.09

Table A2b. Correlation of WAD distance with child pedestrian height

Case No.	1	2	3	4	5	6	7	8	9	10	11	12
Height (cm)	123	130	120	110	120	113	120	115	120	126	110	128
WAD _R (cm)	131	136	100	97	109	103	104	112	111	119	93	118
WAD _R /Height	1.06	1.05	0.83	0.88	0.91	0.91	0.87	0.97	0.93	0.94	0.85	0.92

Table A3a. Calculated injury parameters from adult accident reconstructions

Case No.	1	2	3	4	5	6	7	8
Vehicle speed (km/h)	25	43	26	35	59	43	25	43
HICcar-impact	682	1138	984	980	1397	2278	984	1534
HIC ratio	14.8	0.8	6.4	0.5	2.4	3.9	0.8	0.7
Landing body part	Arm	Head	Arm	Head	Foot	Foot	Foot	Arm
Head injury (MAIS)	2	2	2	2	3	3	1	2

Table A3b. Calculated injury parameters from child accident reconstructions

Case No.	1	2	3	4	5	6	7	8	9	10	11	12
Vehicle speed (km/h)	40	36	23	35	30	24	35	77	40	26	25	30
HICcar-impact	1147	764	367	1041	227	58	851	3788	1182	166	263	725
HIC ratio	1.23	1.10	1.11	1.03	0.51	0.10	1.08	0.77	1.14	0.89	0.33	0.99
Landing body part	Foot	Foot	Head	Foot	Foot	Head	Foot	Head	Foot	Head	Head	Head
Head injury (MAIS)	5	5	1	2	0	1	1	6	5	0	2	1

ASSESSMENT OF VEHICLE RELATED PEDESTRIAN SAFETY

Matthias Kuehn

German Insurance Institute for Traffic Engineering
German Insurance Association
Germany

Robert Froeming

Volker Schindler

Institute for Automotive Engineering
Technical University of Berlin
Germany
Paper Number 05-0044

ABSTRACT

Against the background of upcoming intelligent safety systems, which also will have an impact on passive safety in general and on pedestrian safety in particular, all relevant technical measures have to be quantified in a combined way in order to find most effective solutions.

The article deals with the introduction of an assessment procedure called “**V**ehicle **R**elated **P**edestrian **S**afety - index” (VERPS-index). This test procedure is exemplarily applied to two very different cars. Furthermore, the effectiveness of the uplifting hood applied to the front of these two sample cars is quantified.

Our approach consists of four modules: accident analysis, numerical simulation of kinematic impact parameters, component tests, and quantification of pedestrian safety. Current European component tests use impact parameters which are set more or less independent of the vehicle shape [1]. We propose to use numerical simulations in order to generate vehicle shape dependent test parameters. A weighting procedure based on accident statistics is applied to evaluate the relevance of each tested point on the front of the vehicle regarding its actual impact probability in real life. Thus, the VERPS-index is able to solve many of the disadvantages of a conventional component test compared to a full-scale test.

Based on the VERPS-index we are able to show in detail how the pedestrian safety performance depends on the vehicle front shape and how it differs for adults and children. Technical measures like an uplifting hood can clearly improve the safety performance. However, their effectiveness strongly de-

pends on the individual vehicle's front geometry and differs for adults and children.

INTRODUCTION

13.8 Million accidents occur every year on European roads. These include 38.000 killed and 1.7 Million injured people resulting in costs of around 160 Billion Euros. This corresponds to around 2 % of the European gross national product [2]. These numbers prompted the Commission of the European Community to proclaim the goal to halve the number of road accident victims until 2010 [2]. There are 5.941 pedestrians among the fatalities on European roads [3]. This translates in a death rate for the EU for 2002 of 15.7 killed pedestrians per 1 Million inhabitants. In Australia this figure is 12.3, in the USA 16.4 and in Japan 21.8. Within the EU (EU₁₅, 2002) the rate differs between 6.4 in Sweden and 32.3 in Portugal. In Poland there are 52 killed pedestrians per 1 Million inhabitants [3, 4]. The number of killed vulnerable road users may even be higher in countries with a beginning motorisation, e.g. China.

The high number of pedestrian accidents justifies more safety efforts worldwide. There are different possible starting points:

- avoidance of accidents by measures related to infrastructure, education etc.
- avoidance of accidents by vehicle related, active measures
- mitigation of the consequences of accidents by:
 - reduction of accident severity by braking, steering, etc.

- decrease of the risk inflicted by the pedestrian's first impact on the car by structural design or active elements
- decrease of the dangerousness of the secondary impact on the road
- optimisation of the post crash rescue system

In the following chapters, opportunities are analysed to assess the safety performance of a vehicle concerning a pedestrian impact.

TEST PHILOSOPHIES

There are two different test philosophies in vehicle safety (see Figure 1 and Figure 2). Both of them have specific advantages and disadvantages.

Full-Scale Tests



Figure 1. Typical full-scale test, conducted at the Technical University of Berlin.

In full-scale tests the whole accident event is quite realistically reproduced. In principle, only the human is replaced by an anthropomorphic test device. The required dummies are mechanically complex. Additionally, complex data acquisition is necessary. The preparation of each individual experiment is time consuming. The reproducibility of full-scale-tests of pedestrian-car-crashes is not guaranteed. If conventional, not purpose designed dummies are used, biofidelity is questionable [5, 6]. The WAD (Wrap Around Distance) can not be reliably reproduced compared to PMHS-tests (Post Mortem Human Subject). Possibly the use of the newly developed POLAR II-Dummy can solve these problems and

lead to a different perspective of the full-scale test in the field of pedestrian safety [7].

In principle, numerical simulation has the potential of a comprehensive assessment. Today, vehicle engineers routinely generate detailed numerical vehicle models which can be used to support such a process. But available numerical pedestrian models are not detailed and validated enough to predict injuries accurately. Models which will arise from new approaches may be helpful in the future [7, 8].

Component Tests

Component tests are designed to reproduce just the critical part of the whole accident event. A lot of additional knowledge is needed to interpret the results correctly. In a complex context, for example in a pedestrian accident, a component test with fixed test parameters set independently of the geometry of the vehicle's front may be inappropriate in certain constellations. It is not able to represent these accident events detailed enough with all its variations. A number of national and international expert groups are analysing this problem and try to enhance the procedure which nearly inevitably increase the complexity of the test [9].



Figure 2. Typical pedestrian related component test, conducted on behalf of the Technical University of Berlin.

AN ADVANCED ASSESSMENT PROCEDURE

Head impact by far results in the most severe accident consequences representing almost all fatal injuries in a pedestrian-car-collision. Therefore, our approach is focused on it.

Numerical simulations can provide knowledge about the kinematics of the event for each particular car and for diverse impact conditions. The results of the simulation are used to control a free flying head-form test device. The measured acceleration values provide the basis for the assessment of a particular car.

Our assessment procedure therefore combines the following four modules:

- accident analysis
- numerical simulation
- component test
- quantification of pedestrian safety

In order to quantify pedestrian safety and to make sure that the results are comparable for all forms of vehicles on a linear scale, a Vehicle Related Pedestrian Safety index is proposed (VERPS-index). In addition, it provides the opportunity to assess technical measures applied to the car's front to increase pedestrian safety and allows comparison with active safety measures applied to the vehicle (e.g. brake assist system).

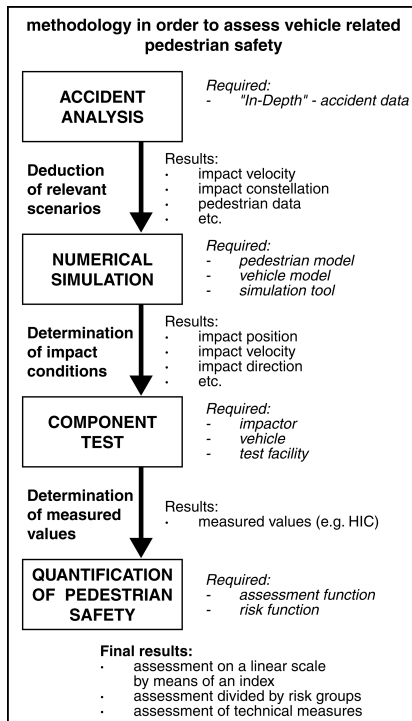


Figure 3. Illustration of the methodology to assess vehicle related pedestrian safety.

Furthermore, the presented method makes it possible to influence the pedestrian friendliness of a product in a very early stage of the vehicle development

process by possibly making geometry changes with minor stylistic or functional effects or by triggering the development of additional pedestrian protection systems.

Accident Analysis

A statistical analysis of pedestrian accidents makes sure, that the input parameters used in the numerical simulations are realistic. It provides the basis for all further deductions and needs a regular update. "In-Depth"- data of the Medical University of Hanover are used [10]. The analysis shows that 90 % of all pedestrian accidents occur with a collision speed of less than 45 km/h, covering around 70 % of the severely injured (AIS3+) and around 95 % of the slightly injured pedestrians. In 71 % of all cases the pedestrian hits the front of the car. Thereby, 92 % of the pedestrians were hit laterally from the right or left side. 94 % of these pedestrians were walking or running the moment prior to the collision. The most frequently injured body parts were the lower extremities (35 %) and the head (33 %). Deadly injuries can be attributed exclusively to the head impact.

Numerical Simulation

For the analysis of the kinematics of the head impact on the front of a vehicle a numerical simulation process has been developed. It is based on the multibody simulation tool MADYMO. The pedestrian is represented by the Full Body Pedestrian Model of TNO. The vehicles are modelled using finite elements. The structure of the vehicle's front is represented using a global stiffness.

Validation of the simulation model was done in three ways. At first, calculated longitudinal throwing distances were compared to those, which resulted from carefully analysed real accidents. At second, the kinematics of well documented PMHS-tests and simulation results for the primary impact were compared. Finally, a very precisely documented real accident was used to compare numerical simulation results to the real accident conditions (see Figure 4) [11]. It could be shown that the simulation model is able to represent the primary impact of a pedestrian to the vehicle front very well. Thus, the model can provide reliable kinematical impact conditions for a component test. It is not intended to predict injuries with this simulation model.

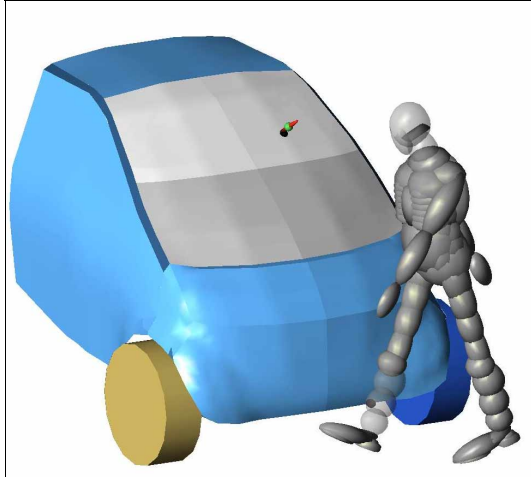


Figure 4. Reconstruction of a real pedestrian-car accident. [11]

For each set of simulations for a VERPS-rating a number of characteristic parameters has to be defined. One group of them describes the impact between car and pedestrian (speed of the car, direction, speed, and size of the pedestrian, location of the first contact between pedestrian and car, angle between pedestrian and car) and is independent of the vehicle. The combination of these parameters results in 32 impact constellations for each analysed vehicle model (see Table 1).

Table 1.

Vehicle specific input parameters.

input parameter	selected values	number of simulations
pedestrian size	four dummy sizes according to TNO-Human-Model family; (6y-child, 5% female adult, 50% male adult, 95% male adult)	4
walking velocity	1.5 m/s and 3.1 m/s	2
angle between pedestrian and vehicle	90° and 75°	2
initial impact location of the pedestrian	two positions along the vehicle front; central (0.0 m), eccentric (0.4 m)	2
simulations per vehicle		32

The other group represents properties of the car (geometry of the vehicle front, braking pitch angle). Additional parameters can be used to include active

safety features like brake assistant, pre-crash sensors, etc.

The impact velocity is set to 45 km/h according to results of the accident analysis. With the help of the accident analysis it can be shown, that the four pedestrian sizes used cover 76 % of all involved persons, if a tolerance of ± 0.1 m in body height is accepted.

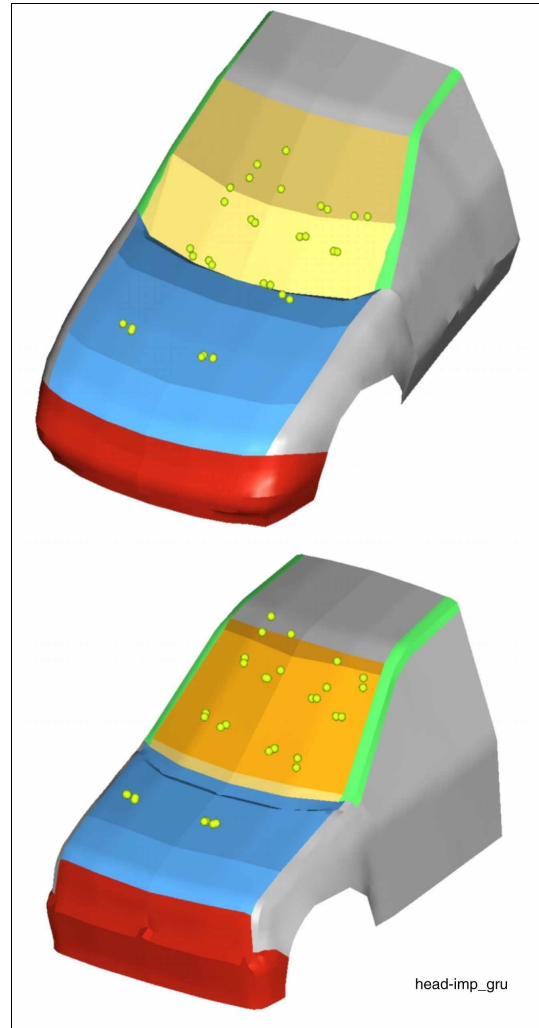


Figure 5. Calculated head impact positions for four pedestrian sizes at $v_C = 45$ km/h. (above: vehicle F, below: vehicle G).

Figure 5 and Table 2 show the calculated head impact conditions for two different cars (distance to impact position = WAD, impact angle = α , impact velocity = v_C). The calculated values represent the geometry of the analysed vehicles and differ considerably from the European directive [1]. Based on the simulation results also the mass of the appropriate head impactors can be allocated.

Table 2.
Calculated head impact parameters for sample cars F and G.

		pedestrian percentile			
		6y-old child	5 % female	50 % male	95 % male
height	h [m]	1.16	1.52	1.74	1.91
$F_k = WAD/h$	F []	1.02	1.08	1.15	1.11
	G []	1.01	1.08	1.14	1.09
WAD	F [m]	1.16-1.20	1.58-1.71	1.92-2.09	2.10-2.27
	G [m]	1.16-1.19	1.57-1.70	1.87-2.01	1.97-2.22
α	F [°]	52	58.5	55.5	56
	G [°]	51	55.5	43.5	48
v_c	F [km/h]	35.4	43.9	49.6	49.9
	G [km/h]	32.3	46.7	48.2	44.4

Table 3 shows calculated head masses of the four pedestrian percentiles and allocates them to the headform masses used in our tests.

Table 3.
Calculated head masses and allocation to existing test headforms. [11]

	h [m]	calculated head mass m_c [kg]	allocated headform mass m_h [kg]
6y old child	1.16	3.5	3.5 (ACEA)
5 %-female	1.53	4.0	3.5 (ACEA)
50 %-male	1.74	4.8	4.8 (EEVC WG 17)
95 %-male	1.92	5.9	4.8 (EEVC WG 17)

The results of the component tests can be represented by HIC values (Head Injury Criterion), calculated from the measured headform accelerations.

They show a typical pattern of potentially dangerous regions at the vehicle front:

- parts of the bonnet with little deformation space beneath
- lateral bonnet edge and transition area between bonnet and wing
- bonnet area directly above the firewall
- lower windscreen frame
- A-pillars
- upper windscreen frame and roof frontal edge

All of these areas are characterized by stiff and hence less deformable vehicle structures. The degree of exposure of a pedestrian to these regions can differ from car to car because of differences in dimensions and styling. A test procedure which stringently dictates meeting of specific test limits will unavoidably produce meaningless ratings in these areas.

Because of different vehicle geometries the potentially dangerous areas for the head impact are affected more or less frequently during a pedestrian impact. Some of these areas might be totally irrelevant for the head impact of a pedestrian (e.g. upper windscreen frame at SUV's). For that reason a weighting of the test results concerning their relevance in pedestrian accidents is necessary.

ASSESSMENT OF VEHICLE RELATED PEDESTRIAN SAFETY

In the following a Vehicle Related Pedestrian Safety Index (VERPS-index) is developed. This index assesses the level of safety which a special vehicle can provide for the head of a pedestrian who is impacted by the front of the car. It allows to assess differences between particular vehicle designs and to compare technical measures applied to the vehicle front. The VERPS-index is the result of the quantification module in the proposed methodology (see Figure 3).

Derivation of the VERPS-index

The VERPS-index for the frontal impact is deduced in three steps from the values M_{ij} measured in the component test:

1. Mapping of M_{ij} to the degree of performance E_{ij} by an evaluation function $B(M_{ij})$.

$$E_{ij} = B(M_{ij}) \quad (1).$$

2. Weighting of the degrees of performances E_{ij} with relevance factors $R_{i,WAD}$ and $R_{j,front}$, deduced from accident analysis.

$$R_{i,WAD} \cdot R_{j,front} \cdot E_{ij} \quad (2).$$

3. Summation of degrees of performance for all subareas of the vehicle front to the VERPS-index.

$$VERPS = \sum_{i=1}^m \sum_{j=1}^n R_{i,WAD} \cdot R_{j,front} \cdot E_{ij} \quad (3).$$

To assess the vehicle front it is necessary to divide it in subareas. For each of them M_{ij} is measured (see Figure 6). Thereby, subindex i describes the longitudinal direction of the vehicle front and subindex j the transverse one.

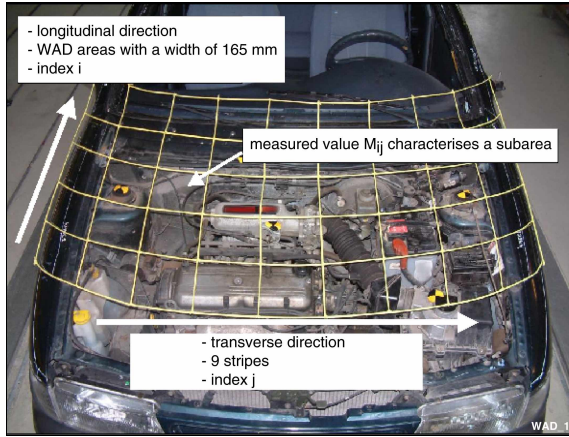


Figure 6. The division of the vehicle front in subareas.

The definition of limit values is an often used possibility to assess measured values. But it allows only a binary assessment. It only distinguishes between good (limit met) and bad (limit exceeded). In order to derive a more refined evaluation an assessment function B can be used to get a functional link between measured values M and the degree of performance E . For the VERPS-index a functional relationship between HIC data and the occurrence of severe head injuries (AIS 3+) is used (Figure 7).

The reduction of a HIC-value by 50 %, e.g. from $HIC = 4.000$ to $HIC = 2.000$, improves the degree of performance E only from $E_{HIC=4000} \approx 1$ to $E_{HIC=2000} = 0,938$ (see Figure 7). In contrast to that an improvement from $HIC = 2.000$ to $HIC = 1.000$ leads

to a significant improvement to $E_{HIC=1000} = 0,244$; this means a probability for the occurrence of severe head injuries of 24,4 %.

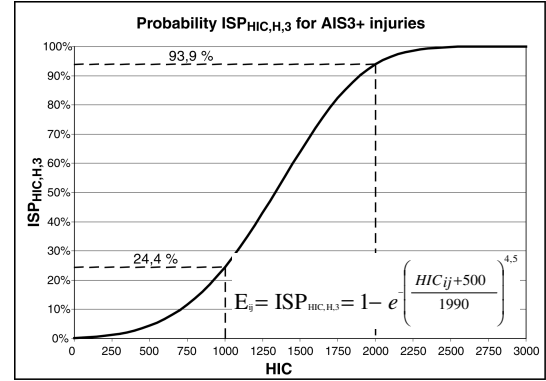


Figure 7. Correlation between measured HIC data and probability of AIS 3+ injuries (ISP – Injury Severity Probability). [based on 12]

In the second step of the calculation of the VERPS-index the degrees of performance E_{ij} are weighted with their relevance in accident events. The importance of a test point obviously depends on the probability of hitting it in real life. In order to deduce the relevance factors, “In-Depth”-accident data of the Medical University of Hanover are used. The relevance factor in the longitudinal direction of the vehicle ($R_{i,WAD}$) describes the correlation between the vehicle specific kinematics factor f_K and the size of the pedestrian. In the transverse direction of the vehicle front an equal distribution for impact locations is assumed. This is supported by accident data.

We calculate the VERPS-index separately for children younger than 12 years and for adults and children older than 12 years. Obviously, other separations are possible. Our choice considers the different requirements of pedestrian safety measures applied to cars for children and adults which result from different body heights. By use of the assessment function $B(M_{ij})$ the VERPS-index can be expressed as follows:

$$VERPS = \frac{1}{9} \sum_{i=1}^m R_{i,WAD} \cdot \sum_{j=1}^9 \left\{ 1 - e^{-\left(\frac{HIC_{ij}+500}{1990}\right)^{4,5}} \right\} \quad (4).$$

Figure 8 shows the division of the vehicle front into subareas and their relevance weights for a sample car.

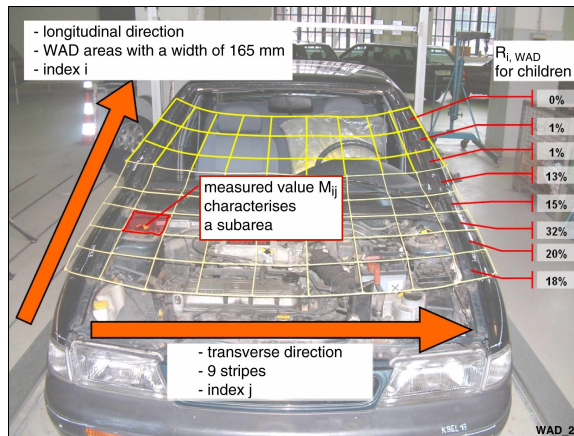


Figure 8. Relevance factors in longitudinal direction ($R_{i, WAD}$) for car F.

The VERPS-index can run between (nearly) zero (no risk for AIS 3+ head injuries) and 1 (maximum risk for AIS 3+ head injuries). A car, which has a HIC-value of 1,000 in all subareas of its front, would have a VERPS-index of $VERPS = 0.244$.

The proposed procedure allows to assess vehicle fronts on a linear scale within the limits of accuracy of the assumptions.

Application of the VERPS-index

The VERPS-index is evaluated for two sample cars. It can clearly be seen, that pedestrian safety has to be assessed separately for children and adults. Pedestrians hit different areas at the vehicle front because of their different body heights. This is the reason why a particular technical measure can positively affect all groups of persons only in exceptional cases.

Two mass-produced vehicles are compared with two modification levels of a possible pedestrian protection system. The first level represents a mechanical system which uplifts the bonnet in the rear area by around 0.1 m in case of a pedestrian impact. In the second level an airbag system is assumed which combines level one measures with an energy absorbing device which covers critical areas of the A-pillars and the lower windscreen frame (see Figure 9). Results can be seen in Table 4.



Figure 9. Implementation of a system to uplift the bonnet by use of an airbag which also covers the A-pillars and the lower windscreen frame. [9]

Table 4.

Assessment of different cars and pedestrian protection systems by use of the VERPS-index.

		vehicle F	vehicle G
production condition	children	0.54	0.63
	adults	0.63	0.24
uplifting bonnet	children	0.22	0.43
	adults	0.60	0.24
uplifting bonnet combined with an airbag	children	0.08	0.11
	adults	0.25	0.17

For vehicle F the VERPS-index for adults could be reduced from 0.63 to 0.25, for children even from 0.54 to 0.08. The marked reduction of VERPS-index for children shows the great potential of active structural measures, if they are applied properly with respect to pedestrian body height and the vehicle dimensions. Head impact areas, which are mainly hit by adults, can only be protected with the uplifting bonnet and the additional airbag to cover A-pillars and lower windscreen frame (see Table 4).

The VERPS-index of 0.24 for adults of vehicle G in production condition is good compared to vehicle F. This can be traced back to the fact, that all relevant head impact areas for adults are in the windscreen area, which is considered uncritically concerning the HIC results unless the windscreen frame area or the A-pillars are included.

Because of the vehicle front geometry of car G an uplifting bonnet alone can protect only a small group

of pedestrians. An additional airbag applied to the lower windscreen frame is able to better protect smaller adults, but the relevant impact areas for taller ones are still not covered. Accordingly the VERPS-index is only reduced from 0.24 to 0.17. For children vehicle G in production condition performs poorer than for adults with an VERPS-index of 0.63, because they quite frequently hit the firewall and the lower windscreen frame with the head. By use of active structural measures the VERPS-performance can be clearly improved. The VERPS-index decreases from 0.63 in series condition to 0.43 for the uplifting bonnet alone and to 0.11 for the uplifting bonnet with the additional airbag.

OUTLOOK

It could be shown that an index can be formulated that allows to assess different vehicles with respect to their pedestrian safety on a linear scale. The VERPS-index allows to compare different vehicles and technical measures like the uplifting hood on the same vehicle concerning their pedestrian protection potential.

We expect, that it will be possible in the near future also to assess active safety measures (e.g. pre crash sensing devices, brake assist systems) on the same scale. The reduction of the collision speed of a vehicle, which can be attained with a certain probability depending on the system layout, can be included in the VERPS-calculation. The reduced collision speed is used as an input parameter for the numerical simulation module. This finally results in an specific VERPS-index for the analysed car.

The comparison of different systems using the VERPS-index also offers the basis for a benefit-cost analysis to identify the most efficient measure in an economic sense [11].

REFERENCES

- [1] European Union (2003): Directive 2003/102/EC of the European Parliament and of the Council of 17 November 2003 relating to the protection of pedestrians and other vulnerable road users before and in the event of a collision with a motor vehicle and amending Council Directive 70/156/EEC. Official Journal of the European Union, L 321, 06/12/2003 P. 0015 – 0025.
- [2] Communication from the European Commission (2003): “European road safety action programme - Halving the number of road accident victims in the European Union by 2010: a shared responsibility”; COM/2003/0311 final, June 2003.
- [3] IRTAD (2004): International Road Traffic and Accident Database (IRTAD). Organization for Economic Co-operation and Development (OECD), <http://irtad.bast.de>, 2004.
- [4] DSW (2004): Deutsche Stiftung Weltbevölkerung, country database, www.weltbevölkerung.de, 2004.
- [5] Stürtz, G. (1984): „Global- und Komponentenversuche zur Fußgängersicherheit“; Forschungsvereinigung Automobiltechnik e.V. (FAT) No. 22, Frankfurt/Main, 1984.
- [6] Eggert, E. (1998): „Experimentelle Untersuchungsmethoden zur passiven Sicherheit bei Fußgänger-Fahrzeug-Kollisionen“; Technical University Berlin, Institute for Automotive Engineering, seminar paper, 1998.
- [7] Sugimoto, T. (2003): „Honda’s Approach to Pedestrian Protection“; VDI conference „Innovativer Insassen- und Partnerschutz - Fahrzeugsicherheit 2010“, ISBN 3-18-091794-6, Berlin, 20.–21.11. 2003.
- [8] Koch, W., Howard, M. (2003): „Verbesserung der Fußgängersicherheit“; Automobiltechnische Zeitschrift (ATZ) 1/2003, volume 105, 2003.
- [9] Kalliske, I., Kühn, M., Otte, D., Heinrich, T., Schindler, V. (2003): „Fahrzeugseitige Maßnahmen zum Schutz des Kopfes eines Fußgängers – eine ganzheitliche Betrachtung“; VDI conference „Innovativer Insassen- und Partnerschutz - Fahrzeugsicherheit 2010“, ISBN 3-18-091794-6, Berlin, 20.–21.11. 2003.
- [10] Otte, D., Krettek, C., Brunner, H., Zwipp, H. (2003):” Scientific Approach and Methodology of a New In-Depth-Investigation Study in Germany so called GIDAS“; 18. ESV conference, proceedings, 2003.

- [11] Kühn, M. (2004): „Weiterentwicklung von Fußgänger-Komponententests“ Fortschritt-Bericht VDI, Reihe 12, No. 573, ISBN 3-18-357312-1, publisher: VDI Verlag, Düsseldorf, 2004.
- [12] ISO 13232: Test Analysis Procedures for Research Evaluation of Rider Crash Protective Devices Fitted to Motorcycles - Injury Indices and Risk/Benefit Analysis. Part 5 Rev. 1, ISO/TC22 Road vehicles, Subcommittee SC22, Motorcycles.

VEHICLE HOOD AND BUMPER STRUCTURE DESIGN TO MITIGATE CASUALTIES OF PEDESTRIAN ACCIDENTS

Jae-Wan Lee

Kyong-Han Yoon

Korea Automobile Test and Research Institute
Korea

Youn-Soo Kang

The Korea Transport Institute
Korea

Gyung-Jin Park

Hanyang University
Korea

Paper Number 05-0105

ABSTRACT

Although the number of pedestrian fatalities and injuries is steadily declining worldwide, pedestrian protection is still an important issue. Extensive researches have been carried out for pedestrian protection in order to establish regulations for pedestrian safety. The automobile hoods and bumpers, which pedestrians frequently collide into during accidents, should be designed for the safety of the pedestrians.

Two analysis methods, a real experiment and computer simulation, are utilized to design safe structures of the hood and the bumper. A real experiment is very expensive while computer simulation has modeling imperfections. It would be optimal to obtain all the data from experiments to identify the design tendency. However, computer simulation is generally used due to budget restrictions.

In this research, a method, which uses an experiment and simulation simultaneously, is developed. Orthogonal arrays are employed to link the two methods. The minimum number of experiments is allocated to some rows of an orthogonal array and the simulations are allocated to the rest of the rows. Experiments should be allocated to have the cases of the experiments orthogonal. Mathematical error analysis is conducted. Based on the proposed methods, a hood and a bumper are designed to protect pedestrians. Real experiments and computer simulations are conducted for the rows of orthogonal arrays. The results show that the errors are distributed uniformly and a precise design is obtained.

INTRODUCTION

With the great number of pedestrian deaths and injuries occurring from automobile accidents, an effort

is being made worldwide to establish automobile safety regulations for pedestrian protection. The hood and bumper, with which pedestrians come in frequent contact, can be designed and manufactured to be pedestrian friendly, effectively decreasing injuries [1-2]. During the development of a safe hood and bumper structures, experiments and computer simulations are used to evaluate their performances. Computer simulations contain many errors from inaccurate modeling and approximation of governing Equations. On the other hand, experiments are considered to be accurate even with the possibility of experimental errors and inaccuracies. In design, it would be the best if all the data could be obtained from experiments. However, an experiment is generally very costly. Therefore, limited experiments are performed in many application fields.

Orthogonal arrays are exploited very well for experiments with a limited number. They are used for the matrix experiments in design of experiments (DOE) [3]. When an experiment is extremely expensive, even the experiments with an orthogonal array are almost impossible to conduct in order to find a good design. In this case, some experiments can be replaced by computer simulations. As mentioned earlier, computer simulation has a large amount of errors [4].

A method is utilized to simultaneously use experiments and computer simulations in an orthogonal array. Experiments and simulations are assigned to the rows of an orthogonal array. The method of the assignment is proposed to minimize the error. The error is reduced since it is distributed evenly. The automobile hood and bumper structures are designed from the results of the orthogonal array. The results indicate that the proposed method finds design variables accurately [5].

EVALUATION OF PEDESTRIAN INJURIES

Pedestrian Accidents

Pedestrian accidents make up a large portion of traffic accidents. In the year 2000, pedestrian casualties numbered 19.0% (7,000) in Europe, 11.3% (4,739) in the U.S., 28.3% (2,605) in Japan, 38.0% (3,890) in Korea, and 50% (19,000) in China. There were also numerous cases of injuries - over 300,000 in Europe, 78,000 in the U.S., 86,000 in Japan and 74,102 in Korea [1-2][6].

Most pedestrian injuries (AIS 2-6) are head, face, and neck injuries, accounting for 36.9% and leg injuries accounting for 32.4% [7]. AIS (abbreviated injury scale) is an index used to classify injuries into 7 levels, from AIS 0 (no injuries) to AIS 6 (death). The greatest causes for head injuries are automobile windshields (33.5%), hood and wing surfaces (19.5%), and window frame and A-pillar (17.2%). The causes for leg injuries are bumpers (61.2%) and vertical parts of the hood (12.1%) [7].

Pedestrian Protection Regulations and Experiments

Impact test for pedestrian protection is implemented as illustrated in Figure 1 [6]. The experiment uses the standards of the impact experiments for the second stage child head model and the first stage lower body model in the Directive 70/156/EEC (2003/102/EC) [8]. The child head model is impacted on the hood. The horizontal impact angle is 50° with the wrap around distance (WAD) between 1,000-1,500mm. Impact speed is 40km/h and the required HIC (Head Injury Criterion) is 1,000 or lower. HIC is calculated from Equation (1) [6][8].

$$HIC = \left[\frac{1}{t_2 - t_1} \int_{t_1}^{t_2} \mathbf{a} dt \right]^{2.5} (t_2 - t_1) \quad (1).$$

where \mathbf{a} is the resultant acceleration measured in units of gravity "g" ($1g = 9.81m/sec^2$), t_1 and t_2 are the two time instances (expressed in seconds) during the impact, defining an interval between the beginning and the end of the recording period for which the value of HIC is the maximum ($t_2 - t_1 \leq 15msec$).

A legform is used for the bumper impact test. Impact is applied to the bumper on at least three points where injuries or shape changes may result. Impact is

imposed at 40km/h horizontally in line with the automobile. The maximum dynamic knee bending angle shall not exceed 21° , the maximum dynamic knee shearing displacement shall not exceed 6mm, and the acceleration measured at the upper end of the tibia shall not exceed 200g [6][8].

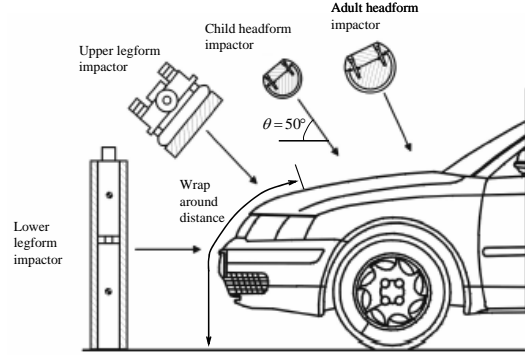


Figure 1. Schematic of impact experiments for pedestrian protection.

A DESIGN METHOD USING ORTHOGONAL ARRAYS WITH EXPERIMENTS AND COMPUTER SIMULATIONS

Using an optimization formulation, a design problem can be expressed as [4][9]:

$$\begin{aligned} & \text{Find } \mathbf{b} \in \mathbb{R}^n \\ & \text{to minimize } f(\mathbf{b}) \\ & \text{subject to } h_i(\mathbf{b}) = 0, \quad i = 1, \dots, k \\ & \quad \quad \quad g_j(\mathbf{b}) \leq 0, \quad j = 1, \dots, l \\ & \quad \quad \quad \mathbf{b}_L \leq \mathbf{b} \leq \mathbf{b}_U \end{aligned} \quad (2).$$

where \mathbf{b} is the design variable vector with n elements, f is the objective function, h_i is the i -th equality constraint, g_j is the j -th inequality constraint, and \mathbf{b}_L and \mathbf{b}_U are the vectors for lower and upper bounds of design variables, respectively. k is the number of equality constraint, and l is the number of inequality constraint. When an orthogonal array is used directly in design, the characteristic values are used by changing the functions in Equation (2).

Design Using Orthogonal Arrays

A full combination of experiments with design candidates can find the best design. However, real

experiments are very expensive. Even computer simulation is costly for crashworthiness. In this case, orthogonal arrays are exploited well to replace the full combination to reduce the number of experiments [3-4][10]. Using the orthogonality of the rows in the orthogonal array, the minimum number of experiments is conducted. After the experiments of the rows are performed, a design is found by analysis of means (ANOM). The error variance is reduced due to the orthogonality [3-5].

Suppose we select the orthogonal array $L_9(3^4)$ where 9 is the number of rows, 3 is the number of levels, and 4 is the number of design variables. As shown in Table 1, an experiment is carried out for each row. The average of the characteristic values from $L_9(3^4)$ of Table 1 is

$$m = \frac{1}{9} \sum_{i=1}^9 \eta_i \quad (3)$$

where η_i is the characteristic value of the i -th row. When factor A is A_3 , the average is m_{A_3} as

$$m_{A_3} = \frac{1}{3}(\eta_7 + \eta_8 + \eta_9) \quad (4)$$

Table 1.
 $L_9(3^4)$ orthogonal array

Exp. No.	Factor assigned				Characteristic value (η)
	A	B	C	D	
1	1	1	1	1	η_1
2	1	2	2	2	η_2
3	1	3	3	3	η_3
4	2	1	2	3	η_4
5	2	2	3	1	η_5
6	2	3	1	2	η_6
7	3	1	3	2	η_7
8	3	2	1	3	η_8
9	3	3	2	1	η_9

Therefore, the effect of level A_3 is $(m_{A_3} - m)$ when additivity is satisfied. Equation (4) is identical to Equation (5) by the additive model [11].

$$m_{A_3} = (\mu + a_3) + \frac{1}{3}(e_7 + e_8 + e_9) \quad (5)$$

where μ is the true average value of η , a_3 is the true value of $(m_{A_3} - m)$ and e_j is the error of the j -th row of Table 1. When we use an orthogonal array to solve the problem in Equation (2), constraints exist. The characteristic function η is usually a function of the objective function f in Equation (2).

For constrained problems, the following augmented characteristic function η_{aug} is defined as:

$$\eta_{aug} = f + \bar{P} \quad (6)$$

$$\bar{P} = \max(0, |h_i|; i = 1, \dots, k, g_j; j = 1, \dots, l) \times s \quad (7)$$

where \bar{P} is a penalty function defined from the maximum violation of the constraints and s is the scale factor. The size of the scale factor determines the way the constraints are considered. The constraints are usually normalized to fairly consider the constraints. η_{aug} is utilized instead of η in constrained problems.

A one-way table is established and the solution from the one-way table is intermediate design 1. The best one from the orthogonal array is intermediate design 2. In other words, η_i , which has the least objective function while constraints are satisfied, is intermediate design 2. Since interactions are not considered, a confirmation experiment should be conducted with intermediate design 1. If a constraint is violated by intermediate design 1, the design is discarded. Otherwise, intermediate design is compared with intermediate design 2 and the better one is selected for the final design [11].

A Method to Simultaneously Consider Experiments and Computer Simulations with an Orthogonal Array [4-5]

The method using experimental and computer simulation results simultaneously with an orthogonal array is explained. For example, if we have four design variables with three levels, orthogonal array $L_9(3^4)$ in Table 1 can be used. The standard deviation for error is σ_e and the standard deviation for the estimate m_{A_3} in Equation (5) is $1/3\sigma_e$. Assume that experiments are performed for rows 1, 5, 9 of the orthogonal array in Table 1 and computer simulations are performed for the rest. Suppose the standard deviation for the experimental error is σ_{ex} and the

standard deviation for the error of computer simulation is σ_{sim} . It is assumed that $\sigma_{ex} \ll \sigma_{sim}$. Then Equation (5) yields

$$m_{A_3} = (\mu + a_3) + \frac{1}{3}(e_{sim} + e_{sim} + e_{ex}) \quad (8).$$

where e_{sim} is the simulation error and e_{ex} is the experimental error. The total error variance σ_E^2 , when each error is independent, is as follows:

$$\sigma_E^2 = \frac{2}{9}\sigma_{sim}^2 + \frac{1}{9}\sigma_{ex}^2 \quad (9).$$

If $\sigma_e \cong \sigma_{sim} \gg \sigma_{ex}$, then the error variance in Equation (9) is much less than the error variance in Equation (5). In rows 1, 5, 9 of Table 1, the design variables A, B, C are distributed so that each level equally appears. This will allow identical decrease in error variance for each level.

DESIGNING AN AUTOMOBILE HOOD AND BUMPER STRUCTURE

An automobile hood and bumper structure is designed to reduce pedestrian injuries. A “variable frontal structure” is installed to the test vehicle. This structure includes the hood and the bumper of a compact car. It allows adjustment of structural members which are design variables. The adjustment is made for each row of the selected orthogonal array. $L_9(3^4)$ orthogonal array is selected for the hood structure and $L_{18}(2^1 \times 3^7)$ orthogonal array is selected for the bumper structure. At the same time, the finite element model is established for each row of the orthogonal arrays.

The flow of the design process is illustrated in Figure 2. A design where only computer simulation results are used for each case in the existing orthogonal array and a design where both experimental and simulation results are used, are compared. A commercial finite analysis program LS-DYNA ([12]) was used for analyzing the hood and bumper structures.

Design of the Hood Structure

For the hood structure, three design variables A, B and C are selected. They are A = height of the striker which is the locking device on the front part of the hood; B = number of holes in the inner frame supporting the hood panel; C = height of the hinge

which is a fastening device on the rear part of the hood [5][13]. For the parameter study of the design variables, impact is applied on three points of the hood at the places between 1,000-1,500mm of the wrap around distance (WAD). The child headform is impacted on the three points.

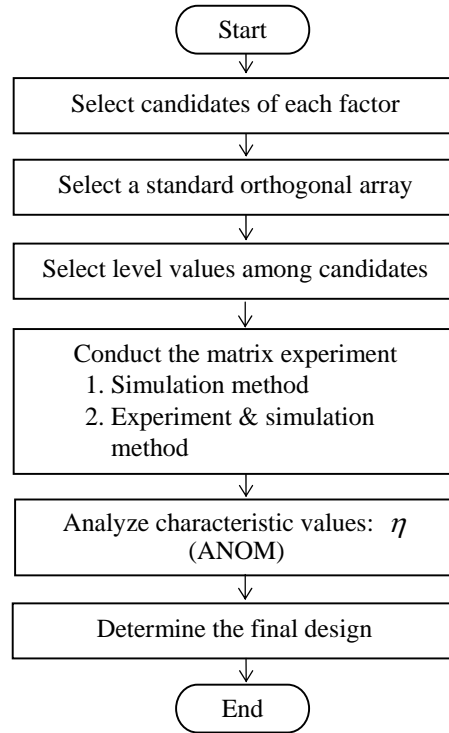


Figure 2. Flow of the design process.

Figure 3 presents the design variables and the impact points. P_1 in Figure 3 affects the striker and the hinge (design variable A), P_2 affects the hood frame holes (design variable B), and P_3 affects the inner structures of the engine room (design variable C) [5][12]. Design variables are determined by considering the tests on these three points. The neighbor of P_3 is stiffer than the other places, therefore, a larger weighting factor is imposed on the characteristic function for P_3 .

The design problem is formulated as:

Find A, B, C

to minimize

$$\eta = 0.3HIC_{P_1} + 0.3HIC_{P_2} + 0.4HIC_{P_3}$$

subject to

$$\begin{aligned} HIC_{P_1} &\leq 1000 \\ HIC_{P_2} &\leq 1000 \\ HIC_{P_3} &\leq 1000 \end{aligned} \quad (10).$$

where HIC_{P_i} is the HIC value at point P_i of Figure 3. The level values for design variables are defined by A (mm) = {0, 10, 20}, B (ea) = {0, 7, 16} and C (mm) = {0, 20, 40}.

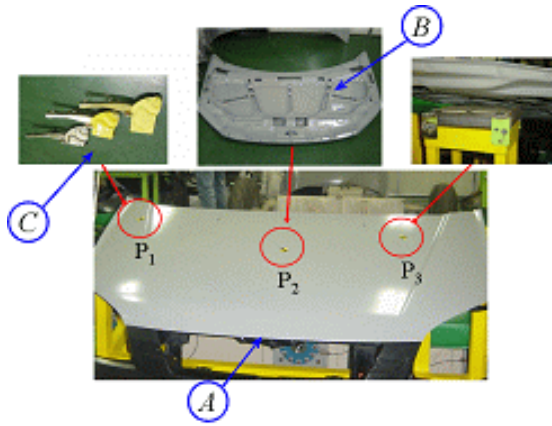


Figure 3. Impact points and design variables of the hood structure.

The Design Process of the Hood Structure Using Computer Simulation

Experiments and computer simulation are performed to evaluate the system. The finite element model is presented in Figure 4. The test facility with a “variable frontal structure,” is shown in Figure 5. The first experiment is performed with respect to the first row of Table 2. For this case, the finite element model is tuned to match the simulation results with the experimental results. Then the finite element model is regarded as the established one. Computer simulations are performed for all the rows of Table 2. The results are shown in Table 2.

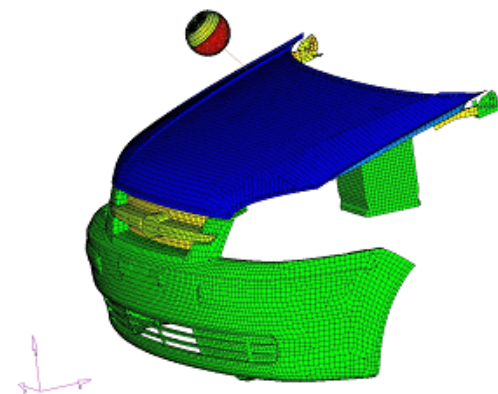


Figure 4. FE model of the child headform impact test.

Table 2.
 $L_9(3^4)$ orthogonal array using computer simulation for the hood structure

Exp. No.	Factor assigned			Characteristic value		
	A	B	C	η	\bar{P}	η_{aug}
1	1	1	1	989.9	204.0	1193.8 \checkmark
2	1	2	2	839.3	25.0	864.3 \checkmark
3	1	3	3	784.0	0.0	784.0
4	2	1	2	955.2	133.0	1088.2 \checkmark
5	2	2	3	832.5	0.0	832.3
6	2	3	1	785.5	0.0	785.5
7	3	1	3	963.8	153.0	1116.8 \checkmark
8	3	2	1	831.8	0.0	831.8
9	3	3	2	814.9	0.0	814.9

η_{aug} is defined from Equations (6) and (10) and the scale factor is set by $s = 1$. Rows 1, 2, 4 and 7 of Table 2 do not satisfy the constraints and are marked by \checkmark on η_{aug} . Through the ANOM (one-way table), intermediate design 1 is found and it is A_2, B_3 and C_3 . A simulation for confirmation is carried out with intermediate design 1. The result is that $\eta_{aug} = 768.0$ and the constraints are satisfied. Intermediate design 2 is selected from Table 2. It is the third row. The two designs are compared and the final solution is intermediate design 1. The final design is: striker height $A = 10$ mm, numbers of hole in hood frame $B = 6$ ea, and hinge height $C = 40$ mm. The simulation for confirmation shows that $HIC_{P_1} = 824.3$, $HIC_{P_2} = 605.7$ and $HIC_{P_3} = 847.6$.

Design by Experiments and Computer Simulation for the Hood Structure

Experiments are performed in the facility in Figure 5. Experiments are prepared for rows 1, 5 and 6 of Table 3 and simulations are prepared for the remaining rows. η_{aug} and the scale factor are defined in the same manner as the previous process. The results with the $L_9(3^4)$ orthogonal array are shown in Table 3. Rows 1, 2, 4, 5 and 7 in Table 3 do not satisfy the constraints and are thus marked by \checkmark in η_{aug} . A_2, B_3, C_3 are obtained as intermediate design 1 from the ANOM (one-way table).

Intermediate design 1 is confirmed by computer simulation. $\eta_{aug} = 768.0$ and the constraints are satisfied. Intermediate design 2 is the third row of Table 3. These results are the same as the previous results. Therefore, A_2, B_3 and C_3 are the final solution.



Figure 5. Child headform impact test setup.

Table 3.
 $L_9(3^4)$ orthogonal array using experiments and computer simulation for the hood structure

Exp. No.	Factor assigned			Characteristic value		
	A	B	C	η	\bar{P}	η_{avg}
1	1	1	1	1056.1	225.5	1281.6 \checkmark
2	1	2	2	839.3	25.0	864.3 \checkmark
3	1	3	3	784.0	0.0	784.0
4	2	1	2	955.2	133.0	1088.2 \checkmark
5	2	2	3	795.0	35.0	830.3 \checkmark
6	2	3	1	785.5	0.0	785.5
7	3	1	3	963.8	153.0	1116.8 \checkmark
8	3	2	1	831.8	0.0	831.8
9	3	3	2	794.6	0.0	794.6

Design of the Bumper Structure

For the bumper test, a legform is impacted on the bumper. A bumper structure is presented in Figure 6. Five design variables are chosen as shown in Figure 6. They are A = distance between the edge of the hood and the edge of the bumper; B = thickness of the bumper foam absorbing the impact energy; C = distance between the edge of the stiffener (a structure to decrease the bend angle of the lower-body) and the edge of the bumper; D = strength of the bumper cross member; and E = bumper height [5][13]. Variable E is different for each vehicle model.

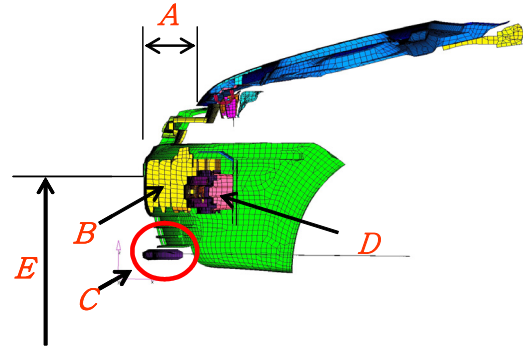


Figure 6. Design variables of the bumper structure.

Since there are five design variables and three levels, $L_{18}(2^1 \times 3^7)$ standard orthogonal array is selected [3]. The values of the design variables from an existing one are set to level 1's. Ones higher than the initial values are set to levels 2 and 3.

The problem is to find the levels of the five design variables to minimize the acceleration, the bending angle, and the shear displacement of the legform. The legform is impacted at a velocity of 40km/h to the center of the bumper structure. Since the acceleration and bending angle requirements are more difficult to satisfy, the corresponding weighting factors are larger. The problem is formulated as

Find A, B, C, D, E
to minimize

$$\eta = (0.45 \times \frac{accel}{200} + 0.45 \times \frac{bend_angle}{21} + 0.10 \times \frac{shear_disp.}{6})$$

subject to

$$\begin{aligned} accel. &\leq 200 \text{ g} \\ bend_angle &\leq 21^\circ \\ shear_disp. &\leq 6 \text{ mm} \end{aligned} \quad (11).$$

where $accel.$ is the acceleration measured at the upper end of the tibia, $bend_angle$ is the maximum dynamic knee bending angle, $shear_disp.$ is the maximum dynamic knee shearing displacement, and η is the characteristic function. Level values for the variables are $A(\text{mm}) = \{78, 105, 132\}$, $B(\text{mm}) = \{25, 50, 75\}$, $C(\text{mm}) = \{\text{none}, -25, 0\}$, $D(\text{ratio}) = \{1, 0.7, 0.5\}$ and $E(\text{mm}) = \{0, 30, 60\}$.

The Design Process of the Bumper Structure Using Computer Simulation

Experiments and computer simulation are performed to evaluate the system. The finite element model is presented in Figure 7. The test facility with a

“variable frontal structure,” is shown in Figure 8. The first experiment is performed with respect to the first row of Table 4. The tuning process of the finite element model is the same as before. Computer simulations are performed for all the rows of Table 4. The results are shown in Table 4.

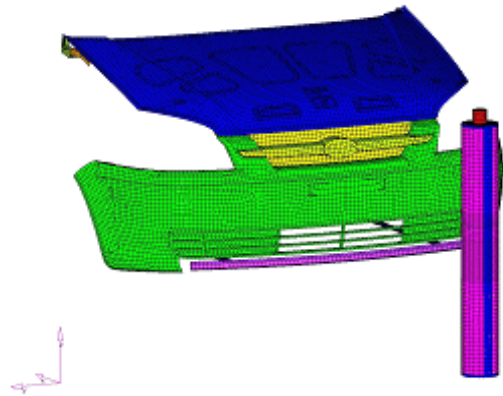


Figure 7. FE model of the lower legform impact test.

Table 4.
 $L_{18}(2^1 \times 3^7)$ orthogonal array using computer simulation for the bumper structure

Exp. No.	Factor assigned					Characteristic value		
	A	B	C	D	E	η	\bar{P}	η_{avg}
1	1	1	1	1	1	1.325	0.688	2.010 ✓
2	2	2	2	2	2	1.063	0.310	1.373 ✓
3	3	3	3	3	3	1.026	0.097	1.122 ✓
4	1	1	2	2	3	1.329	0.557	1.886 ✓
5	2	2	3	3	1	0.782	0.000	0.782
6	3	3	1	1	2	1.152	0.695	1.847 ✓
7	1	2	1	3	2	1.109	0.667	1.775 ✓
8	2	3	2	1	3	1.339	0.538	1.877 ✓
9	3	1	3	2	1	0.997	0.106	1.103 ✓
10	1	3	3	2	2	0.690	0.000	0.690
11	2	1	1	3	3	1.238	0.829	2.067 ✓
12	3	2	2	1	1	0.820	0.000	0.820
13	1	2	3	1	3	1.030	0.104	1.134 ✓
14	2	3	1	2	1	1.098	0.629	1.726 ✓
15	3	1	2	3	2	1.108	0.238	1.346 ✓
16	1	3	2	3	1	0.942	0.065	1.007 ✓
17	2	1	3	1	2	0.983	0.072	1.054 ✓
18	3	2	1	2	3	1.192	0.776	1.968 ✓

η_{avg} is defined from Equations (6) and (11) and the scale factor is set by $s = 1$. All the rows except for rows 5, 10, and 12 do not satisfy the constraints and are marked by ✓ on η_{avg} . Intermediate design 1 is A_3, B_2, C_3, D_3 and E_1 . From the simulation for confirmation, $\eta_{avg} = 0.587$ and the constraints are satisfied. The acceleration is 166.5g, the knee bending angle is 8.3°, and the shearing displacement is 2.1mm. Intermediate design 2 is the tenth row of Table 4. Since intermediate design 1 is better, it is selected as the final solution. The solution is $A = 132\text{mm}, B = 50\text{mm}, C = 0\text{mm}, D = 0.5$ and $E = 0\text{mm}$.

Design by Experiments and Computer Simulation for the Bumper Structure

Experiments are carried out by the facility in Figure 8. Experiments are performed for rows 1-6 of Table 5 where each level of a design variable appears twice. Computer simulations are carried out for the rest of the rows. As shown in Table 5, all the rows except for rows 3, 5, 10, 12 do not to satisfy the constraints and are marked by ✓ on η_{avg} . Intermediate design 1 is A_3, B_2, C_3, D_3 and E_1 .



Figure 8. Lower legform impact test setup.

Computer simulation is conducted for confirmation with intermediate design 1. The results are $\eta_{avg} = 0.587$, acceleration = 166.5g, knee bending angle = 8.3°, and shearing displacement = 2.1mm. The constraints are satisfied. Intermediate design 2 is obtained from Table 5. It is the third row with A_3, B_3, C_3, D_3 and E_3 . Since intermediate design 2 is better, it is chosen as the final solution. The final solution is $A = 132\text{mm}, B = 75\text{mm}, C = 0\text{mm}, D = 0.5$, and $E = 60\text{mm}$. For the final solution, the acceleration is 86.6g, the knee bend angle is 15.2° and the shear displacement is 2.7mm.

Table 5.
 $L_{18}(2^1 \times 3^7)$ orthogonal array using experiments
and computer simulation for the bumper structure

Exp. No.	Factor assigned					Characteristic value		
	A	B	C	D	E	η	\bar{P}	η_{aug}
1	1	1	1	1	1	1.348	0.614	1.962 \checkmark
2	2	2	2	2	2	0.816	0.143	0.957 \checkmark
3	3	3	3	3	3	0.565	0.000	0.565
4	1	1	2	2	3	1.007	0.257	1.265 \checkmark
5	2	2	3	3	1	0.588	0.000	0.588
6	3	3	1	1	2	1.055	0.657	1.712 \checkmark
7	1	2	1	3	2	1.109	0.667	1.775 \checkmark
8	2	3	2	1	3	1.339	0.538	1.877 \checkmark
9	3	1	3	2	1	0.997	0.106	1.103 \checkmark
10	1	3	3	2	2	0.690	0.000	0.690
11	2	1	1	3	3	1.238	0.829	2.067 \checkmark
12	3	2	2	1	1	0.820	0.000	0.820
13	1	2	3	1	3	1.030	0.104	1.134 \checkmark
14	2	3	1	2	1	1.098	0.629	1.726 \checkmark
15	3	1	2	3	2	1.108	0.238	1.346 \checkmark
16	1	3	2	3	1	0.942	0.065	1.007 \checkmark
17	2	1	3	1	2	0.983	0.072	1.054 \checkmark
18	3	2	1	2	3	1.192	0.776	1.968 \checkmark

Discussion

The two methods give the same solution in the design of the hood structure. However, they give different solutions in the design of the bumper structure. The designs are improved in both cases. Computer simulations contain large amount of errors that can change the design results. Therefore, when experiments and simulations are simultaneously used, a more precise solution can be obtained.

CONCLUSIONS

From this research, the followings are concluded:

1) A new method is proposed to use experiments and computer simulation in design. Orthogonal arrays are employed in the design process. Error analysis is conducted for the method. Automobile hood and bumper structures are designed for pedestrian protection by using the proposed method.

2) Designs are carried out in two methods - one utilizing only computer simulation, and one utilizing experiments and computer simulation. The results from the two methods are compared. Precise solution

is obtained from the method by using experiments and computer simulation because the errors are reduced.

3) The final design of this research is for pedestrian protection. More researches are needed to see if the design satisfies other regulations on frontal impacts, offset impacts and bumper impacts, etc.

ACKNOWLEDGEMENTS

This research was supported by the National Transportation Key Technology which is funded by the Korea Ministry of Construction and Transportation. It was also supported by the Center of Innovative Design Optimization Technology, which was funded by the Korea Science and Engineering Foundation. The authors are thankful to Mrs. MiSun Park for correction of the manuscript.

REFERENCES

- [1] UNECE/TRANS/WP.29/AC.3/7, "Proposal to Develop a Global Technical Regulation Concerning the Protection of Pedestrians and Other Vulnerable Road Users in Collision with Vehicles," <http://www.unece.org/trans/main/welcwp29.htm>, 2004.
- [2] Schuster, P. J., "Evaluation of the Real-World Injury-Reduction Potential of the Proposed European Pedestrian 'Leg-form' Impact Test Using a Detailed Finite Element Model of the Lower Limb," Michigan Technological University, 2000.
- [3] Phadke M.S., Quality Engineering Using Robust Design, Prentice Hall, Englewood Cliffs, New Jersey, USA, 1989.
- [4] Park, G. J., "A Design Methodology with Orthogonal Arrays Using Experiments and Computer Simulations," J. of KSME (A), Vol.28, No.7, pp. 885-895(in Korean), 2004.
- [5] Lee, J. W., "Vehicle Hood and Bumper Structure Design to Mitigate Casualties of Pedestrian Accidents," Ph.D. Dissertation, Hanyang University, Seoul, Korea (in Korean), 2004.
- [6] EEVC Working Group 17 Report, "Improved Test Methods to Evaluate Pedestrian Protection Affected by Passenger Cars," European Enhanced Vehicle-Safety Committee, 1998.
- [7] UNECE/TRANS/WP.29/GRSP, "Pedestrian Traffic Accident Data," <http://www.unece.org/trans/main/welcwp29.htm>, 2003.

[8] Commission of the European Communities, "Directive 2003/102/EC of the European Parliament and of the Council of 17 November 2003 Relating to the Protection of the Pedestrians and Other Vulnerable Road Users in the Event of a Collision with a Motor Vehicle and Amending Council Directive 70/156/EEC," Commission of the European Communities, 2003.

[9] Arora, J.S., Introduction to Optimum Design, Elsevier, 2nd Ed., USA, 2004.

[10] Park, S. H., Modern Design of Experiments, Minyoungsa, Seoul, Korea (in Korean), 1991.

[11] Park, G. J., Analytic Methods for Design Practice, Springer-Verlag. Germany (to be published), 2005.

[12] LS-DYNA Ver. 960, "Keyword User's Manual," Livermore Software Technology Corporation, Livermore, CA 94550, 2001.

[13] Han, Y. H. and Lee, Y. W., "Development of a Vehicle Structure with Enhanced Pedestrian Safety," SAE, 2003-01-1232, 2003.